IMPROVED DOCUMENTATION OF CULTURAL HERITAGE USING DIGITAL PHOTOGRAMMETRY WITH VISIBLE AND THERMAL IMAGES FROM UNMANNED AERIAL VEHICLES (UAV)

Dissertation

submitted to and approved by the

Department of Architecture, Civil Engineering and Environmental Sciences
University of Braunschweig – Institute of Technology

and the

Department of Civil and Environmental Engineering
University of Florence

in candidacy for the degree of a
Doktor-Ingenieurin (Dr.-Ing.) /
Dottore di Ricerca in Civil and Environmental Engineering[*)]

by
Saadet Armağan GÜLEÇ KORUMAZ
born 16 September 1981
from Gölcük, Türkiye

Submitted on	5 February 2018
Oral examination on	8 May 2018
Professorial advisors	Prof. Wolfgang Niemeier Prof. Grazia Tucci

2019

*) Either the German or the Italian form of the title may be used

DECLARATION PAGE

I hereby declare that all information in this document has been obtained and presented in accordance with academic rules and ethical conduct. I also declare that, as required by these rules and conduct, I have fully cited and referenced all material and results that are not original to this work.

S. Armağan GÜLEÇ KORUMAZ
05.02.2018

ABSTRACT

Ph.D THESIS

Improved Documentation of Cultural Heritage using Digital Photogrammetry with Visible and Thermal Images from Unmanned Aerial Vehicles (UAV)

S. Armağan GÜLEÇ KORUMAZ

Department of Architecture, Civil Engineering and Environmental Sciences

University of Braunschweig – Institute of Technology

and the

Department of Civil and Environmental Engineering

University of Florence

Tutor (Italy): Assoc. Prof. Grazia TUCCI
(Germany)Prof. Wolfgang NIEMEIER

There is always need for reliable and accurate data for documentation of cultural heritage including archaeological areas. The development in 3D data acquisition has let some technologies use for getting a complete documentation. Close range photogrammetry and terrestrial laser scanning are among the most common used techniques which help to get 3D data acquisition, with high level of detail, accuracy and effective results. However, these techniques are not always the most suitable ones for large archaeological areas, yet aerial images may help to provide a general overview of the area which is fundamental for interpretation and documentation of archaeological sites. Because of the limitations in aerial photogrammetry, UAVs (Unmanned Aerial Vehicles) has become an optimal solution for archaeological areas documentation with its potentials in the context of costs and abilities. To cover large areas at different altitudes, to be able to fly at different altitudes, under different weather conditions, to acquire image with high resolution are among the main advantages of this technology which make it usable and preferable for archaeological documentation. Since UAVs have been rapidly improving in sophistication and reliability, its possibilities aid in archaeological research have recently generated much interest, particularly for documenting sites, monuments and excavations.

In this case study several aerial surveys will be conducted with a UAV mounted thermal camera on an archaeological area. After acquiring aerial images, they will be processed for producing both color and thermal-imagery in related software. Next step will be the alignment of the images in order to build an accurate and georeferenced 3D and mesh model of surveyed area. Then colored and thermal orthophoto mosaics as well as digital surface model (DSM) will be obtained for the documentation. The datasets of thermal images and color images will be collected and compared in order to detect archaeological remains on and under the ground.

Keywords: Aerial Thermography, UAV, Cultural Heritage Documentation, Archaeological Documentation

Acknowledgements

This PhD research has been conducted thanks to a PhD scholarship given by the University of Florence in Italy which is greatly acknowledged. I would like to express my special thanks to Prof. Grazia Tucci and Prof. Wolfgang Niemeier and to for allowing me to conduct this PhD study under their supervision in Geodesy and Photogrammetry Institute in Braunschweig Technical University in Germany, Polytechnic University of Milan in Italy and Selcuk University Faculty of Engineering Department of Geomatics Engineering and for encouring me and my studies with their valuable suggestions. I also would like to give my special thanks to Prof. Ferruh Yıldız (Selcuk University, Department of Geomatics Engineering) and Prof. Elisabetta Rosina (Polytechnic University of Milan, ABC Department) and Assist. Prof. Murat Selek (Selcuk University, Department of Electronics and Automation) for their special support during the research. I also would like to thank GECO laboratory (DICEA, University of Florence) for their big help and support in all this process. I would like to give my special thanks to the people who helped me for my case studies and for providing data. I wish to acknowledge for the cooperation and support to Dipl.-Ing. Ralf Heyen (Geodesist and Assessor of the German Public Survey Administration Board)-CEO&Owner of GRAVIONIC; and from his team Markus Bobbe, Thomas Krüger and Christian Tonhauser for their help and to Martin Lehman from Braunschweig Technical University Geodesy and Photogrametry Institute. For the case studies in Italy, I would like to thank to Simone Orlandini from Microgeo and Marco Salvadori from Microgeo. For the case studies in Turkey, Erkan Baygül from Paksoy Teknik A.ş. is acknowledged. Finally I would like to thank to my colleague Chiara Arrighi for her friendship, guidance and support during my stay in Braunschweig and especillay in Florence.

INDEX

List of Figures

1.INTRODUCTION

Documentation of cultural heritage resources, from a small object to a landscape, is a keystone for their conservation whatever the purpose is to protect them or to make a record. The process is a comprehensive study which requires getting information from different sources for a complete research. This information would help for determination of current situation of the heritage, would be a good guide for decision-making process, would promote to transmit historic knowledge and would facilitate the understanding the values of heritage by humankind. Even though it's a demanding process, detailed documentation serves as primary step for management of cultural heritage. An improved documentation could be used as a tool to support the participation of stakeholders such as public, owners, managers and conservators to all steps of management process.

As a continuous cycle, documentation requires an interdisciplinary work to get necessary information. This information involves extensive data such as sketches, photographs, reports, written descriptions, technical drawings, 3D models, texts etc. Here, the selection and application of proper method and tools become crucial to collect this data when an improved documentation is needed. To decide the most convenient technology, it is indispensable to understand its performance, expected precision and the available resources. The object size, complexity and required accuracy are also the main indicators to choose the appropriate tools and methods. Even though the studies have been proved that there is no certain rule or formula to determine which technique might be the suitable one for any situation, it is certainly mentioned that there should be a strong link between the required output, scale and size.

In last decades, the rapid developments in digital technologies have also affected cultural heritage documentation techniques and reformed the workflow of the practice. Digital tools have led to new openings for each of documentation steps which are planning, data acquisition, data processing, data management and dissemination of the data. Although traditional survey methods are still important and could be used in some cases, technological possibilities have given opportunity to support them in different ways. According to the classification of metric survey techniques by English Heritage, direct and indirect techniques are mainly applied in cultural heritage documentation field (Heritage, 2011). Direct techniques includes hand measurement, levelling, total station and GPS while indirect techniques involves remote sensing, rectified photography, artefact scanner, close range photogrammetry, remote sensing, terrestrial laser scanning, airborne lidar and aerial photogrammetry. In most cases the combination of these technologies and related methodologies regarding their benefits may be the best solution depending on the final product since each of them has some limitations and advantages (Russo and Guidi, 2011; Grussenmeyer et al., 2008; Patias, 2006.).

As a direct technique, hand measurement can provide dimensions and positions of objects and scenes of a few meters, sketches in small size which is sometimes more impractical and not enough for larger objects. In this case, photogrammetry and terrestrial laser scanning could be more suitable by covering larger areas and enabling a

large quantity of three-dimensional measurements to be collected. The studies have shown that photogrammetry has advantages for large amount of data, accurate data, possibility to texture in high resolution and detail, geo-reference data with stereo-viewing capability of the 3D data (Grussenmeyer et al., 2002, Patias, P., 2006). Similarly Terrestrial Laser Scanning technology has high performance in terms of data acquisition speed (Russo and Guidi, 2011) in different field of uses and has advantageous when used appropriately (English Heritage, 2007; Russo and Guidi, 2011).

These both techniques have made it possible to obtain a high level of detail and accuracy and result to be very effective for small and medium-extension areas. However for large areas close range photogrammetry and terrestrial laser scanning are not always the most suitable techniques. Here, the information obtained from aerial or satellite images provide an overview of the study area to complete the documentation. Even they have been used for a long time; such images have some limitations linked to the geometric resolution, inadequate for detailed studies, to the periods of acquisition and to the cost (Lo Brutto et al., 2012). Besides, another challenge of these methods is the difficulty involved in acquiring reliable radiometric information of the complete surveyed area, which can easily be obtained by means of traditional aerial photogrammetry. However, the costs of aerial photogrammetry are usually too high in relation to the limited extension of the surveyed areas. Even the aerial techniques can be an optimal solution in the case of medium-sized and large sites, since the possibility of raising sensors and capturing the information, in many cases it is rather difficult to obtain data at ground level, which can increase the performance of photogrammetry. But these surveys generally require working with large scales and high resolutions.

Due to these restrictions in aerial photogrammetry UAVs (Unmanned Aerial Vehicles) have become alternative solutions for documentation of cultural heritage and archaeological areas because of their relatively low price and capabilities. UAVs were initially used for observation and defensive purposes and then they have started to be used in Research and Development (R&D) as well as civil and commercial fields. In the last years also architecture and geomatics disciplines have been involved to these fields. They have become preferable especially in areas difficult and dangerous to access. Particularly in archaeological areas where there is potential danger to heritage or workers/researchers, they could be used without any risk or damage. The advantages such as the ability to fly in changing weather conditions and in different altitudes, to obtain high resolution and detailed aerial data and to cover large areas with images have included UAVs among the methods used in cultural and archaeological heritage documentation.

Moreover, UAVs have been rapidly improving in sophistication and reliability, its possibilities aid in archaeological research have recently generated much interest, particularly for documenting sites, monuments and excavations. In the 1970s, archaeologists have recognized that aerial images recording thermal infrared wavelengths could be a powerful tool for recognizing surface and subsurface cultural remains, yet technological and cost barriers have largely prevented the widespread application of thermography in archaeological contexts. Despite its potential, archaeological applications of the technology are scarce, largely because few

archaeologists had access to the highly specialized radiometers used by researchers in the 1970s. However in the last years, with new developments in thermal cameras and sensors, it has started to get much interest from the researchers and archaeologists. It is clear that such a kind of technology would help to conservators and decision-makers in decision and documentation process of cultural heritage which are the main objectives of cultural heritage management. Acquired data before excavation would change the process of excavation and would give a new direction to it. Besides, it may help to find deteriorated parts, to observe buried areas where accessibility is too low or hazardous since it is a non-destructive method. In order to get an overview of the survey area, it is needed to be on the archaeological area which is sometimes very dangerous for the surveyor and cultural heritage. In many cases, these kinds of areas are prone to collapse easily that may destruct both surveyor and remains. This technology may prevent this kind of damages and help to get useful data. Moreover, this technique could be used to find buried archaeological walls, roads or to detect water channels, field boundaries as well as architectural remains under the ground in addition to current situation by means of thermal behavior of the materials.

Depending on these general concerns, the study aims to define the capabilities of UAVs for improved documentation of cultural heritage. The study mainly comprises of three parts as theoretical part, case studies and results. For the theoretical part of the thesis, UAV Photogrammetry, Infrared Thermography and Aerial Thermography have been described with their data acquisition and data processing concepts. The theoretical part also concerns about the examples which UAVs are used with color and thermal cameras in cultural heritage and archaeological area documentation field. This part additionally reviews about the current status and future of these techniques.

The second part includes different case studies. In order to analyze the capability of UAVs for cultural heritage documentation, several aerial surveys have been conducted with several types of UAVs in different fields. The case studies have been chosen as different cultural heritage types including a historical building with demolished roof and different archaeological areas. In these fields, UAVs with color and thermal camera have been used to evaluate the performance of UAVs for documentation and detection of archaeological buried ruins. Each case study has been explained with its field work, data processing and results.

Depending on this theoretical and application part, last part of the thesis provides a summary of the thesis related to data results. It involves evaluation of UAVs use in cultural heritage field for improved documentation. It also describes the advantages and limitations of the technology and gives set of recommendations for future researches.

1.1. Aim of the study

The aim of this study is to analyze the capability of UAVs for improved documentation of cultural heritage and to reveal buried architectural ruins with low altitude thermal survey using UAVs. For this aim, the combination of flexible and relatively low-cost a UAV with digital camera and thermal camera has been used on diverse case studies.

Within the frame of the study, the aims of the thesis could be defined as below:

- To review the cultural heritage changing definition by the time and to identify what cultural heritage documentation is; with its steps and components.
- To identify the current situation of cultural heritage documentation techniques with its diverse purposes
- To explore UAV Photogrammetry starting from categories, advantages and limitations including its system composition and regulations
- To examine the workflow, data acquisition and data processing concepts and to understand the current status and the future of UAV photogrammetry
- To identify the use fields of UAV for cultural heritage documentation
- To make a research the principles and parameters of Infrared Thermography including its techniques, data acquisition and data processing concepts
- To define the use fields of thermography for cultural heritage and the principles of aerial thermography for archaeological purposes
- To evaluate the capability of UAVs for archaeological detection for buried structures with low altitude thermal survey
- To indicate the benefits of thermal imagery in archaeological research
- To study the potentials of UAV as a tool for documenting and analyzing for archaeological sites on both the detailed scale and the wider territorial scale by using both color and thermal images.
- To consider the advantage of different scales and the possibilities of color and thermal imagery to arrive at a working heritage information model.
- To check the accuracy of data from UAVs for architectural purposes
- To see the capability of UAVs in indoor applications, to get an idea of problems and try to open new research areas.
- To improve a method in order to document and to reveal underground architectural ruins
- To bring together interdisciplinary specialists in order to collaborate for better documentation of cultural heritage and share their experiences
- To help conservators and decision-makers in decision-making and documentation process of cultural heritage
- To find a solution which may help surveyors on site ; when the accessibility of cultural heritage is very difficult or hazardous
- To provide a valuable complement to regional archaeological surveys, by revealing the likely location of archaeological features across large areas.

- To open new research fields and facilitate many possibilities to make aerial thermography as standard stage in archaeological investigations with imagery data.
- To create a discussion for availability of this technology for other disciplines.

1.2. Content of the study

The study basically consists of three parts in content.

Theoretical part: This part outlines the current situation of cultural heritage documentation with its changing definition and used techniques. Theoretical framework of the thesis gives definition of UAV Photogrammetry, Infrared Thermography and Aerial Thermography with their principles, advantages and limitations, data acquisition and processing concepts with their workflow. This part also reviews the example studies which these techniques are used for cultural heritage documentation purpose.

Case studies: In this section, several UAVs were used in four case studies. Both the size, complexity and the purpose of the projects were different. Besides, different types of UAVs were used with different workflows. Each case study was evaluated in its special condition and each of them involves description of the aim of the study, applied methodology, data acquisition, data processing and the results. In the first case study, a historical building with a demolished roof was chosen and the aim of the project was to see the capability of UAV for historical building documentation. For this, the results were evaluated if the output is enough accurate to draw architectural survey project. In the second case study, UAV survey was conducted on an archaeological area which comprises archaeological ruins. The area dates back to Anatolian Seljuk period and the ruins belongs to the only Seljuk palace survived today. The aim of the study was to check how the orthophoto is accurate. For this aim, the results were checked according to international orthophoto accuracy standards. In the third case study, a UAV with thermal camera was applied to an area where there was an old villa called Villa Medici. The aim of the study was to check the capability of UAV for determination of archaeological buried ruins. The forth case study is another archaeological area, Çatalhöyük where there is a Neolitic settlement. In this case study, another type of UAVwith thermal sensor was used to have 3D model of the area and to make archaeological ruin inspection under the ground.

Conclusions: In the last part of the thesis, while a short summary of the thesis is given, general evaluations were made on obtained results. According to the outputs of the case studies, solved problems and needed further researches were recommended.

1.3. Material and Method
1.3.1. Material

In the field works of each case study, it has been benefited from the current technological possibilities. In the first case study, Quadcopter based on a DJI F450

frame produced by GRAVIONIC whic is equipped with Canon IXUS 220HS 12MP camera was used for aerial survey. The control points were masured with RTK GPS. In the second case study, Smartplanes Freya fixed-wing UAV, for image acquisition Ricoh GR16.1 MP compact camera with 18.3 mm lens was used for aerial survey. In the third case study, AeroMax 600 drone from MicroGeo was used with a camera SONY Alpha 5000 with 14.2 MP resolution. To get tehrmal data OPTRIS PI 450 thermal camera 382 x 288 px with Optical resolution was mounted to same UAVand in different times of the day, several video records were done. GCPs were also measured with GPS. Aerial data of the fourth case study was acquired by two different UAVs. To get all area aeral data e-Bee UAV RTK from Sensefly was used with SONY WX200 color camera with 18.2 MP. For aerial data of inside the shelter, indoor place, Albris Sensefly quadcopter 38 MP digital camera was used. However in this UAV, there was a thermal sensor on UAV which has thermal overlaid (80 x 60 pixels) on main camera stream with 50 degree horizontal field of view. In this case study, GCPs were measured with RTK GPS.

For the processing of aerial data, mainly Agisoft PhotoScan 1.1.5 was used. Only in the fourth case study, to compare two softwares, also Pix4Dmapper Pro (3.2.23) was used. OPTRIS PI Connect Software was used for processing aerial thermal data for snapshots and thermal profiles. Temperature graphs were also prepared in excel. Materials used in each case study are described in their section in detail as well.

1.3.2. Method

Deepending on the the subject of “Architectural Documentation of Cultural Heritage”, the necessities helped to define the problem of the thesis. The needed improved documentation could be supplied by integration of different methodologies and tools. After an extensive literature review, theoretical background has been constituted by reviewing the current status of CH documentation and describing the UAV Photogrammetry and Infrared Thermography (IRT) techniques with their definition, concepts, used fields, field work and data processing steps. These steps were applied into different case studies after decision of them, definition of the aim of the project and the selection of technology. Each case study was described in detail with its each step including data acquisition, data processing and evaluation of the results. Under the guidance of theoretical part information and case studies results, general remarks and recommendation for further researches were done as conclusion.

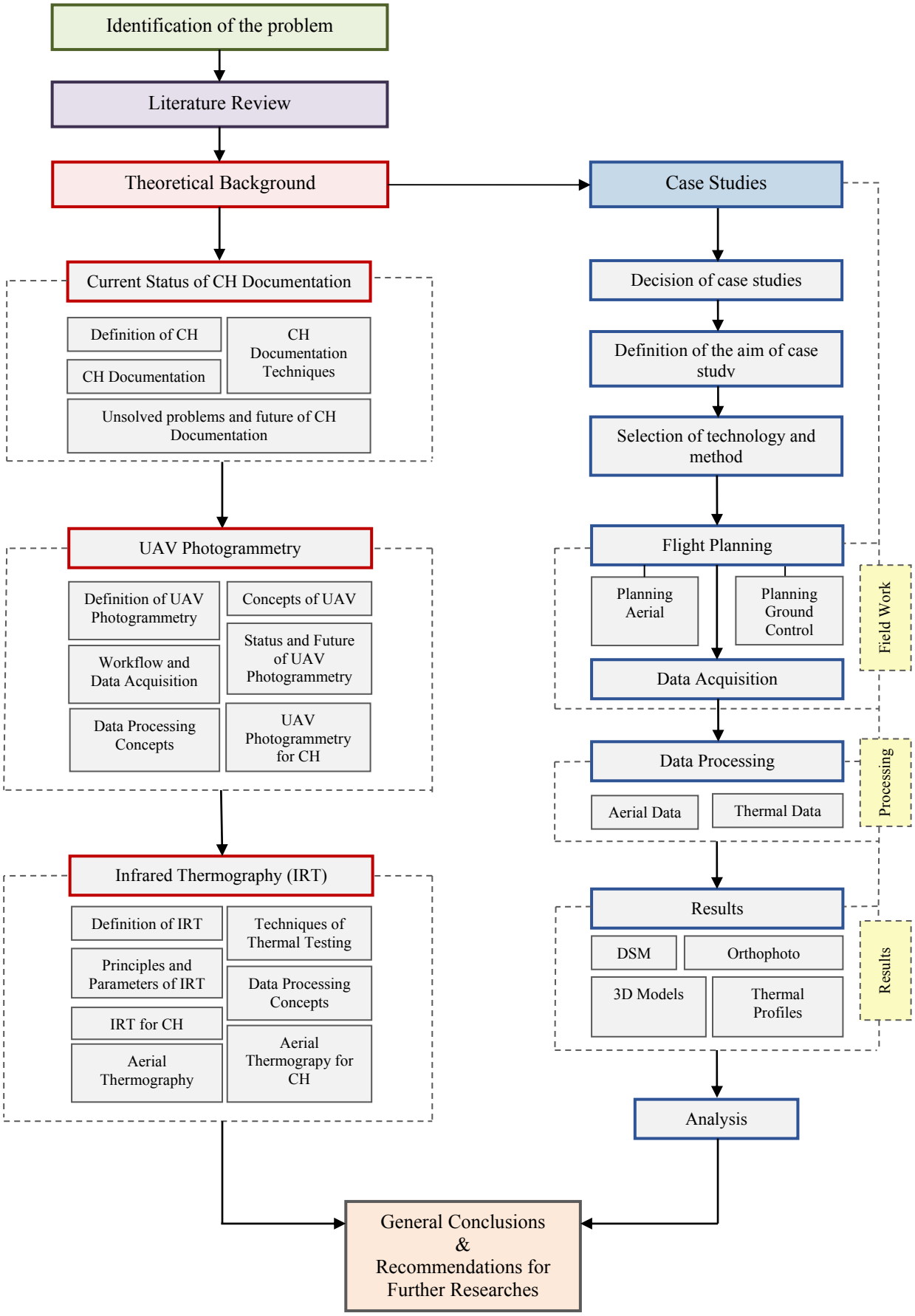

Figure 1.1: Methodology and structure of the thesis

2. CURRENT STATUS OF CULTURAL HERITAGE DOCUMENTATION

2.1. Cultural Heritage Definition

Definition of *cultural heritage* has developed and expanded during the history so its scope in the historical process has differentiated by the time. This definition was limited only to the important monumental structures in the first stages of conservation concept and over time it included civilian buildings, urban and rural areas, and even abstract categories such as culture and arts. According to Vecco (2010), it was firstly used on October 4, 1790 in a petition aimed at the Constituent Assembly by François Puthod de Maisonrouge, while he was trying to convince the emigrants to transform their heritage from family to national (Vecco, 2010). Important events in the historical process have been decisive in the expansion of definition of cultural heritage. The French Revolution in the 18th century is an important milestone in understanding the concept of *heritage*. At the same time, this period was a time when cultural heritage was important, and policies for protection and restoration were developed. The definition of *cultural heritage*, which was firstly started to be used by international organizations in 1931 by the Athens Charter[1], became even more important with the 1964 Venice Charter issued after World War II. After this date it has begun to be perceived as the heritage of humanity(ICOMOS, 1931);(ICOMOS, 1964). In the 1970s, the scope of the definition expanded further including old and rural settlements. Over time it continued to expand by including tangible assets as well as intangible ones. Europe Council (1985), Washington Charter (1987) and UNESCO 1989 Recommendation meetings were mostly effective in this expansion (Europe, 1985);(ICOMOS, 1987);(UNESCO, 1989). In the 2000s, landscape elements became a part of cultural heritage definition then cultural and natural heritage definitions were included. After the 2000s intangible cultural heritage has been included in the scope of heritage (Table 2.1.1)

[1] First International Congress of Architects and Technicians of Historic Monuments

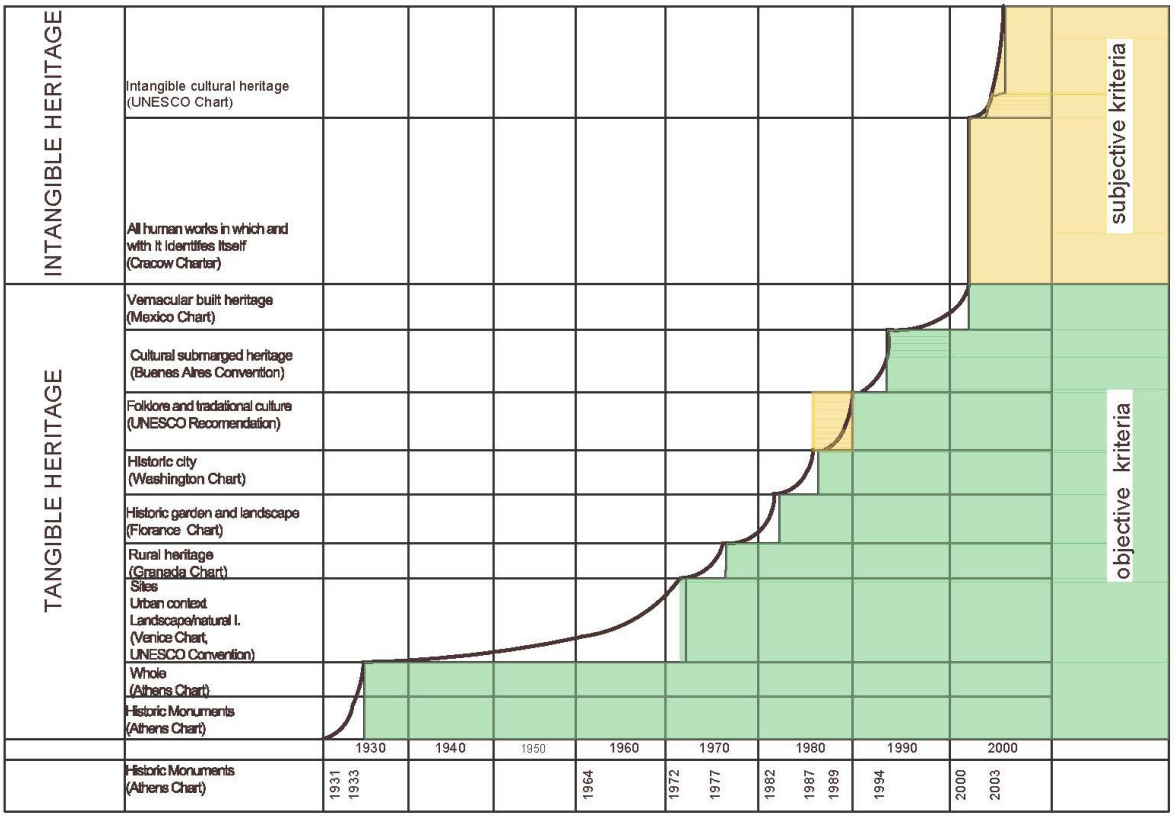

Figure 2.1.1: Changing Cultural Heritage Definition by years (Vecco, 2010).

Over time, the question of what to express, what to cover, how to manage have started to be asked rather than what the cultural heritage is. By the time, the concept of "World Heritage" has developed and the idea that natural and cultural heritage sites are the inheritance of all mankind, not just where they are located, has become widespread and accepted. Today, in addition to the concepts of tangible and intangible cultural heritage, new concepts such as modern heritage, digital heritage and e-heritage have emerged and studies have begun on how to protect and document them. This diversification of heritage concepts has also continued in the field of heritage experience and documentation and it has transformed into a multi-layered structure. The change in the definition and scope of cultural heritage has made conservation and transmission of it more significant for the communities over the time.

In order to transmit of cultural heritage documentation is essential and inevitable. Regarding to the diversity in cultural heritage the documentation techniques has been evolved, changed and new documentation techniques have emerged parallel to cultural heritage definition.

2.2. Cultural Heritage Documentation

Conservation and intervention of cultural heritage requires an interdisciplinary approach which needs the amount of information generated by different specialists. So

the correct recording, documentation, management, dissemination and storage of information become difficult since there are different specialists in the process (Lourenço, Pena, & Amado, 2010).

Cultural Heritage documentation is a complicated process including a range of activities including surveying, testing, analyzing, collecting and monitoring. So as D'Ayala and Smars explanation for documentation; "*The geometry of the object is not the only parameter to be recorded. All specificities making the object unique are meaningful;all potential values – architectural, artistic, historical, scientific and social – are parameters to consider*" it's not enough to document only the geometry of the object (D'Ayala & Smars, 2003).

Furtherly on D'Ayala & Smars's description, the documentation of cultural heritage may be defined as the action of acquiring, processing, presenting and recording the necessary data for the determination of the position and the actual existing form, shape and size of a monument in the three-dimensional space at a particular given moment in time (UNESCO, 1972). The geometric documentation records the present situation of the monuments, as has been shaped in the course of time and is the necessary background for the studies of their past, as well as the studies for their future(Yılmaz, Yakar, Gulec, & Dulgerler, 2007). Similarly Amorim (2011) defines the documentation as complicated process of systematic and comprehensive planning, acquisition, processing, indexing, dissemination of metadata and information graphical and non-graphical (Amorim, 2011). At the end of a documentation project, it is created a huge multimedia database containing information of buildings such as photographs, photographic panoramas, rectified photographs, orthophotos, technical drawings, various types of 3D geometric models, including point clouds, and other kind of data such as videos, audio tapes, interviews, reports, pictures and historical texts, among others.

The scope of the architectural documentation project includes the general characterization of the work being undertaken in their quantitative and qualitative aspects, considering the study of the physical site, the purpose of the surveys, the specification of products to be obtained, data and media formats and execution schedule.(Amorim, 2011)

According to HABS[2], the purpose of the documentation is to conserve an accurate record of historic properties, interventions, changes and everything can be used in preservation and research of cultural heritage (HABS, 1990). Article 16 of the Venice Charter of 1964 set out the responsibilities of those charged with understanding and caring for the historic environment to ensure that '*in all works of preservation, restoration or excavation, there should always be precise documentation in the form of analytical and critical reports, illustrated with drawings and photographs. Every stage of the work of clearing, consolidation, rearrangement and integration, as well as technical and formal features identified during the course of the work, should be included. This record should be placed in the archives of a public institution and made available to research workers. It is recommended that the report should be published*.' (ICOMOS, 1964).

[2] Historic American Building Survey

It can be said that the methodology in architectural documentation includes mainly five parts that can be summarized here:

● The overall planning stage,

that consider all aspects of the work and the objective conditions for it, as well as the financial support and other resources;

● Data acquisition and field work,

when the primary or raw data are captured from in situ studies or compiled from secondary sources, which also involves some other technologies;

● Data processing and analysis, including handling or manipulation,

when the data (primary or secondary) collected are processed to generate the desired products or information and their metadata;

● Management of data

including indexing, storage, retrieval, data security, access, dissemination and publication of the data and information produced for concerned public and, finally,

● Control and documentation of the project,

in which should be analyzed in the various aspects involved in the project's implementation, as well as the assessment procedures used, and product quality grades, and also indicators of income, essential to assist in the planning of future works.

D'Ayala & Smars have also detailed the concepts of cultural heritage documentation as objectivity, values, learning process, continuity, fabric, documentation sets and redundancy in their study (D'Ayala & Smars, 2003). These concepts lead to increasing needs for recording and documentation of CH, which can be shortly defined as,

-***Recording*** and ***collecting*** multi-source, multi-format, multi-content detail with different level of detail and accuracy

-***Processing*** and ***management*** of this data

-***Visualization*** and ***presentation*** of the information with user-friend tools so different kinds of users can acquire using databases, web or even different visualization techniques

-***Sharing*** this information in a secure way with professionals and unprofessional users.

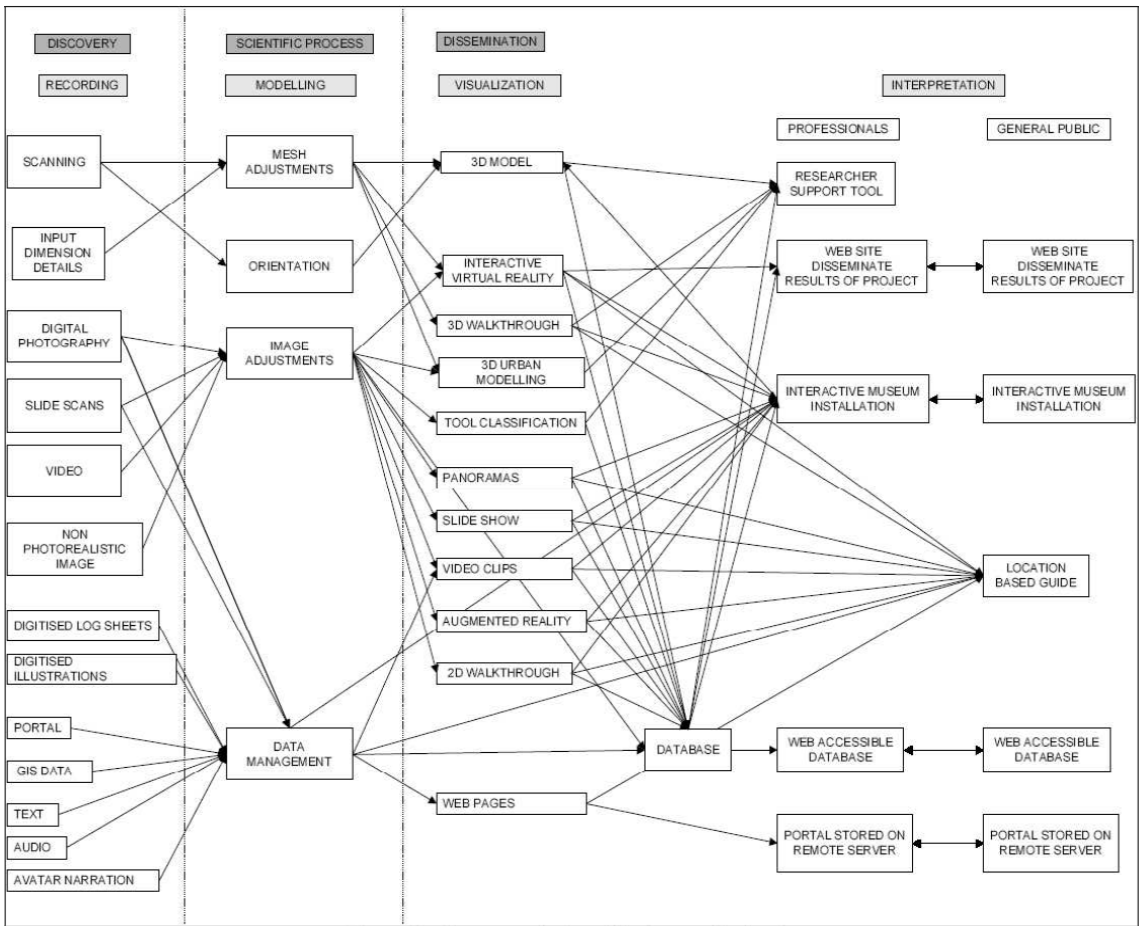

Figure 2.2.1: Techniques used within cultural heritage projects presented at VAST, 2003(Owen, Buhalis, & Pletinckx, 2004).

Owen, Buhalis, & Pletinckx, (2004) put together the needs of cultural heritage process with techniques to be used for each step shown in Figure 2.2.1 (Owen et al., 2004). For recording of CH data, both traditional and modern techniques are used while for processing step it is required to use some special techniques like in the other step visualization. With developing technology visualization techniques changes quickly. For the interpretation of the data using web-sites, interactive museums, portals are available for Professional and unprofessional users.

Even new technologies help for an overall management of CH, due to the complexity of the process, CH documentation has been still difficult. Due to the varying size of the objects, different quality and resolution requirements, level of detail and accuracy needed, CH documentation becomes challenging. Choosing

-Choosing the appropriate technique including software, hardware and equipment

-Deciding to the appropriate methodology

-Designing suitable workflow

-Providing suitable output needed in accordance with technical specifications makes CH documentation challenging (Patias & Santana, 2009).

In order to decide all these steps, the leading parameters become as,

-The size of the object

-The complexity of the object

-Level of detail and
-Needed accuracy
-Required scale

The acquisition of the right survey for the right cost at the right time is a process that requires an appreciation of the balance between the three key elements of the survey:

- Selection
- Measurement
- Communication/presentation(Andrews et al., 2009)

Today with support of technology, different documentation techniques and instruments are available for CH applications changing according to leading parameters mentioned above.

2.3. Documentation Techniques

The evolution of digital technologies has impacted the documentation of cultural heritage. One of the steps that have passed considerable change is maybe the stage of data collection field. Today many different technological tools may be found at affordable prices.

In a documentation project the needs and the aim of the project defines the kind of final product since these needs and the aims will be decisive on the technologies to be employed. Depending on the survey purpose and phase of project documentation several technologies can be employed in the survey field, in data acquisition, data processing, publication and dissemination of information produced. It should, therefore be assessed the resources available for the work, considering the financial, human and technological aspects, so that the expected results can be produced within the requirements of time, cost and quality. This generates a degree of uncertainty for the results, since each experience is unique (Amorim, 2011), (Patias, 2006).

The suitable method for cultural heritage documentation should be chosen considering the needs of research, analysis and conservation. There is no definite way in order to determine which survey technique is the most suitable one in any situation. However the most important links becomes as relationship between the scale required, the selection of data and desired output and the suitable application of the technique is a balance between use of the survey, the precision required and the availability of the resources (Andrews et al., 2009).

There are several classifications of technologies which can be used for CH documentation depending on the leading parameters; *size and complexity of the object*, *level of detail*, *required scale and accuracy*. One of them prepared by Böhler shown in Figure 2.3.1 demonstrates the summary of these techniques in terms of size and object complexity. As it is seen the figure, it can be provided dimensions and positions of a few meter size, with hand measurement technique, close range photogrammetry and terrestrial laser scanner could be more useful in order to get greater number of measurements. Photogrammetry and laser scanning both from air and terrestrial can provide data for larger areas. GPS technique mostly used to collect information about

limited number of points compared to airborne or spaceborn techniques. Laser scanning whether from the air or from the ground enables large quantity of 3D measurements quickly (Heritage, 2011).

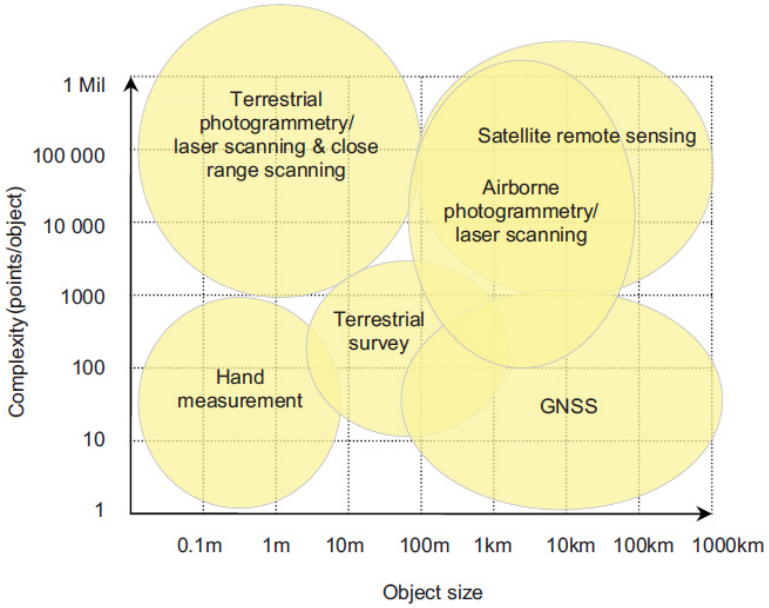

Figure 2.3.1: Three-dimensional survey techniques characterised by scale and object size (derived from Böhler presentation CIPA symposium 2001, Potsdam). (Heritage, 2011)

When the needed accuracy is considered, the classification of the technologies changes. Traditional and digital tools can be recommended with respect to required final output accuracy level. The selection of suitable level of accuracy should be appropriate to the project needs. Figure 2.3.2 below shows the recommended framework for use of recording tools and technologies related to needed accuracy. When low accuracy is sufficient for a documentation, sketches and photographs as traditional tools, CAD measured drawings, GPS , digital photographs, scanning of photographs, digital video and tablet PC can be used as digital recording tools. For midrange accuracy documentation project, in addition to CAD measured drawing and GPS, rectified photos, 3D modelling can be applied as digital tools while hand recording with large and small rectified photographs can be used as traditional recording tools. Digital photogrammetry, total station, GPS, texture mapping, laser scanning techniques are mostly preferable when high accuracy needed and can be supported by traditional tools like rectified photographs and stereophotogrammetry (Letellier, 2007).

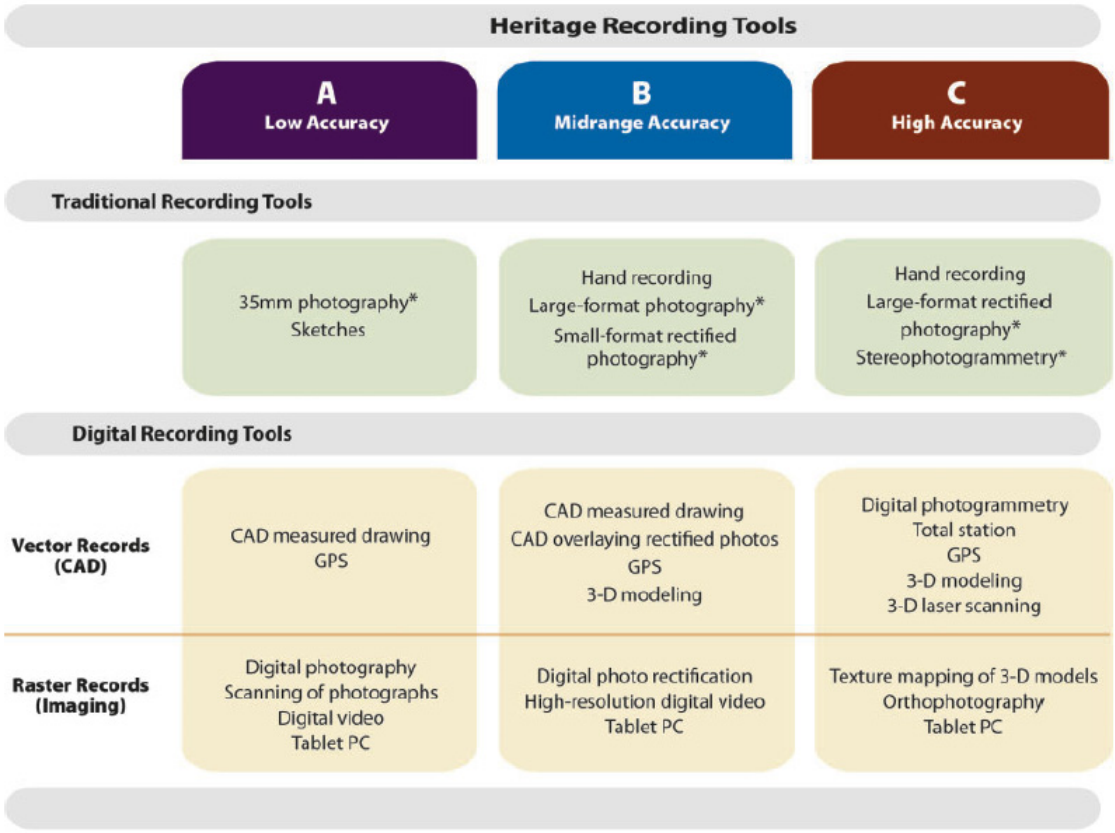

Figure 2.3.2: The relation between recording tools, technologies and accuracy for CH documentation (Letellier, 2007)

Another comprehensive study on classification of applications in terms of the product, methodology and emphasis and their relation with the purpose of the project has been done by English Heritage. The applications are tabled by purpose from small artifacts to city settlements. The products are defined with 2D, 3D vector plans and sections with reconstructions. The methodologies are divided mainly three methods. The study differentiates from others with by emphasis section (Figure 2.3.3) (Bryan, Blake, Bedford, Barber, & Mills, 2009)

Another classification of documentation techniques has been done by Hassani (2015). In the study the categorization based on metric data and acquisition of points' coordinates of the targeted object with or without image was offered shown in Figure 2.3.4 (Hassani, 2015). According to this study, there are mainly three categories: image-based non-image-based and combinative methods. Image-based techniques include photogrammetry (panorama, close range and UAV) and IR cameras while non-image-based techniques comprises traditional terrestrial survey and laser scanner. Apart from these two techniques, photo-laser scanner and structured-light (structured-light, Kinect and DAVID laser scanner) constitutes combinative methods.

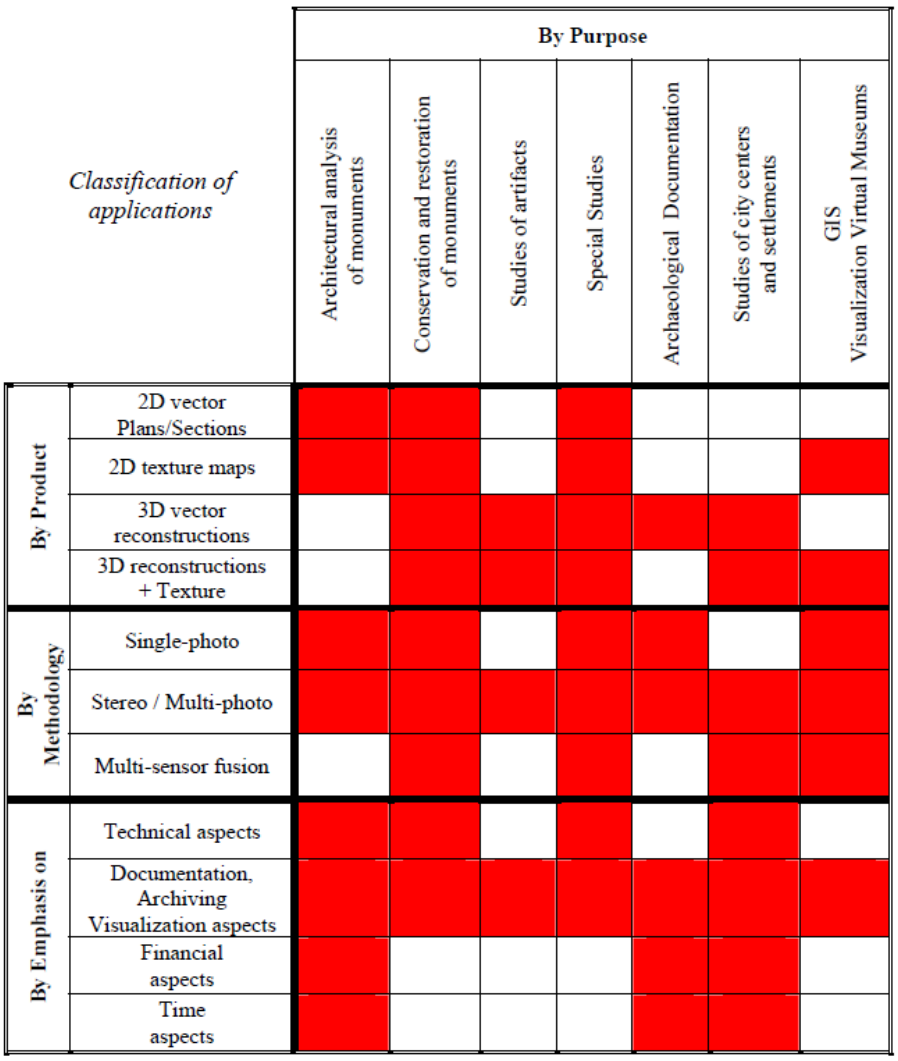

Figure 2.3.3: Technical specifications for CH documentation (Bryan et al., 2009)

Table 2.3.1: The categorization of documentation techniques (Hassani, 2015)

Documentation Techniques	**Image-based**	**Photogrammetry**	**Panorama Photography** **Close-Range Photogrammetry** **UAV**
		IR Cameras	
	Non-image-based	Traditional Terrestrial Survey	Hand Survey Theodolite Measurement
		Laser Scanner	Terrestrial Laser Scanner LIDAR
	Combinative Methods	Photo-laser Scanner	
		Structured-light	Structured Light
			Kinect
			DAVID Lser Scanner

One of the most referred, accepted and detailed categorization of survey techniques ahs been made by English Heritage which is a study adapted from Santana Quintero's study shown in the table 2.3.1 (Bryan et al., 2009). With this study all metric survey techniques are divided mainly two parts called "direct" or "indirect". "Metric

survey" can be defined as: the application of precise, reliable and repeatable measurement methods for heritage documentation (Andrews et al., 2009). These direct and indirect techniques are put together depending on final product, application areas, subject size and limitations in their use.

Table 2.3.2: Summary of metric survey techniques (Bryan et al., 2009)

SUMMARY TABLE OF METRIC SURVEY TECHNIQUES					
TECHNIQUE	**Product**		**Application**	**Subject size**	**Constraints on use**
INDIRECT TECHNIQUES: UNDIFFERENTIATED DATA AT CAPTURE					
REMOTE SENSING	3-D	Wide area landscape records.	Landscape monitoring, water content, mineral reflectance and vegetation health mapping etc.	1-1500Km^2	Dependant on wave band, will not resolve down to centimetric precision in most cases.
AIRBORNE LIDAR	3-D	Topographic mapping.	Landscape mapping and monitoring.	1-500Km^2	Post spacing at sub-metre resolution is costly.
AERIAL PHOTOGRAMMETRY	3-D				Co-ordinated flight plan and ground control.
TERRESTRIAL LASER SCANNING	3-D	Point clouds, surface models.	Building models and drawings.	5-500m^2	Point density must be matched to required information outcome. Congruent image capture needed.
CLOSE RANNGE PHOTOGRAMMETRY	3-D	Photo-maps, CAD drawings, ante-disaster records.	Architectural facade drawings, orthophotos, stereo pairs, surface models.	2-100m^2	Calibrated camera, optimised image capture, object area control, processing software and operator skill.
RECTIFIED PHOTOGRAPHY	2-D	Condition records.	Records of flat facades.	2-50m^2	Only single reference plane scalable.
ARTEFACT SCANNER	3-D	Point clouds, surface models.	Sculpture, relief carving etc.	1-5m^3	Controlled environment required.
DIRECT TECHNIQUES: DATA SELECTED AT CAPTURE					
GPS	3-D	Topographic mapping, point data.	Landscape surveys, inventory mapping, primary orientation to global co-ordinate system.	1-20Km^2	Open sky needed. Height precision can be a problem.
TOTAL STATION	3-D	CAD wire frames, point data.	Topographic mapping, building plans & sections. Precise control network measurement.	0.5-50m^3	Data organisation is needed by code, layer or GIS protocol, trained operators are required.
LEVELLING	2-D	Discrete point height monitoring.	Precise height points.	1-50m	Structural engineers: selected diagnostic points measured for movement monitoring.
DRAWING	2-D	Key detail records, explanatory diagrams.	Structural notes, architectural definition, excavation records.	0.25-5m^3	Selection of information based on subjective domain knowledge.
Table adapted from Santana Quintero, 2003					

2.3.1. Direct Survey Techniques

Direct survey techniques such as measured drawing, GPS (Global Positioning System), Total Station are the techniques which mainly depend on the surveyor's observation skills and proficiency of the surveyor. Direct techniques don't have flexibility like indirect techniques however they are quite effective for many recording tasks. They maximize the expertise of a specialist in the field, contrarily, they minimize post-capture processing and they conduct specific information directly (Bryan et al., 2009)

As a traditional technique ***measured building survey*** using direct measurement and site drawing with sketches remains still highly important and useful. This method can be defined as the supply of metric survey related to buildings or sites and the products can be presented as plans, sections and elevations to be supplied as CAD drawing. Metric requirements of this method is shown in Table 2.3.1.1 below.

Today, this traditional method can be supported by using digital tools like laser levels, digital tape measures which increases the accuracy of the survey and reduce the time. It could be said that for simple and without ornament, this method is still valid. For complex buildings with different angles and deformations, it must be supported by topographic measurement. Another limitation of this method is with high buildings, because of the need of scaffolding, time consuming and has the risk of accidents

Table 2.3.1.1: Tolerance and precision of detail relation(Bryan et al., 2009)

Precision	
Required maximum tolerance for precision of detail	
scale	acceptable precision
1:10	+/- 5mm
1:20	+/- 6mm
1:50	+/- 15mm
1:100	+/- 30mm
1:200	+/- 60mm
1:500	+/- 150mm
No less than 67% of a sample is to be within the stated tolerances and no less than 90% is tobe within 1.65 times the stated tolerances.	

. Even though it's simple to apply by non-experts, requires low-cost equipment and helpful where visibility is limited; it has low accuracy with bigger objects, time consuming, long-field work and it has difficulty in documenting inaccessible features, influenced by human errors (Hassani, 2015). In such cases, it is always better to support this method with topographic method especially with closed polygonal to reduce the errors, to provide better dimensions (Andrews et al., 2009) (Amorim, 2011). As common method for architectural surveys, it relies on a clear sketch and the practitioner should have a strong type-specific knowledge.

Surveying with ***total station*** as direct technique is relatively rapid and precise technique that it is made observations with instrument. Depending on the object size and complexity, the number of the station and traverse can be changed. For this technique, to decide the points to be measured in terms of location and density, the performance of angular and distance measurements for precision are issues to be considered for a successful survey (Andrews et al., 2009). For this technique, the precision is directly related to the condition of the equipment[3] and to the measurement procedure. Even it gives reliable results for all kinds of surveys; this technique is more effective especially in close-range works from 0.25 to 100m. Principle[4] and common errors[5] can be avoided by using the correct application procedure and correct use of instrument (Andrews et al., 2009). It's possible to get precise control data, building surveys, monitoring or physical movements. Additionally, it supports to provide the production of plans, sections and elevations of the building survey and rectified photography. This technique is cost effective if number of points is limited and it gets high accuracy with easy use. However, if it is needed to get more data, the field work may be long, besides it is not possible to document colored data and it requires skilled operator ((Hassani, 2015)

Topography is a method for calculating the coordinates of points inacessible with direct measurement. For the purpose of topographic survey can be defined as the

[3] Most modern instruments measure angles to between 0.5 seconds and 7 seconds of arc, and distances to between 0.1mm and 10mm (the differences dependant largely on price).

[4] Principle errors: Random, systematic and gross errors.

[5] Additive and scalar errors

controlled measurement of natural and artificial landscape features (Bryan et al., 2009). It's a good solution as direct method however the process of determining the coordinates of the point of surveying instruments is too laborious when many points were needed to be determined. With the the automatization of surveying instruments, determining the coordinates of points, distances and angles has been greatly simplified.
Even though topography and direct measurement combination can be used performly in some cases, in many situations new technologies may be needed. As a particular situation, buildings with non-polygonal shapes and buildings with complex ornaments, new demands can be needed when there is a need of 3D representation of the monument.

As another technology used in documentation of cultural heritage is ***GNSS-Global Navigation Satellite System*** and more known one ***GPS-Global Positioning System***. Even in most cases this technology comes as secondarily, it provides the location and coordinates in global geographical system. This technique can be used very effectively with other techniques yet with high accuracy data it mostly becomes expensive and it is not appropriate for indoor measurements.

2.3.2. Indirect Survey Techniques

Indirect techniques such as photogrammetry and laser scanning are used for getting any kind of metric data, especially when the size of the object and its representation needs a high density of point capture and the products of these techniques requires to be processed with careful planning and data is mainly mass. However these techniques provide a smooth data capture when making assessments of risk to valuable or irreplaceable historic fabric.

Imge-based techniques as a part of indirect survey techniques constitute rectified photography, photogrammetry and orthophotography. While rectified photography uses only a single image, photogrammetry requires stereo photography. It should be careful to get a good photograph with these techniques since they are dependent on the line of sight of the camera and all details must be seen clearly in all photos in order to be mapped.

Rectified photography can be defined as a type of survey where single photographs are taken with an image plane of the camera approximately parallel to principal plane of the object. It is useful when the subject surface is flat and detailed. With this technique the main aim is to minimize the errors while taking photography and to do minor adjustments. By taking photograph with high quality camera to the parallel to the object or façade will reduce the errors in consequence of lens distortion. This technique can be applied with low-cost camera and software and don't require to be expert as professional (Bryan et al., 2009).

Another photographic technique ***Orthophotography*** can be used as the purpose of generation "orthophotograph" which can be defined as digital photographic image corrected for scale errors due to tilt and depth(Bryan et al., 2009). Since the

photogrammetry is more expensive than orthophotography, it is important to decide the kind of survey product needed.

Photogrammetric survey is mainly a technique of making precise measurements and drawings from stereo photographs which are overlapping photographs of the same object taken from slightly different positions with metric cameras[6] (Andrews et al., 2009). Today, digital cameras which needs to be calibrated are morely used for photogrammetry. Another classic technique for the documentation ***Photogrammetry*** which was an expensive, needs specialized equipment and experts changed with Digital Photogrammetry by the time. Digital photogrammetry let more simple procedures, reduced the need specialized labor and expert so the process can be used by the architects as well as engineers. In addition to these simplifications, economic aspect of photogrammetry such as to purchase equipment, special cameras, specific software and computers are often less expensive than the investment required previously. It can be said that Photogrammetry solved the problem of registration of complex shapes using stereoscopy and representation through the use of is value curves, white the digital photogrammetry allowed the generation of different types of geometric models (Bryan et al., 2009).

For architectural purposes mainly used two kinds of photogrammetric techniques are close-range photogrammetry and UAV photogrammetry. C***lose range photogrammetry*** is an accurate technique in order to document object's metric data with color and texture in different complexity in short time. It can be used when the accessibility to the object is limited or when the direct measurement on the object would damage to the object. It can be used in many fields in heritage documentation from small artifacts to archaeological sites. Today it has become easier and cost-effective with new cameras. It's a non-contact measurement providing quickly presented data. It is possible to get short field-work, textured and colored data, relatively cheap equipment and data for CAD, however it requires a good network design and planning for ideal photography and it has some limitations in integrity and accuracy and requires skilled operator for data processing. Besides it dependent on the accuracy and resolution of the camera used (Hassani, 2015) (Patias, 2006)

Similarly aerial photogrammetry, it is possible to have real-time capability with fast image acquisition with textured and colored data. For architectural purpose today UAV (unmanned Aerial Vehicle) are used. This system is composed of a light low-cost aerial vehicle with a digital camera and GNSS/INS system. In recent years the use of this system has expanded including documentation and surveying; especially in documentation of cultural heritage and archaeological sites.

It's possible to provide panoramic images, DSM (digital surface models), ortho-ohoto and 3D models with high accuracy. It has real-time capability, fast image acquisition; cover small areas, survey inaccessible or dangerous areas. Among the limitations, it requires skilled experts for getting and processing data, it depends on weather conditions and obstacles limit the integrity and accuracy (Hassani, 2015) (Eisenbeiß, 2009) (Eisenbeiß, 2004).

[6] Cameras that have little or no lens distortion and contain a mechanism for ensuring film flatness.

In recent years, ***3D laser scanning*** shows great versatility for capturing any type of shape and speed of data acquisition. Definition of a laser scanner, adapted from Böhler and Marbs (2002) is '*any device that collects 3D co-ordinates of a given region of an object's surface automatically and in a systematic pattern at a high rate achieving the results in near real time'* (Böhler & Marbs, 2002). This device a kind of "robotic total station" for the mass capture of 3-D coordinate data known as "point cloud" using with rapid-range measurements(Andrews et al., 2009) (Hassani, 2015). Even the technology can be used as terrestrial, it can be also an airborne LIDAR[7]. It is possible to produce detailed geometric models in point clouds, in realistic or false color. The instrument works mainly based on two elements of distance and angle and it has several operate systems[8]. The primary products produced by this type of technology are the geometric models of points and surfaces. Other products are possible processing of primary data. They can be get from a static position (terrestrial laser scanning) or moving platform such an aircraft (airborne laser scanning). This data which can be called as "raw data" may also include additional information such as density and/or color values.

Laser scanners have been used in many diverse applications in cultural heritage documentation depending on the purpose such as: structural or condition monitoring, deformation analysis, making record, spatial analysis, getting a digital geometric model and 3D model (Table 2.3.2.1) (Heritage, 2011). They can be either small objects or complex buildings. Mainly three steps are followed with laser scanner:

-Field survey and data acquisition,

-Editing and data processing and

-Production of final data

The great advantage of this technique is the speed of data capture in the field, and the possibility of working in the dark, if it is not necessary the capture of the surface texture of the object (Amorim, 2011). Laser scanners can provide good results for detailed and irregular objects. Similarly, to other techniques, this one also can be used independently or combined with other techniques depending on the project needs.

Although the 3D laser scanning technology raises the surveying of buildings to another level, the cost for its use in architectural documentation is still expensive and it has limitations in documentation of sharp edges (Rüther, Mtaloand, & Mngumi, 2003). The areas with natural or unnatural obstacles, hidden or unseen points, objects with reflective materials are the reasons causing laser scanner fails to provide accurate data. Rainy weather condition and moisture affects the data as well. It still requires high cost, skilled operators and careful and relatively long data processing process (Amorim, 2011), (Hassani, 2015), (Heritage, 2011).

[7] LİDAR: Light Detection and Ranging

[8] Triangulation, phase comparison and time-of-flight

Table 2.3.2.1: Laser Scanning Techniques used in cultural heritage management activities (Bryan et al., 2009).

scanning system		*use*	*Typical accuracy / operating range*
triangulation-based artefact scanners	rotation range	• scanning small objects /that can be removed from the site) • to produce data suitable for a replica of the object to be made	50 microns / 0.1m-1m
	arm mounted	• scanning small objects and small surfaces • can be performed on site if required • can be used to produce a replica	50 microns / 0.1m-1m
	mirror/prism	• scanning small object surface areas in *situ* • can be used to produce a replica	sub-mm / 0.1m-25m
terrestrial time of-flight laser scanners		• to survey building façades and interiors, resulting in line drawings (with supporting data) and surface models	3-6mm at ranges up to several hundred metres
terrestrial phase-comparison laser scanners		• to survey building façades and interiors, resulting in line drawings (with supporting data) and surface models-particularlay where rapid data and high point density are required	5mm at ranges up to 50-100mm
airborne laser scanning		• to map and prospect landscapes (including in forested areas)	0.05m+ (depending on the parameters of the survey) / 100m-3500m
mobile mapping		• to survey highways and railways • for city models • to monitör coastal erosion	10-50mm / 100-200m
(adapted from Barber, DM,Dallas,Rwa and Mills, JP 2006 "Laser Scanning for architectural conservation". Archit. Conserv 12, 35-52)			

Related to the size of the object, the point density becomes more significant. It's possible to make survey from 1mm point density to 10 m (depending on the instrument capability) (Table 2.3.2.2).

Table 2.3.2.2: Appropriate point densities for various sizes of cultural heritage feature (Bryan et al., 2009)

Appropriate point densities (sampling resolutions) for various sizes of cultural heritage feature			
feature size	example feature	point density required to give 66% probability that the feature will be visible	point density required to give 95% probability that the feature will be visible
10m	large earth work	3500mm	500mm
1m	small earth work/ditch	350mm	50mm
100mm	large stone masonry	35mm	5mm
10mm	flint galleting/large tool marks	3.5mm	0.5mm
1mm	weathered masonry	0.35mm	0.05mm

Another key factor documentation with laser scanning is scale, the point density and the accuracy of measurement required by the project. A simple guide to appropriate point densities is given figure 2.3.2.3 below (Bryan et al., 2009).

Table 2.3.2.3: Required distribution of measured points for photogrammetry, laser scanning, EDM or GPS techniques (Bryan et al., 2009)

Point density/Rate of capture			
Required distribution of measured points			
scale	point cloud	Digitising*	field survey**
1:10	1mm	1-15mm	2-30mm (max. 0.5m)
1:20	3mm	3-30mm	5-60mm (max. 1m)
1:50	5mm	5-50mm	10-100mm (max. 2m)
1:100	15mm	15-100mm	20-200mm (max. 3m)
1:200	30mm	30-300mm	50-600mm (max 5m)
1:500	75mm	75-750mm	0.1-1.5m (max. 10m)

From photogrammetric stereo model or point cloud: the higher value in each range represents the maximum permissible poiint interval.
****For example by electromagnetic distance measurement (EDM) or global positioning system (GPS). Where lineas appear straight or detail is sparse the interval may be increased up to the maximum shown in brackets.***

2.4. Unsolved Problems and Future of Cultural Heritage Documentation

A wide range of use technologies applied in cultural heritage proved the variety of alternatives for documentation of an object. However a single method is insufficient for the desired accuracy and each method has its own advantages and limitations. Cost, time, complexity and size of the object, accessibility, personal skills, instrument capabilities has a significant effect on choosing the most appropriate survey method. In most cases, it is needed to use a single method with the support of other techniques or a combination of different techniques in order to achieve result. If the budget allows, it is the most suitable solution and best possible method.

In order to acquire information in all survey processes require mainly on 3 issue:
-Understanding of techniques and their performance in terms of precision and accuracy
-Understanding of the subject of the documentation
-Presenting the information in accessible, clear and consistent way (Blake, 2010).

Even data capture techniques have increased there is still a lack of standards in data presentation. Standards are as much about work practice as they are about listing quality constraints. The present suite of developing documentation technologies need expert guidance on their application and given the contraction of institutional support for sustaining metric skills.

Acessible technologies like laser scanner is known with its power for 3D data by heritage managers. The standards required to achieve conservation specific data from laser scanner are developing and the indications are that the “magic bullet” of the laser scan isn’t all it appears in the sector.

Digital imagery is becoming ever better in terms of resolution and flexibility. Even the traditional data capture techniques are developing, low-cost web –based tools are emerging which challenge existing standadrs amking the role of heritage bodies in

guiding information users and providers alike in appropriate application ever more urgent (Blake, 2010).

While the level of European technical competence in documentation of spatial data is high, there is no common sdandard about 3D documentation of CH. Despite a general understanding of spatial resolution and accuracy of such documentation and its potential, the standards could be improved by direct cooperation within technical sector. There should be a solution to bridge the gap between CH community and data providers. Thinking about our tangible heritage, we found a broad field of studies and applications –optical measurement techniques- such as digital photography, infrared reflectography[9], traditional colorimetry and spectrophotometry[10], imaging systems for specialist analysis such as computer tomography[11], color, multi and hyperspectral imaging[12], structured-light-based techniques[13], integrated multi-imaging systems other than direct and indirect techniques(Boochs et al., 2014).

Today's technological process offers new possibilities so the list of these techniques continues and develops. Due to the variety of all these instruments, it is almost impossible to possess the respective knowledge required to correctly apply and control all these techniques for individual persons, even if they are technicians experienced in the use of non-contact measuring systems. This is still more demanding for users, who in general are primarily interested in data helping their applications without having to know precisely what type of instruments are available and it's essential to know constraints introduced by the user, or the object respectively. It's of real importance to have a dialog between information user and information provider(Boochs et al., 2014).

As summary, in CH documentation prose, it is faced many complex scenario when considering documentation techniques. Particularly, not oly thinking about 3D model ut rather about the broad brandwidth of data to be provide for whole field of questions to be answered for tangible cultural heritage.

CIPA Heritage Documentation (CIPA, 2014) is the international ICOMOS / ISPRS scientific committee that ensures the right documentation with the existing variety of techniques for preservation, conservation and restoration. A good set of guidelines were undertaken under the RecorDIM initiative (sponsored by The Getty Conservation Institute). CIPA Heritage Documentation encourages and promotes the use of appropriate documentation practice, advises organizations for recording cultural heritage and provides an international forum for exchanging scientific knowledge, ideas and best practices. today's techniques for handling and structuring knowledge are well suited to developing a framework for solving the problem of this vast amount of factors characterizing optical measuring techniques (Boochs et al., 2014).

[9] The techniques is based on a higher transmission of infrared light.

[10] The technique provides accurate information on the optical properties (such as reflectance) and color appearance (such as color coordinates)

[11] An analysis which makes use of various non-optical parts of the electromagnetic spectrum and may enable examination below the surface.

[12] Technique based on many acquisition channels and gives detailed information to the spectral characteristics.

[13] It provides precise spatial models which can be easily combined with color images of the object

However, often they also propose optimal **content of data** based on an anticipation of the requirements an information user might have, without clearly understanding the evaluation process realized by conservators, art historians, curators, archaeologist, and other professionals. This might lead in the same way to non-optimal data as the inverse case, when the information user asks for certain input, without understanding the instruments, their characteristics and constraints. It is therefore of real importance to have a dialog between both sides (information users and information providers) to adjust their **respective perspectives**. This addresses the vocabulary (what does accuracy mean?) and the characteristics of the data (scale, resolution, accuracy, composition...) to be provided in order to optimally serve the work of the various groups of information users (archaeologists, architects, conservators, curators, social scientists, art historians and others). Overall, complexity increases further through the interaction of measuring techniques and the **object** itself. Looking at the variety of objects, we see another list of characteristics having impact on the choice, use and appropriateness of instruments. Aspects like object size (ranging from small artefacts to large sites), shape (rather flat objects or complete spatial geometries), surface morphology (smooth versus ragged or indented), reflectivity (shiny or diffuse), texture (uniform or varying), spectral / color appearance or material composition play their role and may decide upon the quality of results or the feasibility of techniques. Experienced technicians should know these facts and be able to handle their instruments in the right way, but it is not always possible to overcome restrictions without manipulating the object (like the 3D capture of shiny surfaces): what might be suitable from a technical perspective might be strictly forbidden from the user view. It is therefore essential to know constraints introduced by the user, or the object, respectively.

3. UAV PHOTOGRAMMETRY

3.1. Introduction to Unmanned Aerial Vehicle Systems (UAVs)

A simple definition of unmanned aerial vehicles are vehicles with its aircrew removed and replaced by a computer system and a radio-link (Austin, 2010). Another definition and mostly referred in literature is the one by van Blyenburgh. “UAVs are to be understood as uninhabited and reusable motorized aerial vehicles.” States van Blyenburgh, 1999. Even they could be remotely controlled, autonomous, semi-autonomous or combination of these features. When it’s compared to manned aircraft, the main difference between these two systems is that a UAV do not have pilot in the aircraft but it doesn’t mean it flies itself. It can be considered as a part of local or global air transport/aviation which has its rules, regulations and disciplines (Austin, 2010).

UAVs are commonly used in many fields in civil and military use. As well as it is mainly used in aerial photography, mapping and remote sensing, agriculture, conservation (pollution and land monitoring, electricity companies (powerline inspection), fire services and forestry (fire detection and incident control), gas and oil companies (land survey and pipeline security), lifeboat institutions (incident investigations), local authorities (survey and disaster control), meteorological services (forecasting), oil companies (pipeline security), police authorities (search, security and surveillance), river authorities (water course and level monitoring, flood and pollution control), survey organizations (geographical, geological and archaeological survey), water boards (reservoir and pipeline monitoring), as well as for military purpose in navy, army and air force, in computer science, robotics and artificial intelligence as well as photogrammetry and remote sensing.

In the last years, Unmanned Aerial Vehicles (UAVs) have been used in an increasingly broad range of applications, including cultural heritage and archaeology (Eisenbeiss & Sauerbier, 2011), landscape classification (Gini el al., 2012), etc. As for terrestrial applications, the scientific interest was highly focused on the topic of automated aerial triangulation procedure, starting from the autonomous flight control (Bäumker & Przybilla, 2012), up to the image orientation, dense matching, DSM and orthoimage generation (Haala & Rothermel, 2012). Accuracy analyses were usually performed using pre-signalized control points measured with GNSS technique (Kung et al., 2011).(Nocerino, Menna, Remondino, & Saleri, 2013).

3.1.2. Categories of UAVs

Even all UAV systems have many elements other than the air vehicle, they are categorized by their capability, size, power, weight and wings. However it’s possible one system can employ more than one type of air vehicle, with different types of mission. With the technology boundaries are blurred and these classifications are subject to change (Table 3.1.2.1).

Table 3.1.2.1: Classification of Tactical UAVs by the Unmanned Vehicle Systems International Association (International Unmanned Aerial System Community;2008)

Tactical UAVs Sub-categories	Acronym	Max high [m]	Autonomy [hours]	Weight [Kg]
Micro	μ (Micro)	250	1	< 5
Mini	Mini	150-300	< 2	150
Close Range	CR	3000	2-4	150
Short Range	SR	3000	3-6	200
Medium Range	MR	5000	6-10	1250
Medium Range Endurance	MRE	8000	10-18	1250
Low Altitude Deep Penetration	LADP	50-9000	0,5-1	350
Low Altitude Long Endurance	LALE	3000	> 24	< 30
Medium Altitude Long Endurance	MALE	14000	24-48	1500

Austin made a categorization of UAVs based on air vehicle types including the size, range and endurance of the vehicles. According to his categoraization, air vehicle types are HALE (High Altitude-Long Endurance), MALE (Medium Altitude- Long Endurance), TUAV (Tactical UAV), Close Range UAV, MUAV (mini UAV), MAV (Micro UAV) and NAV(Nano UAV) (Austin, 2010). An the more robust classification was drafted by the Unmanned Vehicle Systems International Association shown in figure below (IUASC, 2008)

Similar classification of UAVs has been done by US Department of Homeland security. According to this classification while HALE and MALE type of UAVs remain the same, there are other difference types of UAVs. After HALE and MALE, it becomes LALE(Low Altitude-Long Endurance), LASE Close (Low-Altitude,Short-Endurance, Close Range), LASE, VTOL(Vertical Take-Off&Landing), MAV or NAV likely Austin's classification (Figure 3.1.2.1) (Watts, Ambrosia, & Hinkley, 2012).

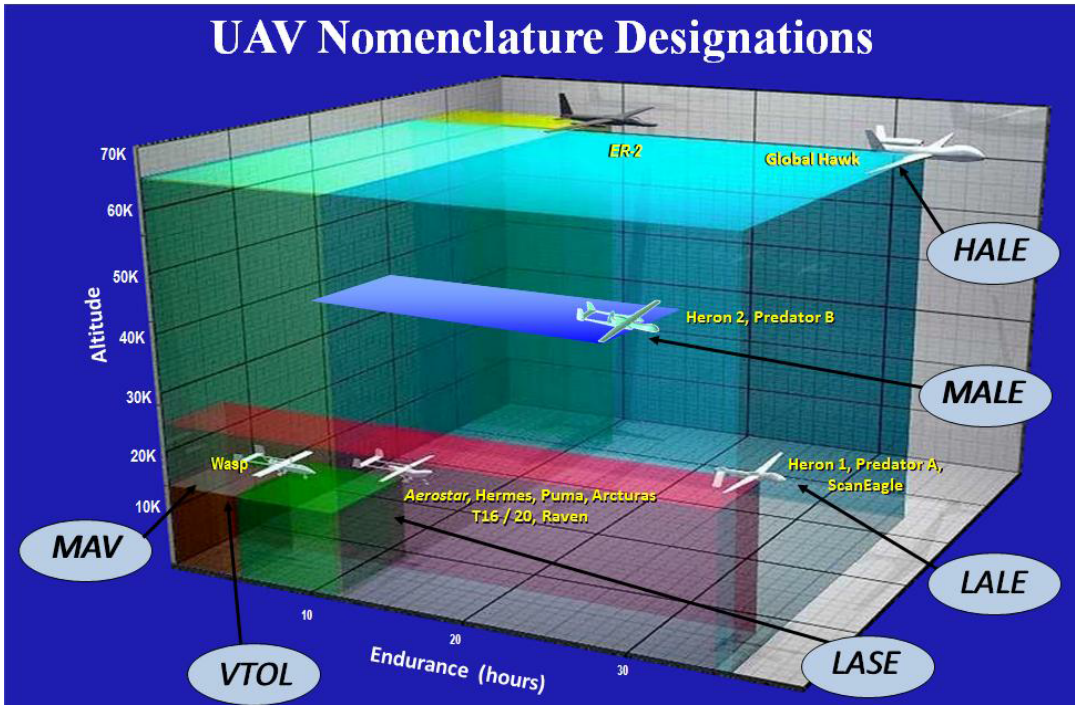

Figure 3.1.2.1: US Department of Homeland Security (Polski, 2004)

NAV *(Nano Aerial Vehicle)* are proposed to be in sycamore seeds and used in swarms for purposes such as radar confusion or propulsion and can be very small for short range surveillance and short missions profile platforms with observation capabilities in confined spaces or hostile environments to enhance situational awareness especially in military applications. They are very small, low altitude, short-duration (Figure 3.1.2.2).

(a)

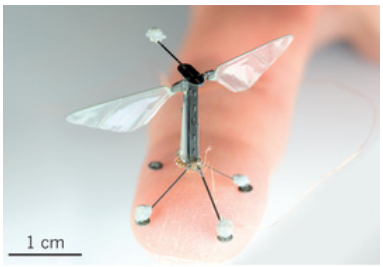

(b)

(c)

Figure 3.1.2.2:NAV and MAV

(a) The 19 g Nano Hummingbird (left) has a camera for live video streaming with ~8 min(Watts et al., 2012)
(b) the 80 mg RoboBee (right) can fly tethered to an external power source(Floreano & Wood, 2015)
(c) Blcak Hornet Nano 2cmx10cm, 18 gram and able to fly up to an altitude of 900 meters(http://www.monitorday.com/)

MAV *(micro/miniature Aerial Vehicle)* was originally defined as "A UAV having a wing-span no greater than 150 mm". It is principally used for urban environments with buildings. It is required to fly slow, to hover and to perch. In order to meet this challenge researches are being conducted into some less conventional configurations: such as flapping wing. However the winged versions have very low wing loads in order to prevent problems in precipitation (Austin, 2010).

VTOL *(Vertical Take-Off&Landing Aerial Vehicle)* UAVs are suitable platforms for remote area operations and quick analysis situations. Their platforms are small, mostly operated with electric motors from rechargable batteries and their durations less than 1 hour. They have an important potential for scientific researches and can be used relatively small size surveys. Their maneuverability can more easily negotiate an urban scale at low altitude. They are generally in development primarily to support military lift and transport operations but they have wider application in science.

(a) (b) (c)

Figure 3.1.2.3 (a) Draganflyer X6 VTOL UAS. Image courtesy Draganfly Innovations, Inc.
(b) Aeryon Scout VTOL UAS. Image courtesy Aeryon Labs, Inc.
(c) LASE and LALE UAS on display at 2005 Naval Unmanned Aerial Vehicle Air Demo. Pictured are (front to back, left to right) RQ-11A Raven, Evolution, Dragon Eye, NASA FLIC, Arcturus T-15, Skylark, Tern, RQ-2B Pioneer, and Neptune. Image Courtesy US Department of Defense (Watts et al., 2012)

LASE *(Low-Altitude,Short-Endurance)* UAVs can be found in many different size and configuration from back-packable, hand-launched platforms to catapult-launch platforms. Today the more common used ones are the ones lightweight and can be hand-launched which has disadvantage of relativeshort-duration capability between 45 min-2 hours (Figure 3.1.2.4)

MALE *(Medium Altitude- Long Endurance)* UAV platforms have a significant role in strategic operations in defense community and also being started to use for civil application areas (Watts et al., 2012). They can fly 5000-15000 m altitude and have 24 hours endurance with in excess of 500 km range (Austin, 2010). They have the capability to support scientific data collection and disaster monitoring, incident management, fire control, wildfire mapping and surveillance. It is appropriate in order to collect data for regional scales and altitudes common to manned aircraft (Watts et al., 2012) (Figure 3.1.2.4).

(a) (b)

Figure 3.1.2.4 (a) NASA Ikhana. Image courtesy NASA.
(b)The NASA SIERRA, shown flying near Svalbard, Norway, 2009. Image courtesy NASA

HALE *(High Altitude-Long Endurance)* UAVs are the platforms which have capability to fly over 15000 m altitude with endurance more than 24 hour. They carry out long-range reconnaissance and surveillance and more in the army and usually operated by Air Forces from fixed bases (Austin, 2010) (Figure 3.1.2.5).

(a) (b) (c)

Figure 3.1.2.5 (a) The Pathfinder HALE UAS. Image Courtesy NASA
(b)The NASA/NOAA Global Hawk HALE UAS. Image courtesy NASA
(c) The Qinetiq Zephyr HALE UAS. Image courtesy QuinetiQ Group, PLC, Farnborough, Hampshire, England(Watts et al., 2012)

A descriptive and comprehensive classification has been made by van Blyenburgh for UAVs, depending on the purpose, mass, range, flight altitude and endurance. According to his classfication, the purposes for UAV use can be divided mainly three task which are tactical, strategical and special/spatial tasks. For tactical purposes UAVs less than 5kg, less than 10 km range at less than 250m with endurance of 1 hour can be used. While UAVs with more endurance which means more than 24 hours can be applicable at more than 2000 km range for strategical purposes.For special tasks different UAVs can be used as shown in Figure 3.1.2.6 (van Blyenburgh, 2006).

		Mass	Range	Flight Alt.	Endurance
Tactical	?	Micro ???	< 5 kg	< 10 km	250 m	1 hour
	Mini	Mini	< 20/25/30/150	< 10	150/250/300	< 2
	CR	Close Range	25-150	10 - 30	3.000	2 - 4
	SR	Short Range	50-250	30 - 70	3.000	3 - 6
	MR	Medium Range	150-500	70 - 200	5.000	6 - 10
	MRE	MR Endurance	500-1500	> 500	8.000	10 - 18
	LADP	Low Alt. Deep Penetration	250-2500	> 250	50 - 9.000	0,5 - 1
	LALE	Low Alt. Long Endurance	15-25	> 500	3.000	> 24
	MALE	Medium Alt. Long Endur.	1000-1500	> 500	5/8.000	24 - 48
Strateg.	HALE	High Alt. Long Endur.	2500-5000	> 2000	20.000	24 - 48
	Strato	Stratospheric	>2500	> 2000	> 20.000	> 48
	EXO	Exo-stratospheric	TBD	TBD	> 30.500	TBD
Sp.Task	UCAV	Unmanned combat AV	>1000	+/- 1500	12.000	+/- 2
	LET	Lethal	TBD	300	4.000	3 - 4
	DEC	Decoys	150-500	0 - 500	50 - 5.000	< 4

= According to national legal restrictions

Figure 3.1.2.6: Different currently existing UAVs according to national legal restrictions based on purpose, mass, range, flight altitude and endurance (van Blyenburgh, 2006)

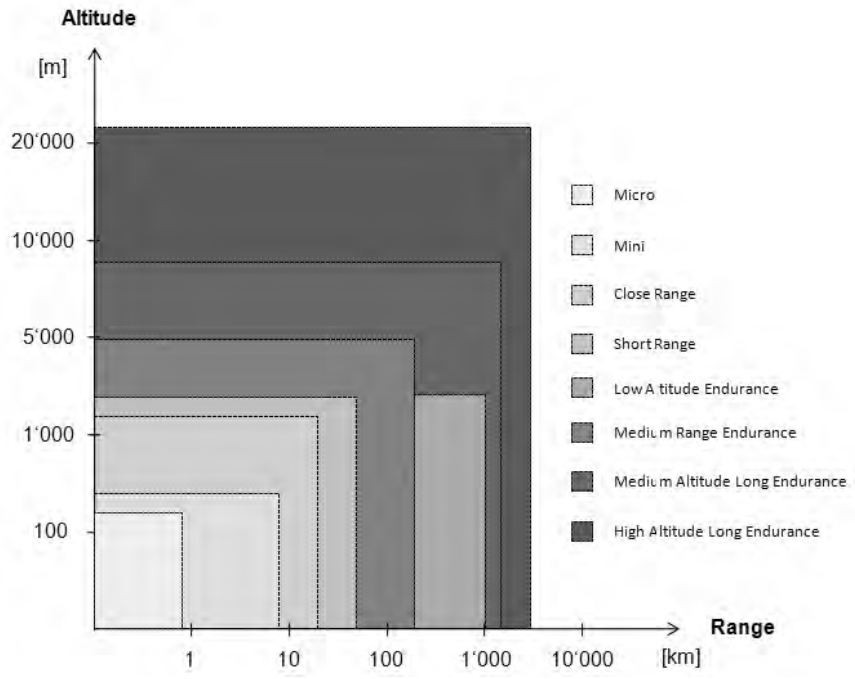

Figure 3.1.2.7: Classification of UAVs depending on range and altitude (Eisenbeiß, 2009).

It should be mentioned that there is no standardized categorization for UAVs in the ISPRS since the classification of UAVs changes from one country to another. So Eisenbeiß made a graph of UAV classification graph adopted from the one by van Blyenburgh (1999) shown in figure 3.1.2.7 (Eisenbeiß, 2009).

UAVs can also be categorized based on their integrated sensors and real-time capability. These factors affect the data processing. Low-cost sensors without GPS/INS requires post georeferencing while sensors with DGPS and IMU have the capability of direct georeferencing. Given accuracy levels in table 3.1.2.2 for the application requirement can change depending on the method applied for georeferencing (Eisenbeiß, 2009).

Table 3.1.2.2: Classification of UAVs regarding to the type of georeferencing, real time capability and application requirements (Eisenbeiß, 2009).

sensors	georeferencing	real-time capability	application requirement	UAV category
No GPS/INS	Post	0	Low accuracy (m)	OM-class
GPS and consumer-grade INS	Post/direct	+	Moderate aacuracy (dm-m)	M-&L- class
DGPS/navigation and tactical grade INS	Post/direct	++	High accuracy (cm)	M-&L-class

UAVs can also be classified based on their power and weight. Eisenbeiß made this classification in the table 3.1.2.3 below (Eisenbeiß, 2009).

Rotary-wing UAVs, also known as vertical takeoff and landing vehicles can be sub-categorized according to their rotors; single, double, four and multi-rotor systems.

Table 3.1.2.3: Range of UAVs currently in use in terms of power and weight (Eisenbeiß, 2009)

	Lighter than air	**Heavier than air**		
		Flexible wing	***Fixed wing***	***Roratry wing***
Unpowered	Balloon	Hang glider	Gliders	Root-kite
		Paraglider		
		Kites		
Powered	Airship	Paraglider	Propeller	Single rotors
			Jet engines	Coaxial
				Quadrotors
				Multi-rotors

Coaxial (double-rotor) systems have increased payload and can be operated higher altitude. They are easier to control and have reduced noise level however use of two main rotors can be resulted in an increased mechanical complexity of the rotor. The single and double rotor systems have more power than four and multi-rotor systems and able to carry more payloads While four-rotor systems have less payload capacity, they are equipped with lighter sensors and low cost systems. Since they are smaller, they are more suitable for indoors but they can be used also outdoor but they are more sensitive to the weather conditions Fixed wings UAVs are generated by forward motion using propellers or jet engines while unpowered UAVs like gliders and ballons are controlled by ropes. This can be limitations in fly altitude and distance to the operator. Besides for the horizontal movement, the operator needs to walk or move by a car. For these unpowered systems the wind influence is greater compared to powered systems. Powered airhsips can stay longer in the air than fixed and rotary wing platforms. Therefore these systtems can be used for long term monitoring tasks and they are more dependent on environmental conditions (Eisenbeiß, 2009).

UAVs can be classified based on their pros and cons depending on range, endurance, weather and wind durability and maneuverability. The endurance of the UAV is influenced by the availability of the radio link and the up-downlink of the telemetry and image data. Besides, endurance depends on the flight autonomy and the amount of fuel (Eisenbeiß, 2009) (Table 3.1.2.4).

Table 3.1.2.4: Classification of UAVs depending on range, endurance, weather condition and maneuverability (Eisenbeiß, 2009)

Type of aircraft	***range***	***Endurance***	***Weather and wind dependency***	***maneuverability***
Balloon	0	++	0	0
Airship	++	++	0	+
Gliders/Kites	+	0	0	0
Fixed wing gliders	++	+	+	+
Propeller&Jet Engines	++	++	+	+
Rotor-kite	++	+	0	+
Single rotor (helicopter)	+	+	+	++
Coaxial	+	++	+	++
Quadrotors	0	0	0	++
Multi-copters	+	+	+	++

3.1.3. Advantages and Limitations of UAVs

3.1.3.1. Advantages of UAVs

UAVs is mainly deigned for particular tasks. It should be decided the final data required which directly affect the design of the system and should be choose the most suitable one depending on the task. It is not possible to conclude that UAVs always have advantages or disadvantages comparing to manned aircraft systems.

Compared to manned aircraft systems they have significant advantages. They can fly in high risk situations without endangering a human life, like natural disaster sites, mountainous and volcanic areas, flood plains, earthquake areas, desert areas etc. Their ability to fly at low altitude close to the object, where manned systems cannot, is another advantages of these systems. They can also be used in areas where access is difficult and manned aircraft is no available or flight permission is no given. The cloudy and drizzly weather conditions are not obstacles since it's possible to fly under the clouds but not possible to get data with manned aircrafts. Another supplementary advantage of UAVs is their real-time capability and fast data acquisition (Eisenbeiß, 2009). It can be said that they are more environmentalist since they are smaller, they have lower mass, they consume less power so produce less emission and noise (Austin, 2010). They can be used for both military and civil applications such as monitoring the environment for nuclear or chemical contamination which puts aircrew at risk. Today UAVs are successfully used for crop-spraying with toxic chemicals. Especially in military tasks, due to its smaller size, it is more difficult for enemy to detect and to strike and aircrew is not under threat of attack(Austin, 2010).

Regarding the cost effect, it can be mentioned that economic expenses of human pilots are not needed to consider. Other issue related to cost is that UAVs on the market more focus on low-cost systems. When it's compared to manned aircraft systems, they are less expensive however depending on the application, the cost can increase. For small-scale applications UAVs can be considered as supplement system. UAV images can be used for high resolution texture mapping on DSMs and 3D models and image rectification.

The implementation of GPS/INS, stabilization systems and navigation units permits precise flights, sufficient image coverage and overlap and gives opportunity to the user to estimate the expected product accuracy before flight (Eisenbeiß, 2009).

3.1.3.2. Limitations of UAVs

Depending on their size, UVAs have limitations in sensor payload in weight and dimension. Low weight sensors mostly small or medium format cameras do it is needed to acquire more images in order to obtain the same image coverage and good resolution. Besides, low-cost sensors are less stable which reduces image quality. Payload limitations require the low weight navigation units which means less accurate results for

the orientation of the sensors. Low-cost UAVs are generally equipped with less powerful engine so they have limitations in altitude.

Even UAVs have some advantages for human beings, they don't benefit from the sensing and intelligence of human being. In unexpected situations, they cannot react as human. Additionally, low-cost UAVs don't have communication with air traffic communications so they are not allowed to flight in line-of-sight. To take full advantage of the impressive flying capabilities of UAVs, like the fully automated operating rotary wing UAVs, there needs to be a well-trained pilot, due to security issues. The pilot should be able to interact with the system at any time and maneuvers. Besides, depending on the local situation of the area, radio frequency for the communication between GCS and UAV has to be selected careful since sometimes radio frequencies may be used by other systems and this can cause signal jamming (Eisenbeiß, 2009).

3.2. Concepts of UAVs

3.2.1. System Composition

An unmanned air vehicle UAV is an aircraft without a human pilot. It is also commonly known as UAS (unmanned aircraft system) or by several other synonymous [14]. However the term Unmanned Aircraft System (UAS) which was adopted by FAA (Federal Aviation Administration) is a terminology UAS whole system including the Unmanned Aircraft (UA) and the Ground Control Station (GCS) (Eisenbeiß, 2009).

UAVs usually have the same elements based upon manned aircraft. The whole system briefly includes (shown in Figure 3.2.1.1 below);

-A control station (CS) which holds the system operators and interfaces between the operators and the rest of the system

-A vehicle or aircraft carrying the payload (which can be diverse types)

-A communication system (is usually achieved by radio transmission) transmitting control inputs to aerial vehicle and returns to payload and visa versa

-A support equipment which may include maintenance and transport items (Austin, 2010)

[14] Remotely piloted Vehicle (RPV), Remotely Operated Aircraft (ROA), Remotely Piloted Aircraft (RPA), Unmanned Vehicle Systems (UVS),

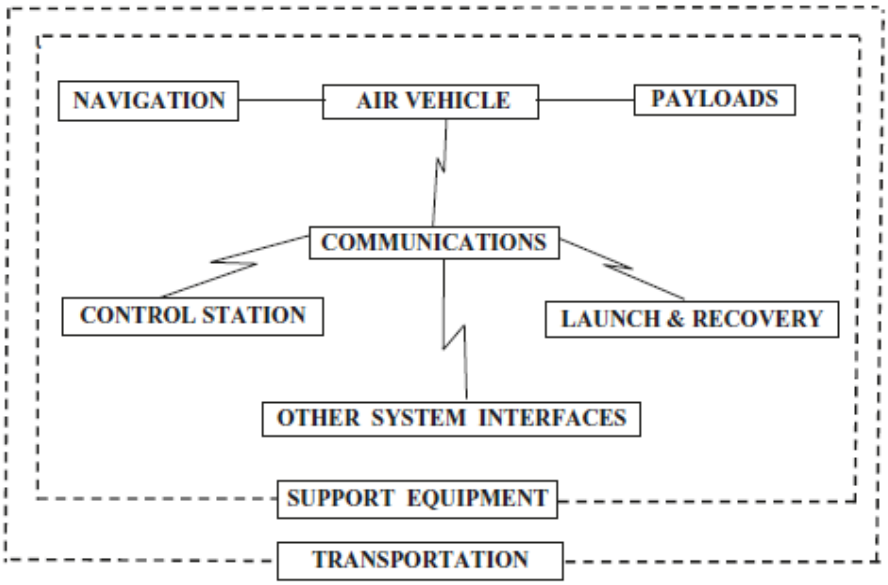

Figure 3.2.1.1: UAV system functional structure (Austin, 2010)

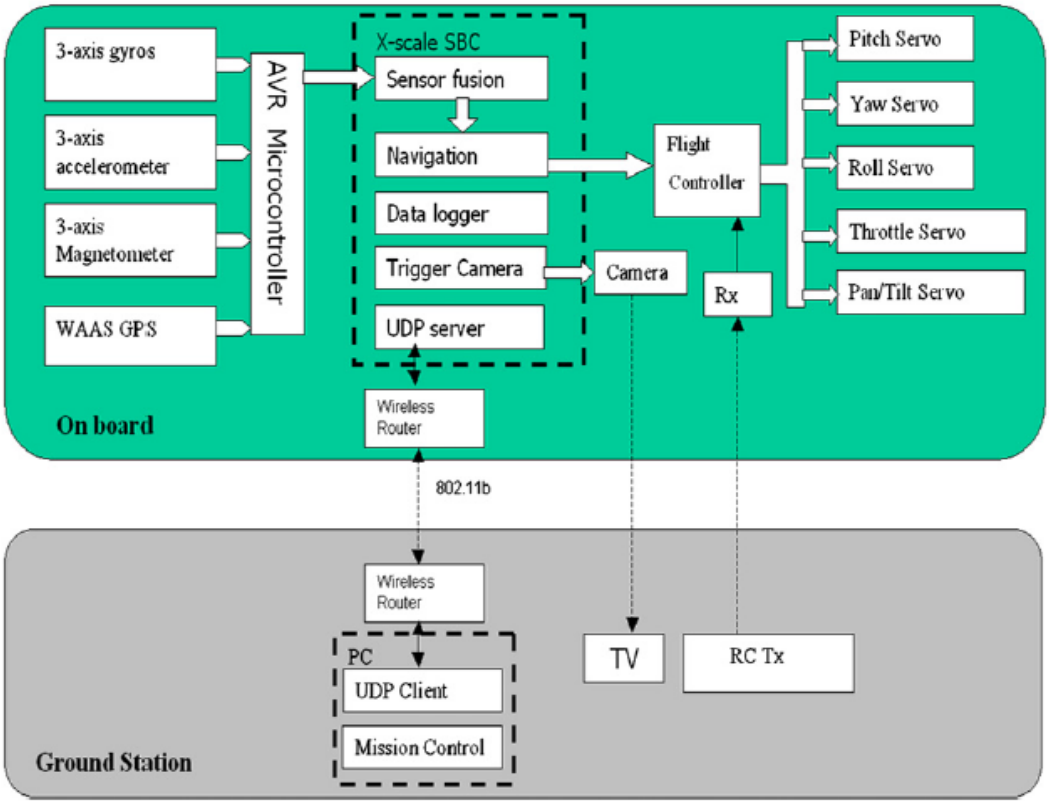

Figure 3.2.1.2:UAV system scheme (Xiang & Tian, 2011)

As system elements, launch, landing, recovery, communication, support etc. have been included in both manned and unmanned systems. Unmanned aircraft must not be confused with model aircraft or with “drone”. A radio- controlled model aircraft is used only for sport and must remain operator side. The operator usually limited to instructing the aircraft to climb or descend and to turn to the left or right. However a

drone can fly out of operator sight being launched into a pre-programmed mission on a pre-programmed course and a return to base. It doesn't communicate and the results of the mission are not obtained from it till it is recovered at base. On the other hand a UAV has some greater and lesser degree of "automatic intelligence". It communicates with its controller and return payload data (visible or thermal images or video), with its primary state information (position, airspeed, heading and altitude). It also transmits the data of its condition and temperatures of components e.g. (Austin, 2010) (Figure 3.2.1.3).

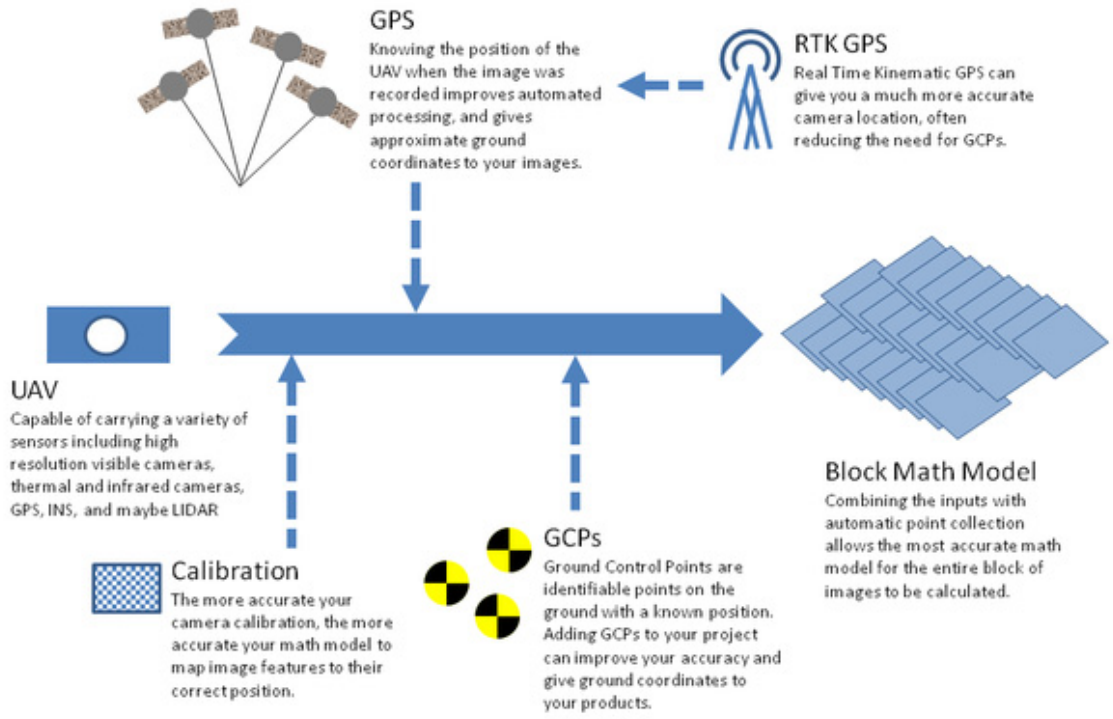

Figure 3.2.1.3: General view of complete process of UAV

Control Station (CS)

The control station is basically the control center of the operation in which the mission planning is pre-planned and man-machine interface. The operators speak to the aircraft via the communication system to direct flight profile and to operate the type of mission payload. The information includes data from payloads, status information of sub-systems and position information. It also houses the systems for communication with other external systems.

The Payload

The type and performance of the payloads is dependent on the needs of the operational task. These can range from less than 200 g to up to 1000 kg. It is also possible that UAV can carry different types of sensors within a payload module or series of modules. The data from these different sensors may be processed and integrated to provide enhanced information. The payloads may be such as daylight cameras, low-light level cameras, thermal imagers, lenses or mounted electro-optic systems, radar imaging payloads, laser target designations as well as dispensable

payloads such as agricultural crop sprayings, water or other fire suppressant materials, for military purposes they can be bombs, rockets or missiles.

The small size and the reduced pay-load of some UAV platforms is limiting the transportation of high quality navigation devices like those coupled to airborne cameras or LiDAR sensors. The cheapest solution relies on MEMS-based inertial sensorswhich feature a very reduced weight but accuracy not sufficient, to our knowledge, for direct geo-referencing. More advanced and expensive sensors, maybe based on single/double frequency positioning mode or the use of RTK would improve the quality of positioning to a decimetre level, but they are still too expensive to be commonly used on low-cost solutions. During the flight, the autonomous platform is normally observed with a Ground Control Station (GCS) which shows real-time flight data such as position, speed, attitude and distances, GNSS observations, battery or fuel status, rotor speed, etc. On the opposite, remotely controlled systems are piloted by operator from the ground station. Most of the systems allow then image data acquisition following the computed waypoints while low-cost systems acquire images with a scheduled interval. The used devices (platform, auto-pilot and GCS) are fundamental for the quality and reliability of the final result: low-cost instruments can be sufficient for little extensions and low altitude flights, while more expensive devices must be used for long endurance flights over wide areas (Remondino, 2014).

However, compared to established workflows based on manned airborne photography,some issues need to be considered. Because of weight and cost restrictions, sensor devices used in UAVs (positioning, camera) are normally of much lower quality compared to professional sensors employed in manned airborne systems. This has as the consequence that in order to achieve the best accuracy for the final mapping product, a significant amount of work concerning signalization and measurement of ground control points (GCPs) is needed. In this context some recent developments concerning GNSS localization are interesting: there is the tendency towards RTK (Real Time Kinematic) devices being integrated onboard commercially available UAV(Gerke & Przybilla, 2016).

Many factors influence the accuracy of the position which is assigned to an image taken during the UAV flight. As the GNSS-RTK board can deliver an absolute position at 2 cm – 3 cm error level, the goal must be to minimize the remaining error coming from uncertainties of the relative alignment of the sensors on board of the UAV and data processing. The following components play an important role in this respect: calibration of offset from camera projection centre to antenna phase centre (boresight alignment), attitude of plane during exposure time, time synchronization, and last but not least a method to identify blunders during bundle adjustment(Gerke & Przybilla, 2016).

The Air Vehicle

The type and performance of the air vehicle is mainly defined by the needs of thes operational mission. The air vehicle carries the payload and subsystems including the communication links, stabilization control equipment, power plant or fulel, electrical

power supplies and mechanisms needed to be launched. Other important factors for the air vehicle are the range, speed and endurance.

Navigation Systems

Navigation systems provides the information where the aircraft is at any moment in time. This may be a part of pre-programmed mission or emergency capability. In fulluy autonomous operations navigation equipment must be carried in the aircraft. Today global positioning system GPS helps for this information since they are available very light in weight and cheap.

An IMU is comprised of triads of accelerometers and gyros, digitization circuitry and a CPU that performs signal conditioning and temperature compensation. The compensated accelerometer and gyro data are output as incremental velocities and angular rates via a serial interface to the PCS typically at rates of 200 to 1000Hz (Mohamed M.R & Hutton, 2001).

Launch, Recovery and Retrieval Equipment

Launch and recovery equipment are required for air vehicles which don't have a vertical flight capability while retrieval equipment is required to transport the aircraft back to its launcher.

Communications

The principal requirement for the communication system is to provide the data links between the CS and the aircraft. The transmission is mostly provided by radio frequency by up-link and downlink. Up-link transmits flight path, real-time flight control commands, control commands and updated positional information. Down-link transmits aircraft positional data, payload imagery or data, and aircraft housekeeping data (fuel, state etc.)

Interfaces

All these systems work together to achieve the performance of the total system. They must be able to operate together so it should be carefully considered the correct functioning of the interfaces.

Support Equipment

Support equipment ranges from operating and maintenance manuaşs to special test equipment and power supplies

.

Transportation

A UAV system is required to be mobile. Transportation is needed for all systems mentioned above.

3.2.2. Regulations

The raising interest among the general public and aviation community imposed the authorities to set up regulations especially in major companies. The regulations mainly divided into two tasks: military and civil.

The published studies for scientific research or public-use don't discuss the regulations of UAVs. Some of scientific journals are beginning to require evidence of adherence to regulations by authors. Behind the restrictions in use of UAVs mainly includes the safety and security of people on the ground and air. The regulations change in response to technology and potential accidents, however general concepts tend to be stable.

In US, Federal Aviation Administration (FAA) controls both manned and unmanned aircraft operations, providing regulations and guidance on airspace restrictions, pilot equipment and performance requirements (http://www.faa.gov/uas/).

In UK, there are two regulatory regimes: military and civil UAVs must follow with the regulations of one or the other. In 1983 the Society of British Aerospace Companies (SBAC) was intended to provide a basis for the certification of UAVs. In 1991 SBAC published a document titled "A Guide to the Procurement, Design and Operation of UAV Systems" which is still relevant today(Austin, 2010). In 2004, the Civil Aviation Authority (CAA) published a comprehensive guide titled " Unmanned Aerial Vehicle Operations in UK Airspace" in 2004 (Eisenbeiß, 2009). For military purposes UK Ministry of Defence UK MOD has a Defence Standard 00-970 (Austin, 2010).

So far the regulations for UAVs differ from one country to another. However European Aviation Safety Agency (EASA) defined that UAVs with a "Maximum Take-Off Mass" (MTOM) over 150 kg have to be certificated by EASA, while less than 150 kg are regulated by the national authorities (Eisenbeiß, 2009).

Main regulatory authorities involved are Joint Aviation Authorities **(JAA)** is an associated body of the European Civil Aviation Conference (ECAC), representing the civil aviation regulatory authorities of a number of European states who had agreed to co-operate in developing and implementing common safety regulatory standards and procedures. It has 29 EU members and 15 non-EU members. Another authority European Organisation for the Safety of Air Navigation, commonly known as **Eurocontrol** is an international organization working to achieve safe and seamless air trafiic management across Eurpoe which was founded in 1960 and has currently 41 member states. The other authority European Aviation Safety Agency **(EASA)**.

In Italy, Ente Nazionale per l'Aviazione Civile (ENAC) - the Italian Civil Aviation Authority, which was established on 25th July 1997, oversees the technical regulation, the surveillance and the control in the civil aviation field. ENAC deals with the diverse regulatory aspects of air transport system and performs monitoring functions related to the enforcement of the adopted rules (http://www.enac.gov.it/)

In Turkey, Sivil Havacılık Müdürlüğü, Directorate General of Civil Aviation (DGCA) is being in charge of regulating the civil aviation industry in accordance with the national and international regulations and standards (http://web.shgm.gov.tr).

3.3. UAV Workflow and Data Acquisition

A typical image-based aerial surveying with UAVs requires mainly to decide the project parameters, a mission planning (flight and data acquisition), image acquisition, data processing and data generation.

Project parameters include all parameters such as flight parameters, camera calibration and Ground Control Points (GCP) measurements, devices and digital photogrammetry parameters. Nex and Remondino (2014) prepared a general workflow and data acquisition and processing pipeline including parameters. According to this pipeline, UAV platforms and flight parameters constitute mission planning. After image acquisition it is possible to get image triangulation with additional parameters such as camera calibration and GCP. AT the end of image triangulation it is possible to get Digital Terrain Models (DTM) or Digital Surface Models (DSM). These outputs can be used for orthoimage generation or for 3D modelling purposes (Nex & Remondino, 2014) (Figure 3.3.1).

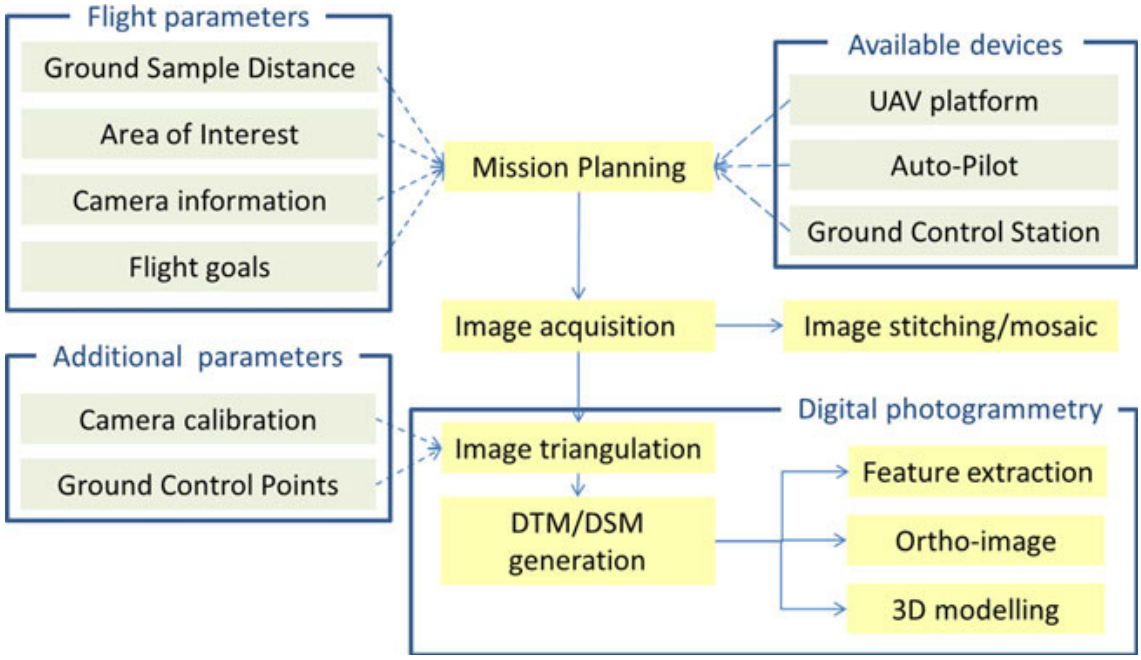

Figure 3.3.1: Typical acquisition and processing pipeline for UAV images (Nex & Remondino, 2014).

3.3.1. Mission Planning

The mission planning including the flight planning and data acquisition is generally planned with related software, the required Ground Sample Distance (GSD) (footprint), and parameters of the digital camera. The parameters such as desired image scale, flight heights are dependent on aim of the flight. Missions for detailed 3D model generatşon requests high overlaps and low-altitude flights to achieve small GSDs, however for emergency surveying or management purpose flights requires to cover large areas in a few minutes, relatively at lower resolution (Nex & Remondino, 2014).

3.3.1.1. Flight Planning Parameters

Depending on the mission, UAV system type and environmental conditions the flight can be done manual, assisted or autonomous. Today with the presence of Global Navigation Satellite System (GNSS) receivers, Inertial Navigation System (INS) guides and improves the acquisition. The navigation system is basically constituted of hardware and software devices. The small size and the reduced payload of some UAVs has limitations to carry on high-quality devices. During the flight this system is observed with a GCS which shows real-time flight data such as position, speed, attitude, distances and GNSS observations, battery or fuel status etc. Regarding the quality of the data, low cost systems can be sufficient for little extensions while it is required more expensive devices with long endurance for larger areas. Expensive UAVs or manned aircraft systems can be a solution to prevent the problems regarding the wind, pilot capabilities, GNSS/INS quality, attitude and location (Nex & Remondino, 2014).

The on-board sensors detect the reflected light energy from the field. In order to clearly record field features and cover the area and to ensure that there is no missing area, many variables required to be considered in flight planning. These variables are the parameters such as flying height, focal length, forward and lateral overlap, required resolution, image scale etc.

In order to product photogrammetric data and aerial images, the most important parameters and formulas can be found in the literature.

-***Image scale*** can be defined as the distance between two points on an image to the actual distance between the same two points. The image scale expresses the average ratio between a distance in the image and the same distance on the ground. It is computed as focal length divided by the flying height above the mean ground elevation. m_b is defined by the flight height above the ground H_g and the focal length of the camera f

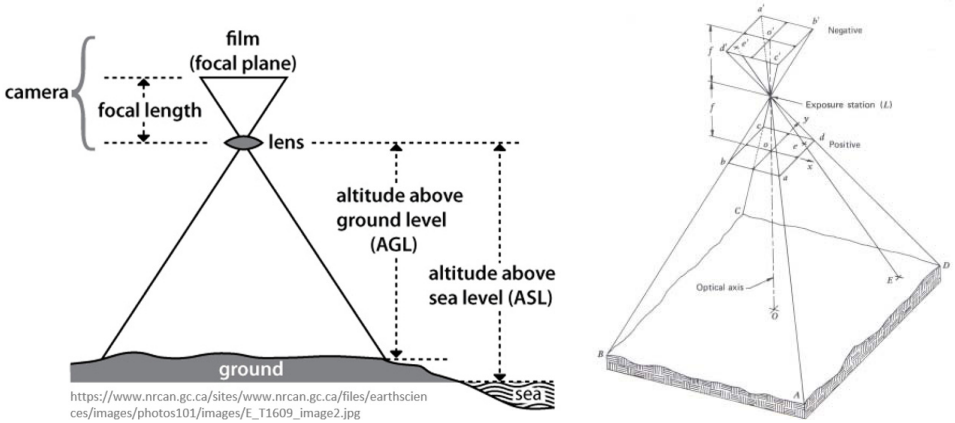

Figure 3.3.2: Image scale in photogrammetry (www.nrcan.gc.ca)

$$m_b = \frac{H_g}{f} \qquad 3\text{-}1$$

-Spatial(ground) resolution/ground sample distance (GSD) can be defined as how much area is represented by a pixel on the image sensor. In other words, it is the minimum distance to distinguish the two goals in the image (He, Li, & Zhang, 2012). The smallest size of the target should be 5-10 times of GSD (He et al., 2012). It determines how much detail can be interpreted from the final image and how many images need to be considered. Two major factors influence the spatial resolution: flying height and the focal length of the sensor. It can be expressed as following equation (Paine & Kiser, 2002)

$$Res = \frac{S_{pixel} * H_f}{f} \qquad 3\text{-}2$$

And the pixel size can be calculated as ;

$$S_{pixel} = W / S_w = H / S_h \qquad 3\text{-}3$$

Where *Res* is the spatial(ground) resolution, S_{pixel} is the pixel size of the image sensor, H_f is the flying height and *f* is the focal length of the camera. Using the same camera, the higher the UAV files, the less ground resolution there will be, and the shorter the focal length, the higher the resolution is.
In pixel size formula *W* is the width of CCD(mm), *H* is the height of the CCD(mm), S_w is the number of pixels for W and S_h is the number of pixels for H (He et al., 2012).
When H increases, GSD decreases, the single image coverage area increases. He, Li, & Zhang (2012) shows the relation between flight height, picture format, coverage area and GSD and the relation between GSD and the mapping scale shwon in Figure 3.3.3 and Figure 3.3.4.

Flight height (m)	100	200	300	400	500	600
Picture format width (m)	100	200	300	400	500	600
Picture format length (m)	150	300	450	600	750	900
Coverage area (km^2)	0.015	0.06	0.135	0.24	0.375	0.54
GSD (m)	0.027	0.053	0.08	0.107	0.133	0.16

Figure 3.3.3: Coverage area with single digital camera image (He et al., 2012)

The mapping scale	**GSD**	**The mapping scale**	**GSD**	**The mapping scale**	**GSD**
1:500	≤0.05	1:1000	0.08 - 0.1	1:2000	0.15 - 0.2

Figure 3.3.4: The relation between the mapping scale and GSD (He et al., 2012).

-Image overlap is the amount by which one image includes the area covered by another image and expressed as a percentage. To map an area with UAV requires a series of images taken multiple flight lines. To guarantee the overage without gaps, the images must contain enough overlaps. Image overlaps mainly contains two types: forward overlap and lateral overlap. The forward overlap –also known as endlap-is the common area on consecutive images along a flight strip. The lateral overlap includes the overlapping areas of images between adjacent flight lines. Figure 3.3.5 illustrates these two types of overlap (Xiang & Tian, 2011).

Appropriate aircraft image coverage is generally designed to provide about 60% forward overlap. This allows stereoscopic viewing of two overlapping images. Lateral overlap between 20% 40% is required for complete area coverage. The usual overlap value cannot be directly used on the UAV system. In order to cover as much as possible of the area with the minimum number of images taken by the UAV system, it is necessary to investigate appropriate overlap values (Xiang & Tian, 2011).

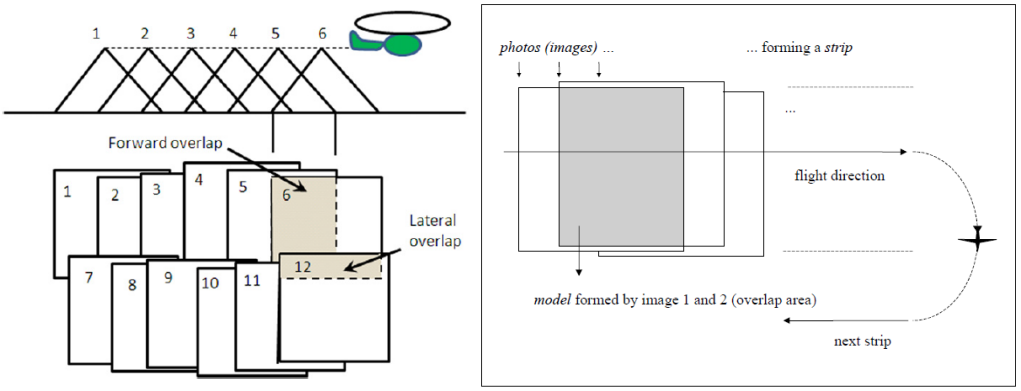

Figure 3.3.5: Forward and lateral overlap (Xiang & Tian, 2011) Photo, strip and overlap (Linder, 2006)

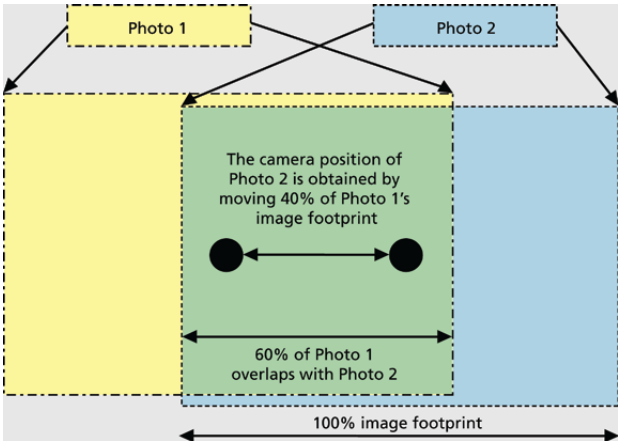

Figure 3.3.6: Image footprint and overlap (Kim,2015)

The length of the baseline is given with p% forward overlap is formulated in Eisenbeiß, 2009 study as;

$$B = S\left(1 - \frac{p}{100}\right)$$

3-3

Where *B* is the baseline, *S* refers to ground distance of the image and *p* is the along track overlap.
Falkner & Morgan, 2002 expressed the forward overlap in their study as (Falkner & Morgan, 2002);

$$g_{end} = s_p * w * \left[\left(100 - o_{end}\right)/100\right] \qquad 3\text{-}4$$

Where
g_{end} =distance between exposure stations
s_p = photo scale denominator (feet)
o_{end} = endlap (percent)
w = width of exposure frame (inches)

Lateral overlap –also known as sidelap- shown in Figure 3.3.7 which refers to the distance between two adjacent flight lines with q% side lap can be calculated as (Eisenbeiß, 2009);

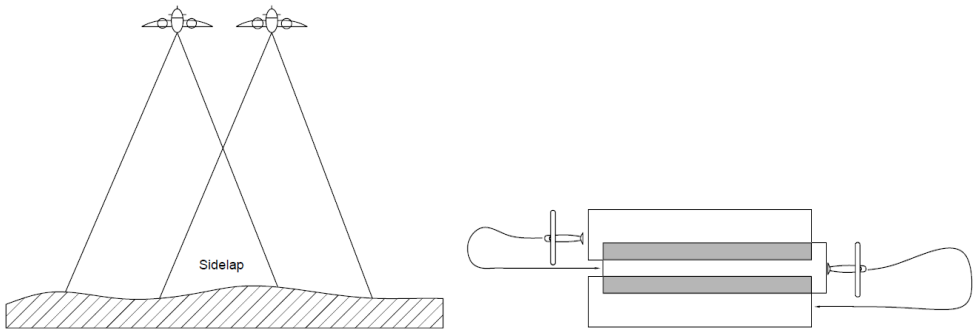

Figure 3.3.7: Sidelap between two (left) and three (right) adjacent flight lines(Falkner & Morgan, 2002)

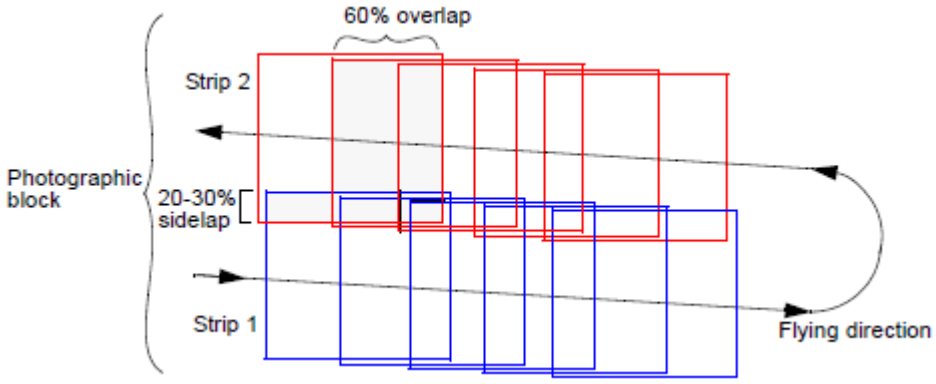

Figure 3.3.8: The relation between sidelap and overlap (https://wiki.hexagongeospatial.com)

$$a = S\left(1 - \frac{q}{100}\right) \qquad 3\text{-}5$$

Where *a* is the distance between flight lines, *S* is the ground distance of the image and *q* is across track overlap.

Falkner & Morgan, 2002 determined the equation for sidelap as ;

$$q_{side} = s_p * w * \left[\left(100 - o_{side}\right)/100\right] \quad 3\text{-}6$$

Where
g side = distance between flight line centers (feet)
Sp = photo scale denominator (feet)
oside = sidelap (percent)
w = width of exposure frame (inches)

When the smallest GSD can not meet the requirement for mapping, or the overlapping degree of the highest point is less than requirement, GSD should be changed, and the relative flight light, GSD of the lowest point, the overlap degree of the highest point should be calculated once more till it meets the requirements (He et al., 2012).

-Stereo coverage allows viewer to observe a pair of two-dimensional photos and see a single three-dimensional image, when using appropriate stereoscopic instruments. In photogrammetry a model is considered as the "neat" area –shown in Figure 3.3.9- that a single stereopair contributes to the total project. This allows for the endlap and sidelap with surrounding photos (Falkner & Morgan, 2002).

$$F_m = S^2 - S \times B \quad 3\text{-}7$$

Where,
Fm= Model area (stereo coverage)
S= ground distance of image
B= Baseline in object space

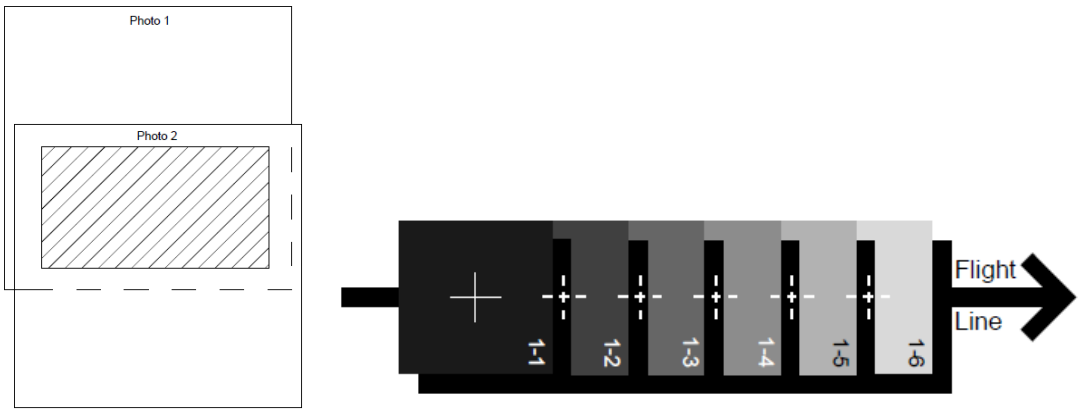

Figure 3.3.9: (left) Neat area of a stereomodel(Falkner & Morgan, 2002)
(right) Flight line and neat models (Burns, 2006)

Stereo coverage and endlap can be adversely affected by the flight trajectory of the aircraft. These are most commonly manifested in either *crab* or *drift*. *Crab* occurs

when constant corrections to the flight path cause the photos to twist with respect to one another. *Drift* occurs when the plane deviates from the intended flightline. Examples of each are shown in the figure below (Caltrans, 2006) .

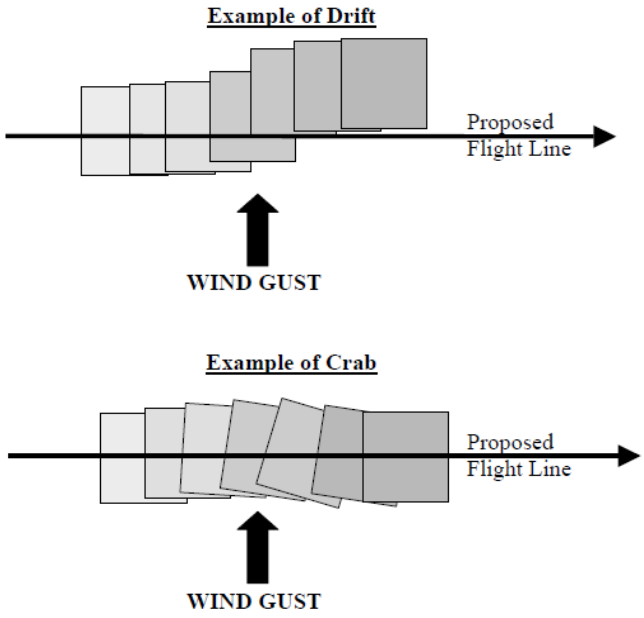

Figure 3.3.10: Wind effect to the flight line: drift and crab(Caltrans, 2006)

-*Accuracy in height* can be calculated with the measurement accuracy in planimetry and the ratio of flight height and baseline in image space. According to Heipke (1999), the measurement accuracy in planimetry is defined through the measurement method and the pixel size. Manually measured points can be defined with an accuracy as low as to 0.5 pixel. Automoatic measurement methods let an accuracy down 0.1 pixel for natural targets for flar terrain and good texture. However for UAV images it can be expected to achieve approximately 0.5 pixel (Eisenbeiß, 2009). The accuracies can calculate as;

$S_x = S_x\,(mes)\ X\ p_x$

$S_z = S_x\ X\ H_g / b$

3-8

Where,
Sx= accuracy in planimetry
Sz= accuracy in height
H_g= Flight height
p_x = Pixel size for digital cameras
b= Baseline in image

3.3.1.2. Flight Path Planning

Exisiting tools for path planning for UAVs to date have been developed for several purposes such as military, robotics, computer visions and artificial intelligence applications. With the development of new tools static and mobile obstacles are known. So local path planners are able to produce fast trajectories.

Nowadays point navigation for UAVs has become as a standard tool. Thus the autonomous flight based on defined points in a global coordinate system I s posiible for most of the UAV systems except for OM-class UAVs since their control is mostly done in the manual or assisted flight modes. So there is a need of integration and adaptation of photogrammetric flights intoı the UAV path planning.

In general UAV mission planning softwares require some additional functions integrated, such as the photogrammetric aerial flight planning tools. For autonomous flights of UAVs, a start and a home point have to be defined. Based on the start point, the mission is set up relative to its coordinate. Besides, some packages allow alos way points, the definition of lines, aths, boundaries and no goes areas. This is especially the case if the UAV mission is completely autonomus like in military applications or for vision recognition based-flights.

Trisirisatayawong and Cheewinsiriwat, 2004 developed a GIS-based flight planning system, which includes parameters like altitude, aircraft position, viewing angle etc. for UAV flight planning. This system depends on the existing GIS software

Combining both the photogrammetric flight planning and the mission planning of UAVs leads to flight planning for UAVs. Since UAVs operate in a transition section between aerial and terrestrial photogrammetry, where the various camera views are available for data acquisition. Eisenbesii made a classification depending on the applications and specifications and tools. According to his classification, 2D flight planning is suitable for docuemnattaion of cities, while for the docuemnatation of facades of strees can be the combination of 2D and circle tool. Circle tool was developed for single objects like buildings. In this case, a flight line defined as circle or ellipse is set around an object.

The area of interest can be defined in a map or orthoimage using GIS, or Google earth, Virtual earth etc. If no information about the area, UAV can provide the image of the area. Defined borders of the area, flight parameters and the flight planning can be generated by tool. The outcome of the flight plan are the coordinates of the image acquisition points and attributes fo the automatic flight which can be integrated into the mission planning software of UAV.

For the photogrammetric processing of UAV data the coordinate systems are needed. This coordinate systems could be global coordinate system[15], local coordinate system[16], platform and device coordinate systems[17] and image coordinate systems[18].

---

[15] Global coordinate systems are described as solar or earth fixed coordinate system, where the coordinate axis are for example defined by means of VLBI (Very long baseline interferometry, SLR (Satellite Laser Ranging), GPS measurements or observation to quasars. These systems have a defined origin; for the geocentric coordinate systems this is the center of gravity of the earth. GPS measurements use the WGS84 (World Geodetic System 1984), which is a geocentric coordinate system. The center of

3.3.1.3. Flight Trajectory and waypoints (exposure station) determination

In flight planning with UAV, determination of desired lines and waypoints (the position of the exposure points) are other flight planning parameters. Flight lines are normally oriented in north-south or east-west direction. The lines are generally parallel to each other. In order to collect the images for a desired area, the UAV flies along the entire length of one strip, then move to the next flight line and flies backwards along the entire length of the next adjacent flight line. This procedure repeats until the desired area is completely covered (Figure 3.3.11).

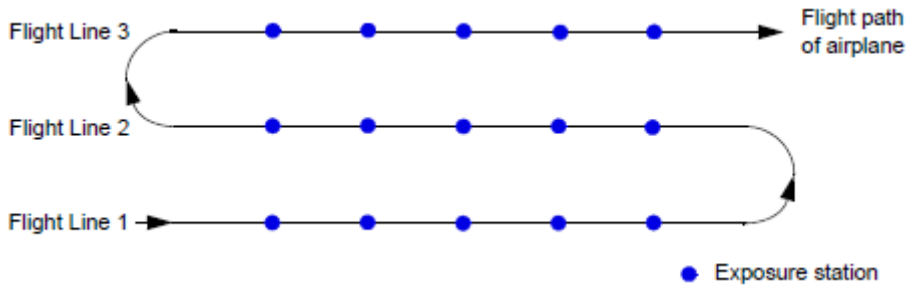

Figure 3.3.11: Exposure Stations Along a Flight Path(https://wiki.hexagongeospatial.com)

Falker&Morgan (2002) and Paine&Kiser (2002) defines the equations for the dimension between flight lines and the number of waypoints (exposure stations) required shown below.

$$D_1 = \frac{\frac{H_f}{f} h_c \left(1 - O_{fO}\right)}{\cos(\theta_c)} \tag{3-11}$$

Where D_1 is the distance between two images in flight line, H_f is the flying height, f is the focal length, h_c is the height of the image sensor, O_{fo} is the forward overlap, Θ_c is the angle between the flight line and heading of the camera called as

---

gravity results from the global equipotential model of the earth. The X-axis is defined through the intersection point of the null meridian and the equator, the Z-axis is equal to the rotation axis of the earth, while movements of the pole are taken into account, the Y-axis completes a right handed coordinate system.

[16] Local coordinate systems are right-handed systems centered at a chosen point P, with the X-axis being a tangent to the local parallel and looking toward East. The Y-axis is tangent to the local meridian and looks toward North, while the Z-axis is directed upwards using orthometric heights (geoid). An example for a local coordinate systems is the Swiss LV03 system.

[17] camera coordinate system depends on the orientation of the camera mounted on the UAV. In the standard configuration, the X-axis of the camera is mounted parallel to the bow direction of the UAV (flight direction), the Z-axis is parallel to the acquisition axis with the normal to the baseline and the Y-axis completes the right-hand-coordinate system. The centre of origin is defined by the projection center of the camera.

[18] The center of the image M' (xM and yM) is defined by means of reference or fiducial points (film based system) or the pixel array (electronic systems). The principal point H' (xp and yp) is defined as the intersecting point of the optical axis and the image plane.

"crab angle". The crab angle is caused by a failure to orient the camera with respect to the planned flight line;

$$D_2 = \frac{H_f}{f} w_c (1 - O_{10}) \sin(\theta_c)$$

(3-12)

Where D_2 is the distance between two flight lines; O_{10} is the lateral overlap, w_c is the width of the image sensor.

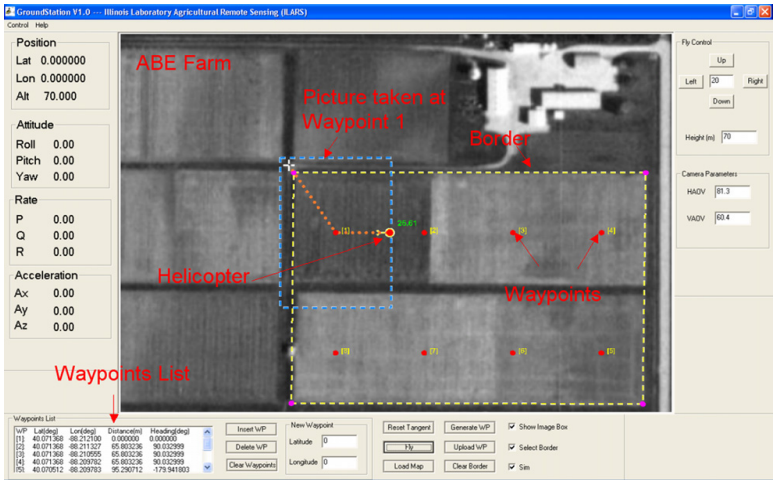

Figure 3.3.12: UAV ground station software

In last years, autonomous flights are heading for image acquisition. However some systems can only be controlled manually. Besides, in some areas autonomous flight is not allowed because of the security reasons. Eisenbeiß (2003) made some investigations on the influence of the manual flight mode compared to the autonomous mode (Figure 3.3.13).

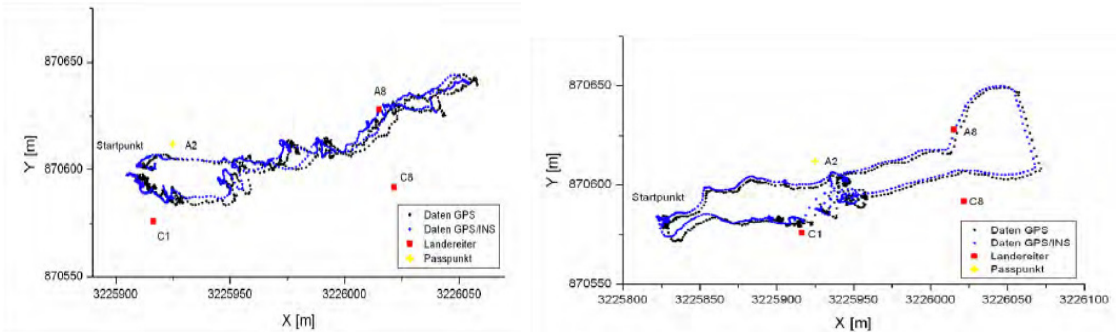

Figure 3.3.13: trajectory of the manually (left) and autonomous controlled flight (Eisenbeiß, 2009)

According to the study, in manually controlled flight it was not possible to get a precise block configuration and successful results, especially under wind conditions. While with autonomous flight, UAV is able to follow pre-defined flight path. In manually controlled systems such as kites and zeppelin, the images distributes irregularly over the desired area and the image cover changes sharply. Besides the orientation and the shape of the images change in many images so block configuration

is insufficient for a good image orientation. It is easier to control and keep stable on a flight trajectory.

While most of the autonomous systems are stabilized so the flight trajectory is more stable. For this, the ideal position and orientation of sensors have to be minimized, movements of the sensors should be avoided and the influences of vibrations have to be reduced. Vibrations of the platform can result in image blurring and errors of the sensors can influence the absolute accuracy[19] of the position. Absolute accuracy between camera and GPS sensors can be neglected for OM and M-class UAVs if the value is less than half meter (Eisenbeiß, 2009). The flight mode has also effect on the stability of the system. The flight mode manual, assisted or autonomous effects the stability of the system and the orientation data. Eisenbeiß (2009) made a study on effect of flight modus on stability and velocity shown in figure 3.3.14.

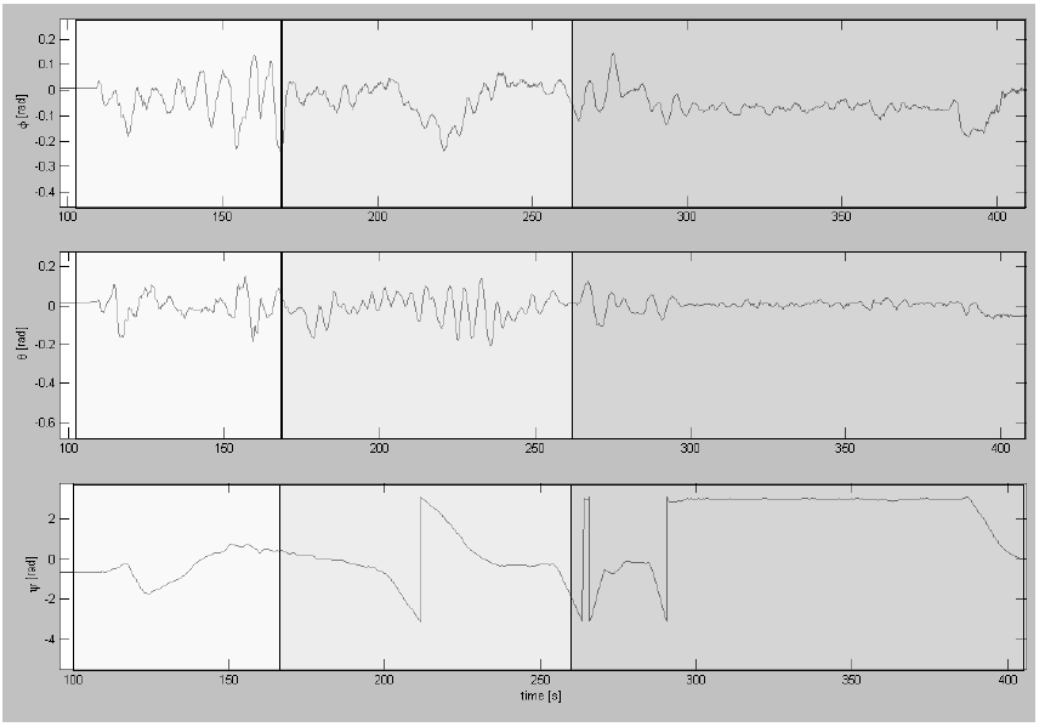

Figure 4-23: Example for the transition between manual (white), assisted controlled (light gray) and autonomous (gray) flight. Upper graph: Roll (Φ) angle around x-axis; Middle graph: pitch (Θ) angle around y-axis; Lower graph: yaw (Ψ) angle around z-axis.

Figure 3.3.14: Example of the transition between manual, assited and autonomous flight and angles (Eisenbeiß, 2009).

[19] Absolute accuracy of low-cost sensors is in the range of several meters.

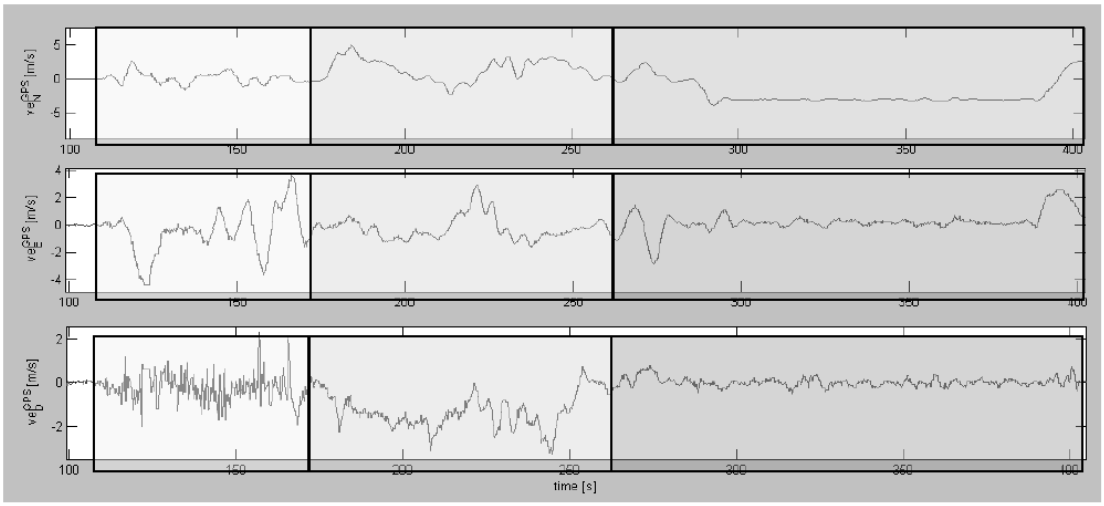

Figure 3.3.15: Example of the transition between manual (white), assited(light gray) and autonomous (gay) flight. Upper graph: velocity-north, middle graph: velocity east, lower graph: velocity height (Eisenbeiß, 2009).

According to his study, during the autonomus flight, the angles were fairly stable in normal wind conditions.

Before starting to a flight with UAVs, the flight trajectory has to be defined. However in many times, predefined flight trajectory can be flown under weather conditions, especially in windy conditions. To be able to compare the difference between predefined flight path and flight trajectory, firstly, the coordinates of the image acquisition centers have to be transformed on to the same coordinate system. The most navigation units use the WGS84 coordinate system. Swisstopo (2005) gave the formula of this transformation (Eisenbeiß, 2009);

$$P\begin{pmatrix} X \\ Y \\ Z \end{pmatrix}_{LV03} = f(WGS84 \rightarrow LV03)\, P\begin{pmatrix} X \\ Y \\ Z \end{pmatrix}_{WGS84} \tag{3-13}$$

According to Stempfhuber and Kirschner (2008), in order to achieve real-time 3D measurement data with accuracy better than1 cm and high temporal resolution, only tracking total stations can be used. This kind of technology is especially suitable for the applications requiring milimeter accuracy in planimetry and height for object distances up to 300m, which is a normal distance of an UAV image strip. The tracking total stations is mainly used for the control of construction machines and seurveying in one-man mode, kinematic measurments in road construction. With this technque, it is possible to achieve and absolute accuracy of few millimeters.

3.4. Data processing concepts

3.4.1. Image Orientation and Camera Calibration

Both image orientation and camera calibration are two principal prerequisites for any metric image reconstruction. Camera calibration relates to the problem of the pixel locations in the image sequence to points in the scene. Each pixel is imaged through perspective projection, it corresponds to a ray of points in the scene. The camera calibration determines the equation for this ray in the absolute coordinate system of the scene and it is needed for both intrinsic parameters[20] and extrinsic parameters[21] (Figure 3.4.1.1.).The position of the camera and camera constant must be determined to relate image plane coordinates to absolute coordinates. Besides, the location of principal point, the aspect ratio and lens distortions must be defined to relate pixel coordinates to positions in the image.

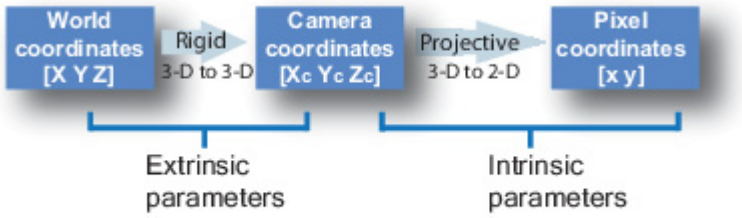

Figure 3.4.1.1.Intrinsic and extrinsic parameters of camera calibration

According to Tsai (2000), camera calibration problem can be summarized and shown as figure below. Where $\mathbf{p}'_0$ is the location of the origin in the image plane, $\mathbf{r}'_i$ is the vector from $\mathbf{p}'_0$ to the image point $\mathbf{p}'_i = (x'_i, y'_i)$, $\mathbf{p}_i = (x_i, y_i, z_i)$ is a calibration point, and $\mathbf{r}_i$ is the vector from the point $(0, 0, z_i)$ on the optical axis to on the optical axis to $\mathbf{p}_i$. If the difference between the uncorrected image coordinates $(\tilde{x}_i, \tilde{y}_i)$ and the true image coordinates (x'_i, y'_i) is due only to radial lens distortion, then $\mathbf{r}'_i$ is parallel to $\mathbf{r}_i$ The camera constant and translation in z do not affect the direction of $\mathbf{r}_i$, since both image coordinates will be scaled by the same amount. These constraints are sufficient to solve the exterior orientation ("Camera Calibration for stereo vision,") (Figure 3.4.1.2).

Photogrammetric cameras (metric) are used where it is needed to get high accuracy measurements; like topographical applications and architectural photogrammetry. While digital cameras are used when lower accuracy measurements are enough. The use of digital cameras for photogrammetric purposes requires calibration due to the fact that elements of non-metric camera internal orientation is not known which is a problem especially for wide-angles lenses because of big distortions.

[20] intrinsic parameters for the camera itself
[21] extrinsic parameters for rigid body transformation

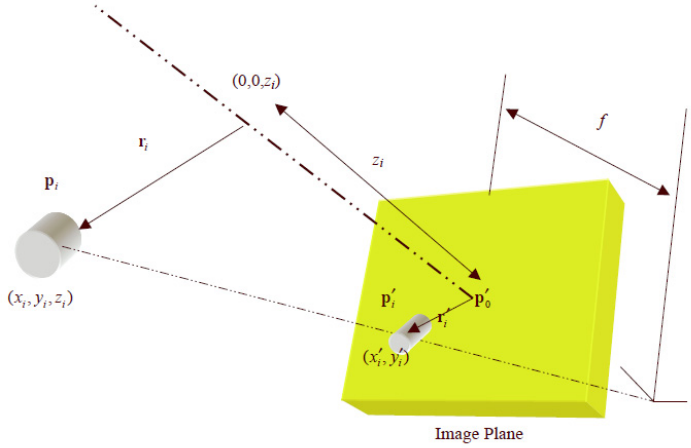

Figure 3.4.1.2: Representation of the camera calibration problem ("Camera Calibration for stereo vision,")

Today non-metric cameras are mountable to UAVs however there is still need to get interior orientation parameters. The problem with non-metric cameras is that stability elements of the interior orientation are not ensured and measurement of fiducial marks associated with principle point is not possible[22](Fryskowska, Kedzierski, Grochala, & Braula, 2016). When lower accuracy is sufficient ,calibration and orientation can be computed simultaneously by self-calibrating bundle adjustment. For aerial cameras it is mostly done in the lab.

There are different methods such as laboratory, test field and self-calibration. In laboratory calibratiom method, a calibraotr is needed and this method mostly applied for the metric cameras. The filed calibration method requires known reference field. The method bases on the images of this test field and the test field consists of a large number of points covering the entire frame. Signalized points are imaged in the picture. They are flat and can be 2D and spatial 3D. Self-calibration is the process of camera calibration performed during the measurement process. This is due to the increased number of images taken, and the necessity of the use of specialized software. The greater the number of images, and thus the greater the number of measured homologous points, the accuracy is higher (Fryskowska et al., 2016).

There are also other studies taht can be found in the literature (Clarke & J.G., 1998; Karras & Mavrommati, 2001; Remondino & Fraser, 2006; Udin & Ahmad, 2014; Wang, Shi, Zhang, & Liu, 2008; W. Zhang, Jiang, & Han, 2010). However there are not many calibration techniques for the images taken from UAVs. But in the last years, there have been several studies also on the calibration of UAV cameras (Fryskowska et

[22] in the images taken with non-metric cameras are not consist of fiducial marks. The role of fiducial marks in the images of the non-metric cameras perform extreme corners of the image pixels.

al., 2016; Gašparović & Gajski, 2016; Perez, Agüera, & Carvajal, 2011; Yanagi & Chikatsu, 2015). Perez et al. (2011) made a study in order to find out interior orientation parameters of a UAV camera and they compared the results of both lab camera calibration based on a flat pattern and a field camera calibration of a UAV camera with Photomodeler Scanner Software. The results show that the field calibration reduced the final total error while RMSs values were similar(Perez et al., 2011) (Figure 3.4.1.3).

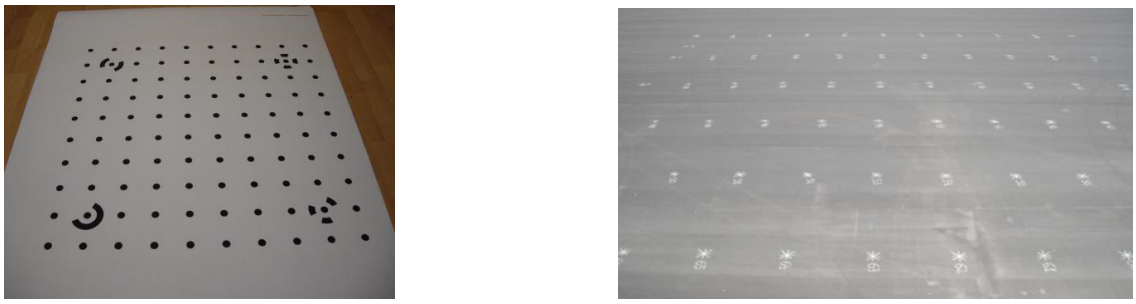

Figure 3.4.1.3: (left)Lab camera calibration pattern (right) Test field calibration surface with the targets points

Fryskowska et al. (2016) prepared a research on calibration of color and NIR UAV cameras in different softwares and compared the results. Udin&Ahmad (2014) made a study on test field calibration on different flying heights. However Colomina et al. (2007) performed in flight-calibration with possible strips at different flying heights (Colomina et al., 2007).

After data acquisition for camera calibration and the image are processed camera calibration parameters as shown in Figure 3.4.1.4 below are acquired. The camera calibration parameters consist of the focal length (c), principal point offset (xp, yp), radial (k1,k2, k3) and tangential (p1, p2,) lens distortion, “affinity” (b1) and different in scale factor (b2) (Udin & Ahmad, 2014)

Parameter	Value
C (mm)	16.6364
x_p (mm)	0.0123
y_p (mm)	0.449
k_1	2.60490e-004
k_2	-1.22048e-006
k_3	-1.16336e-009
p_1	-9.24742e-005
p_2	-1.47364e-004
b_1	-8.37144e-005
b_2	-1.52412e-004

Figure 3.4.1.4: Camera calibration parameters of Sony NEX-5N digital camera(Udin & Ahmad, 2014)

Image orientation and camera calibration require extraction of tie points. It can be done manually by the operator or by fully automated procedures of some commercial softwares such as: PhotoModeler Scanner (Eos Inc.), PhotoScan (Agisoft), LPS(Leica Photogrammetry Suite 8.9-9.2), ORIMA (Orientation Management Spftware), ISDM (Z/I Imaging, Image Station Digital Mensuration). These commercial softwares need

user insteraction or GNSS/INS data in order to extract tie points automatically. However there are also some free web-based and open source softwares (such as Photosynth, 123DCatch, VisualSFM) of which the results are not reliable and accurate enough(Remondino, 2014).

Image orientation is priory required for any task including the computation of 3D coordinates such as Digital Terrain Model (DTM), the computation of orthophotos and the acquisition of the data for Geographic Information Systems (GIS).

Owing to determinative significance of image orientation, it has been always a focus of attention in photogrammetry. Digital photogrammetry holds the completely automating the process of image orientation and image analysis techniques. When an automatic image orientation is available, image orientation can be considered as a preprocessing step in the photogrammetric processing chain (Heipke, 1997). Besides, commercial softwares, Bartelsen et al.(2012) improved several methods in order to orient images also under unfavorable conditions (Bartelsen, Mayer, Hirschmüller, Kuhn, & Michelini, 2012).

3.4.1.1. Interior orientation

Interior orientation defines the internal geometry of a camera or sensor as it existed at the time of data capture and shortly it means the process of camera calibration. It refers to the determination of the parameters describing specific photogrammetric models for mapping geometric primitives such as points, lines and areas from one coordinate system to another one. Interior orientation is primarily used to transform the image pixel coordinate system or other image coordinate measurement system to the image space coordinate system (Figure 3.4.1.5). So image orientation relates to the class of coordinate transformation problems.

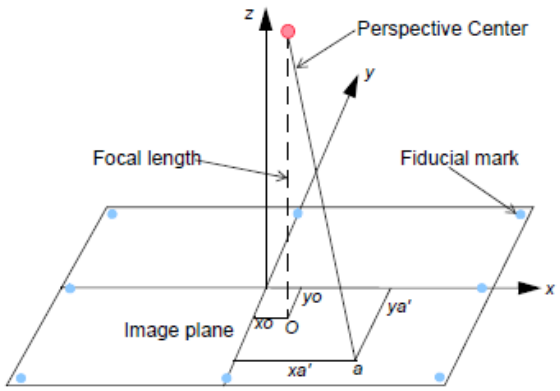

Figure 3.4.1.5: Internal geometry of a camera (https://wiki.hexagongeospatial.com)

Here is the *principal point* is the intersection of the perpendicular line through the perspective center of the image plane. The image plane commonly refers to the focal plane. The *focal length* of a metric camera is accurately determined or calibrated in a laboratory. The image positions of the fiducial marks are measured on the image then

compared to the calibrated coordinates of each fiduacial mark. The measured image coordinates of the fiducial marks referenced to pixel or file coordinate system. And the *lens distortions*[23] exchanges the positional accuracy of image points located on the image plane (Figure 3.4.1.6)

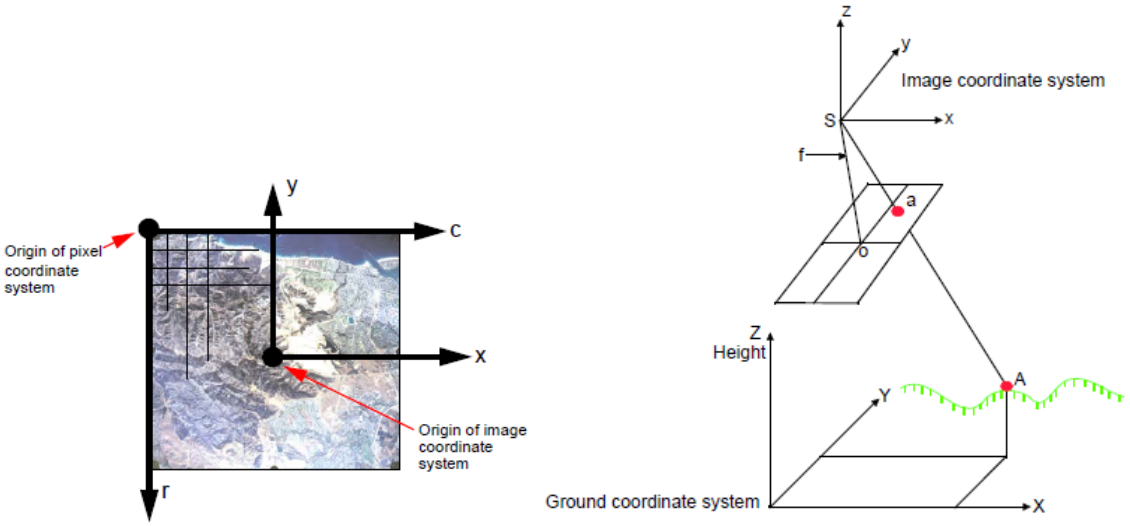

Figure 3.4.1.6: (left)Pixel coordinate system and image coordinate system (https://wiki.hexagongeospatial.com). (right) Image coordinate system and ground coordinate system(https://wiki.hexagongeospatial.com)

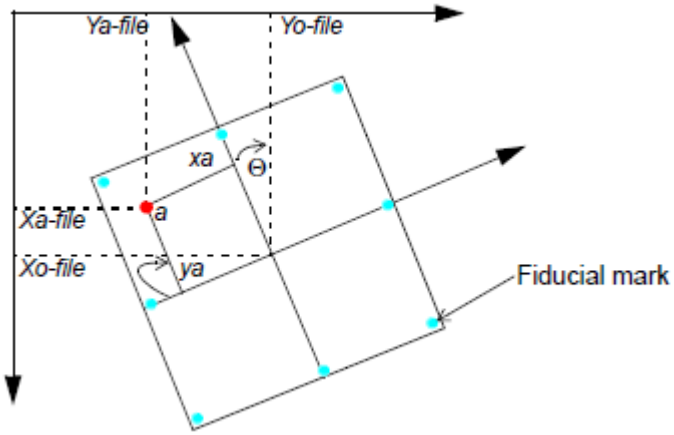

Figure 3.4.1.7: Relationship between the pixel coordinate system and the image space coordinate system(https://wiki.hexagongeospatial.com)

Two-dimensional affine transformation, the relationship between the pixel coordinate system and the image space coordinate system is defined as

$$x = a_1 + a_2X + a_3Y$$
$$y = b_1 + b_2X + b_3Y$$

[23] It happens when the light rays passing through the lens are bent, thereby changing directions and intersecting the image plane at positions deviant from the norm.

The x and y image coordinates associated with the calibrated fiducial marks and the X and Y pixel coordinates of the measured fiducial marks are used to determine six affine transformation coefficients. The resulting six coefficients can then be used to transform each set of row (y) and column (x) pixel coordinates to image coordinates.

For digital cameras, the relation between pixel and image coordinates is fixed and is determined during the calibration procedure in addition to the interior parameters of the camera. Digital photogrammetry gives opportunity to the automation of the image orientation process using image processing and image analysis techniques. In traditional photogrammetry, image orientation is quite complicated and time consuming. So it's clear that an automatic image orientation module will allow a wider use of photogrammetry. And in the computer vision terminology, "image calibration" sometimes includes image orientation (Heipke, 1997). For the automation of the interior orientation several studies have been done (Barazzetti, Remondino, & Scaioni, 2010; Bartelsen et al., 2012; Heipke, 1997; Kersten & Haering, 1997; Pierrot Deseilligny & Clery, 2011)

3.4.1.2. Exterior Orientation

Exterior orientation defines the position and angular orientation associated with an image. The variables defining the position and orientation of an image refer to the elements of exterior orientation.

Exterior orientation parameters of image are geometric parameters of image, that specify its position and orientation in relation to object of photogrammetric survey in a moment of the survey. There are linear and angular exterior orientation parameters of image. Linear exterior orientation parameters of image–coordinates of center of optical image projection in coordinate system of photogrammetric survey object. Angular exterior orientation parameters of image–parameters that define image angular orientation in coordinate system of photogrammetric survey object, slope and rotation angles of image.

The elements of exterior orientation define the characteristcis associated with an image at the time of exposure or capture. It defines ground space coordinates based on image space coordinates and flight information. The elements of exterior information shown in figure 3.4.1.8.

O is the position of the perspective center with respect to the ground space coordinate system (*X, Y, Z*) and *Zo* is the height of the camera above sea level.

The angularor rational elements of exterior orientation describe the relation between the ground space coordinate system (X,Y,Z) and the image space coordinate system (x,y,z). The rotation angles are commonly used to define angular orientation;

omega ω -- a rotation about the photographic x-axis

phi φ -- a rotation about the photographic y-axis

kappa κ -- a rotation about the photographic z-axis

These 6 parameters X,Y,Z and omega, phi ,kappa are called exterior orientation (EO) parameters. In a traditional photogrammetry, EO parameter derived from Aerial Triangulation and it is needed GCP.

Omega, phi, and kappa are defined as being positive if they are counterclockwise when viewed from the positive end of their respective axis.

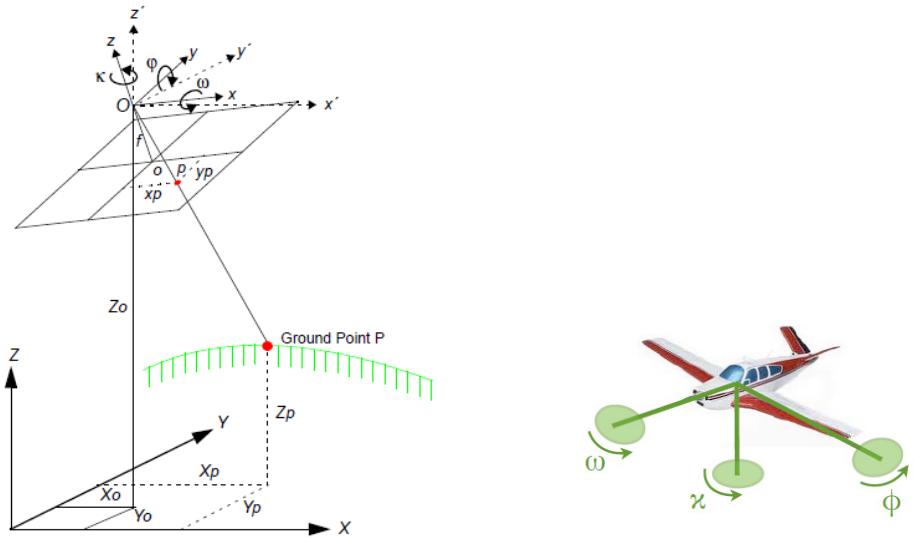

Figure 3.4.1.8: (left)Elements of Exterior Orientation and (right) rotation angles(https://wiki.hexagongeospatial.com)

When the perspective center, an image point and its corresponding groun point are on a straight line for all points on the image, it is called as ***collinearity condition.*** It is used in most photogrammetric operations. The equation below defines the collinearity condition. Collinearity equations can be derived using GCPs and tie points

$$x = -f\frac{a_1(X_A - X_S) + b_1(Y_A - Y_S) + c_1(Z_A - Z_S)}{a_3(X_A - X_S) + b_3(Y_A - Y_S) + c_3(Z_A - Z_S)}$$

$$y = -f\frac{a_2(X_A - X_S) + b_2(Y_A - Y_S) + c_2(Z_A - Z_S)}{a_3(X_A - X_S) + b_3(Y_A - Y_S) + c_3(Z_A - Z_S)}$$

(3-14)

x, y: coordinates of a point on image space
X_A, Y_A, Z_A: ground space coordinates of the point
X_S, Y_S, Z_S: coordinates of the perspective center (lens)
f: focal length

$$
\begin{aligned}
a_1 &= \cos\phi\cos\kappa + \sin\phi\sin\omega\sin\kappa \\
b_1 &= \cos\phi\sin\kappa + \sin\phi\sin\omega\cos\kappa \\
c_1 &= \sin\phi\cos\omega \\
a_2 &= -\cos\omega\sin\kappa \\
b_2 &= \cos\omega\cos\kappa \\
c_2 &= \sin\omega \\
a_3 &= \sin\phi\cos\kappa + \cos\phi\sin\omega\sin\kappa \\
b_3 &= \sin\phi\sin\kappa - \cos\phi\sin\omega\cos\kappa \\
c_3 &= \cos\phi\cos\omega
\end{aligned}
$$

3.4.1.3. Aerial Triangulation versus Direct Georeferencing Technology

Traditionally, in photogrammetry exterior orientation task is solved indirectly using the wellknown method of aerial triangulation (AT) (Figure 3.4.1.9)

Aerial Triangulation is a method in photogrammetry to determine and calculate 3D object coordinates by photogrammetric means, by using photographs exposed from different positions, covering the same object. It solves exterior orientation parameters of each photo and 3D coordinates for all measured object points. The number of points can be divided as tie point, which represents the same location in an adjacent image or aerial photograph and it is used to link the images. While check point is a point of a known coordinate used in aerial triangulation to evaluate the value of the point. The surveyed points in the filed to determine their exact locations are known as control points.Aerial triangulation can be analogue, semi-analytical, analytical or digital (Zomrawi, Hussien, & Mohamed, 2013) The computation of aerial triangulation gives (X, Y, Z omega, phi, kappa parameters).

Aerial Triangulation method was first appeared commercially in the mid-1990s and and since then evolved into a standart for airborne mapping.

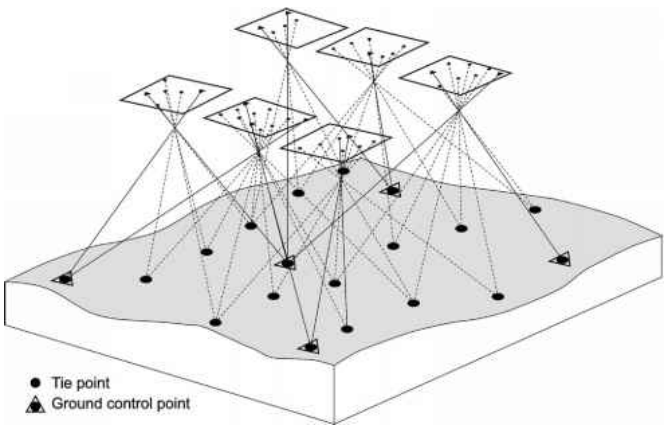

Figure 3.4.1.9: Principle of bundle block adjustment(http://www.tanguayphotomag.biz/)

• In any model, at least 6 well-distributed object points must be measured. It is an old and good tradition to do this in a distribution like a 6 on a dice, the points are then called Gruber points in honour of Otto von Gruber, an Austrian photogrammetrist.
• Neighbouring models must have at least 2 common points. In standard, we will use 3 of the Gruber points (the left 3 for the left model, the right 3 for the right model)(Figure 3.4.1.10)
• Neighbouring strips are connected together with at least one common point per model. As a standard, we will use 2 of the Gruber points (the upper 2 for the upper strip, the lower 2 for the lower strip).
• Each object point must have a unique number. In particular this means that a point has the same number in any image in which it appears. On the other hand, different object points have different numbers (Linder, 2006).

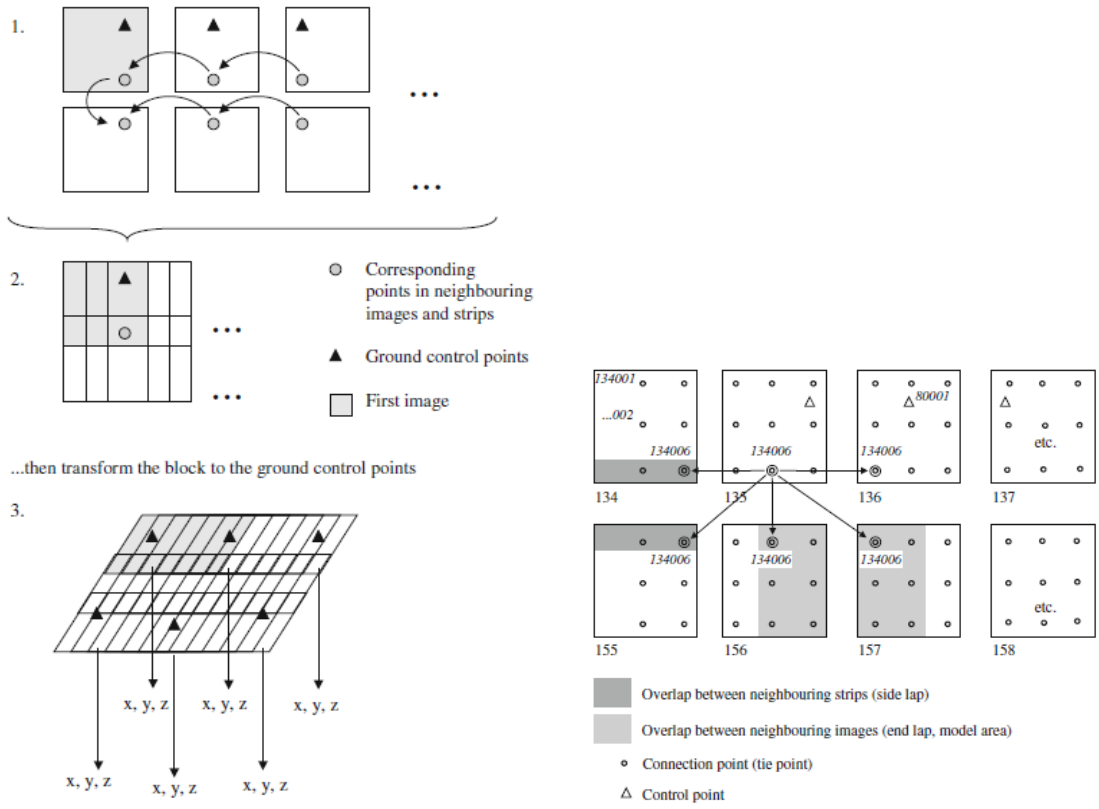

Figure 3.4.1.10:(left)Scheme of aerial triangulation in traditional photogrammetry (Linder, 2006)
(right) Principles of point transfer within a block (Linder, 2006)

• A system for fully automatic aerial triangulation has principally to deal with the appropriate selection of tie point areas and the subsequent point transfer by means of multiple image matching techniques. Tie point areas are here to be understood as patches at the 9 standard positions of an aerial image, also known as Gruber positions(Krzystek, Heuchel, Hirt, & Petran, 1995). Also there are other studies for automatic aerial triangulation by Schenk (1995), (Heipke, 1999; Krzystek et al., 1995; Xiong, 2009)

Although aerial triangulation was essentially improved and expanded to socalled automated aerial triangulation (AAT), the orientation process still suffers from a large

amount of interactive editing and supervision of highly skilled operators. This is especially due to the high computational effort that is necessary for automatic tie point measurement. A reliable matching of tie points is necessary to determine the exterior orientation of each image correctly. With the availability of integrated GPS/inertial systems this situation changes. GPS offers high absolute accuracy position and velocity information. inertial systems provide very high relative accuracy for position, velocity and attitude information, but the absolute accuracy decreases dependent on runtime if the system is working in stand-alone mode and no external update measurements are available. their optimal integration allows fully exterior orientation determination with improved overall accuracy and at higher reliability compared to the stand-alone units.

The integration of GPS and INS was initially undertaken to support reliable commercial aircraft navigation, UAV guidance and control and mobile mapping. This combination of thecnologies may also be referred to as a "GPS-Aided INS" or a "Position and Orientation System (POS)". Even each of these technologies has restrictions, but the integration of GPS (Global Positioning System) and INS (Inertial Navigation System) is a powerful solution for direct georeferencing (DG)[24](Schuckman & Renslow, 2017).

Direct Georeferencing (DG) is the direct measurement of the position and orientation of an airborne mapping sensor -such as a camera or laser scanner- which each pixel or range can be georeferenced to the Earth without the need for ground information collected in the field whic is achieved by Global Navigation Satellite Systems (GNSS) integratedwith inertial measurement sensors. The collected data from GNSS and IMU sensorsa re processed in real-time and in post mission along with data collected from a single or network of GNSS reference stations in order to get precise measurements of the sensor position and orientation exactly at the timeof exposureor scan(Mohamed M.R & Hutton, 2001).

In a direct georefencing system, GPS records *position* of the coordinates (X, Y, Z) and *velocity,* the INS records attitude and orientation (three rotation angles roll, pitch and yaw) of image exposure with respect to the ground with inertial measurement unit (IMU) (Figure 3.4.1.11)

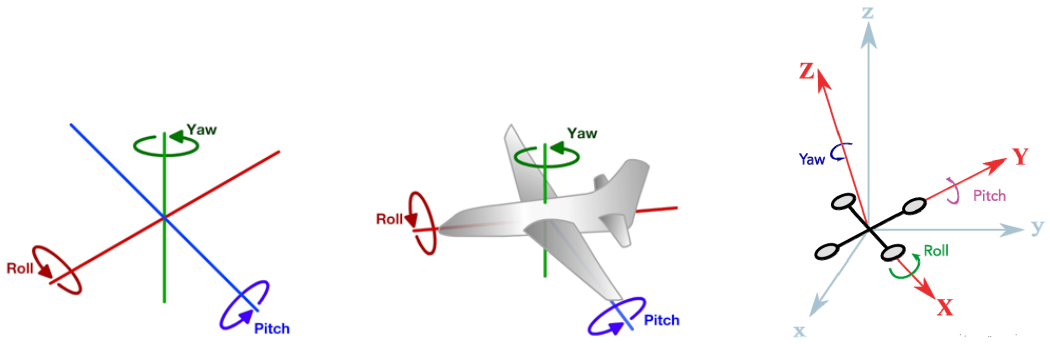

Figure 3.4.1.11:Three rotation angles; roll, picth and yaw (http://theuav.net/)

[24] Amathematical modelling procedure for removing noise, Kalman filter was implemented for lidar collection in the mid-1990s, provide a robust way to estimate and compensate for GPS/INS errors.

Figure 3.4.1.12. gives an overview of the available sensors of UAVs and which sensor can be used in orer to get position and orientation parameters. The interpolation at the exposure times gives the position and orientation of each image; where the projection center is X_o, Y_o, Z_o and the rotation angles r_o, p_o, y_o(Pfeifer, Glira, & Briese, 2012).

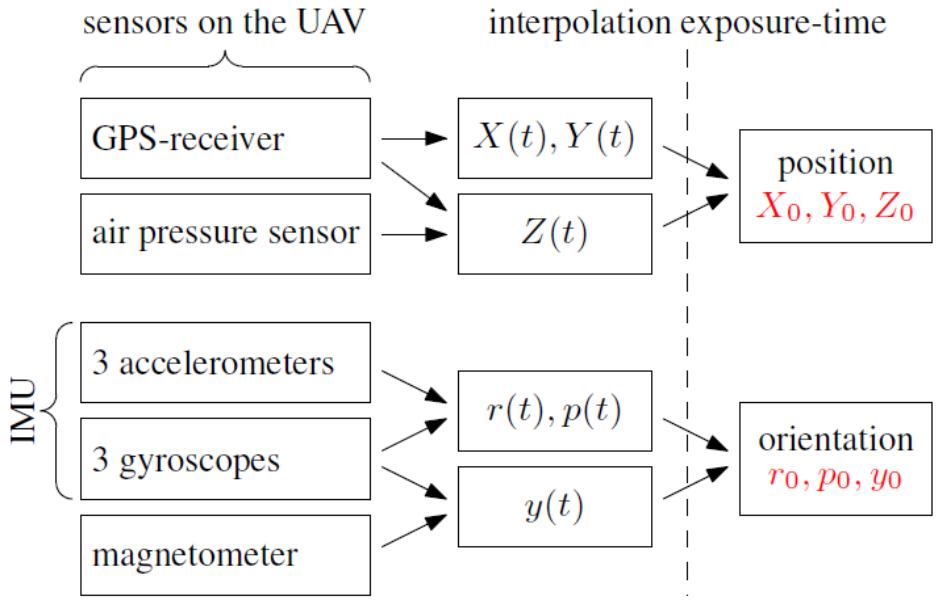

Figure 3.4.1.12: Direct Georeferencing of the images by integration of all available sensors on borad of UAV (Pfeifer et al., 2012)

UAVs are typically equipped with position and motion sensors. Medium weight platforms (with 15 kg payload) can hold a high quality INS while for small platforms, the accelerations and rotation rates are measured with micro-electro-mechanical systems.

The method which exterior parameters recorded directly from GPS/IMU is called Direct Georeferencing. During a flight mission, the direct referencing system records the position and orientation data, typically at a rate of 200hz. The direct georeferencing software interpolates position and orientation of the laser reference point at each time-tag. With this data, 3D ground coordinates of each laser return may be computed

Theoretically it doesn't't require GCP and it can be replaced with Aerial Triangulation process in traditional photogrammetry as shown in Figure 3.4.1.13 (Mian et al., 2015). Haala et al., (2011) compare the results of automatic aerotriangulation to the direct georeferencing positions for a fixed-wing UAV (Haala, Cramer, Weimer, & Trittler, 2011). The advantages of Direct Georeferencing to Aerial Triangulation also been studied by Ip et al. (2006)and they were summarized as large cost saving for GCPs in the field, improved data collection efficiency by reducing or eliminating sidelap requirements, improved point matching efficiency and adjustment accuracy, ability to map in remote locations and ability to map in real-time (Ip, El-Sheimy, & Mostafa, 2006). It gives a shorter time and cheaper in the mapping project, faster in data

processing and simpler workflow with lower cost project at the same accuracy(Rizaldy & Firdaus, 2012). The accuracies are in general at the centimeter level for position and milidegrees range for orientation (Mian et al., 2015). Rizaldy& Firdaus (2012) tested the accuracy of this method and had high accuracy for mapping.Another study on the accuracy and the potential of this system was made by Cramer et al.(2000). They made some accuracy tests on data processing, variable image overlap and baseline length. The presented results proved the high quality of direct exterior orientation measurmenets of direct georeferencing system(Cramer, Stallmann, & Haala, 2000).

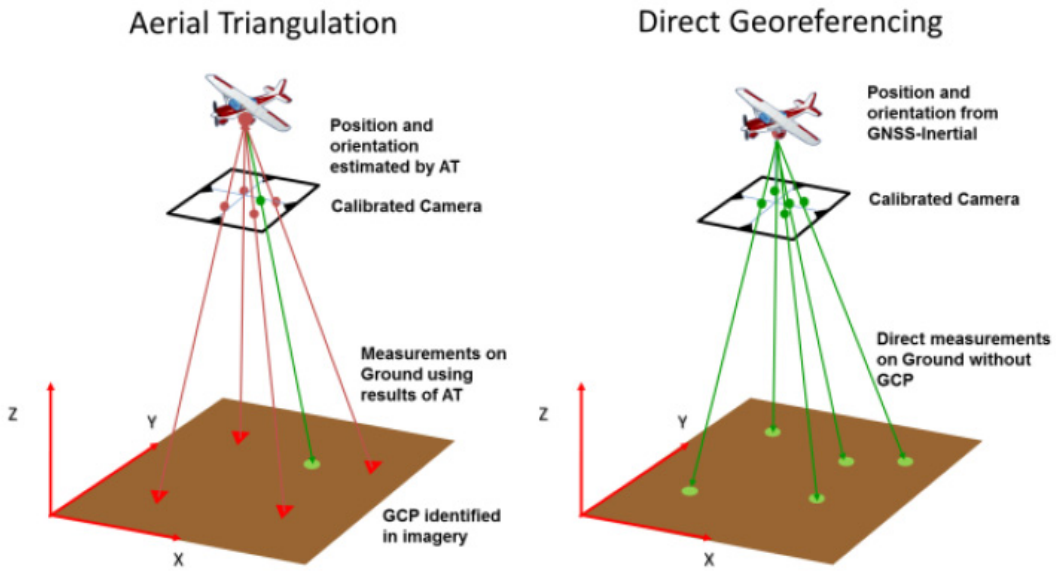

Figure 3.4.1.13: Direct Georeferencing versus Aerial Triangulation (Mian et al., 2015)

Figure 3.4.1.14 and equation (3-11) illustrate the general concept of the airborne DG.

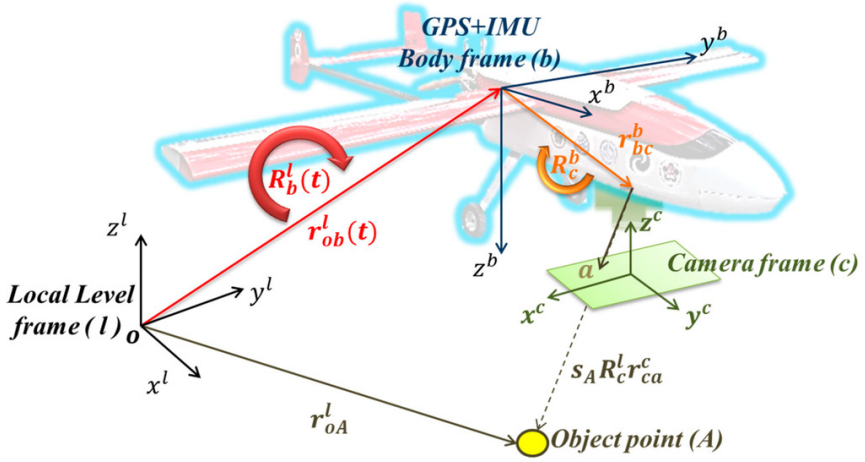

Figure 3.4.1.14: The concept of direct georeferencing in UAV (Chiang, Tsai, Naser, Habib, & Chu, 2015)

With this implementation, the coordinates of a mapping feature can be obtained directly through measured image coordinates(Chiang et al., 2015).
This procedure works based on *a priori* knowledge of various systematic parameters, as shown in the following representation:

$$\mathrm{r}^{\mathrm{l}}_{\mathrm{oA}} = \mathrm{r}^{\mathrm{l}}_{\mathrm{ob}}(\mathrm{t}) + \mathrm{R}^{\mathrm{l}}_{\mathrm{b}}(t)\left(s_A \mathrm{R}^{\mathrm{b}}_{\mathrm{c}}\mathrm{r}^{\mathrm{c}}_{\mathrm{ca}} + \mathrm{r}^{\mathrm{b}}_{\mathrm{bc}}\right) \tag{3-11}$$

In the formula, the "r" means a vector and "R" means a rotation matrix. Their superscripts and subscripts represent the frame. But the subscript of vector means start-point and end-point of this vector.

$\mathrm{r}^{\mathrm{l}}_{oA}$ is the coordinate vector of feature point (A) in the Local Level frame (LLF, l-frame);

$\mathrm{r}^{l}_{\mathrm{ob}}(t)$ is the interpolated coordinate vector of the navigation sensors (INS/GPS) in the l-frame;

S_A is a scale factor, determined by stereo techniques, laser scanners or a Digital Terrain Model (DTM);

$\mathrm{R}^{l}_{\mathrm{b}}(t)$ is the interpolated rotation matrix from the navigation sensor body frame (b-frame) to the l-frame;

(t) is the time of exposure, *i.e.*, the time of capturing the images, determined by synchronization;

$\mathrm{R}^{\mathrm{b}}_{\mathrm{c}}$ is the rotation matrix from the camera frame (c-frame) to the b-frame, determined by calibration;

$\mathrm{r}^{\mathrm{c}}_{\mathrm{ca}}$ is the coordinate vector of the point (a) in the c-frame (*i.e.*, image coordinate); and

$\mathrm{r}^{b}_{\mathrm{bc}}$ is the vector between the IMU center and the camera perspective center in the b-frame, determined by calibration.

Even there is high photogrammetric potential for direct georeferencing of UAVs, there are relevant factors which may influence the accuracy of DGS (Table 3.4.1.1). Depending on the error type DGS accuracy changes. Errors in interior orientation have an impact on accuracy as systematical error more than 1m while this impact changes between more than 4 meters and 1 meters if the error is related to exterior orientation. Lack of synchronisation between GPS and camera induces non systematic error more than 4 meter, while if the eroors depends on GPS, accuracy may become less than 4 meter. When there is an instability of the platform especially due to atmospheric variations, which cause significant variation in the image of covered area, forward and sidelap overlaps (Graça, Mitishita, & Gonçalves, 2014),

also the accuracy is affected by 5-9 meters erros on accuracy. The external factor wind gusts influence the UAV speed, image overlap and block stability can cause more than 5 meters impact on accuray, while DEM has less than 5 meters(Grenzdörffer, Engel, & Teichert, 2008). Also the vertical extension of the objects or the limited or impossible visibility of satellite makes hard use of GPS and so DGS(Barazzetti, Remondino, Scaioni, & Brumana, 2010)

Table 3.4.1.1: Factors influencing the direct georeferencing of UAVs (Grenzdörffer et al., 2008).

Source of error	Problem	Possibility of correction	Impact on accuracy*
Interior orientation			
Changes of centre point	With zoom lenses of consumer cameras in the centre point may change	Given:camera calibration before the flight or simultaneous calibration	Systemical error, > 1m
Changes of focal length	With zoom lenses of consumer cameras the focal length may change	Given: camera calibration before the flight or simultaneous calibration	Systemical error, > 1m
Radial distorsion	Nearly constant over time	Generally not necessary, but correction available with every calibration	Systematic, increase toward image corner
Exterior orientation			
Time synchronization between GPS and camera	Unknown exposure time of camera, related to GPS time stamp	Given: Synchronisation of camera and GPS	Nonsystematic error, > 4m
GPS	No DGPS	Given: use of DGPS-Logger / postprocessing	Large (<4m)
Exposure delay	Unknown, variable	Given: measurement of the exposure delay and examination of delay pattern	Systematical error, 1-3m
Instability of the platform	No vertical images, due to winds and accelerations	Not given	Nonsystematic error, 3-5°, 5-9m
External factors			
DEM (constant height value)	Differences in elevation in the area, no DEM available	Given: application of a better/more accurate DEM/ortho rectification	Nonsystematic error < 5m
JPG-Compression	Poor image quality/problems at automatic tie point generation	Given: may be reduced by lower compression/more storage space	Small < 0.5m
Wind gusts	Influences the speed of the UAV, image overlap, block stability	Partly given: await weather with low winds	Large (> 5m)
Image motion	Image motion due to high speeds at low altitudes above ground of the UAV, No FMC	Given: use of camera with a large pixel size per CCD-element and short exposure intervals	Medium (> 5m)

If the navigations sytems doesn't work efficiently or it is not possible to get GPS data for geo-referencing, indirect geo-referencing can be performed in mainly two ways -import at least three GCPs in the bundle adjustemnt solution, treating them as weighted observations inside the least squares minimization[25].

[25] The quality of the bundle is influenced by the redundant control information and additional check points can be used.

-use a free-network approach in the bundle adjustment and apply only at the end of the bundle[26] in order to bring the image netwrok results into a desired reference coordinate system[27].

3.4.1.4. Block Configuration and Ground Control Points

The flight with UAVs is normally can be done in *manual*, *assisted*(semi-autonomous) or *autonomous* mode. Like the other parameters, this mode vary according to the goal of the flight, platform type, environmental conditions. GNSS/INS navigation devices lead to use the autonomous flight (take-off landing and navigation) and the image acquisition. The image network quality is mainly based on the flight mode. In manual mode, the image overlap and the geometry of acquisition is generally very irregular. With low-cost navigation system, waypoints are more on straight and the geometry of the acquisition is more regular, while image overlap is still irregular. Autonomous mode of flight and image acquisition provides much more regular overlap and the geometry of the acquisition, as shown in Figure 3.4.1.15(Remondino, 2014)

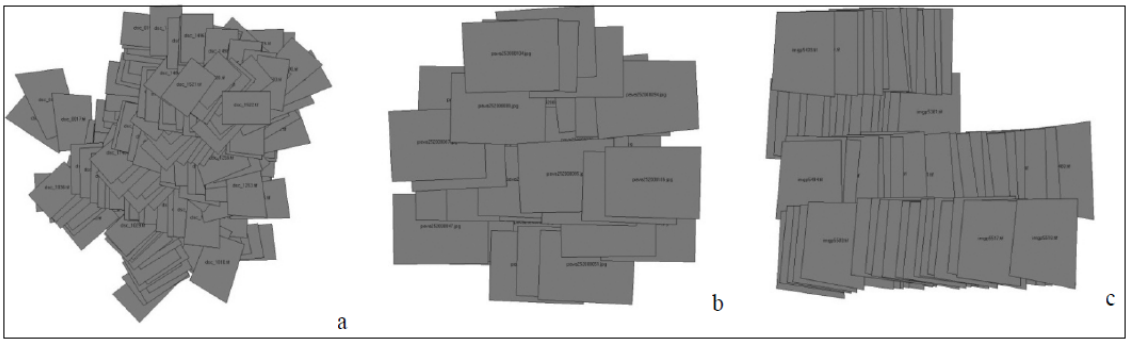

Figure 3.4.1.15: Different modalities of the flight execution delivering different image block's quality: a) manual mode and image acquisition with a scheduled interval; b) low-cost navigation system with possible waypoints but irregular image overlap; c) automated flying and acquisition mode achieved with a high quality navigation system (Remondino, 2014)

The presence of GNSS/INS devices together with navigation systems can improve the image acquisition. The navigation system, generally called -auto-pilot-, comprises of software and hardware and provides to perform a flight in accordance with pre-planned flight and communicates with the platform during the mission. However the small size UAVs has limitations on holding high quality navigation devices so the suitable and cheap solution relies upon micro electro-mechanical systems (MEMS). Even they are in reduced-weight, the accuracy is not sufficient for direct georeferencing. In general in case of light weight and low-cost platforms, a regular overlap cannot be provided since also they are affected by weather conditions like wind, pilot capabilities, GNSS/INS quality. So they can be more suitable for little extensions and low altitude flights, while more expensive devices can be used for long extensions and long endurance over wide areas.

UAV-based image block capturing needs the interior parameters of the camera during bundle adjustment (self-calibration). According to Cramer (2001), in this case

[26] Helmert transformation
[27] The solution is onyl based on the integrity and quality of the multi-ray relative orientation.

cross flight patterns and different flying heights might provide more reliable self-calibration process. Gerke & Przybilla (2016) made several tests with a fixed-wing UAV on accuracy analysis of photogrammetric UAV image blocks and they analyzed the effect of RTK-GNSS and cross flight patterns on accuracy of UAV image blocks. (Gerke & Przybilla, 2016). Another study on block deformation and analysis of UAV images by Nocerino et al. (2013). They made several qualitative and quantitative analyses using different UAV configuration for digital documentation of an archaeological area (Nocerino et al., 2013).

Digital images from UAVs can be processed by using the traditional photogrammetric method or some Computer Vision (CV) field softwares. The traditional photogrammetric method aims to get high accuracy in point coordinates and in 3D modelling, while with CV softwares mainly try to get a quick processing and effective final product. Traditional photogrammetric method has some difficulties on the images georeferencing and the block configuration, especially when image position and attitude is far from achieved in the survey. However with CV softwares, the image processing is faster, easier, orthoimages and 3d products requires less time and control and the accuracies are calculated with computed parameters. The photogrammetric softwares require operatorintervention in check of EO parametres in the process or check of calibration parameters or in the manual selection of points. The computation time is longer than CV softwares(Gini et al., 2013). Gini et.al (2013) made a study on block configuration comprasions with traditional photogrammetric softwares and CV softwares. They used several software Erdas-LPS, EyeDea, Agisoft Photoscan and Pix4UAV for block adjustment and evaluated results in terms of digital surface model (DSM), orientation parameters and accuracies.

Regarding the automated orientation of image blocks with UAVs proposed a fast and accurate methodology and tested this methodology on different dataset of images with different UAVs shown in Fgure 3.4.1.16. The results show that the usefulness of the developed automated procedure to support UAV data processing, to reduce the processing time in all the cases where the direct orientation is not accurate or in the case in which GPS/INS cannot be used at all. (Barazzetti, Remondino, & Scaioni, 2010; Barazzetti, Remondino, Scaioni, et al., 2010).

Field surveying for photogrammetric control has mainly two steps. The first step is to set up a network of basic control consisting of horizontal and vertical benchmarks in the project area. It can also be established by GPS techniques. The second step involves establishing photo control points by means of surveys based on the basic control network. These photo control points can be in different types and sizes are connected by short traverses, intersections or loops (Figure 3.4.1.17)

If GCPs are used for the purpose of orientation of stereo models for topographic map, each stereo model should have three horizontal and four vertical control points. The horizontal points should be widely spaced and vertical points should be in the corners of the neat model. In traditional distribution, one stereo model should have three GCPs in the first model and use pass points only for a number of photos, then three GCPs in the fourth or fifth model. For a strong relation of GCPs, pass points should be

collected in the area of 3-way overlap between the images and GCPs should be well distributed in the block (Figure 3.4.1.18).

Block 1 – Milan	Block 2 – Copan	Block 3 – Pava	Block 4 – Veio
Nikon D200 20 mm lens – 80 images 3872×2592 pixels pixel size 6.1 µm	Nikon D2Xs 35 mm lens – 70 images 4288×2848 pixels pixel size 5.5 µm	Pentax Optio A40 8 mm lens – 32 images 4000×3000 pixels pixel size 1.9 µm	Pentax Optio A40 8 mm lens – 87 images 4000×3000 pixels pixel size 1.9 µm
Manual flight	Autonomous flight	Manual flight	Autonomous flight
			
			
	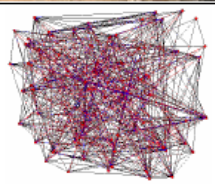	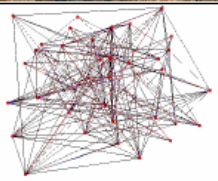	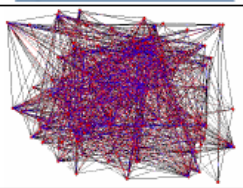
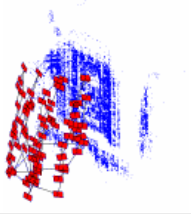	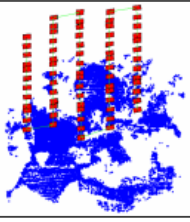	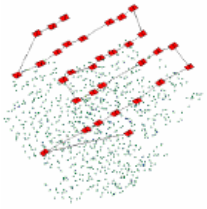	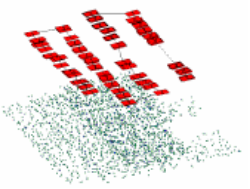

Figure 3.4.1.16:Some features of the image blocks used in the reported experiments: (1) main characteristics of the images; (2) flight mode; (3) example of an image for each block; (4) images of the UAV used; (5) visibility map (red dots are the images and blue lines give their connections); (6) orientation results after the photogrammetric bundle adjustment(Barazzetti, Remondino, Scaioni, et al., 2010)

Figure 3.4.1.17: Different types of GCPs.

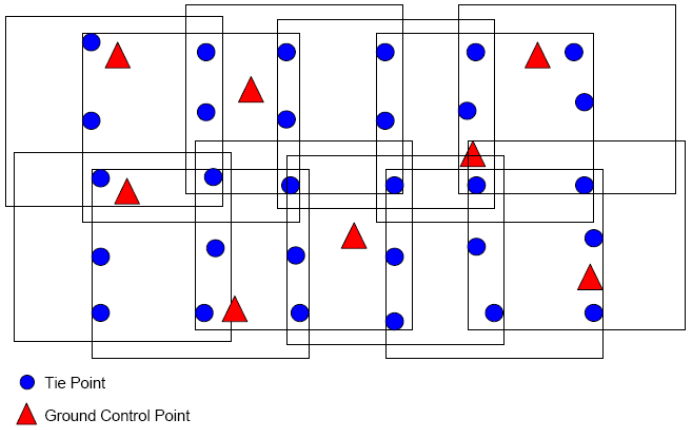

Figure 3.4.1.18: Traditional Ground Control Point Distribution(https://wiki.hexagongeospatial.com)

Tie point is a point that ground coordinates of it is not known, but it is visuable and recognizable in the overlap area between two or more images. The corresponding image positions of tie points appearing on the overlap areas of multiple images. Ground coordinates for tie points are computed in block triangulation. The points can be measured either manually or automatically. Mainly nine points in each image are sufficient for block triangulation. However selecting and measuring tie points are very time consuming and high-cost (Remondino, Del Pizzo, Kersten, & Troisi, 2012b; Z., A., & I., 2011). In order to deal with these problems Automatic Tie Point Extraction (ATİPE) method has been used in photogrammetry field. The method is based on developing procedure to extract tie points from set of images for the successive bundle adjustment phase. There are several valuable research on this task (Barazzetti, Remondino, & Scaioni, 2009);2010; Remondino et al. 2011;2012; (Gini et al., 2013; Z. et al., 2011).

When GPS is used, number of vertical control points can be reduced and for a block adjustment with the projection center coordinates determined by kinematic GPS positioning, control points are required only in the block corners. In order to get sufficient reliability, two control points should be located in each corner. With GPS projection center coordinates, the adjustment can be processed with at least four control points However, additional and well-distributed control points increase the reliability and accuracy of the blocks (Figure 3.4.1.19).

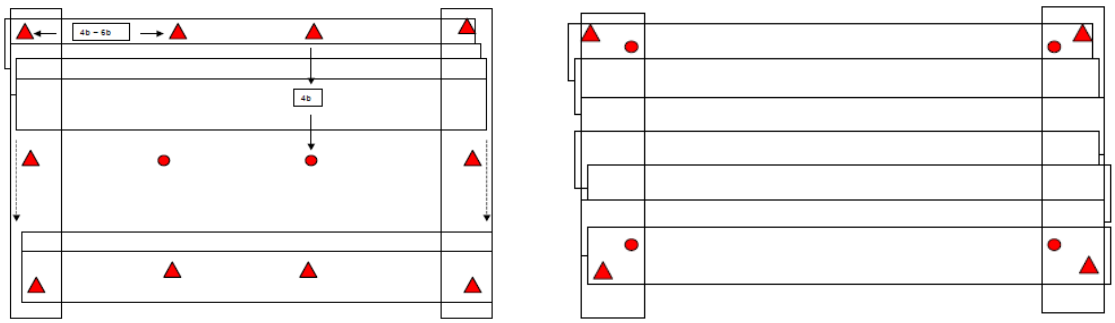

Figure 3.4.1.19(left)Control Point Distribution for Blocks with Cross Strips (%60 sidelap)
(right)Control Point Distribution for GPS Blocks (%60 sidelap)
(https://wiki.hexagongeospatial.com)

The distribution of GCPs is not only need for the accuracy of the image blocks, it is also needed for determination of block deformations. When GCPs were introduced into the bundle adjustment the errors were reduced by a factor of 3, and they became even smaller when oblique images were used (Nocerino et al. 2013). Here the distribution of GCPs become a significant task. ELtohamy and Hamza (2009) evaluated the effect of GCPs location and distribution on accuracy of remote sensing images (ELtohamy & Hamza, 2009) and UAV images for mapping studies (Tahar, Ahmad, Abdul Aziz, Mohd Akib, & Mohd Naim, 2012), georeferencing of UAV images (Skarlatos, Procopiou, Stavrou, & Gregoriou, 2013) and in 3D reconstruction of UAV images (Caroti, Martínez-Espejo Zaragoza, & Piemonte, 2015). Similarly Gerke et. al. (2016) made a research on two different areas in order to see the impact of GCPs distribution and cross flight on UAV image blocks accuracy. So they compared different GCPs configurations. As result of their study, it was obtained that when more GCPs are used, the typical error reduces (Figure 3.4.1.20) .

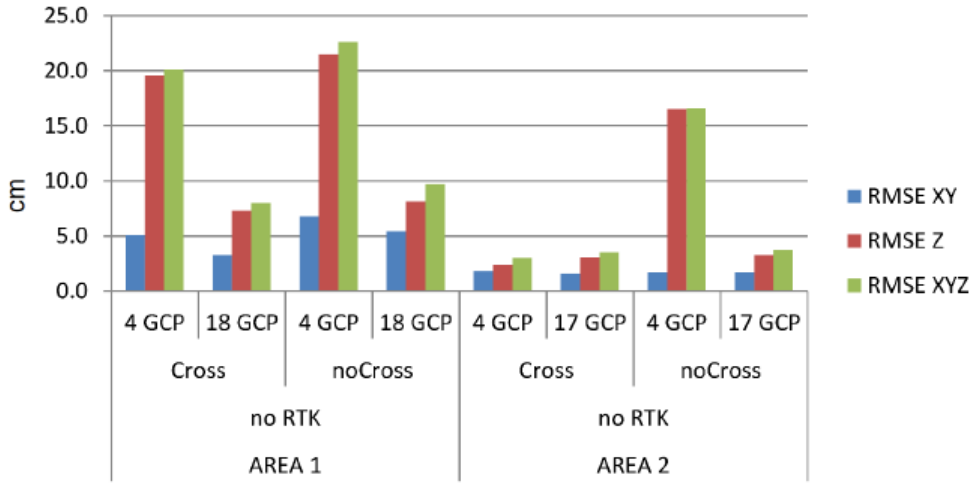

Figure 3.4.1.20: RMSE of residuals at check points in area 1 and 2, with RTK disabled. Left columns with cross pattern used, right without. GCP: number of control points. In area 1, the number of check points is 31 if four and 17 if 18 GCPs are used. In area 2, the number of check points is 30 in case of four GCPs and 17 in case of 17 GCPs (Gerke & Przybilla, 2016)

GCPs has a significant role in order to get better photogrammetric results. The studies show that the more GCPs is the more accurate photogrammetric results. There are several studies related to optimal number of GCPs today. One of them was prepared by Prajwal et. al. (2016). They used different combination of GCPs derived from DG and RTK-GPS in order to get accuracy throughout the pathway of a UAV from 600m (Prajwal, Jain, Srinivasa, & Karthik, 2016). Another study on evaluation of GCPs numbers in UAV blocks was done by Tahar, 2013. In the study, six GCP configurations (figure 3.4.1.21) were tested to determine the best photogrammetric results for UAV photogrammetry. Two main photogrammetric result orthophoto and digital elevation model were used for the test and the configurations with more GCPs provided more accuracy (Tahar, 2013) (Figure 3.4.1.22).

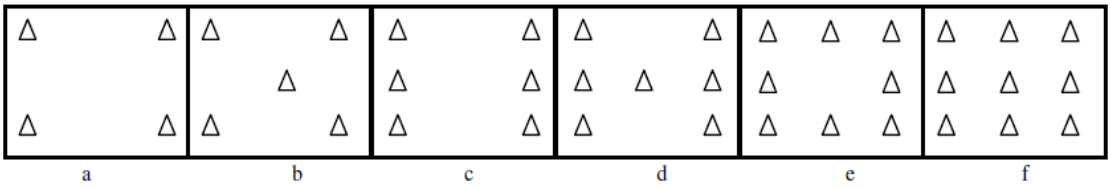

Figure 3.4.1.21: Ground Control Point Configurations for Photogrammetric Block (a) 4GCP, (b) 5GCP, (c) 6GCP, (d) 7GCP, (e) 8GCP, (f) 9GCP

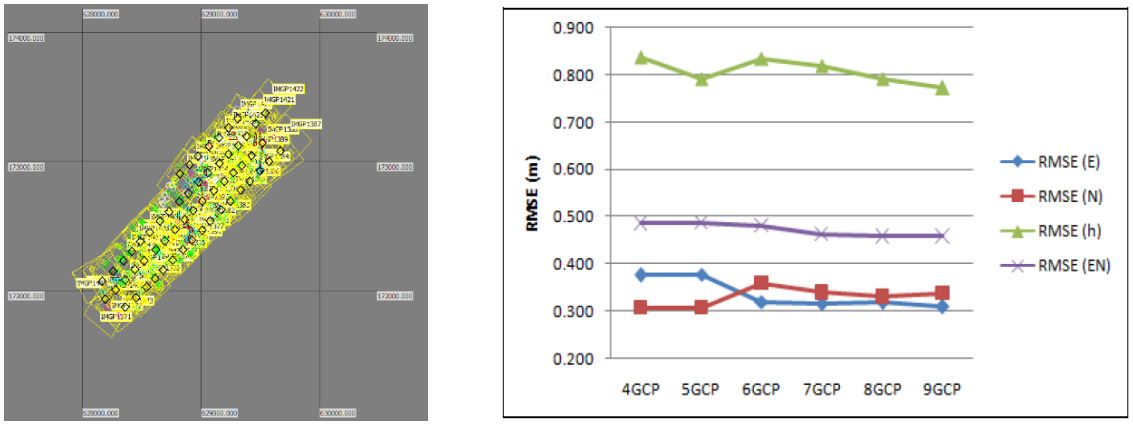

Figure 3.4.1.22: (left) Photogrammetric Block for 60 UAV Images
(right)Line Graph for RMSE Value based on Different Number of GCPs (Tahar, 2013)

Except for the studies related to GCPs distribution and number, also the size of GCPs is a research topic. Yılmaz et. al. (2004) made research on the most suitable size of GCP for High Resolution Satellite Images (HRSI). In the study, different GCPs have been set up in the field at different sizes (Yilmaz, Yakar, Mutluoglu, & Yildiz, 2004). For GCP size, there is strong relation between the focal length, the flight height and pixel size. Ground resolution is the minimum distance to distinguish two goals in the image however it doesn't mean the minimal size to recognize the ground object in the image (Xie, Lin, Gui, & Lin, 2012). According to He at. Al .(2012), the smallest size of GCP recognizable from the image should be the 5-10 times of GSD (He et al., 2012). GSD can be calculated as following equitation below:

$$\mathrm{GSD} = \frac{H}{f}\mu$$

$$\mu = \frac{W}{S_W} = \frac{H}{S_H}$$

where H is flight height (m), f is focal length (mm), GSD is ground sampled distance (m), μ is pixel size (μm), W is the width of CCD (mm), H is the height of CDD(mm), SW is the number of pixels for W, SH is the number of pixels for H.

3.4.1.5. Products: DSM, DTM and Orthoimages

With a typical photogrammetric pipeline, 3D results like DSM (Digital Surface Model) or DTM (Digital Terrain Model) (Figure 3.4.1.23), contour lines, textured 3D models, vector data, etc. can be produced, in a reasonable automated way.

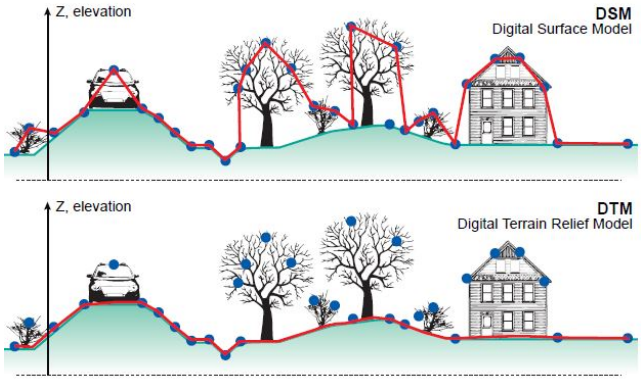

Figure 3.4.1.23: The difference of DTM and DSM (http://www.charim.net)

In order to get DSM from UAV images, classical photogrammetric workflow (Figure 3.4.1.24) or Computer Vision (CV) techniques (Figure 3.4.1.25) can be used (Bhandari, Oli, Pudasaini, & Panta, 2015). According to Bhandari et al. (2015), CV techniques have better results for georeferencing the images and generating DSM.

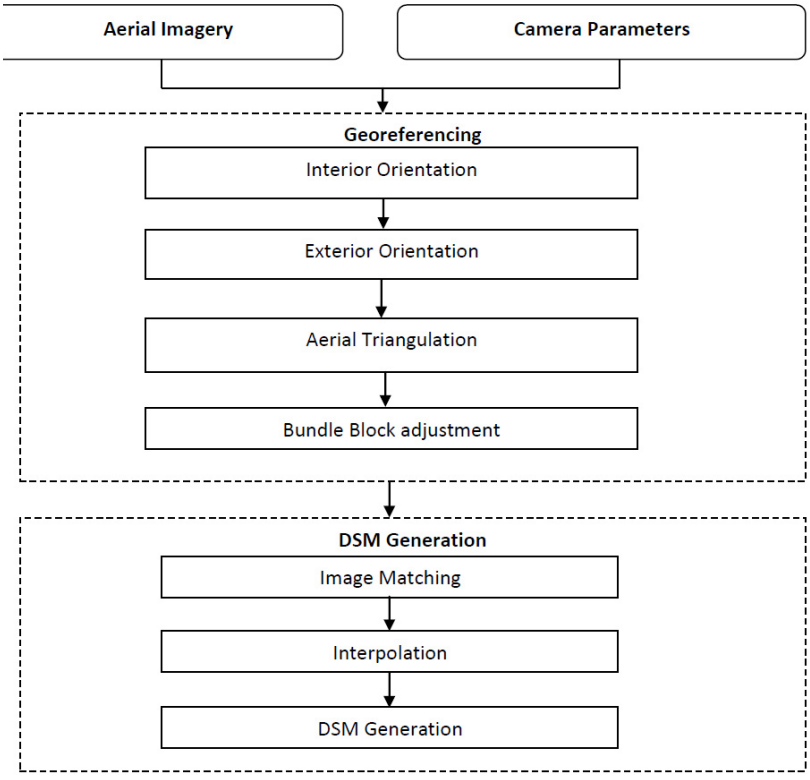

Figure 3.4.1.24: General Photogrammetric process for generating DSM from UAV images (Bhandari et al., 2015)

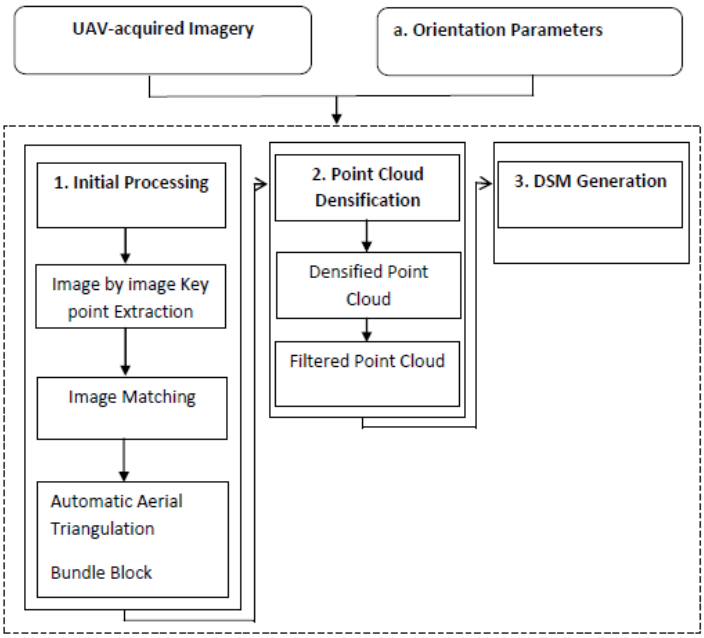

Figure 3.4.1.25: General workflow for modern computer vision techniques (Bhandari et al., 2015)

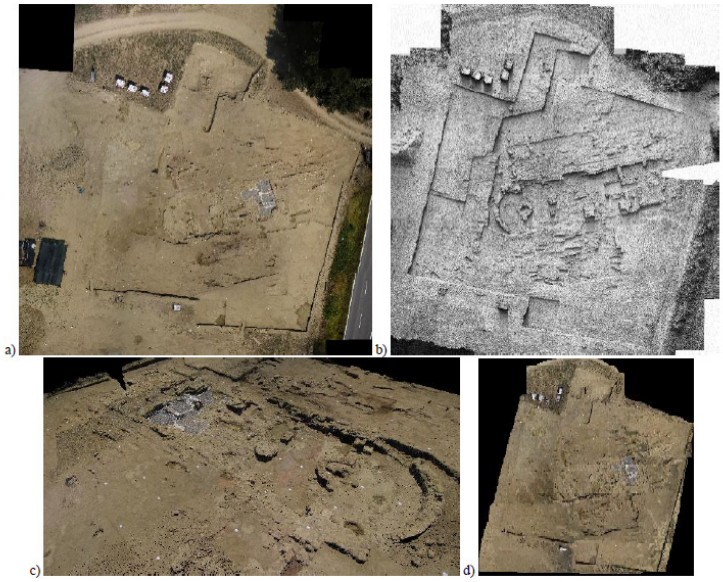

Figure 3.4.1.26: A mosaic over the excavation area in Pava (a), the derived DSM, shown in shaded mode (b), a closer view of the textured 3D model (c) and the produced orthoimage (d).(Remondino, Barazzetti, Nex, Scaioni, & Sarazzi, 2011)

Digital Elevation Model (DEM), one of the product of UAV photogrammetry, can be defined as a digital model or 3D representation of a terrain surface created from elevation data. A DEM can be a raster file consist of each record with 3D element usually associated with geographic coordinates. Digital Terrain Model (DTM) is a DEM shape of the ground, while Digital Surface Model (DSM) is a DEM of the shape of the surface (including vegetation, infra-structures etc.). In photogrammetry, DEMs are a by-product resulting from the interpolation of extremely dense 3D point clouds extracted from imagery. The quality of a DEM depends on horizontal and vertical accuracy. In order to check DEM accuracy, RMSE and standard deviation (SV) calculations can be

used (Rock, Ries, & Udelhoven, 2011). However the best accuracy is achieved by applying image matching and data filtering algorithms(Remondino et al., 2015).

DEM generation from UAV images normally follows the SFM pipeline framework as shown in Figure 3.4.1.28.(Ruiz, Diaz-Mas, Perez, & Viguria, 2013). First SFM algoritms are employed to acquire 3D model from triangulating correspondences between images in the scene. In this case camera parameters are needed in order to calculate a projection matrix for each image. Then GPS data is used to eliminate the uncertainty of the first model. After the optimization point clouds are computed and triangulated to increase the spatial resolution (Jiang et al. 2009). The result 3D point cloud is smoothed and filtered by eliminating noisy data. Then the dense point cloud is interpolated using a mesh-grid generator. Each these techniques and algorithms can be effected by several factors. However the studies show that the final accuracy is more affected by the quality of input data than by the specific algorithms (Ruiz et al., 2013)

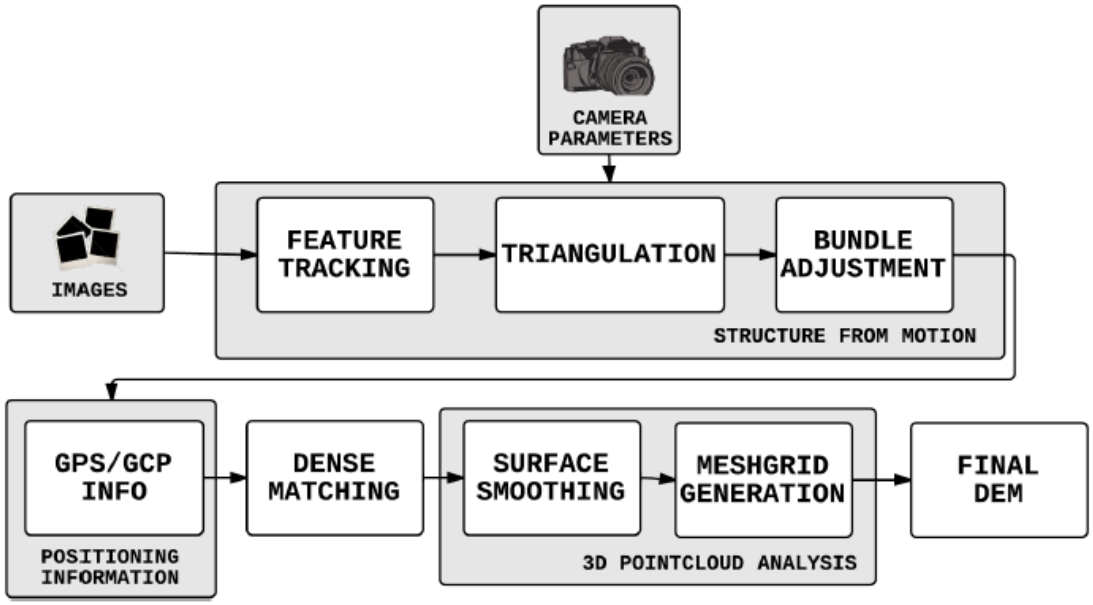

Figure 3.4.1.27: Flowchart of DEM generation algorithms(Ruiz et al., 2013)

Following the oriented images in UAV photogrammetry process, in order to achieve 3D reconstruction and modeling, the surface measurement, orthophoto creation and feature extraction steps are followed. Reconstruction can be done with interactive procedures or automated matching techniques (Eisenbeiss & Zhang, 2006; Haala, 2011; Remondino et al., 2011; Remondino, Del Pizzo, Kersten, & Troisi, 2012a; Remondino et al., 2012b; Remondino et al., 2015; Wierzbicki, Kedzierski, & Fryskowska, 2015). The output is sparse or dense point cloud. According to Remondino (2014) dense matching techniques algorithms should be able to extract dense point clouds in order to define the object's surface and its main geometric discontinuities. This point clouds are needed to be structured and interpolated. Dense point clouds are generally preferred in case of surface reconstruction while sprase clouds are preferred for man-made scenes like buildings (Remondino, 2014).

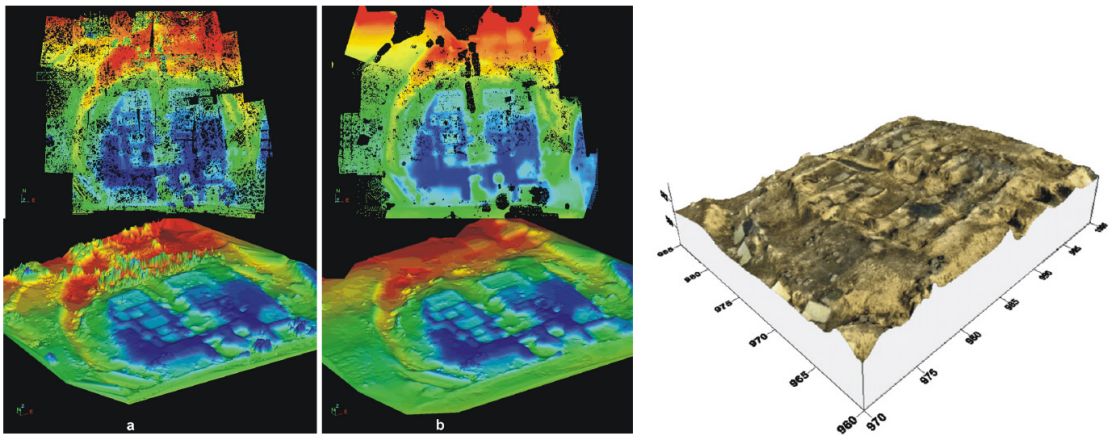

Figure 3.4.1.28: (left)a) Raw digital elevation model after image matching; b) Edited digital elevation model. Point mesh (above) and triangulated surface (below) are represented in both cases.
(right) 3D model of the area (Mozas-Calvache, Prez-Garca, Cardenal-Escarcena, Mata-Castro, & Delgado-Garca, 2012)

Even it is possible to acquire DSMs and orthophotos, their accuracy is an important topic for UAV photogrammetry. The accuracy of UAV products can be validated with geodetic terrestrial survey data. Haarbrink and Eisenbeiss (2008) made four case studies and they checked the accuracies with geodetic terrestrial data. The results were quite in high resolution and accuracy in DSMs(Haarbrink & Eisenbeiß, 2008). The accuracy evaluation of orthophoto was checked in a study by Rinaudo et al. (2012)(Rinaudo, Chiabrando, Lingua, & Spanò, 2012). In order to check the accuracy of orthophoto also the root mean square error (RMSE) can be used and the studies Show that it is possible to achieve at sub-meter accuracy with UAVs (Ahmad, 2011; Azmi, Ahmad, & Ahmad, 2014; Caroti et al., 2015). RMSE is used to measure of the differences between observed coordinates and reference coordinates. The results show the accuracy values of the dataset and can be calculated by following equitation:

$$RMSE = \sqrt{\frac{\sum (N_i - N_j)^2}{n}}$$

Where N_i is observed values and N_j is refereence values and n is number of points.

3.5. Status and future of UAV photogrammetry

The studies about UAV photogrammetry in the last years show that UAV technology has been used in diverse applications. Even though the automation process is demandable, the study results indicate that it is possible to get better results with autonomous process. Although the automation process has reached to a satisfactory level for automated tie point extraction and DSM generation, a high percentage of the time is spent for image orientation and GCPs measurements, especially when direct

geo-referencing couldn't be fulfilled. The time effort in a typical UAV-based photogrammetric workflow is shown in figure 3.5.1 below, according to the research of (Remondino, 2014)

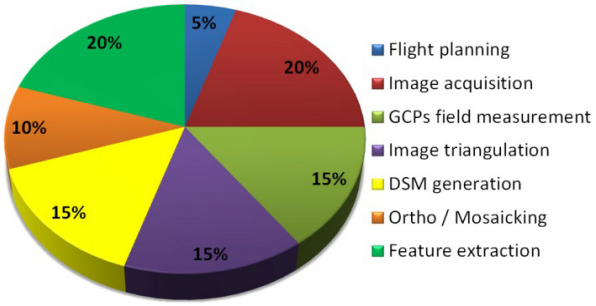

Figure 3.5.1: Approximate time effort in a typical UAV-based photogrammetric workflow (Remondino, 2014).

The measurement of GCPs has a significant role with UAV image blocks since It affects the accuracy of the results. The accuracy of the topographic network has effect on the image triangulation and GSD of the image. In researches, 2-3 pixels for RMSE are reported as normal.

It is clear that UAV have recently received a lot of attention since they are relatively cost, gives opportunity for quick data processing and outputs. To compare to traditional airborne platforms, UAVs decrease operational costs and reduce the risk of operator. Their great advantages could be their ability to deliver spatial data with high resolution and to be used in critical situations (in high risk situations, inaccessible areas, areas with some limitations with aircrafts etc.) where to get 3D data is quite difficult. High resolution data can be used to get dense point cloud, texture mapping, orthophoto, mosaic map. Besides their real-time capability for data acquisition, data transfer processing. While fixed UAVs can cover wider areas, rotary wing UAVs have the possibility of take-off and land vertically. When it is not required very accurate 3D data, depending on the hardware and software, it is possible to complete remote sensing solutions. Besides the aerial photographs, depending on the platform, UAVs can get terrestrial data.

Regarding the payload-systems, the cameras generally employed to UAVs are mostly small and medium format and low-cost cameras. In order to obtain the same coverage of traditional airborne systems with high resolution, it is recommended to use automated and reliable software for better results and less processing time. Today there are some reliable on-shelf solutions even in low-cost. Although sensor requirements depend on the mission of the flight and project objectives, advances in sensors and system components can also create new opportunities for innovative UAVs applications. Battery weight and maximum time for charge causes limitations in UAV missions. So the future directions may include the development and incorporation of solar powered battery components for UAVs.

The stability of UAVs is a significant issue, especially in windy areas. Even the camera and platform stabilizers help to solve this problem, used another way to solve this problem is to take images during the flight continuously and use the best one for image process (Remondino, 2014). The payload limitation obstructs the use of low

weight GNSS/IMU systems which enforce direct-georeferencing solutions. New low-weight and reliable navigation systems are available however their cost is not still low.

Even though it is quite difficult to make a prediction of future regulations for UAV, it should be the first thing to ensure the safety of the public and this will bring increased reliability and safety systems. Another important task is reliability and security of the communication links. It is believed that it will be quite useful if a UAV could be capable of continued safe flight and controlled flight with minimal risk in case of loss of communication links (Dalamagkidis, Valavanis, & Piegl, 2008). The regulations of UAVs are still under development in countries to be able to define UAVs application areas with technical specifications. The lack of precise rule frameworks and long process for flight permissions cause the limitations on the use of UAV.

It seems that the most possible development should be related to payload, autonomy and stability tasks as well as real-time construction. Real-time processing is needed to fill the gap between remote sensing and variable-rate aerial applications. Data analysis is a significant step of a UAV process so the data must be analyzed carefully. To develop a user-friendly image processing software analyzing data from UAV immediately could be a goal for future of UAV (Lan, Thomson, Huang, Hoffmann, & Zhang, 2010). Wendel et al. (2012) tried a new live reconstruction system capable of generating live dense reconstructions based on data from a micro UAV. Results are visualized in real-time on a tablet interface. They captured diverse indoor and outdoor scenes on-the-fly. As they mentioned, they will continue to their studies by extending their system capability in outdoor reconstruction and their results can be improved by adapting the tracking approach. To research multiple volumes indexed by GPS, compass and depth data for large spaces in outdoor scenes could be a topic of another study (Wendel, Maurer, Graber, Pock, & Bischof, 2012). Similarly Konoglie&Agrawal (2008) and Nuechter et al. (2007) tried SLAM (Simultaneous Localization And Mapping) method for real-time visual mapping (Konoglie & Agrawal, 2008; Nuechter, Lingemann, Hertzberg, & Surmann, 2007).

It seems that lab-post processing will remain compulsory for high accuracy need applications. The acquisition of image blocks especially in case of large scale objects and non-flat objects is still an issue. In case of reduced endurance is used for UAV, it is necessary to have two or more flights. Since image acquisition at different time affects the quality of DSM and orthophoto. It can be another task needed to be improved. In last years, other new researches have been started on using new sensors on-board such as thermal and multi-spectral cameras.

3.6. UAV Photogrammetry for Cultural Heritage

Following the developments in image capturing and processing, UAVs have become an alternative in cultural heritage domain and have been started to be successfully used in diverse projects. Since they have the ability to perform in high risk situations without any danger for researcher and they can reach the places where men cannot, they have become standard platforms in cultural heritage sector. Their cost-

effectiveness, less economic limits, real time data capability, fast data acquisition and small-size features have made them strong alternative in heritage documentation projects. In cultural heritage area UAV applications are mainly focused on documentation, observation, monitoring, mapping, 3D modelling and 3D reconstruction (Remondino et al., 2011) as well as producing digital maps, digital orthophoto, digital elevation model (DEM) and digital surface models (DSM) (Patias, Grussenmeyer, & Hanke, 2008).

In documentation and modelling of cultural heritage, images are generally taken from the ground level for façade information and to detect the features on façades. However in many cases, it is difficult to get the photos of the roof of the buildings and to get an overview from the top with the building surrounding. In this sense UAVs enable to capture the images from the roof and to see the surrounding of the building in larger view. Some previous studies in literature can be found in use of UAV images for documentation of a unique building (Fiorillo, Fernández-Palacios, Remondino, & Barba, 2013). In addition to aerial images, UAVs also give possibility to get oblique images for complete documentation. It is possible and easier to get information and observe also building façades with oblique images. Many researches used data acquired from oblique images for building 3D models with UAV (Aicardi et al., 2016; Feifei, Zongjian, Dezhu, & Hua, 2012; Höhle, 2013). Oblique images make possible to record of historical objects with a vertical direction and they may be used for 3D photorealistic model production and façade views which also give opportunity to make analysis and determination of materials. With the help of this method, details in the vertical dimension can be seen, recorded and visualized. Here, high accuracy recording should be considered so the details have to be recognized. In the case of oblique images, the choose of the best flight planning approach in order to cover the whole object with the minimum time of flight still remain the main problem(Aicardi et al., 2016).

Another capability of UAVs can be mentioned as their ability of integration with other documentation techniques which helps to a complete documentation (figure 3.6.2)(Campana, 2014). The combination of UAVs and terrestrial systems for monuments can also be found in literature for different case studies (Eisenbeiss, Lambers, & Sauerbier, 2005; Püschel, Sauerbier, & Eisenbeiss, 2008) as well as for the purpose of architectural photogrammetry (Zischinsky, Dorffner, & Rottensteiner, 2000). The applications with the integration of UAVs with such systems are considered as successful practices in cultural heritage study areas (Patias et al., 2013).

(a) (b)

(c) (d)

Figure 3.6.1: (a)S.Maria's Chapel in Novalesa Abbey (Italy) (Aicardi et al., 2016)
(b)The employed multi-rotor platform used for the image acquisition
(c)Schema of the circular flight for oblique images acquisition
(d) ContextCapture

Archaeological documentation is other research and application field in which UAVs have been effectively and mostly used in last years. In archaeology (and cultural heritage) projects there is always a need for a rapid and accurate documentation of objects. Since the process is dynamic, it requires fast and preferably non-immersive documentation techniques. Even though fast, accurate, cheap modelling and visualization of archaeological areas is a demand, there are some justifications making this demand difficult. The complexity of archaeological areas and their geometric and radiometric features can be considered the first one among these reasons. The second reason is more related with its conceptual interpretation since it is a scientific document. These make a need for new methods instead of traditional ones for archaeological documentation.

String grids, basic traditional methods, mostly do not provide accuracy standard which architects need. Simple survey of the site similarly can only provide a layout with a few accurate points connected with vectors, without any further information. Besides, the two methods both need extra people working within archaeological site for a defined period of time, which increases the economic cost, as well as the possibility of accidental destruction of important findings. Additional security precautions should be

taken in order to prevent any possible damage to the surveyor or archaeological remains (Ioannidis, Potsiou, Soile, & Badekas, 2000).

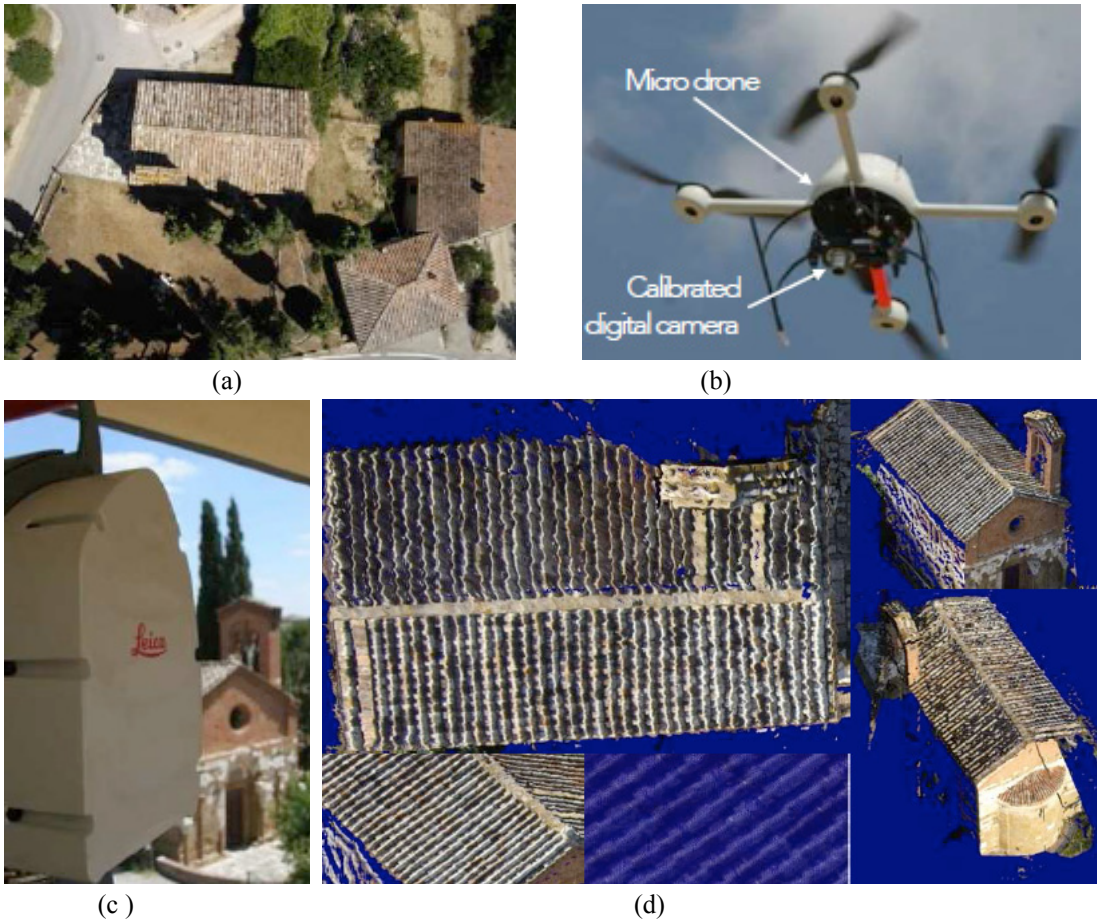

Figure 3.6.2: (a) Aerial photo of Villore Parish Church, Italy
(b) The employed drone with digital camera for aerial data
(c)Terrestrial laser scanning for terrestrial data
(d)Combination of terrestrial and aerial data as integrated approach (Campana,2014)

Another used traditional techniques like tracing with wet paper and pencil/crayons, free-hand drawing, photography, plaster moulding, latex and wax rubbing to record inscriptions or significant details on the surfaces cannot reproduce the degree of detail and accuracy required by today's researchers and conservators (Diaz-Andreu, Hobbs, Rosser, Sharpe, & Trinks, 2005)

Since archaeological data is extremely complex from a geometric point of view and existing methods of 3D modelling lead to large simplifications. In addition, the data also should be easily scalable to support different levels of visualization quality. Detailed geometric information about archaeological sites can be obtained by using laser scanning methods as well as topographic surveying, photogrammetric techniques and Terrestrial Lidar Acquisitions (Apollonio, Gaiani, & Benedetti, 2011; Brown, Chalmers, Saigol, Green, & D'Errico, 2001);(Lerma, Navarro, Cabrelles, & Villaverde, 2010);(Chiabrando et al. 2011). These techniques made it possible to obtain a high level of detail and accuracy and result to be very effective, especially for small or medium-extension archaeological sites (up to tens of hectares). However, for large

archaeological sites close range photogrammetry and terrestrial laser scanning are not always the most suitable survey techniques; whereas, the information obtained from aerial or satellite images provide an overview of the study area, which is fundamental for the interpretation of archaeological structures. In fact, images obtained by metric aerial cameras (film and digital) or by high resolution satellite sensors have been used in archaeology for long time (Cowley, 2010). It should be pointed out that such images have some limitations linked to the geometric resolution inadequate for detailed studies, to the periods of acquisition (which does not always correspond to a given particularly useful date for the purposes of the archaeological work) and ultimately to the cost (Lo Brutto, Borruso, & A., 2012). Besides, another main objection of these methods is the difficulty involved in acquiring reliable radiometric information of the complete surveyed area, which can easily be obtained by means of traditional aerial photogrammetric flights. However, the costs of aerial photogrammetry are usually too high in relation to the limited extension of the surveyed areas. Moreover, the flight altitudes of aircraft equipped with aerial photogrammetric cameras are not able to supply suitable images for the production of large-scale maps (higher than 1:500) and the flight of motor aircraft over archaeological sites is often forbidden. Another problem is that the sites that have to be surveyed are sometimes in remote areas. Even the aerial techniques can be an optimal solution in the case of medium-sized and large sites, since the possibility of raising sensors and capturing the information, in many cases it is rather difficult to obtain data at ground level, which can increase the performance of photogrammetry. Any conventional photogrammetric project can fit to that block geometry even in the case of cartographic surveys at limited archaeological sites. But these surveys generally require working with large scales and high resolutions. As a result, conventional airborne photogrammetric surveys can be unfeasible because of the limited site extent, the large scale required, the expected low flight height, speed of the aircraft and the relatively high cost of the technique (Mozas-Calvache et al., 2012). The use of alternative techniques based on close range photogrammetry and laser scanning from light and low height platforms can be a solution for these problems (Gomez-Lahoz & Gonzalez-Aguilera, 2009; Mozas-Calvache et al., 2012).

After Giacomo Boni used a balloon in order to take aerial photographs of the Foro Romano at the end of 19th century (Campana, 2014) , then Whittlesey reported on the use of a tethered balloon for archaeological documentations in the first time in 1970, which he actually started in 1967 (Eisenbeiß, 2009), the archaeologists have understood the need of acquiring low-altitude aerial imagery for documentation, monitoring, conservation and cultural resource management. Up to today diverse kinds of manned and un-manned platforms have been used in archaeology in order to lift camera. Among them, there are mats, poles, booms, towers as well as kites, balloons, blimps and helikites (figure 3.6.3 and figure 3.6.4)(Campana, 2014).

Figure 3.6.3: Manned platforms for archaeological photograph (Campana, 2014; http://www.ai-journal.com/articles/10.5334/ai.1319/)

(a) (b)

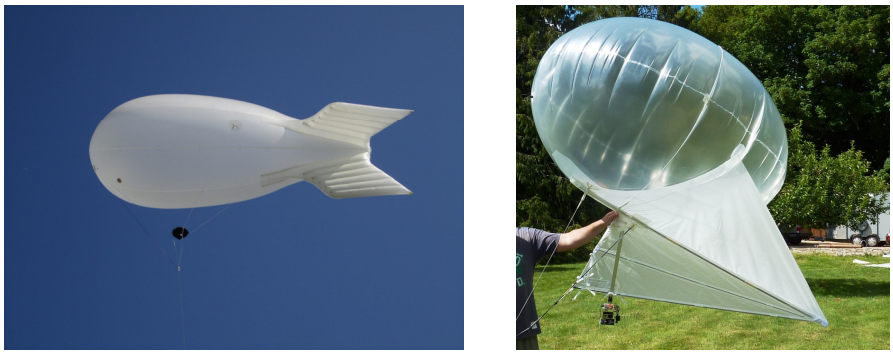

(c) (d)

Figure 3.6.4: Unmanned platforms for archaeological photography
(a)Kite(https://commons.wikimedia.org/wiki/File:Kite_aerial_photo.jpg)
(b) Balloon (Campana, 2014)
(c) Blimp (http://eijournal.com/news/industry-insights-trends/earth-observation)
(d) Helikite (http://www.helikites.com)

According to Verhoeven et al. (2008), each of these methods has own advantages and disadvantages:

-Although the platforms of mats, poles, booms and towers are cost effective, stable and very easy to move, their moderate operational height is no more than about 20 m.

-Even though the kites have been used since 1970s since they are not expensive and can carry up to several kilograms, the wind affects their performance.

-Balloon photography is pretty flexible and easy to perform. However balloons and blimps become difficult to position and to hold in windy conditions. On the other hand helium is expensive and difficult tofind.
-Helikites (the combination of helium-filled balloon with kite wings) are difficult to control and manage (Campana, 2014).

The main difference between traditional close-range applications and UAV photogrammetry for archaeological purposes is the opportunity to control the platform and ability to collect stereo pairs which allow generating 3D models.

It can be found many diverse research and studies about use of UAV for archaeological purposes. Some of them can be mentioned as generated color orthophotos, DEMs, 3D models and thermal images for observation of archaeological areas (Remondino et al., 2011; Rinaudo et al., 2012)UAV for documentation of archaeological excavations (Anuar et al., 2013; Sauerbier & Eisenbeiss, 2010) and for several ancient sites (Skarlatos, Theodoridou, & Glabenas, 2004), for burial mounds (Hendrickx et al., 2011), for modelling archaeological heritage (Eisenbeiss et al., 2005; Verhoeven, Loenders, Vermeulen, & Docter, 2009), for archaeological remains (figure 3.6.5) (Haubeck & Prinz, 2013) and for 3D mapping (Bendea, Chiabrando, Giulio Tonolo, & Marenchino, 2007)

(a) (b) (c)

Figure 3.6.5: (a) MikroKopter (Quadro XL) with the attached Fuji FinePix Real 3D W3 stereo camera during a flight mission at the survey site Doliche (photo by R. Dylka, 2012)
(b) Orthophoto mosaic (rotated) of ca. 70 m2 of the excavation site in Doliche derived from a digital terrain model that was created out of a stereo image pair
(c) Detail of an orthophoto with overlaid drawings. Flight altitude was approx. 12m; the photo reveals an offset of up to 20cm (Haubeck & Prinz, 2013)

There are also several studies in literature related to the methodology for surveying and the process of the UAV data for archaeology. Hendricx et al. (2011) used a microdrone in order to collect data and presented the challenges of the process of the methodology(Hendrickx et al., 2011). Another study about the methodology was done by Mozas-Calvache et. al. (2012) with a UAV system. They described the complete methodoloy for performing photogrammetric surveying of archaeological sites using UAV system. They also demonstrated the viability of this methodology in windy weather conditions (Mozas-Calvache et al., 2012). Chiabrando et al. (2011) dealt with the acquisition and processing of low-height aerial imagery acquired by UAVs and RPVs(Remote Piloted Vehicles), in order to provide large-scale mapping to support archaeological studies. Similarly Lo Brutto et al. (2012) used a UAV system for

surveying an archaeological site to carry out a complete documentation of the site through the production of a DSM (Digital Surface Model) and an orthophoto image (figure 3.6.6) (Lo Brutto et al., 2012). Then they evaluated the results within two different image processing workflows: a typical photogrammetric approach and computer vision approach.

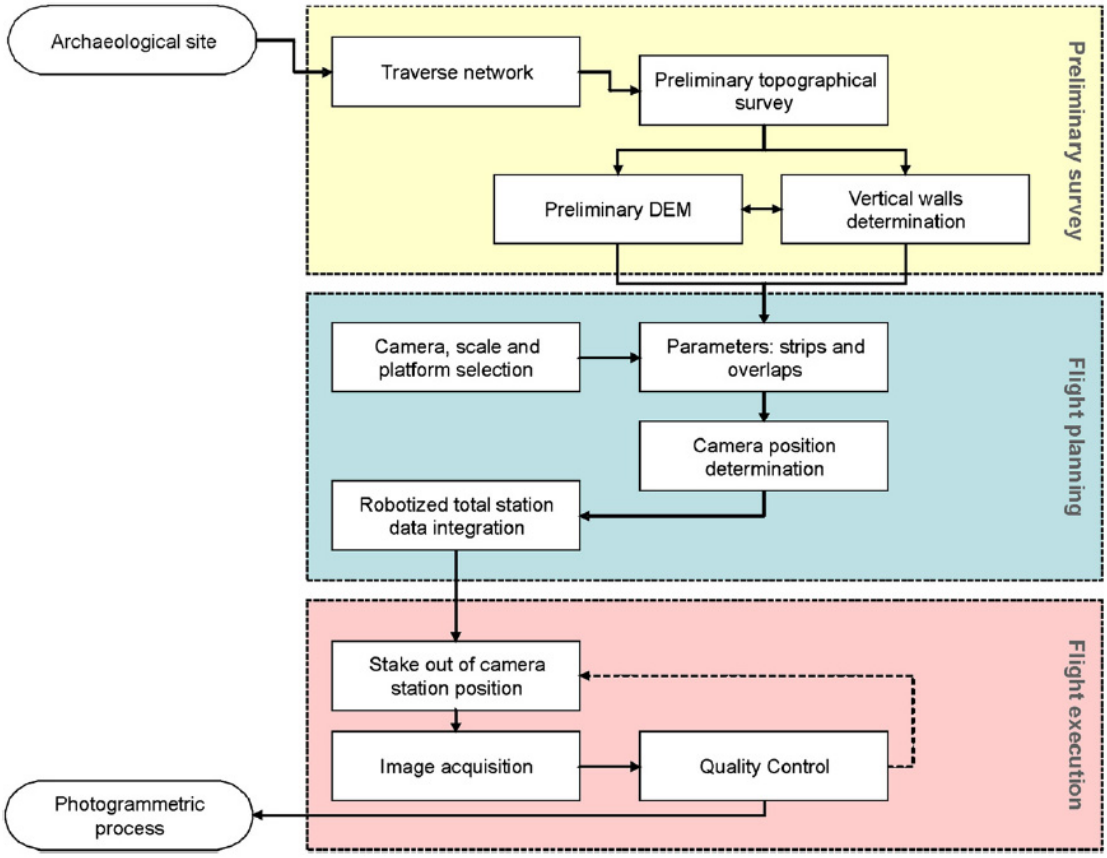

Figure 3.6.6: Methodological approach for archaeological sites documentation with UAVs (Mozas-Calvache et al., 2012)

There have been several studies based on the combination of different techniques with UAV for archaeological documentation. Researches have showed that the combination of photogrammetry and aerial photograph with UAV can be an ideal solution when the archaeological area is not heavily wooded and the structures are not protected by a roof (figure 3.6.7-8)(Mouget & Lucet, 2014). The integration of low-altitude aerial photogrammetry and mobile GIS has also enabled documentation and analysis at a level of detail. The considerable advantage of this approach is the multiple media and forms of presentation it produces such as: vector-based representations in both 2D and 3D, raster-based, continuous surface representations via visible-light orthomosaics and point clouds (Wernke, Adamas, & Hooten, 2014). Some studies have showed that the combination of terrestrial laser scanning and UAV photogrammetry allow a fast yet accurate recording of archaeological site and its stone architecture in high resolution and with high accuracy (Lambers et al., 2007). 3D model based on range and laser scanner image data can serve as a valuable data for archaeological analysis and better understanding of the construction techniques. A part of the research on investigation of new methodologies for integration of different techniques is the

combination of geometric and thermal analysis from UAV platforms for archaeological documentation(Brumana et al., 2013). The combined inspection of both thermal and color images in GIS allow to discover buried traces as well as documentation.

Figure 3.6.7: (left)Spreading Wings S800 hexacopter with the Sony Nex-7 camera
(right) Orthophoto of the archaeological site of Cempoala, Greece (Mouget & Lucet, 2014)

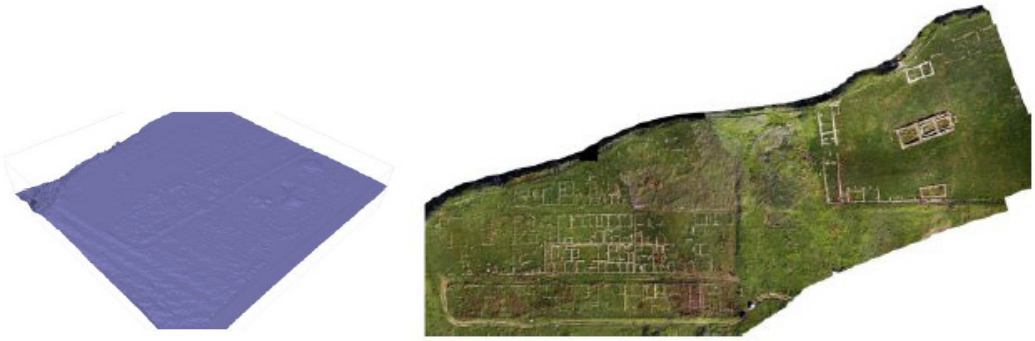

Figure 3.6.8: DSM (left) and orthoimage (right) of the archaeological site of Himera (Lo Brutto et al., 2012)

4. INFRARED THERMOGRAPHY (IRT)

4.1. Introduction to Infrared Thermography (IRT)

Non-destructive testing is defined as comprising test methods used to examine or inspect a part or material or system without impairing its future usefulness and it includes noninvasive medical diagnostics. This technique has been mainly used to search material integrity of the test object in order to find if there is something wrong with the material. These methods are means for inspecting materials and structures without disruption or impairment of serviceability and make possible internal properties or hidden discontinuities to be revealed. Nondestructive testing has become vital in research, development, design and manufacturing areas. The contribution of non-destructive testing has been approved especially in the medical field and computer and aerospace industries.

These tests are mainly used to identify the variations in structure, changes in surface, to measure the thickness of materials and determine the features of other industrial products. According to a report by National Materials Advisory Board (NMAB) Ad Hoc Committee on Nondestructive Evaluation classified techniques into six major method categories: visual, penetrating radiation, magnetic-electrical, mechanical vibration, thermal and chemical/electrochemical, presented in Table 4.1.1 below (Trimm,2010)

Table 4.1.1.Nondestructive testing method categories (Trimm,2010)

Categories	Objectives
Basic Categories	
Mechanical-optical	Color; cracks; dimensions; film thickness; gaging; reflectivity; strain distrubition and magnitude; surface finish; surface flaws; through-cracks
Penetrating radiation	Cracks; density and chemistry variations; elemental distributions; foreign objects; inclusions; micro porosity; misalignment; missing parts; segregation; shrinkage; thickness; voids
Electromagnetic-electronic	Alloy content; anisotropy; cavities; cold work; local strain; hardness; composition; contamination; corrosion; cracks; crack depth; crystal structure; electrical conductivities; flakes; heat treatment; hot tears; inclusions; ion concentrations; laps; lattice strain; layer thickness; moisture content; polarization; seams; segregation; shrinkage; state of cure; tensile strength; thickness; disbonds
Sonic-ultrasonic	Crack initiation and propagation; cracks; voids; damping factor; degree of impregnation; degree of sintering; delaminations; density; dimensions; elastic moduli; grain size; inclusions; mechanical degradation; misalignment; porosity; radiation degradation; structure of composite; surface stress; tensile, shear and compressive strength; disbonds; wear
Thermal nad infrared	Anisotropy, bonding; composition; emissivity; heat contours; plating thickness; porosity; reflectivity; stress; thermal conductivity; thickness; voids; cracks; delaminations; heat treatment; state of cure; moisture; corrosion
Chemical-analytical	Alloy identification; composition; cracks; elemental analysis and distribution; grain size; inclusions;
Auxiliary Categories	
Image generation	Dimensional variations; dynamic performance; anomaly characterization and definition; anomaly distribution; anomaly propagation; magnetic field configurations
Signal image analysis	Data selection, processing and display; anomaly mapping, correlation and identification; image enhancement; separation of multiple variables; signature analysis

According to Trimm (2010), the objective of each method is to provide information on specific objectives and specific attributes to be measured, detected and defined shown in figure below. The objective of each method is to provide information about discontinuities and seperations, structure or malstructure, dimensions and metrology, physical and mechanical properties, composition and chemical analysis, stress and dynamic response, signature analysis and abnormal sources of heat (Table 4.1.2).

Table 4.1.2: Objectives of nondestructive testing methods (Trim,2010).

Objectives	Attributes Measured or Detected
Discontinuities and separations	
Surface anomalies	Roughness; scratches; gouges; crazing; pitting; inclusions and imbedded foreign material
Surface connected anomalies	Cracks; porosity; pinholes; laps; seams; folds; inclusions
Internal anomalies	Cracks; separations; hot tears; cold shuts; shrinkage; voids; lack of fusion; pores; cavities; delaminations; disbonds; poor bonds; inclusions; segregations
Structure	
Microstructure	Molecular structure; crystalline structure and/or strain; lattice structure; strain; dislocation; vacancy; deformation
Matrix structure	Grain structure; size; orientation and phase; sinter and porosity; impregnation; filter and/or reinforcement distributions; anisotropy; heterogeneity; segregation
Small structural anomalies	Leaks (lack of seal or through-holes); poor fill; poor contact; loose parts; loose particles; foreign objects
Gross structural anomalies	Assembly errors; misalignment; poor spacing or ordering; deformation; malformation; missing parts
Dimensions and metrology	
Displacement; position	Linear measurement; separation; gap size; discontinuity size; depth; location and orientation
Dimensional variations	Unevenness; nonuniformity; eccentricity; shape and contour; size and mass variations
Thickness; density	Film; coating; layer; plating; wall and sheet thickness; density or thickness variations
Physical and mechanical properties	
Electrical properties	Resistivity; conductivity; dielectric constant and dissipation factor
Magnetic properties	Polarization; permeability; ferromagnetism; cohesive force
Thermal properties	Conductivity; thermal time constant and thermoelectric potential; diffusivity; effusivity; specific heat
Mechanical properties	Compressive, shear and tensile strength (and moduli); poisson's ratio; sonic velocity; hardness; temper and embrittlement
Surface properties	Color; reflectivity; refraction index; emissivity
Chemical composition and analysis	
Elemental analysis	Detection; identification; distribution and/or profile
Impurity concentrations	Contamination; depletion; doping and diffusanst
Metallurgical content	Variation; alloy identification, verification and sorting
Physiochemical state	Moisture content; degree of cure; ion concentrations and corrosion; reaction products
Stress and dynamic response	
Stress; strain; fatigue	Heat treatment, annealing and cold work effects; residual stress and strain; fatigue damage and life (residual)
Mechanical damage	Wear; spalling; erosion; friction effects
Chemical damage	Corrosion; stress corrosion; phase transformation
Other damage	Radiation damage and high frequency voltage breakdown
Dynamic performance	Crack initiation and propagation; plastic deformation; creep; excessive motion; vibration; damping; timing of events; any anomalous behavior
Signature analysis	
Electromagnetic field	Potential; strength; field distribution and pattern
Thermal field	Isotherms; heat contours; temperature; heat flow; temperature distribution; heat leaks; hot spots; contrast
Acoustic signature	Noise; vibration characteristics; frequency amplitude; harmonic spectrum and/or analysis; sonic and/or ultrasonic emissions
Radioactive signature	Distribution and diffusions of isotopes and tracers
Signal or image analysis	Image enhancement and quantization; pattern recognition; densitometry; signal classification, separation and correlation; discontinuity identification; definition (size and shape) and distribution analysis; discontinuity mapping and display

It should be considered that none of non-destructive testing method is fully revealing and only one method or technique is not sufficient for specific purposes. In many cases, it takes a series of test methods to do a complete nondestructive test.

Infrared thermography (IRT) is a non-invasive method which can be used for gathering information about the condition of historic buildings. Using IRT, information about the building's elements, their location, shape, material characteristics and state of decay can be obtained that may not be noticeable from visual examination. Heat ¯owing in a material is altered by the presence of anomalies and IRT investigation uses this principle to map localized differences in surface temperature caused by changes in heat ow. This allows a map of inner anomalies to be obtained.(Spodek & Rosina, 2009)

Temperature which is an objective comparative measurement is mostly considered the key for plant maintenance and one of the most measured quantities in industrial process. Temperature and thermal behavior of the object, plants and materials are the main factors for infrared and thermal imaging. In the last years, infrared sensors have become less expensive and more reliable so this noncontact measurement technique has become progressively desirable. Today it is possible to get computer aided predictive maintenance and full image thermal control of products and process are possible with developing computer technology.

While infrared imaging technology was first developed for military applications, the first applications of IRT to buildings and artistic objects can be found in the scientific literature of the 1970s.1,2,3,4 The most common approach was qualitative analysis based on the comparison between an area under investigation and a comparable zone which was sound. In the 1980s, thermal mathematical models were developed improving qualitative evaluations of temperature distribution in building materials. During the latter part of the 1980s, cultural heritage IRT laboratory applications started in order to de®ne more reliable procedures for ®eld applications. To de®nitively develop a quantitative approach, thermal anomalies have been related to the local thermal characteristics of the materials and to the defects of the examined part.5 Controls became reliable due to speci®c algorithms applied in signal processing and the development of new generations of thermocameras.(Spodek & Rosina, 2009)

Infrared spectrum was firstly revealed by William Herschel (1738-1822) who was the Royal astronomer for King George III of England and who accidentally discovered Uranus on March, 1793 and this accident has led to his discovery of infrared rays. Using a mercury thermometer, he noticed that the maximum elevation of temperature happened beyond the red band where no radiation was visible and the heating is located in a specific part of spectrum so it depends on wavelength[28] (Maldague).

In the twentieth century, with many developments in industry, thermal and infrared testing was collected in a search of United States patents. And during World War II many patents are released and application areas included detection of soldiers, ships, icebergs and communication.

[28] He also defined the difference between heat and light. He also demonstrated that quantitative measurements are possible in electromagnetic spectrum using the mercury thermometer. He also showed that transmission of invisible rays is affected by material properties (Maldague….)


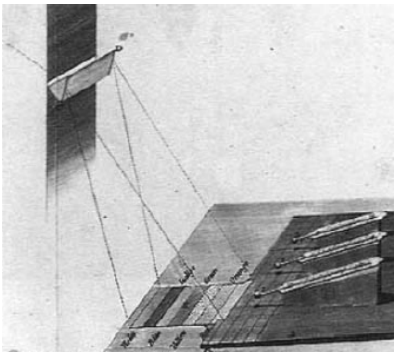


(a) (b) (c)

Figure 4.1.1:(a)Portrait of William Herschel
(b)Thermometer placed in shadow near red side of color spectrum
(c) prism used by Herschel (Maldague)

After World War II, many new research and developments were produced especially for military purposes. In 1960s other many applications had been started to apply in diverse fields such as medicine, environment industry, science and military. In 1992, edition of ASNT Recommended Practice No. SNT-TC-1A included provision for infrared and thermal testing(Maldague). Today IR Thermography has found many application areas including testing of metal, aerospace applications, electric-power applications, chemical and petroleum applications as well as infrastructure and conservation of energy both for new and historical buildings.

4.2. Standards and Specifications for Infrared and Thermal Testing

Standards and specifications[29] for infrared and thermal testing are mainly in three basic areas: equipment, process and personnel.

-Standards for equipment and materials include electronic and optical equipment.
-Standards for test techniques are published by The American Society For Testing and Materials and other organizations.
-For the test personnel there is a recommendation of ASNT Recommended Practice No.SNT-TC-1A (Trimm,2010).

4.3. Principles and Parameters of IR Thermography

4.3.1. Principles of Infrared Thermography

The terms *infrared* and *thermal* can be used in lieu of the other in many context. Mainly the term *thermal* refers to the physical phenomenon of heat, involving the movement of molecules. *Infrared* (beyond the color red) indicates radiation between the visible and microwave regions of the electromagnetic spectrum shown in figure 4.3.1.

[29] Standards and practices for infrared thermal testing can be found in Trimm,2010.

Infrared and thermal testing includes temperature and heat flow measurement in order to predict or diagnose failure which requires contacting devices [30] or non-contacting devices[31] or combination of both (Jones & Kaplan).

When a surface becomes hot, there are atomic particles rising energy leads to a corresponding increase in temperature and emitted energy. Ther thermal energy of atomic particles produces an electromagnetic energy known as *infrared radiation.* When infrared radiation fall on a surface, the absorbed energy is converted into heat (Figure 4.3.1)(Jones & Kaplan).

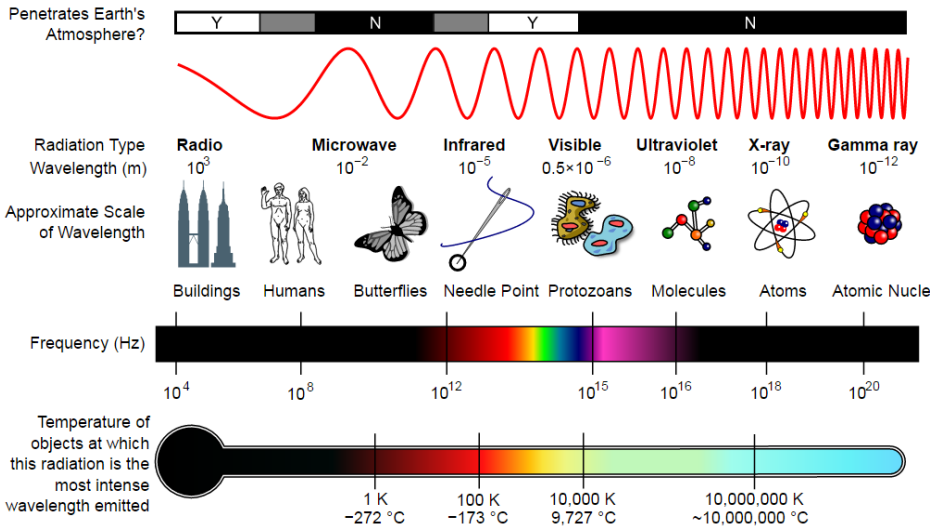

Figure 4.3.1: Electromagnetic spectrum (Jones & Kaplan)

Infrared testing can be performed by either active or passive techniques. Active techniques include heating or cooling the material to generate the required heat flow and thermal gradients. Passive techniques include applications where the material contains its own internal source of heat[32] and in stable conditions passive tests are normally applied (Jones & Kaplan) (figure 4.3.2).

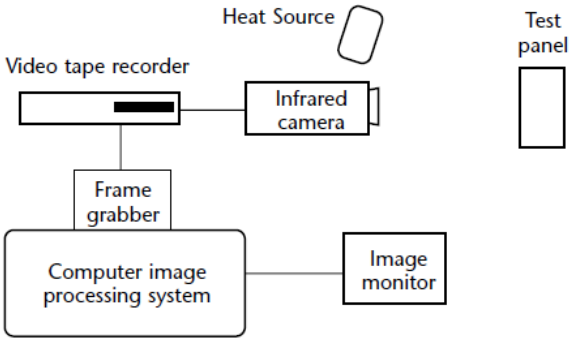

Figure 4.3.2:Typical infrared inspection system diagram(Jones & Kaplan)

[30] Contacting devices include thermometers of various types, thermocouples, thermopiles, thermochromic coatings.

[31] Non-contacting devices include convection (heat flux) devices, optical pyrometers, infrared radiation thermometers, infrared line scanners and infrared thermal imaging (thermographic) equipment.

[32] Such as an inservice heater element or the human body

Infrared thermography is a non-destructive, non-intrusive, non-contact mapping of thermal patterns on the surface objects. It is usually used to diagnose thermal behavior and to assess the performance of equipment and the integrity of materials, products and processes. The infrared thermal imaging equipment used in infrared thermography is available in many configurations and with diverse complexity. The thermal maps produced by infrared thermal imaging instruments are called as *thermogram*. Infrared and thermal methods are mainly based on the principle that heat flow[33] in material is changed by the presence of some types of anomalies. These changes in heat flow cause localized temperature differences in the material surface. The imaging or study of such thermal patterns is known as *thermography.*

According to Maldague (1999), thermography is a technique used to see unseen(Maldague) where it uses the distrubition (–graphy) of surface temperatures (thermo-) to assess the structure or behavior under the surface. Mainly thermography refers to a contact technique to record a distribution of surface temperatures whereas infrared thermography is a contactless technique. In 1970s the term thermography came to usually mean noncontact, infrared thermography(Maldague).

The fundamental equiation of infrared thermography relates the irradiance N_{cam} (spectral radiant power incident on a surface per unit area) received by the camera to the radiance emitted from the surface under consideration N_{sur} at a given temperature T with N_{env} being the radiance emited by the surrounding environment considered as a blackbody. The equation is

$$N_{\text{cam}} \approx \varepsilon N_{\text{sur}} + \left(1 - \varepsilon\right) N_{\text{env}}$$

IRT uses an infrared camera to detect and record infrared energy and produce a thermal image recording of the surface temperature of a building. An infrared camera has specialized sensors to detect incident infrared radiation, which is gathered through a lens capable of transmitting infrared waves affecting the sensors' electrical conductivity. This data is converted into a visual image, called a thermogram (or temperature map), of the surface under investigation. The sensors do not respond to visible light so the camera only captures infrared radiation either emitted or re¯ected off an object. Data can therefore be gathered in low or no visual light situations.(Spodek & Rosina, 2009).

4.3.2. Parameters of IR Thermography

During an IR thermographic investigation of structures or materials, there are diverse physical properties need to be considered. All properties can be classified as below:

-thermal properties(conductivity, diffusivity, effusivity, specific heat),

-spectral properties (emissivity, absorption, reflection, transmission) and

[33] Heat flow can happen by conduction, radiation, convection or a combination of these.

-other properties (porosity, volumetric mass, physiological water content)(Avdelidis & Moropoulou, 2004).

4.3.2.1. Thermal Properties

Thermal **conductivity** is the property of a material to conduct heat[34] . Even the materials at the same temperature make us to have different sensations because of difference in their heat transfer. Copper, aluminum, gold and silver are good heat conductors while wood, plastic and rubber are poor heat condustors which they can be used as insulators (figure 4.3.3).

There are mainly four factors (*k, A, ΔT, d)* affecting the rate at which heat is conducted through a material. These factors are included in equation below:

$$\frac{Q}{t} = \frac{kA\Delta T}{d}$$

The letter Q(joules) represents the amount of heat transferred in a time t(second), k is the thermal conductivity constant for the material, A is the cross sectional area of the material transferring heat, ΔT is the difference in temperature between one side of the material and the other, and d is the thickness of the material. These factors can be seen visually in the diagram below.

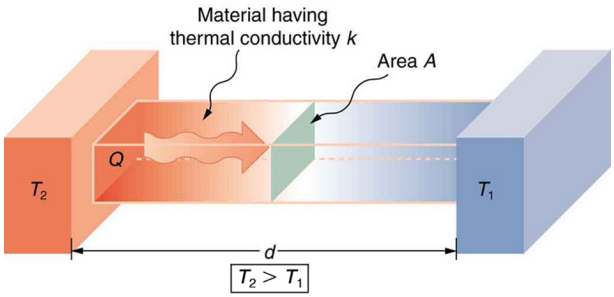

Figure 4.3.3: Heat conduction occurs through any material, represented here by a rectangular bar, whether window glass or walrus blubber. (Image Credit: Openstax College Physics) (https://www.khanacademy.org/science/physics/thermodynamics/specific-heat-and-heat-transfer)

Thermal **diffusivity** is the thermophysical property that defines the speed of heat propagation by conduction during changes of temperature. The higher thermal diffusivity, the faster the heat propagation. Thermal diffusivity depends on the thermal conductivity, specific heat capacity and density. This can be realized with the following equation:

$$a = \frac{k}{\rho C_p}$$

[34] It's evaluated in terms of Fourier's Law for heat conduction.

Where *a* (m^2/s) is the thermal diffusivity ($m^2\ s^{-1}$), *k* is the thermal conductivity ($W\ m^{-1}\ K^{-1}$), *p* is the density ($kg\ m^{-3}$) and *Cp* is the specific heat capacity ($J\ kg^{-1}\ K^{-1}$).

Another factor to be considered in IR thermographic survey is thermal **effusivity** value of materials. Thermal effusivity is sometimes called as the heat penetration coefficient and it is defined with equation below. A material's thermal effusvity is a measure of its ability to exchange thermal energy with its surroundings. Materials with low effusivity values will increase the temperature rapidly.

$$e = \sqrt{k\rho C_p}$$

Where e is the thermal effusivity ($W\ s^{1/2}\ m^{-2}\ K^{-1}$). Thermal diffusion length can be expressed by

$$\mu = \sqrt{\frac{\alpha}{\pi f}}$$

where *f* is the frequency (Hz).

4.3.2.2. Spectral Properties

Emissivitiy is the measure of object ability in emitting energy as thermal radiation. It is mainly a ration of the total energy radiated by a given surface at a given temperature to the total energy radiated by a blackbody at the same temperature as given by Stefan-Boltzmann law.

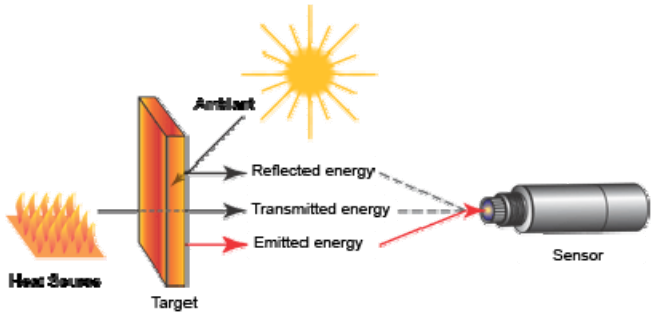

Figure 4.3.4: Emissivity

Here the emitted energy indicates the temperature of the object. A blackbody is a hypothetical radiation source which delivers the maximum radiation energy theoretically possible at a given temperature. It has an emissivity of 1.0 and all real materials have emissivities between 0 and 1.0. The effect of emissivity on the radiation curve is given in figure 4.3.5 below.

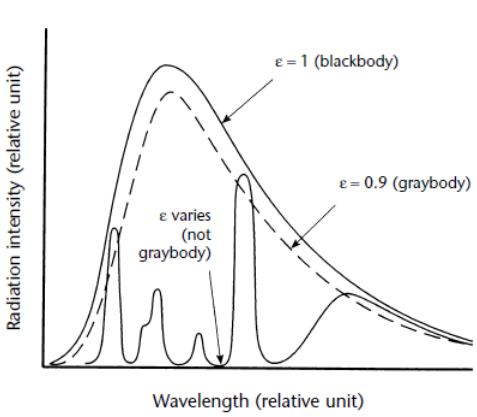

Figure 4.3.5: Emissivity effect on radiation from surface of emissivity ε with hypothetical intensity.

According to Wien's displacement law, the wavelength of maximum intensity is computed simply by dividing 2897 by the temperature of the surface.

$$\lambda_{max} = \frac{b}{T}$$

Where b is the wien displacement constant $(2897\ \mu m \cdot K^{-1})$, T is temperature (Kelvin),and λ_{max} is maximum wavelength (micrometer). Higher temperatures yield lower wave lengths (figure 4.3.6)(Luhmann, Ohm, Piechel, & Thorsten, 2010).

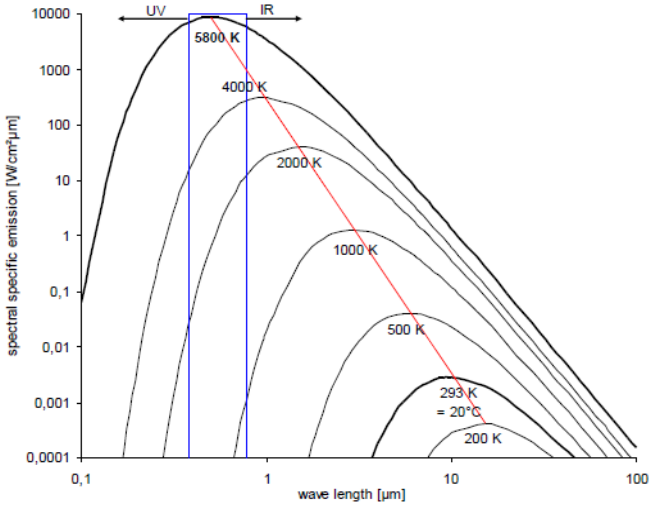

Figure 4.3.6: Spectral specific emission

Emissivity changes according to surface condition and composition. Smooth materials have lower emissivities than rough materials. Polished metals have lower emissivities than oxidized or corroded metal surfaces. Nonmetals usually have higher emissivities than metals. High emissivity surfaces give better results in infrared thermography. Surfaces with high emissivity which means poor reflector, emit higher intensity radiation so provides larger signal for infrared dedector. Low emissvity surfaces tend to reflect radiation which contributes to the noise of the test. High emissivity surfaces absorb more radiant energy that can be effective in inducing a thermal gradient in the

test sample. Figure 4.3.7 Shows a list of of typical surface emissivities for different materials (Jones & Kaplan)

Material	Emissivity Range (0 to 1.0)
Metallic	
Highly polished aluminum, silver, gold, brass, tin	0.002 to 0.04
Polished brass, copper, steel, nickel, chromium, platinum, clean mercury	0.03 to 0.08
Dull, smooth, clean aluminum and alloys, copper, brass, nickel, stainless steel, iron, lead, zinc	0.08 to 0.20
Rough ground or smooth machined castings; steel mill products, sprayed metal, molten metal	0.15 to 0.25
Sooth, slightly oxidized aluminum, copper, brass, lead, zinc	0.20 to 0.40
Bright aluminum, gilt, or bronze paints	0.30 to 0.55
Heavily oxidized and rough iron, steel, copper, aluminum	0.60 to 0.85
Nonmetallic	
White or light colored paint, plaster, brick, tile, porcelain, plastics, asbestos	0.80 to 0.95
Snow at 263 K (–10 °C or +14 °F)	0.85
Red, brown, green, buff and other colors of paint, tile, inks, clays or stone; glass and translucent plastics; glass fiber composites; ice crystals; oil; varnish	0.85 to 0.95
White bond paper, sand, wood (planed oak)	0.90
Carbon black, asphalt, carbon fiber composites, matte black paints, tar	0.90 to 0.97
Concrete	0.92
Brick (common red)	0.93
Water	0.96
Human skin	0.98

Figure 4.3.7: Total radiation emissivities at all wavelengths (Jones & Kaplan)

Emissivity changes can create several errors in radiometric detection methods, unless something is done to keep emissivity constant. The emissivity problem can be reduced by special design of the radiometer system(Jones & Kaplan).

Absorption in IR refers to the heat transfer that occurs between two bodies and it can be through conduction, convection or radiation. In absorption electromagnetic energy is transformed into internal energy of the absorber like thermal energy.

Heat **transmission** is the thermal energy betwwen physical systems. The rate of heat transfer is dependent on the temperatures of the systems and the properties of the intervening medium through which the heat is transferred. The three fundamental modes of heat transfer are conduction, convection and radiation (https://en.wikipedia.org/wiki/Heat_transfer)

IR Thermography imaging system measures the energy emitted from a ground surface only. However the temperatures measured on the surface of the ground depend on the subsurface conditions. So the measurement of the temperature of ground cover surface becomes important. However there are various parameters affecting the surface temperature measurements that need to be considered such as sunlight (solar radiation), clouds, ambient temperature, wind and moisture. Weil (2001) explains these parameters on his study about leak testing for infrastructure (Weil, 2001) (figure 4.3.8)

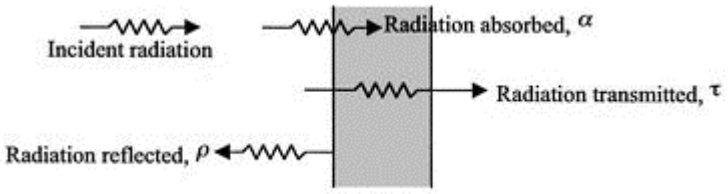

Figure 4.3.8: Radiation surface properties (Weil, 2001)

IR Thermography testing should be performed during times of the day or night when the **solar radiation** produce the most rapid heating or cooling of the ground surface. **Clouds** absorb and scatter infrared radiation which effects of slowing the heat transfer process between sky and ground. So IR Thermal testing should be performed during times of little or no cloud cover in order to allow efficient energy transfer.
It can be said that **atmospheric temperature** has a negligible effect on the accuracy of testing since the important consideration is the rapid heating or cooling of the ground surface on the contrary **wind** has a negative cooling effect on surface temperatures. Measurements should be taken at wind speeds of less than 6.67 $m \cdot s^{-1}$ ($15mi \cdot h^{-1}$). **Moisture** on the ground is a significant parameter affecting the results. Since moisture tends to disperse the surface heat and mask the temperature differences and so subsurface anomalies. So IR Thermal testing shouldn't be performed when the ground has water or when it's wet(Weil, 2001). Equations of effects of moisture on thermal parameters can be found in detail in Rosina, 2001 (Rosina & Grinzato, 2001).

4.3.2.3. Other Properties

4.3.3. Camera Calibration

A normal digital camera registers the visible light emitted by the sun and reflected by the surface. A thermal camera, instead, registers mostly the 'invisible light' directly emitted by the surface.

As thermal imaging has found applications in many commercial and medical fields, the need to test these devices to recognized standards is becoming increasingly important. Thermographic cameras can be divided mainly two types: cooled and uncooled cameras. The cooling is necessary for semiconductor materials operations. Without cooling, the sensors would be blinded or flooded by their own radiation. The main drawbacks of these cameras are the cost in production and run, and cooling is energy-intensive and time consuming. Uncooled cameras typically have a sensor operating at ambient temperature, or a sensor stabilized at a temperature close to ambient temperature. They use small temperature control elements. To stabilize the temperature helps to reduce image noise. Since they don't need coolers, they are smaller and less costly. However their resolution and image quality tend to be lower than cooled detectors (Figure 4.3.9).

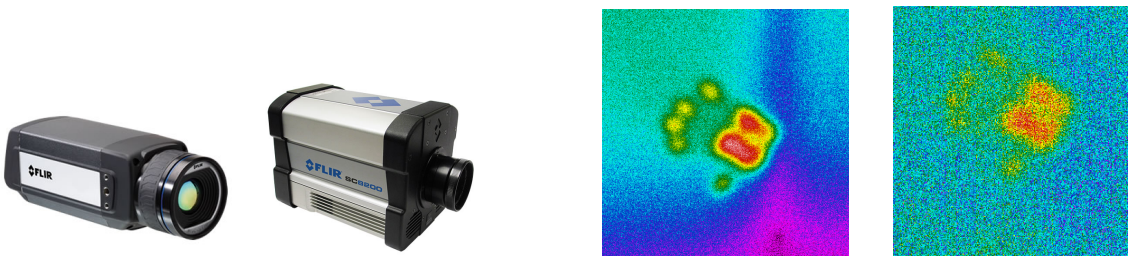

(a) (b) (c) (d)

Figure 4.3.9: (a)uncooled camera FLIR-A655sc (640x480 Resolution)
(b)cooled camera FLIR-SC8300 (1344x784 Resolution)
(c) Cooled thermal camera image of handprint on wall
(d) Uncooled thermal camera image of handprint on wall(http://www.flir.com)

According to DeWitt and Nutter (1989), a radiometer, where each individual pixel of an IR camera can be determined, measures the radiant flux of the object and generates an output signal which, as a result of the calibration, is proportional to the temperature of the object. A radiometric IR camera displays as accurately as possible the true temperature of a black body. The calibration is used here to calculate a temperature proportional output signal (IR image) from the measurement signal (raw image) taking into account all technical and physical properties of the IR camera. Flow chart of a radiometric calibration is shown in figüre 4.3.10(Budzier & Gerlach, 2015).

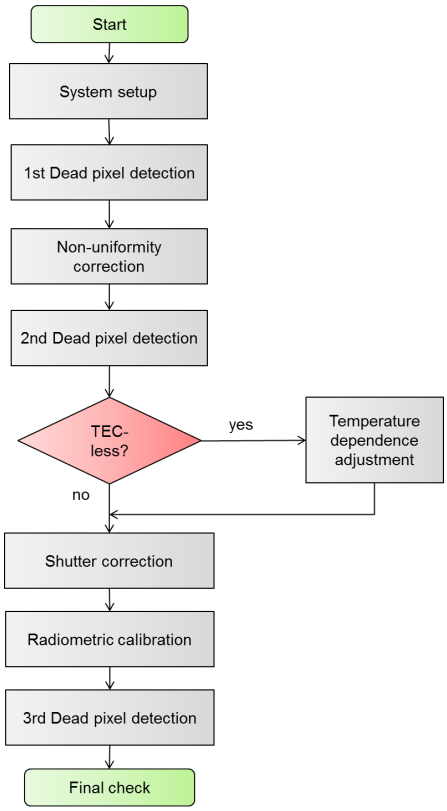

Figure 4.3.10: Flow chart of radiometric calibration (Budzier & Gerlach, 2015)

Even though the subjects of greatest interest have only a small temperature difference compared with the background, there are set of performance metrics for thermal imagers. Noise equivalent temperature difference, subjective and objective minimum resolvable temperature difference, minimum detectable temperature difference and modulation transfer function are typical parameters that may need to be measured in a testing laboratory. Those metrics require the presentation of a target with a precisely known thermal contrast. Frequently four-bar targets are used to determine the minimum resolvable temperature difference (Figure 4.3.11) (Imrie, 2009). Despite commonly use of four-bar targets (a) in fugre 4.3.11 and checkerboard targets (b) different kinds of targets are also used for camera calibration (Luhmann et al., 2010). It should be considered that there is relationship between calibration pattern and calibration results. It was determined that the results obtained with the large size calibration template are more correct according to the results of the smaller size templates (Durgut & Akçay, 2016).

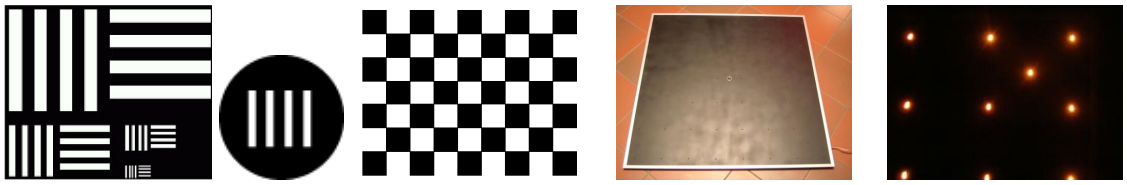

(a) (b) (c) (d)

Figure 4.3.11:(a)Different type of four-bar targets(Imrie, 2009)
(b)Checkboard target (www.google.com/patents/US20120069193)
(c-d)Plane test field with active and burning lamps (Luhmann et al., 2010)

Calibration and measurement procedures such as blackbody calibration and non-linearity correction, point spread function measurement, emissivity measurement and true temperature measurement for thermal cameras can be found in Lane and Whitenton (2015) (Lane & Whitenton, 2015). Beside Machin, Simpson and Broussely (2008) made a research on how the accurate calibration of thermal imagers can be obtained through the use of appropriate and available metrology tools (Machin, Simpson, & Broussely, 2008). Another study was made on calibration of uncooled thermal infrared cameras by Budzier and Gerlach(2015). In their study they discussed the mathematical and physical principles of calibration based on radiometric camera models and presented the individual stages of calibration for uncooled cameras (Budzier & Gerlach, 2015). Luhmann et al. (2010) tried five different thermal cameras with different targets for calibration and camera calibration results showed that standard thermographic cameras yield high distortion values and large shifts of principal points(Luhmann et al., 2010).
Beside laboratory test method, there are also some in-situ calibration methods run for thermal cameras (Martiny, Schiele, Gritsch, Schulz, & Witting, 1997; Pineda, Montés, Sánchez, Bensadoun, & Ruiz, 2012).

Thermal cameras need imaging sensors sensitive to wavelengths usually between 2.5 and 15µm. Depending on the detector technology, temperatures between -30 and +400 can be detected by common thermographic cameras. The geometric resolution of imaging devices is limited by diffraction. The diameter of the Airy disk d depends on the aperture (f-number k) and the wavelength:

$$d = 2.44 \cdot \lambda k$$

Equation makes clear than the pixel sizes of thermal sensors can be much larger than for standard color cameras. Most thermal imaging sensors provide pixel sizes between 30 and 50 µm (Luhmann et al., 2010). Sensors could be quantum detectors or thermal detectors. Thermal detectors use the effect that a temperature change of the detector element leads to a change of the electrical properties of the detector. These changes can be measured and transformed into intensity values. Even though they are less sensitive and slower than quantum detectors, hence they are less expensive und usually applied for applications like building monitoring (Luhmann et al., 2010)

4.4. Techniques of Infrared and Thermal Testing

Infrared thermography mainly uses two kinds of infrared cameras: scanning radiometers and focal plane array in one or two dimensions[35]. A radiometry comprises of optics collecting and focusing or image the received infrared radiation on a sensitive detector. The detector converts the infrared radiation into an electrical signal(Maldague). Scanning radiometers have an internal temperature reference seen by detectors during scanning so the output signal is directly calibrated in temperature. Focal plane arrays, scanning is not needed since the infrared image of the scene is directly imaged on the detector matrix(Maldague).

In thermography mainly two techniques are used: active and passive thermographic techniques.

4.4.1. Passive Thermography

The principle of thermography is energy conservation so an essential parameter to measure in order to assess proper operation becomes temperature. The passive thermography approach is used when the object of interest has sufficient thermal contrast with respect to the background in order to be detected. This abnormal temperature profiles represents a potential problem, often referred to as the *delta T*[36] (ΔT) or the *hot spot*. A (ΔT) of 1 to 2 K (1 to 2°C≅ 2 to 4°F is generally found suspicious, 4K (2°C≅ 2 to 7°F) is a strong evidence of abnormal behavior(Maldague). In passive thermography the aim is to localize anomalies(Maldague). Typical applications include; surveillance, medicine (oral lesions, breast surgery), monitoring (structures,

[35] One-dimensional is useful when inspecting moving objects, the second dimension provided by the displacement

[36]

urban areas etc.), humidity assessments, insulation, electrical components etc (Figure 4.4.1).

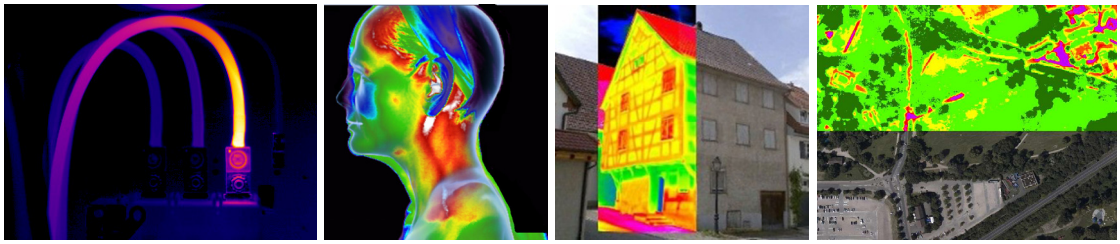

(a) (b) (c) (d)

Figure 4.4.1:(a) (http://ecmweb.com)
(b)(http://www.oregonnaturalmedicine.com/breast-thermography/researcharticles)
(c)(http://www.viaduct-diadrasis.net/methods/17)
(d)(http://globalmrr.com/aerotherm/)

4.4.2. Active Thermography

Active thermography is based on the detection and recording by an infrared camera of thermal radiations on object surface. In order to detect the defects, heating or cooling becomes necessary to inspect object thermal state.
In active thermography, heat flow is induced by an energetic excitation of the test object which can be done in a transmissive or a reflective setup. The resulting heat flow is influenced by interior material layers and defects. These in homogeneities can be captured on the object surface by high-precision thermographic cameras (Figure 4.4.2).
Main advantages of active thermography are:
-It has possibility to perform one-side inspection
-Carried out in real-time
-Appropriate for many materials and multi-layer structures
-Relatively unaffected by object geometry and well adopted for large surfaces(Maldague, 2013).

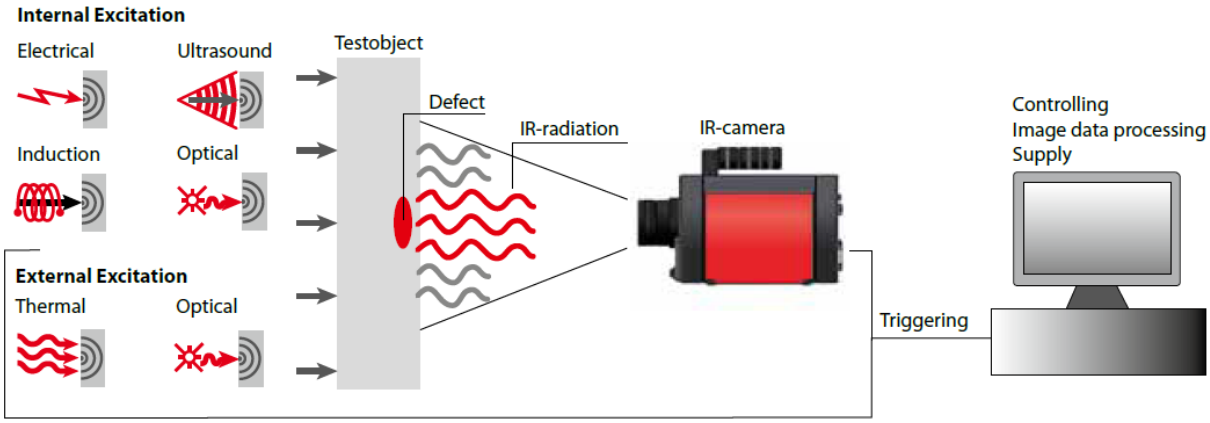

Figure 4.4.2: Active Thermography (InfraTEC GmbH)

Active thermography includes different techniques which are mainly: lockin thermography, pulsed thermography, step heating thermography and

vibrothermography. Each of these techniques has different application areas (shown in figure 4.4.3) (Maldague)

4.4.3. Pros and Cons of Existing Techniques

The non-contact nature of IRT is advantageous because it allows for investigation of delicate or sensitive surfaces. As long as a direct line of sight is available, data can be collected from a distance, eliminating the need for lifts or scaffolding. IRT can be applied repeatedly to monitör conditions, evaluate the effects of treatments, and observe anomalies and changing conditions over a lengthy period of time.(Spodek & Rosina, 2009)

Table 4.4.1: Applications of infrared thermographic techniques(Maldague, 2013)

Technique	Process Control	Discontinuity Detection	Material Characterization
Passive Thermography	Carton sealing line inspection, automobile brake system efficiency, heat dissipation of electronic modeluse, recycling process identification, printed circuit borads, glass industry(bottles,bulbs), welding process, metal (steel) casting Bearings, fan and compressors, pipelines, steam traps, refractory lining, rotating kilns, turbine blades, electric installations, gas leaks	Walls, moisture evaluation, roofs, assemblies Liquid level in tanks	Glaze thickness on ceramics, crush tests investigation
Lockin Thermography (active)	Aircraft structural component inspection, loose bolts detection Plastic pipe inspection Radar absorbing structure investigation	Crack identification, disbanding, impact damage in carbon fiber reinforced plastics	Adhesion strength, anisotropic material characterization, coating thickness in ceramics, moisture evaluation Depth profile of thermal conductivity or diffusivity
Pulsed Thermography (active)	Aircraft structural component inspection, solder quality of electronic components, spot welding inspection Water entrapment in buildings and fresco delamination	Metal corrosion, crack detection, disbanding, impact damages in carbon fiber reinforced plastics, turbine blades, subsurface defect characterization (depth, size, properties) in composites, wood, metal, plastics	Thermophysical properties (diffusivity etc.), underalloyed and overalloyed phases in coatings on steel, moisture, anisotropic material characterization
Step heating Thermography (active)	Degradation of erasable programmable read only memory chips Ppaer structure (cockling)	Defects in adhesive and spot welded lap joint	Thermal conductivity measurement in carbon fiber reinforced plastics Coating thickness measurement
Vibrothermography (active)	Failure analysis	Coating wear, fatigue test, closed crack detection	Variations in viscoelasticity and emissivity

All thermographic techniques have advantages in fast surface inspection, ease of deployment especially on one side, safety, easy modelling, appropriate to perform on many different areas and they are valuable tool. Despite these advantages, they have

also some critical points need to be considered carefully and sometimes can be disadvantage. Variable emissivity, losses in cooling, absorption of infrared signals by the atmosphere can be some disadvantages. Besides, it is not easy to get uniform heating (for active procedures) and thermal contrasts have to be recorded by fast infrared cameras. There is also a need of straight corridor between infrared camera and target in order to get data. Passive thermography is non-contact and non-interaction with specimen however it doesn't work well if there isn't natural thermal contrast. Even active thermography is non-contact technique, it is difficult to get homogeneous test surface (Table 4.4.1 and 4.4.2)(Maldague).

It has been shown that it is theoretically possible to overcome IRT's depth limitations of a few centimetres beneath the outer surface. However, even with this development the reality is that obstacles remain to the extensive application of IRT during field testing for layers that are deep inside walls. This is primarily due to the difficulty in getting a proper thermal solicitation of the surface, and thus a return signal, which can be detected by the thermocamera and unequivocally related to the researched defect instead to any surface anomaly.(Spodek & Rosina, 2009)(Figure 4.4.2).

Table 4.4.2:Advantages and limitations of infrared thermographic techniques(Maldague,2013)

Technique	Advantages	Disadvantages
All thermographic techniques	Fast, surface inspection Ease of deployment Deployment on one side only Safety (no harmful radiations) Ease of numerical thermal modelling Ease of interpretations of thermograms Great versatility of applications Sometimes unique tool (corrosion around rivets)	Variable emissivity Cooling looses (convection/radiation causing perturbing contrasts) Absorption of infrared signals by the atmosphere (especially for distances greater than a few meters) Difficulty to get uniform heating (active procedures) Transitory nature of thermal contrasts requiring fast recording infrared cameras Need of straight viewing corridor between infrared camera and target (although it could be folded through first surface mirrors) Limited contrasts and limited signal to noise ratio causing false alarms-measurement of a few degrees above background at around 300K Observable defects generally shallow
Passive thermography	No interaction with specimen No physical contact	Works only if thermal contrasts naturally present
Lockin thermography (active)	No physical contact Large inspected surface-several m² simultaneously Phase and modulation images available Modulated ultrasonic heating (for some applications, might require physical contact or bath immersion)	Require modulated thermal perturbation Require observation for at least one modulation cycle (longer observation with respect to pulsed thermography) Thickness of inspected layer under the surface related to the modulation frequency (unknown defect depth might require multiple experimentations at different frequencies)
Pulsed thermography (active)	No physical contact Quick (pulsed thermal stimulation: cooling or heating)	Requires apparatus to induce the pulsed thermal perturbation Computation of thermal contrasts require a priori knowledge of defect free zone in field of view Inspection surface limited (-0.25 m ² maximum)
Step heating thermography (active)	No physical contact	Requires apparatus to induce the pulsed thermal perturbation Risk of overheating the specimen
Vibrothermography (active)	Reveal close cracks	Difficulty to generate mechanical loading Thermal patterns appear only at specific frequencies Physical contact to induce thermal stimulation

4.5. Data processing concepts and solutions

During the years diverse methods for thermal data analysis suited in thermography. Beside traditional techniques coming from computer vision, several specific methods have been developed. These unique techniques are sometimes based on the underlying heat-conduction physics. These methods are required either at image processing or processing stages.

In processing IR images some effects should be considered. These can be defined such as:

-Vignetting
-Fixed pattern noise(FPN) in focal plane array(FPA)
-Presence of dead pixels in FPA matrix
-Radial distortion

Among the thermography techniques pulsed thermography has become a common approach. All these approaches diverge primarily by the way the specimen thermally stimulated. For the enhancement of the signatures there are several techniques including: thermal contrast computation, normalization, pulsed phase thermography, principle component thermography, 1st and 2nd derivatives. Among these techniques thermal contrast is the most common and simpler one. Various thermal contrast definition exist but they all share together the need to know a sound area (SoA) location within the field of view. Absolute thermal contrast $C^a(t)$ at location of pixel p at time t is defined as

$$C^a(t)=\Delta T(t) = T(t) - Ts(t)$$

Where $T(t)$ is the temperature at time t at p and $Ts(t)$ is the average temperature at time t for the SoA (Ibarra-Castanedo, Gonzalez, Klein, Pilla, & Vallerand, 2004).

IR data processing and analysis it can be found several studies in literature in detail (ASHRAE, 2011; GRTI, 2008; Ibarra-Castanedo et al., 2004; Suresh, Pardha sardhi reddy, Vinod, Ravi Chandra sekhar, & Ghali, 2015).

4.6. Thermography for Cultural Heritage and Historical Buildings

IR Thermography is mainly applied with similar procedures for modern and historical buildings. However historical buildings have some special peculiarities that may affect the regular procedure. Walls of historical buildings generally are irregular shape and their thickness, structure, construction technique or layers may vary in several parts. So the procedure must be followed by trained personnel. Even though there are some nondestructive techniques developed for industrial purposes, they can not be useful for historical buildings thick walls. For ancient buildings, usually nondestructive technique can be applied. In the processing of data, it should be very careful since historical buildings have oftenly heterogeneous colors, materials and thickness, many false alarms may be seen in the data. In this case, the processing of raw thermograms

and using software filter based on visual analysis are effective tools to reduce undesired information. The surface temperature[37] may give information about the inside structure. The heat is transferred more quickly throughout the most cohesive materials or materials with high thermal diffusivitiy. Differences of surface temperature based on thermal properties of elements[38] can be visualized at appropriate time as *footprint* of their shapes on the plaster since any thin delamination reduces the heat transfer so gives signal on the structure. Brick, concrete, stone, adobe and cast iron masonry have oftenly a protective slab that prevents weather damage to the structure. The optical and thermal properties of this slab affect any information regarding inner layers. Conservation of ancient coatings is often an object of thermographic investigation since the surface of finishing materials shows different colors and porosity. Optical characteristics of the materials can be important in order to evaluate the cleaning and restoration treatments of the surface. Thermal properties of such materials are known but hardly determinable (Rosina & Grinzato, 2001).

The purpose of investigation with IR Thermography is mainly the detection and evaluation of thermal anomalies and discontinuities because of decay and hidden elements of the building. For historical buildings IR Thermography is mainly used to determine the existence, position, shape and dimension of structural elements, bricks and stones under the plaster. Besides, thermography characterizes different materials and gives opportunity to monitor thermal and hygrometrical conditions of the surface. Moreover thermography can be applied to investigate optical signal related to discontinuities of the surface. Temperature and humidity measurements help to estimate thermal anomalies of the structures. Especially depending on the direction, different facades of the buildings may show diverse surface temperature values.

The ultimate objectives of IRT are the detection and evaluation of thermal anomalies (which may be the result of decay), the discovery of hidden elements in a building and the exploration of variation in elements that may have the same visual appearance. The primary applica- tion for historic buildings is the investigation of inner layers and structural elements a few centimetres beneath plaster or stucco, and in masonry construction. Applications on wood-frame construction have determined the location of internal wood framing and structural members. IRT is also used to identify and monitor diffusion of moisture on or near the surface of masonry walls by determining the correspondence between actual distribu- tion of moisture and visual damage.(Spodek & Rosina, 2009)

Even though the capacity and the ability of infrared thermography technique in the literature are well documented, it becomes more important when it is considered the investigation of historic structures. Infrared thermography, both active and passive technique, is widely used in many applications including the assessment of structural and historical materials and techniques. IR thermography is applied also for the evaluation of conservation interventions such as cleaning of surfaces, consolidation applications, restoration of masonry, the disclosure of tesserae on plastered mosaic

[37] Thermographic readout refers to the surface temperature. It's a function of heat flow crossing the wall and local boundary conditions.

[38] Such as thimber, brick, stone.

surfaces (Avdelidis & Moropoulou, 2004), in assessment of structural timber elements (Kandemir-Yücel, Tavukcuoglu, & Caner-Saltik, 2007) and monitoring of built heritage(Rosina et al., 2004). Besides, IR Thermography has been applied for detect and disclose artificial and in-depth defects on structures (Meola, 2007), for hidden structures like niches or burned openings (Grinzato, Bressan, Marinetti, Bison, & Bonacina, 2002; Imposa, 2010), for monitoring and (Rosina et al., 2004) and consolidation (figure4.6.1) (Paoletti, Ambrosini, Sfarra, & Bisegna, 2013). Another important and advantageous field of IR Thermography is the detection of moisture and rising damp in historical buildings (figure 4.6.2) (Grinzato et al., 2002; Ludwig, Redaelli, Rosina, & Augelli, 2004; Moropoulou, Avdelidis, Koui, Delegou, & Tsiourva, 2001; Rosina & Grinzato, 2001; Tavukçuoğlu, Düzgüneş, Caner-Saltik, & Demirci, 2005). Moreover, it should be mentioned that IR Thermography is a potential tool for damage characterization and crack mapping (Grinzato et al., 2002; Kordatos, Exarchos, Matikas, Stavrakos, & Moropoulou, 2012). These features make IR thermography to be considered as an assessment tool for the preservation and conservation of cultural heritage.

(a) (b) (c)

Figure 4.6.1:(a) The Church of Santa Maria ad Cryptas fron side thermogram, Spetember, 2007
(b)Naked eye analysis, 2009
(c) Thermogram, May, 2010 (Paoletti et al., 2013)

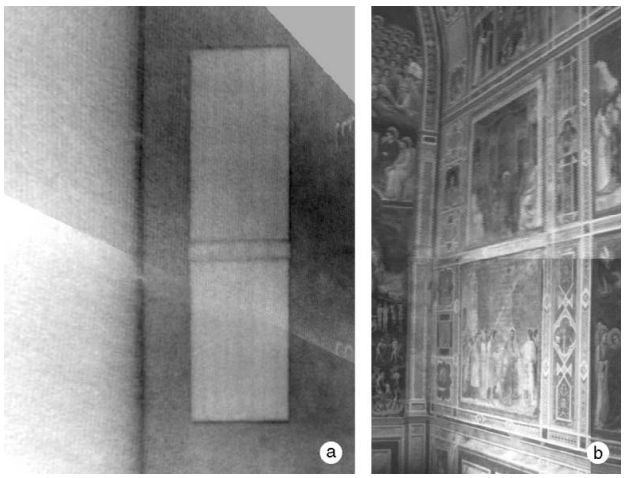

Figure 4.6.2 (a) Thermogram of the west-side surface, close to the south corner, corrected for the perspective distortion; a hidden structure bearing the fresco is detected. (b) The image of the west-side wall corresponding to the thermogram of (a) (Grinzato et al., 2002)

IR thermography has been used more than 25 years in buildings and historic structures monitoring (Avdelidis & Moropoulou, 2003) however the interpretation of thermographic survey can be complex depending on the application. During an IR thermographic investigation of structures or materials, all properties such as thermal properties(conductivity, diffusivity, effusivity, specific heat), spectral properties (emissivity, absorption, reflection, transmission) and other properties (porosity, volumetric mass, physiological water content) have to be considered (Avdelidis & Moropoulou, 2004).

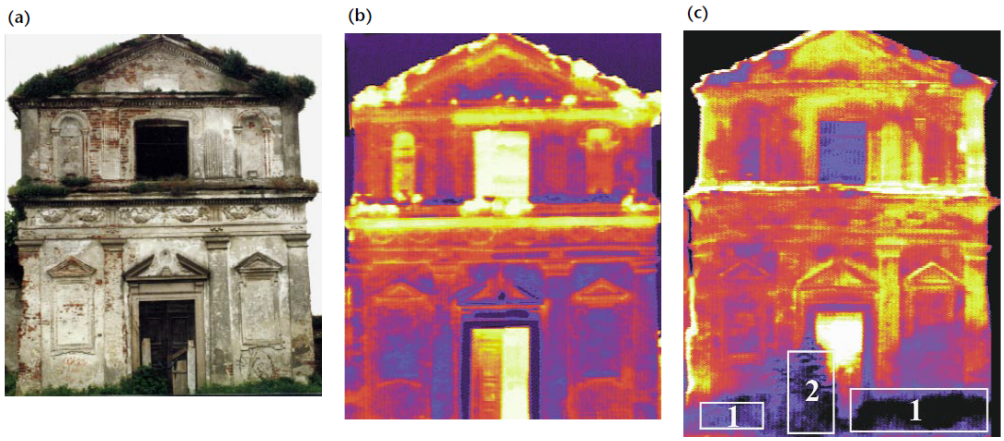

Figure 4.6.3: Facade of Oratory of Guardia di Sotto, Italy. (a) visible light photograph; (b) thermogram of façade does not reveal any moisture (21 November 1995, air temperature 280 K=7°C=45°F, relative humidity 57 percent, clear sky; (c) passive thermogram (16 June 1997, air temperature 296K=23°C=73°F, relative humidity 67 percent)(Rosina & Grinzato, 2001)

Except for material and structural analysis IR Thermography can be used with combination of different recording methods for documentation and analysis of paintings as well as historical structures. IR thermography can be used with the combination of close-range photogrammetry for 3D modelling and texturing (Rizzi, Voltolini, Girardi, Gonzo, & Remondino, 2007) (figure 4.6.4) with the combination ultrasonic velocity in order to assess the condition of structural elements in terms of their state of preservation (Kandemir-Yücel et al., 2007), with georadar techniques (Imposa, 2010) for hidden structures, geophysical methods (Carlomagno, Maio, Meola, & Roberti, 2005).

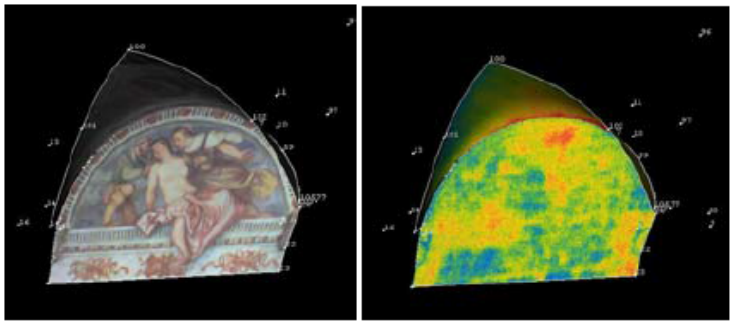

Figure 4.6.4: A detail of the internal courtyard, reconstructed using digital visible images and afterwards textured using also IR data (Rizzi et al., 2007)

4.7. Aerial thermography

Aerial thermography is a remote sensing technique displaying the apparent temperatures of objects in a scene. Infrared radiation was firstly discovered by Sir William Herschel, a German born, British astronomer in 1800. Infrared thermography includes the measurement and visualization of this infrared radiation. The first prototype infrared line-scanner, united with and infrared detector, was developed for military applications in 1946. By the 1960s, the technology was commercially available. During the energy crisis in 1970s infrared thermography ensured suitable visual images of "heat loss" which supported to promote energy conservation[39]. In 1980s analysis software and electrical cooling systems and in 1990s focal plane array[40] instruments were developed (Madding, Orlove, & Kaplan, 2003). Today temperature measurements can be applied by using imaging systems including many pixels. The thermal infrared sensors (TIR) on the market can get fairly small matrices, the largest of which is 640x512 pixels. These values lead limitations in aerial thermography, particularly on flight time.

Except for building heat loss projects, aerial thermography has been used in many commercial applications including thermal profiling of buildings (Mauriello & Froehlich, 2014), brick deck delamination (Ellenberg, Kontsos, Moon, & Bartoli, 2016), dump monitoring(Strakova & Reznicek, 2013) for vegetation monitoring(Berni, Zarco-Tejada, Suarez, & Fereres, 2009), for water stress detection(Zarco-Tejada, González-Dugo, & Berni, 2011), environmental contamination (figure 4.7.1)(Lega et al., 2012) and forensics(Lega & Teta, 2016), energy consumption and identifying potential leaks (Hagman & Lefebvre, 2012), people and animal search and rescue (Hammerseth, 2013), insulation purposes for houses(Allinson, 2007), sensing plant disease in agriculture(Mahlein, Oerke, Steiner, & Dehne, 2012) and for mapping (figure4.7.2) (Turner, Lucieer, & Watson, 2011). Moreover there are developing systems working with the combination of different sensors in order to use in heat loss mapping (Hagman & Lefebvre, 2012).

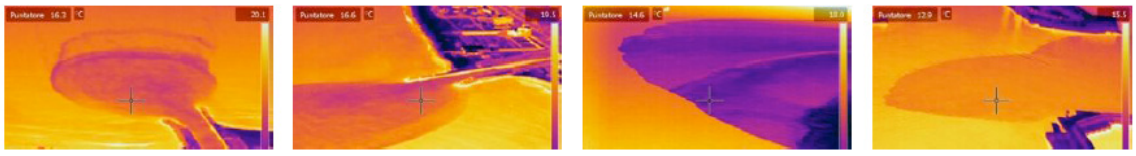

Figure 4.7.1: Example of pattern shapes of mixing zones with particular geometry and thermal profile that permits to suppose a change in material/pollutant concentration (Lega et al., 2012)

Aerial thermography can also be used for detection of subsurface defects in components and samples as non-destructive technique. Typically the component is heated actively or passively and the time-dependent and/or frequency-dependent effects

[39] All instruments of this period had a single detector but rotating mirrors or prisms were used tos can a line or scene. The sensors had to be cooled using compressed gases.

[40] Staring array

on the surface temperature are analyzed to reveal the location and depth of the defect(Allinson, 2007).

Figure 4.7.2(a) Oktokopter multispectral camera (b)Vineyard point cloud (c) Example TIR image of vineyard (Turner, Lucieer, & Watson, 2011)

Infrared sensors typically operate in the short wave (3-5µm) or long wave (8-14µm) portions of the infrared spectrum. The sensor basically converts incoming infrared radiation into an electrical signal. The relationship between the magnitude of this signal and the magnitude of the incoming radiation depends on the type of detector and the optics, filters and electronics that comprise the sensor (Allinson, 2007).
The use of thermography in aeroplanes to produce images of the ground is part of the wider field of remote sensing. This aerial thermography has a number of applications in the literature.

4.8. Aerial Thermography for Archaeology

IR Thermography make possible a fast, non-contact and non-destructive detection of the artifacts. The detection of buried objects using aerial thermography is mainly based on the difference in thermal conductivity between the object and the surrounding environment (soil) and this difference make object possible recognizable mode of emission and called as “thermal signature” of the artefact (Santulli, 2007). Principle factors to be considered in the detection of buried objects using IR thermography can be mainly classified as soil surface temperature (presence of vegetation or soil surface coverage), soil nature (chemical composition), climatic variations (temperature/humidity cycles during day and night), buried object characteristics (geometry, dimension, materials), buried object position (depth and orientation) and thermal excitation such as natural (solar), long pulse (microwave) or short pulse (UV, IR, normal lighting) (Santulli,2007). Several studies have demonstrated that thermography can detect features at or near the ground surface such as pits, ditches and field boundaries as well as buried architectural features up to a half meter below the ground (e.g., Perisset and Tabbagh, 1981; Lunden, 1985; Bellerby et al., 1990).

Archaeological sites consist of different materials such as stone walls, clay floors, organically-enriched middens, stable or removed top soil. Thermal infrared energy is emitted from an object instead of being reflected. The thermal behavior of the material (cooling or heating) makes thermal signals. Several quantities defining the thermal behavior of the target are conductivity, density, emissivity and specific heat. Thermal properties of each material and the subsurface thermal gradient are all relevant. A convenient measure, thermal inertia is proportional to the response of the ground to thermal energy (Giardino and Haley, 2006).

The principle of aerial thermography for archaeology is directly related with fundamental difference between the thermal characteristics of remains above and under the ground. Because of their different composition, content and density, each material emits and reflects different rate thermal radiation. These varieties give opportunity to detect archaeological ruins on and under the ground.

For detection of buried objects, several studies have been done with diverse methods including geo-radar (Lester & Bernold, 2007), electromagnetic induction (Bell, Barrow, & Miller, 2002), electrical impedance tomography (Church, Mcfee, Gagnon, & Wort, 2006), neutron backscattering (Cruz Silva, 2009), gamma rays (Brooks, Buffler, & Allie, 2004), laser-doppler vibrometry (Abe & Sugimoto, 2009) of which each of them has advantages and drawbacks (Santulli, 2007).

Table 4.8.1: Emissivity values of some non-metal materials (values from Infrared-USA.com; www.infrared-thermography.com ; www.omega.com ;www.optotherm.com)

Material	Emissivity
Asphalt	0.95
Red brick	0.93
Lime clay brick	0.43
Glass	0.85
Clay	0.95
Clay tiles	0.33
Cloth	0.95
Copper, polished	0.07
Copper, oxidized	0.87
Black elec tape	0.97
Granite-rough	0.90
Grass	0.98
Ice	0.95- 1.00
Iron, not oxidized	0.05
Iron, oxidized	0.74
Limestone	0.95- 1.00
Paper	0.85- 1.00
Plastic	0.95
Soil, dry	0.92
Soil, wet	0.95
Sand	0.90
Sandstone	0.67
Snow	0.80 to 0.90
Water	0.90- 0.95
Wood	0.80- 0.95
Wood (sawdust)	0.75
Zinc (polished)	0.02

In last years, the detection of buried objects using IR techniques has been widely studied (Balsi & Corcione, 2005; Boras, Malinovec, Stepanic, & Svaic, 2000, 2002; Hadas, Wilner, & Ben-Yosef, 2003; Muscio & Corticelli, 2004; Stepanic, Malivovec, Svaic, & Krstelj, 2004). The use of IR thermography makes possible a fast and non-

contact detection of the artefacts; in particular detection of landmines and buried archaeological artefacts.

As non-destructive technique IR for buried objects system performance mainly depends on three elements: capability of the method (or combination of methods) employed, the state of environment surrounding of the buried object and human factor (skills of the operator) (figure 4.8.1)(Santulli, 2007). Besides, the soil character affect the response of buried object and increase the difficulty for discrimination (Araneo & Celozzi, 2003). In this case, in order to increase the probability of detection and to decrease the probability of false indications, some systems for data fusion or sensor vision are needed according to Müller (2003).

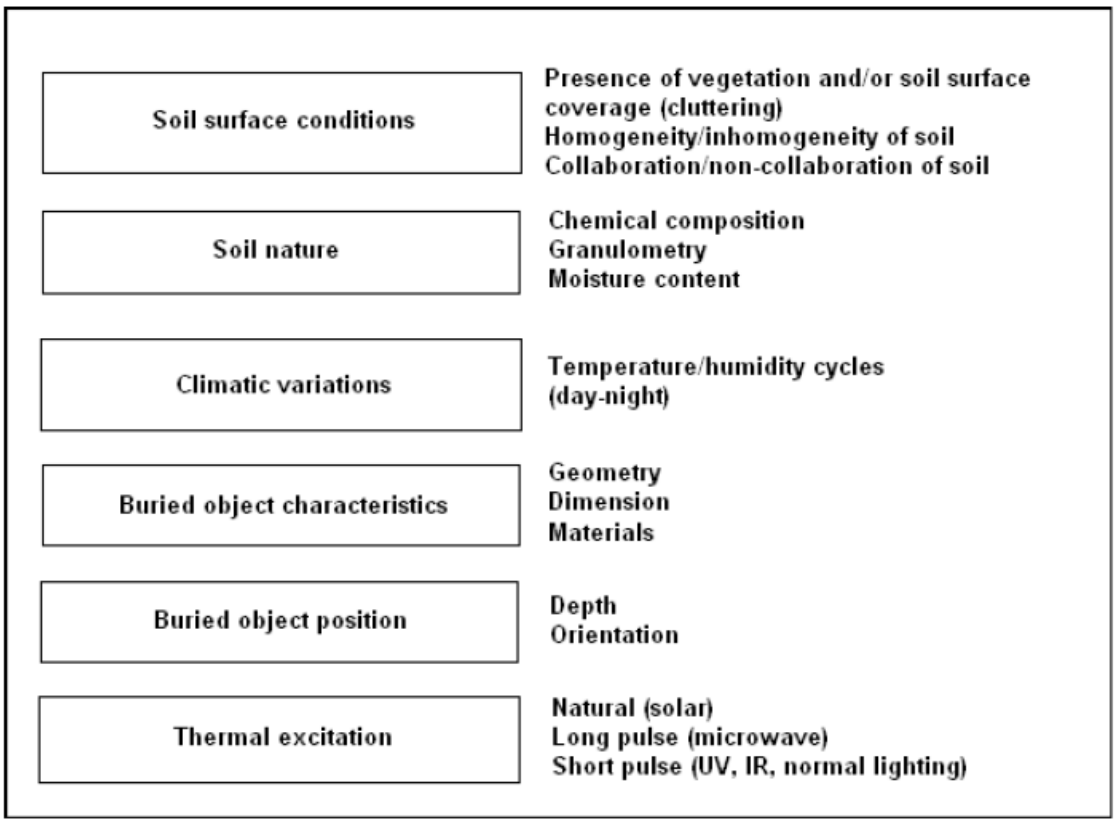

Figure 4.8.1: Principal factors to be considered in the detection of buried objects using IR thermography (Santulli, 2007)

The effects of water and soil density were another thermal prospects studied by Stanjek and Faßbinder (1995). As the soil density increases, the heat capacity increases as well. Stone walls contain less water and higher heat diffusivity and lower heat capacity which means it can be observed strong cooling when the air temperature drops (Stanjek and Faßbinder, 1995). In general, dense materials—stone, packed earth—tend to resist temperature change and retain the day's warmth . Moist areas tend to be cooler owing to the effects of evaporation, temperature variations occur across plant types caused by evapotranspiration, the cooling mechanism of plants, and vegetated surfaces generally are much cooler than bare, open earth (Scollar et al. 1990).

The detection of buried objects using passive thermography is mainly based on the difference in thermal conductivity between the object and the soil which allows

seeing recognizable emission "thermal signature" of the artefact. Another important and key thermal property is the volumetric heat which describes the heat capacity of a material. The relation between volumetric heat and conductivity defines other thermal property called diffusivity (detailed described in section 4.3.2.1). A material with high conductivity and low volumetric heat will have high diffusivity, means that heat travels quickly without being retained (Table 4.8.2). So the material with low conductivity and high volumetric heat will retain more heat. One of the main and mostly referred thermal property thermal inertia defines the material tendency to resist changes in temperature. If a material has high thermal inertia (like water), is heat up and cool down slowly. While the soil heat more quickly in the sun and cool just as fast at night. With the help of this property, estimating the potential strength of anomalies in different context becomes easier (Cool, 2015).

Table 4.8.2: Thermal conductivites of some rocks, environment features and archaeological remains

Geological rocks and objects	**Thermal Conductivity, W / m °C**
Clay	0.25-1.08
Sand	03.-2.95
Limestone	2.0-3.0
Sandstone	2.5-3.2
Dolomite	2.0-4.2
Basalt	2.2-3.5
Gabbro	2.0-2.3
Marble	1.7-1.9
Granite	2.2-3.5
Granodiorite	2.5-3.0
Brick	0.6-1.2
Conglomerate	2.4-2.9
Dry soil	0.3
Woodland soil	0.8
Rock Salt	5.3-7.2
Massive pyrite-polymetallic ore	7-10
Environment features	
Air	0.026 (25 ^{o}C)
Water	0.59 (25 ^{o}C)
Bitumen	0.2
Snow(fresh)	0.1-0.2
Snow(old)	05.-1.8
Ice	2
Archaeological remains	
Wood	0.09-0.14
Isolated cavity	0.05
Ceramics	1.8-2.1
Glass	1.1-1.2
Paper	0.4-0.6
Slag	0.5-1.0
Iron	29.6 (25 ^{o}C)
Gold	317
Lead	35
*****Note: many kinds of archaeological remains are composed from geological rocks and contain environment features***	

Périsset and Tabbagh (1981) set up several experiments on these thermal properties and they designed a software to analyses thermal behaviors of different models. Beside the software, they made experiments with physical models and they compared the results with computer ones. One of their physical experiment was to duh a ditch into a limestone subsoil and bury it in topsoil, buried building materials in sand and in gravel and collected the data with ARIES scanning radiometer. From this experience, they concluded that:

-If the superficial layer increases in thickness or conductivity and decreases in diffusivity, the thermal signature of the feature will reduce.

-Features located in low conductivity and low diffusivity subsoil will have a stronger thermal signature.

Even aerial thermography has been used since the 1970s, archaeologists have recognized that aerial images with recording thermal infrared wavelengths of light (7.5-13 μm) could be a powerful tool for recognizing both surface and subsurface cultural remains after 1970s (Berlin, Ambler, Hevly, & Schaber, 1977). However limitations in technology and cost have prevented the widespread application of aerial thermography in archaeological contexts at the beginning. The use of aircraft or satellite imagery made this method difficult to access due to its cost and lack of flexibility. Beside the high cost of the system, aerial data generally don't provide suitable images for the production of large-scale maps and the relatively high flight altitude is able to detect only large structures not the small ones (Poirier, et al. 2013). Although the thermal images could be acquired by Remote Sensing, the spatial resolution of these images has not enough qualities to reveal archaeological ruins aircraft with TIMS (Thermal Infrared Multispectral Scanner) and advanced sensors (Buck, Sabol, & Gillespie, 2003; Challis, Kincey, & Howard, 2009; Sever & Wagner, 1991). Moreover, some restrictions related to aircraft motor and height doesn't always permit to fly over the area. Likewise, sometimes archeological areas are in remote areas which prevent to fly over the site.

Aerial thermography is mainly dependent on temperature response of buried objects. In theory, modelling the temperature response of a buried object requires the knowledge of equation for turbulent heat flux which can be bi-dimensional or mono-dimensional model in a soil assumed dry and homogeneous (Moukalled, Ghaddar, Kabbani, Khalid, & Fawaz, 2006). In practice, modelling of buried object geometry requires evaluating thermal inertia in the soil above the object. Thermal inertia I is defined as:

$$I= (k\rho C)^{1/2}$$

Where k is the bulk thermal conductivity, ρ is the bulk density and C is the specific heat capacity. In order to evaluation of thermal inertia, the measurement of the content moisture and chemicals in the soil are required since they affect the value of ρ. However the variations of soil characteristics are not so much critical for object recognition. The measurement of soil heat flux and infrared radiation temperature permits to evaluate thermal inertia (Sun, Zhu, Tang, Su, & Zhang, 2000).

How an archaeological target behave thermally can get by considering thermal inertia values (Table 4.8.3). In the morning, as the sun's heat is focused on the ground, a subsurface feature may be detected as a positive or negative anomaly. A feature that enhances drying would be visible as a positive anomaly in the morning and a negative anomaly in the evening. While a feature that traps moisture results in a negative anomaly in the morning since moisture effectively lowers the thermal inertia. In the evening, this situation reverses since the thermal gradient will be from the ground to the atmosphere. Archaeological features may be detected with thermal prospecting only if the physical properties of the feature differ enough to cause a visible contrast in the imagery (Giardino and Haley, 2006). To maximize archaeological visibility, thermal imagery has to be collected at a time of day when the contrast in thermal inertia is highest between the archaeological target and the background soil and ground cover. Besides, the entirety of the survey area must be covered with as little temporal variability as possible in order to reduce drift in thermal values across a single mosaicked scene (Casana, 2014). Experimental data from the 1970s show that in some cases the ability of early morning thermal imagery to reveal micro-relief can be used to extensively map archaeological remains (Scollar et al., 1990). Related to thermal inertia, the potential strength of thermal anomalies depends on the relative thermal inertias of the archaeological feature and surrounding subsoil in which it is embedded. Because of their different thermal inertia, archaeological features display different thermal properties. So thermography application should be conducted when the temperature of materials are still adjusting and differences are at their maximum (Cool, 2015).

Table 4.8.3: Thermal inertia of some materials (Giardino and Haley, 2006).

Material	Thermal Inertia (P)
Basalt	0.053
Clay soil (moist)	0.042
Granite	0.056
Gravel	0.033
Limestone	0.045
Marble	0.0056
Obsidian	0.035
Quartzite	0.074
Sandstone	0.075
Sandy gravel	0.050
Sandy soil	0.024
Serpentine	0.059
Shale	0.041
Slate	0.049
Water	0.036

Another parameter to be considered is the presence of vegetation since it affects the soil heat capacity. Besides, moisture should be mentioned as other factor effecting thermal survey. Even though higher moisture facilitates buried object detection, at higher depths it is required a longer cooling phase. Although several studies have indicated that thermography can detect features at or near the ground surface up to half meter below the ground (Bellerby, Noel, & Branigan, 1990), the depth still remains as

main factor for good results. Researches show that it's quite difficult to acquire archaeological thermal data in situation where the area is covered with dense vegetation and/or deeply buried. It should be mentioned that the time of the performance is another significant factor. Experimental studies in literature prove that in order to get satisfactory results, IR thermography should be performed in absence of sunlight or in case thermal contrast owed to solar irradiation is negligible for the detection of buried objects (Santulli, 2007). Furthermore in order to maximize archaeological visibility, thermal imagery has to be collected in time when the contrast in thermal inertia is highest between the archaeological surface and the background soil and ground cover. Normally, the night time is considered as the best time for performing aerial thermography since at night, the ground surface temperature is more directly dependent on the thermal characteristics of the ground. During the night, vegetation creates a very strong signature, as the water in trees and plants tends to retain heat much more readily than the dry desert soils. Investigators could, for example, exploit diurnal and seasonal differences in the appearance of archaeological features to enhance their visibility or determine their depth. Similarly, the differential thermal properties of vegetation could be used to indirectly detect archaeological features, as could the subtle topographic relief that is recorded in early morning thermal imagery (Cool, 2015). However this situation is more valid for calm and clear nights. Also Scollar et al. (1990) emphasized the role of vegetation in thermal imaging. Dead or inactive plants have poor heat conduction, instead the temperature of living plants is regulated by transpiration, not by the surface they grow. The vegetation hide the thermal behavior of subsurface features. However some subsurface features like stone walls impede the growth of roots and plants.

Another way to minimize the effect of heterogeneous surface is to perform in clear weather during the early morning (Lunden, 1985). Also diurnal and seasonal differences enhance the visibility of archaeological remains and helps to determine the depth of the ruins(Casana, Kantner, Wiewel, & Cothren, 2014). Buried ruins under the ground influence the drainage capacity of the ground. As mentioned before, water content is the most important factor for the thermal behavior of the ground. For satisfied results, differences in infiltration in the ground should produce temperature differences at the surface of the ground at certain times.

According to Lunden (1985), a suitable time for registration is spring time when the surface of the ground is drying out and the fields are without crops. Besides the ground is warming up in the spring and the higher thermal inertia appears in soil profile so it strengthen the temperature anomalies (Lunden, 1985). Additionally, the surveyed area must have as little as possible temporal variability to reduce drift in thermal values in for mosaicked scene (Casana et al., 2014).

Although today it is possible to find high resolution thermal cameras (up to 640x512 pixels), thermal cameras still have low resolution compared to color light cameras. In this case, to maximize the camera's view and have better results, reducing the altitude during aerial survey could be a solution. Increasing the altitude of UAV will reduce the image resolution while the increase the speed of UAV result in an excessive number of blurred images (Casana et al., 2014). The target size also another important issue for aerial thermographic survey. The targets should be made of material with low

thermal emissivity such as aluminum or plastic so they can appear dark (cold) on thermal image.

According to Périsset and Tabbagh (1981) experiments, the ideal time for thermal imaging is during the period of change, generally two or three days after a reversal heat flux, when the temperature difference between features is at maximum. Périsset and Tabbagh (1981) also focused on several thermal properties which helps to understand the behavior of heat in soil as described detailed in section 4.3.2.1. Depending on these thermal properties, the temperature difference between the target and its surrounding is directly related with heat flux which refers rate and direction of travel of heat. When its considered the soil, while the soil is warming, heat is traveling to the ground means there is a positive heat flux. Oppositely, when the soil is cooling, heat is travelling into the air and heat flux becomes negative. The larger heat flux value (in positive or in negative direction), the faster the change is happening. Slow transient heal flux variation determines when an anomaly will be at its most visible. It means that, during a week of warm weather all materilas have become heated, then following week of cold weather materilas with low thermal inertia will cool quickly while materials with high thermal inertia will remain warm (Cool, 2015). Kwamme (2004) states that since the sun heats the ground surface, making it difficult to detect temperature contrasts between various features, thermal imaging tends to be most productive before sunrise and after sunset. Although the surface cools rapidly after sunset, evening images tend to better show near-surface temperature contrasts affected by the day's sunshine while pre-sunrise images made after a full night of cooling tend to better reveal deeper thermal variations. (Kwamme, 2004).

Except from Périsset and Tabbagh (1981) studies, Scollar et al. 1990, assumed that deeply buried features may not be directly affected by diurnal flux and seasonal heat flux changes are not useful for archaeological prospection since the surface changes during the year by vegetation, humidity, plowing, heat flux crate so much noise that anomalies are hidden (Scollar et al. 1990). Besides according to Scollar et al. 1990, if the surface layer is composed of homogenous material, it uniformly dampen the thermal responses of any underground features. In this case as Périsset and Tabbagh (1981) stated that a thick surface layer or a layer with low diffusivity decrease the strength of anomalies. Scollar et al. declared that these parameters impede the visibility of anomalies. If the surface layer is heterogonous means if there are human agricultural and construction activities or archaeological materials or etc., thery are mostly affected by diurnal variations and they are most visible in the afternoon. Depending on these observations, Scollar et al. (1990) defined the appropriate time to carry out a thermal survey as,

-to make measurements in without cloud weather to record anomalies due to micro relief

-to take readings during the morning so the effects of diurnal variation on surface heteregonues do not hide deeper weak anomalies. In this case a flight in the first half of the night could be useful

-to fly after a sufficiently well-marked long variation in transient flux.

Today with the developments in UAV and thermal sensors, UAV can be an alternative for aerial thermal imaging in order to detect buried archaeological objects.

5. CASE STUDIES

5.1. Hotel Harzburger Hof, Badharzbourg,Germany

5.1.1 Introduction and aim of the study

Architectural heritage documentation is an activitiy which requires getting information from different sources for complete and comprehensive analysis. It involves huge multimedia data containing different information. Eventhough traditional survey methods are still important and useful in some cases; technological possibilities have given oppurtunity to support digital technologies. In this case, choosing the appropriate technology, procedure and workflow is always a challenging and depends on the size, complexity and the level of required accuracy of the project (Patias et al., 2008). Beside different innovative systems such as Terrestrial Laser Scanning in architectural documentation field, also UAVs have become one of the most promising techniques. Their capability of data acquisition with high resolution, considerable potential in terms of accuracy, cost and ability have allowed them to be used in several applications in architectural documentation process scuh as 3D documentation, monitoring and recording.

In some cases, it becomes quite difficult to have a complete data for architectural object. In these cases only one method would not be enough. It can be get terrestrial data with traditional methods, topography, photogrammetry or terrestrial laser scanning, how ever aerial data may be lack. Even the aerial techniques can be an optimal solution in the case of medium-sized and large sites, since the possibility of raising sensors and capturing the information, in many cases it is rather difficult to obtain data at ground level, which can increase the performance of photogrammetry. But these surveys generally require working with large scales and high resolutions. As result, conventional aerial photogrammetric surveys can be unfeasible because of the limited site extent, the large scale required, the expected low flight height, speed of the aircraft and the relatively high cost of the technique. In the last years relatively low-cost Unmanned Aerial Vehicles (UAVs) have become popular for rapid and accurate documentation of cultural heritage. They have been started to be used in order to get missing aerial data especially if the heritage is under risk, or it’s difficult and dangerous to reach the top of the heritage;

The aim of this study is to research the potentials of UAVs for architectural documentation of cultural heritage with required scale for inacessible and dangerous areas. The study presents preliminary results in which the capabilities of this technique in architectural documentation. The main goal was to make an accuracy assesstment of the values and the orthophoto and to see if the accuracy is enough for desired scale architectural documentation project.

5.1.2. Harzbourgher Hof Hotel, Bad Harzburg

Harzburger Hof is an old Hotel in Bad Harzburg, Germany. It was built as Deluxe Hotel with casino on 1874 and it had an honorable reputation and was considered a s a top adreess in the wellness-hiking city. However, the quality of the substance was significantly reduced in the 1990s, with the changing og the owner of the hotels. And the necessary modernization work was not carried out totally, it was done only partially which was not enough for the hotel. For a number of years, the building had a reputation as a senior citizen's residence. By the time, due to the water problems in the foundation, water entered to the playroom so that the casino couldn't open for long periods of time and thus deacy began. And it was the victim of fire three times in the past. In Spetember 2013, it burned starting from the second and third floor. The connection to the casino collapsed with creating a big hole. In 21 May 2014 the building was badly destroyed because of a great fire. The upper three storeys of the wooden building were completely destroyed (http://www.haz.de/Nachrichten/Der-Norden/Uebersicht/Der-Abstieg-eines-Prunk-Hotels-Der-Harzburger-Hof-in-Bad-Harzburg;
http://www.ndr.de/nachrichten/niedersachsen/braunschweig_harz_goettingen/Harzburger-Hof-Verschwindet-der-Schandfleck; http://www.rottenplaces.de/main/harzburger-hof-6886/)

Figure 5.1.1: Harzburger Hof Hotel fire (http://mittenmang-bs.blogspot.com.tr/2014/05/harzburger-hof-1874-2014-in-memoriam.html)

Figure 5.1.2 (a)Fire on the roof(www.noz.de) (b)View from the roof (www.nordharz-portal.de)

The building is planned to be renovated and reused as hotel in the future. In order to draw of the project, an architectural firm needed the survey of the roof for survey project. For this, we made survey of the roof with UAV.

Figure 5.1.3: Harzburger Hof Hotel, 2014 (http://www.rottenplaces.de/main/harzburger-hof-6886/)

Figure 5.1.4: Harzburger Hof Hotel, 2014 (http://www.rottenplaces.de/main/harzburger-hof-6886/)

5.1.3. Methodology

For aerial image processing Agisoft PhotoScan 1.1.5 was used for image processing. Agisoft PhotoScan is an image-based 3D modelling solution aimed at creating professional quality 3D content from still images. The adopted workflow for the processing of the UAV images of Harzburger Hof Hotel is given in Figure 5.1.5 below.

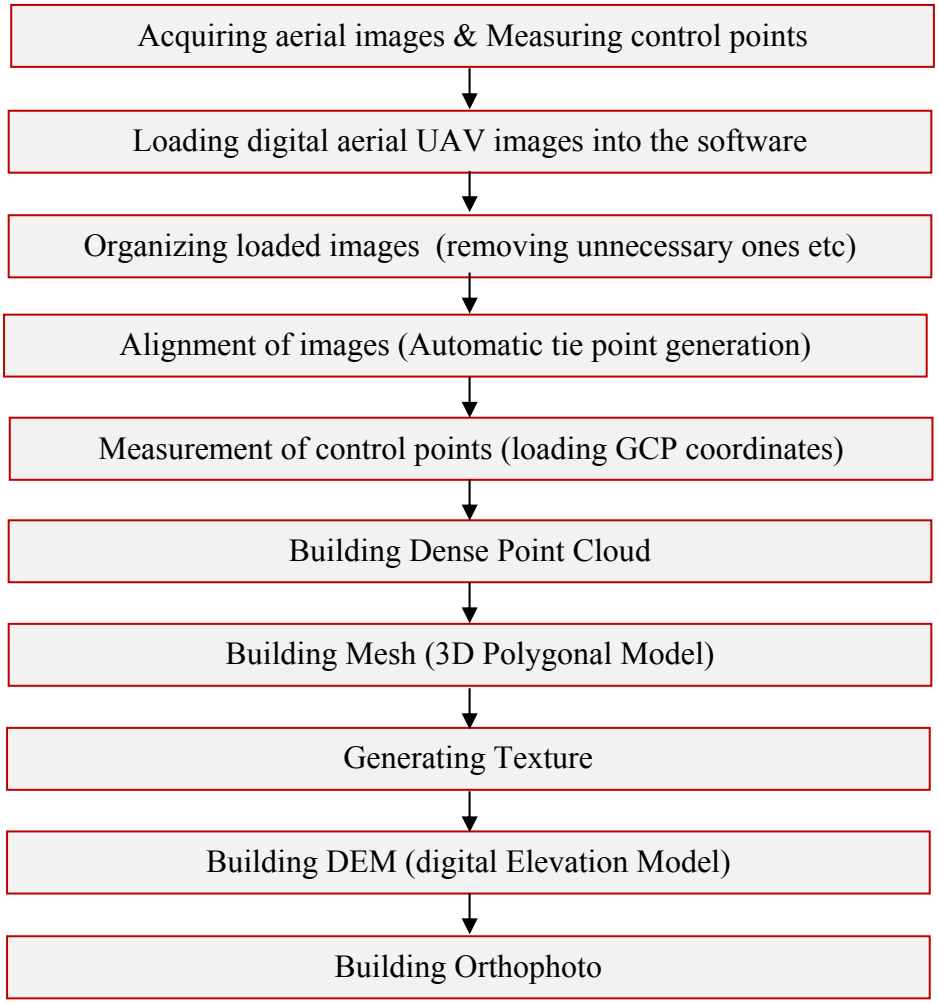

Figure 5.1.5: Workflow of UAV images processing for Harzburger Hof Hotel

5.1.4.Field Work

In the field survey, 6 ground contorl points were arranged a part of the area and they were measured with GPS (figure 5.1.6).

In 2014, during the aerial survey of Harzburger Hof Hotel, the UAV system which is a prototype Quadcopter based on a DJI F450 frame produced by

GRAVIONIC[41]. The system is equipped with Canon IXUS 220HS 12MP camera calibrated before (Figure 5.1.8). The electronic equipment includes APM2.6 autopilot with external GPS and magnetometer. For the flight, Mission Planner 1.3.7. software was used for managing flight path (Figure 5.1.7)

Figure 5.1.6: Measurement of control points and GCP with GPS

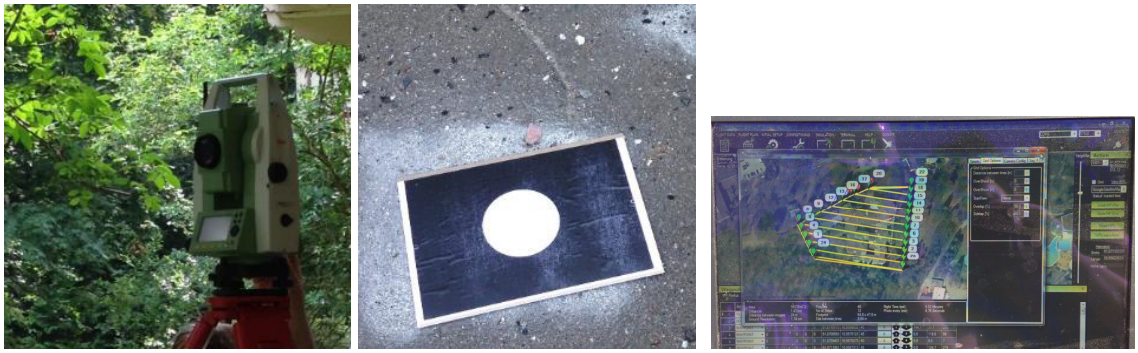

Figure 5.1.7: Leica TS09 Total Station (left), ground control points (A4 size) (middle), Mission planner software

The flight planning was done in the area. The area was approximately 10.178 m². The distance between images 24m and the ground resolution was set 1,74 cm. The number of strips were 12 and the footprint was 64,6 x 47,6 m while the distance between lines was 9,04m and the photo was taken in each 4,76 seconds. Overlap was %50 and sidelap was %86 and the flight height was 43.25 meters (table 5.1)

[41] GRAVIONIC- German Geo Services- was founded in 2007 as a spin off of the Institute of Flight Guidance and Control (IFF) of the Technical University of Braunschweig, Germany. http://www.gravionic.com/

Figure 5.1.8: Quatcopter by GRAVIONIC (left) and CANON IXUS 220 HS (right)

Table 5.1.1: Technical Parameters of quatcopter and camera

Technical Parameters Quatrocopter by GRAVIONIC	
Type	Quadcopter
Dimensions	1.03 m between opposite rotor shafts
Wieght (incl. supplied camera&battery)	2.65 kg approx.(depends on configuration)
Recommended payload mass	0.80 kg
Maximum payload mass	1.25 kg
Maximum take-off weight	5.55 kg
Cruising speed	15 m/s
Max climb rate	7,5 m/s
Wind resistance	Steady pictures up to 6 m/s
Maximum flight time	Up to 45 minutes (depends on payload and wind)
Fligth radius	Minimum 500 m using radiocontrol, with waypoints up to 40 m
Ceiling altitude	Up to 1,000 m
Take-off altitude	Up to 4,000 m about sea level
Autopilot&control	IMU, magnometer, barometer&GPS/GNSS
Operating temperature	-10 to 50 ℃
Humidity	Max %90
Integrated payload – CANON IXUS 220 HS	
Main camera	
Still images resolution	12.1 MP resolution
Resolution	7152x5368
Focal length	35 mm
Digital zoom	5x

5.1.5. Data Processing

After the setting of project parameters (described in section 5.1.3.), the images were taken by quatrocopter drone described ins ection 5.1.3. For this project 210 images were used. After alignment of the images, we had sparse point cloud model with 119.198 points in high accuracy and disabled pair selection parameters with tie point limit[42] was 1.000 (while recommended value is 4000) (figure 5.9).

[42] Tie point limit parameter allows to optimize performance fort he task and doesn't generally effect the quality of further model. Recommended value in the software is 4000. Too high or too low tie point limit value may casue some parts of the dense point cloud model to be missed.

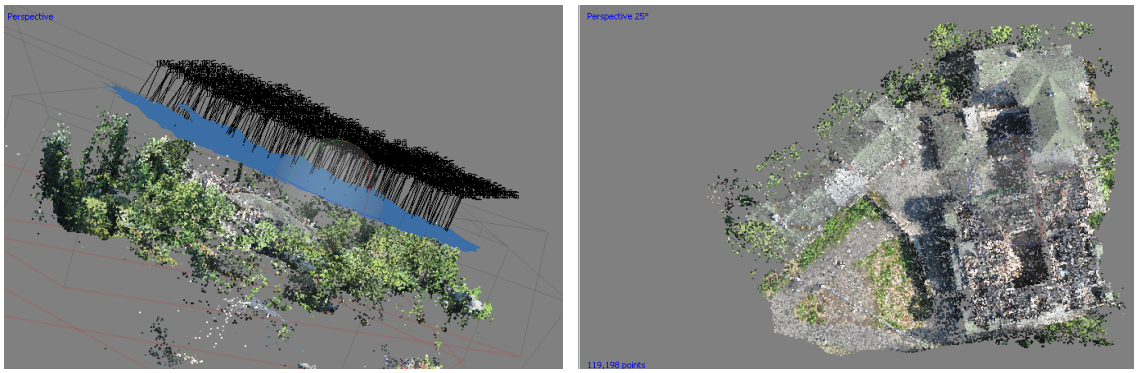

Figure 5.1.9: Image alignment and camera positions (left), sparse point cloud model with 119,198 points after image alignment (right)

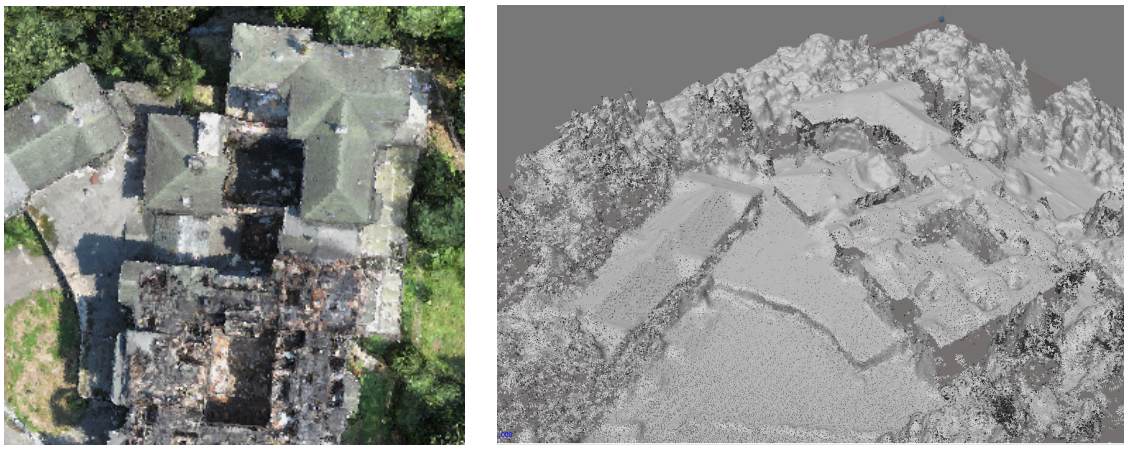

Figure 5.1.10: Dense point cloud data (left) and dense point cloud classes in Photoscan (right)

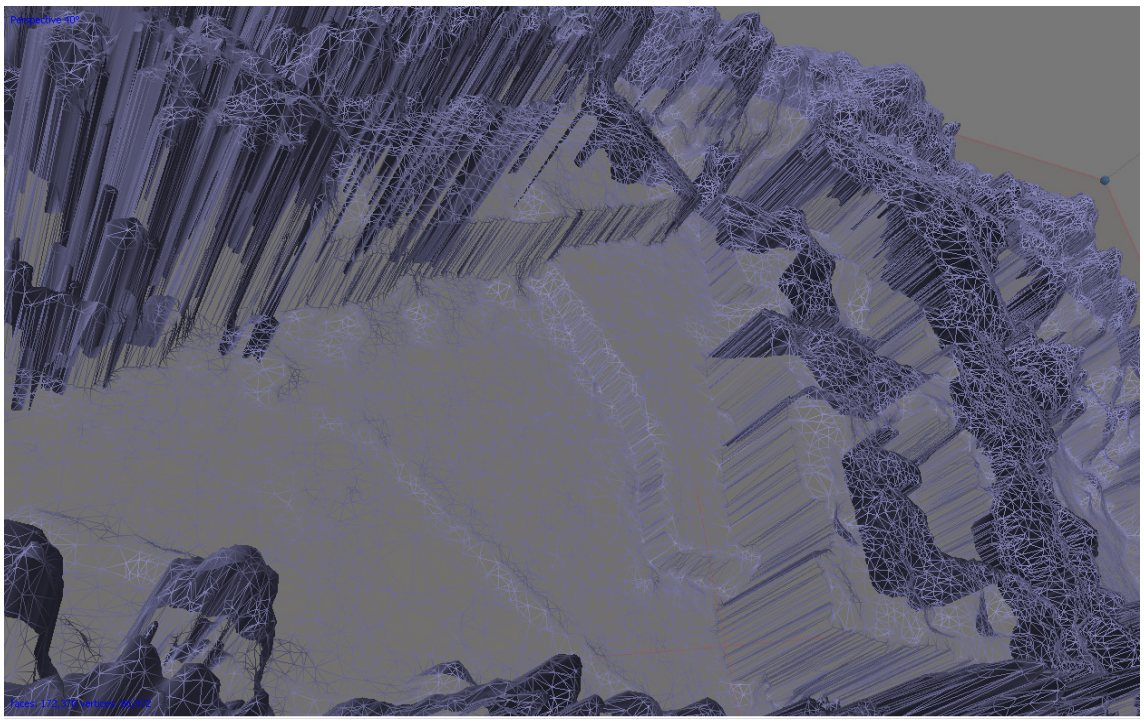

Figure 5.1.11: Detail of frame model

Figure 5.1.12: Detail of textured model

Figure 5.1.13: Dense point cloud with texture

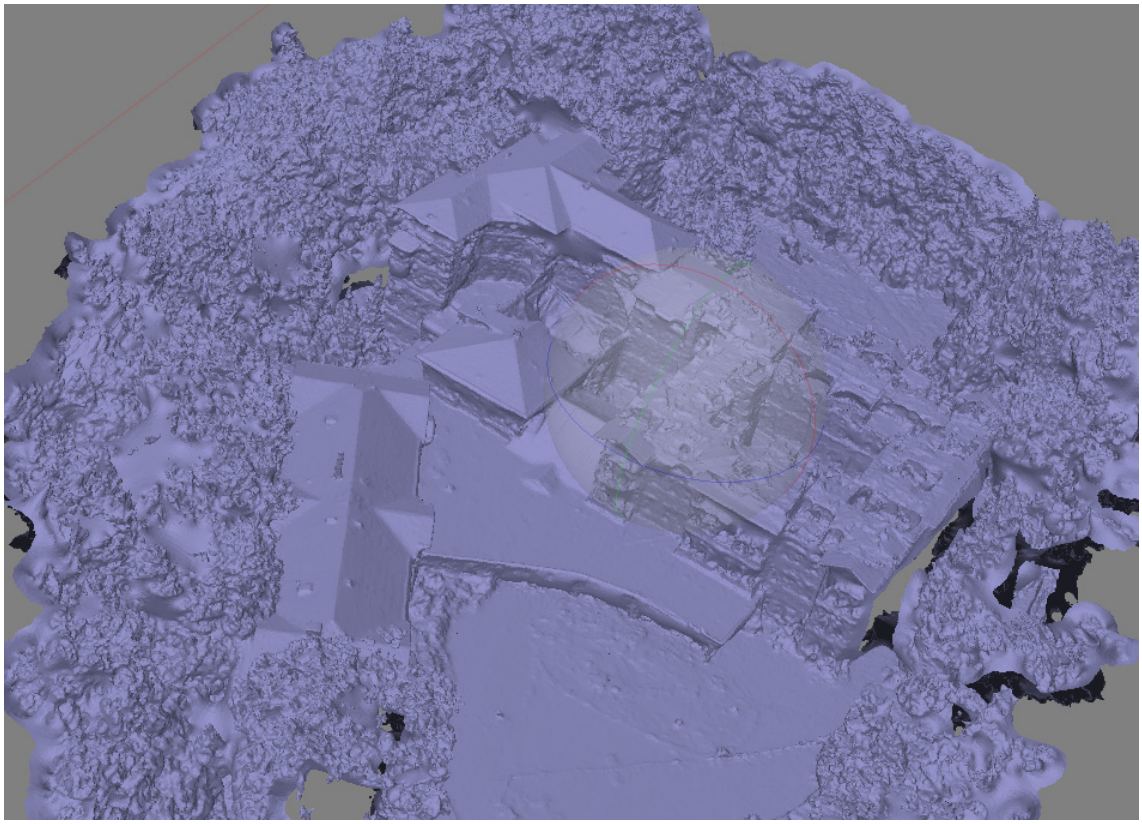

Figure 5.1.14: Mesh model with 172,370 face and 86,972 vertexes

Figure 5.1.15: Textured model details from the roof

5.1.6. Results and discussion

The use of UAVs for cultural heritage documentation has increasing interest in last decades. Beside documentation, they have been preferable for modelling, mapping and monitoring purposes as well. The other potentials of them such as their cost, flexibility, high resolution made them a strong alternative. Especially for the risky areas such as this case study, they have become a good solution.

In this work, the mini UAV system quadcopter produced by GRAVIONIC was used for aerial data acquisition. The data was processed in Agisoft Photoscan 1.1.5 build version. The results were satisfied for us. Since it was possible to reach only two floors of the building, GCPs were organized around the building (Figure 5.1.16-17). There were also some other control points on the surface of the building however they were not used for the processing. All field work was done in 1 day and project processing and all parameters are shown in table 5.1.2 below.

The case study presented in this paper is only the first results of the documentation of a historical building. It was a kind of experience to see the potentials of UAVs in order to get detailed documentation for especially inaccessible areas or dangerous/risky places. The use of UAV platforms can be an optimal solution for these kinds of places. Besides, they can be efficiently used to generate orthophotos and 3D models with or without texture.

Generated orthophoto has 1.3503 cm/px ground resolution with 0.94 px error and 19662x17251 px size. The details were seen in the roof and the orthophoto was suitable to draw a survey project in scale of 1:50. The areas with deformation were visible on the roof. So,b it could be exported to CAD file to prepare 2D survey project. The generated Digital Elevation Model was in 0.216048 m/px resolution and 21.4239 points per sqm point density. The main difficulty was on the walls and vertical surfaces. Because of the wind, there are some parts with deformation. The other difficult part was the modelling of the trees. It was enough to put them in 2D project however for 3D modelling and in height there were missing parts.

Table 5.1.2: Project parameters

Project parameters	
Flight Height	43.25 m
Ground resolution	0.013503 m/px
Coverage area	0.0463079 sq/km²
Sidelap	%86
Overlap	%50
Number of strips	12
Number of images	210
Number of GCP	6
Aligned cameras	209
Coordinate System	DHDN / 3- degree Gauss-Kruger zone 4 (EPSG::31468)
Dense point cloud points	861,008
Tie points	119,198
Projections	458,804
Reprojection error	0.940818 px
Faces	172,370
Vertices	86,972
Orthomosaic size	19662x17251 px

This study aimed to get data of the roof of the building. The next step for this study could be to combine this data with TLS data for a complete documentation. Besides, UAV system could be used to get also vertical images of the façades.

Figure 5.1.16: Location of GCPs

Label	X error (m)	Y error (m)	Z error (m)	Error (m)	Projections	Error (pix)
1	-0.000598	0.012122	0.013847	0.018413	54	0.313309
10	0.041477	-0.001152	-0.009054	0.042470	26	0.738818
2	-0.002753	0.003114	-0.002521	0.004861	35	0.342735
3	0.008567	-0.009910	-0.004116	0.013731	33	0.374147
4	-0.000797	-0.027301	-0.011187	0.029515	31	0.194430
9	-0.046049	0.023228	0.013267	0.053254	12	0.328548
Total	**0.025570**	**0.016026**	**0.009985**	**0.031786**	**191**	**0.400857**

Figure 5.1.17: GCPs RMSE in Agisoft Photoscan

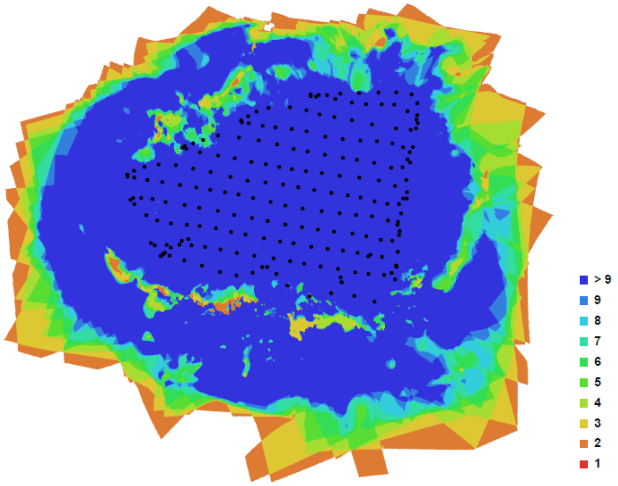

Canon IXUS 220 HS Camera Calibration Parameters			
Resolution	4000x3000	F	2828.01
Type	Frame	B1	0.340109
Cx	5.63841	B2	0.322671
Cy	33.518	P1	0.00131651
K1	-0.0365912	P2	0.00198238
K2	0.0190306	P3	0
K3	-0.00408081	P4	0
K4	0		

Figure 5.1.18: Camera locations and image overlap in Agisoft Photoscan (left) and camera calibration parameters (right)

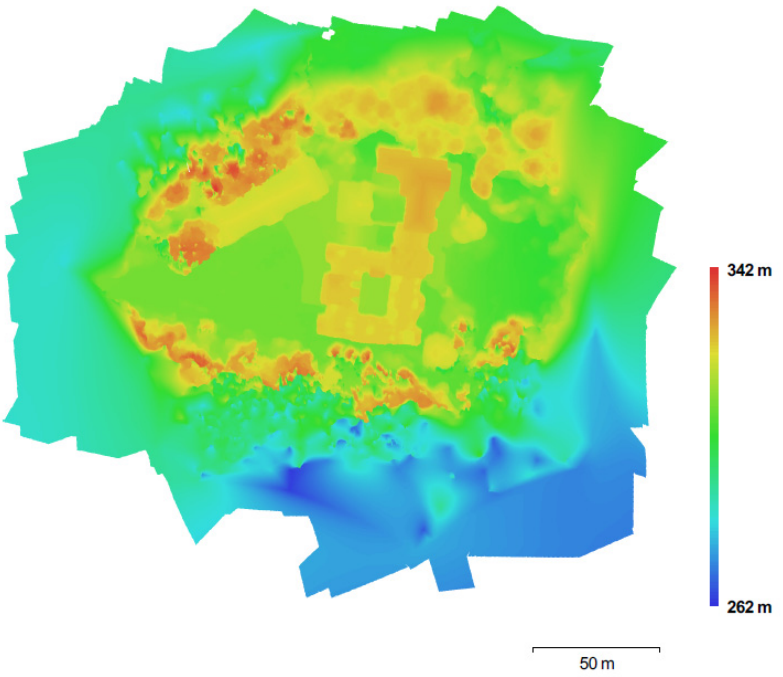

Figure 5.1.19: Digital Elevation Model (DEM) in resolution 0.216048 m/px and 21.4239 points per sqm point density

Figure 5.1.20: Orthophoto with 1,3503 cm ground resolution and 19662x17251 px

Figure 5.1.21: Details from orthophoto

5.2. Kubad-Abad Palace, Beysehir, Turkey

5.2.1. Introduction and aim of study

For large archaeological sites close range photogrammetry and terrestrial laser scanning are not always the most suitable survey techniques; whereas, the information obtained from aerial or satellite images provide an overview of the study area, which is fundamental for the interpretation of archaeological structures. In fact, images obtained by metric aerial cameras (film and digital) or by high resolution satellite sensors have been used in archaeology for long time (Cowley, 2010). It should be pointed out that such images have some limitations linked to the geometric resolution inadequate for detailed studies, to the periods of acquisition (which does not always correspond to a given particularly useful date for the purposes of the archaeological work) and ultimately to the cost (Lo Brutto et al., 2012). Besides, another main objection of these methods is the difficulty involved in acquiring reliable radiometric information of the complete surveyed area, which can easily be obtained by means of traditional aerial photogrammetric flights. However, the costs of aerial photogrammetry are usually too high in relation to the limited extension of the surveyed areas. Moreover, the flight altitudes of aircraft equipped with aerial photogrammetric cameras are not able to supply suitable images to produce large-scale maps (higher than 1:500) and the flight of motor aircraft over archaeological sites is often forbidden. Another problem is that the sites that have to be surveyed are sometimes in remote areas (Chiabrando, Nex, Piatti, & Rinaudo, 2011). Even the aerial techniques can be an optimal solution in the case of medium-sized and large sites, since the possibility of raising sensors and capturing the information, in many cases it is rather difficult to obtain data at ground level, which can increase the performance of photogrammetry. Any conventional photogrammetric project can fit to that block geometry even in the case of cartographic surveys at limited archaeological sites. But these surveys generally require working with large scales and high resolutions. As a result, conventional airborne photogrammetric surveys can be unfeasible because of the limited site extent, the large scale required, the expected low flight height, speed of the aircraft and the relatively high cost of the technique (Mozas-Calvache et al., 2012). The use of alternative techniques based on close range photogrammetry and laser scanning from light and low height platforms can be a solution for these problems (Gomez-Lahoz & Gonzalez-Aguilera, 2009; Lasaponara, Coluzzi, Gizzi, & Masini, 2010; Mozas-Calvache et al., 2012).

UAVs have been used for large scale purposes such as mapping (Everaerts, 2008; Sofia Udin & Ahmad, 2012), mapping of plateau (Tianyun, Xiaocheng, Defang, Yonghe, & Hongliang, 2015), mapping of coastal areas (Darwin, Ahmad, & Zainon, 2014) and mapping for archaeological areas (Bendea, Chiabrandao, Giulio Tonolo, & Marenchino, 2007)

In this study a practical application of a UAV system was used for large scale mapping of an archaeological area in Beyşehir town of Konya.It was taken as an example to demonstrate the feasibility of UAV data processing for archaeological area large-scale mapping.

5.2.2. Kubad-Abad Palace, Beyşehir

Kubad-Abad Palace is a complex mentioned by the famous Saljuk historian Ibn Bibi (Figure 5.2.1). It was constructed upon the order of Aleaddin Keykubad I (1120-1236)[43] which was established as the summer residence of Sultan in the Anatolian Seljuk period and is the only Seljuk palace survived today. The palace lies on the south-west of Lake Beyşehir (Figure 5.2.2), west of Konya and located 3 km north of the town of Gölkaya. The location of the palace was found by the Konya Museum Director Zeki Oral in 1949, after the refers[44] abouth the location. The first excavations started in 1965-1966 by Katharina Ottodorn, in 1967 by Mehmet Önder. From 1980, the excavations continue by a team of archaeologist under the direction of Prof. Rüçhan Arık.

Figure5.2.1:Kubadabad Palace and Beyşehir

Figure 5.2.2: Beyşehir in google earth

[43] There are no structures remaining in the palace that bear inscriptions relating to construction. It is dated according to the testimony of the famous traveller Ibn Bibi, dendrochronological tests performed on wooden fragments retrieved from the ruins, and the style of tiles.

[44] Ibrahim Hakkı Konyalı and after him Prof. Dr. Osman Turan pointed out that the palace should be around Beyşehir.

The palace consists of various structures mainly including Great Palace on the north side of the site and the small palace on the south of it, a boat house on the shore of the lake and small pavilions surrounding it, the walls of an inner courtyard and other ruined structure of which the functions have not been known yet (Figure 5.2.4). The Great Palace in size of 50 m x 35 m is the largest building of the complex and consists of three main sections: a palace building, a courtyard and a terrace extending to the lake. The Small Palace has also similar plan with thicker and more regular walls. Both buildings have the plan is of large and small rooms on either side of an axis determined by an *iwan*[45] once used as the throne room and the forecourt. The structures were constructed with rubble stone (Arık, 2000; Daş, 2017).

Beside the structure, the palace is significantly famous with its tiles decorating the walls of structure (Figure 5.2.3). Most of these tiles are star or square shaped mostly with traditional colour turquoise and in dimension of 20x24 cm. They are decorated with figurative motifs in lustre or underglaze techniques. The influence of Central Asian traditions is felt in decoration compositions[46]. Typical tiles are white, eight-pointed stars and have delicate figural paintings of humans and animals, including some of the best in Anatolian Seljuk representational art. Painted with an underglaze in turquoise, green, purple, and blue, these figural tiles are set on a background of cruciform-shaped turquoise tiles with arabesque motifs in black (Arık, 2000).

Figure 5.2.3: Some tiles from Kubad Abad Palace excavations, in Konya Kratay Museum

[45] An iwan is a rectangular hall or space, usually vaulted, walled on three sides, with one end entirely open.
[46] The Sultan and courtiers are shown in sitting cross-legged.

Figure 5.2.4: Kubadabad Palace on Google Earth

5.2.3. Methodology

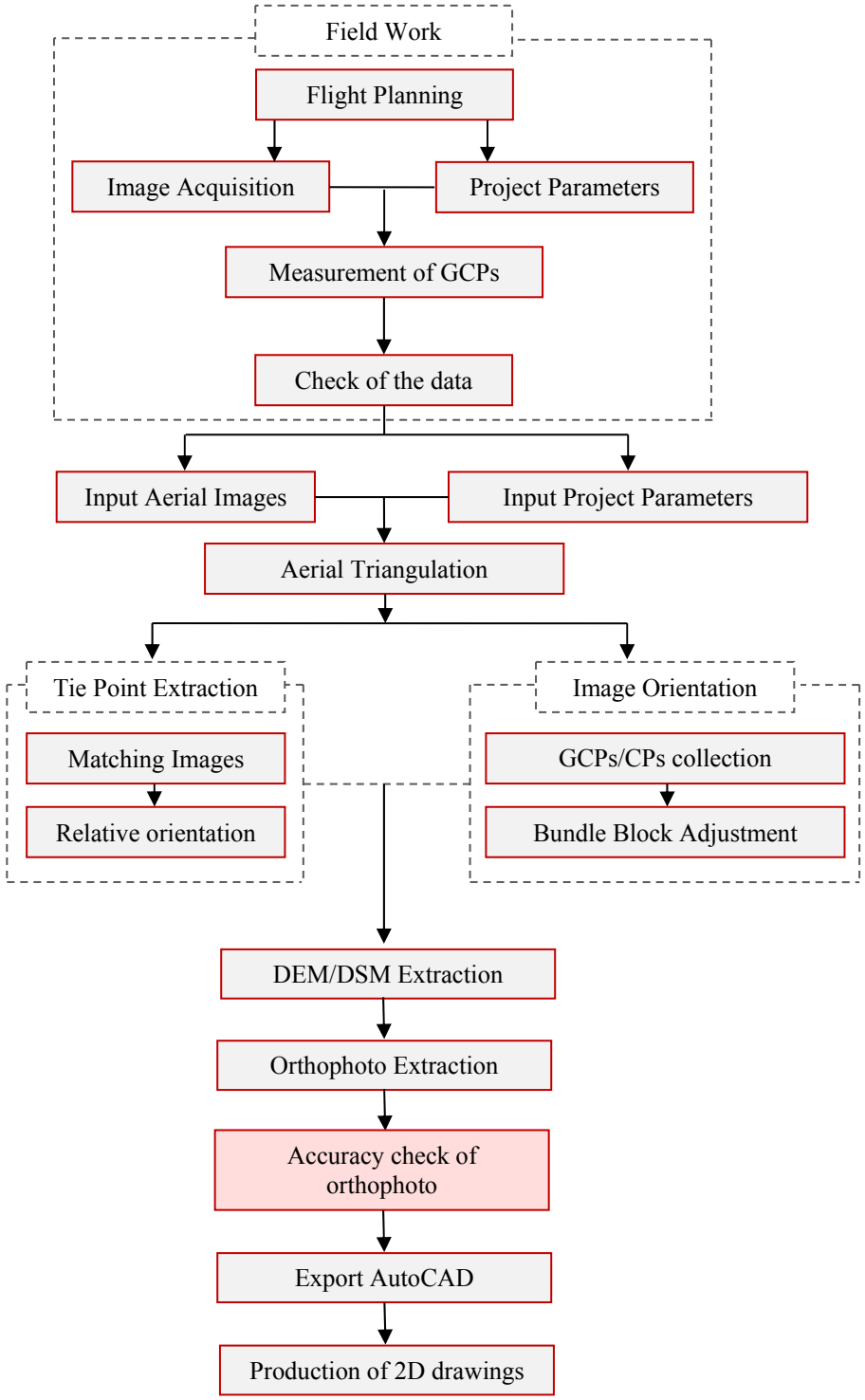

Figure 5.2.5:Methodology of the study

5.2.4. Field Work

UAV for aerial data

In order to get aerial data Smartplanes Freya fixed-wing UAV was used which is 1.2 m span, covered EPP wing, molded polycarbonate fuselage. It is 1.1.-1.5 kg with 50 min.-1.40 min flight time. It has different flight modes suc as auto, assisted and manual and wind rating 13 m/s with payload capacity between 200-600 gr (Figure 5.2.6).

Figure 5.2.6:Smartplanes Freya UAV(http://smartplanes.se/) (left); Ricoh GR camera (right)

For image acquisition Ricoh GR16.1 MP compact camera with 18.3 mm lens. Was used. Image resolution was 4928x3264 in 4.78 x 4.78 µm.

Table 5.2.1:Technical parameters of Smartplanes Freya UAV and Ricoh GR camera

Technical Parameters of Smartplanes Freya UAV	
Type	Fixed wing aircraft
Dimensions	1.2 m span
Wieght (incl. supplied camera&battery)	1.2 kg
Motor	1electric motor
Radio link range	868 MHz, 900 MHz up to 6 km
Max wind	13 m/s
Max cruise speed	16 m/s
Maximum flight time	50 min. – 1 h 40 min.
Autopilot&control	IMU, magnometer, barometer&GPS/GNSS
Operating temperature	-20 to 40 ℃
Integrated payload RICOH GR	
Main camera	
Still images resolution	16.1 MP resolution
Resolution	4928x3264
Focal length	18.3 mm
Pixel size	4.78 X 4.78 µm
GSD (Ground sample distance)	1-20 cm / px (depend on flight height)

In the field, totally 14 GCPs were measured with GPS RTK. The flight was carried out in autonomus mode with a trained pilot. Since archeological area was asked to survey with surrounding, the flight height was calculated according to the area size. The flight height was 159 m. The flight trajectory and the image acquisition points were calculated depending on the scale, camera parameters, flight height, dimension of the

area and the overlap. For the flight trajectory Ground Control Station software was used. At the end of field work, 903 images were taken in mainly 30 strips in 2 flight time. In the first flight 435 photos were taken, while in the second flight 468 photos were taken. Image acquisition overlap was %60 and sidelap was %80. Flight mission was completed in 1 part since the duration of the UAV was enough to complete the area.

5.2.5. Data Processing

In this study, for aerial image processing PhotoScan 1.1.5 was used. Image alignment was carried out with 373 cameras and 14 GCPs. The coordinate system of the project was selected TUREF / TM 33 (EPSG::5255). The images was aligned with 68,572 tie points and 14 GCPs (Figure 5.2.7-8).

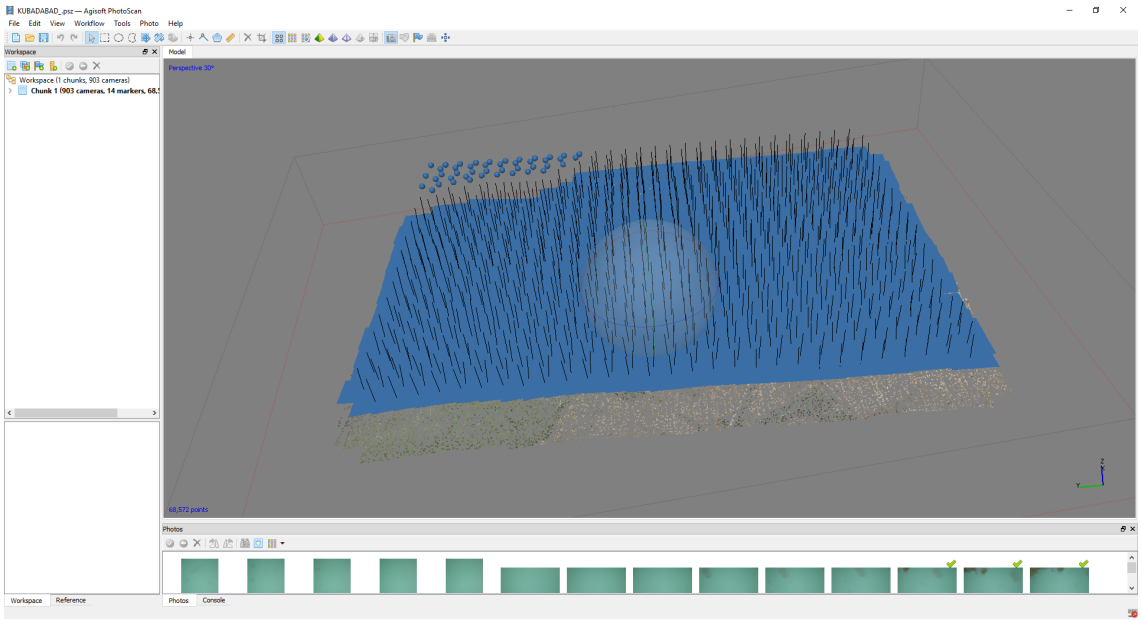

Figure 5.2.7: Camera positions in Agisoft PhotoScan

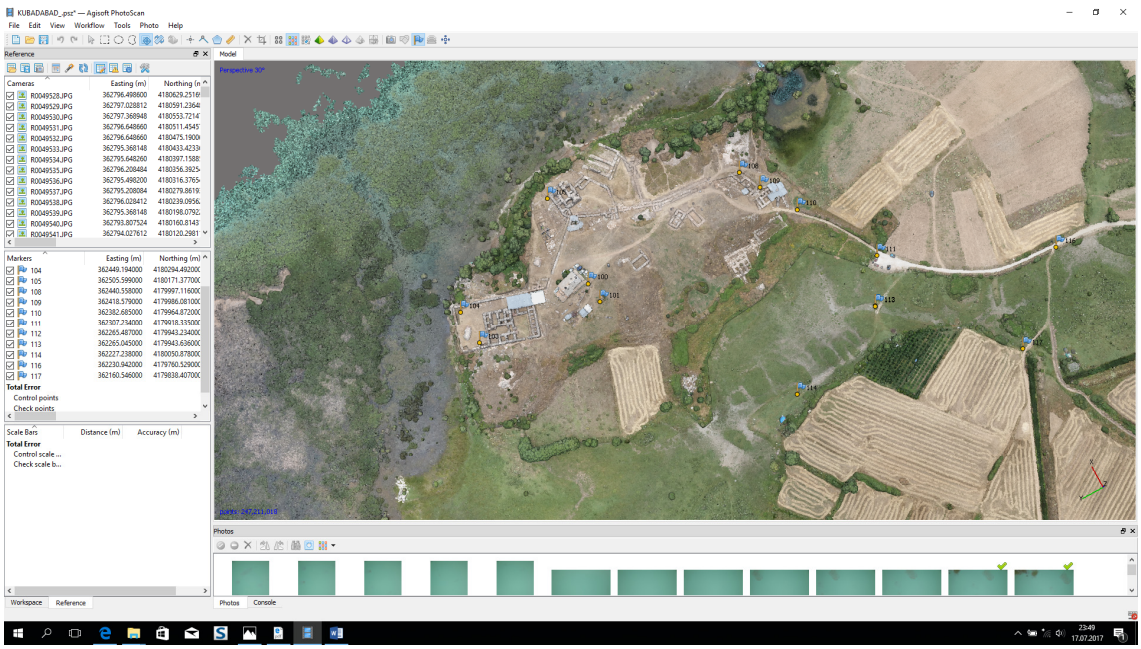

Figure 5.2.8: GCPs positions and in Agisoft PhotoScan

At the end of image alignment, total error was 0.061943 m for GCPs and 0.324 pixel (Figure 5.2.9).

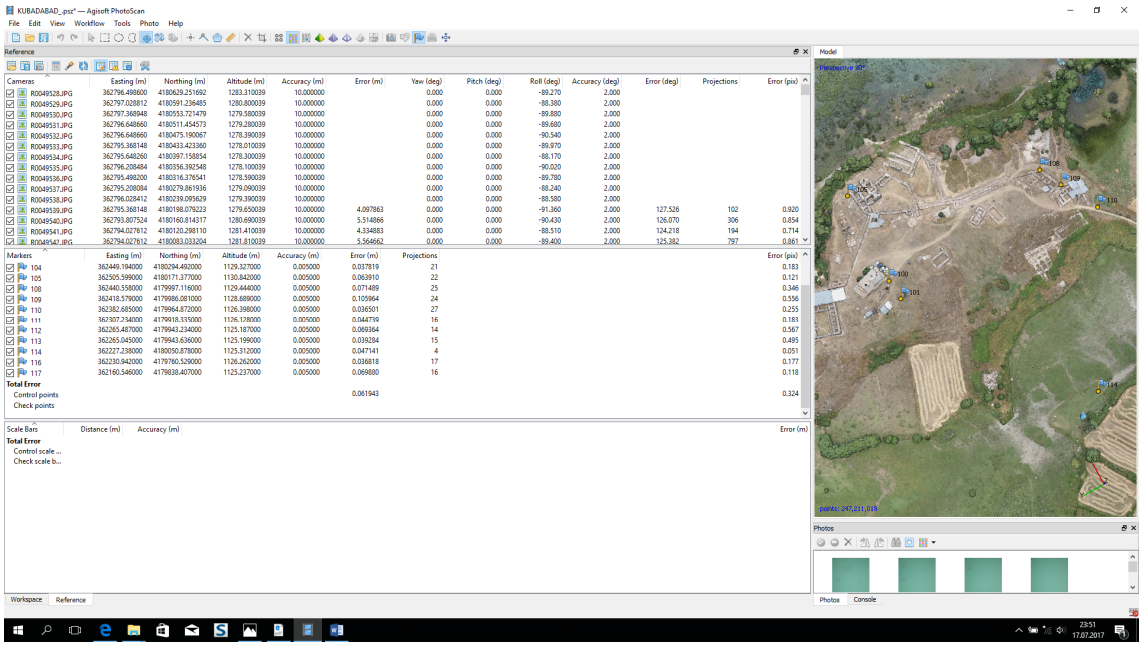

Figure 5.2.9: Camera positions and erros (on the top) and GCPs positions and erros (below).

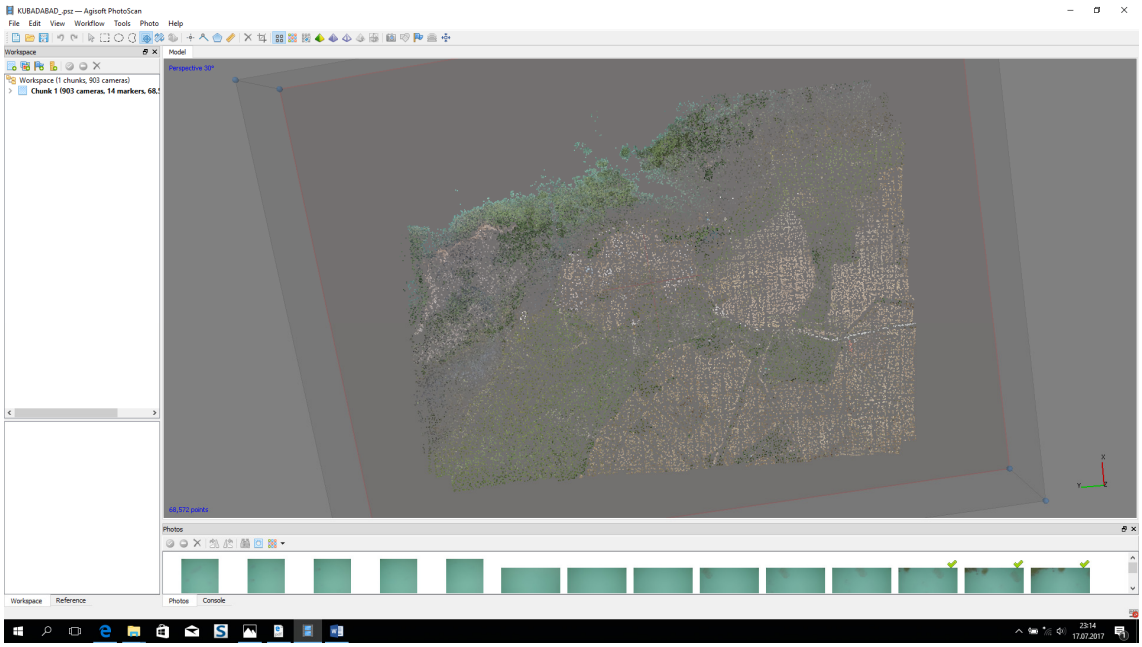

Figure 5.2.10: Point cloud model with tie points in Agisoft PhotoScan

Then dense point cloud model was created in high quality parameter. After the process dense point cloud model had 247,211,018 points. (Figure 5.2.11)

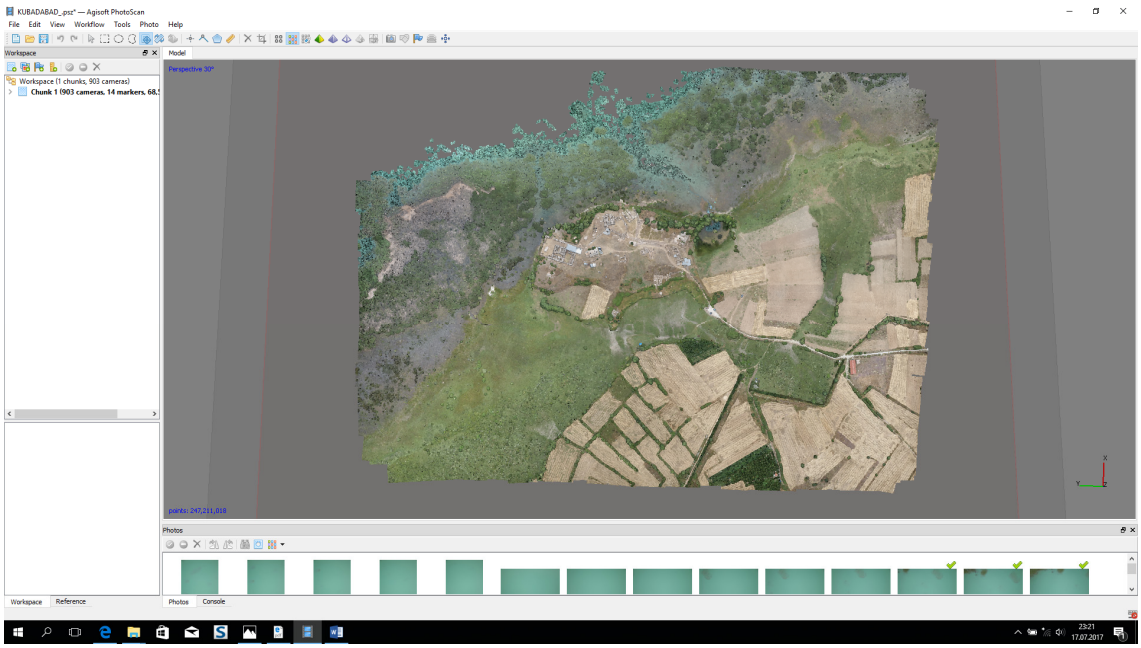

Figure 5.2.11: Dense point cloud model with 247,211,018 points

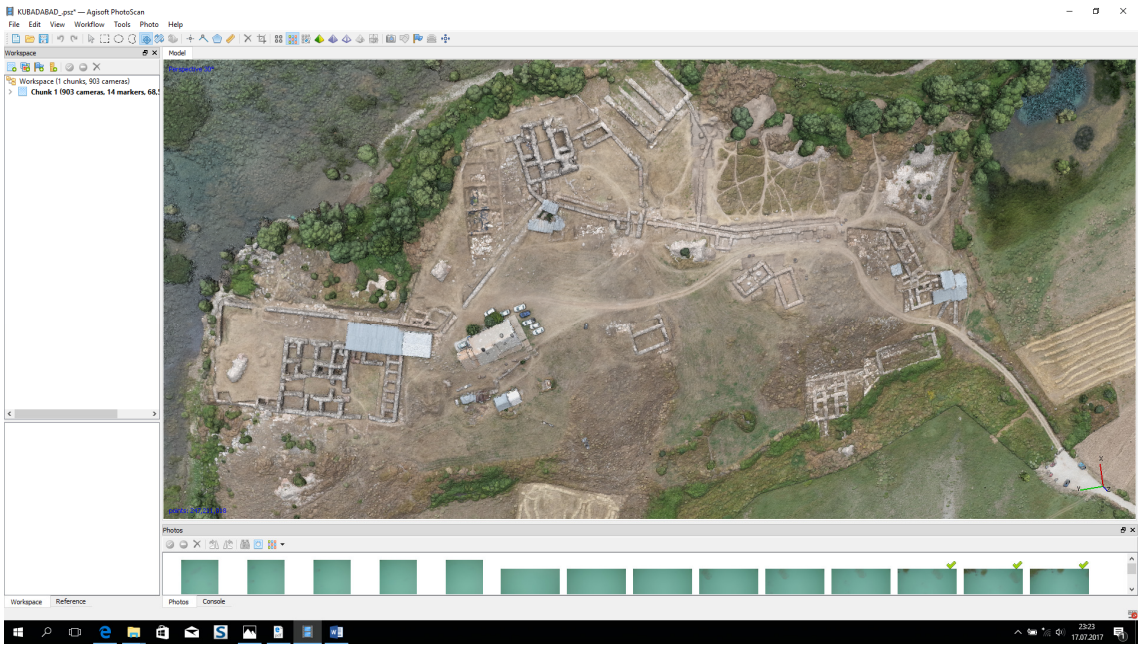

Figure 5.2.12: A part of dense point cloud model with 247,211,018 points

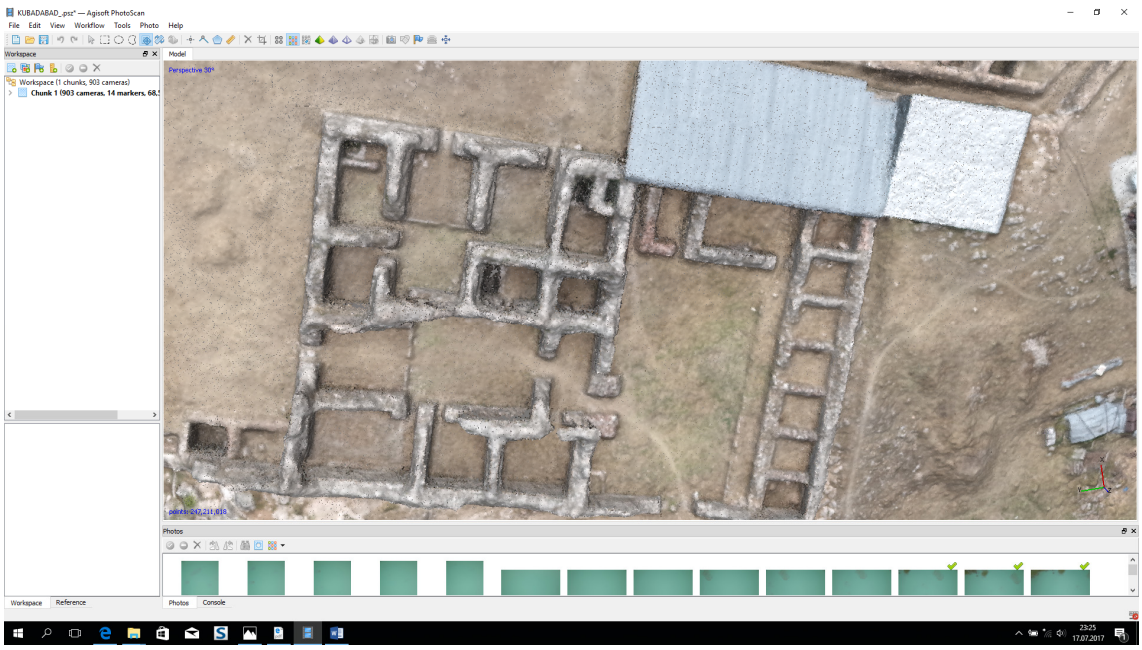

Figure 5.2.13: Detail of Grand Palace in dense point cloud model

After the dense point cloud model, mesh model was processed and at the end it was acquired 49,813,987 faces and 24,715,739 vertices mesh (Figure 5.2.14).

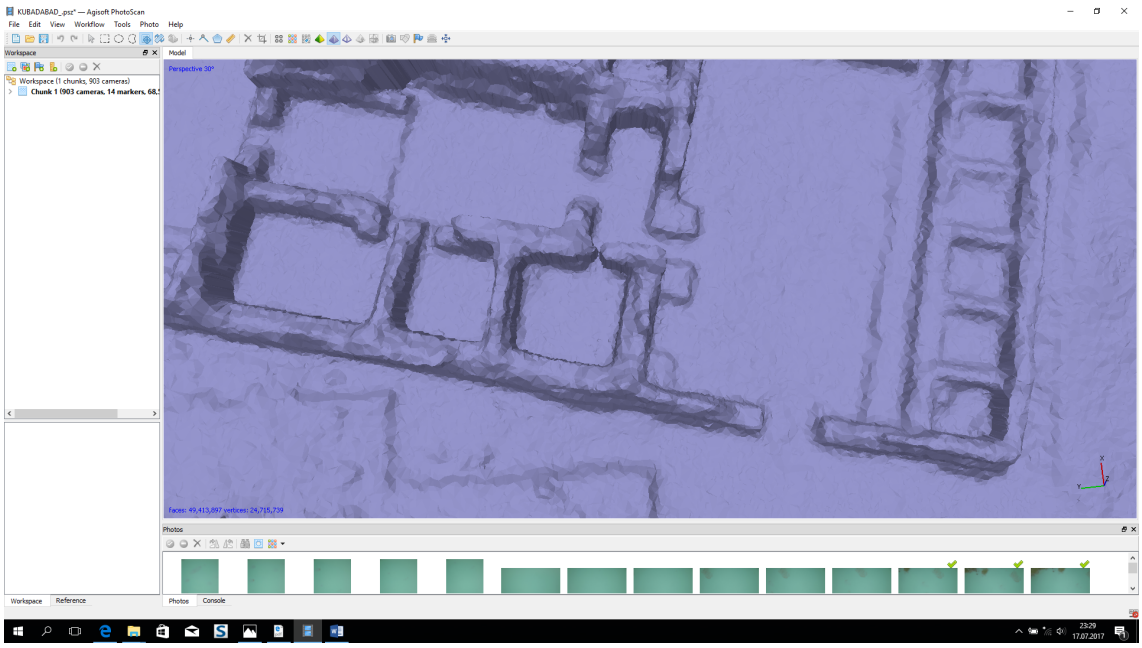

Figure 5.2.14: Detail from a part of Grand Palace in mesh model

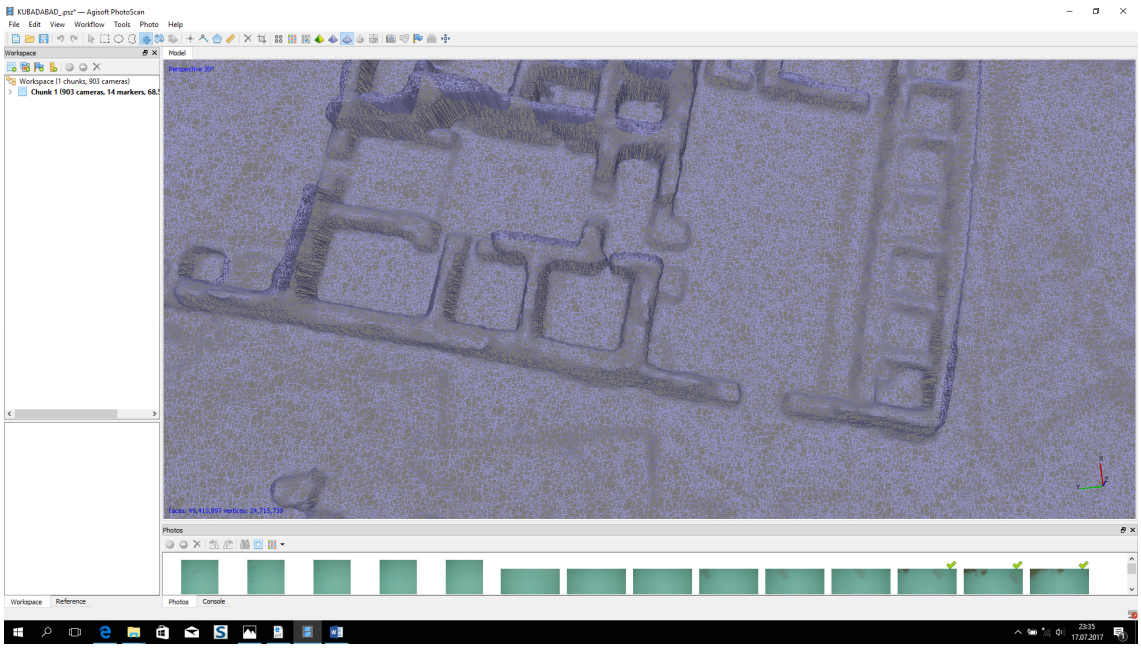

Figure 5.2.15: Detail from a part of Grand Palace in frame model

5.2.6.Results and discussion

Based on this study, the digital aerial imagery of Smartplanes UAV can be used of r large scale mapping of archaeological areas. The obtained data was satisfied in terms of accuracy and resolution. All field work was done in 1 day and project processing and all parameters are shown in table 5.2.2. below.

1.22 km² area was covered with 3.77 cm/px ground resolution and with 0.772 px reprojection error with Richor GR camera (Table 5.2.2.). Because of the nice weather and high stability of UAV, camera locations were quite stabile on archaeological area. There were just some deformation of camera locations on the north west part of the area for a couple of centers. The camera locations error was 0.961439 m in X, 3.34197 m in Y, 4.76581 in Z and totally 5.89967m (Table 5.2.2). Camera calibration parametrs are given in table 5.2.3.

Table 5.2.2: Project parameters

Project parameters	
Flight Height	159 m
Ground resolution	3.77 cm/px
Coverage area	1.22 km²
Sidelap	%80
Overlap	%60
Number of strips	30
Number of images	903
Number of GCP	14
Aligned cameras	859
Coordinate System	TUREF / TM 33 (EPSG::5255)
Dense point cloud points	247,211,018
Tie points	68,572
Projections	611,032
Reprojection error	0.772 px
RMS reprojection error	0.324 px
Faces	49,413,897
Vertices	24,715,739
DEM resolution	7.55 cm/px
Orthomosaic size	26,390x35,636

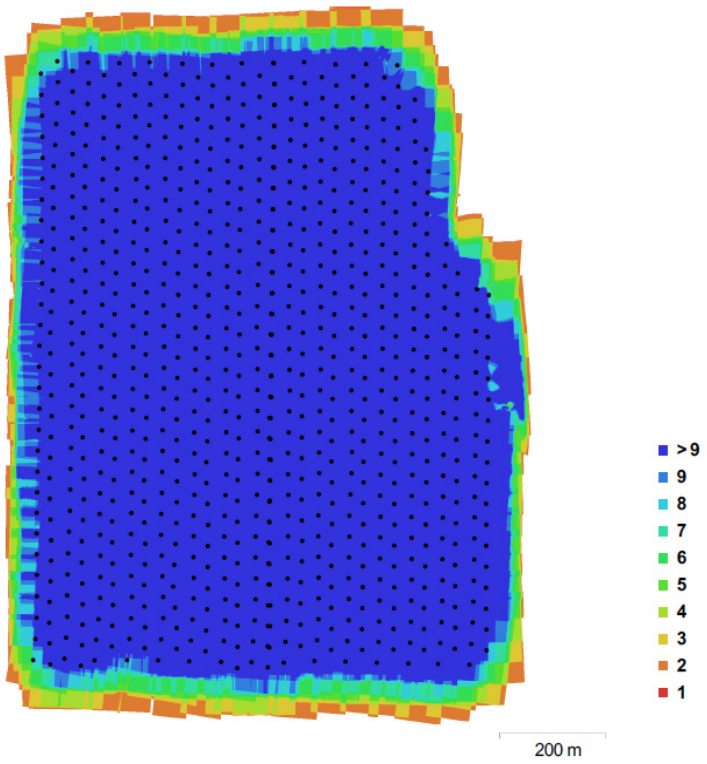

Figure 5.2.16: Camera locations and image overlap in Agisoft Photoscan

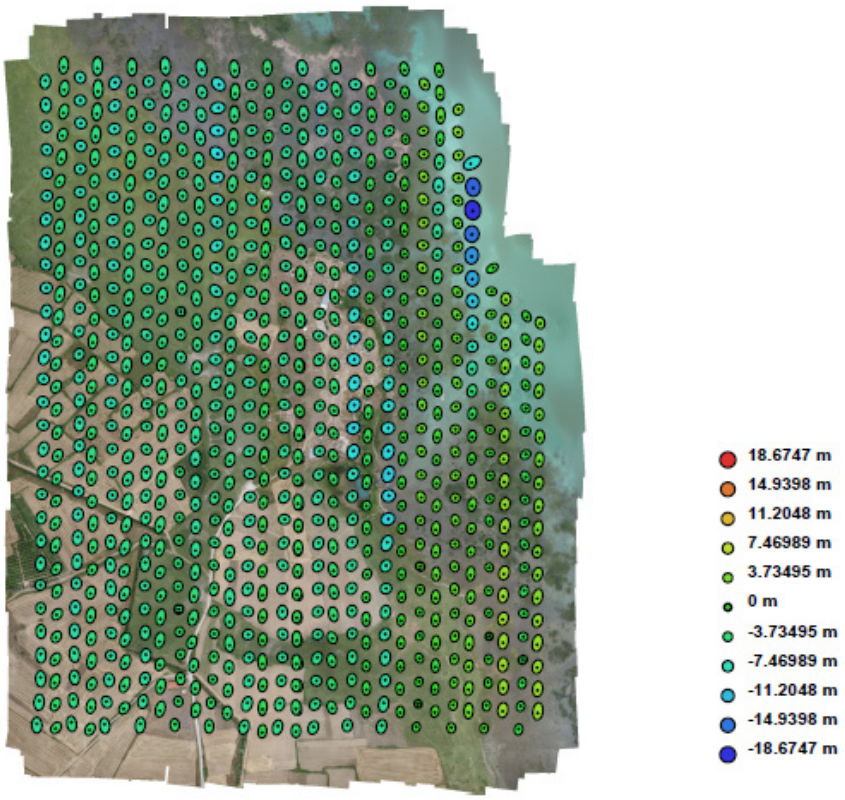

X error (m)	Y error (m)	Z error (m)	XY error (m)	Total error (m)
0.961439	3.34197	4.76581	3.47752	5.89967

Figure 5.2.17: Camera locations and error estimates. Z error is represented by ellipse color. X,Y errors are represented by ellipse shape. Estimated camera locations are marked with a black dot.
Table5.2.3: Camera calibration parameters

Richor GR 18.3 mm Camera Calibration Parameters			
Resolution	4928x3264	F	3872.84
Type	Frame	B1	0.441328
Cx	-6.25894	B2	2.37701
Cy	11.7735	P1	-0.000308219
K1	-0.0723221	P2	2.6913e-05
K2	0.091206	P3	0
K3	-0.0196215	P4	0
K4	0		

14 GCPs RMSE values were in 4.06257 cm in X, 3.32436 cm in Y, 3.28841 cm in Z and in total 6.19432 cm and 0.324 px (Figure 5.2.18)

Figure 5.2.18: GCPs locations

Count	X error (cm)	Y error (cm)	Z error (cm)	XY error (cm)	Total (cm)	Image (pix)
14	4.06257	3.32436	3.28841	5.24937	6.19432	0.324

Figure 5.2.19: GCPs RMSE values in total

Label	X error (cm)	Y error (cm)	Z error (cm)	Total (cm)	Image (pix)
100	6.11981	5.95244	-1.88219	8.74221	0.269 (23)
101	4.45511	-2.77318	3.11042	6.10027	0.310 (24)
103	-4.27609	-1.04231	-2.03174	4.84761	0.266 (18)
104	-3.38464	-1.1302	1.253	3.78194	0.183 (21)
105	3.75177	-5.17337	-0.0764271	6.39103	0.121 (22)
108	-0.994673	2.90823	6.45443	7.1489	0.346 (25)
109	-8.0377	3.28298	-6.07461	10.5964	0.556 (24)
110	2.599	-2.00871	-1.59175	3.65012	0.255 (27)
111	2.75833	1.93097	2.94591	4.47386	0.183 (16)
112	-3.95106	2.24095	-5.24227	6.93643	0.567 (14)
113	2.49822	-1.3361	2.72138	3.92839	0.495 (15)
114	-1.66697	4.1478	-1.49671	4.71415	0.051 (4)
116	-3.39311	-0.623031	-1.28622	3.68181	0.177 (17)
117	3.72089	-5.57416	1.97885	6.988	0.118 (16)
Total	**4.06257**	**3.32436**	**3.28841**	**6.19432**	**0.324**

Figure 5.2.20: GCPs RMSE values

Reconstructed DEM model resolution was also satisfied. The resolution of DEM was 7.55 cm/px and point density of the model was 176 points/m² (Figure 5.2.21)

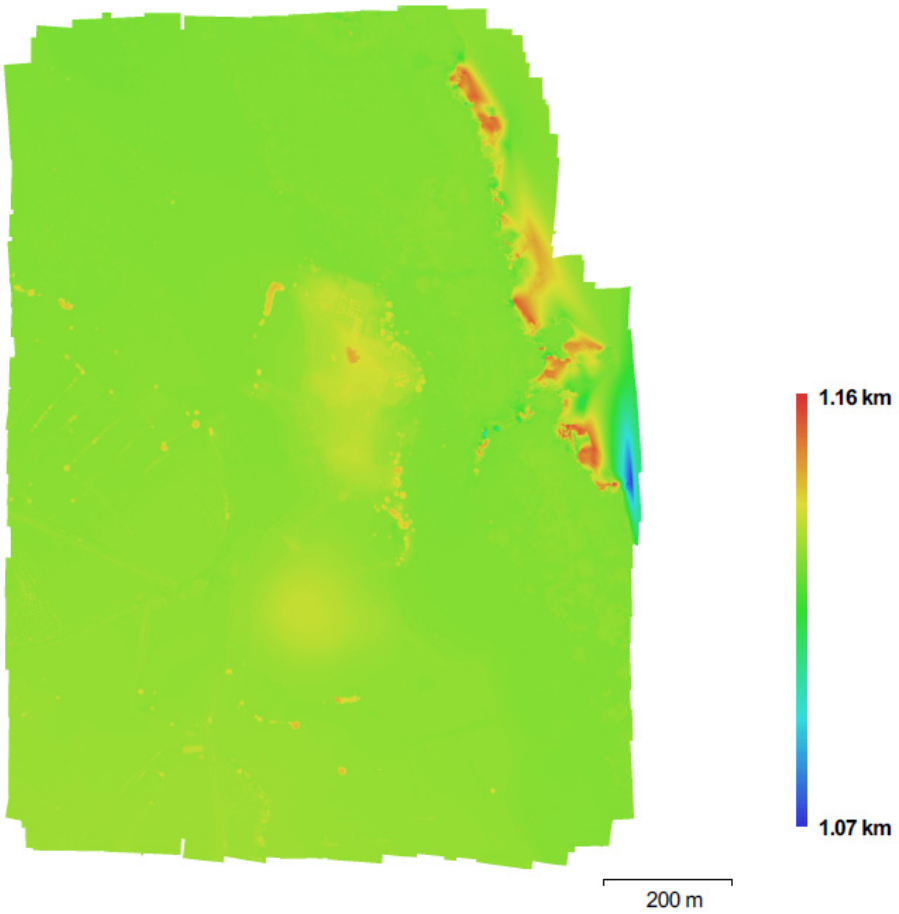

Figure 5.2.21: Reconstructed DEM model in 7.55 cm/px resolution and 176 points/m²

The final orthophoto size was 26,390x35,636 and 1.72 GB file size (Figure 5.2.22)

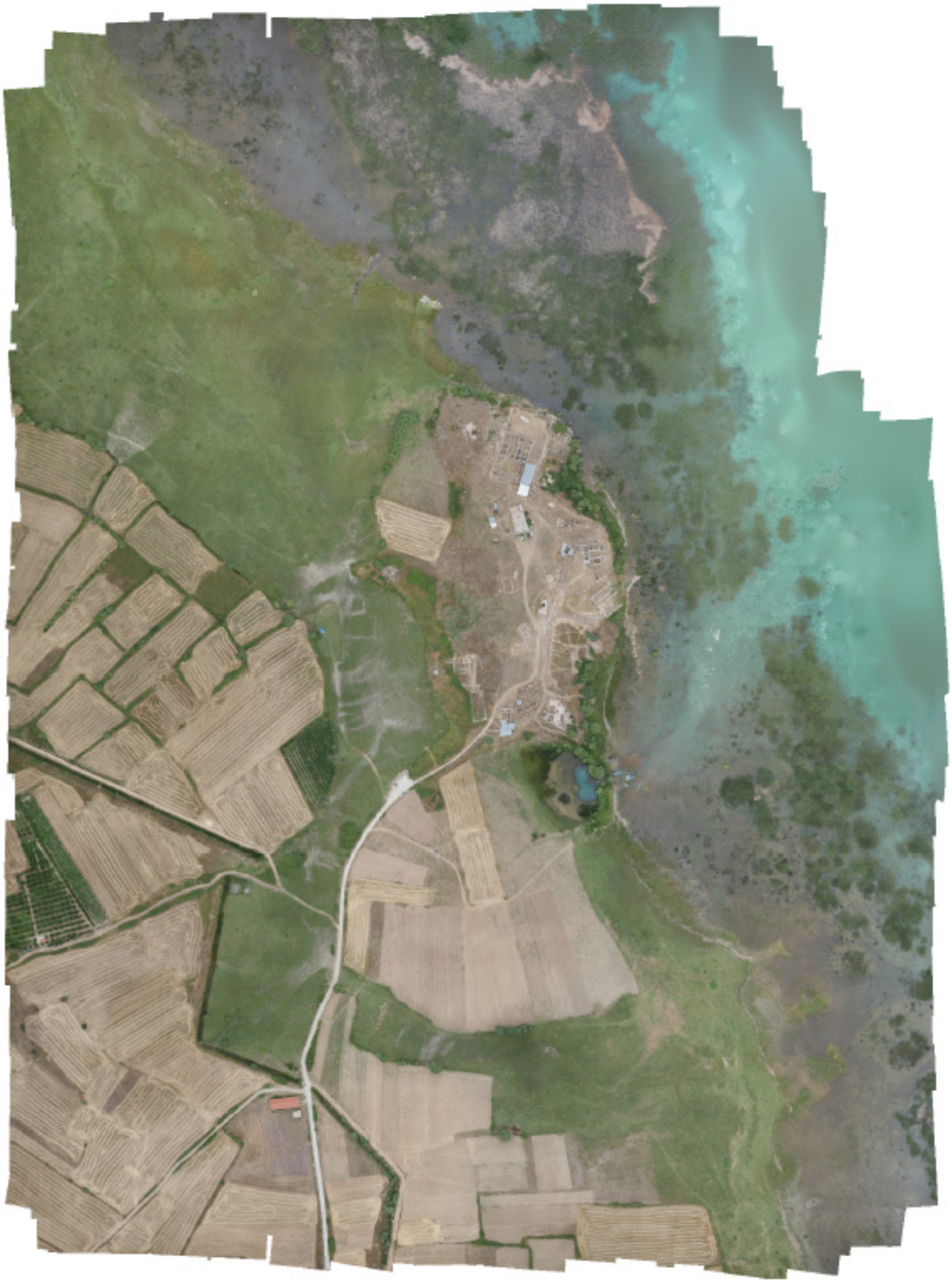

Figure 5.2.22: Orthophoto of the arcaeological area

Figure 5.2.23: Detail of The Grand Palace and Small Palace from Orthophoto

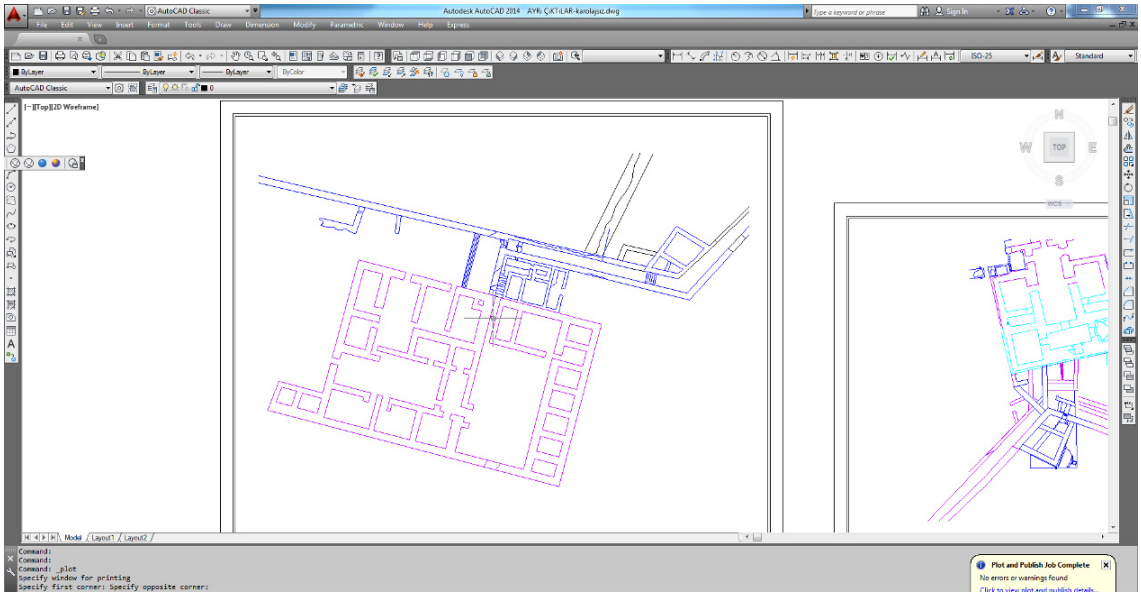

Figure 5.2.24: Drawing of archaeological area in AutoCAD

In this study, an aircraft model UAV was used in order to get large scale mapping and 2D drawings of archaeological area. For this project, the data was quite dense it was difficult to manage the data. This kind of big areas, hardware should be powerful enough. Since the management of the data was difficult, data processing took time and even to take the printscreens from the computer took time and caused crash in the computer.

The resolution of the final orthophoto is is high even the single structures like stones can be seen in orthophoto and 3D model. The main difficulties were on vertical

walls however since their height was not so mcuh from the ground, it was possible to draw in AutoCAD for 2D purpose. For these kinds of parts it would be better to make laser scanning and to combine both data sets. For the future work, it is aimed to combine both data and to prepare a reconstructed model of the area. According to the experience, UAV data can be used for large scale mapping (more than 1:500) and 2D drawing.

To check the data accuracy, ASPRS (The American Society for Photogrammetry and Remote Sensing) published a draft report in 2014 was taken as reference. ASPRS is a scientific association founded in 1934 and their mission is to advance knowledge and improve understanding of mapping sciences to promote the responsible applications of photogrammetry, remote sensing, geographic information systems (GIS) and supporting technologies (www.asprs.org). They published ASPRS Accuracy Standards for Digital Geospatial Data in March 21, 2014 with the objective to replace the existing ASPRS Accuracy Standards for Large- Scale Maps (1990) and the ASPRS Guidelines, vertical Accuracy Reporting for Lidar Data (2004) to better address current technologies.

The standard defines specific accuracy classes and associated RMSE thresholds for digital orthoimagery, digital planimetric data and digital elevation data. Accuracy classes have been revised and upgraded from the 1990 standard to address the higher accuracies achievable with newer technologies. The standard also includes additional accuracy measures, such as ortho seam lines, aerial triangulation accuracy, horizontal accuracy of elevation data and the required number and spatial distribution of check points. The standard is intended to be technology independent and the base standard upon which future work can build.

Specific Requirements

For all data sets, testing may not be required but always recommended. However specific requirements must be addressed in the project specifications.

When testing is required, horizontal accuracy shall be tested by comparing the planimetric coordinates of well-defined points in the data set with coordinates of the same points from an independent source of higher accuracy. Vertical accuracy shall be tested by comparing the elevations in the data set with elevations of the same points as determined from an independent source of higher accuracy.

When errors are normally distributed, accuracy can be performed with RMSE values, standard deviations, mean errors, maximum and minimum errors, and unit-less skew kurtosis values. When errors are not normally distributed, alternative methods can be used. If the number of test points (check points) is sufficient, testing and reporting can be performed using 95 th percentile errors.

When testing is required, horizontal accuracy can be tested by comparing the planimetric coordinates of well-defined points in the data set with coordinates of the same points from an independent source of higher accuracy. Vertical accuracy can be tested bt comparing the elevations in the data set with elevations of the same points as determined from an independent source of higher accuracy.

Check point accuracy, density, distribution and place requirements

Both the number of points and their spatial distribution play an important role in the accuracy evaluation of any geospatial data. Prior guidelines and accuracy standards typically specify the required number of check points and, in some cases, the land-cover types, but there is no requirement for defining and/or characterizing the spatial distribution of the points. While it is not a simple process and there is no practical method available at this time, characterizing the point distribution by some measure and, consequently, providing a quality number is undoubtedly both realistic and necessary. ASPRS encourages research into this topic, peer reviewed and published in *Photogrammetric Engineering and Remote Sensing* for public testing and comment.

The independent source of higher accuracy for QA[47]/QC[48] check points should be at least three times more accurate than the required accuracy of the geospatial data set being tested. For accuracy testing, well-defined points must be easily recognizable on the ground. Elevation data do not normally include clearly- defined point features. Vertical accuracies are to be tested using elevations interpolated from a Triangulated Irregular Network (TIN) generated from the elevation data set. Vertical check points should be surveyed on flat or uniformly-sloped terrain, slopes of 10% or less in order to minimize interpolation errors.

Distribution of the check points is a specification which should be defined by data provider and the end user. For digital orthophoto accuracy or planimetric data accuracy be based on less than 20 check points. However check point density and distribution are based primarily on empirical results and simplified area based methods.

Using metric units, ASPRS recommends 100 static vertical check points for the first 2500 square kilometer area within the project. This provides a statistically defensible number of samples on which to base a valid vertical accuracy assessment. For horizontal testing of areas >2500 km², clients should determine the number of additional horizontal check points, if any, based on criteria such as resolution of imagery and extent of urbanization.

For vertical testing of areas >2500 km², add 5 additional vertical check points for each additional 500 km² area. Each additional set of 5 vertical check points for 500 km² would include 3 check points for NVA[49] and 2 for VVA[50]. The recommended number and distribution of NVA and VVA check points may vary depending on the importance of different land cover categories and client requirements.

[47] Quality Assurance
[48] Quality Check
[49] Non-Vegetated Vertical Accuracy
[50] Vegetated Vertical Accuracy

Table 5.2.4: Recommended number of check points based on area

Project Area (Square Kilometers)	Horizontal Accuracy Testing of Orthoimagery and Planimetrics	Vertical and Horizontal Accuracy Testing of Elevation Data sets		
	Total Number of Static 2D/3D Check Points (clearly-defined points)	Number of Static 3D Check Points in NVA	Number of Static 3D Check Points in VVA	Total Number of Static 3D Check Points
≤500	20	20	5	25
501-750	25	20	10	30
751-1000	30	25	15	40
1001-1250	35	30	20	50
1251-1500	40	35	25	60
1501-1750	45	40	30	70
1751-2000	50	45	35	80
2001-2250	55	50	40	90
2251-2500	60	55	45	100

According to ASPRS Standards, it the area is equal or smaller than 500 km², to test horizontal accuracy of orthoimage and planimetric data, it is recommended 20 clearly-defined 2D/3D check points. In order to check vertical and horizontal accuracy test of elevation data sets,
-if the area is non-vegetated, 20 check points,
-if the area is vegetated , 5 check points,
And totally 25 3D check points are recommended (Table 5.2.24)

In Kubadabad project, the project area was 1.22 km² and in totally 14 GCPs were used and the area was vegetated (Figure 5.2.25).

Figure 5.2.25: GCPs location

Horizontal and vertical accuracy assessment

Horizontal accuracy is the horizontal component of the positional accuracy of a data set with respect to a horizontal datum, defined at the 95% confidence level[51]. Horizontal accuracy is to be assessed using root-mean-square-error (RMSE) statistics. While vertical accuracy is to be assessed using RMSE statistics in non-vegetated terrain and 95th percentile statistics in vegetated terrain.

Horizontal accuracy for digital orthoimagery

According to ASPRS standards, there are mainly three primary standard accuracy classes which can be applied to digital orthoimages.

Horizontal Class-I: In this class, accuracies apply to highest accuracy survey-grade geospatial data for more-demanding engineering applications

Horizontal Class-II: The accuracies apply to standard, high accuracy mapping-grade geospatial data.

Horizontal Class-III: This class and larger class products refer to lower-accuracy visualization-grade geospatial data.

Class N showed in the table below applies to any additional accuracy classes that may be needed for lower accuracy projects.

Table 5.2.5: Horizontal Accuracy Standards for Digital Orthoimagery depending on the pixel size

Horizontal Data Accuracy Class	$RMSE_x$ and $RMSE_y$	Orthophoto Mosaic Seamline Maximum Mismatch	Aerial Triangulation or INS-based RMSEx RMSEy and RMSEz
I	Pixel size x 1.0	Pixel size x 2.0	Pixel size x 0.5
II	Pixel size x 2.0	Pixel size x 4.0	Pixel size x 1.0
III	Pixel size x 3.0	Pixel size x 6.0	Pixel size x 1.5
…..			
N	Pixel size x N	Pixel size x 2N	Pixel size x 0.5N

*Pixel size here is the pixel size of the final digital orthoimagery, not the GSD of the raw image that is used to establish the horizontal accuracy class.

For accuracy classes I, II and III, Table B.1 provides horizontal accuracy examples and other quality criteria for digital orthoimagery produced from imagery having ten common pixel sizes.

Horizontal accuracy,

$RMSE_x = \text{sqrt}[(x_{data,t} - x_{check,t})^2/n]$

$RMSE_y = \text{sqrt}[(y_{data,t} - y_{check,t})^2/n]$

[51] Confidence level: The percentage of points within a dataset that are estimated to meet the stated accuracy. Ex: 95% confidence level means that 95% of the positions in the data seyt will have an error with respect to true ground position that are equal to or smaller than the reported accuracy level.

RMSEx, the horizontal linear RMSE in the X direction (Easting)

RMSEy, the horizontal linear RMSE in the Y direction (Northing)

$x_{data,i}$ and $y_{data,i}$ are the coordinates of the *i* th check point in the dataset
$x_{check,i}$ and $y_{check,i}$ are the coordinates of the *i* th check point in the independent source of higher accuracy (in the model)
n is the number of check points tested
i is an integer ranging from 1 to n

Horizontal error at point *i* is defined as sqrt[(x data, i - x check, i)² +(y data, i - y check, i)²].

Horizontal RMSE, $RMSE_r$ is the horizontal root-mean-square error in the radial direction that includes both x- and y- coordinates

RMSEr = sqrt[$x_{data,i}$- $x_{check,i}$)²+($y_{data,i}$- $y_{check,i}$)²/n]

= sqrt[RMSEx² + RMSEy²]

If RMSEx = RMSEy,

RMSEr = sqrt(2*RMSEx²) = sqrt(2*RMSEy²)

= 1.4142*RMSEx = 1.4142*RMSEy

It is assumed that systematic errors have been eliminated as best as possible. If error is normally distributed and independent in each the x- and y-component and error, the factor 2.4477 is used to compute horizontal accuracy at the 95% confidence level (Greenwalt and Schultz, 1968). When the preceding conditions apply, Accuracyr , the accuracy value according to NSSDA, shall be computed by the formula:

Accuracyr = 2.4477 * RMSEx = 2.4477 * RMSEy
= 2.4477 * RMSEr /1.4142

Accuracyr = 1.7308 * RMSEr

Regarding Kubadabad Project, RMSE values of GCPs are given in table …..and table… shows the total RMSEx, RMSEy and RMSEz values.

Label	X error (cm)	Y error (cm)	Z error (cm)	Total (cm)	Image (pix)
100	6.11981	5.95244	-1.88219	8.74221	0.269 (23)
101	4.45511	-2.77318	3.11042	6.10027	0.310 (24)
103	-4.27609	-1.04231	-2.03174	4.84761	0.266 (18)
104	-3.38464	-1.1302	1.253	3.78194	0.183 (21)
105	3.75177	-5.17337	-0.0764271	6.39103	0.121 (22)
108	-0.994673	2.90823	6.45443	7.1489	0.346 (25)
109	-8.0377	3.28298	-6.07461	10.5964	0.556 (24)
110	2.599	-2.00871	-1.59175	3.65012	0.255 (27)
111	2.75833	1.93097	2.94591	4.47386	0.183 (16)
112	-3.95106	2.24095	-5.24227	6.93643	0.567 (14)
113	2.49822	-1.3361	2.72138	3.92839	0.495 (15)
114	-1.66697	4.1478	-1.49671	4.71415	0.051 (4)
116	-3.39311	-0.623031	-1.28622	3.68181	0.177 (17)
117	3.72089	-5.57416	1.97885	6.988	0.118 (16)
Total	**4.06257**	**3.32436**	**3.28841**	**6.19432**	**0.324**

Figure 5.2.25: RMSE values of GCPs

According to the table,

RMSEx = 4.06 cm

RMSEy = 3.32 cm

RMSEz = 3. 29 cm

For testing horiontal accuracy,

If it s accepted as RMSEx ≅RMSEy,

$$RMSE_{xy} = \frac{(RMSE_x + RMSE_y)}{2}$$

$$RMSE_{xy} = (4.06 + 3.32)\ /2$$

$$RMSE_{xy} = 3.69$$

According to ASPRS Standards,

$RMSE_{xy} \leq RMSE_x$ means

$3.69 \leq 4.06$

$RMSE_r = \sqrt{RMSE_x^2 + RMSE_y^2}$

$RMSE_r = \sqrt{4.06^2 + 3.32^2}$

$RMSE_r = 5.24$ cm

According to the Standards, horizontal accuracy at 95% confidence level should be ≤ 2.45 *X which means for this project is,

$Accuracy_r$ = 1.7308 * $RMSE_r$ should be ≤ 2.45 *X

$Accuracy_r$ = 1.7308 * 5.24
= 9.06

2.45 *X = 2.45 * 3.69
= 9.04

Table 5.2.6: Horizontal accuracy values depending on the x values

Horizontal Accuracy Class	$RMSE_x$ and $RMSE_y$ (cm)	RMSEr (cm)	Horizontal Accuracy at 95% Confidence Level (cm)	Orthoimagery Mosaic Seamline Mismatch (cm)
X-cm	**≤X**	**≤1.41*X**	**≤2.45*X**	**≤ 2*X**

Table 5.2.7: Horizontal Accuracy/Quality Examples Standards for Digital Orthoimagery

Horizontal Accuracy Class $RMSE_x$ and $RMSE_y$ (cm)	**$RMSE_r$ (cm)**	**Orthoimage Mosaic Seamline Maximum Mismatch (cm)**	**Horizontal Accuracy at the 95% Confidence Level (cm)**
0.63	0.9	1.3	1.5
1.25	1.8	2.5	3.1
2.50	3.5	5.0	6.1
5.00	7.1	10.0	12.2
7.50	10.6	15.0	18.4
10.00	14.1	20.0	24.5
12.50	17.7	25.0	30.6
15.00	21.2	30.0	36.7
17.50	24.7	35.0	42.8
20.00	28.3	40.0	49.0
22.50	31.8	45.0	55.1
25.00	35.4	50.0	61.2
27.50	38.9	55.0	67.3
30.00	42.4	60.0	73.4
45.00	63.6	90.0	110.1
60.00	84.9	120.0	146.9
75.00	106.1	150.0	183.6
100.00	141.4	200.0	244.8
150.00	212.1	300.0	367.2
200.00	282.8	400.0	489.5
250.00	353.6	500.0	611.9
300.00	424.3	600.0	734.3
500.00	707.1	1000.0	1223.9
1000.00	1414.2	2000.0	2447.7

According to the table…..horizontal accuracy examples for digital orthophotos, the values of Kubadabad project are between the required values of ASPRS Standards with the value,

$RMSE_{xy}$ = 3.69 cm
$RMSE_r$ = 5.24 cm
$Accuracy_r$ = 9.06 cm

Table 5.2.8: Horizontal Accuracy/Quality Examples for High Accuracy Digital Planimetric Data

ASPRS 2014				Equivalent to map scale in	
Horizontal Accuracy Class $RMSE_x$ and $RMSE_y$ (cm)	$RMSE_r$ (cm)	Horizontal Accuracy at the 95% Confidence Level (cm)	Approximate GSD of Source Imagery (cm)	ASPRS 1990 Class 1	ASPRS 1990 Class 2
0.63	0.9	1.5	0.31 to 0.63	1:25	1:12.5
1.25	1.8	3.1	0.63 to 1.25	1:50	1:25
2.5	3.5	6.1	1.25 to 2.5	1:100	1:50
5.0	7.1	12.2	2.5 to 5.0	1:200	1:100
7.5	10.6	18.4	3.8 to 7.5	1:300	1:150
10.0	14.1	24.5	5.0 to 10.0	1:400	1:200
12.5	17.7	30.6	6.3 to12.5	1:500	1:250
15.0	21.2	36.7	7.5 to 15.0	1:600	1:300
17.5	24.7	42.8	8.8 to 17.5	1:700	1:350
20.0	28.3	49.0	10.0 to 20.0	1:800	1:400
22.5	31.8	55.1	11.3 to 22.5	1:900	1:450
25.0	35.4	61.2	12.5 to 25.0	1:1000	1:500
27.5	38.9	67.3	13.8 to 27.5	1:1100	1:550
30.0	42.4	73.4	15.0 to 30.0	1:1200	1:600

Ground Sample Distance GSD is the linear dimension of a sample pixel's footprint on the ground. In ASPRS Standards, GSD is assumed to be the value computed using the camera focal length and camera height above average mean terrain. (Further details, calculation and studies can be found in section 3.4.1.4). In Kubadabad project GSD can be calculated as;

$$GSD = \frac{H}{f}\,\mu$$

$$\mu = \frac{W}{S_w} = \frac{H}{S_h}$$

where H is flight height (m), f is focal length (mm), GSD is ground sampled distance (m), μ is pixel size (μm), W is the width of CCD (mm), H is the height of CDD(mm), S_w is the number of pixels for W, S_h is the number of pixels for H.

In this project,

H is 159 meters and f *is 18.3* mm.

$\mu = 4.78\ \mu m$

$$GSD = \frac{159\,000}{18.3} 4.78\ \mu$$

$$GSD = 8688.5 * 4.78$$

$$GSD = 41531.14\ \mu$$

$$GSD = 4.15\ cm$$

According to ASPRS Standards, depending on the horizontal accuracy values, GSD value should be between 1.25 and 5.0 cm. when $RMSE_{xy}$ value is between 2.5 and 5 cm. In our study, GSD value 4.15 cm is among this interval with 3.69 cm $RMSE_{xy}$.

Vertical accuracy for digital elevation data

Vertical accuracy is the measure of positional accuracy of a data set with respect to a specified vertical datum. According to ASPRS accuracy standards, elevation data has mainly ten accuracy levels relevant to technologies such as mobile mapping systems, unmanned aerial systems, airborne or satellite imagery, lidar or IFSAR[52].

$RMSE_z$ = sqrt[$(z_{data,i} - z_{check,i})^2/n$]

Where

$z_{data,i}$ is the vertical coordinate of the i th check point in the dataset.
$z_{check,i}$ is the vertical coordinate of the i th check point in the independent source of higher accuracy
n = the number of points being checked
i is an integer from 1 to n

It is assumed that systematic errors have been eliminated as best as possible. If vertical error is normally distributed, the factor 1.9600 is applied to compute linear error at the 95% confidence level (Greenwalt and Schultz, 1968). Therefore, vertical accuracy, $Accuracy_z$ reported according to the NSSDA[53] shall be computed by the following formula:

$$Accuracy_z = 1.96 * RMSE_z$$

Table 5.2.9: Accuracy standards for digital elevation data

[52] Interferometric Synthetic Aperture Radar (IFSAR)

[53] National Standard for Spatial Data Accuracy

Vertical Accuracy Class	Absolute Accuracy			Relative Accuracy (where applicable)		
	$RMSE_z$ Non-Vegetated (cm)	NVA at 95% Confidence Level (cm)	VVA at 95th Percentile (cm)	Within- Swath Hard Surface Repeatability (Max Diff) (cm)	Swath-to-Swath Non-Vegetated Terrain ($RMSD_z$) (cm)	Swath-to-Swath Non-Vegetated Terrain (Max Diff) (cm)
X-cm	**≤X**	**≤1.96*X**	**≤3.00*X**	**≤0.60*X**	**≤0.80*X**	**≤1.60*X**

Absolute accuracy is a measure that accounts for all systematic and random errors in a data set.

In Kubadabad porject, $RMSE_z$ = 3. 29 cm

$Accuracy_z$ =1.96 * 3.29 = 6,49 cm (NVA at 95% Confidence Level)
$Accuracy_z$ = 3*3.29 =9,87 cm (VVA at 95 th percentile)

Table 5.2.10: Vertical Accuracy/Quality Examples for Digital Elevation Data

According to ASPRS Standards, horizontal and vertical accuracy should be reported as

Vertical Accuracy Class	**Absolute Accuracy**			**Relative Accuracy (where applicable)**		
	$RMSE_z$ Non-Vegetated (cm)	NVA at 95% Confidence Level (cm)	VVA at 95th Percentile (cm)	Within-Swath Hard Surface Repeatability (Max Diff) (cm)	Swath-to-Swath Non-Veg Terrain ($RMSD_z$) (cm)	Swath-to-Swath Non-Veg Terrain (Max Diff) (cm)
1-cm	1.0	2.0	3	0.6	0.8	1.6
2.5-cm	2.5	4.9	7.5	1.5	2	4
5-cm	5.0	9.8	15	3	4	8
10-cm	10.0	19.6	30	6	8	16
15-cm	15.0	29.4	45	9	12	24
20-cm	20.0	39.2	60	12	16	32
33.3-cm	33.3	65.3	100	20	26.7	53.3
66.7-cm	66.7	130.7	200	40	53.3	106.7
100-cm	100.0	196.0	300	60	80	160
333.3-cm	333.3.	653.3	1000	200	266.7	533.3

in the following.

"This data set was **tested** to meet ASPRS Positional Accuracy Standards for Digital Geospatial Data (2014) for a 5 (cm) $RMSE_x/RMSE_y$ Horizontal Accuracy Class.

Actual positional accuracy was found to be $RMSE_x = 4.06\ (cm)$ and $RMSE_y = 3.32\ (cm)$ which equates to +/- 9.04 cm at 95% confidence level."

"This data set was **tested** to meet ASPRS Positional Accuracy Standards for Digital Geospatial Data (2014) for a 5 (cm) $RMSE_z$ Vertical Accuracy Class. Actual NVA accuracy was found to be $RMSE_z = 3.29\ (cm)$, equationg to +/- 6.49 cm at 95% confidence level. Actual VVA aacuracy was found to be +/- 9.87 cm at the 95th percentile."

5.3. Villa Medici, Pratolino, Italy

5.3.1. Introduction and aim of the study

There have been several methods such as geo-radar, electromagnetic induction, gamma rays, laser vibrometry used for buried archaeological objects. These methods are listed depending on their advantages and drawbacks in Santulli (2009) as it is shown in the table below (Table 5.3.1).

Table 5.3.1: Methods, advantages and drawbacks of methods for buried archaeological objects

Method	Advantages	Drawbacks
Geo-radar	Transportability, absence of contact, possible selection of most adapted frequency band	Reflections of both soil surface and the antenna used require a very broad detection band to have a resolution lower than 10 mm, and often data filtering methods are needed
Electromagnetic induction	Ease of detection for known types of buried objects, e facility in obtaining a uniform magnetic field with remote sensing	Strong dependence on geometry and orientation of the buried object, usually avoided by the use of normalized electromagnetic spectra
Electrical impedance tomography (EIT)	Possibility and relative ease of measuring conductivity perturbations and simulate realistic conditions per la presence of the object. Advantageous for the detection on humid soil and underwater	Problems with electrical contact can be revealed in case the soil is very dry. Strong dependence of detection reliability from object geometry
Neutrons	Easy detection of small quantity of explosive substances also at significant depths (up to 300 mm)	Performance limited from presence of humidity and strongly dependent on objects scale. Need to evaluate neutron distribution to reduce false alarms. Virtual impossibility of detecting buried objects other than landmines
Gamma rays	Portability and auto-feeding. Inspection at depths exceeding 80 mm.	Dependence on density, not necessarily related to the presence of the buried object. Need for simulations and probabilistic evaluations to reduce levels of error. Resonance effects due to the substances present in the object (e.g., explosives, dust), and therefore need to know in advance its nature and composition.
Laser-Doppler vibrometry (LDV)	Capable of ensuring detection by comparing the ratio of the velocity magnitude of the ground surface over and away from the target, and the presence of wave-like or scattering phenomena. The dimension of the buried object can be measured, with suitable excitation wavelength	Requires acoustic excitation, in which case detection reliability is strongly dependent on the acoustic relaxation time of the soil surface

With recent developments in technology, the detection of buried objects using another method "*thermography"* has also started to be studied in archaeological areas. Many scientific papers are available in the literature some of which are shown in the table below (Table 5.3.2).

Table 5.3.2: Some works on the application of IR thermography to the detection of buried objects (Table is updated version of Santulli ,2007)

Author/s	Year	Aim of the study
Agassi & Ben Yosef	1997	Effect and parametrization of vegetation in Thermographicdetection of buried objects
Boras et al.	2000	Use of active thermography for detection analysis based on the mutual influence of the system scanning capacity and the quality of thermograms
Hadas *et al.*	2003	Evaluation of the effect of soil anisotropy and sunlight on parameters for thermal transport for objects detection
Stepanic *et al.*	2004	Study of the effect of object orientation on the signal obtained on the thermograms
Martinez *et al.*	2004	Comparison of thermographic detection results with a tridimensional model of heat flux transport
Muscio & Corticelli	2004	In-lab reproduction of thermographic tests for buried objectsdetection with parametric evaluation of scale-effect
Blasi & Corcione	2005	Adoption of a detection system based on a concentrated heat source and a non-contact thermometer mounted on a suspended transportation system exploring the soil surface
Meola et al.	2005	Application of infrared thermography and geophysical methods for defect detection in architectural structure
Rowlands et al.	2007	Detection of exposed and subsurface archaeological remains using multi-sensor remote sensing
Thành	2007	establishment of a forward thermal model for shallowly buried objects and validation of the forward thermal model by comparing the simulations with measured data acquired in an outdoor minefield
Martínez et al.	2004	iterative procedure to classify the detected perturbations as mines or nonminers and to estimate their depth of burial.
Eppelbaum	2009	Noise elimination, calculation of terrain relief and effective interpretation of temperature anomalies

In general, thermography can be described as a non-destructive evaluation technique, whose performance depends on three elements: the intrinsic detection capability of the method (or combination of methods) employed, application-related factors, in particular the state of environment surrounding the buried object, and the human factor, connected with the skills of NDE operators (Santulli, 2009). By the time, using thermography with aerial images started to be used in archaeology field.

Aerial thermography has attracted the archaeologists for their excavation since 1970's. They have recognized that the aerial images recording thermal infrared wavelengths of light could be a tool for identification of surface and subsurface cultural remains (Casana, et al. 2014). One of the primary attractions for archaeologists is to be a non-destructive remote-sensing method for archaeological investigations (Kvamme 2008b). However, to have access to technology and the cost were the main obstacles to make this technology widespread in archaeological area (Casana, 2014). Despite the potential of this technology, few archaeologists had access to the highly specialized radiometers as remote sensing technique (Scollar et al. 1990). Besides, thermal images acquired from civilian satellites such as Landsat and ASTER have too low spatial resolution to reveal most archaeological features. Sever and Wagner (1991) used remote sensing data in order to analyze prehistoric roadways in Chaco Canyon and their resolution was only 5m. Additionally, Challis et al. (2008) made a study to investigate

the potential of multispectral methods of airborne remote sensing for geological and archaeological prospection in the archaeologically rich area. In their study, they mention that even the multispectral techniques have capacity in rapid and broad area coverage combined with a data collection beyond the visible spectrum, the flights are expensive and they add that there is no sense in which a single multispectral flight could substitute for a season of opportunistic flying using conventional photography (Challis et al. 2008). Another attractive reason for archaeologists is the usability of data for different purposes. This data can help to archaeologist to make analyze, to use information in different ways, in different scales (from a small scale to a larger context), to derive plan of entire area, to focus on specific area/s for needed or further studies. Even though it was mentioned about the cost of technology as barrier in the past, this method can get data in relatively limited time with limited budget and labor in last years (Kvamme 2008b). While new technologies are constantly being developed, tested, adapted and added to the toolbox, aerial thermography has become one of the most recent innovative technologies in last years (Cool, 2015).

The main principle behind aerial thermography mainly depends on material's thermal behaviors. Due to their composition, density and moisture content, materials on and below the ground surface absorb, emit, transmit, and reflect thermal infrared radiation at different rates (Casana et al. 2014). And these materials can be visible if they have sufficient contrast in thermal inertia, a product of a material's thermal conductivity and its volumetric heat capacity (Perisset and Tabbagh, 1981), and if the image is acquired at a time in the diurnal cycle when such differences are pronounced (Casana et al. 2014). Several studies have demonstrated that thermography can detect features at or near the ground surface such as pits, ditches and field boundaries as well as buried architectural features up to a half meter below the ground (e.g., Perisset and Tabbagh, 1981; Lunden, 1985; Bellerby et al., 1990; Casana et al. 2014)).

Among the early studies to apply aerial thermography were geologists and they employed this method for geological detection and until 1960's, as mentioned before, it was not realized the potential of thermal imaging for archaeological purpose (Cool, 2015). In 1966, the National Aeronautics and Space Administration conducted a thermal survey of the San Francisco volcanic field northeast of Flagstaff, Arizona. The NASA and USGS scientists discovered three groups of parallel linear anomalies in the thermograms (Berlin et al.,1977). In 1969, Schaber and Gumerman determined some linear thermal anomalies in ancient agricultural fields. The anomalies were to be basalt ridges with low thermal inertia tend to warm quickly and buff soil swales with high thermal inertia tend to remain cooler (Schaber and Gumerman, 1969). Similarly, Berlin et al. (1977) made a thermal survey on agricultural plots to measure ridge-swale pairs (Berlin et al. 1977).

After these early aerial imaging studies, aerial thermography started to be used for archaeological inspection. Among the earliest studies of aerial thermography, Périsset and Tabbagh did several, valuable and significant studies about this issue. Beside their theoretical studies, they also carried out several field-based studies. For their studies, they used ARIES radiometer mounted on a low-flying aircraft. One of

their studies was the survey of the necropolis of La Tombe in Seine et Marne, France. They have revealed a square enclosed with aerial thermal photographs. In their later studies, they surveyed several known Neolitic ditches in Seine et Marne, France and they also took samples of soils and flew in different seasons to achieve the best thermal response. In another study, they used aerial thermography for defining the location of a deserted village at St Vincent. They found large rectilinear anomalies as cold stone foundations (Cool,2015).

Furtherly, Scollar (1990) made a research with aerial thermography. He carried out three days after the transient heat flux and found some structure foundations as cold anomaly. Another survey by Scollar was done at a Gallic and Gallo Roman Complex at Maillys, France. It was found several cold anomalies indicated a road, a Roman camp and Iron Age rural settlement (Scollar,1990). Ben-Dor et al. (1999) conducted one of the earliest digital video aerial thermography on the Bronze Age settlement in Tel Leviah, Israel. He used a helicopter with infrared video imaging radiometer in order to reveal buried structures made of basalt. Buck et al. (2003) used FLIR IQ Series 821 thermal imagery mounted on a tripod to detect obsidian ceramic artifacts underground. Another study was carried out by Hayel et al. (2002). They used a helium blimp mounted FLIR Agema 570 thermal camera for detection of archaeological features in late prehistoric site Mississippi. Kwamme (2006) deployed a hand-held camera to a kite. Haley (2005) also mounted a handheld camera to a manned powered parachute in North Dakota. His results are inspiring in their possibilities as they reveal much of what can be seen in more traditional geophysics, as well as distinct features not recorded by other methods. One of the most systematic studies was undertaken at late prehistoric mound center in Mississippi, where thermal imagery acquired with a handheld camera suspended from a helium blimp was used to successfully document subsurface house remains as well as the diurnal variation in their thermal values (Haley et al., 2002; Giardino and Haley, 2006). Another study was conducted by Lunden (2006) using a helicopter with infrared imaging radiometer in Dalecarlia, Sweeden. They made flight in an August night and observed temperature variations which could be linked to archaeological remains. In 2013 Brumana et al. used an Octocopter with FLIR T620 thermal camera for detection of ancient roads, land plot boundaries, site plans and underground caves in archaeological site of Isola Comacina (Comacina Island) in the Lago di Como (Lake Como) Lombardy, Northern Italy. The aim of the study was to investigate new methodologies to get heritage information model. One of the last, systematic and successful study was done by Casana et al. (2014). They used CineStar 8 UAV with FLIR Tau camera and their surveys were conducted at the Chaco-period Blue J Community in northwestern New Mexico. They could reveal previously undocumented architectural features in Blue J and Chaco Canyon in New Mexico.

This study presents a result of a case study to improve a methodology for collection of thermal images using a UAV and to evaluate the availability of the technique for detection of archaeological buried features. Here it is presented a case study carried out on an area that was an Italian Villa called Villa dei Medici in Pratolino Park, Florence in Italy. In the study a UAV was used with thermal camera recorder. Results of the study indicate the potential of aerial thermography for revealing archaeological buried ruins.

5.3.2. Villa Medici, Pratolino, Italy

Villa Demidoff is the current name of the ancient Medicean Paggeria of Pratolino, Parco Mediceo di Pratolino which is located on the Florentine hills along the Via Bolognese heading into the Mugello valley. It's just fifteen minutes from Florence and north on Bolognese road through the little town of Pratolino[54] (Figure5.3.1-2-3).

Figure 5.3.1:Medici Park, Pratolino in Google Earth

Figure 5.3.2: The borders of Medici Park, Pratolino (left) and the place of Villa Medici in the park (right)

[54] The name derives from the Word "prato" which means "field" in Italian

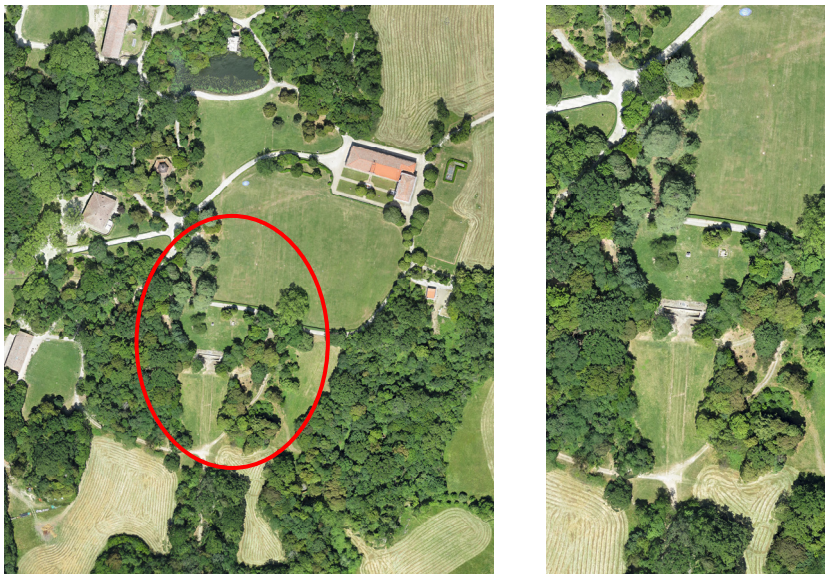

Figure 5.3.3: The studied area in Medici Park, Pratolino on the eft and in detail on the right

Francesco I de' Medici who was the Grand Duke of Tuscany asked to Bernardo Buontalenti to design a villa and a large park in 1568. He built a magnificent Renaissance villa surrounded by a wonderland park with water fountains and grottoes, beautiful gardens filled with delicate plants adn flowers. The park project was completed in 1585 and Bountalenti laid it out to be a fantasy land where nature and technology blended to create a symbolic journey that would introduce the visitor to the Grand Duke's phlosophical thought. The park has great interest with its artificial grottoes, water tricks and statues and it was started to be called as "the graden of wonders". In 1818, Joseph Frietsch elarged the park from twenty hectares to eighty hectares and gave a new English look garden. Today The Medici Garden is a public Park, which conserves several basins, statues grottoes and in particular, the splendid statue of the Colossus of the Apennines (1579-1580) by Giambologna. There are lawns and woods of tall oaks and cedars and large plane tress. The park was the largest of the estates of the Medici family with a Northern entrance in front of The Fountain of Jupiter. In 1872 the park was sold to the Russian Prince Paolo II Demidoff, who restored the buildings within the property and enlarged on of the remaining outer structures into a villa and the park was renovated. In 1981, the Florence Province Council bougth the property to turn it into a public park.
https://www.discovertuscany.com/mugello/pratolino-park.html
http://architetturaquattrocentocinquecento
http://brunelleschi.imss.fi.it/itineraries/place/ParcoMediceoPratolinoVillaDemidoff.html
http://www.tuscanyvacation.us/IT/vacanza_toscana/ville_firenze/villa_pratolino.html#.WXuapLpuJMM

The Medici Villa which had a complex of artificial grottoes complex with water tricks and automatons is lost today.

Figure 5.3.4: Pratolino Park and Villa Medici (1736)

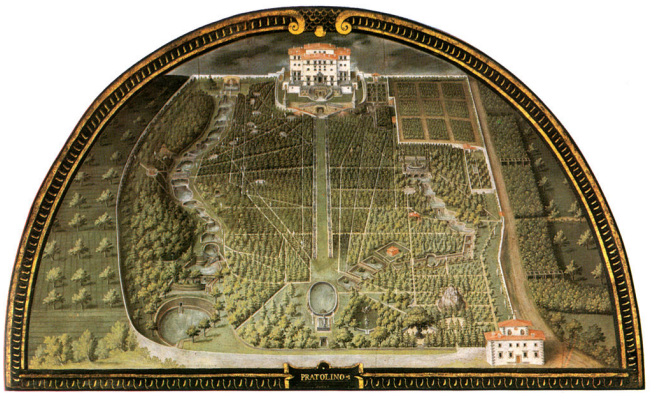

Figure 5.3.5: Pratolino Park and Villa Medici

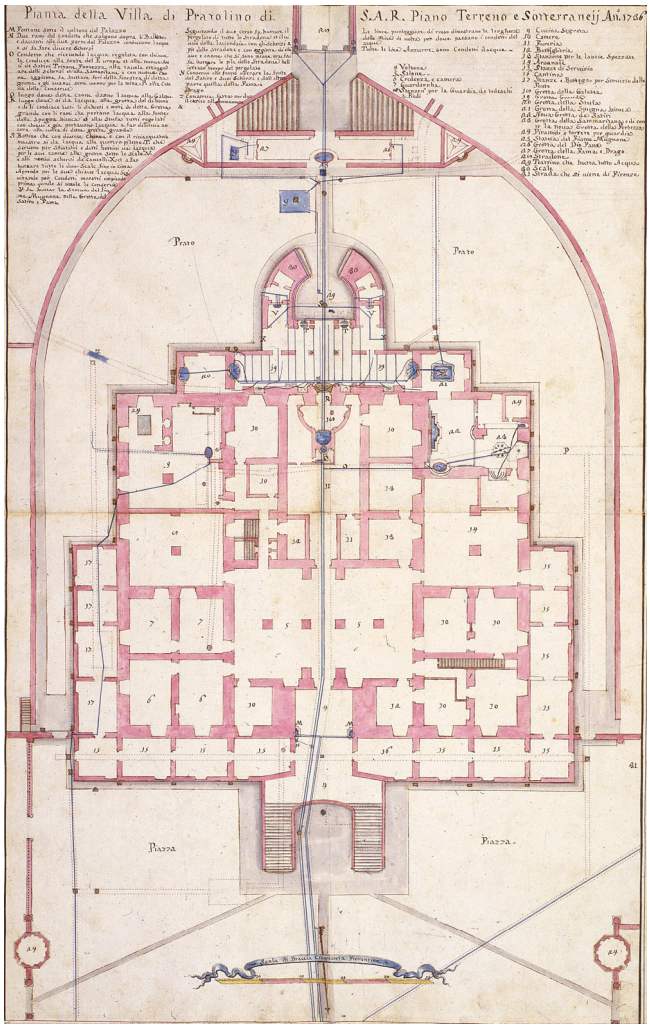

Figure 5.3.6: Plan of Villa Medici (1736) Dotted lines of red show the width of the mine at a time for where the water ends. All blue lines demonstrate the water lines.

In 2009, Desideri prepared a report[55] about Villa Medici and the name of the study is Archaeological Diagnostics and (Sondaj) Stratigrafic Surveys in Villa Medici Archaeological Area. During the month of July 2009, it was completed a new field survey of non-destructive geophysical prospections (survey), through geoelectric tomography, with the specific purpose of archaeological diagnosis, in order to acquire more information on the underground, for a more circumstantial/ detailed and effective planning of archaeological surveys.

The field survey of prospection it became necessary in consideration of the obtained results of a field survey, conducted in 2002, which proved insufficient for the development of a program of archaeological surveys. In such occasion infact, the greater effort for the identification of underground water pipes, prospectings were

[55] Dottt. Andrea Vanni Desideri, "Relazione sulla campagna 2009 di indagini archeologiche nell'area della Villa Medicea di Pratolino: Diagnostica Archeologica e Sondaggi Stratigrafici", Province di Firenze, Istituzione Parco Mediceo di Pratolino, 31 December 2009.

conducted on a limited grass surface overlying the fountain of the Mugnone (about 50x50 cm), to identify the remains of the villa using the electromagnetic method, georadar and geoelectric. In addition to the limit resulting from too low surface under investigation, the results obtained by used method had allowed to detect traces of partial wall structures relative to some rooms of the villa, in particular in its S and W parts (Figure 5.3.6-7).

In prevision of the field work of archaeological surveys, Director of the park and Superintendence of Archaeological Heritage of Toscany, have therefore expressed the need to carry out a new field works for further diagnosis with non-destructive instruments, focused on specifically, in terms of location and used methodologies, the acquisition of more detailed information on underground archeology, in order to program surveys with greater topographic precision.

Based on the needs identified in such agreements and, particularly, specific characters and archaeological purposes, the new work of prospection - designed by those who write archaeological and topographical aspects, in accordance with Director of Medici Park of Pratolino and Superintendence of Archaeological Heritage of Toscany, it was conducted a research group under control of Prof. Paolo Mauriello, Department of Science and Technology for Environment and Territory from the University of Molise.

The surveys were designed to cover basically the entire surface of the villa, taking into account the historical cartography, especially in the ground floor of the Royal Villa of Pratolino (B. S. Sgrilli, 1742), ground floor of the Villa of Pratolino Ser. Grand Duke of Tuscany (1736), and reference points on the ground. The result was an area of 100 x 80 m with the major axis basically coincident with the axis of the NS villa with prospecting method.

The first result consists in the identification the *entire planimetric extension of the villa*, at the end of prospecting, results so exactly placed in the Regional Technical Map. According to these surveys, the area is to obtain in estimate of about 90 x 70, major axis oriented NS, slightly rotated toward E.

Restitution drawing in about 1 m depth underground (Figure 5.3.7) shows that *planimetric plan of the villa is good conservated*, at least in its foundation elements, from the end of its south part (semicircular stairs) located approximately 10 m from the current balustrade of fountain Mugnone to the end of N (principle stairs) corresponding to the arrival of the road from the Customs. It 'also detectable substantially the good conservation of the walls of the building foundation, so that it is possible to recognize, with a considerable level of detail, each single room documented in the Plan of the Ground Floor already mentioned, which it is perfectly stackable.

Figure 5.3.7: (up): Planimetric restitution of resistivity tomography at 1 m depth from the surface by Campagna, 2009. (down): Planimetric restitution of electromagnetic anomalies by Campagna, 2002 (Desideri, 2009).

In the complex architecture of the villa the followings were identifiable:

-the bases of the four pillars supporting the vault of the *Enormous Entrance Room* and so-called *other rooms for different uses;*

-*the Cave of the Samaritan woman* and the basic element of the central table, as indicated by Giovanni Guerra (1598) " *Water play table in various jokes with eight places for the guests where always cool/fresh contests*" and described by Sgrilli (1742); Cave of Galatea and the similar table, also indicated in the drawing by Giovanni Guerra, in Riccardian news (XVI-XVII century) and from Sgrilli (1742);

-foundations of the semicircular scales body S are also recognizable, where they hosted the *Grotticella della Donnola* and la "*Grotticella dei Ranocchi*";

-the two bodies supporting main scale N face, with their small rooms underlying; -it is also visible the tunnel of the water pipe axial of the villa, exactly as it appears in the Plan of the Villa of Pratolino of S.A.R. ground floor and basement floor in 1736; the two areas of high resistivity at the southern angle of plant of the villa can indicate the materials of results or collapse of angular *Pyramids*.

The place is located to the west of the previous one for an extension of about 8.80x8.45 m, and contrary to what is shown in test 1, here the structural remains are only 0.21 m from the ground. The stratigraphic sequence is also here substantially well preserved, except for a pit built for planting, which has profoundly affected the ridge of one of the masonry and can be dated, based on the context of artifacts contained in the filling soil, within the XX century.

At this stage, much of the masonry of the sage on the south-eastern corner of the caves is made. The first activity corresponds to 10 which constitutes the perimeter masonry of caves and support to the terrace. The structure appears to be constructed with discontinuous foundations consisting of lowered arches of low relief, armed on the ground, resting on quadrangular pillars made of narrow ditch.

Some details of the masonry and the system of conductive ducts suggest that the structure of the system has been completed for later stages. Moreover, extensions and additions are also deduced from the archive series, for example the probable secondary construction of the "Copper Putte" fountain under the noon window in the Stove Cave, described by Sgrilli in 1742 but which does not appear in most documents Ancient ones and, among them, especially in the Pratolino Villa of SAR Ground Floor and Underground Year 1736 (Figure 5.3.8).(Desideri, 2009).

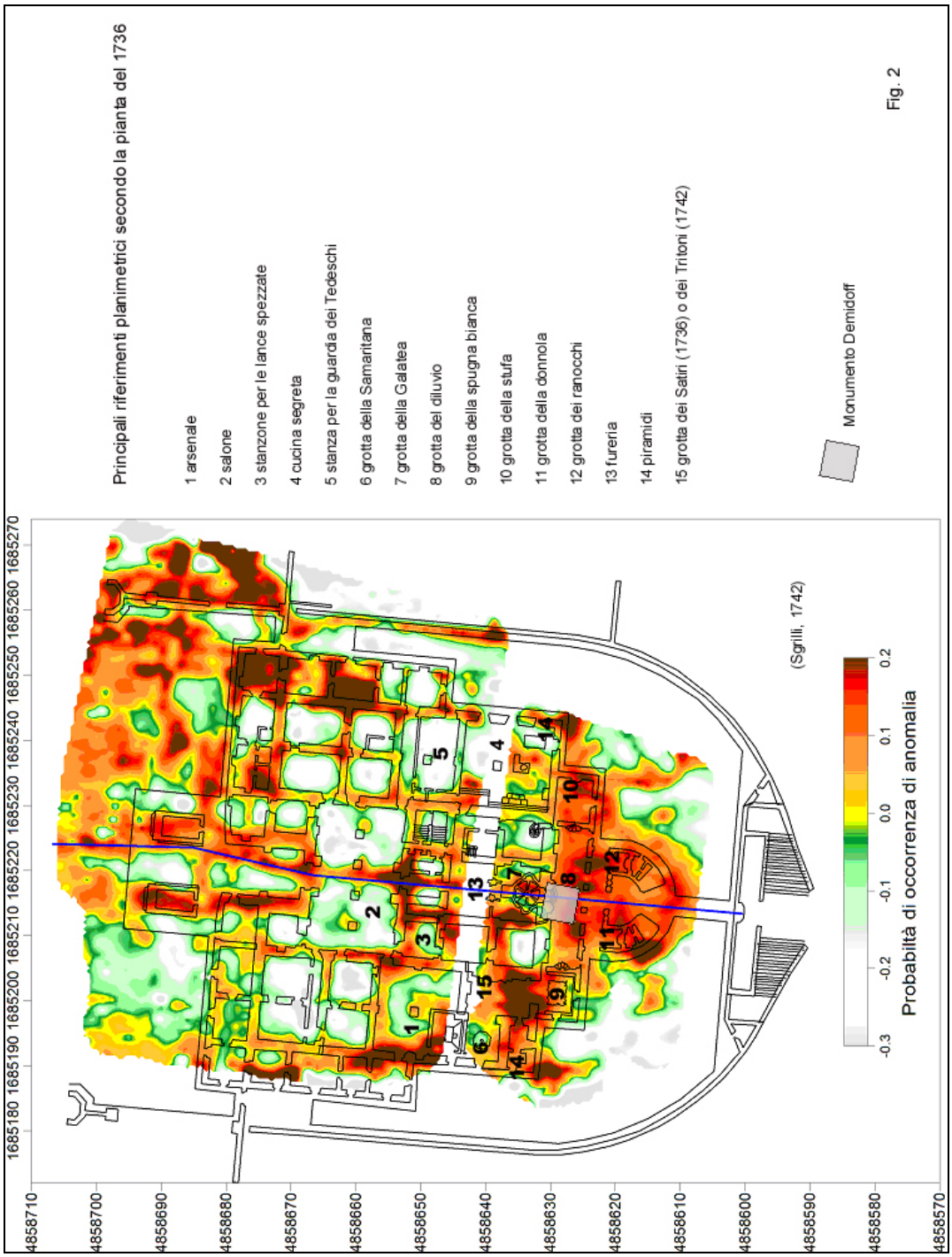

1: arsenal
2: lounge
3: room for broken spears
4: secret kitchen
5: rooms for the guard of the Germans
6: samaritan cave
7: galatea cave
Demidoff monument
8: food cave
9: white sponge cave
10: stove cave
11: weasel cave
12: cave of frogs
13: orderly room
14: pyramids
15: cave of Satyrs

Figure 5.3.8: Planimetric restitution of resistivity tomography at 1m from the surface by by Campagna, 2002 (Desideri, 2009).

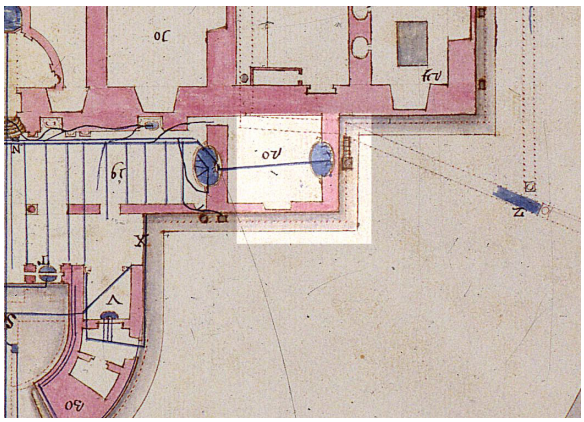

Figure 5.3.9: Plant of 1736 with highlighted area corresponding to Grotta della stufa (Stove cave). (Desideri, 2009).

Figure 5.3.310: Zenital sight stove cave (Desideri, 2009).

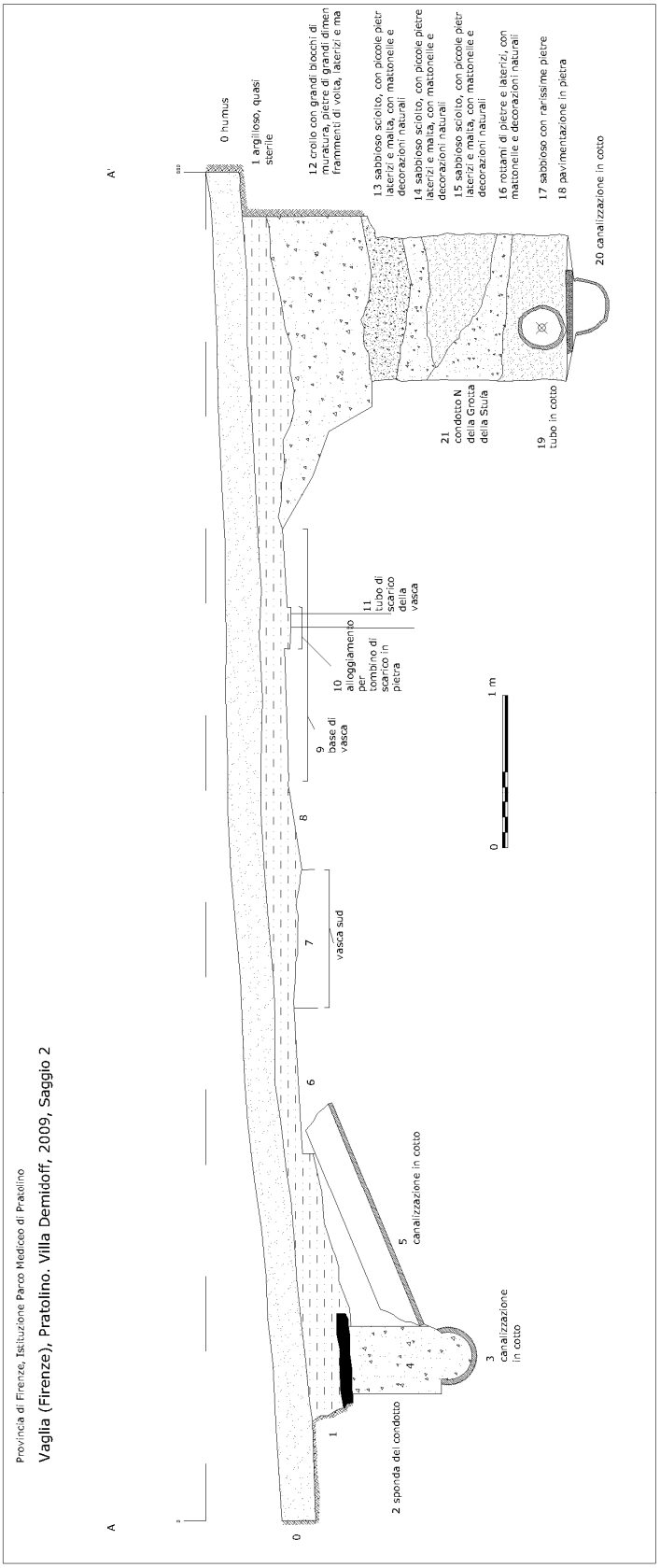

0: humus
1: almost sterile yellowish clay
2: duct shore
3: terracotta channel
5: terracotta channel
7: south tub
9: bathtub base
10: housing for stone drainage
11: tub drain pipe
12: collapsed large blocks of masonry, partd of brick vaults
13-14-15: loose sandy, with small stone bricks and mortar, with tiles and natural decorations
16: Stones and bricks with tiles and natural decorations
17: sandy with very rare Stones
18: stone flooring
19: brick pipe
20: brick channel
21: stone door of cave of North

Figure 5.3.11: Stratigraphic section A-A' (S-N)(Desideri, 2009).

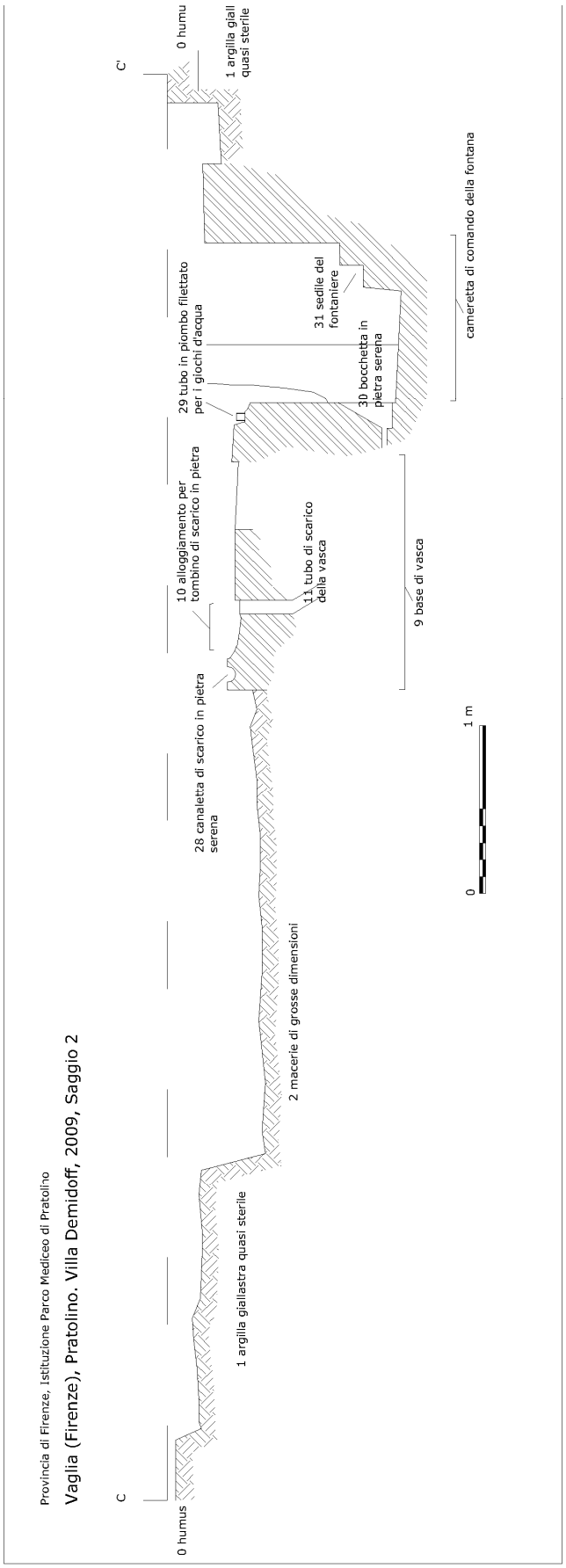

0: humus
1: almost sterile yellowish clay
2: big size rubbles
9: bathtub base
28: stone drainage channel
10: housing for stone drainage
11: tub drain pipe
29: threaded lead tube for water games
30: nozzle in sandstone
31: fountain seat

Figure 5.3.12: Stratigraphic section C-C' (W-E) (Desideri, 2009).

This change may be accompanied by the different composition of the masonry of the corresponding tub, here in bricks instead of mixed material as elsewhere. It is also evident that the chimney chamber of the stove groove is the result of a modification of an already functioning plant. At this stage, in the southern wall of the duct, a breach was made which, by short steps was accessed to the control room which was first portrayed with certainty Pratolino Villa Plant Ground Floor 1736 (Figure 5.3.10).

Abandoning the hydraulic system. The maintenance maintenance (and therefore use) of the plant is documented by the level of sandy loose soil and sterile deposited inside the duct and which covered the brickwork pipe protecting it from the collapse of the vault of phase 5. It's dating dates back to 1764, when Ruggieri describes how the Flood Cave hydraulic systems are still working.

The operation is here documented by the collapse material that fills the duct and covers the basal structures. In the first case, at the end of a series of levels of masonry material and cave decoration elements, it is conceivable that a collapse of the upper walls of the villa has invested and caused the collapse of a large portion of the pipe duct whose scrap permanently fills the duct light. The stratigraphic series closes with the preparation of yellowish surface smoothing clay, followed by humus

Most of the collections collected in the 2009 excavation campaign come from the area 2. Among the materials are represented almost exclusively parts of the parietal and floor decorations of the cave and therefore relate to the archaeological phases 1 and 2 and among them are particularly abundant the fragments Tiled tiles floor tiles. The latter are distinguishable in two types: the rectangular ones with a blue background and an orange frame which, based on the remains of pavement preserved in situ in the upper cave of the Appellate Giant, had to be related to the rigging along the walls, while the white square squares formed the central floor mat.

The Stove Cave floor had to be built over terracotta tiles (Figure 5.3.11-12) supported by "suspensurae" which determined an interspace, on the type of ancient hypocaust. Particular areas of the pavement were also made with mosaics of black and white river pebbles, of which fragments were found. Interestingly, contrary to what emerged in the wonders at the Giant Appennine, where such floors were attributed to the Demidoff phase of the monument, the data collected in the area 2 documented the presence of pebble floors from the most Ancient phases of the villa (Desideri, 2009).

5.3.3.Methodology

In this case study, the methodolgy is consist of mainly two workflow. One of them is related to get color images processing to get orthophoto and the other one is aimed to get thermal orthophoto. The process followed for color orthophoto was regular workflow for UAV photogrammetry. The steps followed for thermal orthophoto are also similar to aerial photogrammetry workflow. Only after data acquisition with thermal camera, the video record was opened in thermal camera special software Optris PI Connect (2.9.2147). After the Project parameters set up, the snapshot were acquired and saved as .TIFF format to be able to get thermal orthopoto in PhotoScan software. At the end of getting orthophotos, they were scaled and overlapped to check possible anomaly places. General methodolyg of case study is given Table 5.3.13. Then thermal

data processing was done which will be detailed described in section 5.3.5. Aerial Thermal data processing.

Figure 5.3.13: General methodology of case study

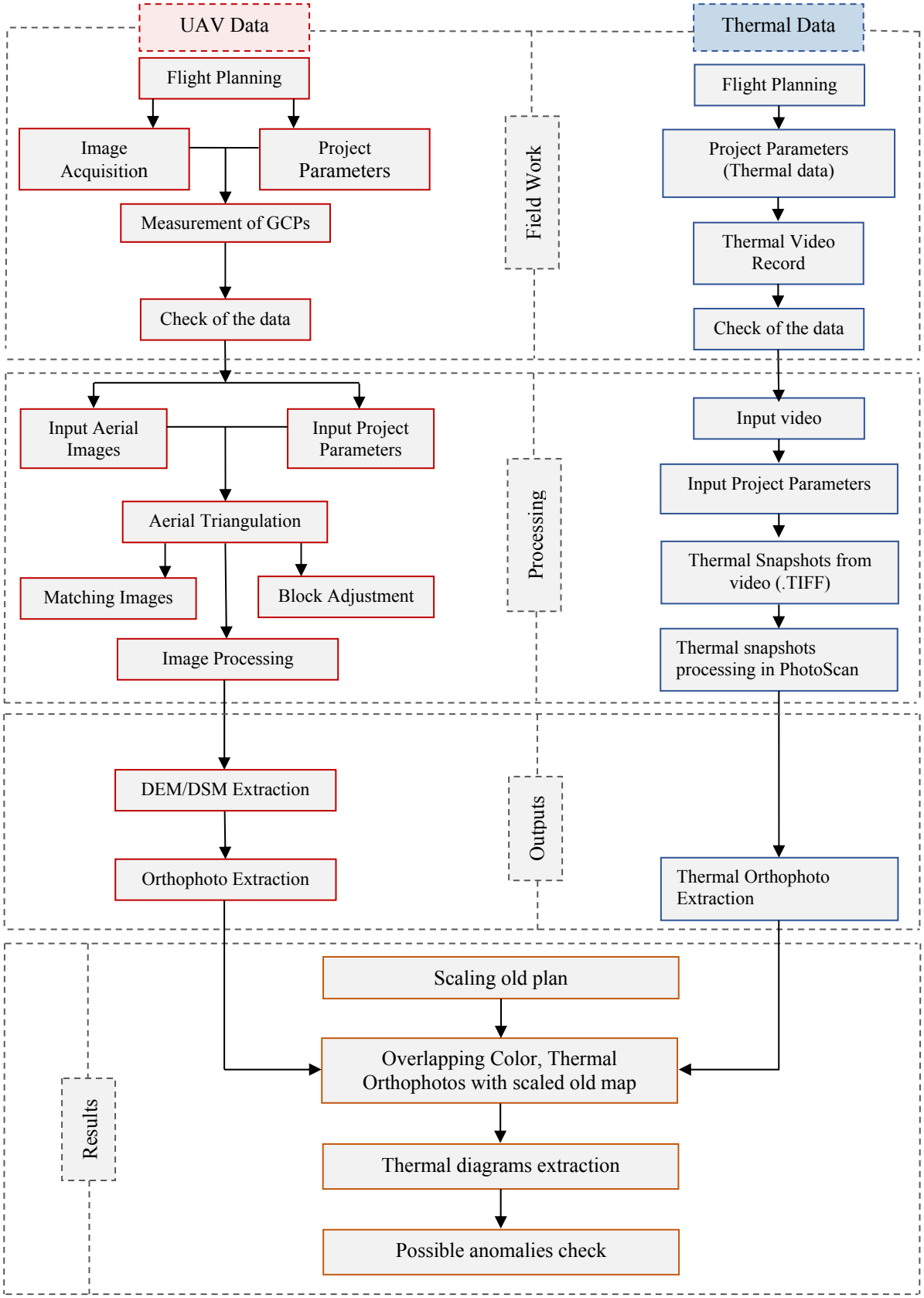

5.3.4.Field Work

UAV for aerial data

UAVs offer key advantages for archaeological aerial imaging, especially for covering large areas, their ability to fly at fixed height and speed helps for aerial thermography image acquisition since image acquitision is highly time-sensitive. To maximize archaeological visibility, thermal images need to be collected at a time of day when thermal inertia is highest between the archaeological target and background and the surveyed area must be covered with little temporal variability in order to reduce drift in thermal values in thermal mosaic scene.

In this project, AeroMax 600 drone from MicroGeo was used with a camera SONY Alpha 5000 with 14.2 MP resolution, 22 mm focal lenght, 5.16 µm pixel size(Figure 5.3.14) . The AeroMax is a multirotor drone 3.9 kg with 4 motors. Maximum speed of it is 11 m/sn and climb rate is 7 m/sn and the maximum flight time is 12 minutes with operating temperature between -10 to 40 ℃ (Figure 5.3.15)

Figure 5.3.14: AeroMax600 drone with main camera (left) and with thermal camera (right)

Figure 5.3.15: SONY Alpha 5000 camera (left) and OPTRIS PI 450 thermal camera (right)

In the field, several flights were made with AeroMax 600 drone with thermal camera Optris PI 450. Thermal camera was not able to tkae images instead it was used with its video record. Its measurement speed was max. 80 Hz with 383 X 288 px optical resolution. It can take measuremnets in the range of -20 ℃ - 900 ℃ with spectral range between 7.5 to 13 µm (table 5.3.3).

Table 5.3.3: Technical parameters of AeroMax 600 UAV

Technical Parameters AeroMax 600 UAV	
Type	Multirotor
Wieght (incl. supplied camera&battery)	3.9 kg
Motor	4 electric brushless motors
Max airspeed	Automatic flight: 11 m/s
Max climb rate	7 m/s
Maximum flight time	Up to 12 minutes (in autonomous mode)
Autopilot&control	IMU, magnometer, barometer&GPS/GNSS
Operating temperature	-10 to 40 ℃
Payloads (cameras)	
Main camera SONY Alpha NEX-5	
Still images resolution	4592 x 3056
Resolution	14.2 MP
Focal length	22 mm
Sensor size	23.7 x 15.6 mm
Pixel pitch	5.16 µm
Thermal camera-OPTRIS PI 450	
Still images / video	Video
Measurement speed	80 Hz
Optical resolution	382 x 288 px
Temperature range	-20 ℃ - 900 ℃
Spectral range	7.5 to 13 µm
Field of view (FOV)	62°

In these kinds of case studies, especillay when it is worked with therma lcaera, both for safety reasons and technical requirements, the field work must be operated with a trained pilot. Additionally, an operator with thermal background is preferred for checking the data and controlling thermal image acquisition in the field. A trained pilot from MicroGeo helped and operated this case study with us.

While working on large areas with thermal camera, it is not possible to collect all images in one flight. It would be possible to collect a large number of images or longer video record from a lower height however the short flight time of UAV, max. 12 minutes, made this impossible and impractical. In order to cover larger area, it could be solution to increase the flight height however the number of blurring images cooul increase. For thermal image acquisition the flight height was choosen 25 m ,with 2,4 cm ground sampling distance (GSD) for thermal image and image footprint was 23.99 x 18.02 m with 30 Hz speed which enables to extract images from the video with %80 or greater overlap. Because the flight time limitation of UAV it was not possible to complete all area in one flight. Totally 5 thermal flight was conducted on the field. They were at 7.38 am with flight duration 10 minutes, 8:43 am with 8 minutes flight duration, 9:16 am with 10 minutes flight duration, 15:16 pm with 7 minutes flight duration and 19:00 pm with 8 minutes flight duration. Sensor size of the camera was 23.99 x 18.02 (WxH).

In the field, two flights were conducted for completion of the area with UAV payload with SONY Alpha NEX-5 camera with 22mm focal lenght. The flight height

was set 50.5 m and the images were acquired at 11:21 am and 12:01 am with 10 minutes flight duration. Thesidelap was %60 and overlap was %40, the distance between two lines were 16.36 m and the baseline was 135 m. The GSD was 1 cm (0.0106748 m / px). At the end of two flights, totally 108 images were acquired.

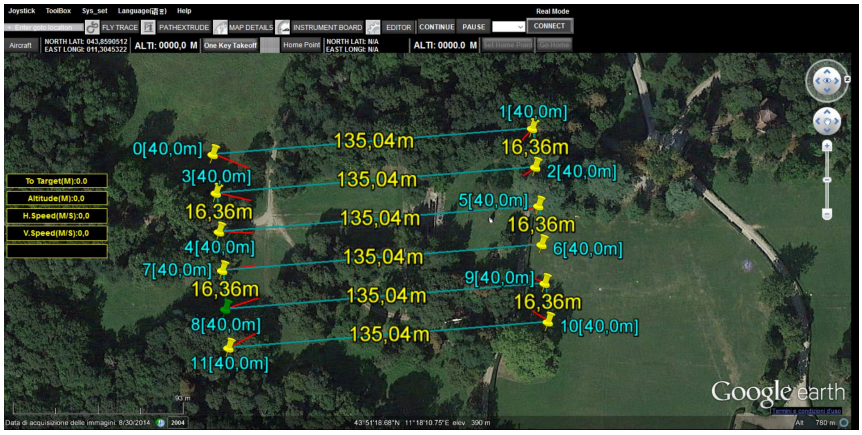

Figure 5.3.16: Flight planning in DJI Ground Control Station

The flight trajectory and the image acquisition points were calculated depending on the scale, camera parameters, flight height, dimension of the area and the overlaps in DJI Ground Control Station software. 108 images were acquired in 6 strips and all field survey was completed in one day.

During the survey, for the georeferencing of the images, totally 12 GCPs (black and white A4 size targets) were placed in the surveyed area. Using a total station, theri position were recorded within the coordinate system. In order to process thermal images 15 aluminium sheeting targets were used since it has very low thermal emissivitiy so they tend to appear dark in thermal images and video. The targets were in different size. We had 5 targets in 40 x 40 cm, 50 x 50 cm and 60 x 60 cm in order to be able to see them in low resolution video record.

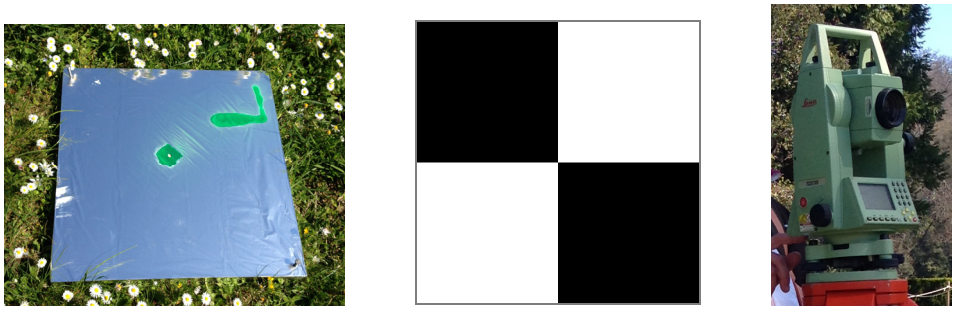

Figure 5.3.17: Aluminium sheet covered targets for thermal imagery (left) and black&White targets for aerial color imagery (middle) and total station used to measure control points (right

Except from two flights with UAV with SONY camera, 5 more fligths were conducted in the area with thermal camera. For thermal flight, the flight height was 25 m with 30 Hz flight speed .

Thermal flights was done in different period of day to see diurnal temperature change on area. The five thermal flight begun at 7:38 am and continued at 8:43 am, 9:16 am, 3:16 pm and 7:50 pm on 25 m height. According to Lunden (1985), a suitable time for registration is spring time when the surface of the ground is drying out so this field

survey was conducted at 8th April 2015. We tried to collect images at early in the morning, in the afternoon and just after the sunset. Since the duration of UAV in the area is max. 11 minutes, we couldn't have thermal and color data of all area in one flight. We divided the area mainly three parts (Figure 5.3.18). So we were able to get color orthophoto with two flights and thermal orthophoto with one flight. Since the temperature was changing, thermal orthophoto could be created with snapshots from 7:38 am flight.

Table 5.3.4: Summary of flight times, temperature, duration and weather conditions during aerial surveys

Time	Camera	Duration	Part	Temperature	Humidity
7:00 am	Optris PI450	10 min.	2 nd part	-1 ℃	%72
8:43 am	Optris PI450	8 min.	3 rd part	3 ℃	%68
9:16 am	Optris PI450	10 min.	1&2 nd part	6 ℃	%68
11:20 am	SONY Alpha NEX-5	9 min.	1&3 rd part	10 ℃ with wind 3 km/h	%43
12:05 am	SONY Alpha NEX-5	10 min.	2 nd part	12 ℃ with wind 2 km/h	%33
3:16 pm	Optris PI450	7 min.	3 rd part	17 ℃with wind 10 km/h	%22
7:50 pm	Optris PI450	8 min.	2 nd part	16 ℃ with wind 16 km/h	%45

Figure 5.3.18: Divided parts of the surveyed area

5.3.5.Data Processing

Aerial Color Data Processing

In this study, for aerial image processing PhotoScan 1.1.5 was used. Image alignment was carried out with 99 cameras of 108 with 27 GCPs (Figure 5.3.19-20). The images were aligned with 23, 438 tie points(Figure 5.3.21).

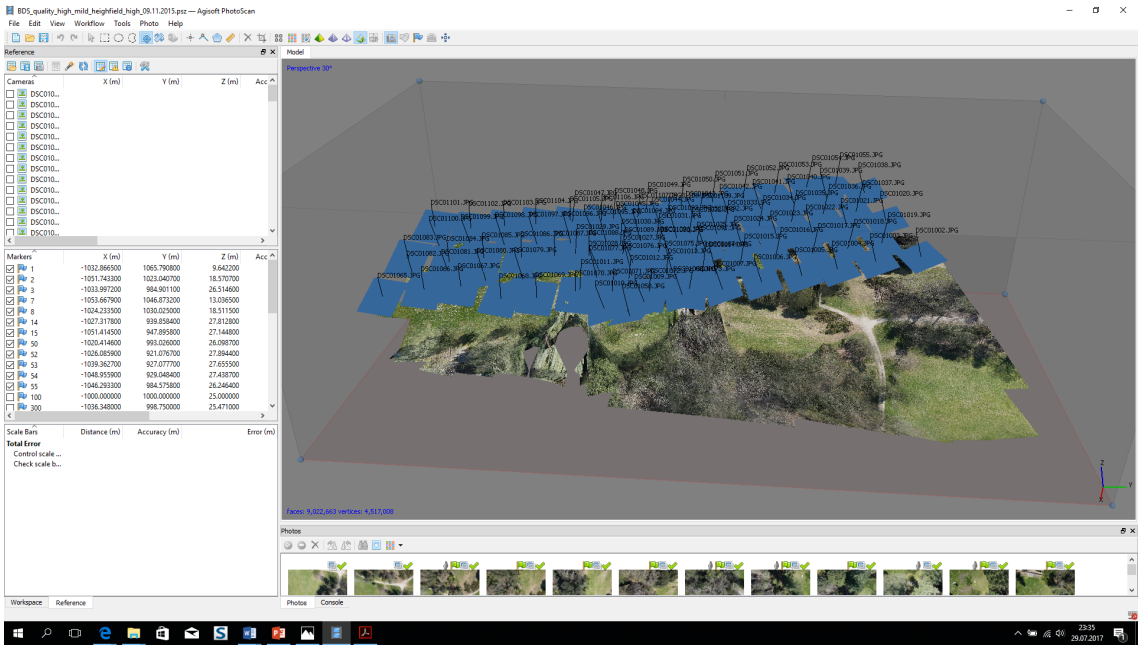

Figure 5.3.19: Camera positions in Agisoft PhotoScan

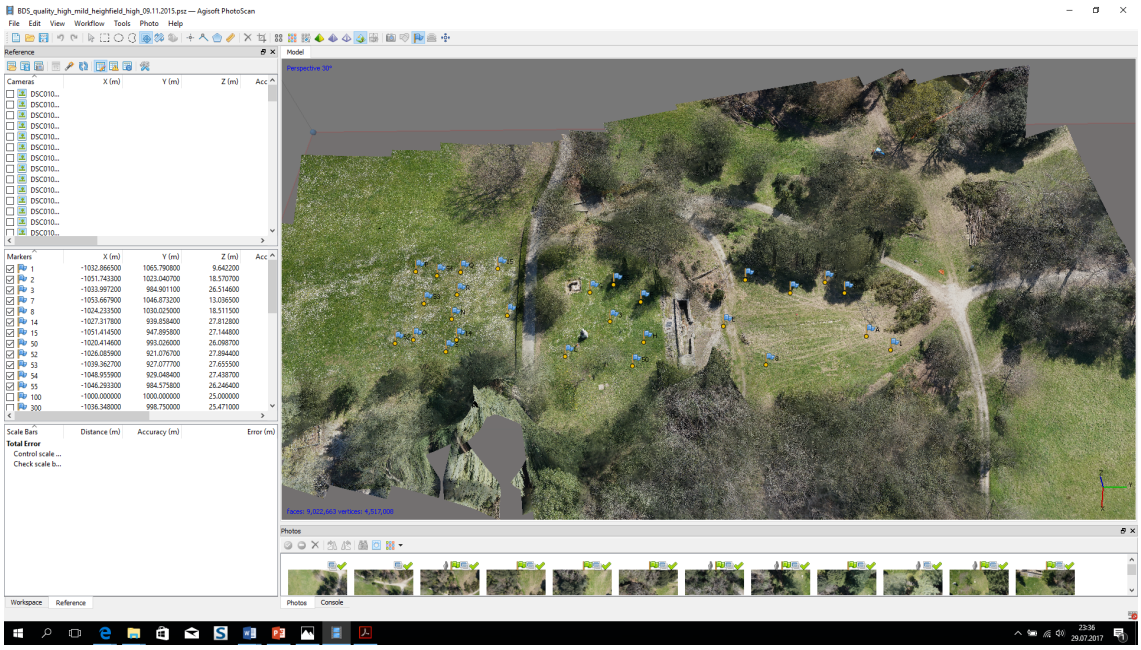

Figure 5.3.20: GCPs positions and in Agisoft PhotoScan

At the end of image alignment, total error was 0.027358 m for GCPs and 0.632 pixel.

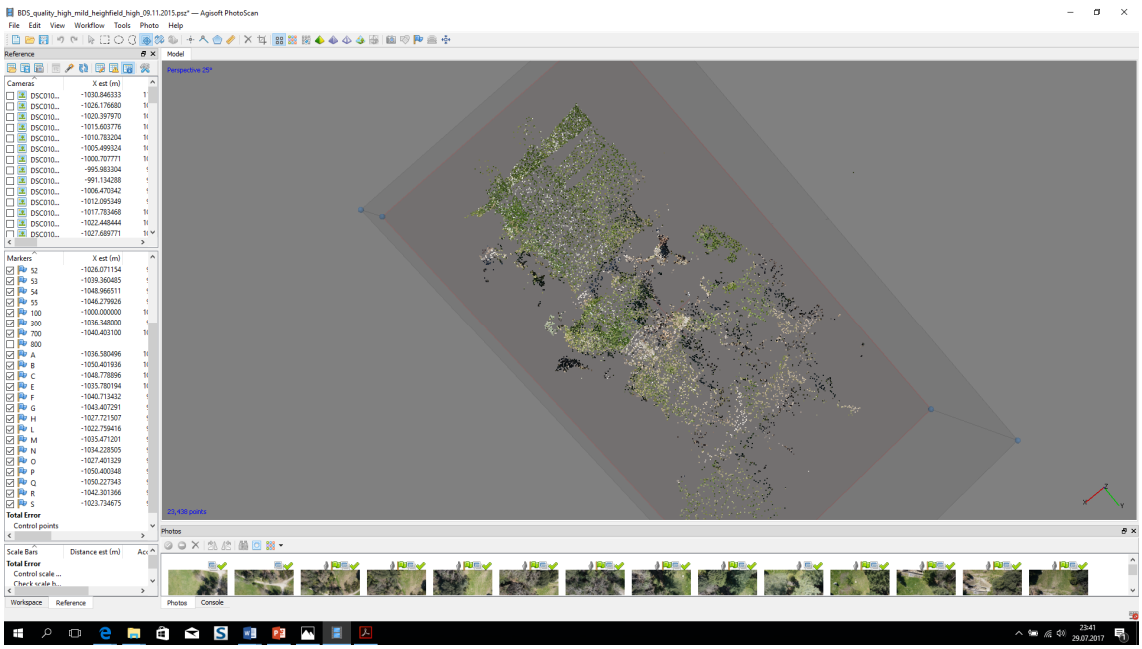

Figure 5.3.21: Point cloud model with 23, 438 tie points in Agisoft PhotoScan

Then dense point cloud model was created in high quality parameter. After the process dense point cloud model had 45, 398, 256 points. (Figure 5.3.22)

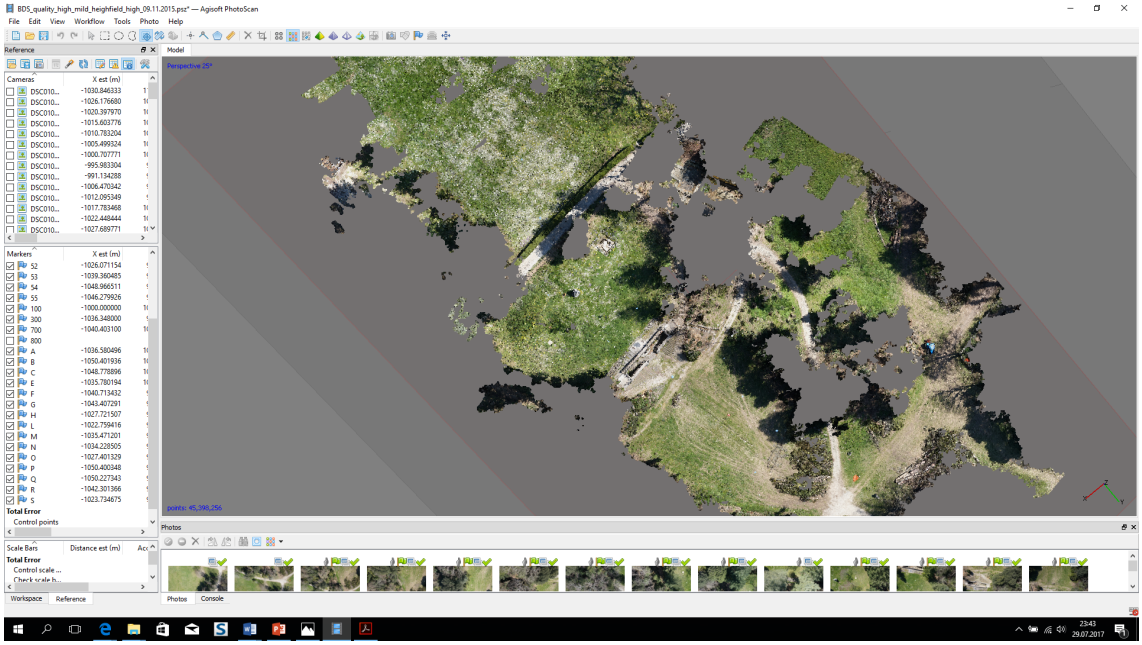

Figure 5.3.22: Dense point cloud model with 45, 398, 256 points

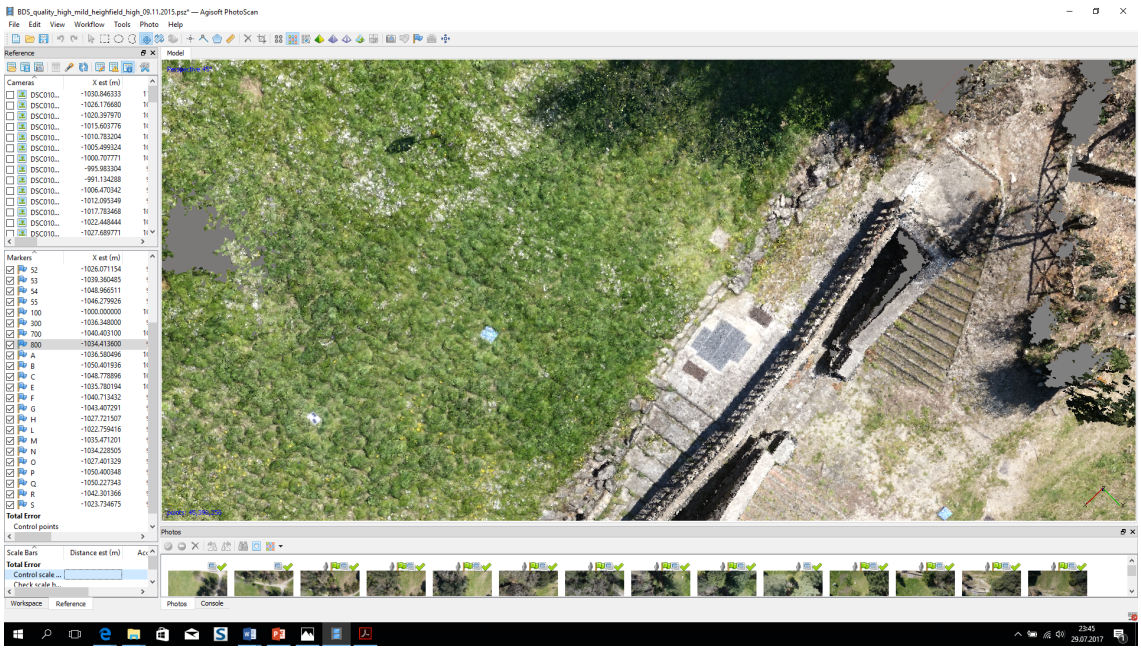

Figure 5.3.23: Detail in dense point cloud model

After the dense point cloud model, mesh model was processed and at the end it was acquired 9,022,663 faces and 4,517,008 vertices mesh (Figure 5.3.24).

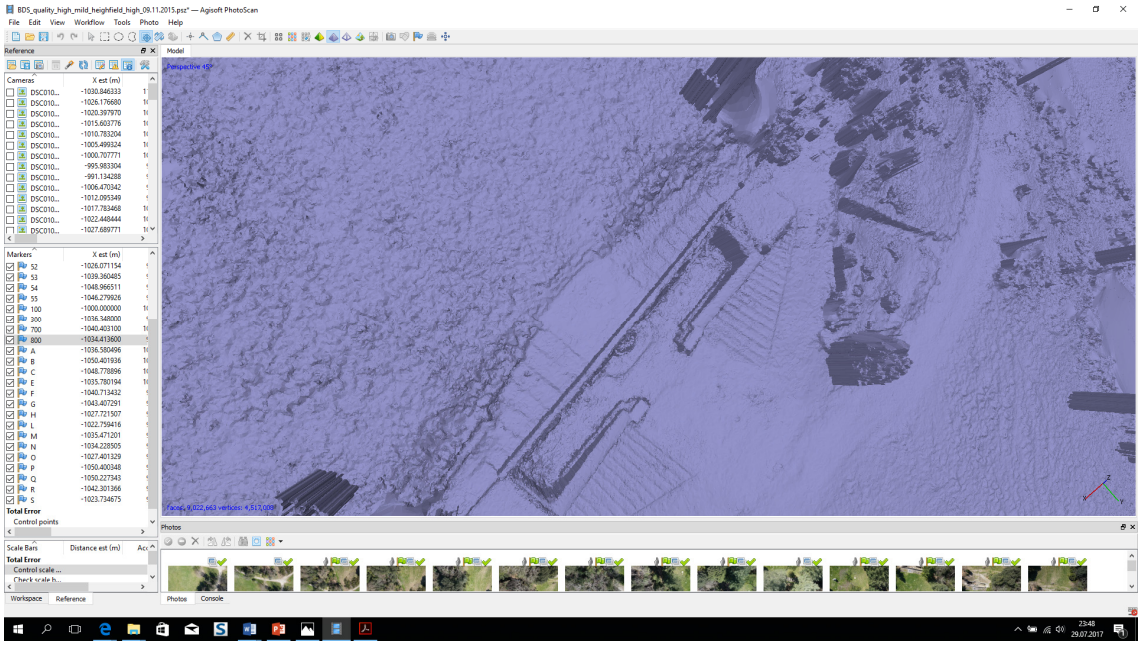

Figure 5.3.24: Detail in mesh model

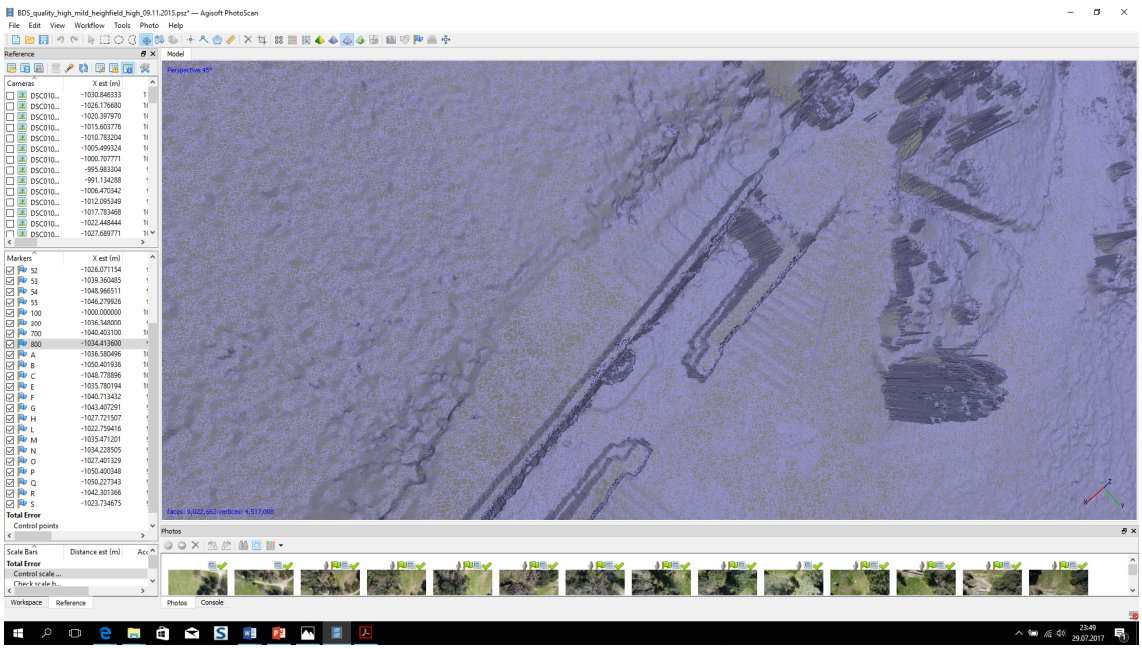

Figure 5.3.25: Detail in frame model

Aerial Color Data Results

0.0382 km² area was covered with 1.07 cm/px ground resolution and with 1.78 px reprojection error with Sony Alpha NEX-5 camera. The camer calibration parameters are given in table 5.3.5.

Table 5.3.5: Project parameters for color aerial data

Project parameters	
Flight Height	50.5 m
Ground resolution	1.07 cm/px
Coverage area	0.0382 km²
Sidelap	%60
Overlap	%40
Number of strips	5-6
Number of images	108
Number of GCP	27
Aligned cameras	99
Coordinate System	Local Coordinate System
Dense point cloud points	45,398,256
Tie points	23,438
Projections	84,301
Reprojection error	1.78 px
RMS reprojection error	0.632 px
Faces	9,022,663
Vertices	4,517,008
DEM resolution	2.13 cm/px
Orthomosaic size	8,192 x 8,192

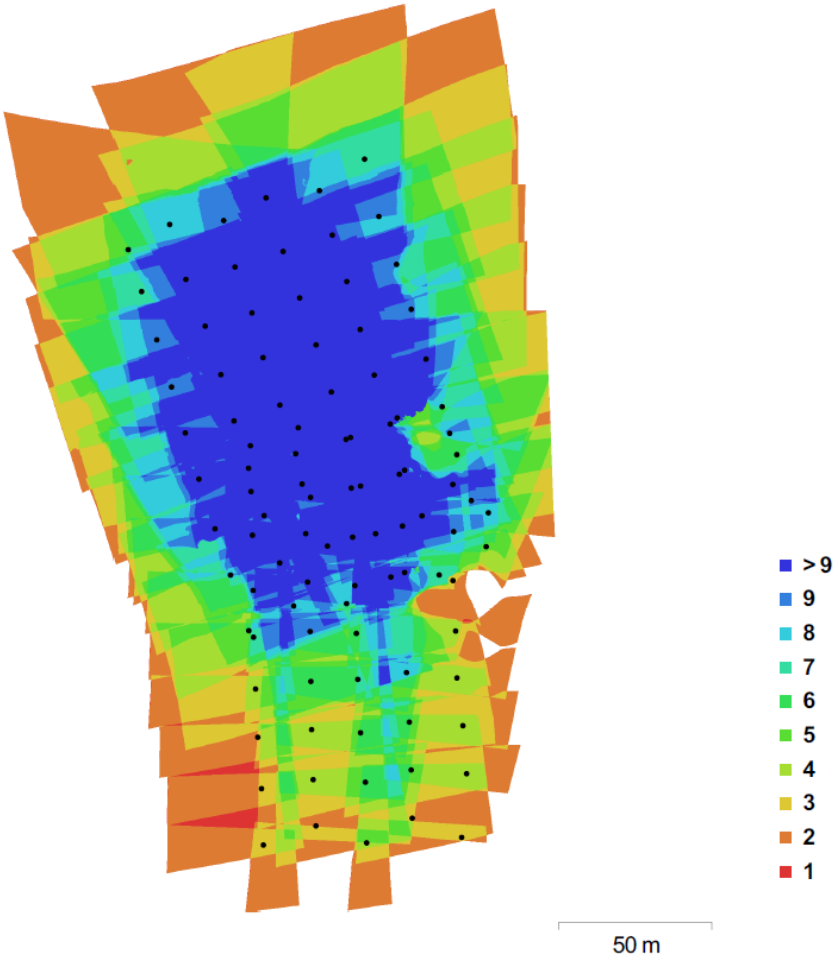

Figure 5.3.26: Camera locations and image overlap in Agisoft Photoscan

Table 5.3.6: Camera calibration parameters

Sony Alpha NEX-5 22 mm Camera Calibration Parameters			
Resolution	5456x3632	F	5241.83
Type	Frame	B1	-1.3486
Cx	-63.7104	B2	19.1937
Cy	52.6104	P1	-0.000267941
K1	-0.0495716	P2	-0.00312287
K2	0.284889	P3	0
K3	-0.0564159	P4	0
K4	0		

27 GCPs RMSE values were 1.04843 cm in X, 1.55077 cm in Y, 1.99509 cm in Z and in total 2.73577 cm and 0.632 px (Figure5.3.27).

Figure 5.3.27: GCPs locations

Count	X error (cm)	Y error (cm)	Z error (cm)	XY error (cm)	Total (cm)	Image (pix)
27	1.04843	1.55077	1.99509	1.87192	2.73577	0.632

Figure 5.3.28: GCPs RMSE values in total

Reconstructed DEM model resolution was also satisfied. The resolution of DEM was 2.13 cm/px and point density of the model was 2.190003 points/m² (Figure 5.3.29)

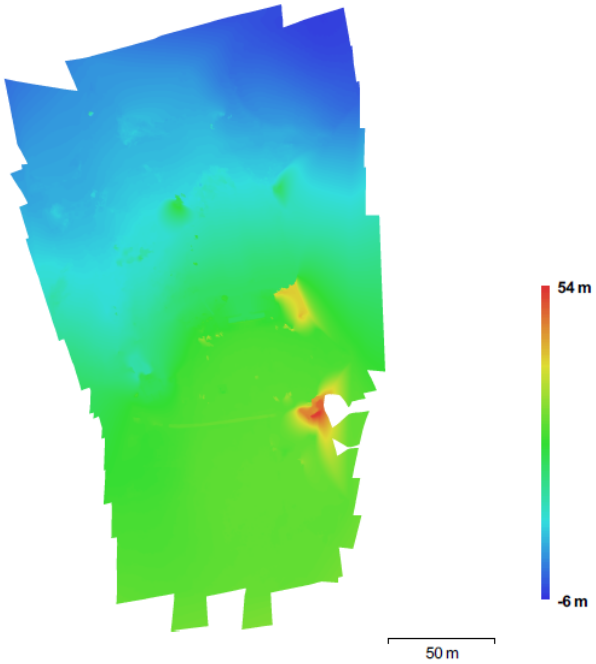

Figure 5.3.29: DEM model

Label	X error (cm)	Y error (cm)	Z error (cm)	Total (cm)	Image (pix)
1	-1.49041	1.77279	0.563623	2.38365	0.481 (11)
2	0.925807	-2.01287	-0.209518	2.22546	0.578 (13)
3	0.871849	-2.21501	1.12937	2.63474	0.749 (12)
7	-0.462267	0.216197	-1.90458	1.97177	0.674 (11)
8	0.937869	1.93144	0.332868	2.17275	0.316 (9)
14	-1.30446	0.285347	1.64727	2.1205	0.447 (6)
15	-0.239745	0.150815	-0.276676	0.395945	0.390 (8)
50	0.419633	-2.57726	-0.352988	2.63495	0.527 (16)
52	1.47464	1.68587	0.687111	2.34283	0.107 (5)
53	0.221549	0.848143	-1.15718	1.45172	1.064 (5)
54	-1.06111	1.02883	0.890064	1.7253	0.443 (6)
55	1.33735	-2.08349	-0.230392	2.48647	0.606 (12)
A	-1.16961	1.90904	-0.914181	2.4183	0.539 (14)
B	-0.923582	0.775432	-0.621256	1.35656	0.395 (14)
C	0.230369	1.09916	0.883335	1.42881	0.599 (13)
E	0.580632	0.111665	-1.1143	1.26145	0.455 (13)
F	0.39675	-1.65033	2.37174	2.91653	0.594 (12)
G	1.37095	-1.5179	0.091275	2.0474	0.588 (10)
H	0.669268	-2.19572	1.60985	2.8037	0.496 (14)
L	0.48844	-2.61875	-0.563466	2.72286	0.490 (7)
M	0.379882	-0.896397	-4.98845	5.08256	0.465 (7)
N	-1.55049	1.53903	3.76852	4.35595	1.116 (6)
O	2.19711	2.16059	-2.80598	4.16761	1.547 (4)
P	-0.894767	-0.479368	-4.00654	4.13313	0.224 (3)
Q	-1.52429	1.0559	0.983147	2.0988	0.941 (6)
R	-0.896592	1.35854	4.51868	4.80291	0.834 (6)
S	-1.01751	0.377925	-0.583273	1.23221	0.999 (8)
Total	**1.04843**	**1.55077**	**1.99509**	**2.73577**	**0.632**

Figure 5.3.30: GCPs RMSE values

Figure 5.3.31: Orthophoto of the surveyed area

Aerial Thermal Data Processing

Eventhough aerial thermography has been used since 1970s in archaeological field, archaeologist have recognized the advantages of this technique for reconizing both surface and subsurface remains. Even this method was more expensive, with the use of UAVs this technique has been strated to be used in archaeology. There are several studies done whic are descried in detail in section 4.8. with aerial thermography used fields and related works (see section 4.8).

The aim of this stufy to present a methodology for cellection of thermal images using a UAV in order to reveal subsurface cultural features of and archaeological area. To try this method, aerial surveys both color and thermal were conducted on a Villa Medici which is located in Pratolino Park in Florence. The methodology aims to produce data of traditional archaeological remains in terms of feature visibility, and to get data in non-destructive way with minimum cost.

Thermal Data Processing

For aerial thermal data processing, firstly a thermal orthophoto was created in PhotoScan (Figure 5.3.36). To be able to get a thermal orthophoto, needed thermal snapshots were saved as .TIFF format from the video in Optris PI connect. For this, the 7:38 am flight which was carried out early in the morning was choosen. Beginning from the 36th seconds (when the UAV got the optimum and stable flight height), in each 5 second, it was taken a snapshot, which means %80 sidelap for each image. In total, 72 snapshots were saved as .TIFF from the video and they were imported to PhotoScan as photo.

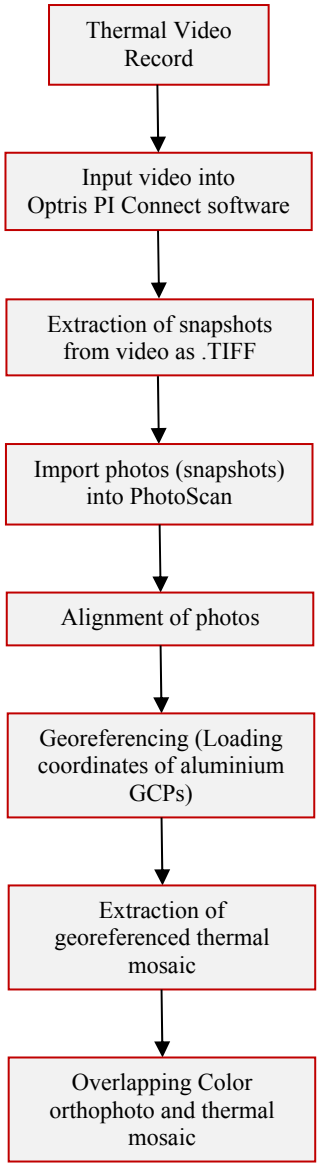

Fure 5.3.32: Workflow of georeferenced thermal mosaic

In Photoscan software, firstly the photos were aligned. After the alignment of the photos, aluminium sheet covered GCPs were georeferenced with the same reference system of color images in Photo Scan and thermal orthophoto was created (Figure5.3.32-33-34).

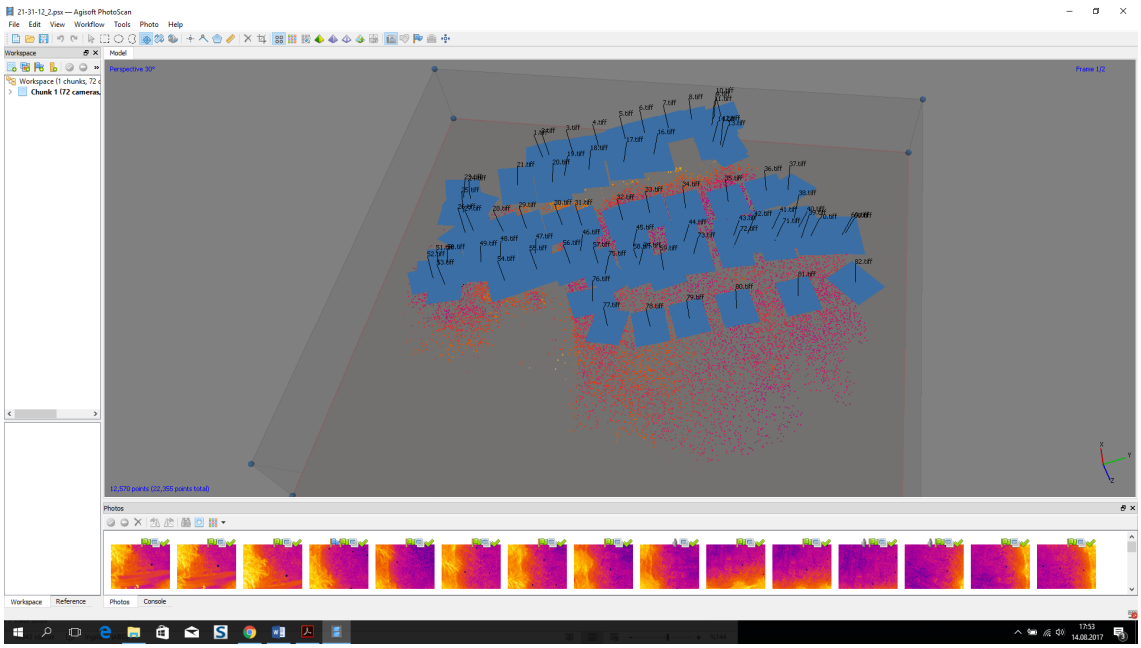

Figure 5.3.33: Camera positions in PhotoScan

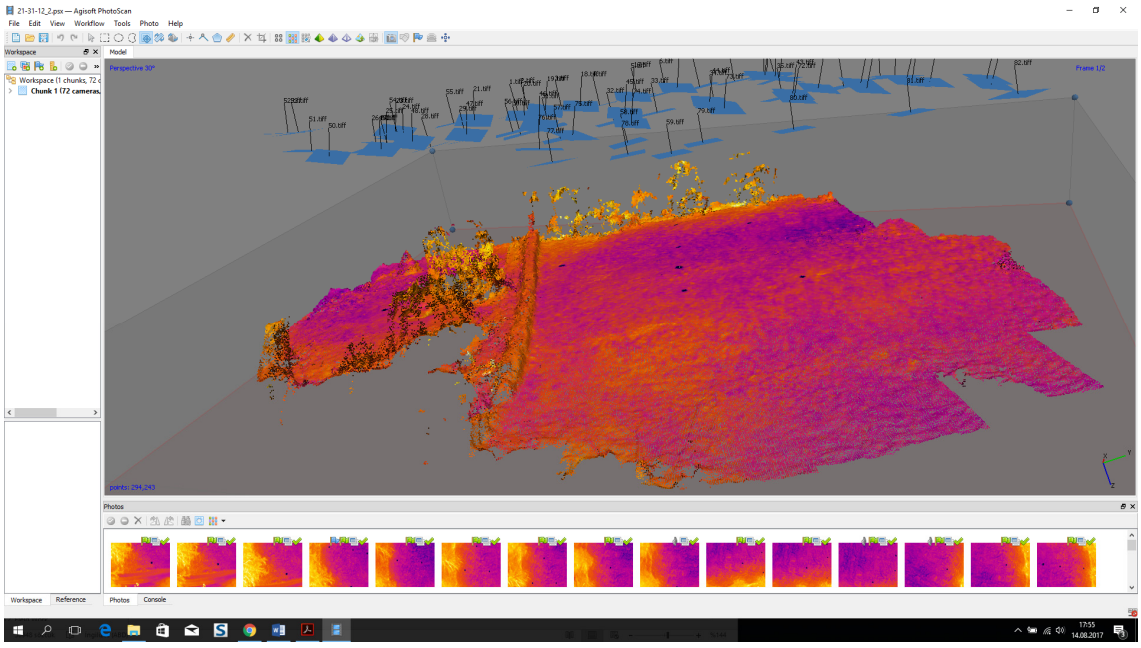

Figure 5.3.34: Dense point cloud model with 294,243 points in PhotoScan

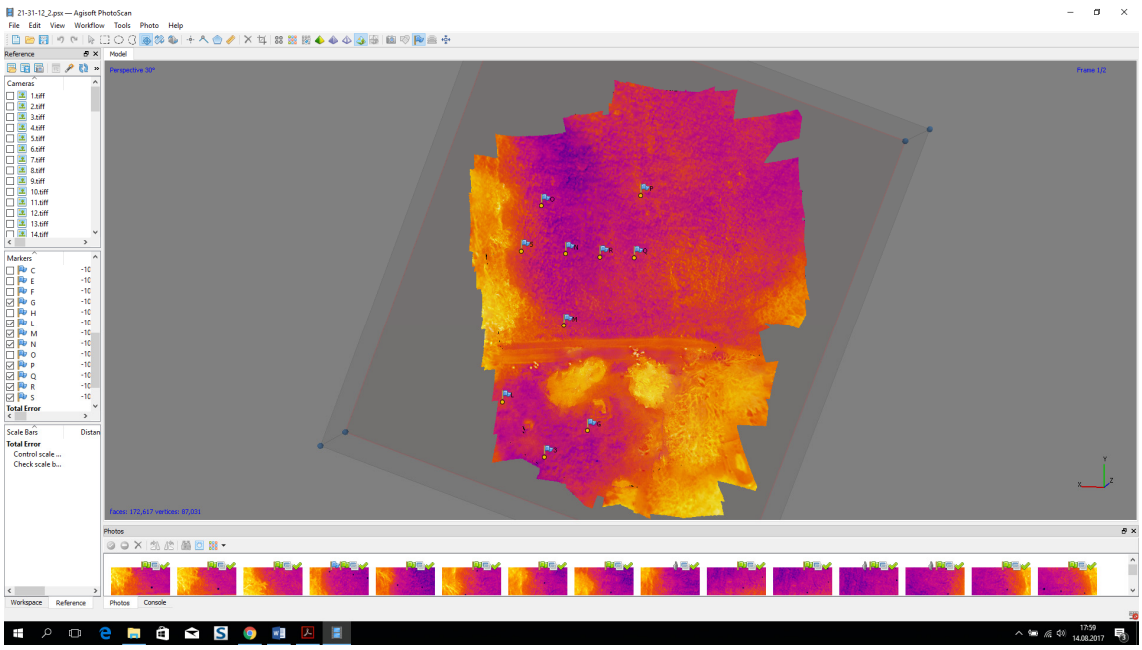

Figure 5.3.35: Georeferenced aluminium GCPs in PhotoScan (textured model)

After getting georeferenced thermal mosaic in PhotoScan, it was overlapped with color orthophoto (Figure 5.3.36).

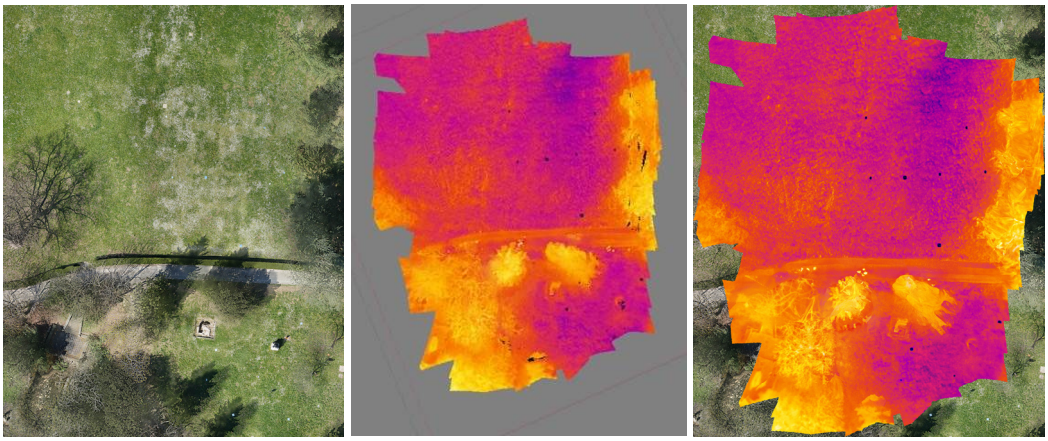

Figure 5.3.36: (left) A part of color orthophoto, (middle) Thermal orthophoto in PhotoScan, (right) overlapped color and thermal orthophoto with aluminium sheet covered targets in black

Villa Medici had important spaces during the history. For estimation of the anomalies under the ground, old plan of the Villa (Sgrilli, 1742) was an important data and indicator about the building. The old plan of the Villa Medici was scaled in AutoCAD and overlapped with orthophoto in AutoCAD (Figure 5.3.38).

They were set in the same scale to see how the building was located on the area with help of some reference points and scale. It was aimed to have an idea of possible ruins locations under the ground. To have an idea for possible anomalie areas, the same possible areas were determined in thermal video. After input of thermal parameters, several snapshots were saved as .csv file. These .csv files were imported to excel then thermal profile graphs were prepared in excel. According to these temperature profiles, overall evaluation was made. The workflow for thermal images processing is given Figure 5.3.37 below.

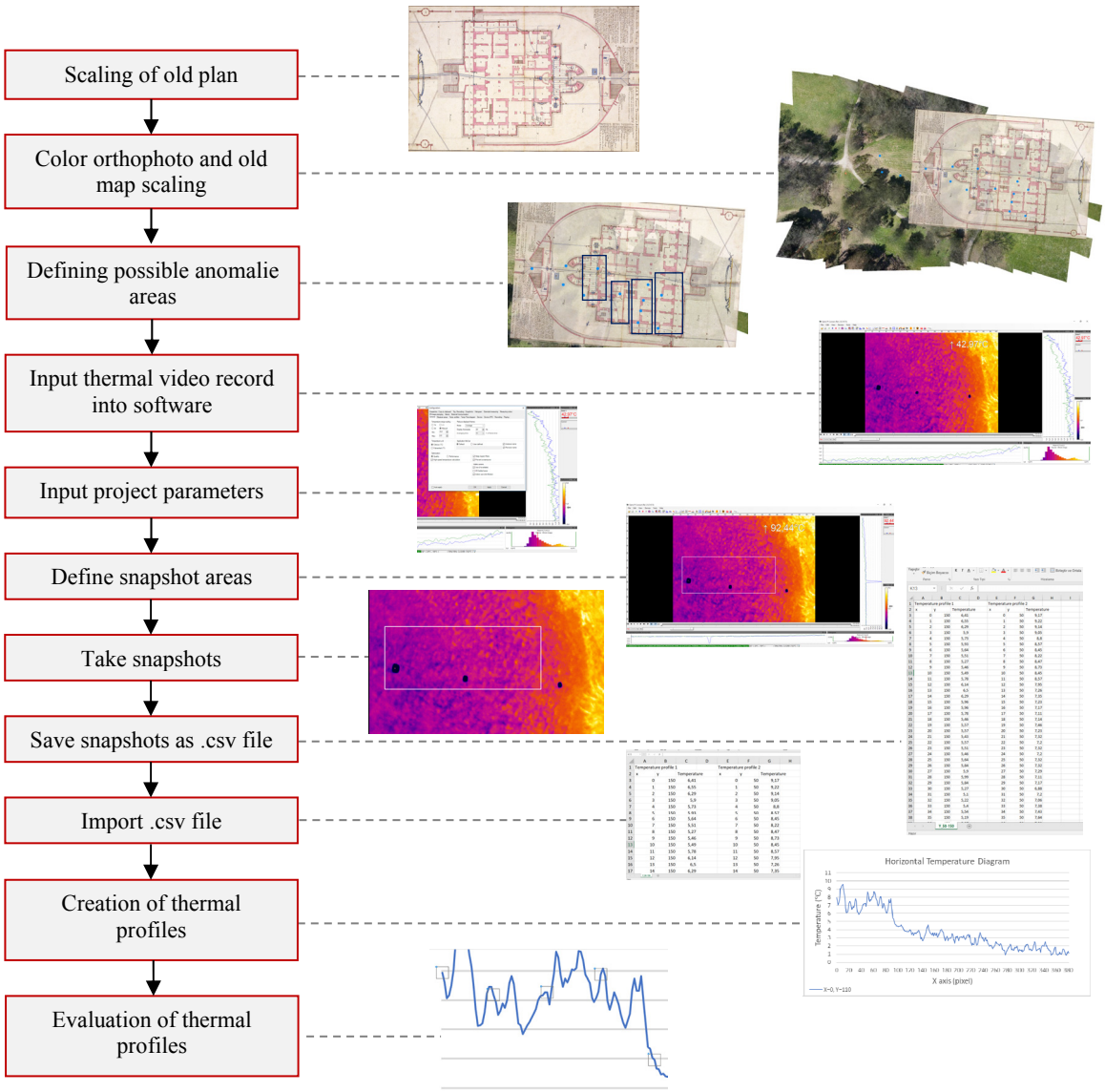

Figure 5.3.37: Detailed workflow for processing thermal images

Figure 5.3.38: Overlapped map of color orthophoto and and old map with GCPs in blue

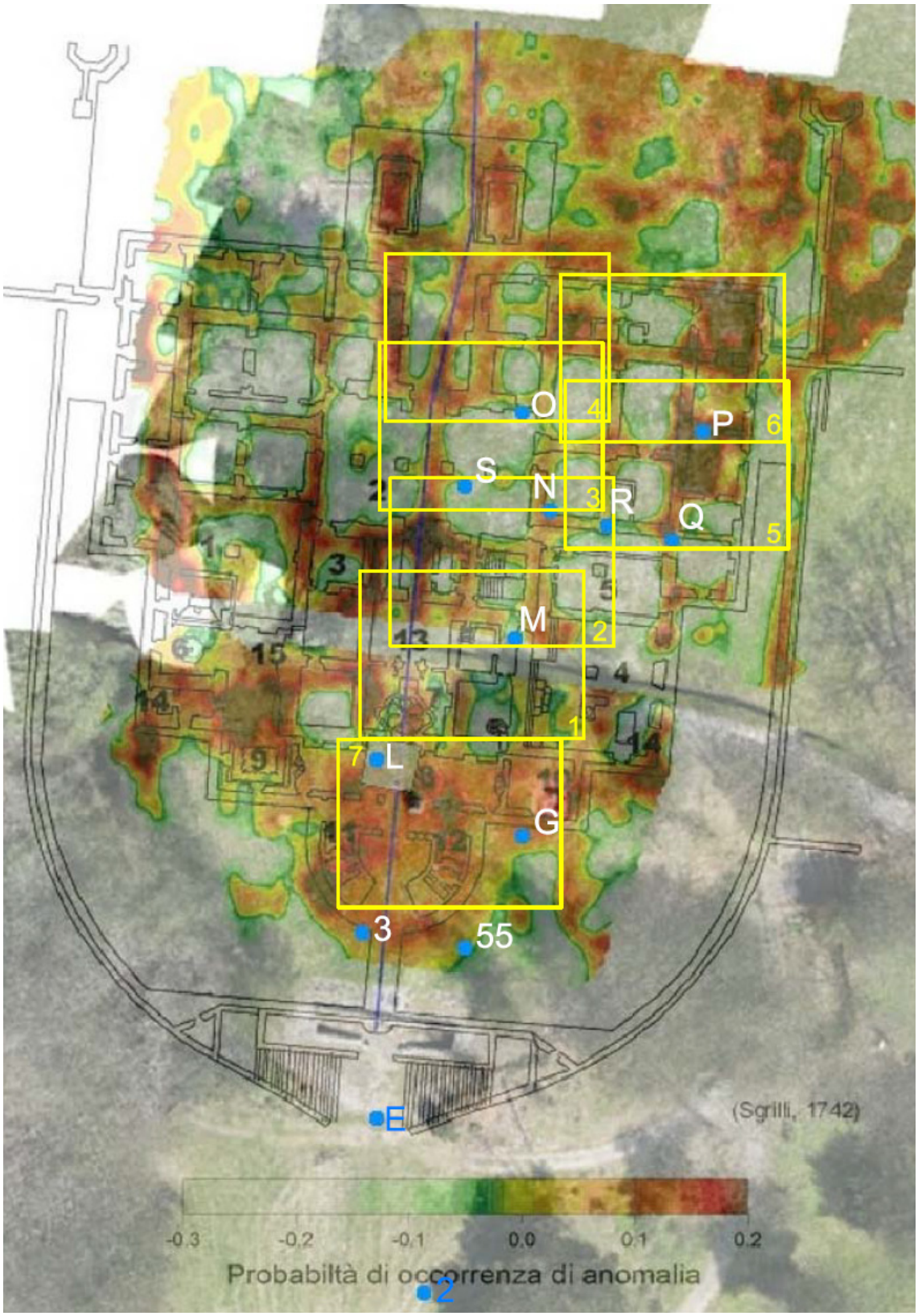

Figure 5.3.39: Frames dividing the area for thermal anomalies (frames and the number of frames are in yellow and control points are in blue)

With the reference of this overlapped map, all area divided in snapshots area. For maximum visibility, thermal parameters were entered to the software. Emissivity

value was set 0.98 for grass since the area was grassed. Ambient temperature was set -1□. Depending on thermal camera features, each snapshot 382 x 288 px corresponds 23.99 m width and 18.02 m height on object surface. And each pixel equals to 6.283 cm on the object surface (Figure 5.3.40).

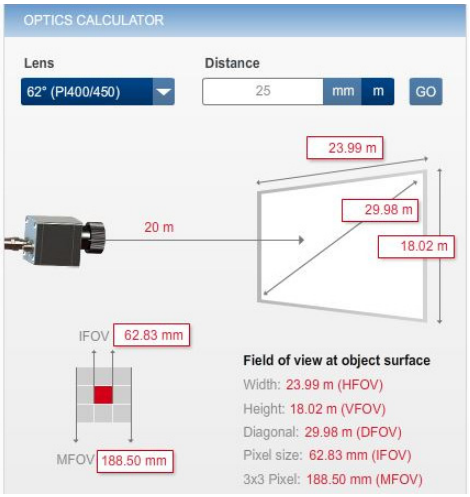

Figure 5.3.40: Optris PI 450 FOV at object surface

In order to cover area, it was divided totally 7 frames. Mostly the frames were taken from 7:00 am and 7:50 pm flight means mainly 1 st and 2 nd part of the area (Figure 5.3.39) where the Villa located on. Each frame was divided to several parts (approximately 1.20 m) to check the anomalies. Since the sides of the area was covered with trees, they were seemed as hot areas. Eventhough there was the probability of archaeological features under the trees, it was not possible to interprate the data on these parts. Since the survey was conducted on March, the grass was not so grown however vegetation makes difficult to process thermal data. The best images for archaeological visibility is 7:00 am flight. The sunrise time was 6:57 am. After this flight, since the ambient temperature increases and the sun warms vegetation, it rises the noise and the temperature difference decreses so the visibility becomes more difficult. While 7:00 am flight has sunlight over the trees and the surface features differently reflect thermal radiation since some parts of the area was covered with fresh small camomiles, while some parts were still soil. Subsurface features far less apparent in 3:16 because of the sun. Also the visibility is relatively high in 7:50 pm flight, just after the sunset which was 7:45 pm. However, a part of this video is not good and has too much noisy. In this project, temperature profiles showing temperature difference are taken reference more than visibility. So each snapshot was saved as .csv file and was converted to temperature profiles as graphs in excel. Also the temperature differences are more defined in 7:00 am flight and 7:45 pm flight. When it's considered and compared the same places in different times, there are some areas cooler than environment in the mornig and warmer in the evening.

5.3.6.Results and discussion

The excavation at 2009 show that the structural remains of the villa are only 0.21 cm from the ground and the stratigraphic sequence is well presented. As it can be seen A-A' (S-N) section of the first excavated area, stove cave) as in Figure 5.3.11-12, protected layers are composed of humus, clay, tiles, stones, bricks and soil. As it's seen in C-C' (W-E) section, after humus and clay vertically, large rubbles can be seen on the floor. Stone drainage channel and the tube for the chanel give us information about what kind of materials there are in the subsoil. It is also mentioned that, the maintenance of the plant is provided by the level of loose sandy soil and located in the duct which covered the brickwork pipe protecting it from the collapse of the vault. In the excavation, collapsed materials such as masonary material, cave decoration elements, broken and collapsed fragments of upper walla. Among the materials collected from the excavation, there are aslo parietal and floor decorations. Floor tiles are distinguishable in mainly two types the rectangular ones with a blue background and an orange frame which, based on the remains of pavement preserved in situ. While the white squares formed the central floor mat. However, excavated area "Stove Cave" floor had to be built over terracota tiles. Particular areas of the floor were also made with mosaics of black and white river pebbles which were found. These pebble floor were also documented in Demidoff monument area (Desideri, 2009).

Depending on the excavation results, it cann not be said there is a certain material under the ground. Each material found in the area has different thermal properties. Considering their emissivity, (pg:200) (non-metaliclerde 0.80-0.95)
-Soil (dry-wet): 0.92-095 ε
-Red Brick: 0.93 ε
-Clay: 0.95 ε
-Clay tiles: 0.33 ε
-Sand: 0.90 ε
-Sandstone: 0.67 ε
-Grass: 0.98 ε

Considering their thermal conductivity (W/m.℃) (pg:199)
-Soil (dry): 0.3 ℃
-Brick: 0.6-1.2 ℃
-Clay: 0.25-1.08 ℃
-Sand: 0.3-2.95 ℃
-Sandstone: 2.5-3.2 ℃

Considering the thermal inertia (P), (pg:196)
-Clay soil: 0.042
-Sandy soil: 0.024
-Sandstone: 0.075
-Brcik, stone have high thermal inertia.

As detailed described in Chapter 4.3 (pg:195), emissivity, thermal conductivity and thermal inerta helps for detection of buried archaeological targets. In the morning, a subsurface feature that enhances drying would be visible as positive anomaly while it reverses in the evening.Potential strength of thermal anomalies depends on the relative inertias of the archaeological feature and surrounding subsoil. If the material has high thermal inertia, It heats up and cool down slowly. While the soil heat more quickly in the sun and cool just as fast as night. With the help of this property, estimating the potential strength of anomalies in different context becomes easier (Cool, 2015).

According to Périsset and Tabbagh (1981) studies, depending on the thermal properties, the temperature difference between the target and its surrounding is directly related with heat flux. Another key thermal property is the volumetric heat and cconductivity relation. A material with high conductivity and low volumetric heat, will have high diffusivity, means that heat travels quickly. However the material with low conductivity and high volumetric heat will retain more heat.

Périsset and Tabbagh (1981)

-If the superficial layer increases in thickness or conductivity and decreases in diffusivity, the thermal signature of the feature will reduce.

-Features located in low conductivity and low diffusivity subsoil will have a stronger thermal signature.

Scollar et al. (1990) emphasized the role of vegetation in thermal imaging. Dead or inactive plants have poor heat conduction, instead the temperature of living plants is regulated by transpiration, not by the surface they grow. The vegetation hide the thermal behavior of subsurface features. However some subsurface features like stone walls impede the growth of roots and plants.

As the soil density increases, the heat capacity increases as well. Stone walls contain less water and higher heat diffusivity and lower heat capacity which means it can be observed strong cooling when the air temperature drops (Stanjek and Faßbinder, 1995). In general, dense materials—stone, packed earth—tend to resist temperature change and retain the day's warmth. Moist areas tend to be cooler owing to the effects of evaporation, temperature variations occur across plant types caused by evapotranspiration, the cooling mechanism of plants, and vegetated surfaces generally are much cooler than bare, open earth (Scollar et al. 1990).

In the content of this study, the area was divided several parts and thermal profiles of each part was taken as temperature diagram to see the temporal difference between the soil and possible underground materials. Totally seven frame was taken from all area and from each frame, several temperature diagrams were carried out. The frames are mostly depend on the morning flight. Also the evening flights were tried to be matched with their evening flights.

The first frame taken from 7:00 am flight was a little upper part of the road which divides the area (Figure 5.3.39). In this part there is only one target, named "M", to be referenced. As mentioned before, thermal snapshot 382x288 px corresponds to 23.99 m(w; in X axis) and 18.02 m (h; in Y axis) on object area. In this snapshot, Y=150 was taken as reference line since the lower part of the frame is mostly covered

by road. Upper part of the reference line was divided five parts with 20 or 30 pixels which means 120- 180 cm on object area. The other lines are Y= 120, Y=110, Y=90, Y=70 and Y=50. Temperature profiles were created of each of these lines y exporting them as .csv file to excel and all temperetaure profiles of the snapshot created as shown in figure 5.3.41 (Figure 5.3.41).

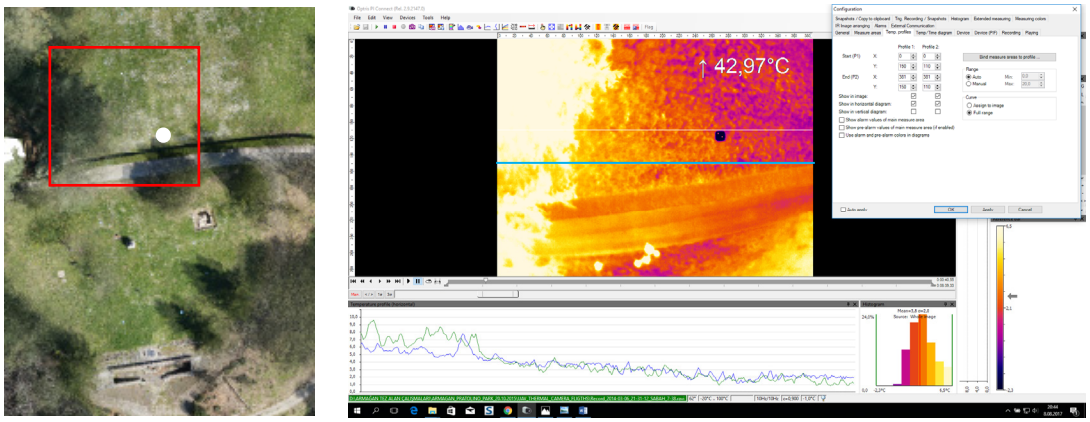

Figure 5.3.41: (left) The first frame of the area with red rectangle and aluminium M target with white point. (right) the thermal frame of the area displayed on the left and aluminium target in black and blue line indicates Y=150 reference line and white line indicates Y=110.

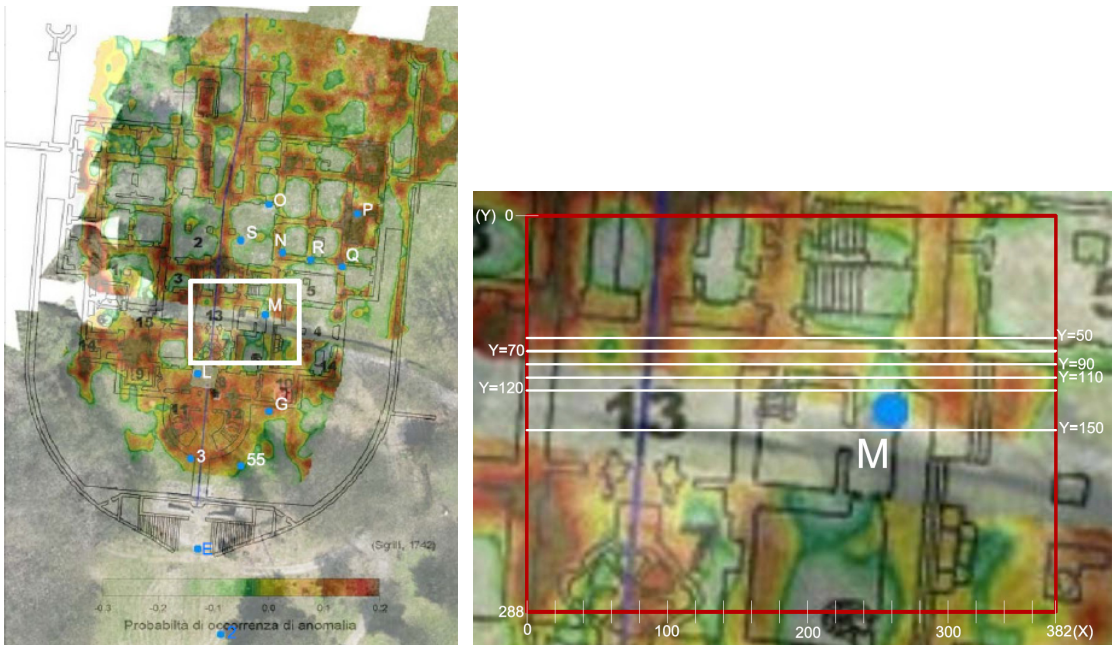

Figure 5.3.42(left) Orthophoto and anomaly map from Desideri, 2009 and the first frame area with white rectangle.
(right) Horizontal temperature diagram lines showing Y=150, Y=120, Y=110, Y=90, Y=70 and Y=50

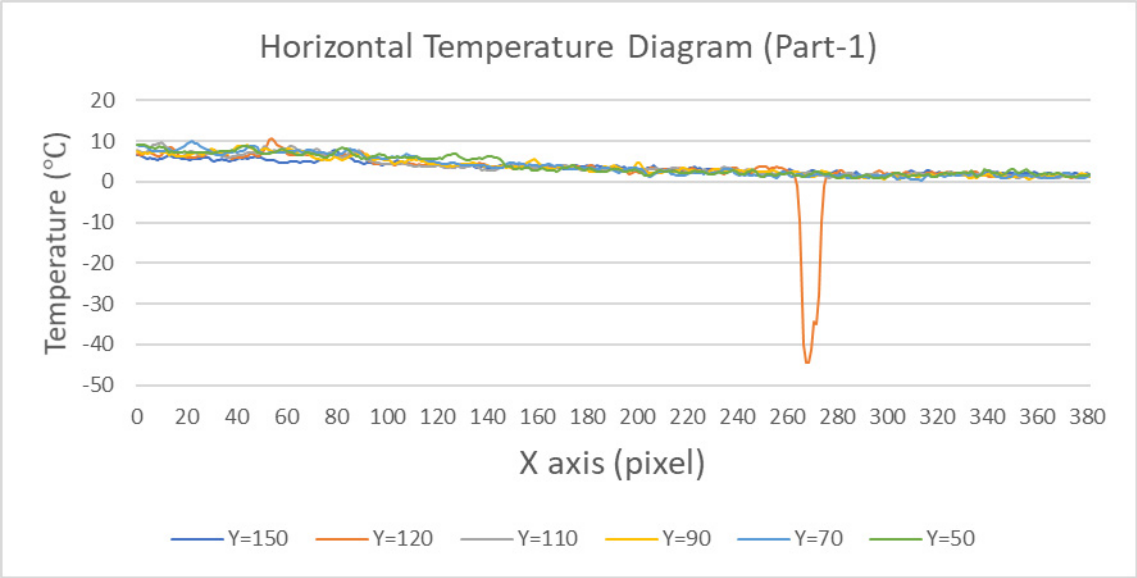

Figure 5.3.43: Horizontal temperature diagram of the first snapshot

In Y=120 line, between 260 and 280 pixels, the temperature decreases suddenly because the line passes over aluminium target. When it is not considered, it is easier to recognize temperature difference between the lines (Figure 5.3.43).

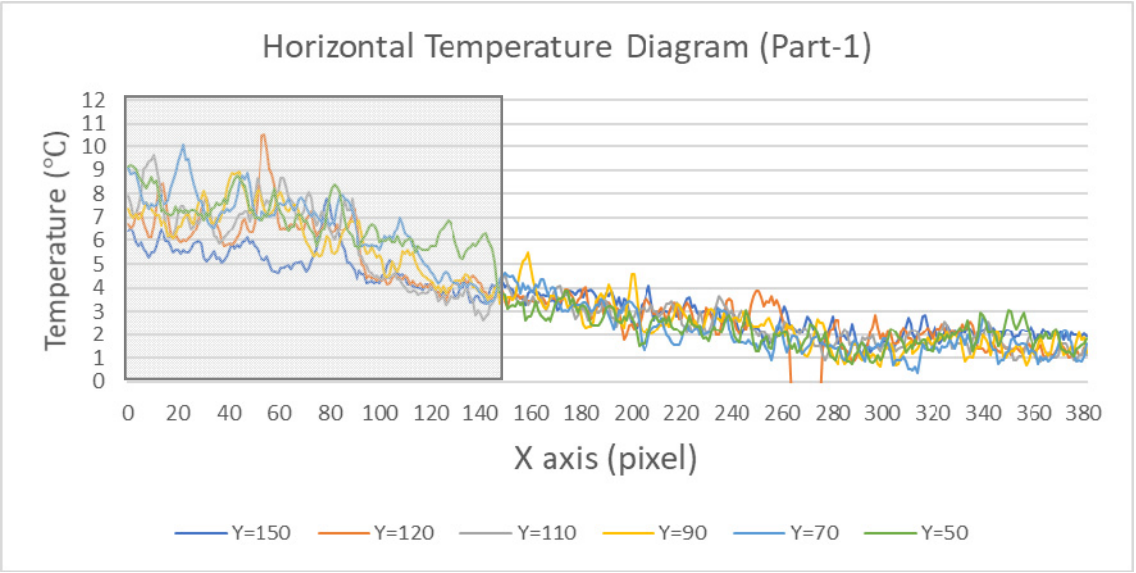

Figure 5.3.44: Horizontal temperature diagram of the first snapshot with reduced temperature scale. Grey rectangle indicates the area where a big tree is.

Each line of this snapshot was affected by big tree's thermal reflection until X=150 px in the snapshot. It is shown as grey rectangle in temperature diagram. When the temperature diagrams are examined closely, in Y=120 line between 240-260 pixels temperature increases suddenly. Similarly, while Y=120 and Y=110 has almost the same temperature, Y=150 still remains warmer between X=340 and X=380 pix (Figure

5.3.44). According to Cool (2005), materials with high thermal inertia remain warm heats up and cool down slowly, while materials with low thermal inertia cools quickly.

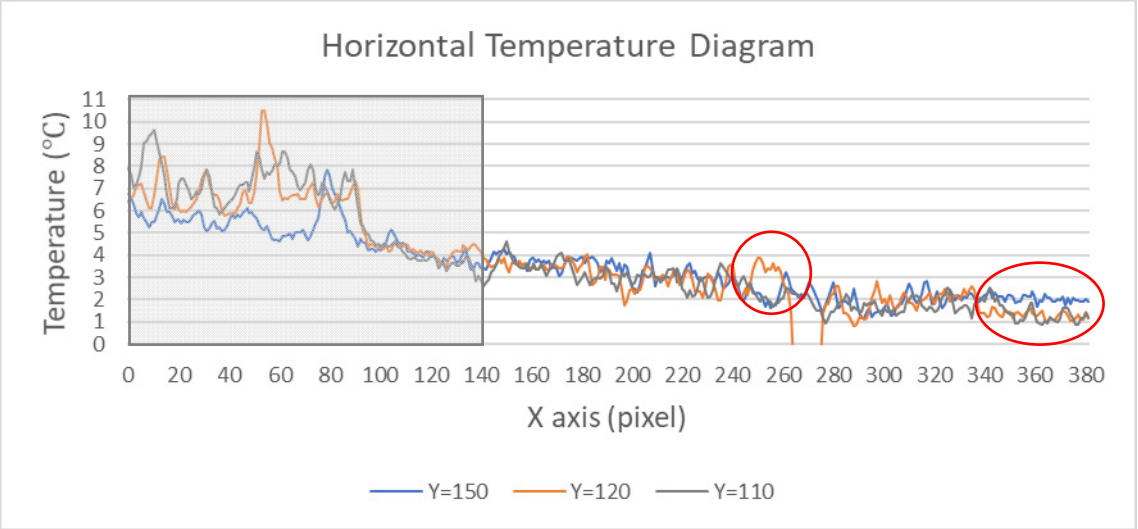

Figure 5.3.45: Horizontal temperature diagram of Y=150, Y=120 and Y=110 Grey rectangle indicates dense vegetation area with trees of snapshot.

When it's moved to Y=90 line, it was seen a rapid temperature decrease in X=200px adn Y=90 line remains warmer than Y=70 between X=200 and 280 px. Most apperant temperature difference is seen Y=50 line between X=340 and X=360 px. With the reference Périsset and Tabbagh (1981) study, while the soil is warming, there is a heat flux and larger heat flux value, the faster the change is happening (Figure 5.3.46).

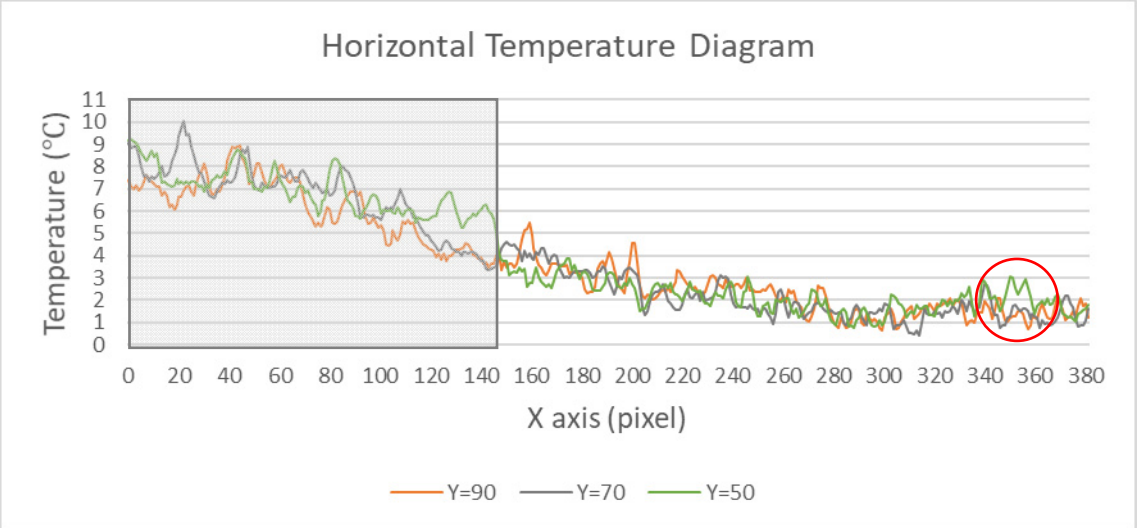

Figure 5.3.46: Horizontal temperature diagram of Y=90, Y=70 and Y=50. Grey rectangle indicates dense vegetation area with trees of snapshot.

The same area was acquired also in 7:50 pm, after the sunset and temperature profiles of the same lines were prepared in order to compare. In Y=110 line, while there is no big temperature difference in the morning (Figure 5.3.47), there is a quick temperature

decrease in the evening flight between 340-370 px. The same decrease continue till Y= 50px (Figure 5.3.46). It may point out a featurewhich enhances drying and cools faster than the soil or a feature with low thermal inertia. In other words, a feature may be an anomalie of a material with high conductivity and low volumetric heat means high diffusivity that heat travels quickly.

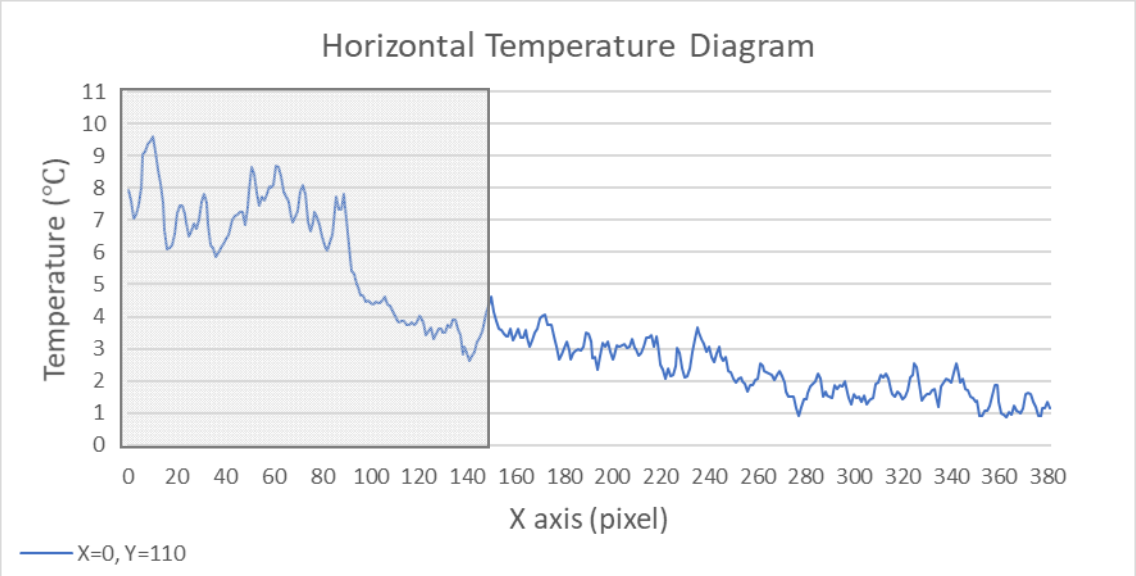

Figure 5.3.47: Horizontal temperature diagram of Y=110 at 7:00 am flight.

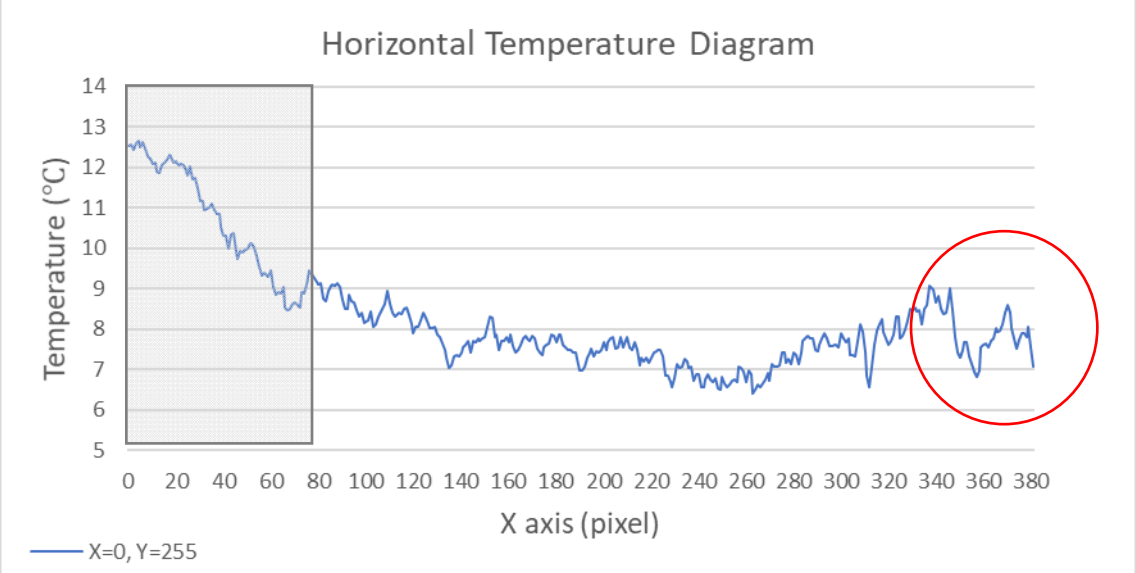

Figure 5.3.48: Horizontal temperature diagram of Y=110 at 7:50 pm flight.

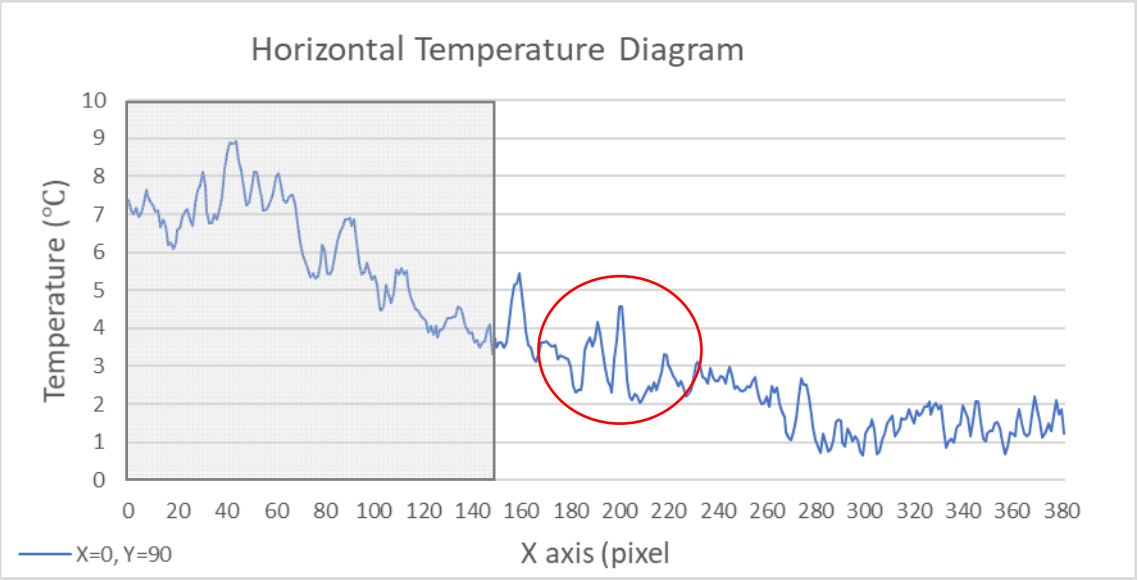

Figure 5.3.49: Horizontal temperature diagram of Y=90 at 7:00 am flight.

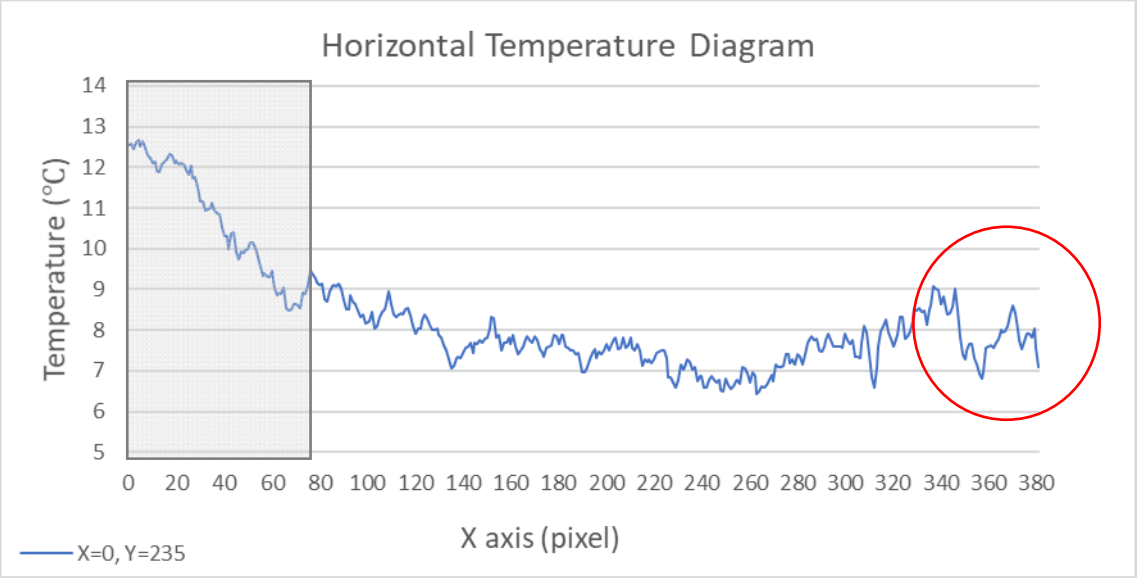

Figure 5.3.50: Horizontal temperature diagram of Y=90 at 7:50 pm flight.

Conversly, in Y=90 line, at 7:00 am flight, between X=160-200 px there is a positive heat. The material with low conductivity and high volumetric heat remains more heat than surrounding (Figure 5.3.49).

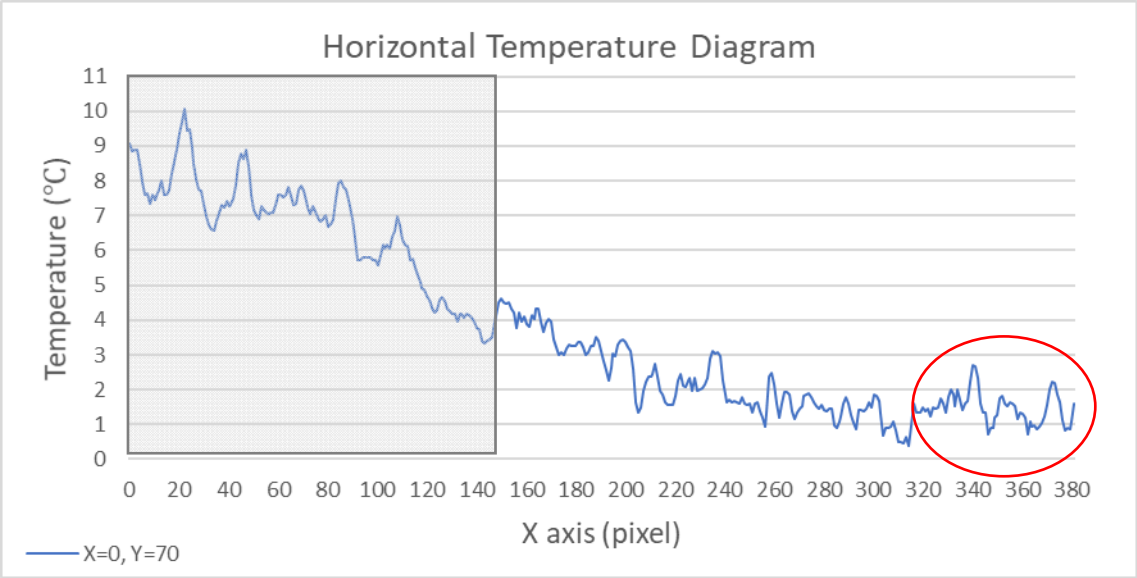

Figure 5.3.51: Horizontal temperature diagram of Y=70 at 7:00 am flight.

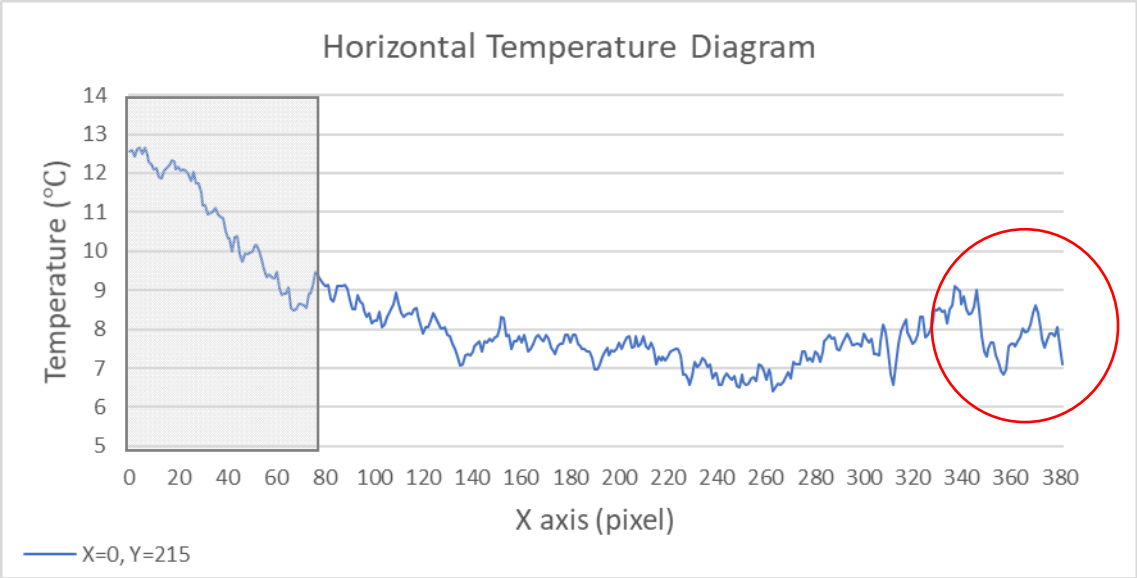

Figure 5.3.52: Horizontal temperature diagram of Y=70 at 7:50 pm flight.

Y=70 line, after 340 pixel, both in the morning and in the evening flight, the temperature stand the higher according to surrounding (Figure 5.3.52).

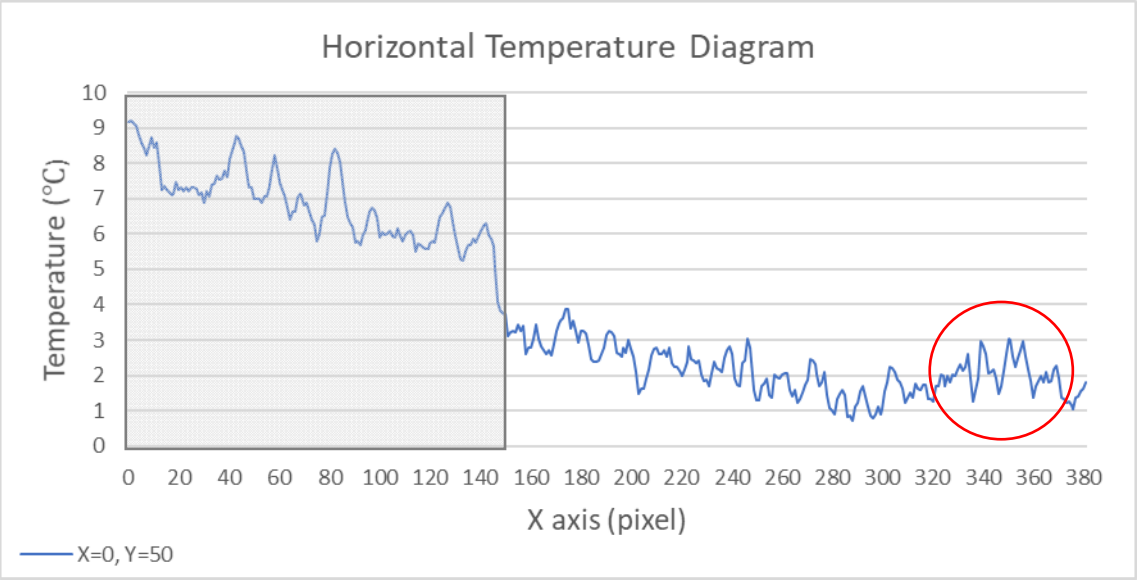

Figure 5.3.53: Horizontal temperature diagram of Y=50 at 7:00 am flight.

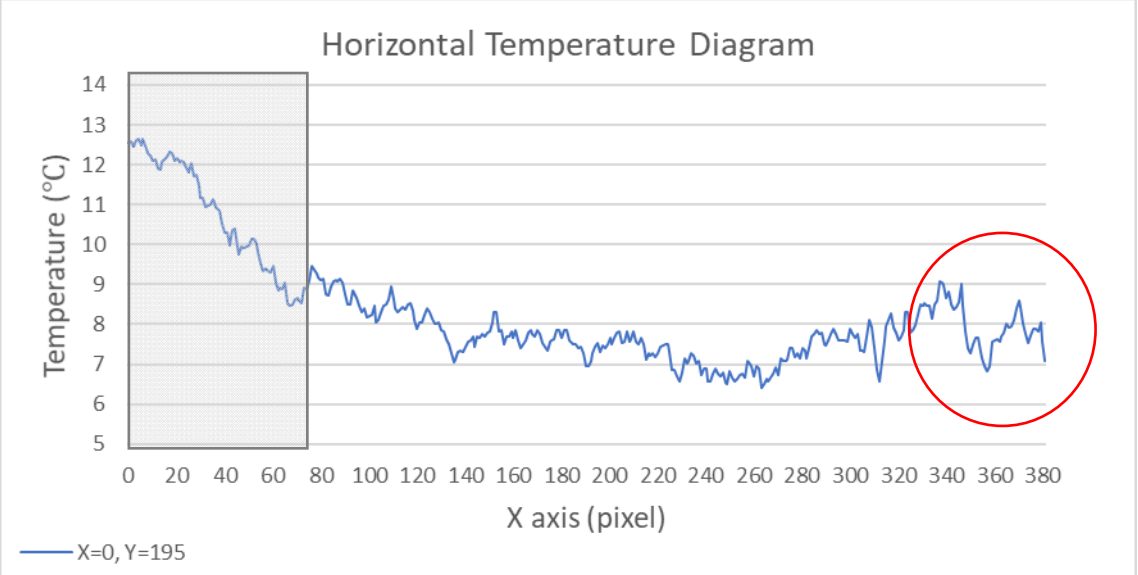

Figure 5.3.54: Horizontal temperature diagram of Y=50 (Y=195 in the evening flight snapshot) at 7:50 pm flight.

And in Y=50 line between 340-360 px it can be seen almost 2℃ increase in the morning, whilte it decreases again almost 2℃ in the evening flight. It may have a material heats up and cool down fastly (Figure 5.3.53).

When the temperature profiles are compared with Desideri anomaly map, it can be seen that strong anomalies in Desideri anomaly map can be seen after 300 px similarly temperature profiles of this part in the thesis (Figure 5.3.52)

According to Giardino and Haley, (2006) study, a feature that enhances drying would be postivie anomaly in the morning and negative anomaly in the evening. Kwamme (2004) also states that the surface cools rapidly after sunset, evening images show better near-sufrace temperature contrats. With the continue of the first frame,the previous snapshot of 7:00 am was taken as reference (Y=210) and the following (upper

part)was divided in each 40 pixel for the first two parts then divided two parts with 25 pixels.

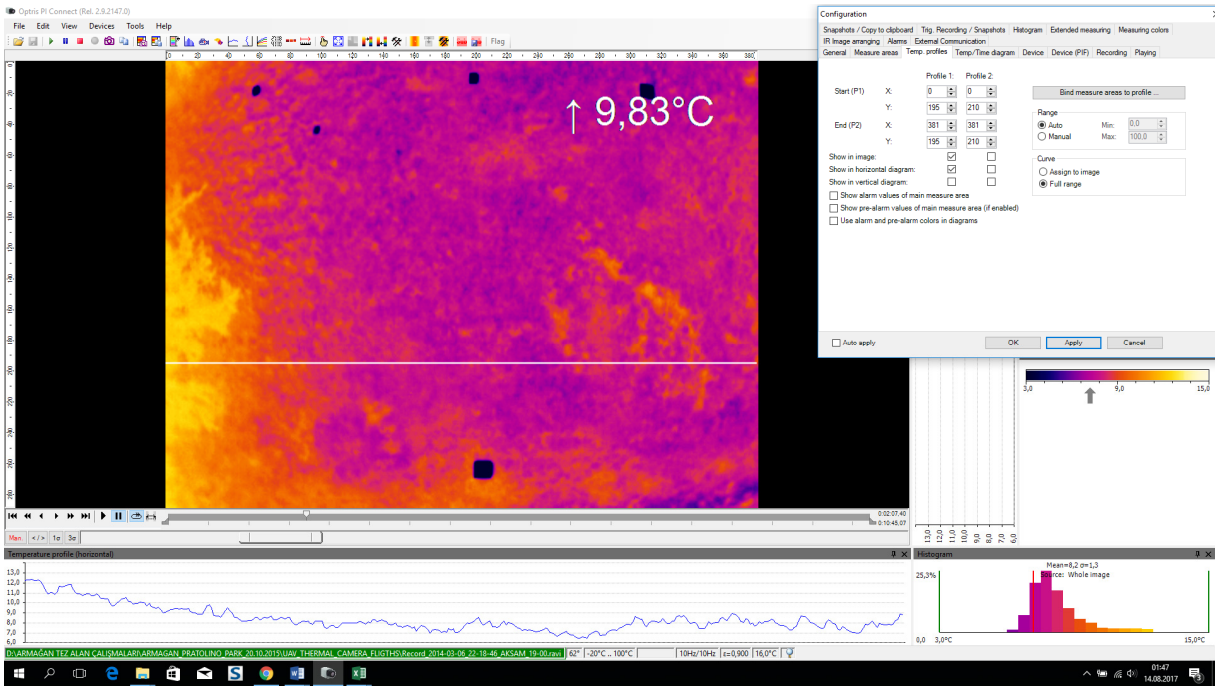

Figure 5.3.55: 7:50 pm flight with reference target of previous snapshot below. The white line displays Y=195 px.

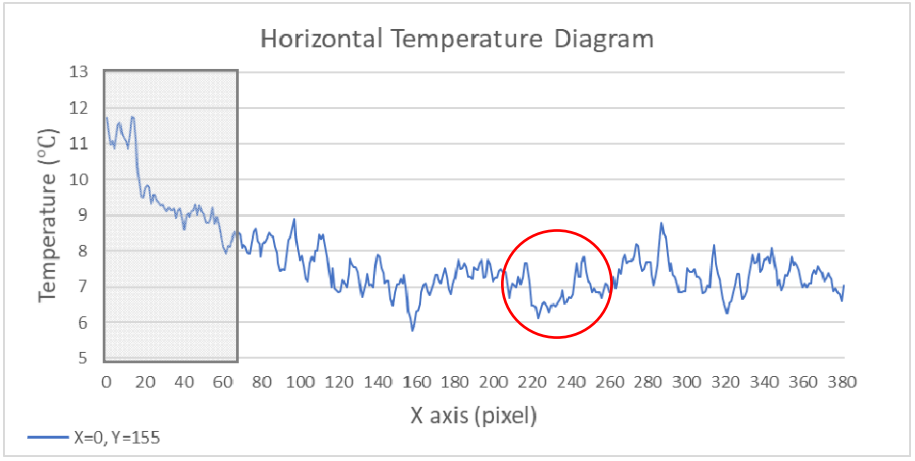

Figure 5.3.56: Horizontal temperature diagram of Y=155 at 7:50 pm flight.

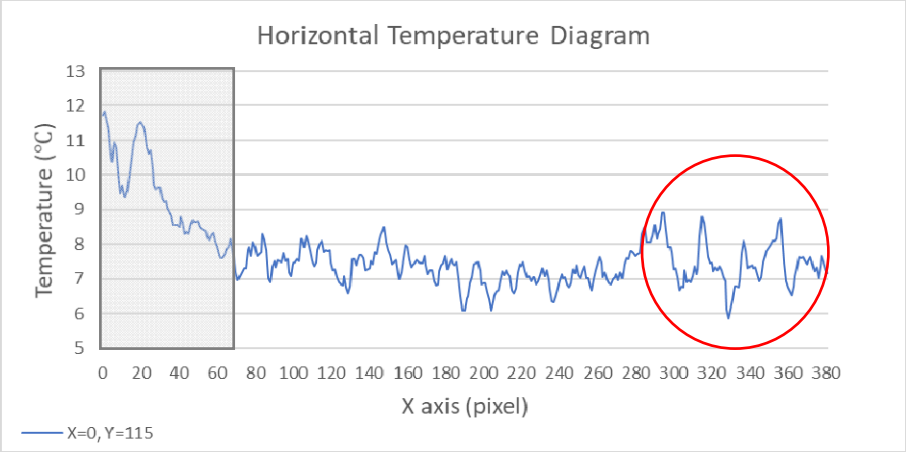

Figure 5.3.57: Horizontal temperature diagram of Y=115 at 7:50 pm flight.

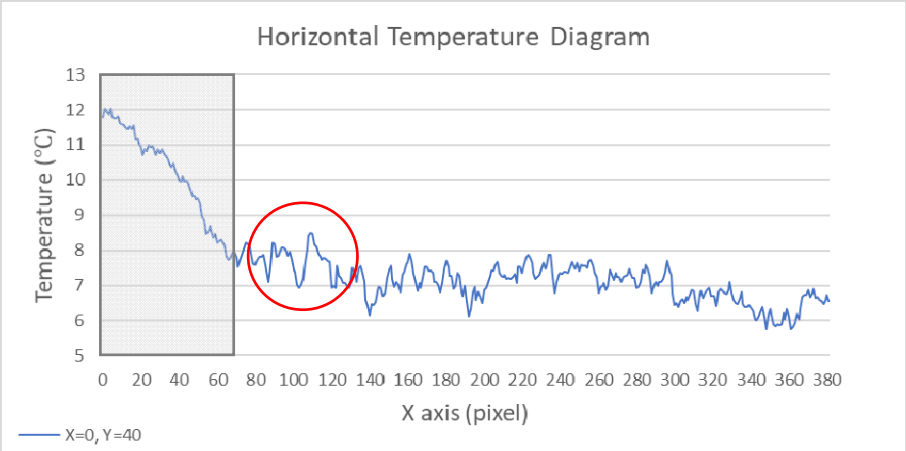

Figure 5.3.58: Horizontal temperature diagram of Y=40 at 7:50 pm flight.

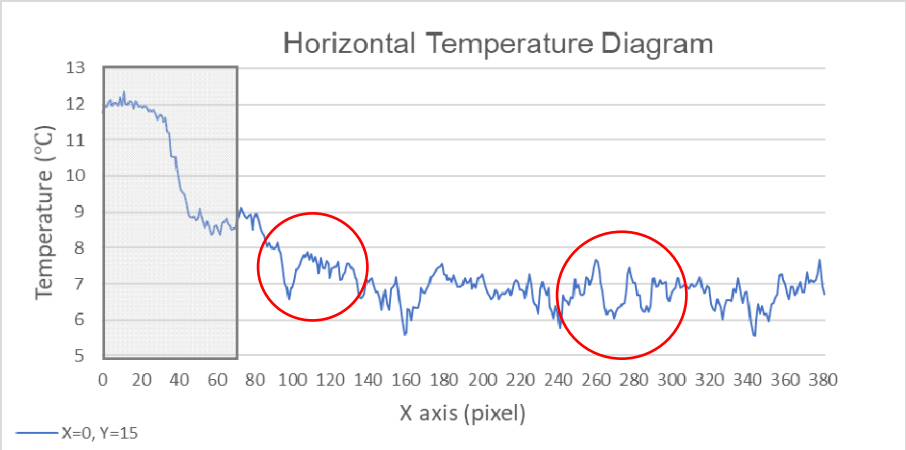

Figure 5.3.59: Horizontal temperature diagram of Y=15 at 7:50 pm flight.

As the evening flight is observed, in Y=155 and in Y=115 line in this frame, there are strong temperature changes in between 200-240 px in Y=155 and between 280-360 px in Y=115 (Figure 5.3.56-57). This may refer to a material with high conductivity and low volumetric heat and with high diffusivity which means that heat travels quickly without being retained. While, in Y=40 line, it should be referred a material with low conductivity and high volumetric heat so it remains more heat (Figure 5.3.58). Also it

has been seen strong decrease in temperature in Y=15 line at 7:50 pm flight between 100-140 px and 260-300 px(Figure 5.3.59).
The second frame was taken from 50 pixel higher from the previous target and from 7:00 am flight. Y=200 was the reference line and the upper part was divided each 40 pixel (Figure 5.3.60). This area includes four targets, M, S, N and R.

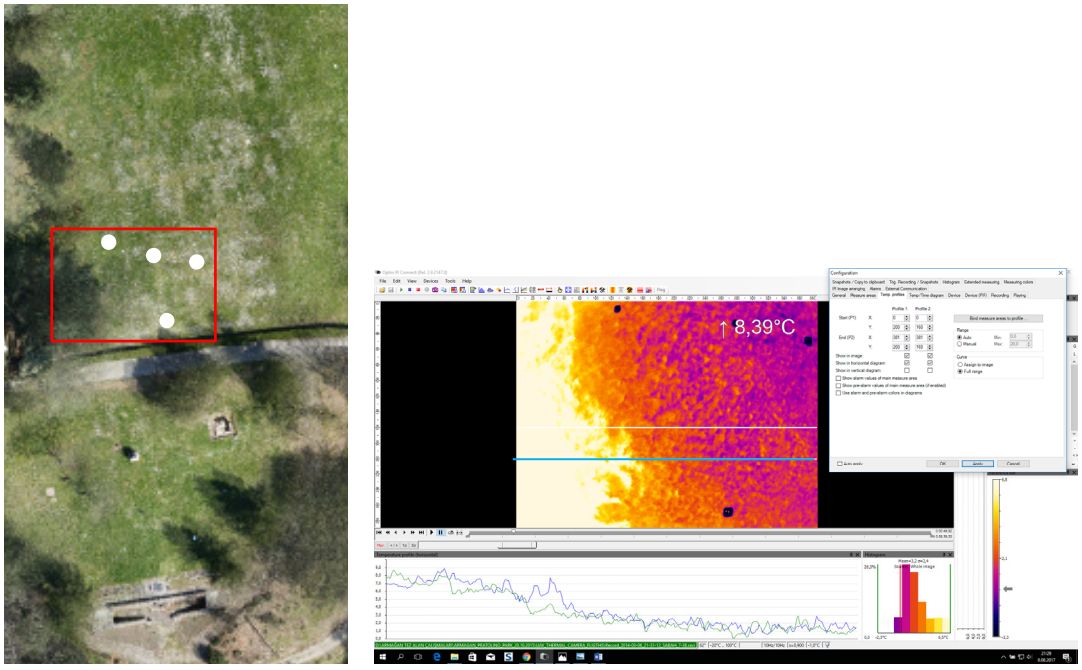

Figure 5.3.60: (left) The second frame area with red rectangle and aluminium target with white point, (right) the thermal frame of the area displayed on the left and aluminium target in black and white line indicates Y=200 reference line in blue and Y=160 in white

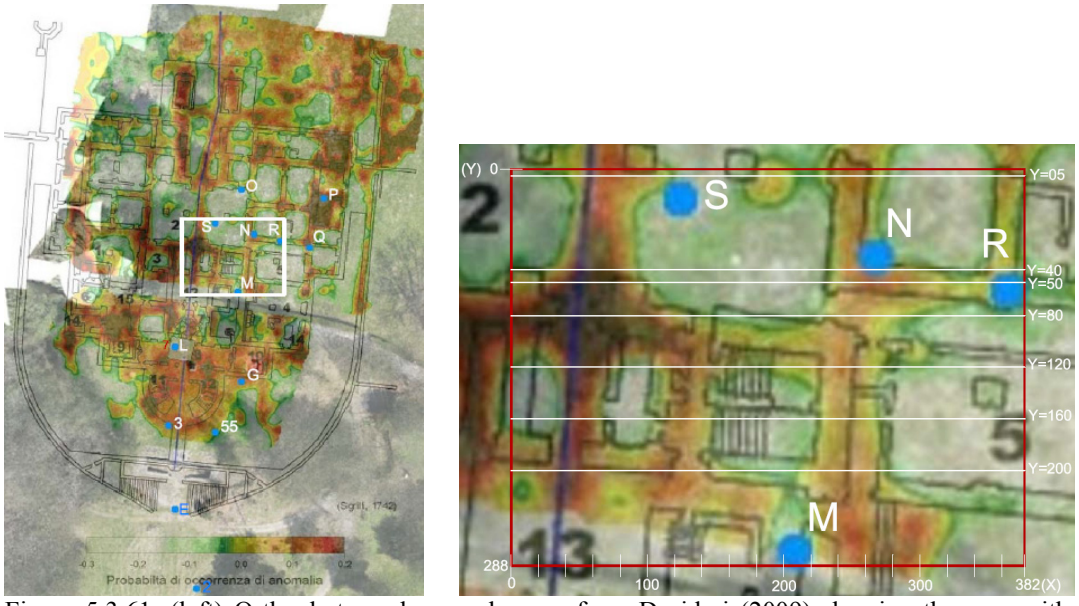

Figure 5.3.61: (left) Orthophoto and anomaly map from Desideri (2009) showing the area with white rectangle.
(right) Horizontal temperature diagram lines showing Y=150, Y=120, Y=110, Y=90, Y=70 and Y=50.
Considering all temperature profiles of this frame, no big temperature changes are seen. Only in Y=160 line, between 320-350px, the temperature increases (Figure 5.3.62),

similarly like in Y=5 between the same px. In Y=160 line, between 280-300 px, the temperature decresases, likewise in Y=5 line has strong temperature decrease in X=130px (Figure 5.3.62)

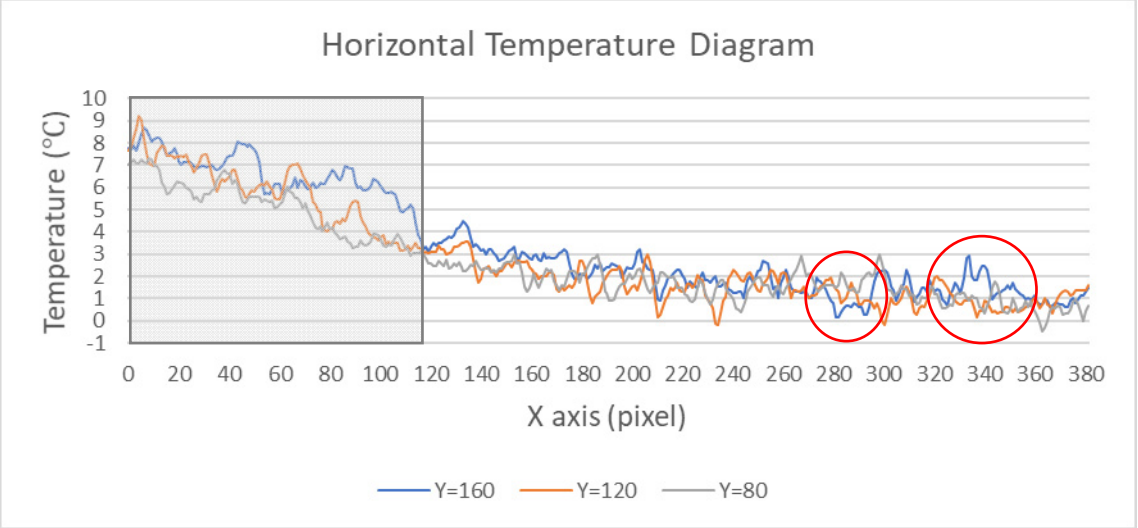

Figure 5.3.62: Horizontal temperature diagram of the second from Y=160, Y=120 and Y=80. Grey rectangle indicates dense vegetation area with trees of snapshot.

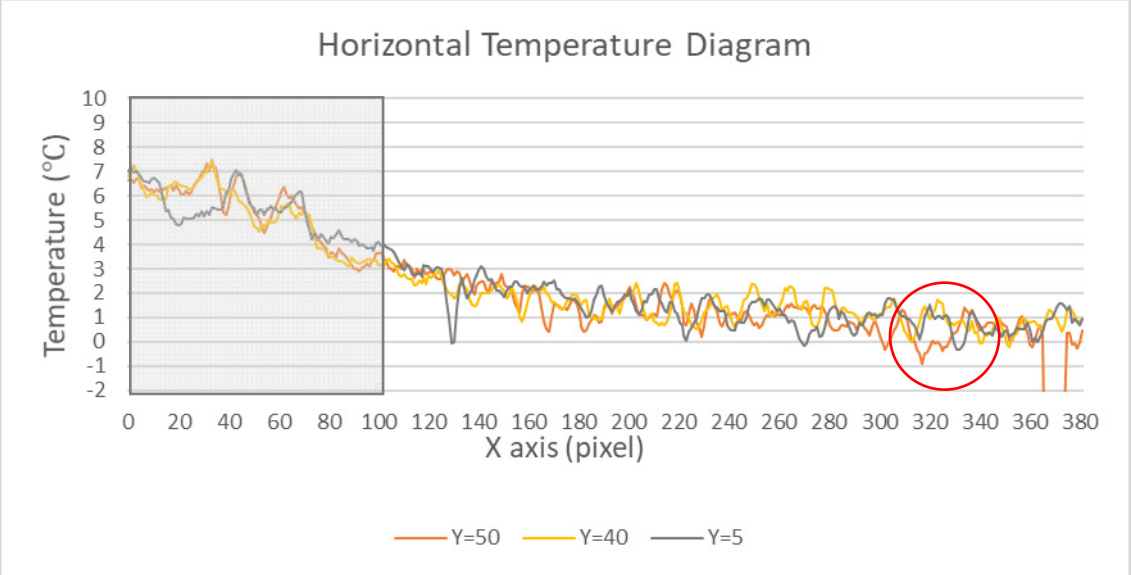

Figure 5.3.63: Horizontal temperature diagram of the second frame Y=50, Y=40 and Y=05. Grey rectangle indicates dense vegetation area with trees of snapshot.

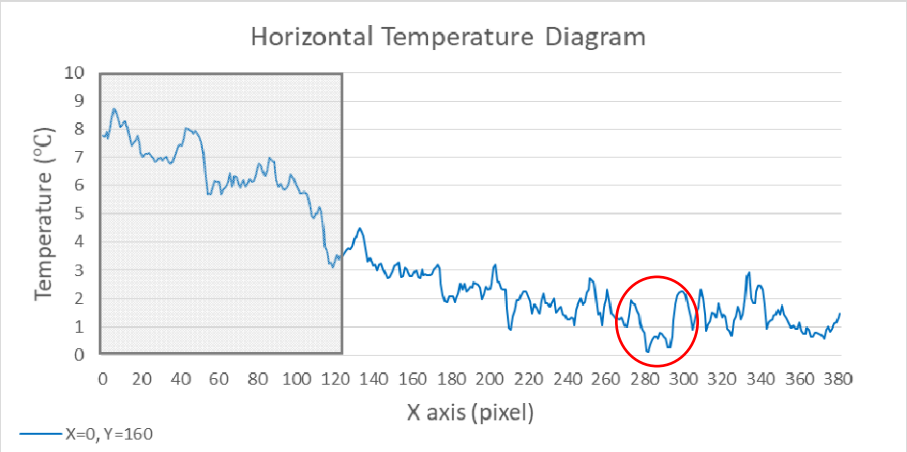

Figure 5.3.64: Horizontal temperature diagram of Y=160 at 7:00 am flight.

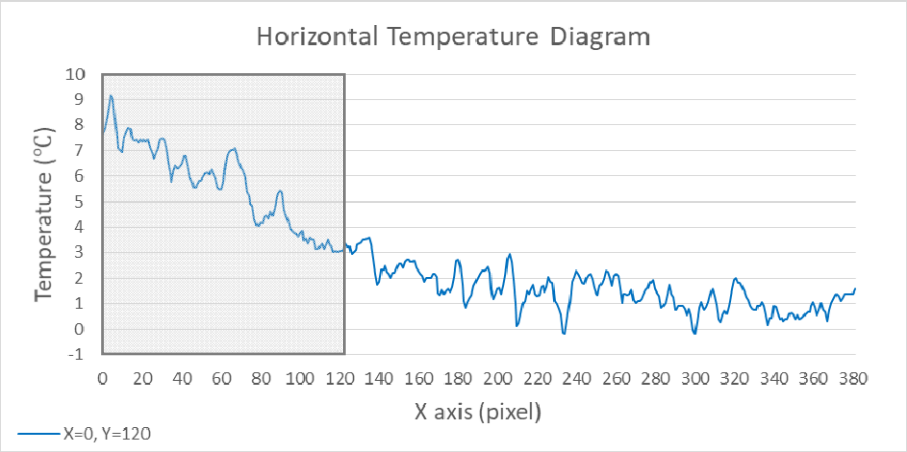

Figure 5.3.65: Horizontal temperature diagram of Y=120 at 7:00 am flight.

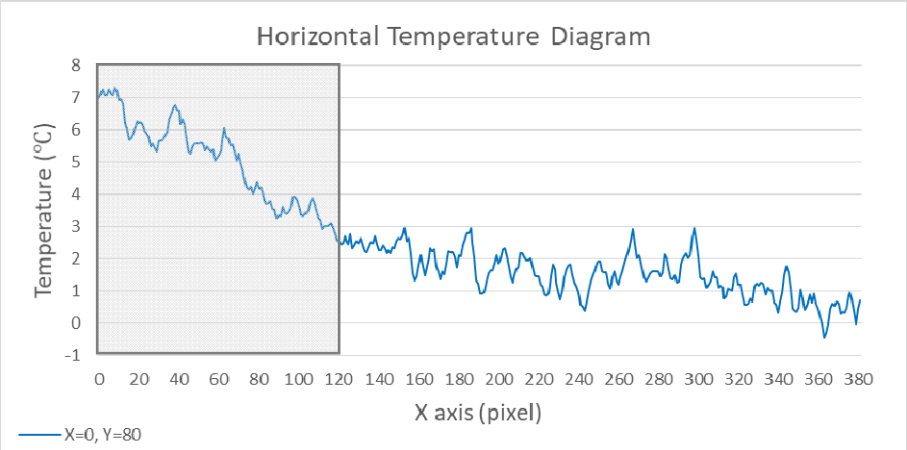

Figure 5.3.66: Horizontal temperature diagram of Y=80 at 7:00 am flight.

When considering Y=50, 40 and 5 lines (figure 5.3.63), and 80 lines(figure 5.3.62), it can be seen that temperature doesn't change sharply. It may be subsoil has almost the same or similar material.

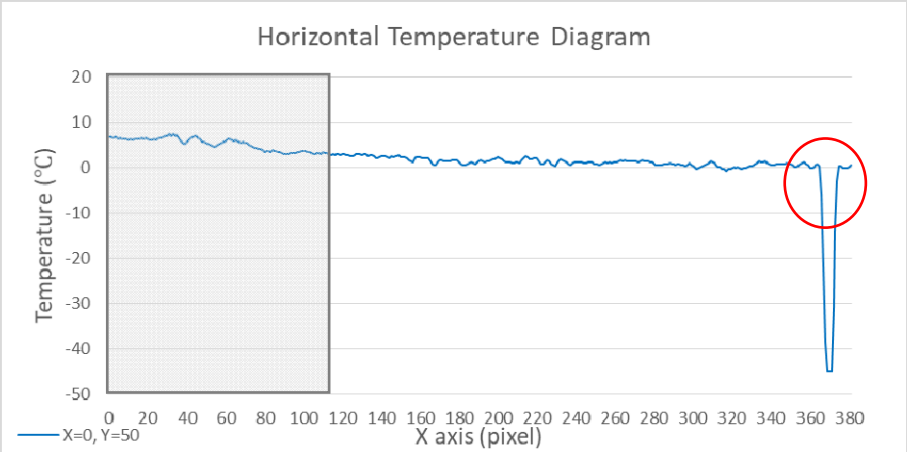

Figure 5.3.67: Horizontal temperature diagram of Y=50 at 7:00 am flight.

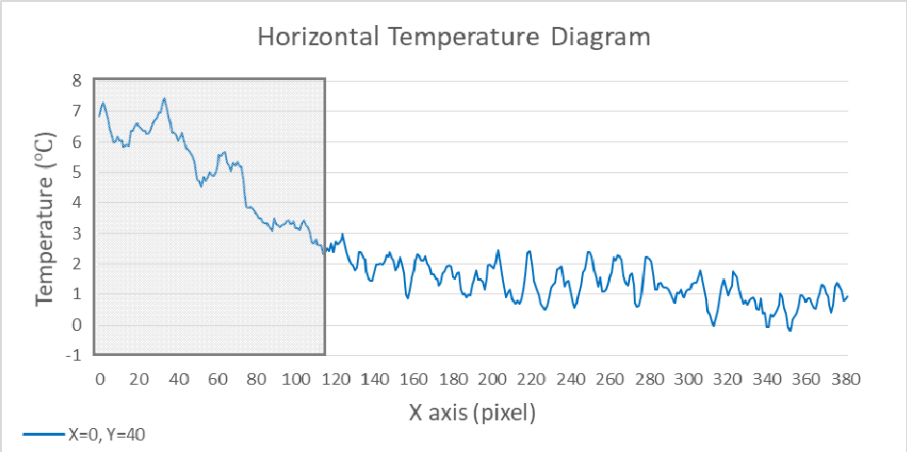

Figure 5.3.68: Horizontal temperature diagram of Y=40 at 7:00 am flight.

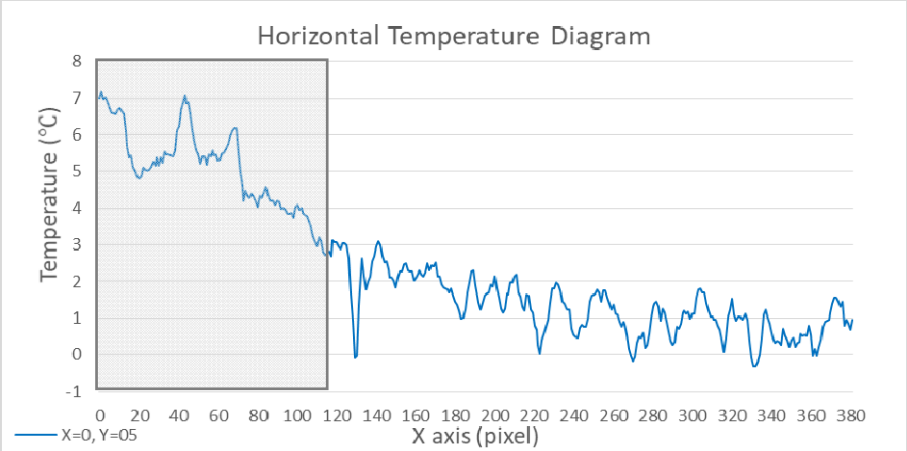

Figure 5.3.69: Horizontal temperature diagram of Y=5 at 7:00 am flight.

Regarding Y=50, 40 and 5 lines, a strong temperature change can be easily seen in temperature diagram of Y=50, between 360-380 px, since the line pass over aluminiuget. Just after Y=50, the line Y=40 goes without strong temperature changes while it can be seen slight changes in Y=5 line, especially between 180-280 px Figure 5.3.67-68-69).

The third frame was taken from with the reference of targets of previous snapshot from the line Y=270 from 7:00 am flight and the upper part was divided each 40 pixel (Figure 5.3.70). The targets in this frame are N,O,S.

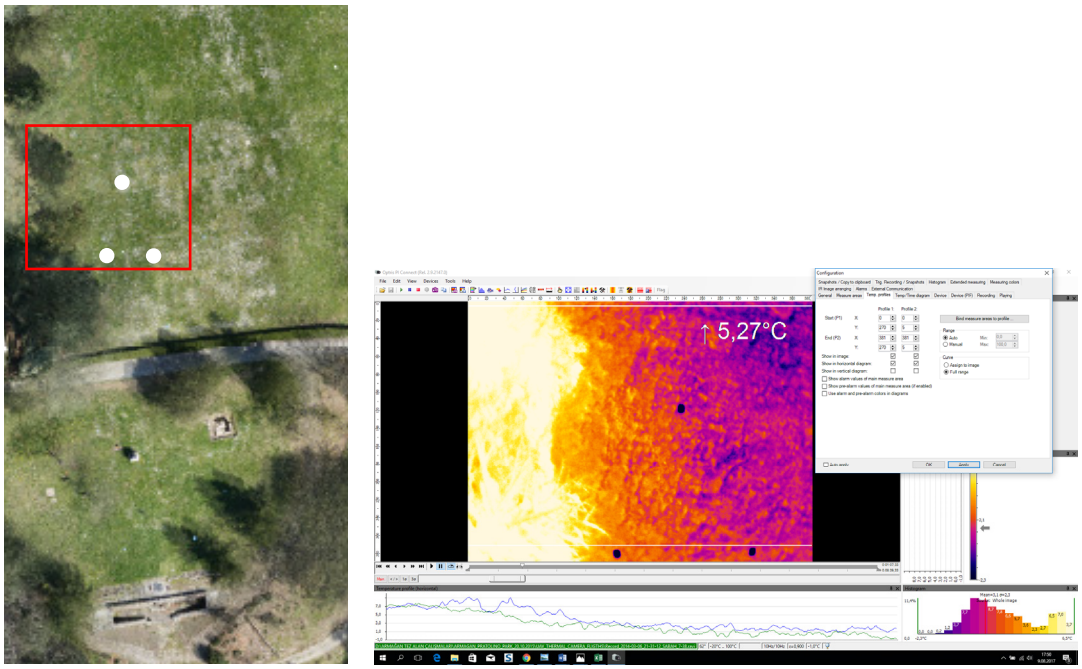

Figure 5.3.70: (left) The third frame area with red rectangle and aluminium targets with white points, (right) the thermal frame of the area displayed on the left and aluminium targets in black and white line just upper parts of the targets indicates Y=270 reference line.

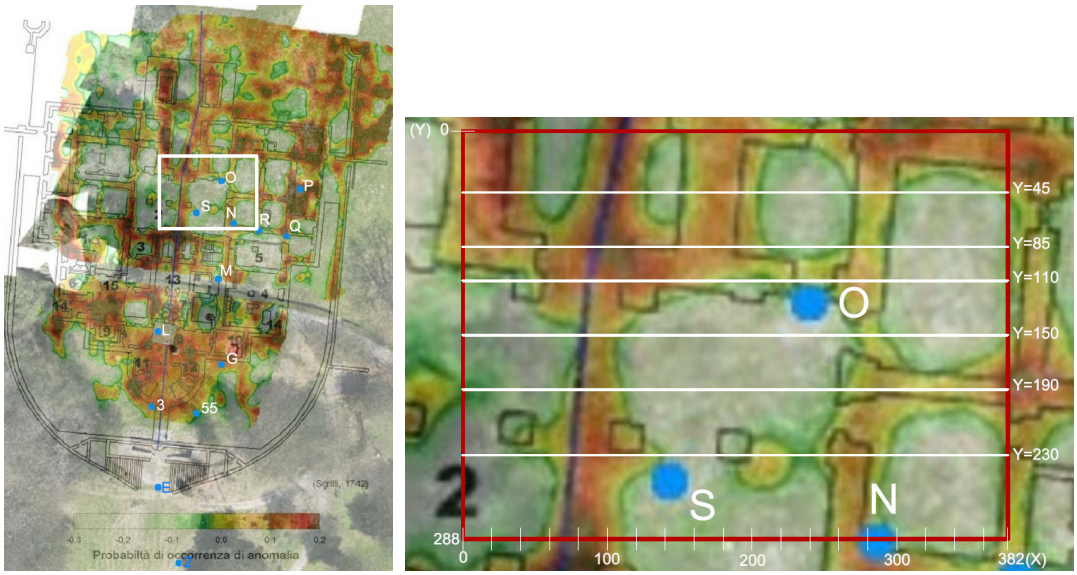

Figure 5.3.71: (left) Orthophoto and anomaly map from Desideri (2009) showing the area with white rectangle.(right) Horizontal temperature diagram lines showing Y=150, Y=120, Y=110, Y=90, Y=70 and Y=50.

In this frame, till X=120 px, it was vegetated area with trees so the reflection was high and temperature was seeming high in the profile. When the first part of the frame is evaluated, while the temperature profile of Y=190 and Y=230 shows similarity

between 160-200 pixel, Y=150 line slightly differs. Similarly, while Y=190 and 150 have similar temperatures between 330-360, Y=230 has lower temperature (Figure 5.3.72)

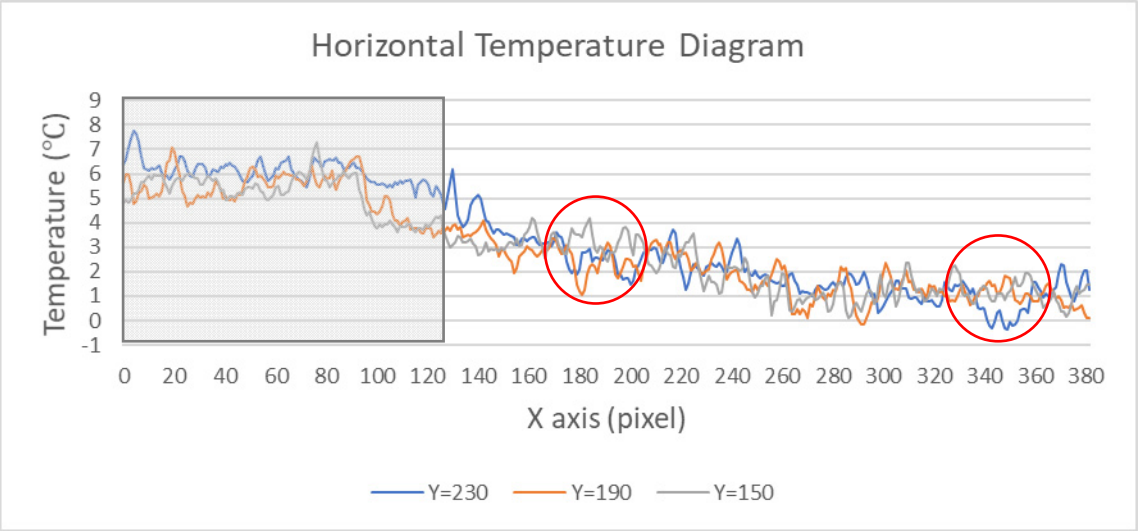

Figure 5.3.72: Horizontal temperature diagram of the third frame Y=230, Y=190 and Y=150 at 7:00 am flight. Grey rectangle indicates dense vegetation area with trees of snapshot.

In Y=230 line, it can be seen temperature differences in X=200-220 and X=320-360 px at 7:00 am flight (Figure 5.3.72). It was discovered similar temperature differences also in the evening flight. However, because of the location of UAV, it was not possible to get exactly the same frame in the evening flight (Figure 5.3.73). The UAV was slightly different position in horizontal axis approximately 80 px on east direction. Thus, to comparison of the profiles should have considered according to this difference. When considered this difference, thermal difference in X=330-360 in the morning flight corresponds X= 240-270px. In this same area, the temperature is lower in the morning and still remains lower in the evening. Similarly,temperature in X=300px in the morning flight and X=220 px in the evening have lower temperature during the day. Conversly, temperature decreases in X=240-300 px in the morning, however in the evening the same area which corresponds to X=160-220px keeps the heat while the soil is cooling (Figure 5.3.75).

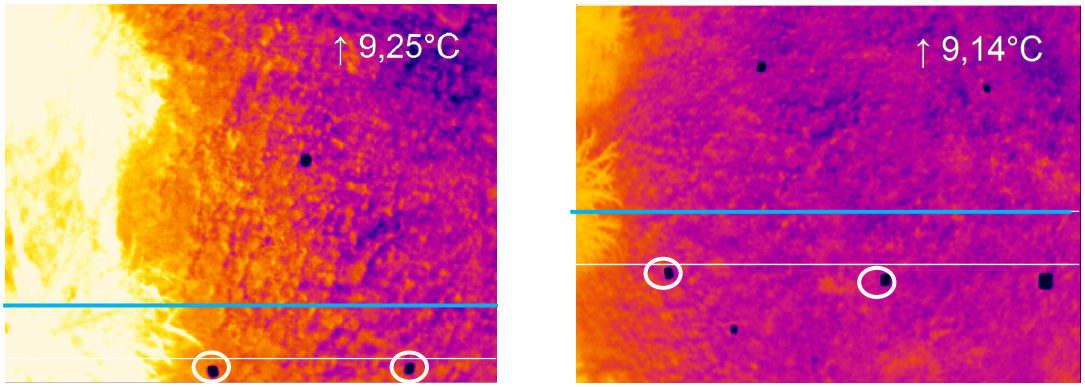

Figure 5.3.73: The snapshot of Y=230px line in blue at 7:00 am flight (left) and 7:50 pm (right). And the reference targets in white circles. While the white line refers Y=270 px which was used as reference.

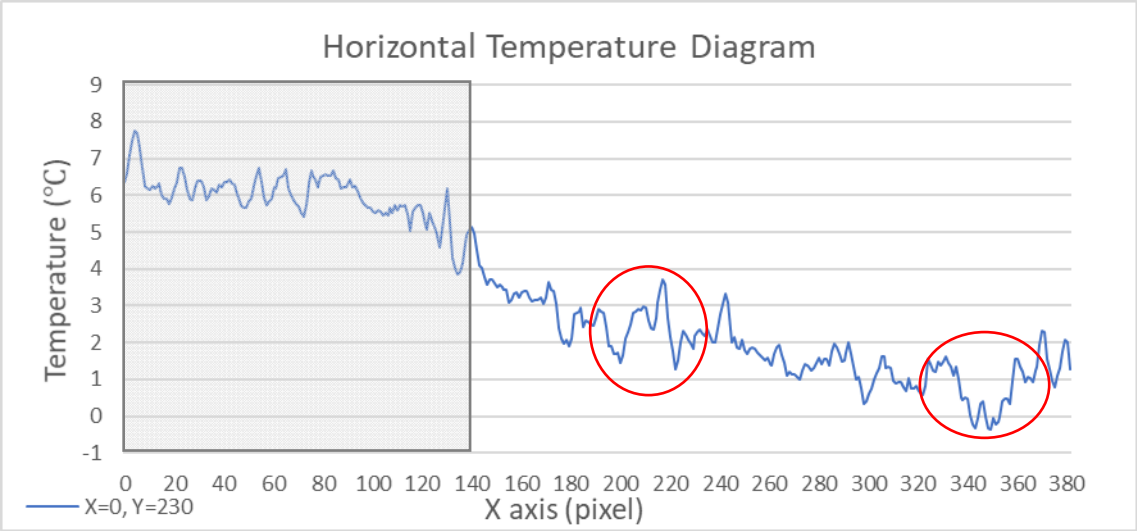

Figure 5.3.74: Horizontal temperature diagram of the third frame Y=230 at 7:00 am flight. Grey rectangle indicates dense vegetation area with trees of snapshot.

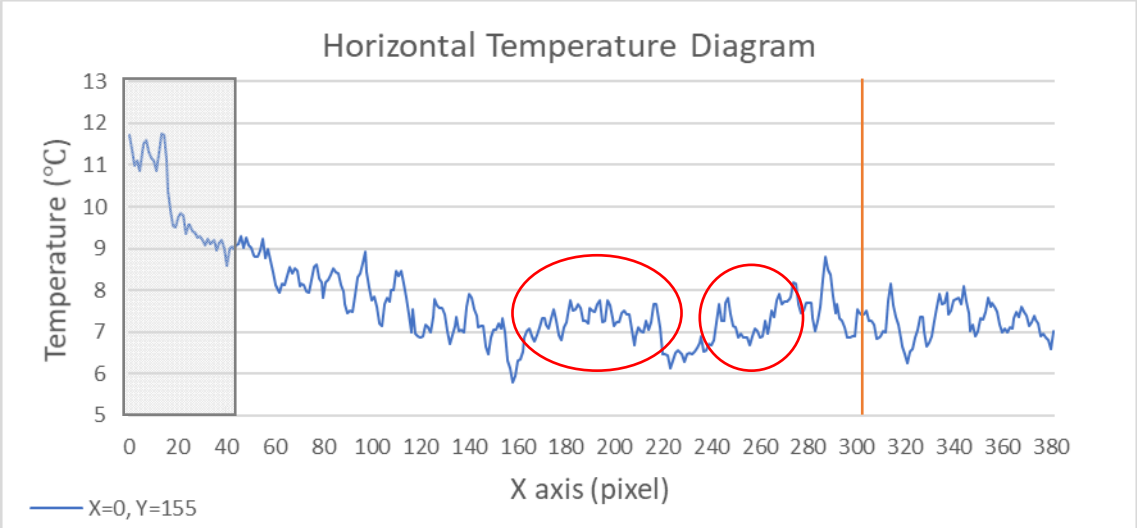

Figure 5.3.75: Horizontal temperature diagram of the third frame Y=230 at 7:50 pm flight. Grey rectangle indicates dense vegetation area with trees of snapshot and orange line displays the border of morning flight screen.

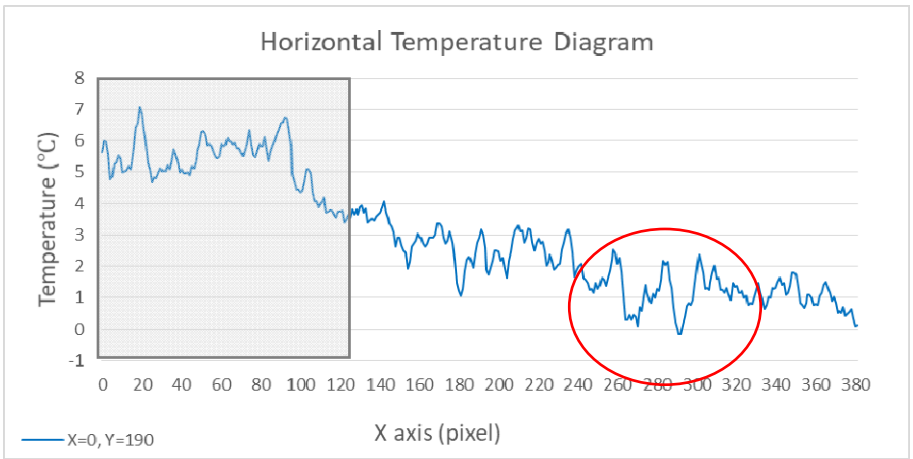

Figure 5.3.76: Horizontal temperature diagram of Y=190 at 7:00 am flight of the third frame

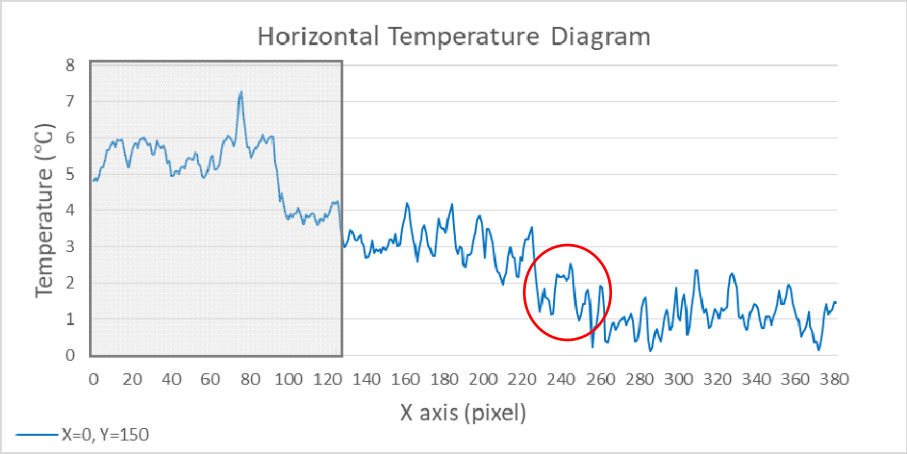

Figure 5.3.77: Horizontal temperature diagram of Y=150 at 7:00 am flight of the third frame

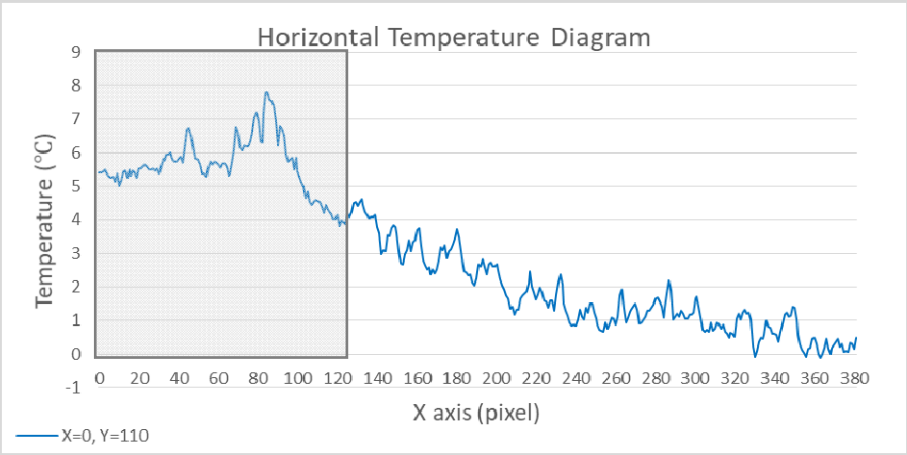

Figure 5.3.78: Horizontal temperature diagram of Y=110 at 7:00 am flight of the third frame

In Y=190 line, between 250-300 px, some waves show lower temperature compared to the surrounding, early in the morning. Even the px between 220-250 becomes higher temperature in Y=150 line while no strong change is visible in Y=110 line.

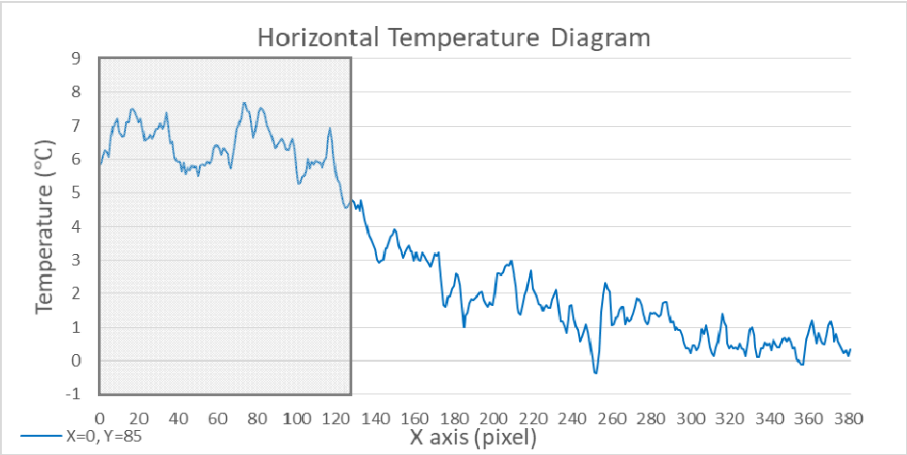

Figure 5.3.79: Horizontal temperature diagram of Y=85 at 7:00 am flight of the third frame

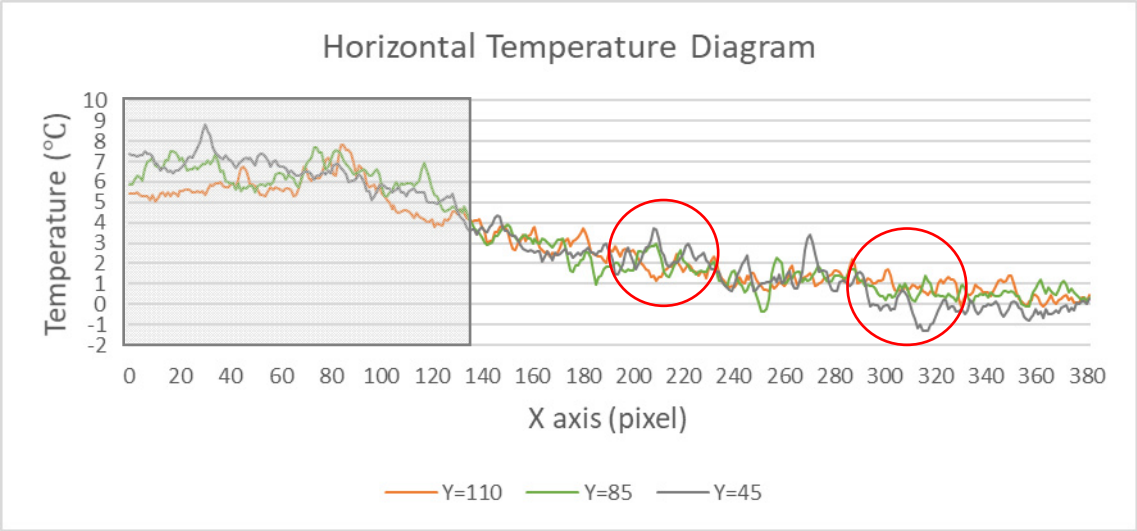

Figure 5.3.80: Horizontal temperature diagram of the third frame Y=110, Y=85 and Y=45 at 7:00 am flight. Grey rectangle indicates dense vegetation area with trees of snapshot.

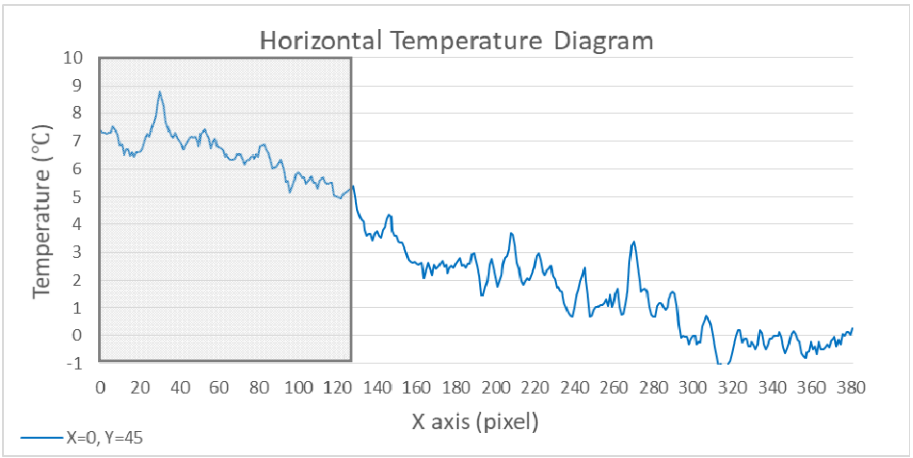

Figure 5.3.81: Horizontal temperature diagram of Y=45 at 7:00 am flight of the third frame

In X=210 px, Y= 100 line has lower temperature than Y=85 and Y=45 line, while they have similar temperature. However more recognazible temperature changes are visible in Y=45 line in X=270px and X=300-330 px. Even the sun heats the ground surface, homogenously, the profile of Y=45 in X=300-330 px could be a signal for material with low thermal inertia or a material traps moisture.

The fourth frame was taken from with the reference of targets of previous snapshot from the line Y=270 from 7:00 am flight and the upper part was divided several pixels (Figure 5.3.82).

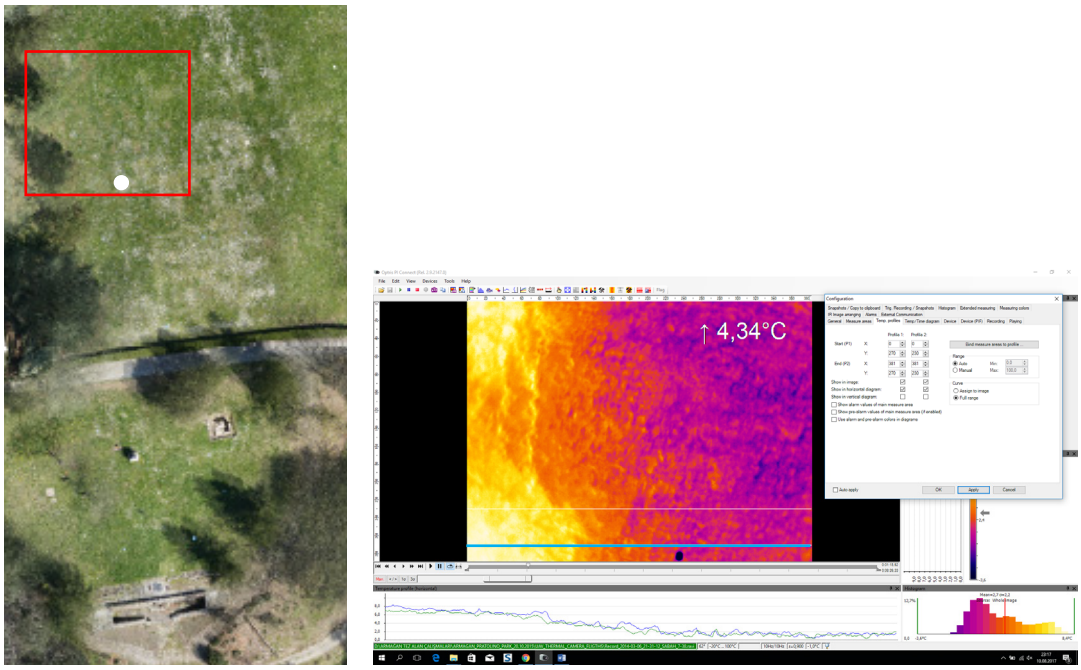

Figure 5.3.82: (left) The fourth frame area with red rectangle and aluminium targets with white points, (right) the thermal frame of the area displayed on the left and aluminium target in black and blue line just upper parts of the targets indicates Y=270px reference line and the upper of this line is Y=230px.

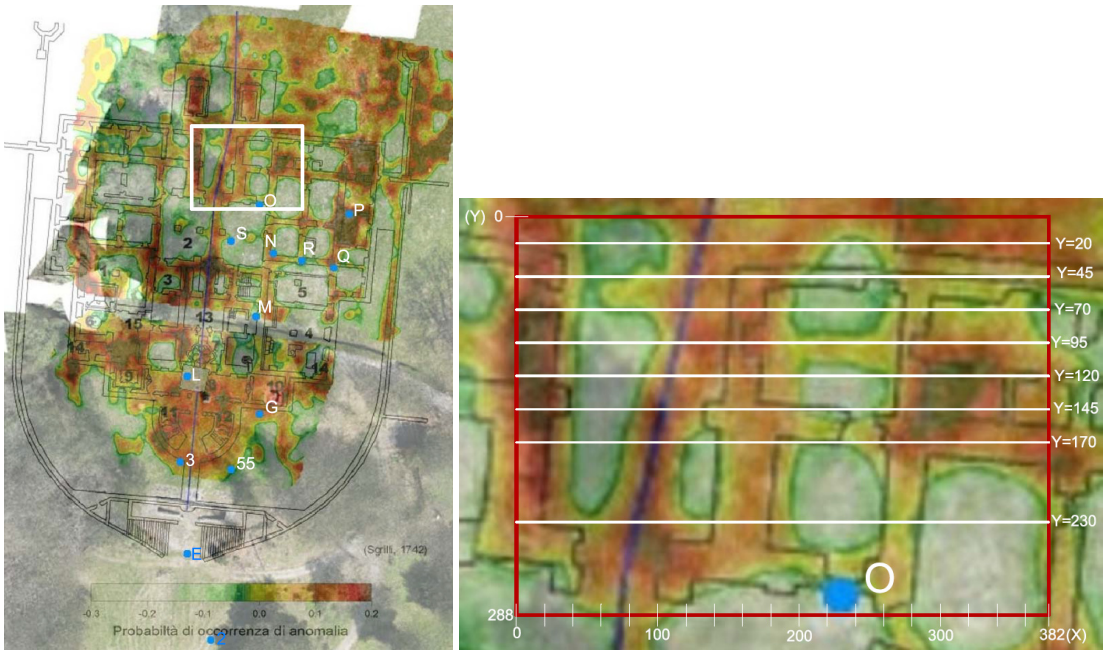

Figure 5.3.82: (left) Orthophoto and anomaly map from Desideri (2009) showing the area with white rectangle.(right) Horizontal temperature diagram lines showing Y=230, Y=170, Y=145, Y=120, Y=95 and Y=70, Y=45 and Y=20.

In the fourth frame, temperature difference is seen mostly Y=20 and Y=95 line. When it's compared with other lines, Y=20 has higher temperature in X=260-280 px and X=320-340 px and X=350-370 px. While Y=45 and Y=70 has similar temperatre profile, Y=95 has different profile with rising temperature at X=160-200; 220-240 and

especially 320-350 px. Similar to that profile, Y=145 has higher temperature at X=160-180 and 340-370 px (Figure 5.3.82).

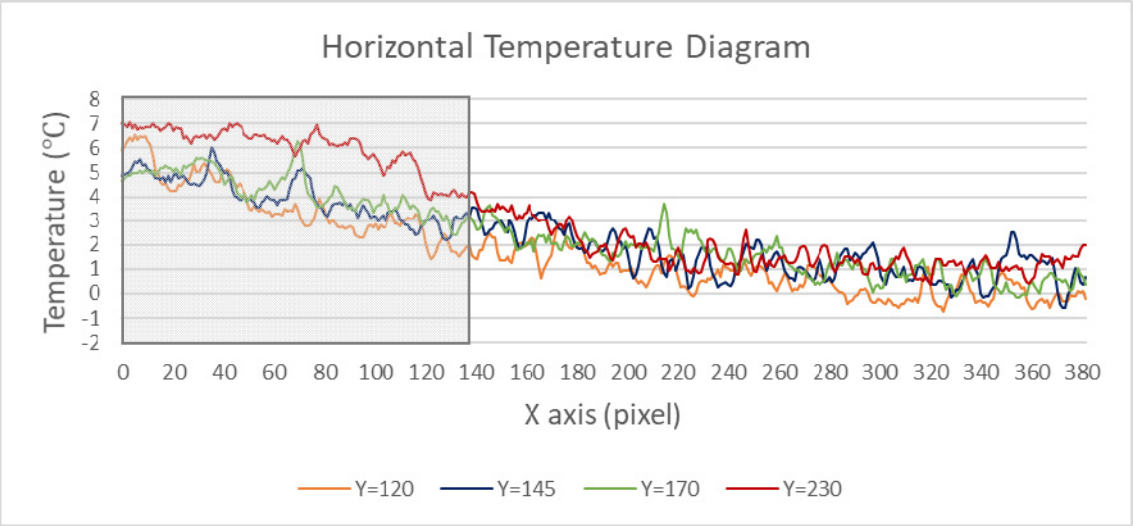

Figure 5.3.83: Horizontal temperature diagram of the third frame Y=120, Y=170, Y=145 and Y=230 at 7:00 am flight. Grey rectangle indicates dense vegetation area with trees of snapshot.

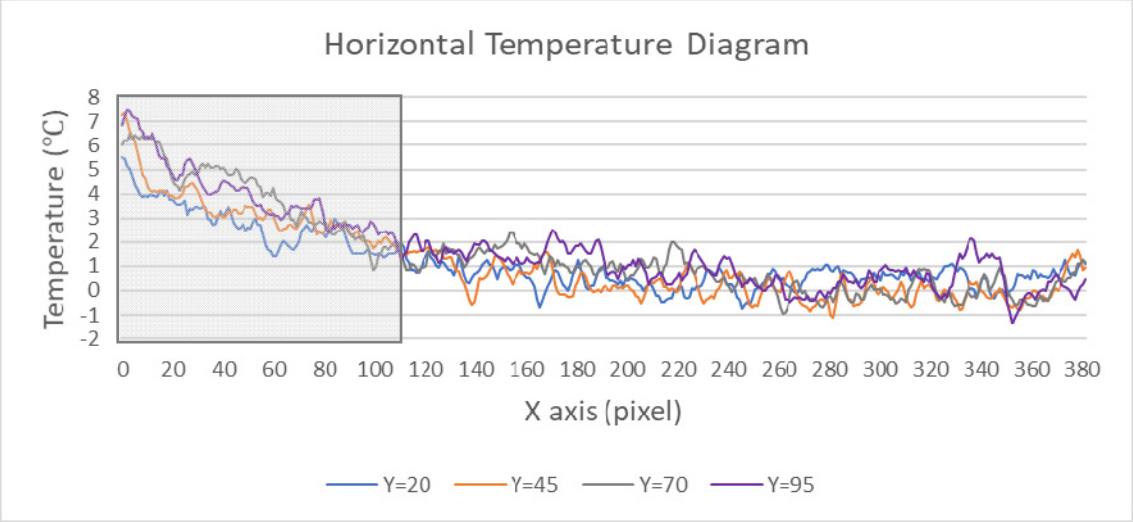

Figure 5.3.84: Horizontal temperature diagram of the third frame Y=20, Y=45, Y=70 and Y=95 at 7:00 am flight. Grey rectangle indicates dense vegetation area with trees of snapshot.

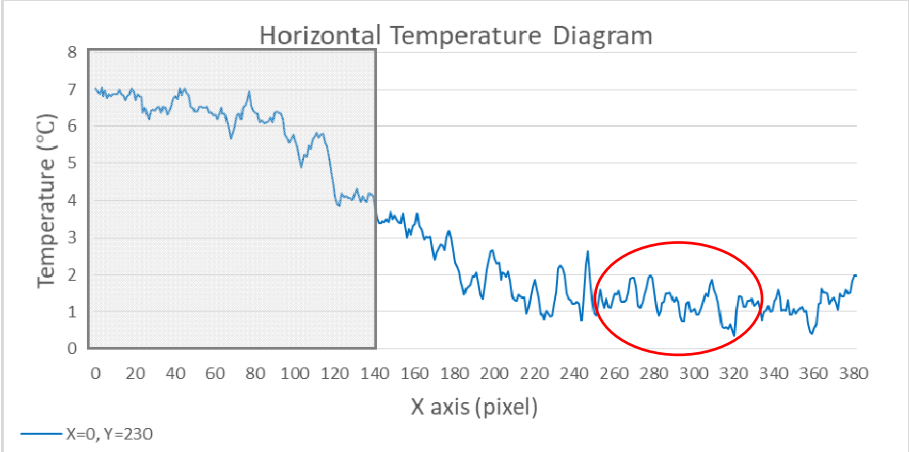

Figure 5.3.85: Horizontal temperature diagram of Y=230 at 7:00 am flight of the fourth frame

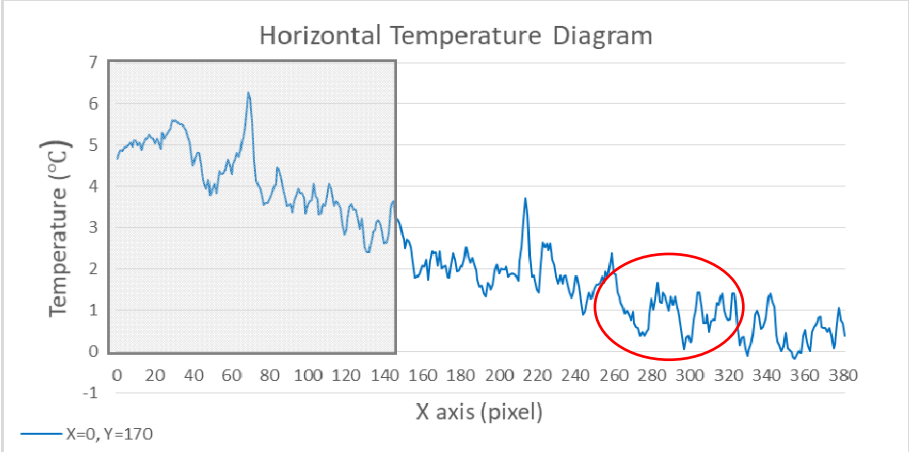

Figure 5.3.86: Horizontal temperature diagram of Y=170 at 7:00 am flight of the fourth frame

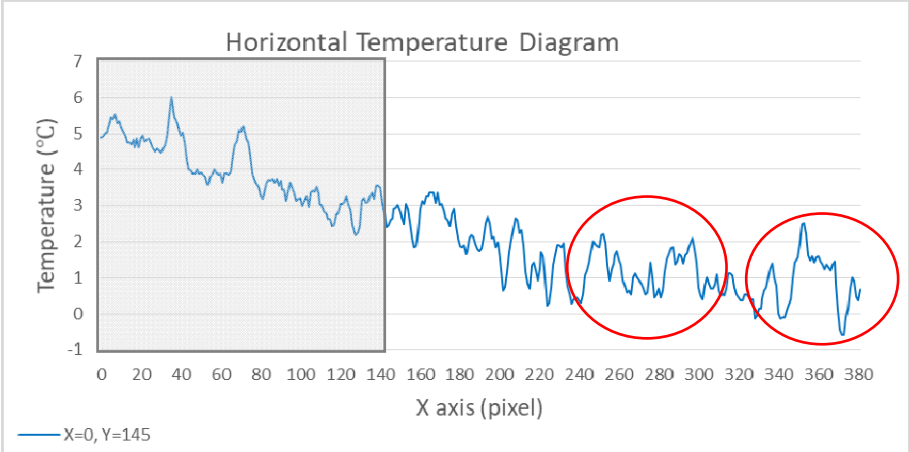

Figure 5.3.87: Horizontal temperature diagram of Y=145 at 7:00 am flight of the fourth frame

It can be observed that 240-300 px shows similar thermal response in Y=145 and Y=230 line. The temperature has almost around 2℃ while it slightly decreases in Y=170 line. 340-380 px shows to have high temperature between 320-380 px adn continues in Y=120 and temperature starts to decrease in Y=70. Besides Y=95 has high temperature between 320-360 px.

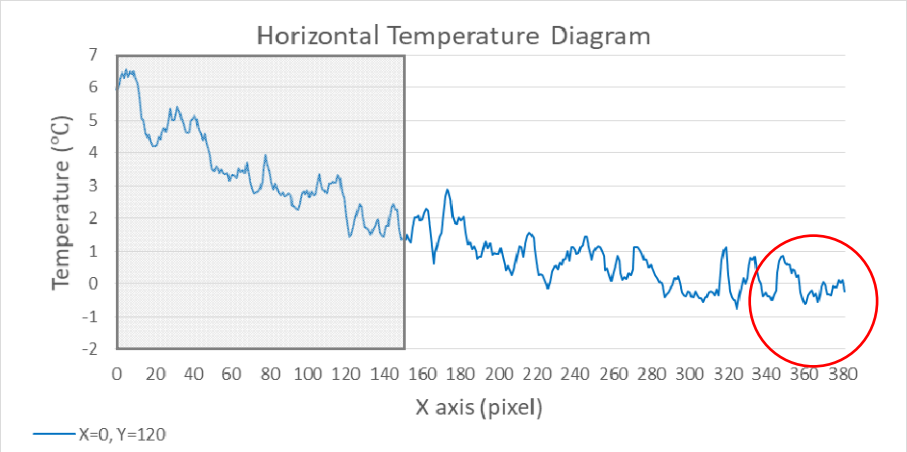

Figure 5.3.88: Horizontal temperature diagram of Y=120 at 7:00 am flight of the fourth frame

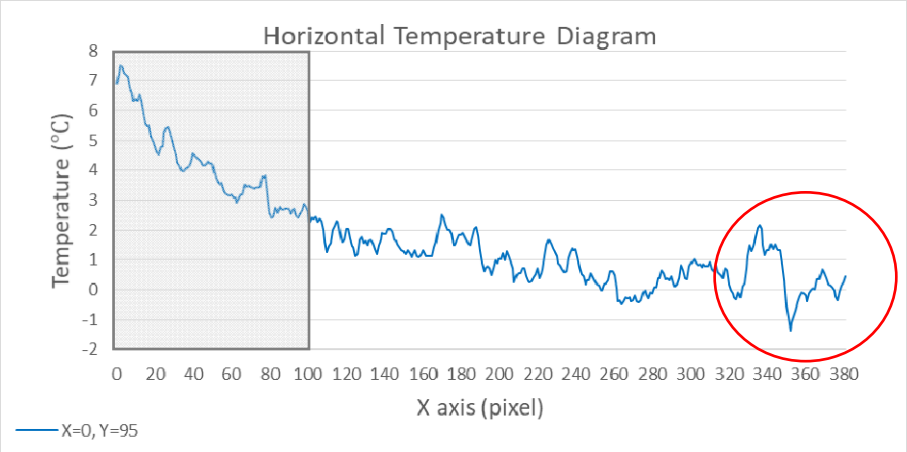

Figure 5.3.89: Horizontal temperature diagram of Y=95 at 7:00 am flight of the fourth frame

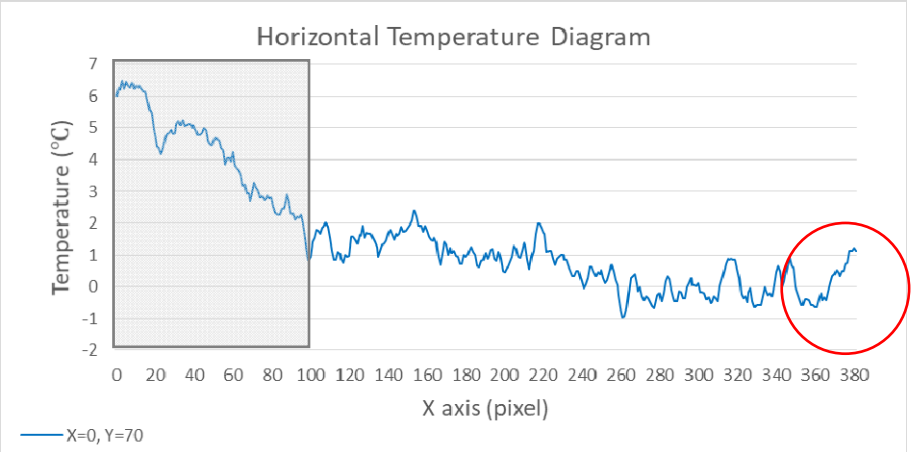

Figure 5.3.90:Horizontal temperature diagram of Y=70 at 7:00 am flight of the fourth frame

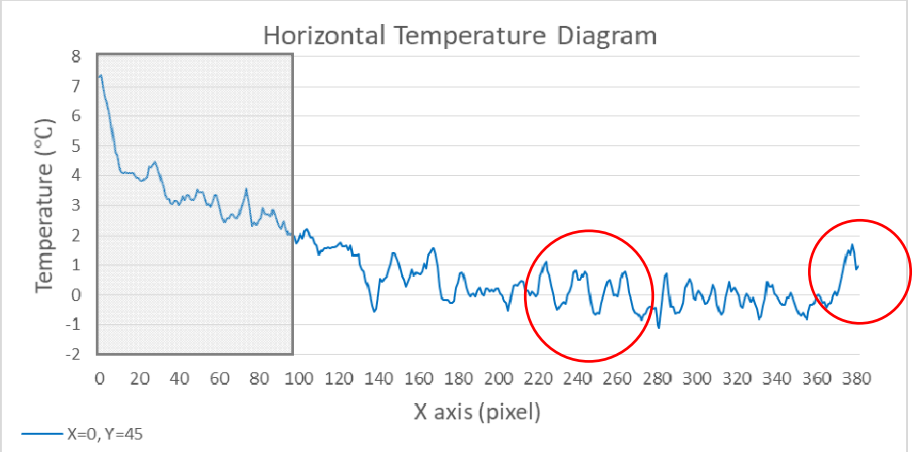

Figure 5.3.91: Horizontal temperature diagram of Y=45 at 7:00 am flight of the fourth frame

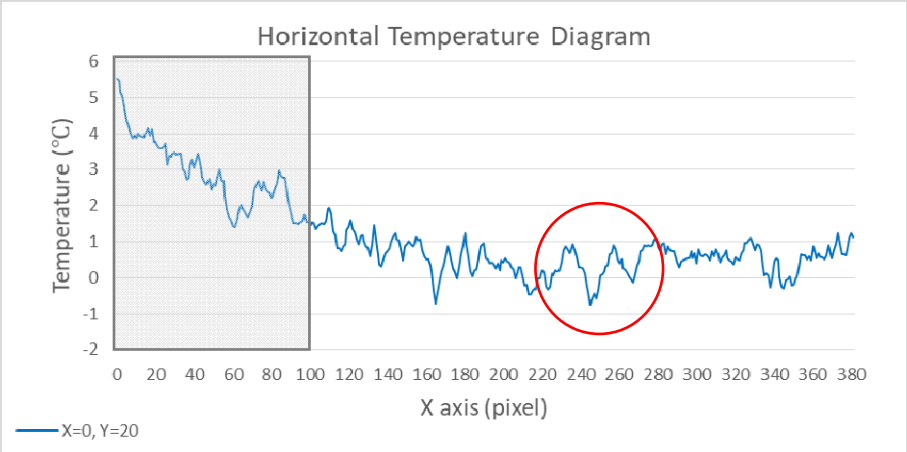

Figure 5.3.92: Horizontal temperature diagram of Y=20 at 7:00 am flight of the fourth frame

220-280 px have also show similar temperature and thermal behaviour in Y=45 and Y=20 (Figure 5.3.91- 92). However in Y=45 line, it can be seen sharp temperature decrease in 360-380 px.

The fifth frame was one of the non-tree frame of the area. So the temperature scale is smaller than other profiles. There was no tree in any side of the area. Some parts of the ground was covered with camomille like other parts but also there were small areas without any vegetation. This part showed high anomalies in Diverise, 2009 report. Thus this part was divided approximately each 25 pixel. In order to take refence, aluminium targets were used as it was in other frames. The line just up of the target was accepted as reference as Y=270 (Figure 5.3.93).

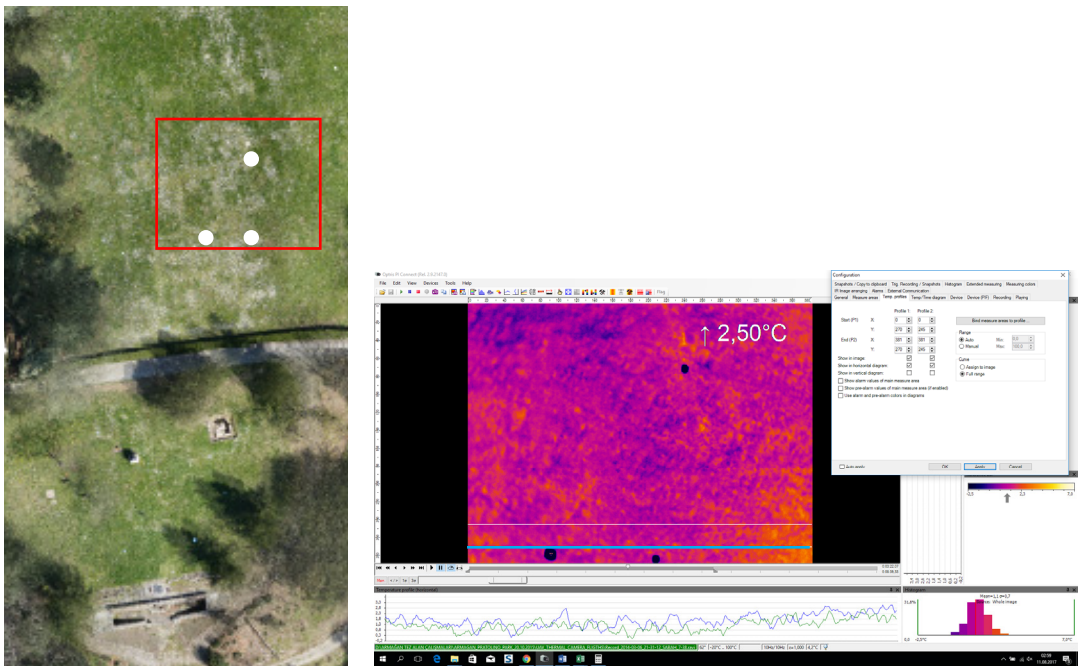

Figure 5.3.93: (left) The fifth frame area with red rectangle and aluminium targets with white points, (right) the thermal frame of the area displayed on the left and aluminium target in blacks and blue line just upper parts of the targets indicates Y=270px reference line and the upper of this line is Y=245px.

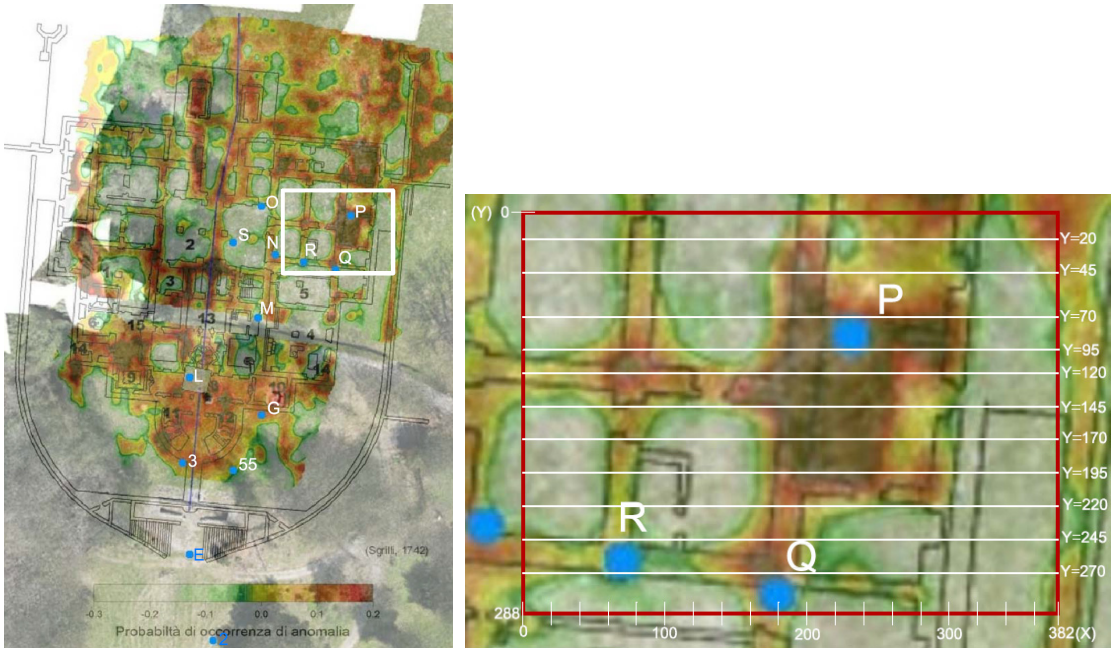

Figure 5.3.94: left) Orthophoto and anomaly map from Desideri (2009) showing the area with white rectangle.(right) Horizontal temperature diagram lines showing Y=270, Y=245, Y=220, Y=195, Y=170, Y=145, Y=120, Y=95, Y=80, Y=70, Y=45, Y=20.

In this frame, X=0-20 px range, temperature decreases slightly in during Y=245 and Y=195, temperature increases on the other lines. However the most visible temperature differences are seen in line Y=220 at X=40, 60 and between 100-120 pixels and at X=150 px it reaches maximum temperature. After a slight decrease, it increases again at X=170-190 while in the same range Y=245 has the lowest temperature. Aslo

while Y=270 and 220 has close temperatures at X=220 and 260, Y=245 has lower temperature (figure 5.3.94).

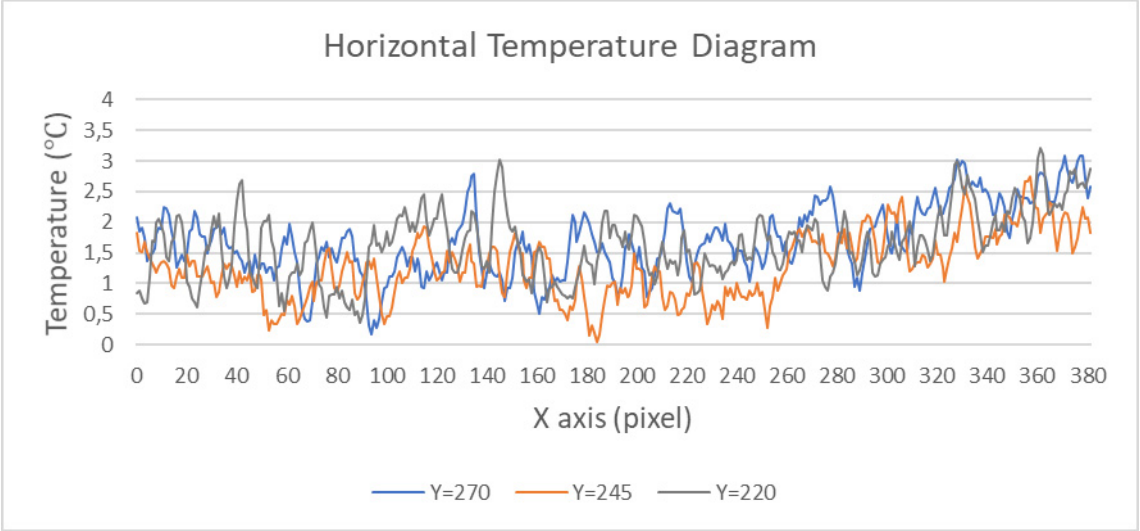

Figure 5.3.95: Horizontal temperature diagram of the fifth frame Y=270, Y=245, Y=220 at 7:00 am flight.

Regarding to Y=270, Y=245 and Y=220 line, it can be seen temperature changes till 3℃. Between 0-60 px, Y=245 and Y=270 have similar temperatures, Y=220 line behaves different from them.When Y=245 has 1-1.5℃ between 120-140 px, this temperature becomes almost 3℃ in Y=270. Similarly, while Y=220 and Y=245 between 200-220 px, Y=270 has higher temperature. Contrastly, in Y=245 line in 180 px, temperature decreases (Figure 5.3.95).

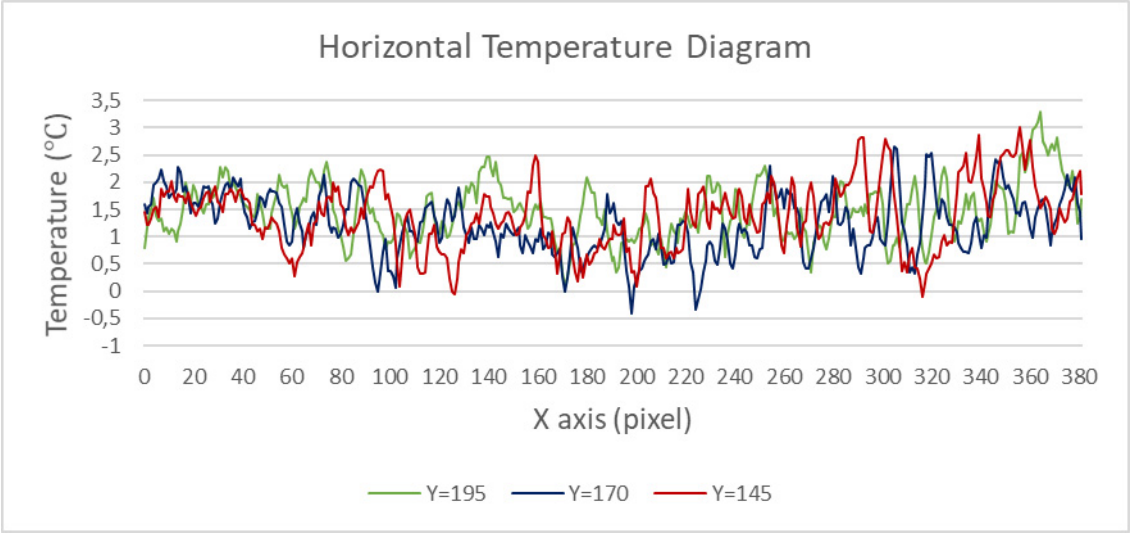

Figure 5.3.96: Horizontal temperature diagram of the fifth frame Y=195, Y=170, Y=145 at 7:00 am flight.

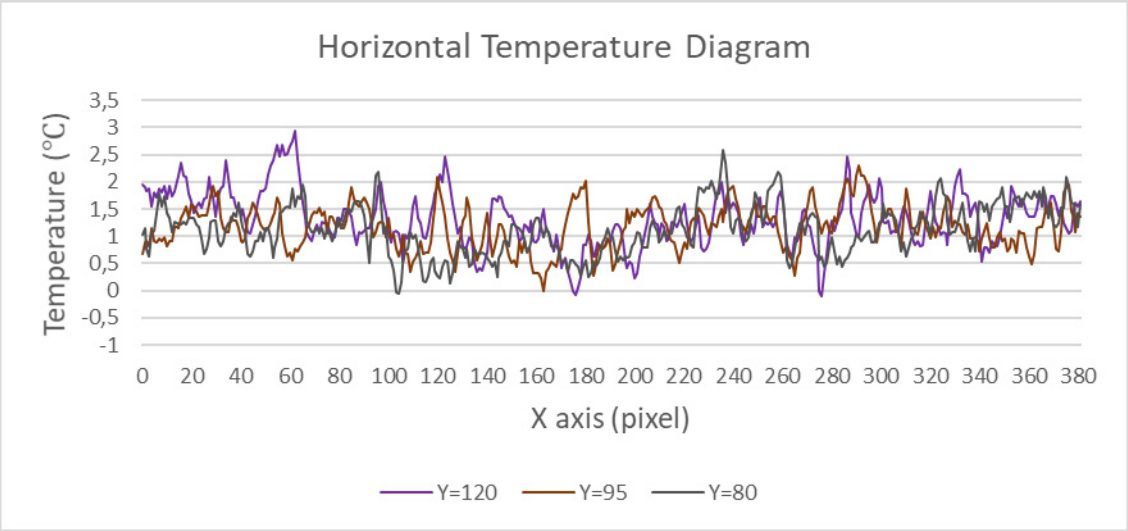

Figure 5.3.97: Horizontal temperature diagram of the fifth frame Y=120, Y=95, Y=80 at 7:00 am flight.

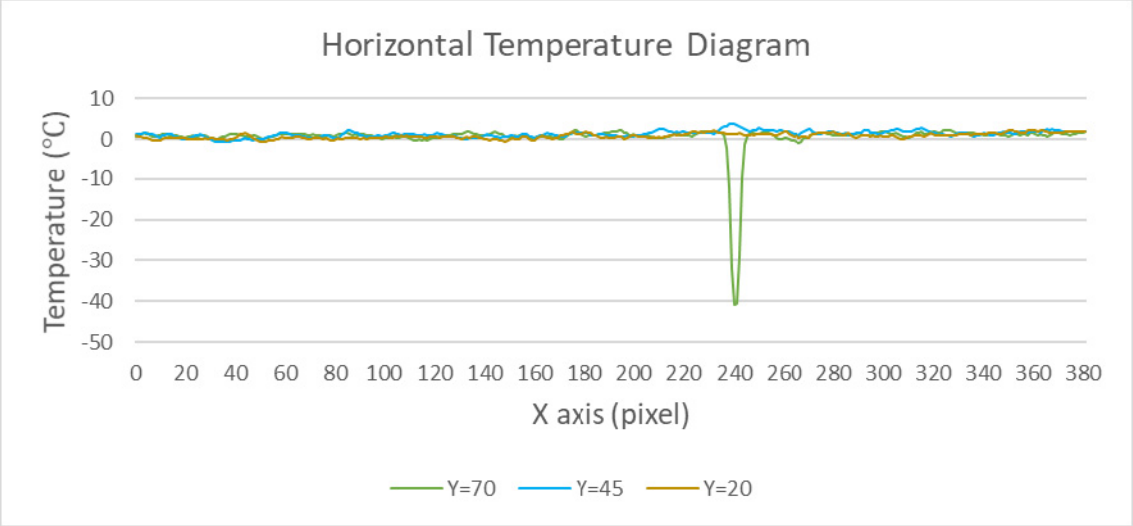

Figure 5.3.98: Horizontal temperature diagram of the fifth frame Y=70, Y=45, Y=20 at 7:00 am flight (with aluminium target between 230-250 px)

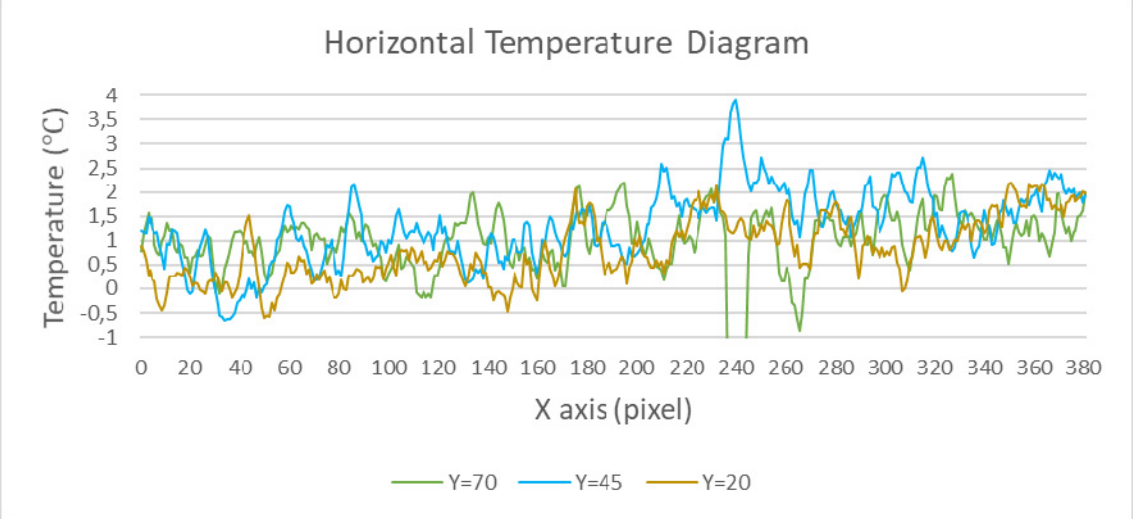

Figure 5.3.99: Horizontal temperature diagram of the fifth frame Y=70, Y=45, Y=20 at 7:00 am flight

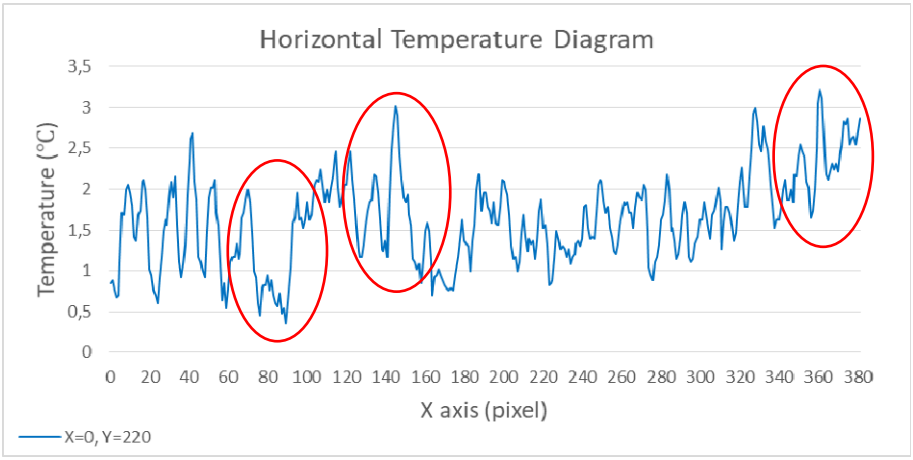

Figure 5.3.100: Horizontal temperature diagram of Y=220 at 7:00 am flight of the fifth frame

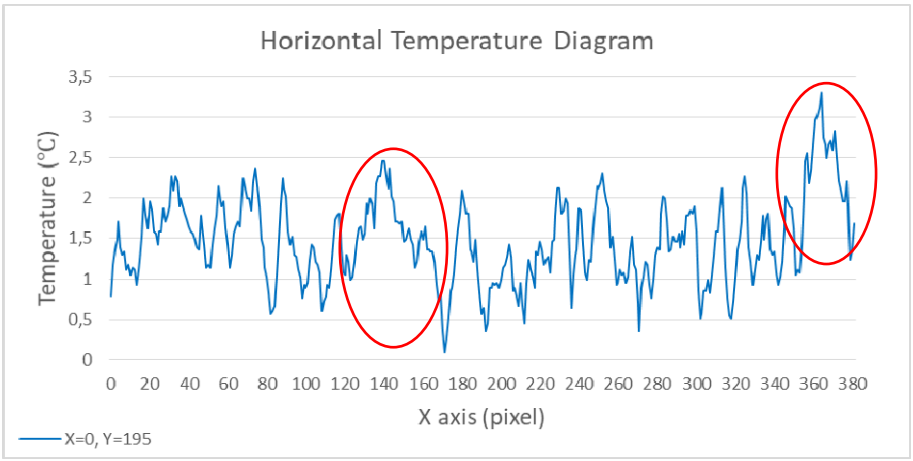

Figure 5.3.101: Horizontal temperature diagram of Y=195 at 7:00 am flight of the fifth frame

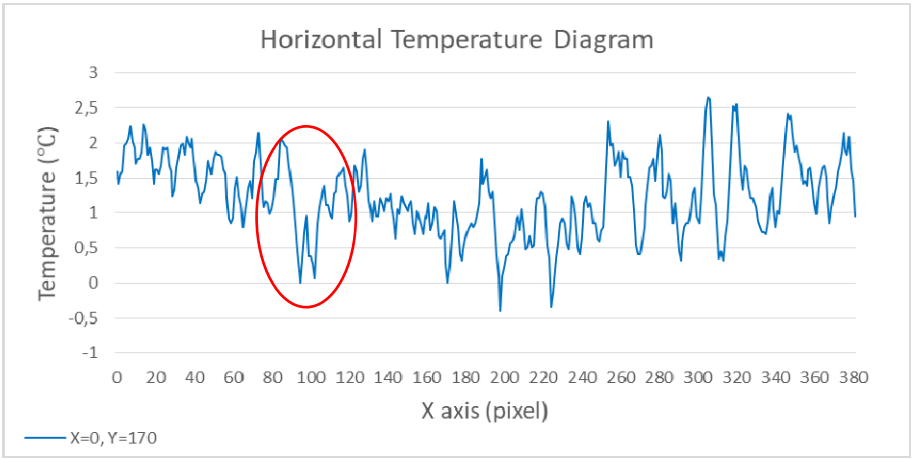

Figure 5.3.102: Horizontal temperature diagram of Y=170 at 7:00 am flight of the fifth frame

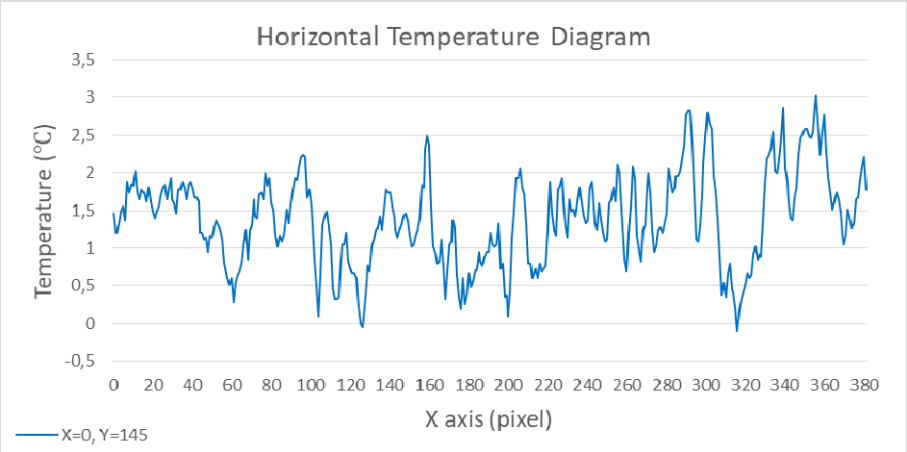

Figure 5.3.103: Horizontal temperature diagram of Y=145 at 7:00 am flight of the fifth frame

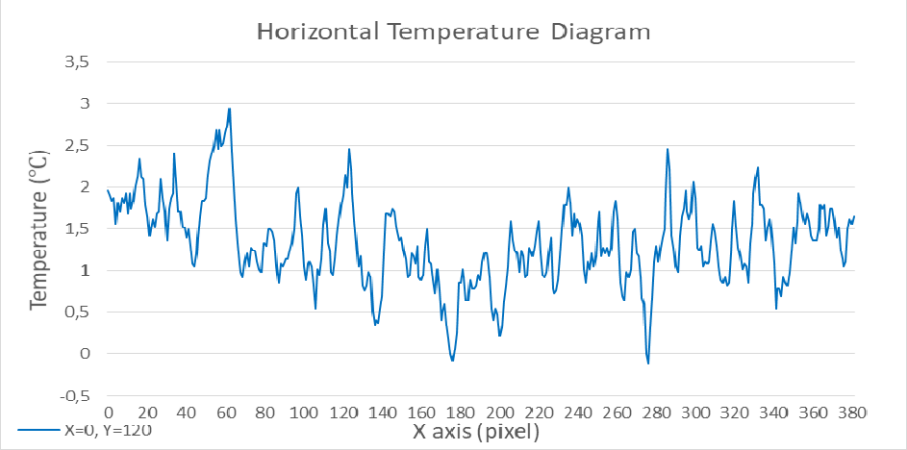

Figure 5.3.104: Horizontal temperature diagram of Y=120 at 7:00 am flight of the fifth frame

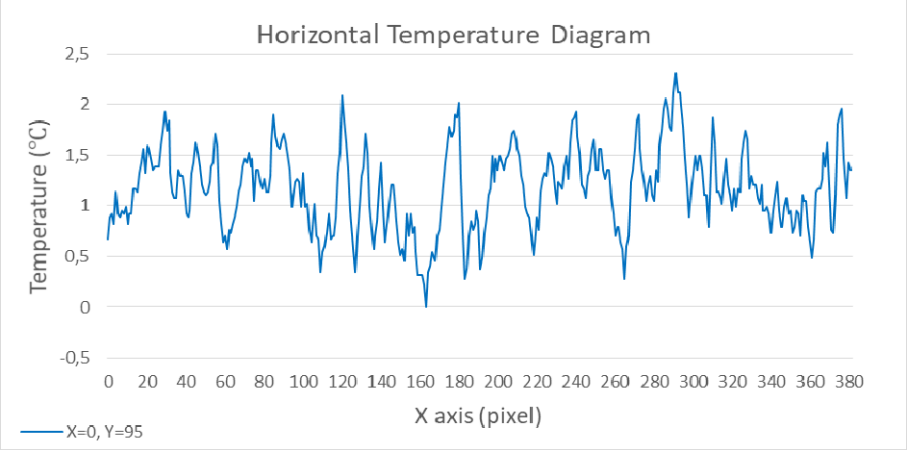

Figure 5.3.105: Horizontal temperature diagram of Y=95 at 7:00 am flight of the fifth frame

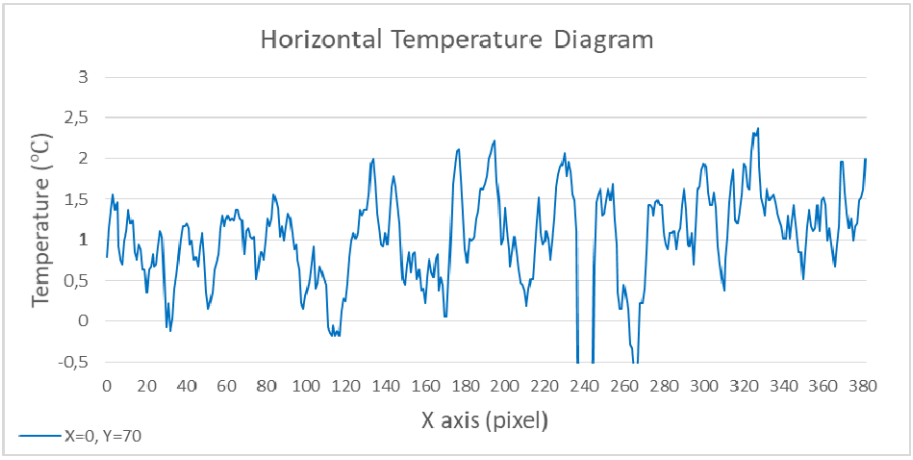

Figure 5.3.106: Horizontal temperature diagram of Y=70 at 7:00 am flight of the fifth frame

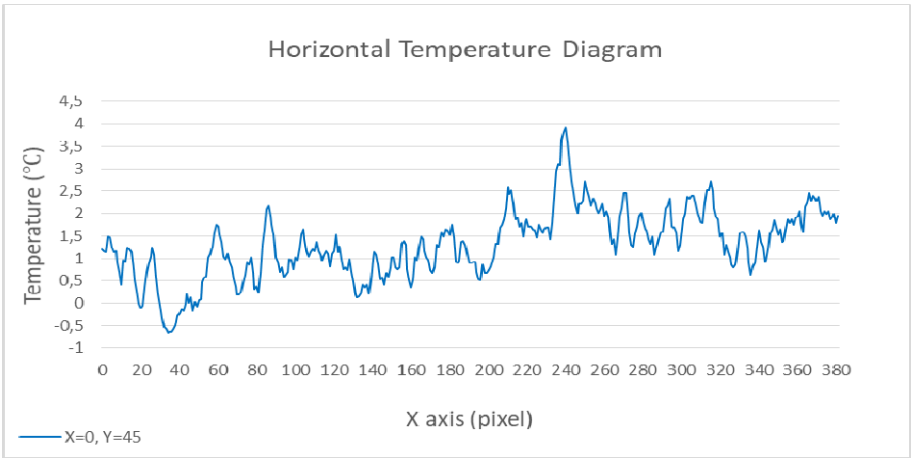

Figure 5.3.107: Horizontal temperature diagram of Y=45 at 7:00 am flight of the fifth frame

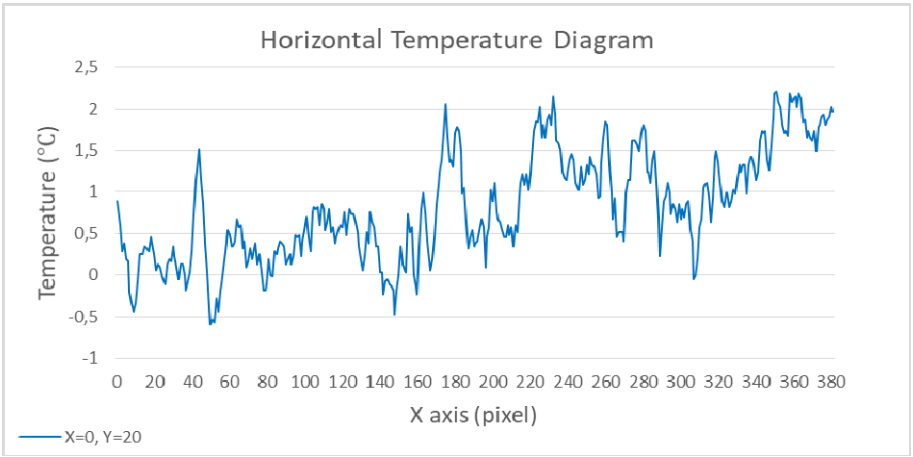

Figure 5.3.108: Horizontal temperature diagram of Y=20 at 7:00 am flight of the fifth frame

The sitxth frame was one of the non-tree frame of the area. So the temperature scale is smaller like fifth frame. There was no tree in any side of the area. Some parts of the ground was covered with camomille like other parts but also there were small areas without any vegetation. This part showed high anomalies in Diverise, 2009 report. In order to take refence, aluminium targets were used as it was in other frames. The line just up of the target was accepted as reference as Y=270 (Figure 5.3.109).

Figure 5.3.109: (left) The sixth frame area with red rectangle and aluminium target with white point, (right) the thermal frame of the area displayed on the left and aluminium target in black and blue line just upper parts of the targets indicates Y=270px reference line and the upper of this line is Y=245px.

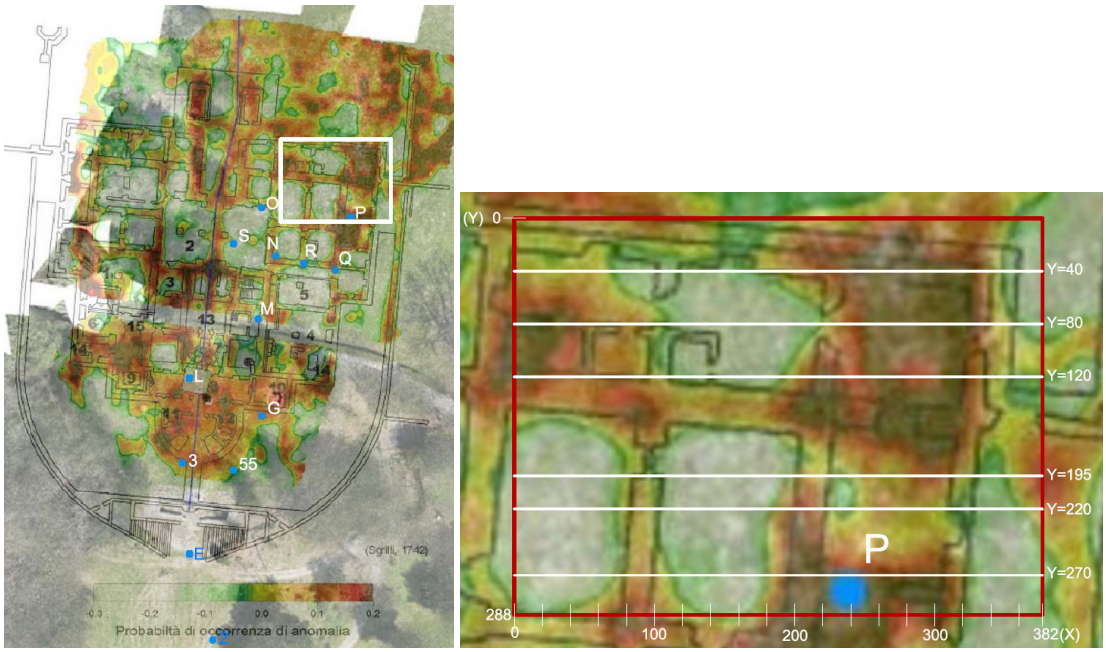

Figure 5.3.109: left) Orthophoto and anomaly map from Desideri (2009) showing the area with white rectangle.(right) Horizontal temperature diagram lines showing Y=270, Y=220, Y=195, Y=120, Y=80, Y=40.

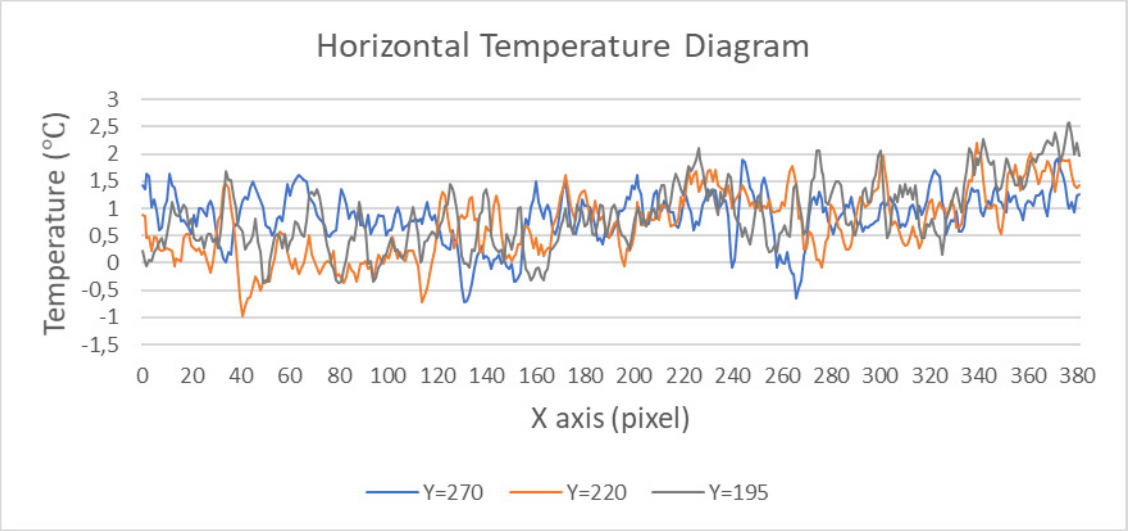

Figure 5.3.110: Horizontal temperature diagram of the sixth frame Y=270, Y=220, Y=195 at 7:00 am flight.

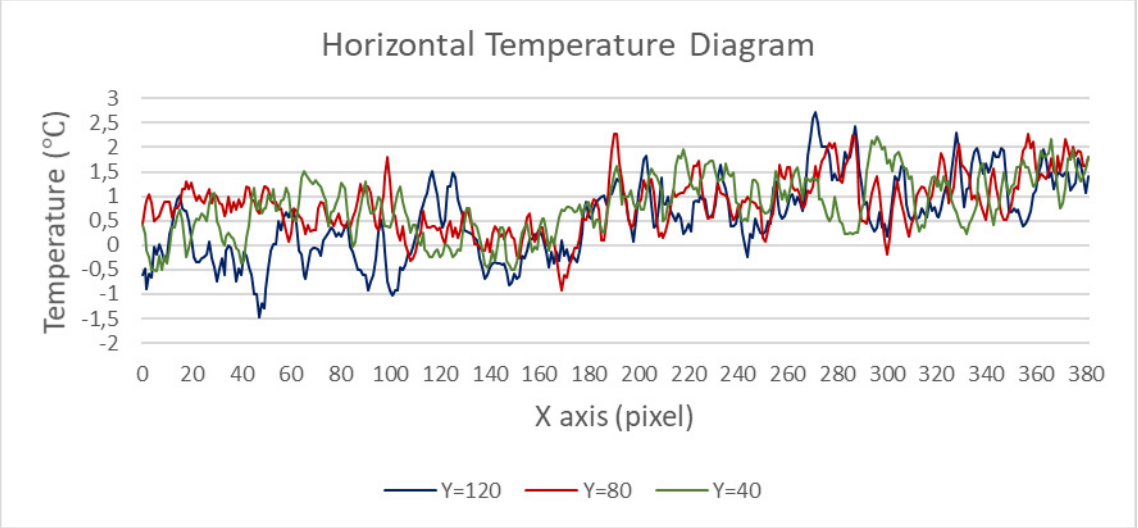

Figure 5.3.111: Horizontal temperature diagram of the sixth frame Y=120, Y=80, Y=40 at 7:00 am flight.

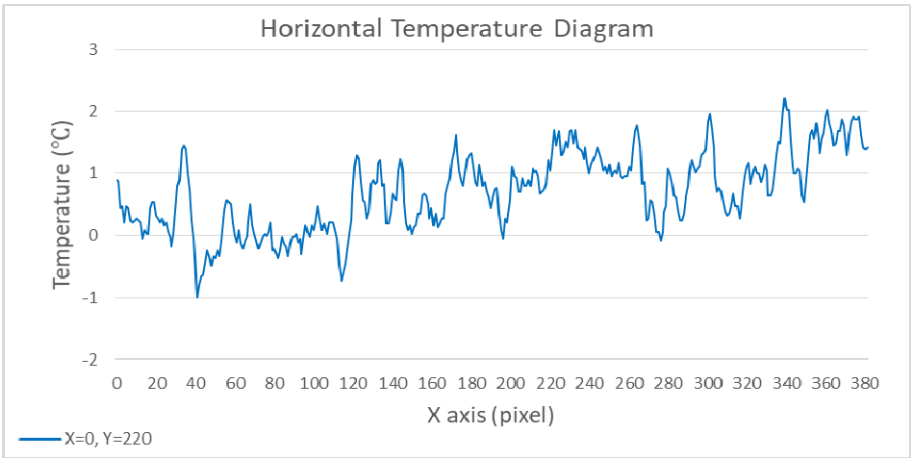

Figure 5.3.112: Horizontal temperature diagram of Y=220 at 7 am flight of the sixth frame

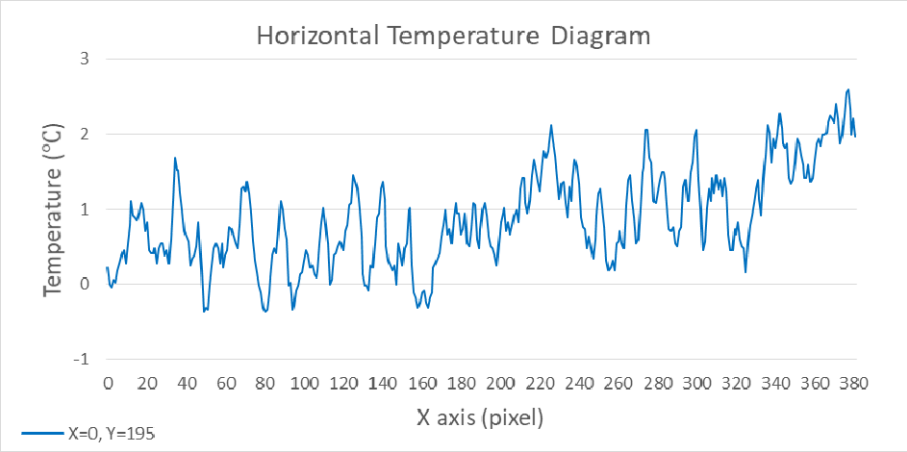

Figure 5.3.113: Horizontal temperature diagram of Y=195 at 7 am flight of the sixth frame

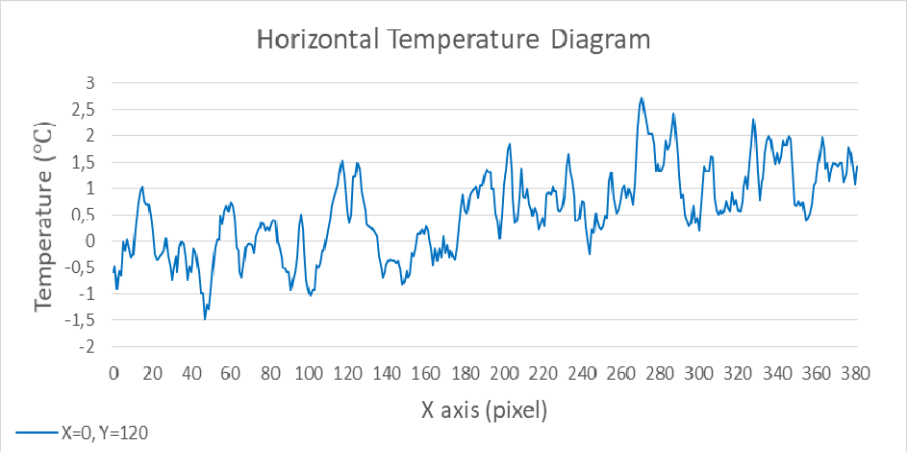

Figure 5.3.114: Horizontal temperature diagram of Y=120 at 7 am flight of the sixth frame

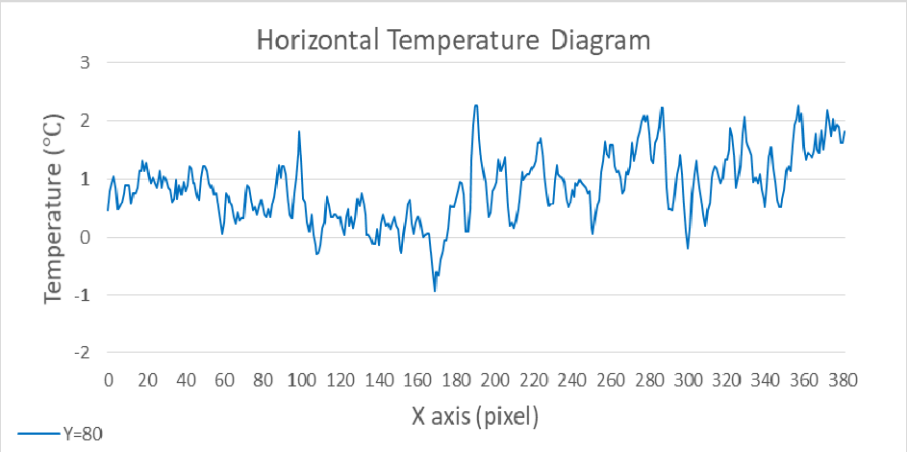

Figure 5.3.115: Horizontal temperature diagram of Y=80 at 7 am flight of the sixth frame

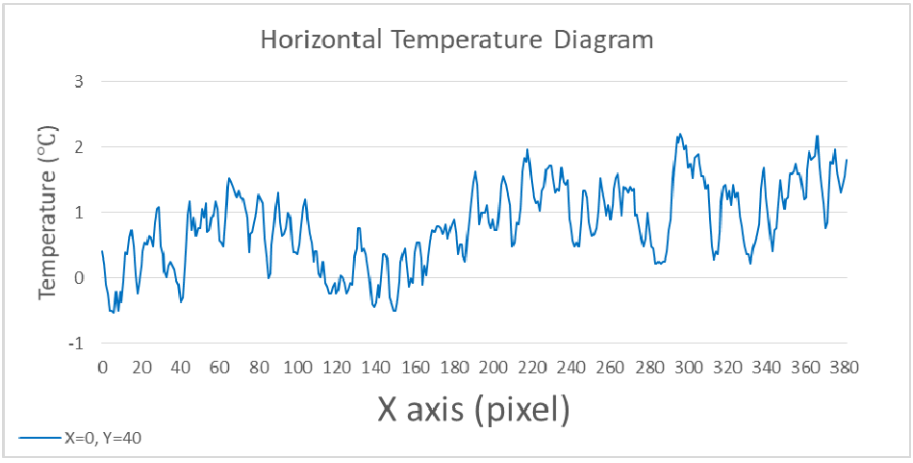

Figure 5.3.116: Horizontal temperature diagram of Y=40 at 7 am flight of the sixth frame

The seventh frame was one of the non-tree frame of the area. This frame was 9:16 am flight.

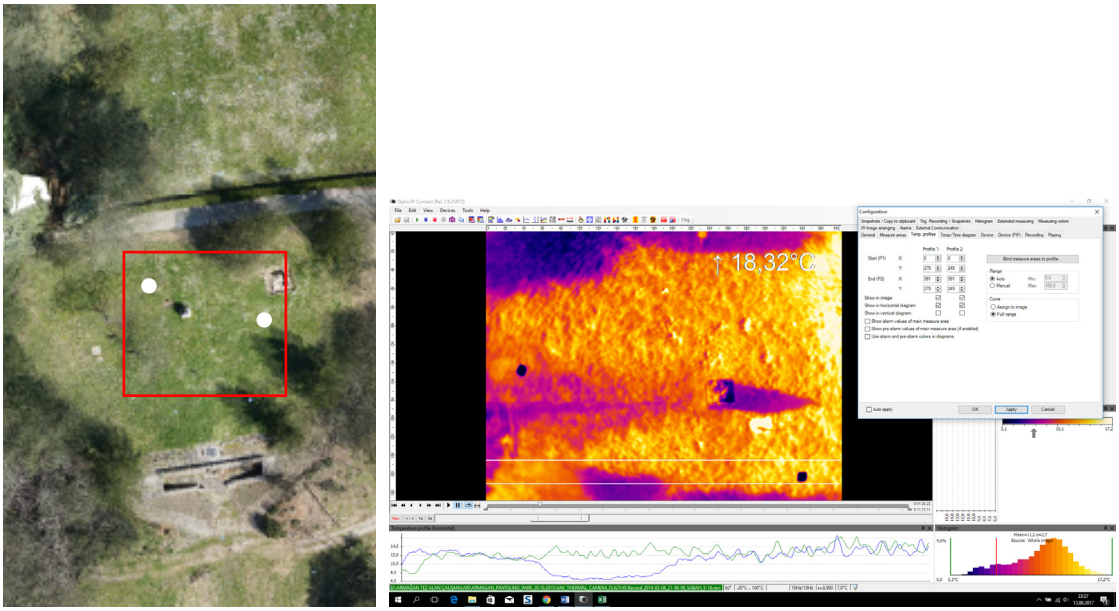

Figure 5.3.117: (left) The sixth frame area with red rectangle and aluminium target with white point, (right) the thermal frame of the area displayed on the left and aluminium target in black and blue line just upper parts of the targets indicates Y=270px reference line and the upper of this line is Y=245px.

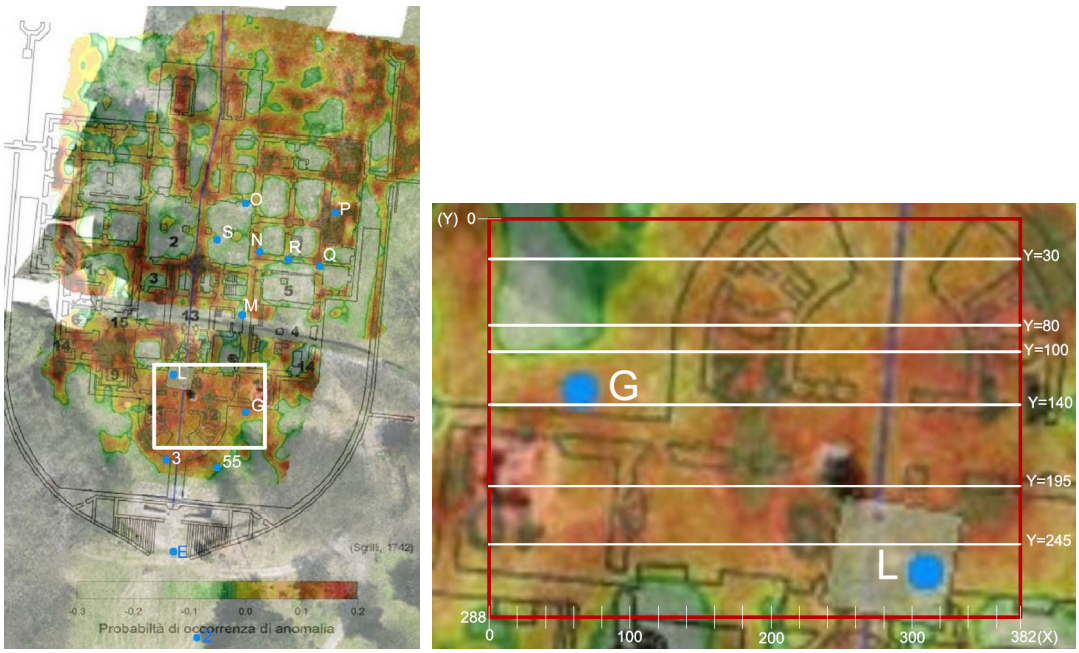

Figure 5.3.118: left) Orthophoto and anomaly map from Desideri (2009) showing the area with white rectangle.(right) Horizontal temperature diagram lines showing Y=245, Y=195, Y=140, Y=100, Y=80 and Y=30.

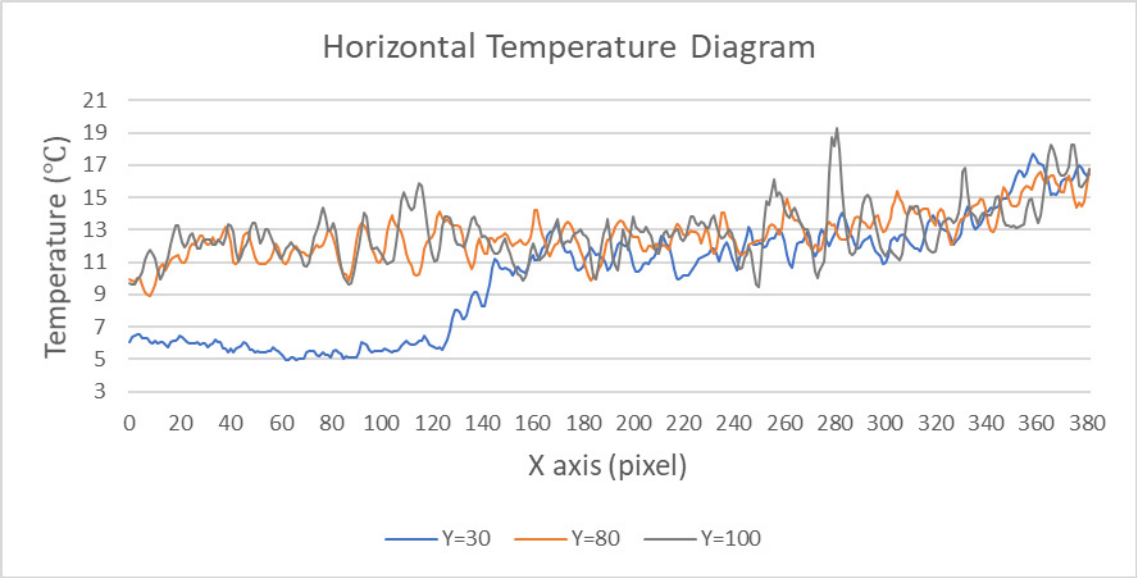

Figure 5.3.119: Horizontal temperature diagram of Y=30, Y=80 and Y=100 at 9:16 am flight of the seventh frame

In Y=30 line it can be observed low temperature because of shadows of trees. While befor the trees, Y=80 and Y=100 the temperature is close to each other. Y=80 an Y=100 diagram is smiliar till 100-120 px, while in Y=100 line, there is a temperature increase between 100-120 px likely between 240-280 px (Figure 5.3.119).

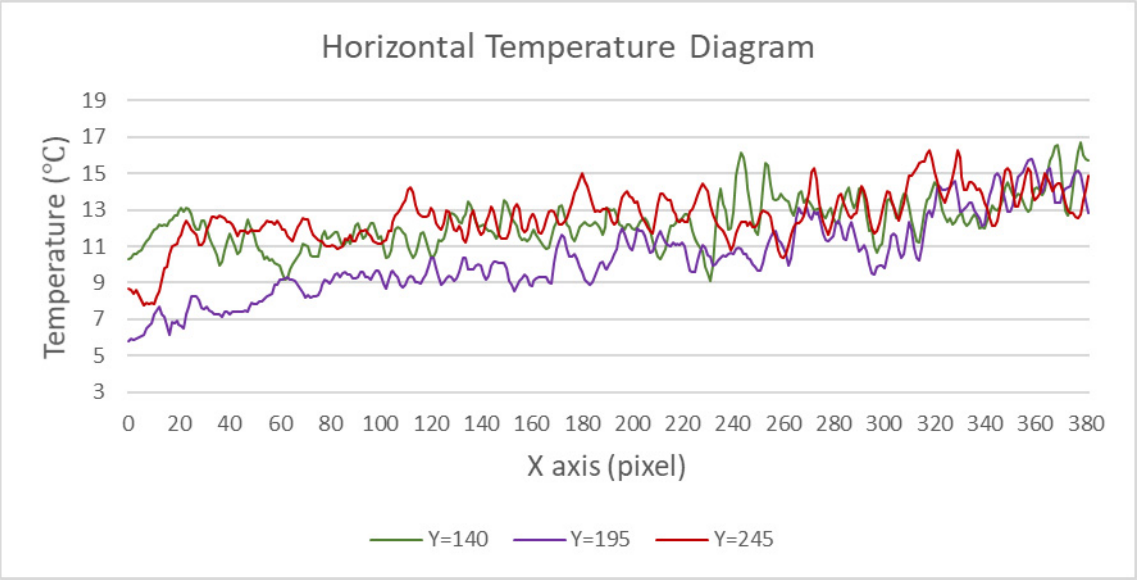

Figure 5.3.120: Horizontal temperature diagram of Y=140, Y=195 and Y=245 at 9:16 am flight of the seventh frame

In Y=140, Y=195 and Y=245 line, only Y=195 line has slightly difference and lower temperature profile from Y=140 and Y=245. More stronger difference can be seenbetween 160-200 px. Besides, in Y=245 line between 300-340 px (figure 5.3.120).

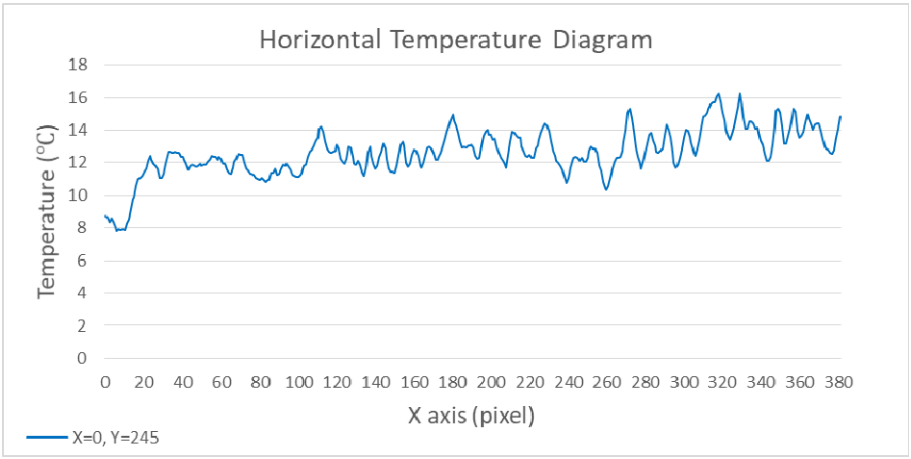

Figure 5.3.121: Horizontal temperature diagram of Y=245 at 9:16 am flight of the seventh frame

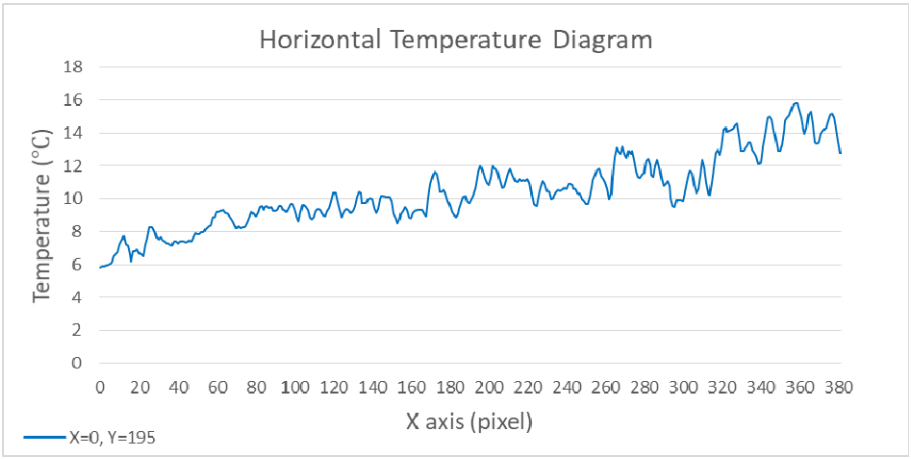

Figure 5.3.122: Horizontal temperature diagram of Y=195 at 9:16 am flight of the seventh frame

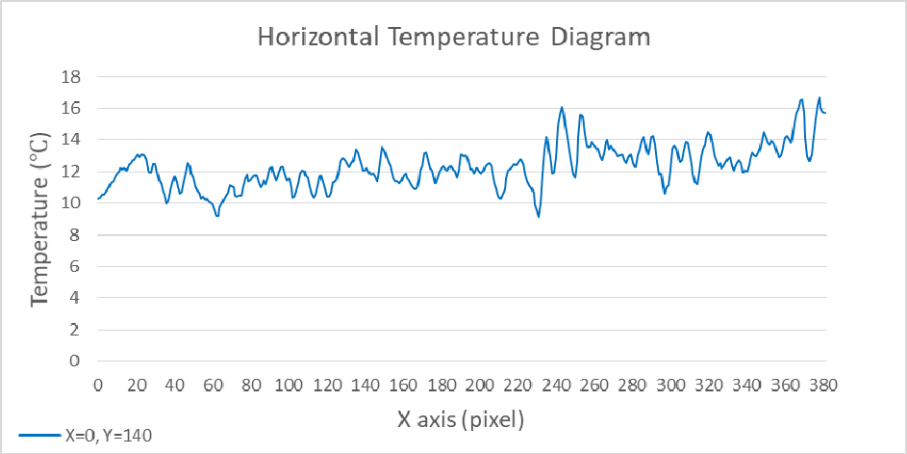

Figure 5.3.123: Horizontal temperature diagram of Y=140 at 9:16 am flight of the seventh frame

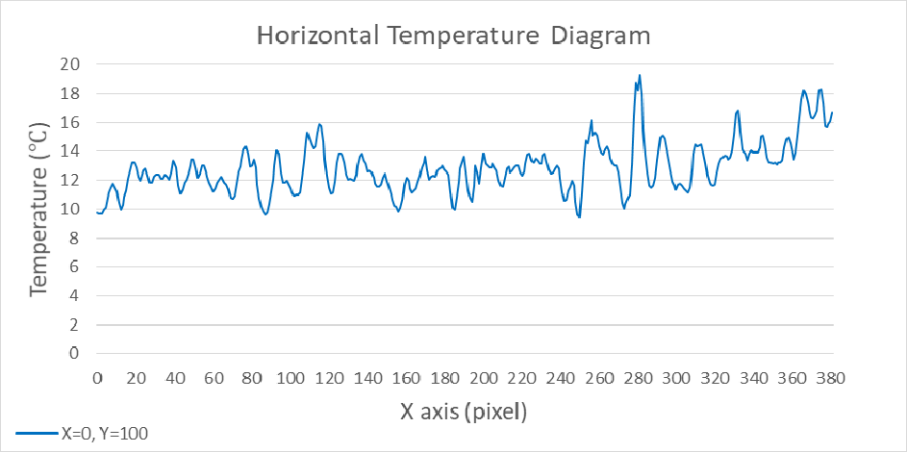

Figure 5.3.124: Horizontal temperature diagram of Y=100 at 9:16 am flight of the seventh frame

When it's observed Y=100 and Y=140 line, temperature increase can be seen in between 260-280 px and temperature increase after 300 px in Y=140, Y=100, Y=80 and Y=30. If it's compared with Desideri anomaly map, this areahas strong anomaly that could be sign of any ruin.

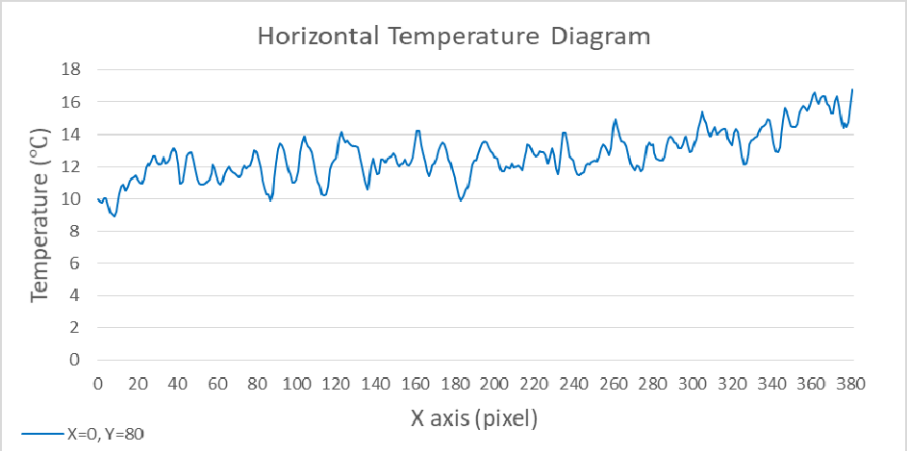

Figure 5.3.125: Horizontal temperature diagram of Y=80 at 9:16 am flight of the seventh frame

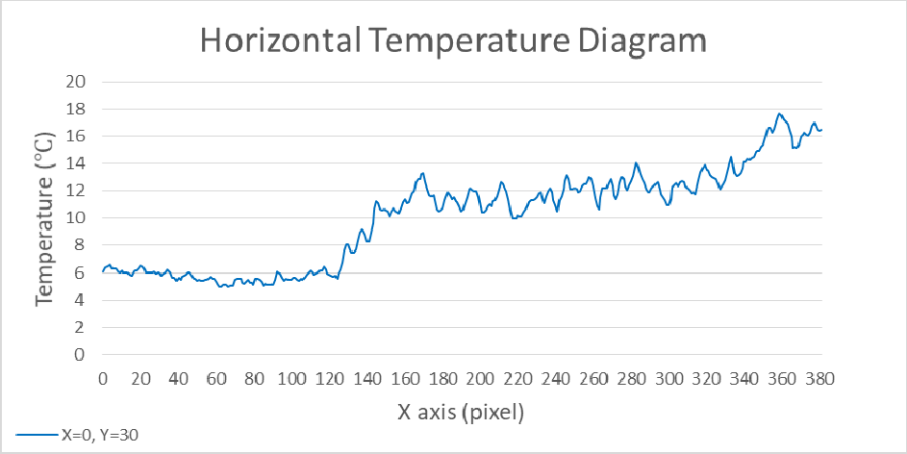

Figure 5.3.126: Horizontal temperature diagram of Y=30 at 9:16 am flight of the seventh frame

5.4. Çatalhöyük Archaeological Area, Konya, Turkey

5.4.1 Introduction and aim of the study

In archaeology and cultural heritage related projects there is often need for a rapid and accurate documentation of the objects. Since the process is dynamic, it requires fast and preferably non-immersive documentation techniques. Besides, the technique inevitably should be suited to cover the complete area (Sauerbier & Eisenbeiss, 2010). Even though fast, accurate, cheap modelling and visualization of archaeological areas is a demand, there are some justifications making this demand difficult. The first reason for this difficulty is directly related with the complexity and geometric and radiometric features of archaeological areas, while the second one is more related with its conceptual interpretation since it is a scientific document. These reasons make a need for new methods instead of traditional ones for archaeological documentation. String grids and basic traditional methods may not provide accuracy standard which architects need in many situations. Simple survey of the site similarly can only provide a layout with a few accurate points connected with vectors, without any further information. These methods both need extra people working within archaeological site for a defined period of time, which increases the economic cost, as well as the possibility of accidental destruction of important findings. Additional security precautions should be taken in order to prevent any possible damage to the surveyor or archaeological remains (Ioannidis et al., 2000). Another used traditional techniques like tracing with wet paper and pencil/crayons, free-hand drawing, photography, plaster molding, latex and wax rubbing to record inscriptions or significant details on the surfaces may not reproduce the degree of detail and accuracy required by today's researchers and conservators (Diaz-Andreu et al., 2005). Besides it takes time to prepare it for drawing which could be only 2D.

In last decades, there has been an increasing demand in the digital documentation of archaeological sites and artefacts with development of new technologies. In this sense, three-dimensional photo-realistic models allow to document, manage and analyze the shape and dimension of the represented objects with a high degree of accuracy and resolution with the potential for recording.

Archaeological data is extremely complex from a geometric point of view and existing methods of 3D modelling lead to large simplifications. In addition, the data also should be easily scalable to support different levels of visualization quality. Detailed geometric information about archaeological sites can be obtained by using terrestrial laser scanning methods as well as topographic surveying, photogrammetric techniques and Terrestrial Lidar Acquisitions (Apollonio et al., 2011; Brown et al., 2001; Lerma et al., 2010). These techniques made it possible to obtain a high level of detail and accuracy and result to be very effective, especially for small or medium-extension archaeological sites (up to tens of hectares).

Besides use of these technologies, in the last years, it can be seen extensive use of light aerial platforms or unmanned aerial vehicles (UAV) combined with digital non

metric cameras for archaeological documentation. In archaeological areas, some parts could be dangerous or difficult to reach. In many time, even though it is reachable areas, it may damage to archaeological area or object to walk on it as well as to try to make survey. For these reasons UAVs has started to be a solution.

Since UAVs have been rapidly improving in sophistication and reliability, its possibilities aid in archaeological research have recently generated much interest. With this rapid development in use of UAVs for archaeological areas, in las years there has been an increased interest in aerial thermography with UAV. Even though this detection method has been used in archeology since the 1970s but the use of aircraft or satellite imagery made this method difficult to access due to its cost and lack of flexibility. Beside the high cost of the system, aerial data generally don't provide suitable images for the production of large-scale maps and the relatively high flight altitude is able to detect only large structures not the small ones. Although the thermal images could be acquired by Remote Sensing, the spatial resolution of these images has not enough qualities for architectural documentation. Moreover, some restrictions related to aircraft motor and height doesn't always permit to fly over the area. Likewise, sometimes archeological areas are in remote areas which prevent to fly over the site.

In this project, archaeological area Çatalhöyük was surveyed with terrestrial laser scanning and mini UAV with color and thermal camera.

There were mainly two aims of this project: The first aim was

-to combine both terrestrial laser scanning data and aerial data from a mini UAV in order to improve and get a complete documentation of archaeological area Çatalhöyük.

The second one was

-to investigate the potential of UAVs with thermal camera for buried architectural ruins. For this aim, the combination of flexible and relatively low-cost a UAV with thermal digital camera was used on a case study for archaeological detection.

5.4.2. Çatalhöyük Archaeological Area

Çatalhöyük is one of the most ancient and prominent of the archeological sites in Turkey. It was built in the Neolithic period, and located near the town of Çumra district within the province of Konya, 52 km South east of the city (Figure 5.4.1).

Figure 5.4.1: Çatalhöyük from the satellite (image from google earth)

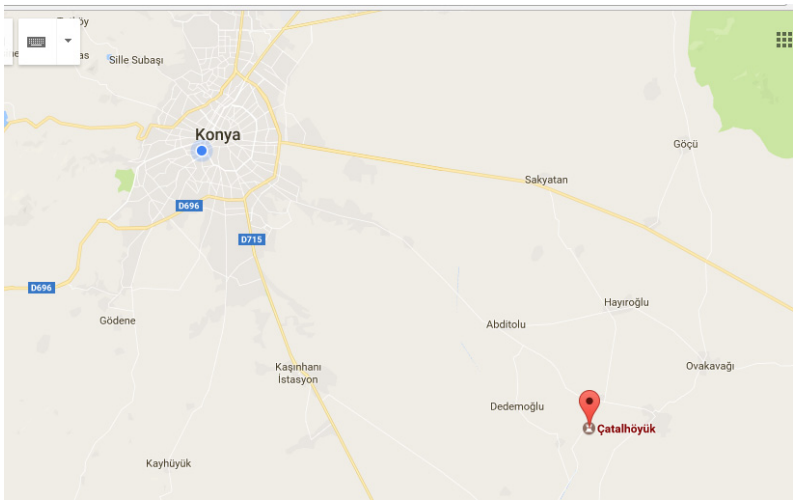

Figure 5.4.2: Çatalhöyük and Konya (image from maps google)

Çatalhöyük consists of two hills form the 37 ha site on the Southern Anatolian Plateau. The taller eastern mound contains eighteen levels of Neolithic occupation between 7400 BC and 6200 BC, including wall paintings, reliefs, sculptures and other symbolic and artistic features (Figure 5.4.3-4). Together they testify to the evolution of social organization and cultural practices as humans adapted to a sedentary life. The western mound shows the evolution of cultural practices in the Chalcolithic period, from 6200 BC to 5200 BC. Çatalhöyük provides important evidence of the transition from settled villages to urban agglomeration, which was maintained in the same location for over 2,000 years. It features a unique streetless settlement of houses clustered back to back with roof access into the buildings(http://whc.unesco.org/en/list/1405)

Figure 5.4.3: The excavations in Çatalhöyük, near Konya, discussed the long-standing archaeologists who represented the geometric figures resembling a settlement croquis below a settlement dating back to 8,600 years ago. The British archaeologist James Mellaart and some later archaeologists interpreted a wall-painted leopard skin, pointing to the leopard motifs frequently found at Çatalhöyük, and the geometric patterns below them. For others, two-tiered paintings such as Mount Hasan represented the volcanic eruption and the rising volcanic bombs or semi-solid lava fragments.(www.arkeolog.tumblr.com)

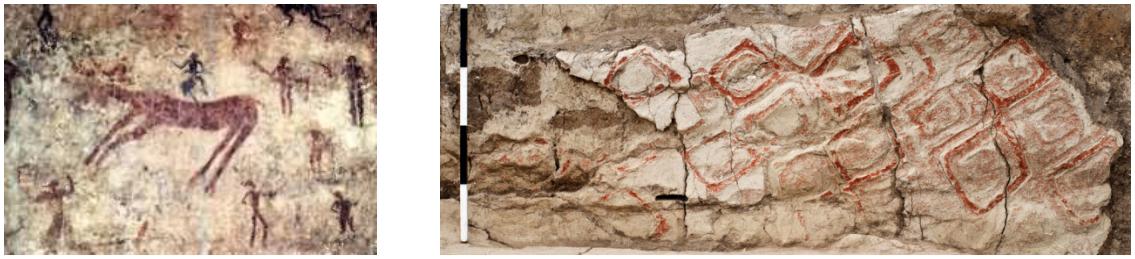

Figure 5.4.4: Examples of some wall paintings (www.catalhoyuk.com)

Figure 5.4.5: Çatalhöyük in Neolitic period (www.aktuelarekoloji.com.tr)

This site was first discovered in the late 1950s and excavated by James Melaart between 1961 and 1965 (Figure 5.4.4). The site rapidly became internationally famous due to the large size and dense occupation of the settlement, as well as the spectacular wall paintings and other art that was uncovered inside the houses. Since 1993, an international team of archaeologists, led by Professor Ian Hodder of Stanford University, has been carrying out new excavations and research, in order to shed more

light on the people that inhabited the site (Figure 5.4.5). In July 2012, Çatalhöyük was listed on the UNESCO World Heritage List. The Turkish Cultural Foundation (TCF) has been a sponsor of the Çatalhöyük excavation project for multiple years. The TCF grants were allocated to build a shelter over the excavation site, and to help improve access and informational signage on the site. TCF worked with the Global Heritage Fund in California on this project. To further expand its knowledge on Çatalhöyük, TCF has been taking its Teacher Study Tours to Çatalhöyük for many years (http://www.turkishculture.org/archaeology/catalhoyuk-1023.htm)

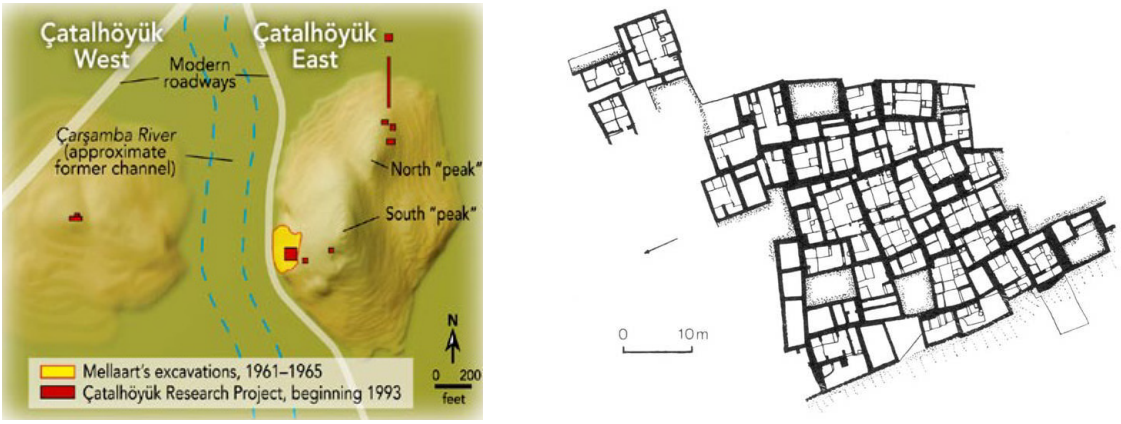

Figure 5.4.6: (left).Site of Çatalhöyük, located in the semiarid Konya Basin of Anatolia (now central Turkey), comprises two mounds that accumulated as the settlement's inhabitants repeatedly built, tore down, and rebuilt their mud-brick houses. The eastern mound, dating from 9,400 until 8,000 years ago, has two "peaks," suggesting that the population may have been divided into two intermarrying kin groups. The western mound was occupied from about 8,000 until 7,700 years ago.Map by Joe LeMonnier (http://www.naturalhistorymag.com/htmlsite/master.html?http://www.naturalhistorymag.com/htmlsite/0606/0606_feature.html). On the(right)….Plan of James Mellaart's excavations showing the dense house layout.source: (http://www.newtowninstitute.org)

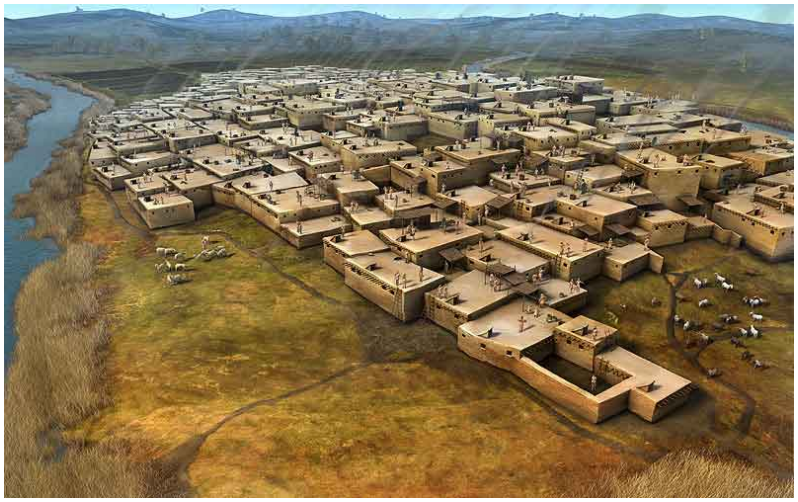

Figure 5.4.7: three dimensional illustration of Catalhoyuk source: http://delalhambra.multiply.com/journal/item/10/Th e_cradle_of_civilization_Wiege_der_Zivilisation (http://www.newtowninstitute.org)

Architecture in Çatalhöyük

One of Çatalhöyük's most defining attributes was its inhabitants' gradual, continuous building and rebuilding of their houses. These houses were very important to all aspects of their lives: material, social and ritual. Houses were roughly rectangular and closely built together with no streets in-between. Instead, people moved around on roofs and accessed their homes down a wooden ladder via an opening in the ceiling(http://www.catalhoyuk.com/site/architecture). (Figure 5.4.8).

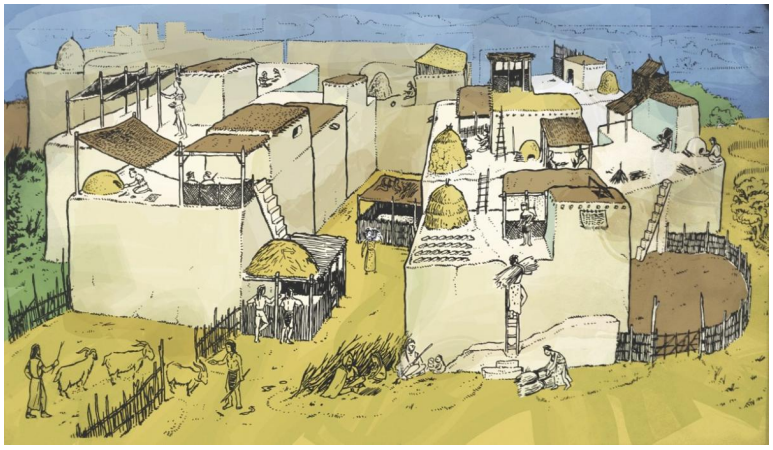

Figure 5.4.8: Reconstruction of Çatalhöyük showing the importance of the roof spaces. Illustration by John Swogge (http://www.catalhoyuk.com/site/architecture)

All the houses found at Çatalhöyük are different in shape and size, yet most follow a general layout. Each central room had an oven below the stairs where people carried out domestic tasks such as cooking. Raised platforms within the rooms were used for sleeping and other domestic activities. Beneath these platforms inhabitants buried their dead. Side rooms were accessed off the central room providing essential storage areas (Figure 5.4.9-10)

Figure 5.4.9: A reconstruction showing the use of space and the layout of a typical house. Illustration by Kathryn Killackey(http://www.catalhoyuk.com/site/architecture)

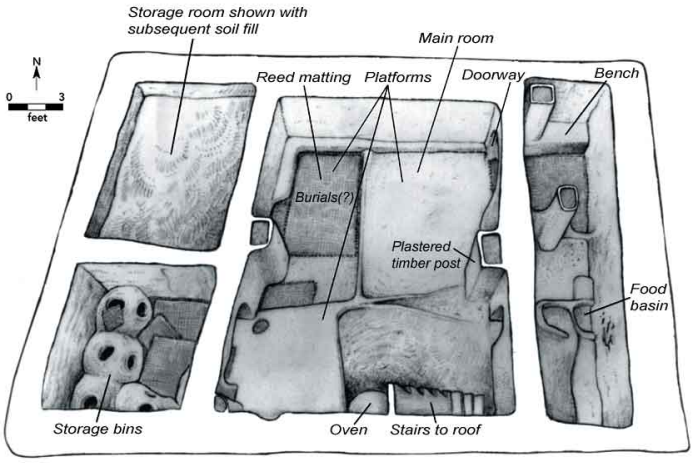

Figure 5.4.10: Lower parts of walls, floor, and the main furnishings of a typical house at Çatalhöyük are depicted in this artist's reconstruction. The house was inhabited about 8,500 years ago, and excavated by the author's team in 1998 and 1999. The floors have not yet been excavated, but on the basis of similarities with other buildings at the site, the archaeologists expect to find burials beneath the mat-covered northwest platform (http://www.naturalhistorymag.com/htmlsite/master.html?http://www.naturalhistorymag.com/htmlsite/0606/0606_feature.html)

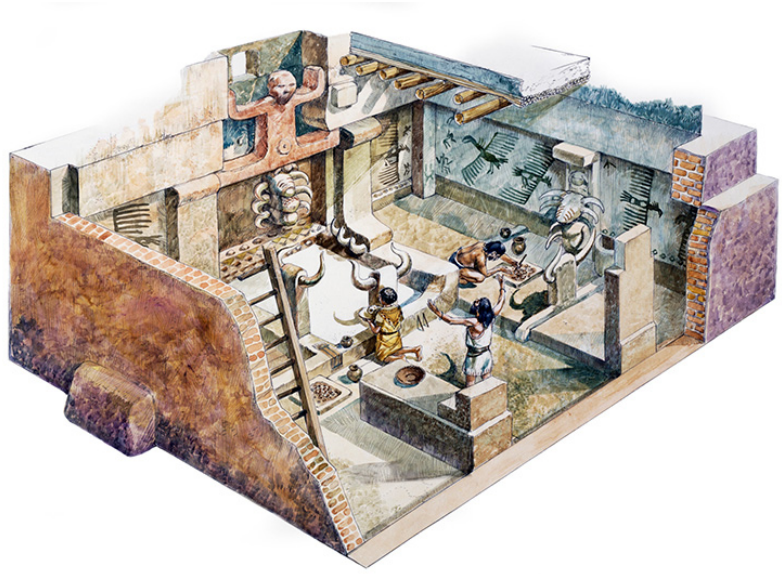

Figure 5.4.11: An illustration of Çatalhöyük house , drawing by De Agostini Picture Library((http://www.nationalgeographic.com.tr/makale/kesfet/catisma-kesfedilmeden-once/2625)

Being built on a mound of alluvial clay and on the bank of a now dry river, it housed mostly farmers. The inhabitants of this agricultural settlement lived in mud-brick houses, which were stacked next to each other so closely as if they had been welded. Therefore, there was no street - pattern on the ground level between the dwellings, but the access to the interiors was provided by holes in the ceilings, which were reached through exterior ladders and stairs. The ground circulation was replaced

by the rooftops where most of the daily activities took place when the weather allowed. It also appears that in later periods they had even built communal ovens on the rooftops. According to findings, the life cycle of a house coincided with the life of an extended family. The renewal of the houses was succeeded by partial demolition and rebuilding on the basis of the debris. This resulted in the approximately sixty feet high mound which consists of almost eighteen levels of settlement. These were the reasons that drove Mellaart to state the the vision of the builders of Çatalhöyük was far removed from the disorderly and random agglomeration of freestanding huts and hovels characteristic of the Protoneolithic period. Hand and foot seem to have been the standards of measurement with four hands to a foot. Houses are invariably of rectangular plan and the lines of the walls are as straight as the eye could make them. Because of the habit of building one structure on top of the other, using the old walls as foundations, a certain homogeneity of plan was created(http://www.newtowninstitute.org).

Figure 5.4.12: Excavation area of eastern mound, north peak

Figure 5.4.13: Excavation area of eastern mound, south peak

5.4.3. Documentation of all area

In Çatalhöyük, mainly 2 different field works were done. The first field work was done in eastern mound north peak inside the shelter. The second one was outside the shelter. Also orthophoto of the whole area was acquired (Figure 5.4.18). In order to get the whole area orthophoto e-Bee UAV RTK from Sensefly was used with SONY WX200 Color camera (Figure 5.4.14)

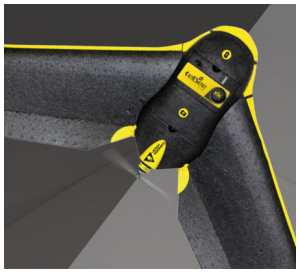

Technical Features of SONY WX COLOR	
Resolution	18.2 MP
Image resolution	4896 x 3672
Ground resolution at 100 m	2.75 cm/px
Sensor size	6.16 x 4.63 mm
Pixel pitch	1.26µm
Image format	JPEG

Figure 5.4.14: e-Bee UAV RTK by Sensefly (left), SONY WX 220 Color camera (middle) and camera technical features (right).

For the field work the flight was conducted on 102m flight. The whole area was calculated as 0.43 km². Images were acquired with %80 sidelap and %65 overlap. For image acquisition and flight trajectory eMotion software was used. According to these parameters the number of strips were 11 and totally 169 images were acquired (figure 5.4.16). Image processing was done in Agisoft Photoscan 1.2.7. build 3100.

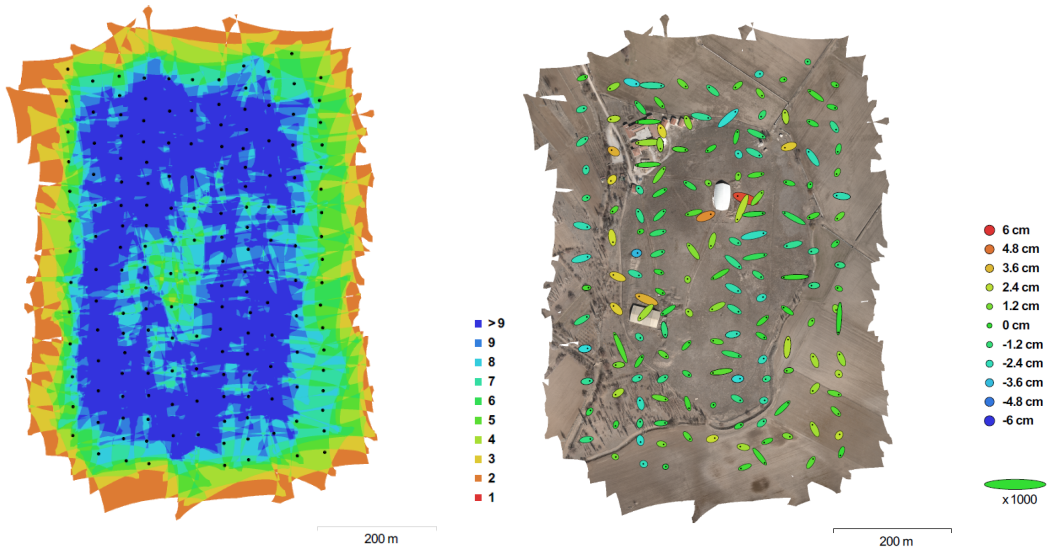

Figure 5.4.15: Camera locations and image overlap (left), camera locations and error estimates(right). Z errors is represented by ellipse color. X,Y errors are represented by ellipse shape. Estimated camera locations are marked with a black dot.

Table 5.4.1. Average camera location errors

Average Camera Location Error				
X error (cm)	**Y error (cm)**	**Z error (cm)**	**XY error (cm)**	**Total error (cm)**
1.36006	1.03135	1.66294	1.70688	2.38302

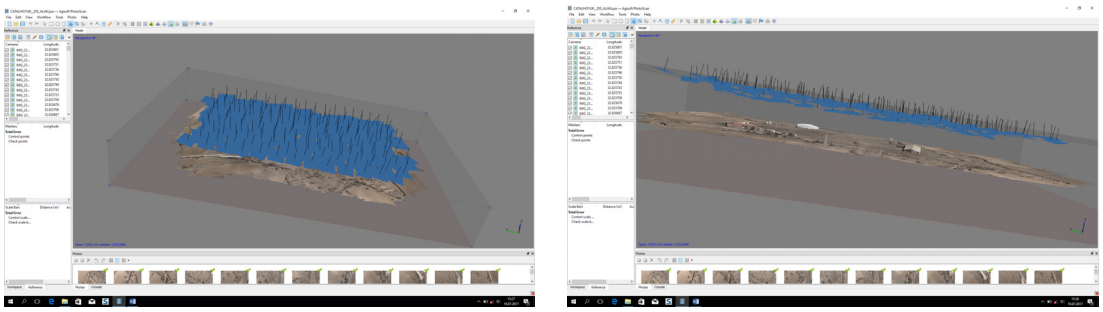

Figure 5.4.16: Camera positions of the area in Agisoft Photoscan

The alignment was carried out with 169 images with 424,331 tie points while dense cloud model had 106,059,194 points (Figure 5.4.16).

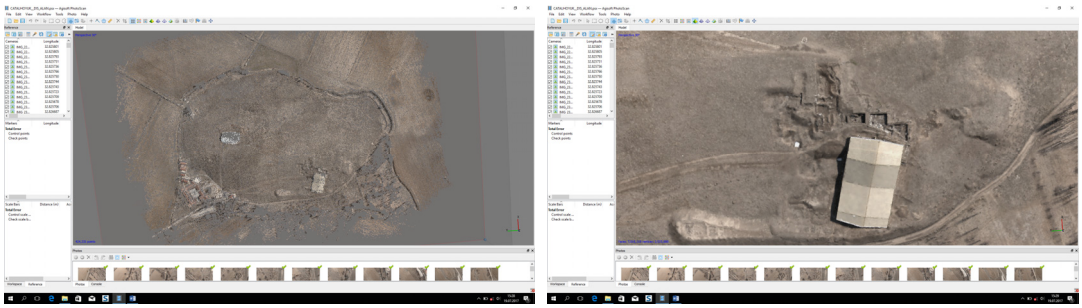

Figure 5.4.17: Point cloud model with 424,331 tie points in Agisoft PhotoScan (left)
Detail from dense Point cloud model with 106,059,194 points in Agisoft PhotoScan (right)

Reconstructed DEM is with 6.46 cm/px and 240 points/m² (Figure 5.4.18).The size of DEM is 11,063x16,086 with and 6.46 cm/px and 240 points/m² point density.
Generated orthophoto has 3.23 cm/px ground resolution with total RMSE 0.583975 px error. Orthomosaic size is 19,448x26,943 (Figure 5.4.18)

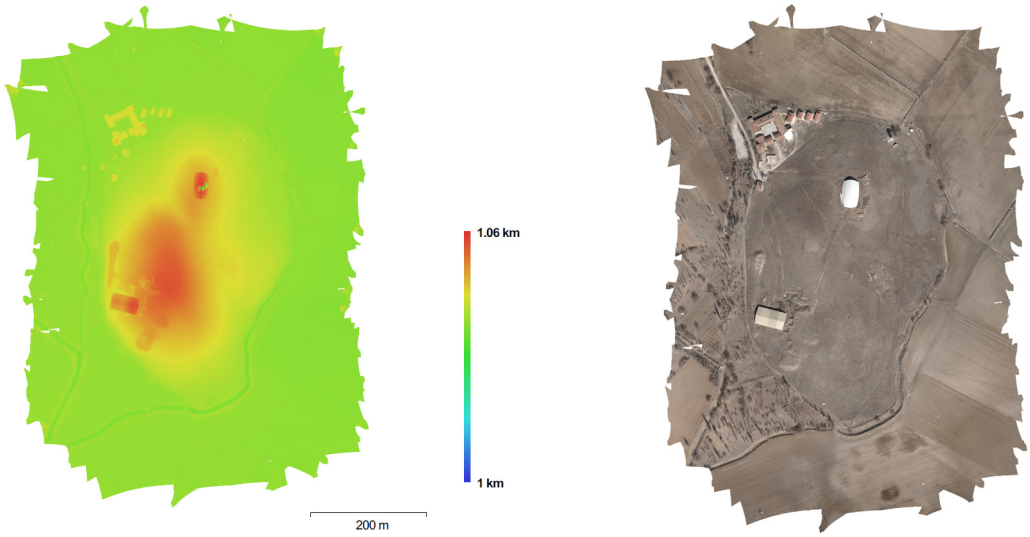

Figure 5.4.18: Reconstructed digital elevation model with 6.46 cm/px and 240 points/m² (left)
Generated orthophoto (right)

5.4.4. Eastern Mound North Peak Archaeological Area –inside the shelter

5.4.4.1.Field Work

After the orthophoto production of all area, the main study field was carried out inside the shelter. The studies regarding to this area have showed that this part of archaeological area contains eighteen levels of Neolithic occupation between 7400 BC and 6200 BC, including wall paintings, reliefs, sculptures and other symbolic and artistic features. In this area, several flights with color and thermal camera and TLS field work carried out for mainly two aims. One aim of this project was to combine and compare terrestrial laser scanning and UAV point cloud data while the second aim was to combine color and thermal data to check the anomalies since to define the anomalies is an input and may guide future excavataions.

Terrestrial laser scanner and a UAV system employed in this study, field work was conducted in cooperation with PAKSOY Teknik. For aerial data Albris Sensefly quadcopter, for terrestrial data FARO Focus 3D 120 Terrestrial Laser Scanner (Figure 5.4.19) was used.

The photogrammetric processing of the aerial images was carried out in both Agisoft Photoscan and Pix4D. For alignment of the point clouds several targets were used. Terrestrial laser scanning data set was registered in Scene software. For comparison and combining both point cloud data, Cloud Compare software was used.

Also 5 thermal flight was conducted in different times over the archaeological area inside the shelter without GPS. Some control points were used for registration of

data in Scene and Agisoft Photoscan. In order to combine the data, same control points were used for registration of point clouds data in Cloud Compare software.

Terrestrial Laser Data

FARO Focus3D 120 is a phase-based laser scanner. It captures objects in range from 0.6 m to 120 m with distance accuracy up to ±2 mm. Similar to other phase-based scanners, it is characterized by a high measuring speed at a maximum of 976.000 measuring points per second. The scanner is equipped with an internal color camera. A built-in 8 mega-pixel HDR camera captures detailed imagery easily This integrarted colour camera is able to get photorealistic 3D colour scans with up to 70 megapixels resolution and parallax-free colour overlay to the scan data in exreme ligthining conditions.

The scanning of the field was completed in one day and the whole areas was covered with 12 scans. The scanning was done only on the edges of the excavation area since it was forbidden to walk on archaeological area. Since the scanning was carried out only from the edges of the area, there were some missing parts in the data (Figure 5.4.21). Totally 515.726.448 million of points were acquired in 12 scan files. The point spaceing was 1-3 cm. After the alignment, a registered point cloud data 515,726,448 million points were acquired.

Figure 5.4.19: Terrestrial Laser Scanning with FARO Focus3D 120

UAV for aerial data (inside the shelter)

Even though there is an increasing research in UAVs due to their wide range applications, full autonomy is one the main milestone development in UAV system (Ehsan & McDonald-Maier, 2009; Vanblyenburgh, 2006). For the autonomy, the UAV needs a navigation system which gives information about the status of the vehicle and sends this information to the controller. The common navigation system in large scale

UAVs is the Inertial Navigation System coupled with the Global Positioning System (INS/GPS) (as described in detail in section 3.4.1.3). However, for small UAVs or indoor applications, there is a need for alternative navigation strategies (Ehsan & McDonald-Maier, 2009). This is because of mainly two reasons. INS/GPS system is relatively expensive and needs a good access to the GPS signal which is not available or diffciult to connect in case of indoor applications (Mohamed, Patra, & Lanzon, 2011).
Several indoor navigation schemes has been studied by many UAV research groups (Ehsan & McDonald-Maier, 2009; Valavanis, 2007; J. Zhang, Wu, Liu, & Chen, 2010). Among proposed techniques vision-baesd systems (computer vision systems) has achieved considerable interest (J. Zhang et al., 2010) since they are lightweight, passive and produce rich information about the motion of the vehicle (Kendoul, Fantoni, & Nonami, 2009; Mohamed et al., 2011). For using vision based navigation systems, the possible path of the UAV needs to be known. Images of the surrounding environment of the UAV's flying path are taken and analyzed to identify the basic features of this path before the flying mission commences. Then, the real time images taken from on-board camera(s) during the flight mission are compared with the visual memory of the vehicle to identify the known features and estimate the motion of the UAV (Mohamed et al., 2011). The vision-based information is integrated with other sensors such as GPS/gyroscope to refine and correct the estimation of the UAV's motion. However this requires a good GPS signal and it is not practical for indoor environments adn urban territories (Mohamed et al., 2011).

Figure 5.4.20: Measurement of the soil temperature and humidity

While computer vision based systems are being developed and researches are being continued to tackle with software and hardware problems, other navigation systems have been developed. One of them, a laser based navigation system has been developed in which the projection of four diode spots on the ground is used to estimate the dimensional position of the helicopter (Barabanov & Romaev, 2009). Another new indoor navigation strategy which is the combination of computer vision based and laser based was proposed by Mohamed et al, 2011. The systems used the location of three laser dots generated by the tree laser beams fixed to the body of the vehicle to identify the status of the UAV, fusing data estimatiom method like Extended Kalman Filter or additional GPS/IMU sensors (Mohamed et al., 2011).

Since there is shelter on excavation area, it was limited to fly on a definite height. The shelter height starts from 5.5m and the hightest point it becomes 7m meters.

For this study it was used Albris Sensefly quadcopter (56 x 80 x 17 cm), 1,8 kg.with up to 22 min. flight time with thermal sensor (Figure 5.4.21). It's main camera is 38 MP with GSD is 1mm/pixel at 6m and 1 cm/pixel at 60m with 63 degree horizontal field of view. Thermal camera has thermal overlaid (80 x 60 pixels) on main camera stream with 50 degree horizontal field of view (https://www.sensefly.com/drones/albris.html)

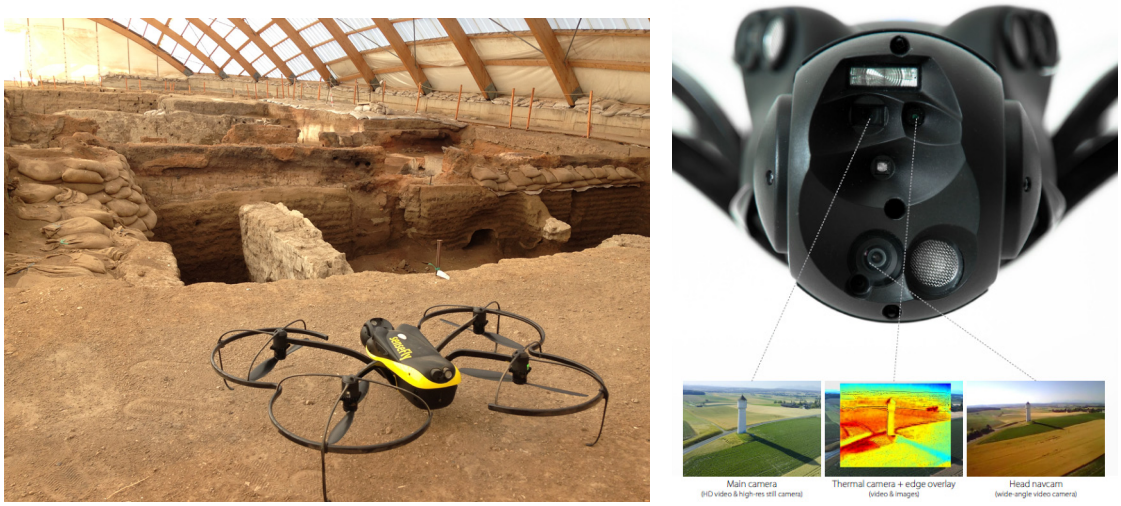

Figure 5.4.21: Albris Sensefly UAV in Çatalhöyük excavation area (left), (right) Albris Sensefly sensor payload system-main camera (left), thermal camera(middle), wide-angle video-camera(right

The lower part of the shelter was always problem during the field work. Thus, instead of autonomous flight, manuel flight with remote control (RC) was carried out in this area for data acquisition. For the flight control, eMotion3 was used. This quadcopter has 3 different flight modes (automatic, interactive and manual), able to fly up to 22 minutes with autopilot&control system. This UAV system is a sensor-rich platform with wide camera breadth. It's stabilized TripleView camera head which allows the user to switch between HD and thermal video imagery, live during the flight besides it can be captured high-resolution still images on demand (Figure 5.4.21).It was an advantage to get color and thermal data at the same time since the system has ability 80x60 pix thermal overlaid on color image.

This kind of field work operations requiresa trained piot for safety reasons, since especially landing in these kinds of areas has to be controlled. Besides, an operator with photogrammetric background is preferred for checking the image acquisition. The main units of UAV platform and integrated payloads are given in Figure 5.4.22.

Due to the difficulties on the area, take off and landing were controlled by the pilot and the actual flight mission was controlled by the operator via the flight control station. The flight trajectory was controlled via eMotion3 software. Because of the shelter changing height, the flight height was fixed at 4,81 height. The lowest part of the shelter is in 5.5 m and the highest part of the shelter is 10 m. The manual flight was controlled with remote control so it was difficult to control UAV.

The flight trajectory and the image acquisition points were calculated depending on the scale, camera parameters, flight height, dimension of the area and the overlap. For the flight planning it was the idea to have a high overlap for the accuracy.

Table 5.4.2: Technical parameters of Albris Sensefly UAV

Technical Parameters Albris Sensefly UAV	
Type	V-shaped quadcopter
Dimensions	56x80x17 cm
Wieght (incl. supplied camera&battery)	1.8 kg
Motor	4 electric brushless motors
Radio link range	Up to 2km with 2.4 GHz & 5 GHz ISM bands
Max airspeed	Automatic flight: 8 m/s –Manual flight: 12 m/s
Max climb rate	7 m/s
Wind resistance	Automatic: up to 8 m/s – Manual: up to 10 m/s
Maximum flight time	Up to 22 minutes
Autopilot&control	IMU, magnometer, barometer&GPS/GNSS
Operating temperature	-10 to 40 ℃
Integrated payloads (cameras)	
TripleView head	
Main camera	
Still images resolution	38 MP resolution
Resolution	7152x5368
Focal length	8.02 mm
Pixel size	1.4x1.4 μm
GSD (Ground sample distance)	1 mm/px at 6m 1 cm/px at 60m
Video	HD (1280X720 px)
Horizontal field of view	63 degrees
Digital zoom	6x
Thermal camera	
Still images / video	Thermal (80x60 px) overlaid on main camera stream
Horizontal field of view	50 degrees
Edge enhancement	Yes
Head navcam (visual sensor)	
Video	VGA (640X480 PX)
Video live streaming range	Up to 2 km
Horizontal field of view	100 degrees

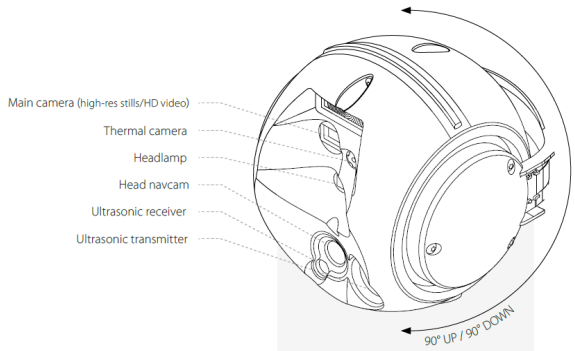

TripleView head
*180 ° vertical range of motion *6x digital zoom *Approx. 1 mm still image resolution at 5m *Active gimbal stabilization *Unobstructed field of view

Figure 5.4.22: TripleView head of Albris SenseflyUAV

At the end of field work, 373 images were taken in mainly 5 strips. It was the first time to use this UAV system in closed area also with thermal camera. Total field work was completed in one day.

Methodology

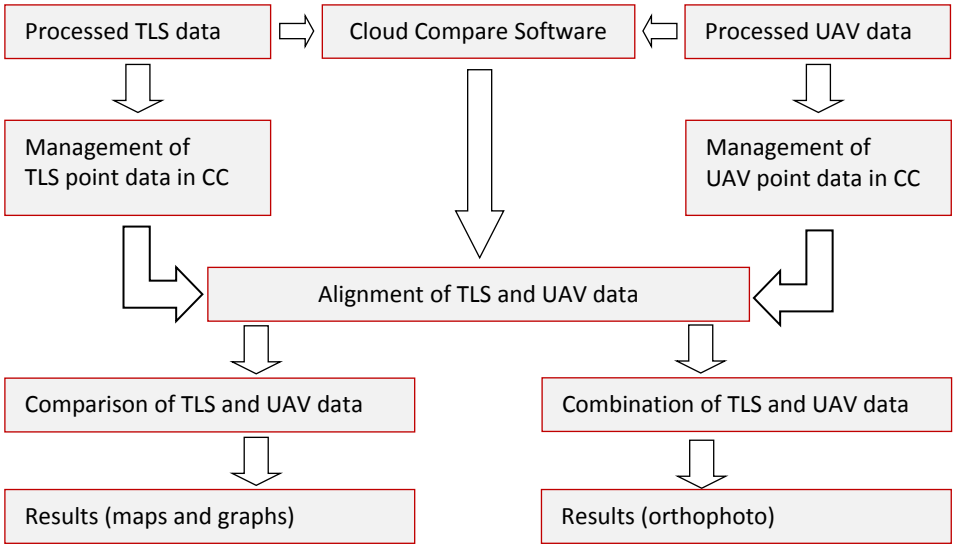

Figure 5.4.23: Simplified workflow for combination and comparison of TLS and UAV point cloud data in Cloud Compare software

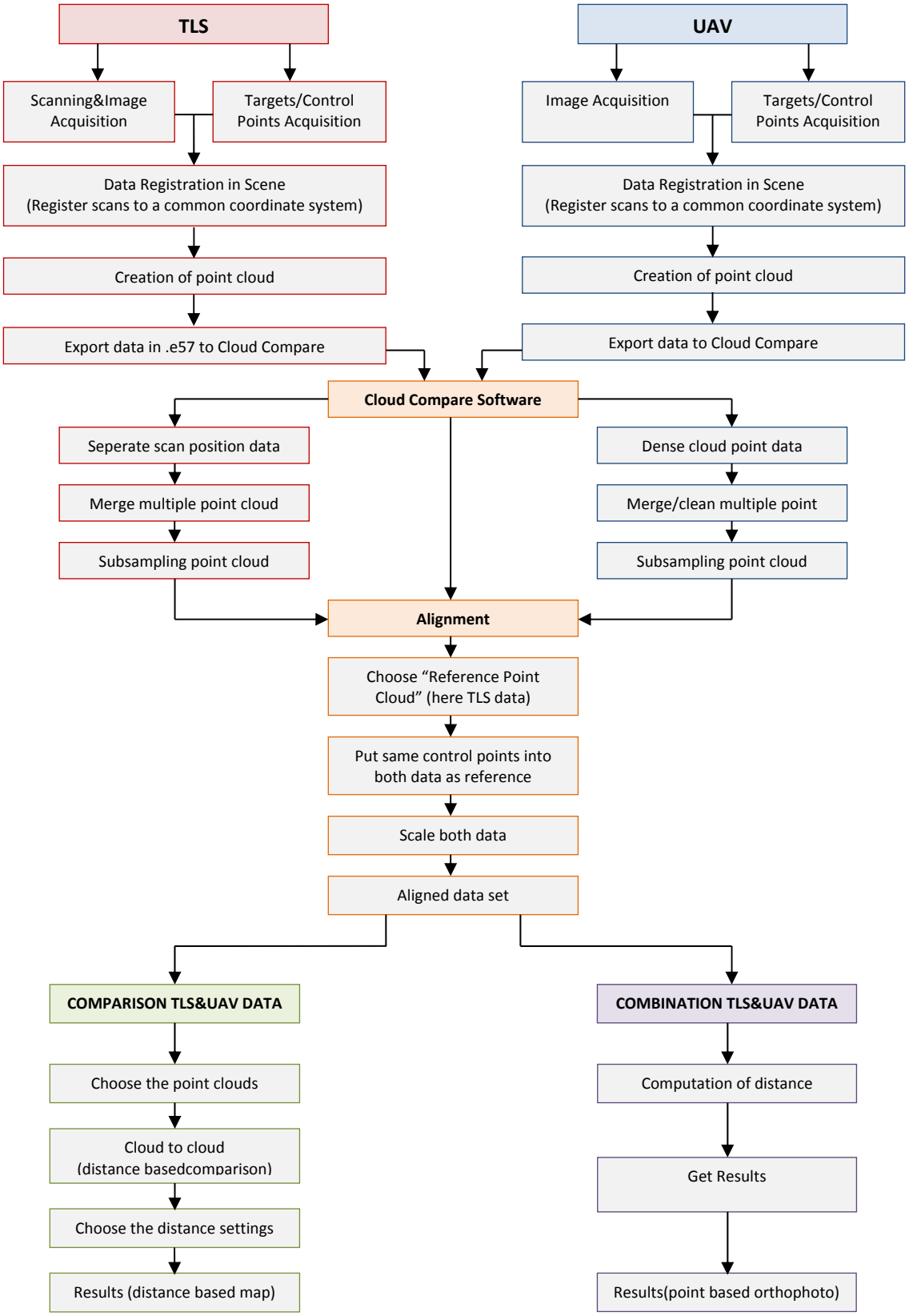

Figure 5.4.24: Detailed workflow of for combination and comparison of TLS and UAV point cloud dat

5.4.4.2.Data Processing

In this study, for aerial image processing PhotoScan 1.1.5 was used. Image alignment was carried out with 373 cameras. The coordinate system of the project was selected WGS 84 (EPSG::4326) (Figure 5.4.25-26).

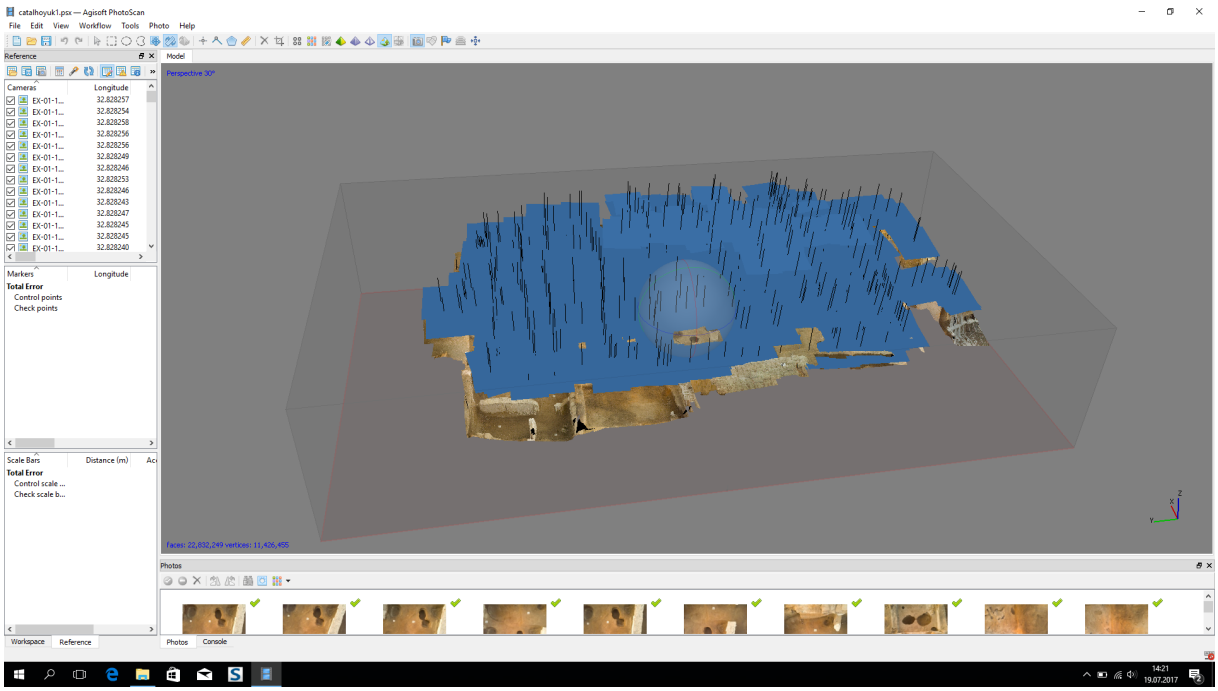

Figure 5.4.25: Camera positions in Agisoft PhotoScan

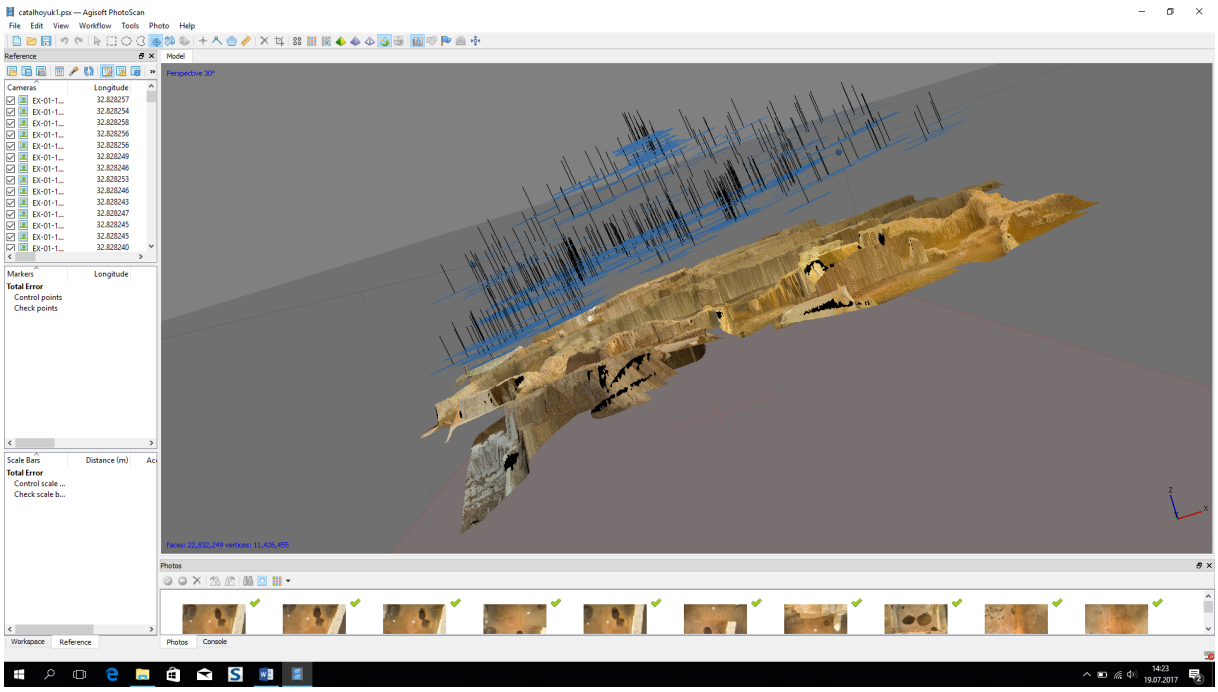

Figure 5.4.26: Camera positions in Agisoft PhotoScan

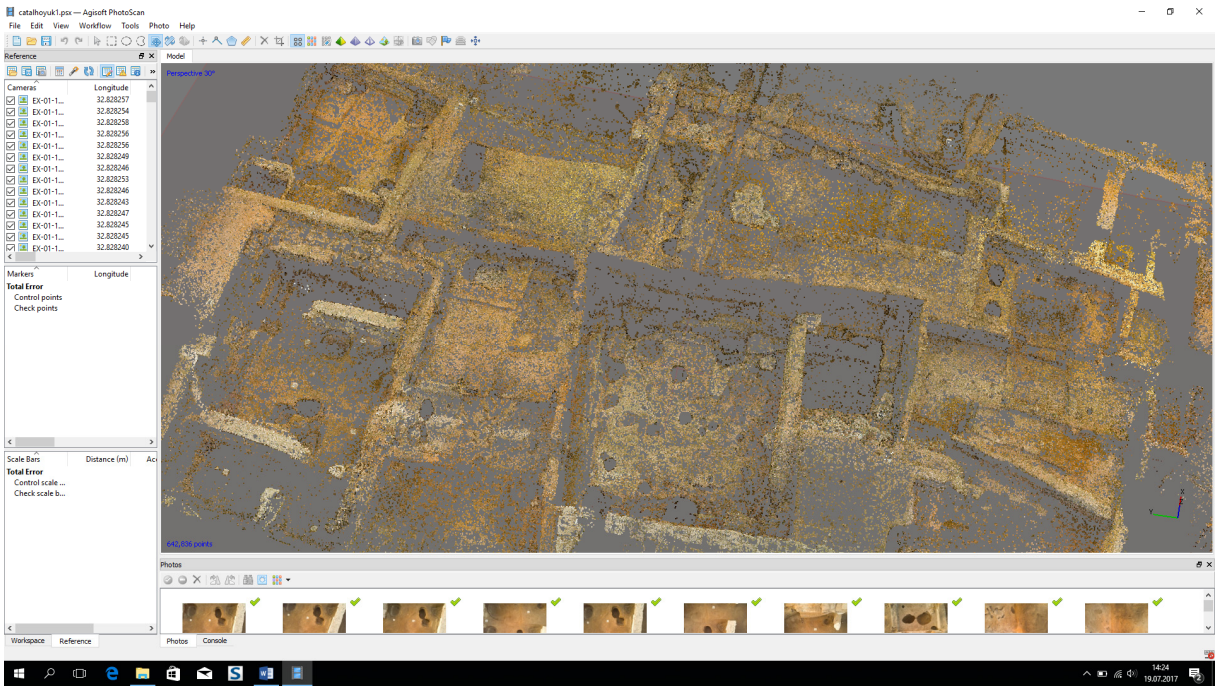

Figure 5.4.27: Point cloud model with 642,836 tie points in Agisoft PhotoScan

Then dense point cloud model was created in high quality parameter. After the process dense point cloud model had 345,091,208 points. (Figure5.4.28)

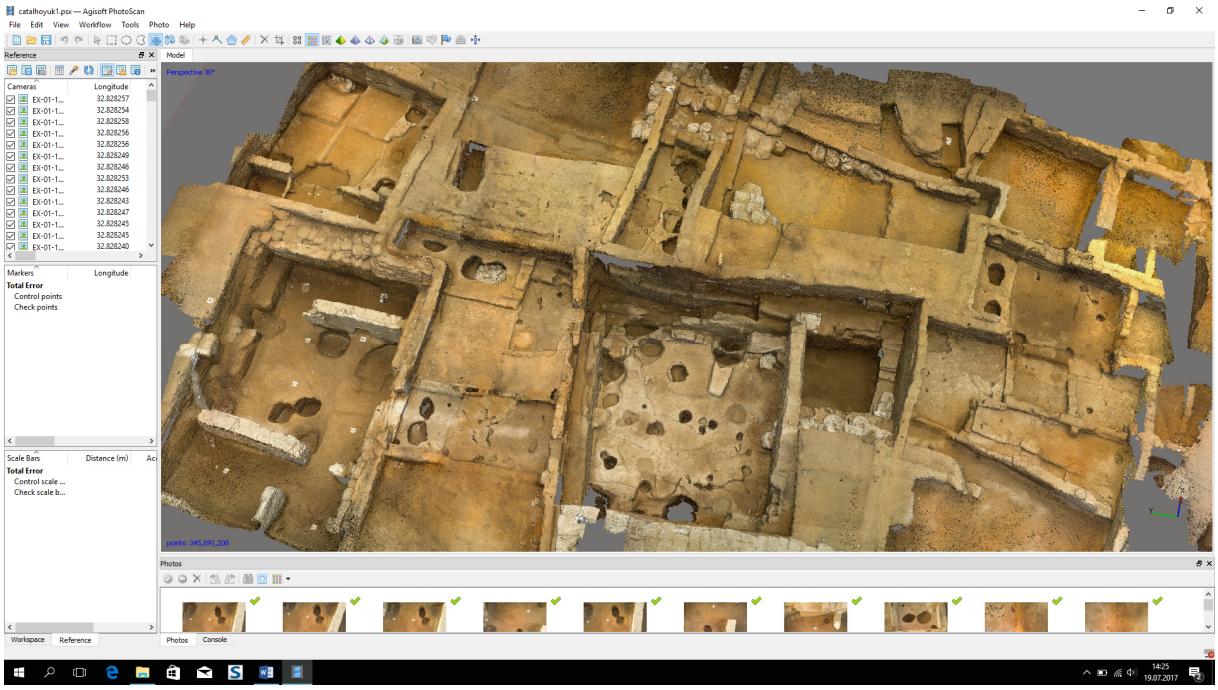

Figure 5.4.28: Dense Point cloud model with 345,091,208 points in Agisoft PhotoScan

After tehe dense point cloud model, mesh model was processed and at the end it was acquired 22,832,249 faces and 11,426,455 vertices in mesh model (Figure 5.4.29).

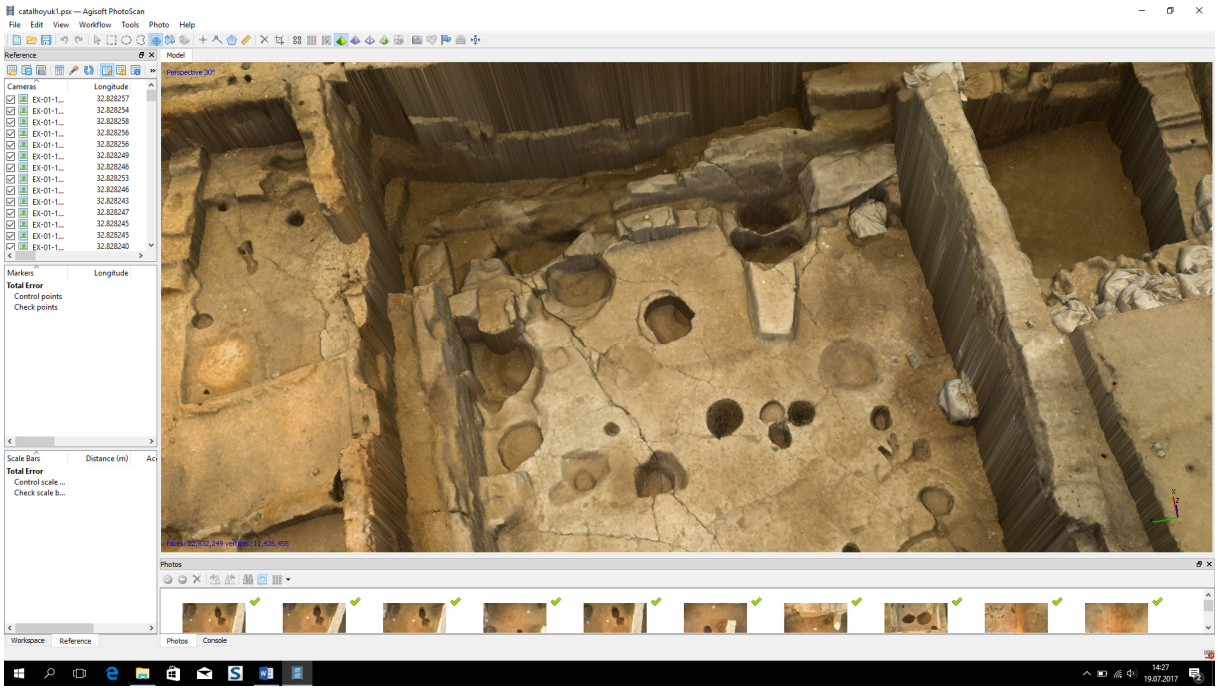

Figure 5.4.29: Detail of shaded model in Agisoft PhotoScan

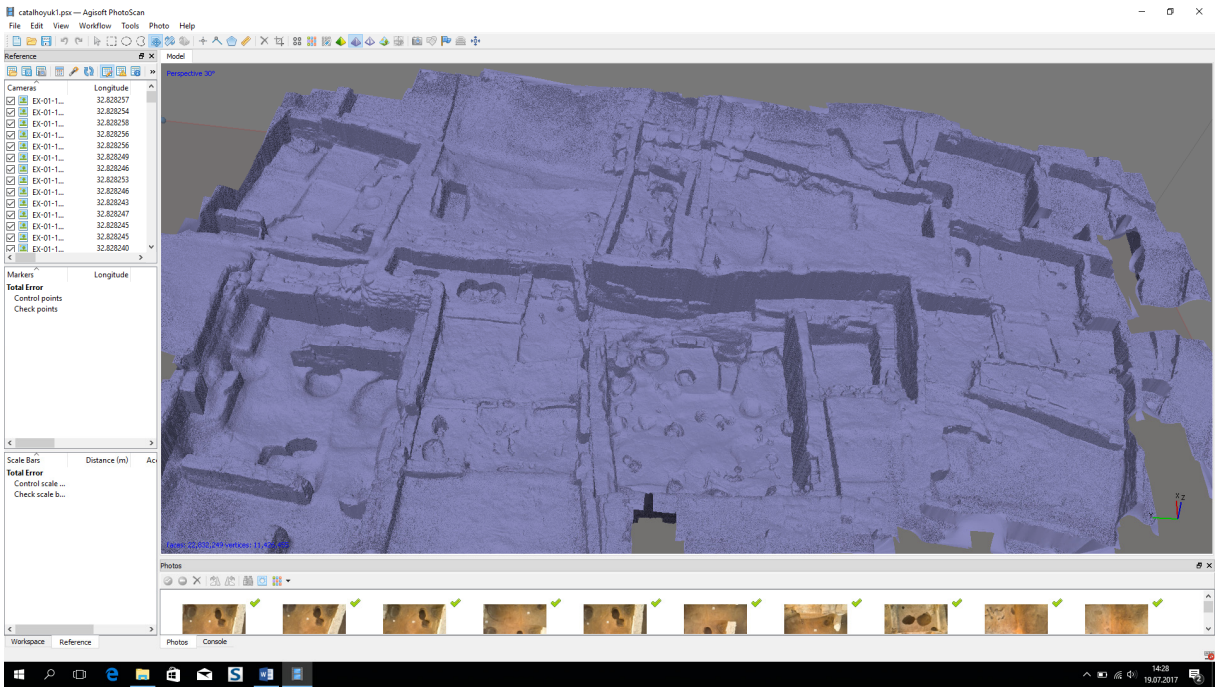

Figure 5.4.30: Solid model with 22,832,249 faces and 11,426,455 vertices in Agisoft PhotoScan

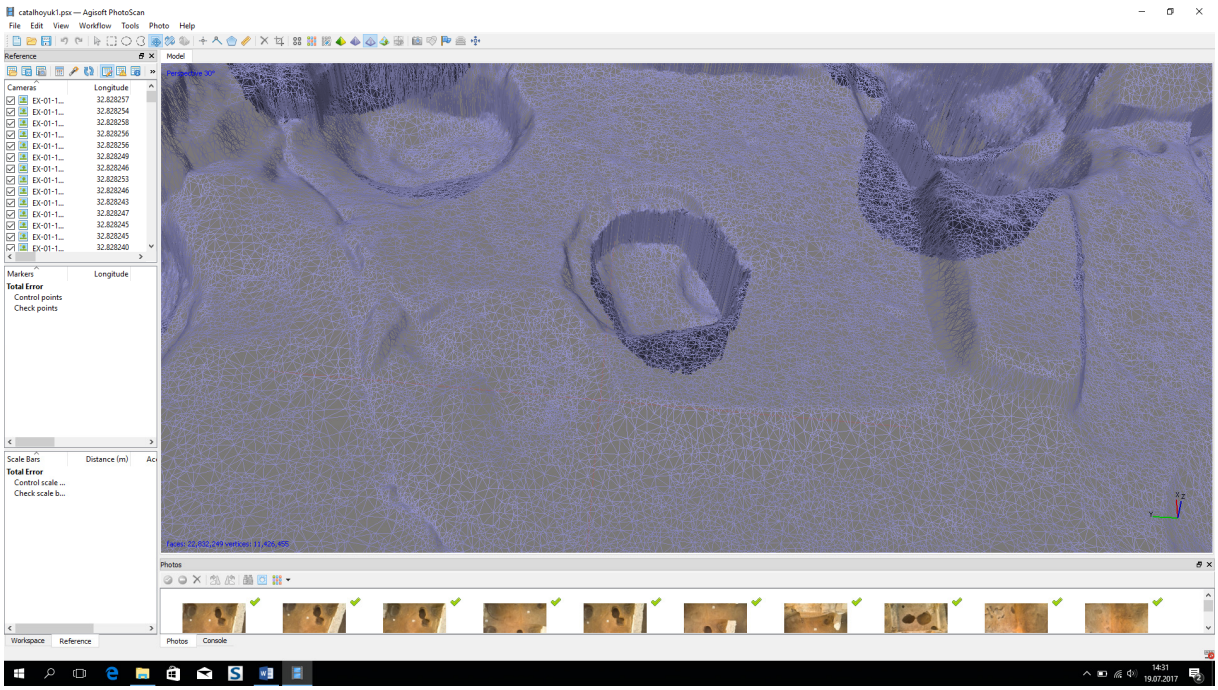

Figure 5.4.31: Detail of frame model in Agisoft PhotoScan

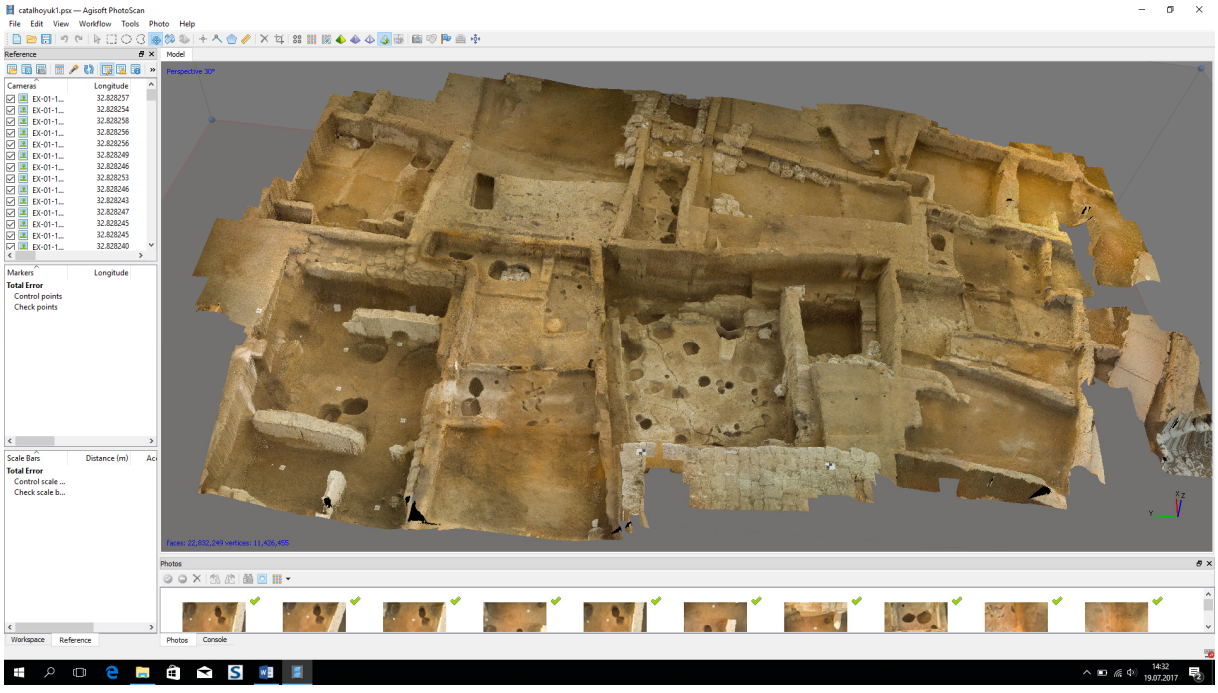

Figure 5.4.32: Textured model in Agisoft PhotoScan

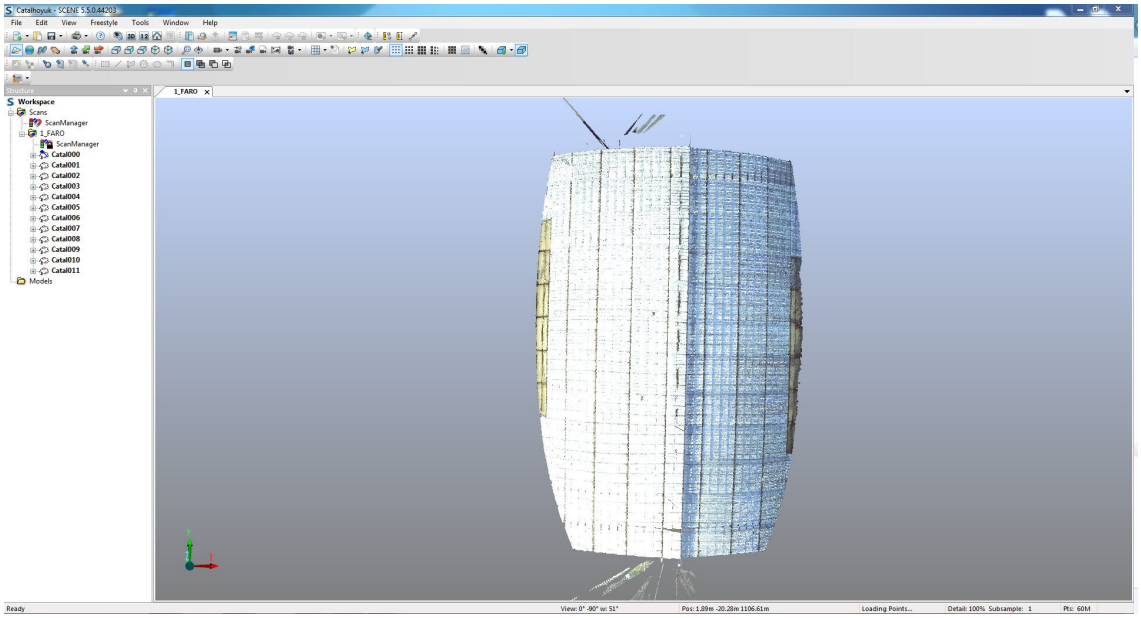

Figure 5.4.33: TLS data point cloud after the alignment in Scene software

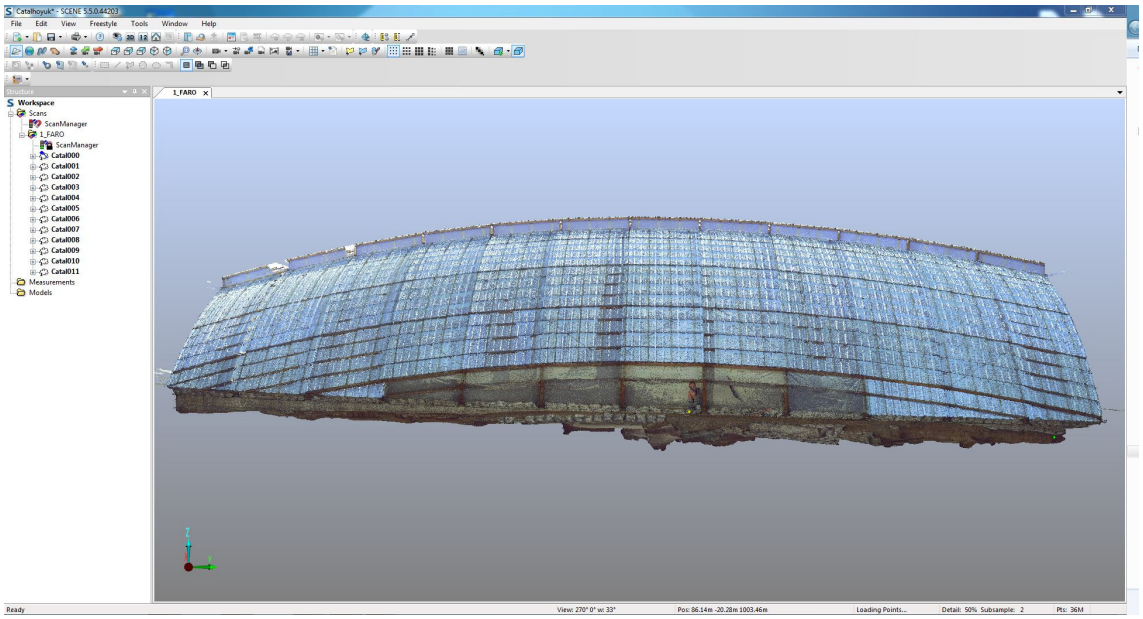

Figure 5.4.34: TLS data point cloud after the alignment in Scene software

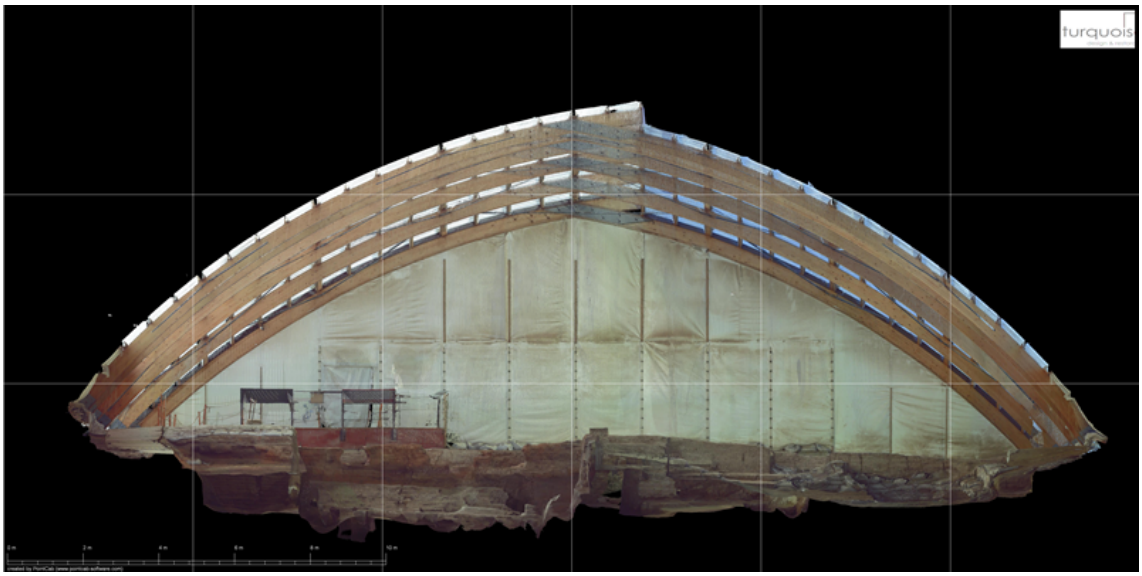

Figure 5.4.35: Cross section or archaeological area from TLS data point cloud data in Scene software

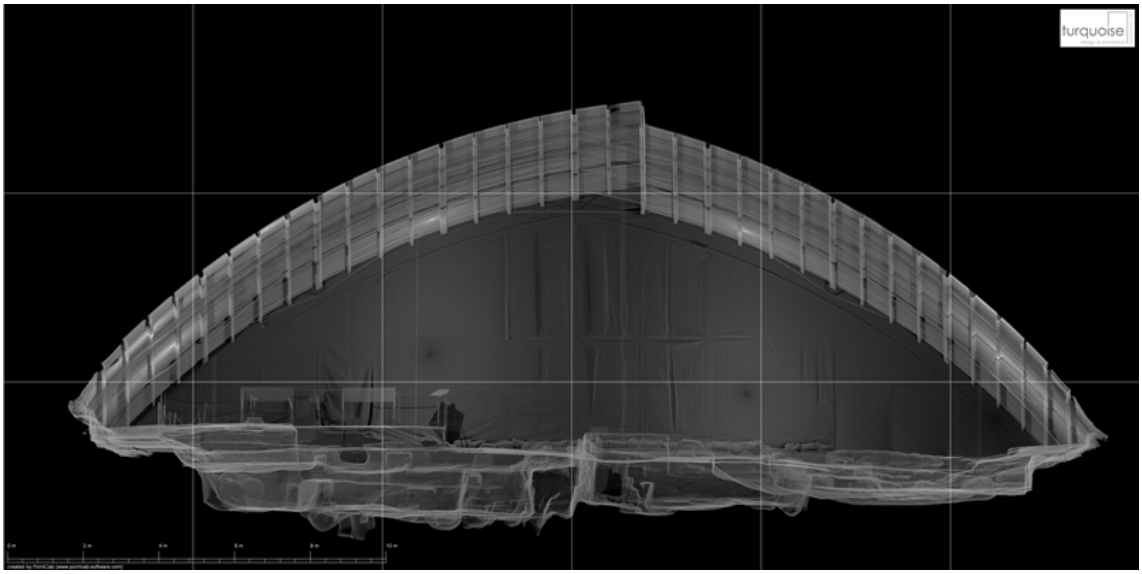

Figure 5.4.36: Cross section or archaeological area from TLS data point cloud data in Scene software

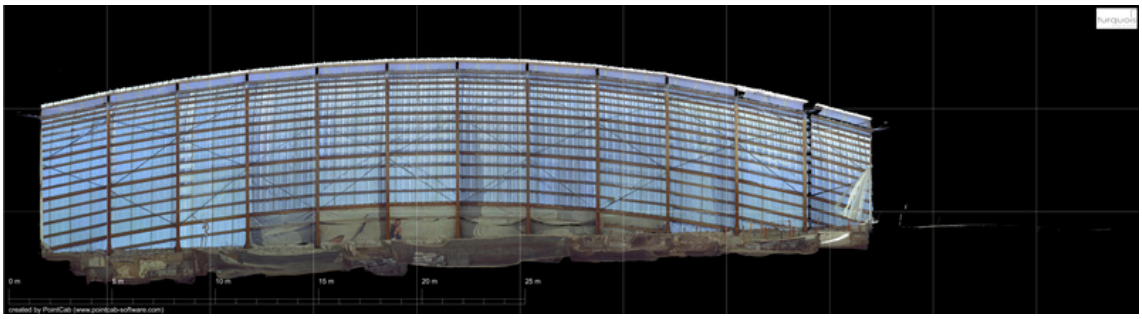

Figure 5.4.37: Longitudinal section or archaeological area from TLS data point cloud data in Scene software

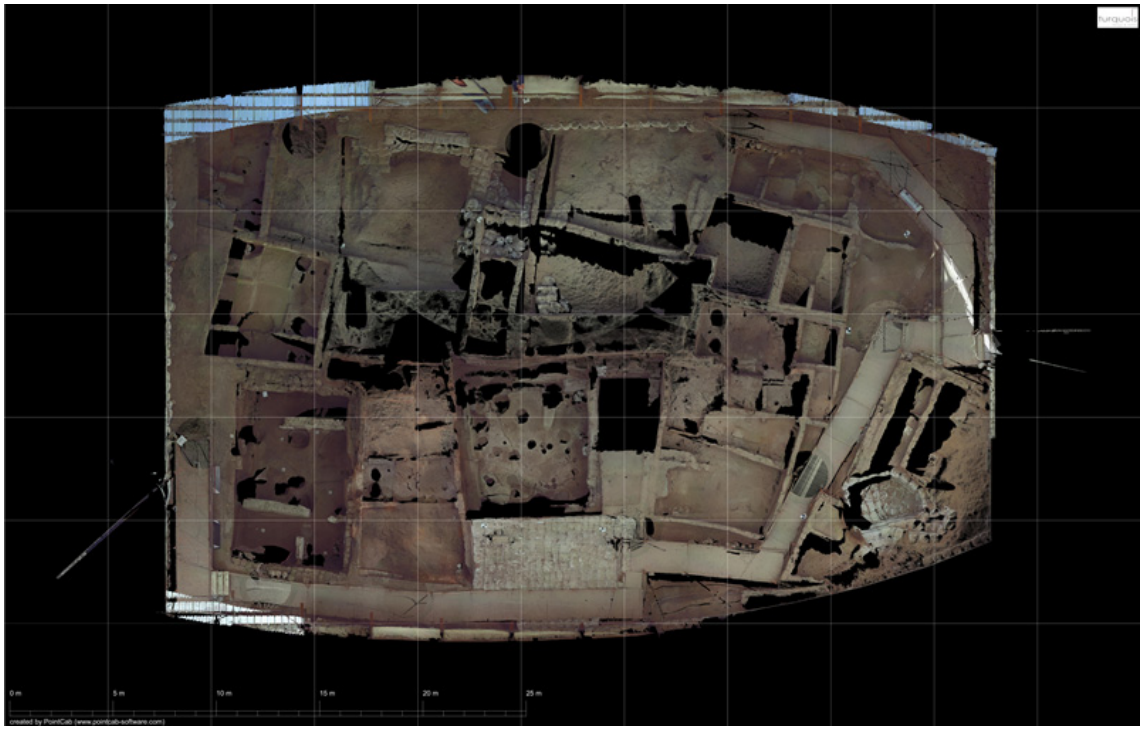

Figure 5.4.38: Plan of archaeological area without shelter from TLS data point cloud data in Scene software

5.4.4.3. Results and discussion

Aerial Data Results

In this case study, there were mainly two aims one of which was to compare point cloud data of TLS and UAV and the other one was to combine both point cloud data in order to get a complete documentation of the archaeological area. For these aims two data acquitison techniques were used. The UAV data results were satisfied while there were some missing parts in TLS data. Since it was not possible to make survey inside and on the archaeological area, TLS was not capable to get data from all parts of the area. However, since the UAV data was good, it helped to fill the balnks of TLS data. It was main aim to provide a new methodology for archaeological area documentation. Studies have already shown that only one method is not sufficient for complex area documentation.

The total covered area was 633 m² from 4,81 m height. The ground resolution was 0.813 mm/px with reprojection error 1.12 px while RMSE error was 0.18372 px. Since the flight could be completed in manual mode, the camera locations error was higher: 0.609059 m in X, 1.92749 m in Y, 4.18157 m in Z and totally 4.64453m.

Table 5.4.3: Project processing parameters in Photoscan

Project parameters	
Flight Height	4,81 m
Ground resolution	0.813 mm/px
Coverage area	633 m²
Number of strips	-
Number of images	373
Number of GCP	-
Aligned cameras	373
Coordinate System	WGS 84 (EPSG::4326)
Dense point cloud points	345,091,208
Tie points	642,836
Projections	2,294,575
Reprojection error	1.12 px
RMS reprojection error	0.18372 (1.1176 px)
Max reprojection error	0.557164 (59.0106 px)
Mean key point size	4.9406 px
Faces	23,006080
Vertices	11,426,455
DEM size	17,302x28,962
Orthomosaic size	26,962x45,059

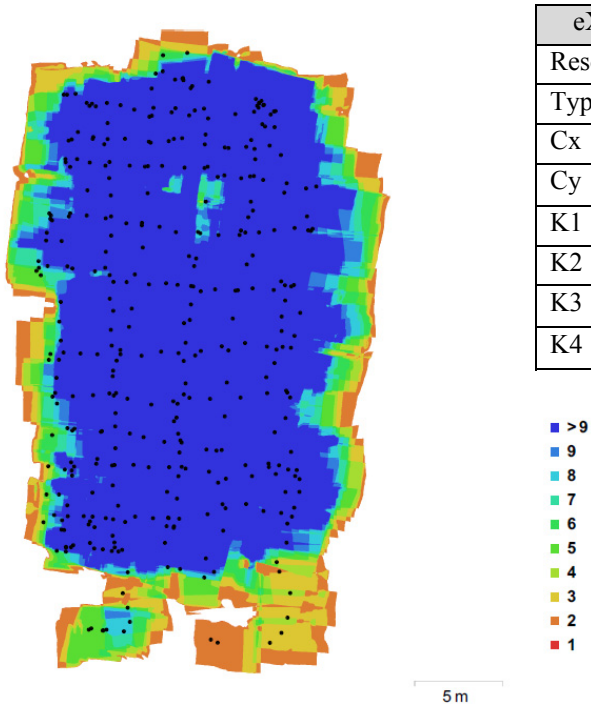

eXom (8.02 mm) Camera Calibration Parameters			
Resolution	7152x5368	F	5663.29
Type	Frame	B1	-0.629973
Cx	16.2675	B2	-0.274737
Cy	88.6356	P1	0.000500948
K1	0.230724	P2	-0.00057726
K2	-0.519592	P3	0
K3	0.0816669	P4	0
K4	0.458725		

Figure 5.4.39: Camera locations and image overlap (manual flight) (left)

Camera calibration parameters (right

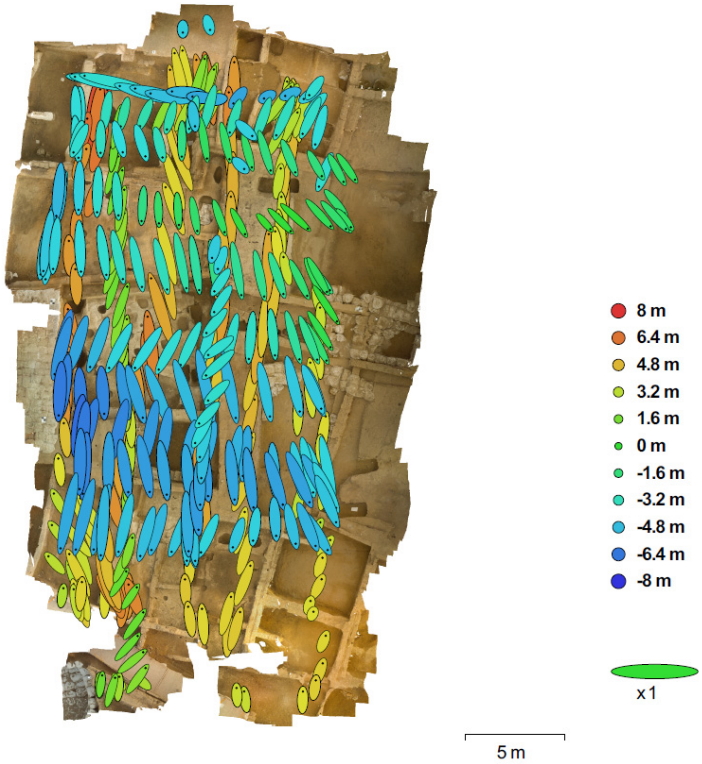

Figure 5.4.41: Camera locations and error estimates. Z erros is represented by ellipse color. X,Y errors are repsresented by ellipse shape. Estimated camera locations are marked wth a black dot.

Table 5.4.4: Average camera location errors

Average Camera Location Error				
X error (m)	**Y error (m)**	**Z error (m)**	**XY error (m)**	**Total error (m)**
0.609059	1.92749	4.18157	2.02142	4.64453

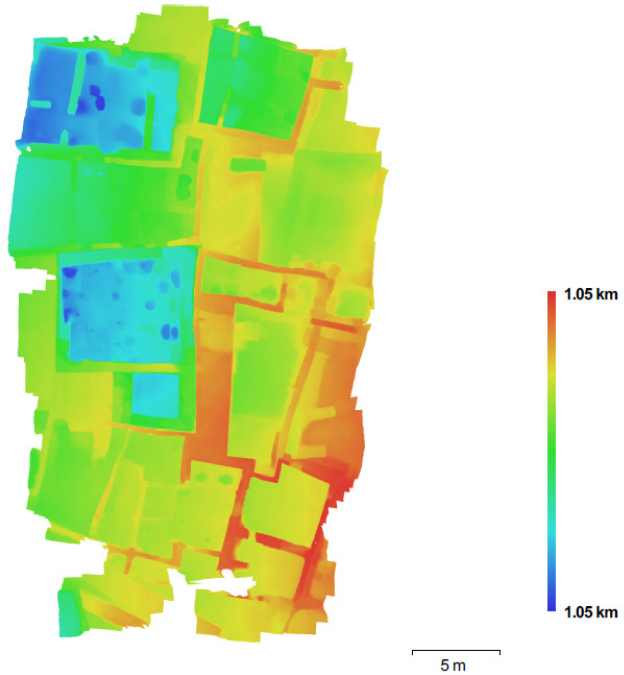

Figure 5.4.40: Reconstructed digital elevation model with 1.63 mm/pix and 37.9 points/cm²

Figure 5.4.41: Orthophoto of archaeological area in Photoscan

Comparison and combination of TLS and UAV point cloud data

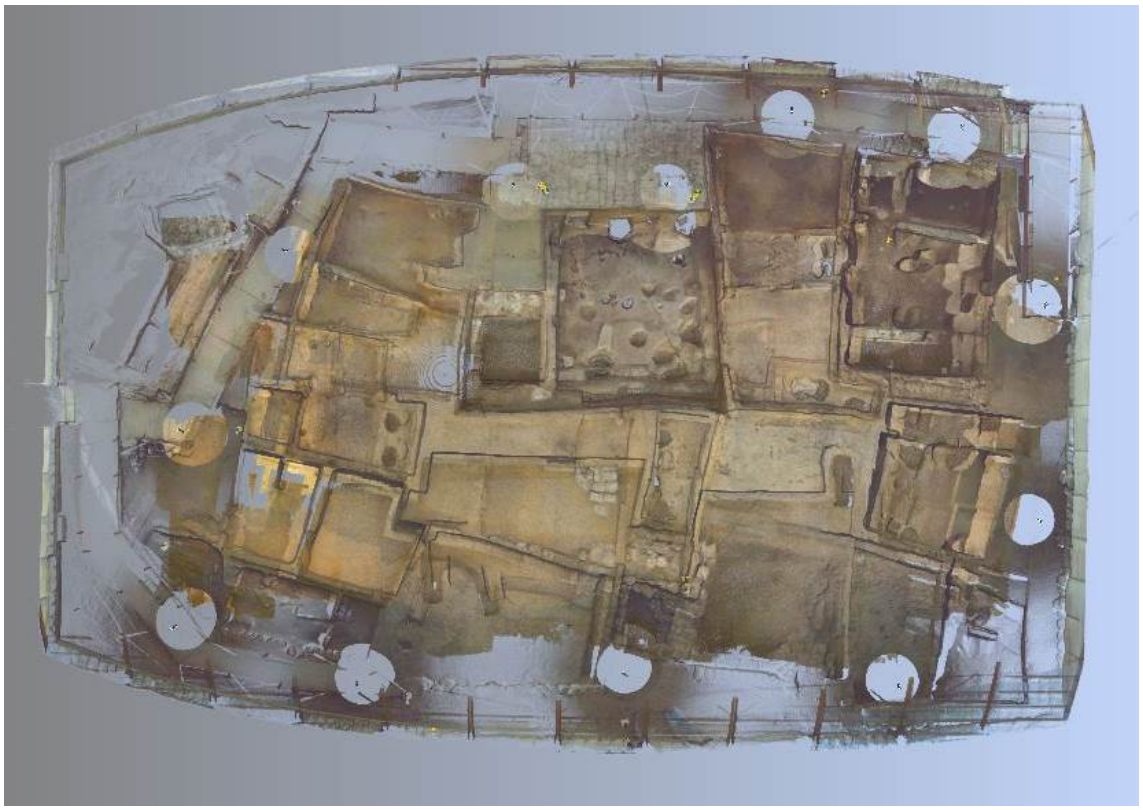

Figure 5.4.42: Registered TLS and UAV point cloud data in Cloud Compare

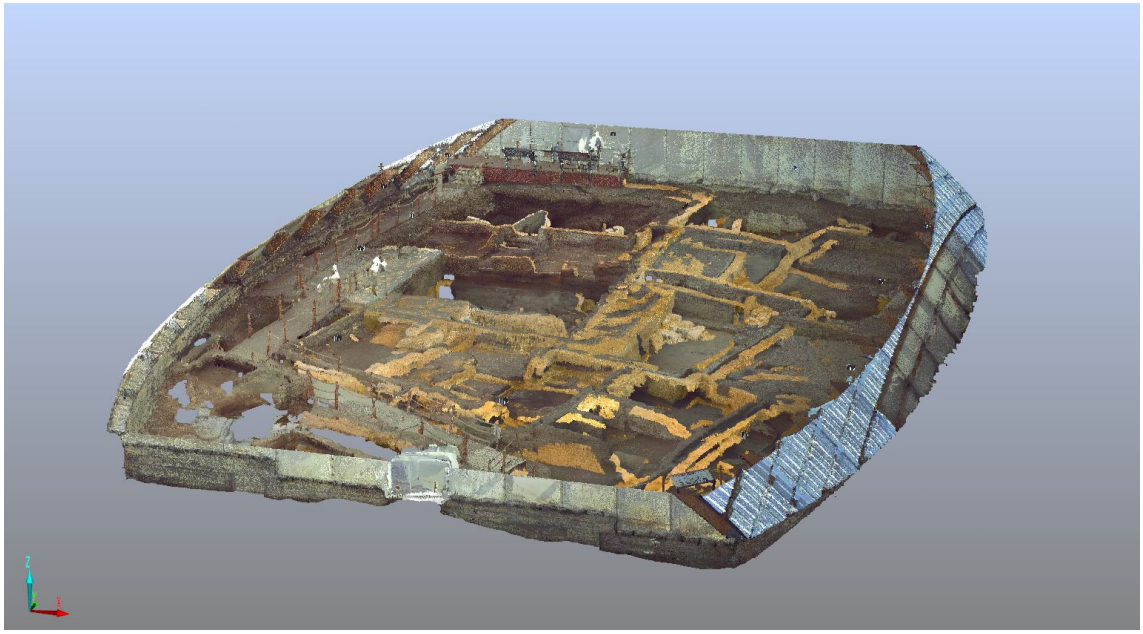

Figure 5.4.43: Registered TLS and UAV point cloud data in Cloud Compare

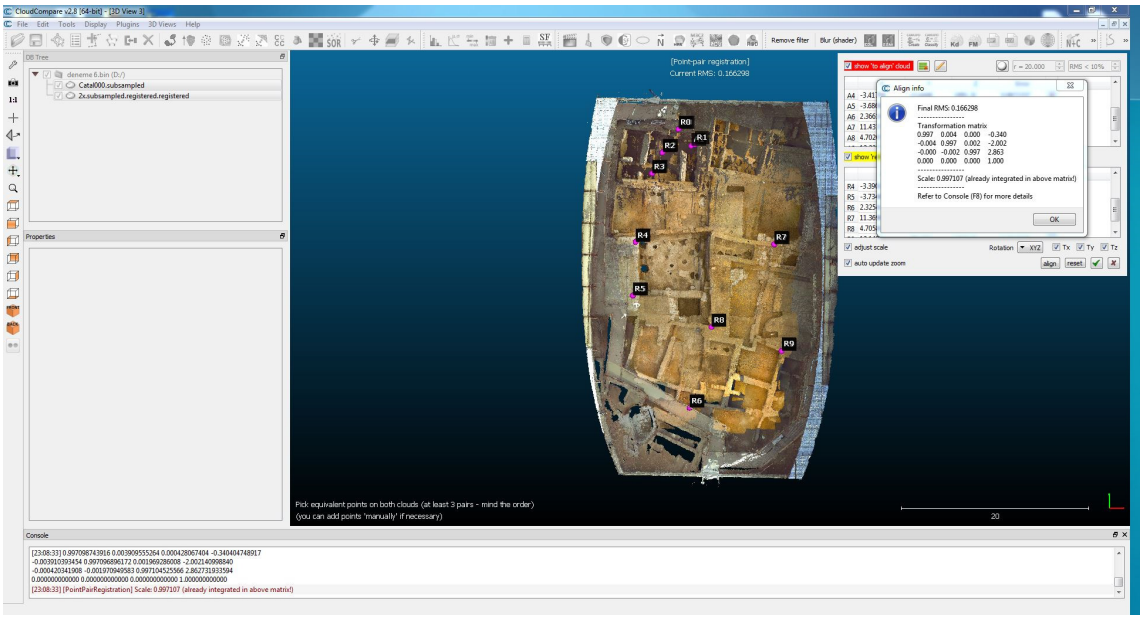

Figure 5.4.44: TLS and UAV point cloud data and reference points for registration of two data in Cloud Compare Software

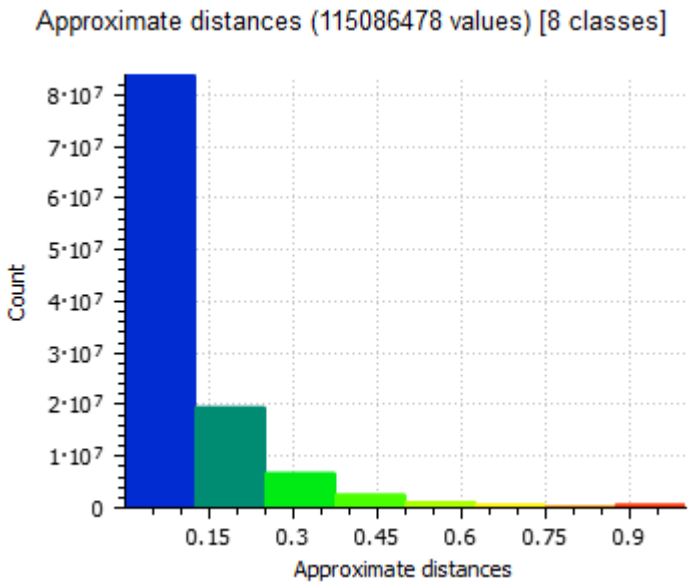

Figure 5.4.45: TLS and UAV point cloud data histogram

In the archaeological surveyed area, totally 8 classes of different distance has been calculated between two point cloud data. The point clouds of TLS and UAV overlapped with till 9 cm difference. In all sides of the area, UAV point cloud data is more missing than UAV data, while, in the middle TLS data is more missing. Since it was forbiiden to put TLS into the archaeological area, we were not allowed to go to and get data from the center of the area. While, in the center of the surveyed area UAV data is more stronger and has much more point cloud data. So in lower parts of the area where TLS data is missing, overlapping difference becomes till 9 cm. For the other parts, mainy 3-4 cm difference is observed (figure 5.4.46-47).

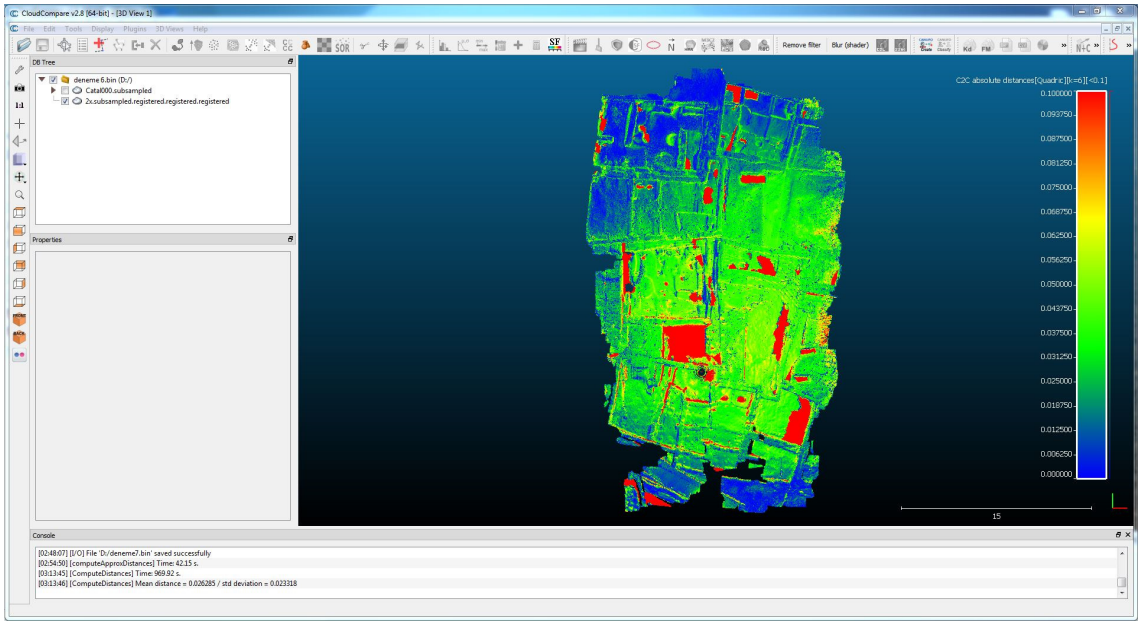

Figure 5.4.46: TLS and UAV point cloud data registration

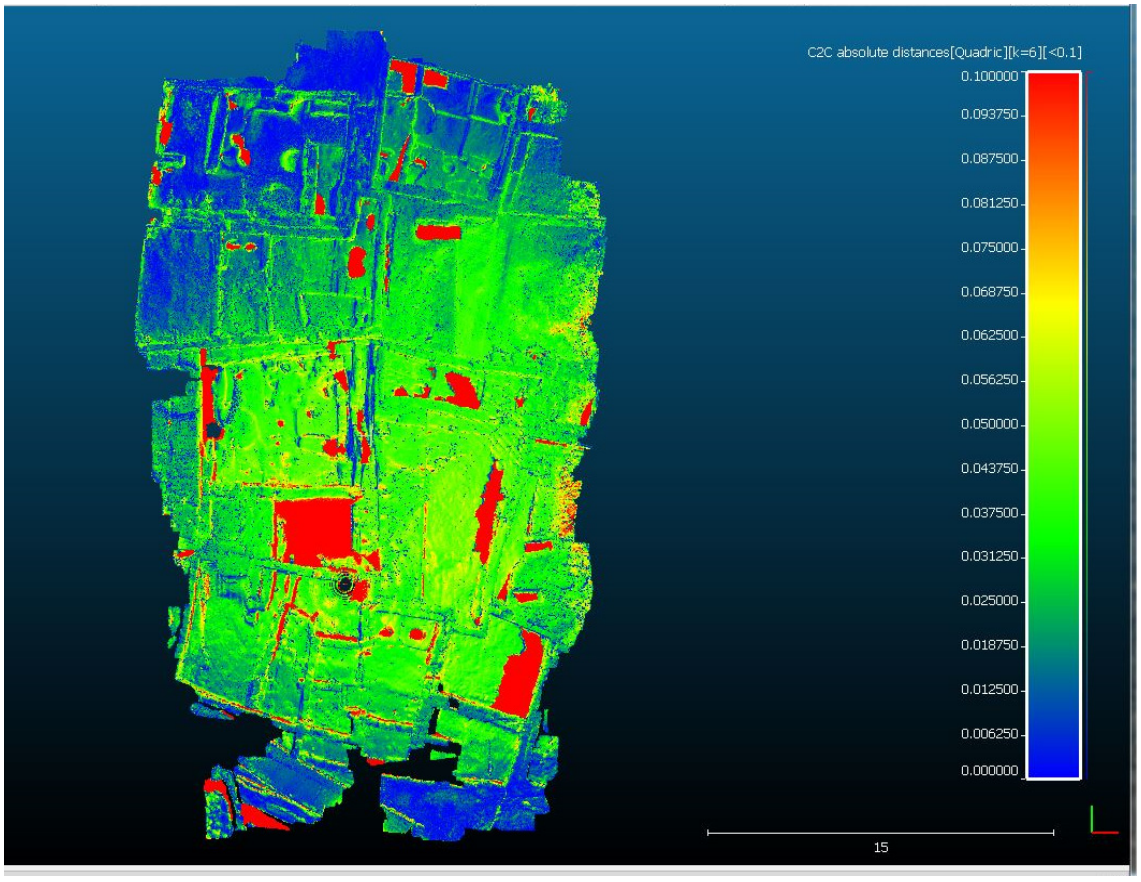

Figure 5.4.47: TLS and UAV point cloud data registration

QAerial thermal data results

On Eastern Mound North Peak Archaeological area of Çatalhöyük, 6 surveys were conducted, collecting five thermal and one color photographic datasets. Each flight took approximately 10 minutes from take off to land. The thermal flights were started at 7:50 am and continued with 10:38 am, 13:29 am, 17:25 am and 18:51 pm. The sunrise was 7:15 am and sunset was 6:48 pm. The flight height was average 4.81 m however because of the changing height of the shelter and manual flight it sometimes became lower. It was strictly forbideen to walk on the area so an unexcavated area, entrance was chosen as ground control station. On the days of survey, the temperature variability was 20□. The temperature difference between outside and inside was 6.3℃ in the morning and after the beginning of late afternoon, temperature difference between outside and inside started to increase and became 12.5℃ in the evening. The difference between soil temperature and indoor temperature was very less in late morning 6.1℃ in the morning the difference became 9.8℃ in the afternoon and 12.7℃ in the evening. Moisture of the area was %43 in the morning and increased in the late morning till %70, while in the evening it was only %20. Mositure of the soil was always in low level.

In the first 7:30 am flight, it was get 130 thermal images, while 155 from 10:38 am flight, 171 from 1:29 pm flight, 139 from 5:25 pm flight and 149 from 7:00 pm. Alignment of thermal images and the creation of orthophoto of thermal images was not possible since it can't get raw thermal images without overlapping.

The best images for visibility were 7:30 am and 7:00 pm flights, while in 10:38am and 1:29 pm, archaeological subsoil features are less apperant. In 7:00 pm flights, it can be easily seen the features retaining and relieving the heat. Especially on the floor of the rooms strong thermal signals can be seen in the evening flights.

Table 5.4.5: Çatalhöyük Eastern Mound North Peak Thermal Flight Details

Çatalhöyük Thermal flight details (06.03.2016)						
Parameters	EM-NP	EM-NP	EM-NP	HILL	EM-NP	EM-NP
Flight height	4.81m	4.81m	4.81m	63m	4.81	4.81
Time	7:30am	10:38am	1:29pm	4:21pm	5:25pm	7:00pm
℃ (indoor)	8.6℃	11.6℃	25.8℃	23.4℃	22.4℃	18.7℃
℃ (outdoor)	2.3℃	9.9℃	17.5℃	12.8℃	14.3℃	8.2℃
℃ (soil)	0.5℃	10℃	16℃	17℃	18℃	16℃
moisture (inside)	%43	%70	%25	%20	%20	%20
moisture (outside)	%67	%66	%20	%48	%39	%55
moisture (soil)	low	low	low	low	low	low
Number of images	129	155	171	40	139	149

ÇATALHÖYÜK THERMAL DATA (MORNING AND EVENING) RELATED TO AREAS -1

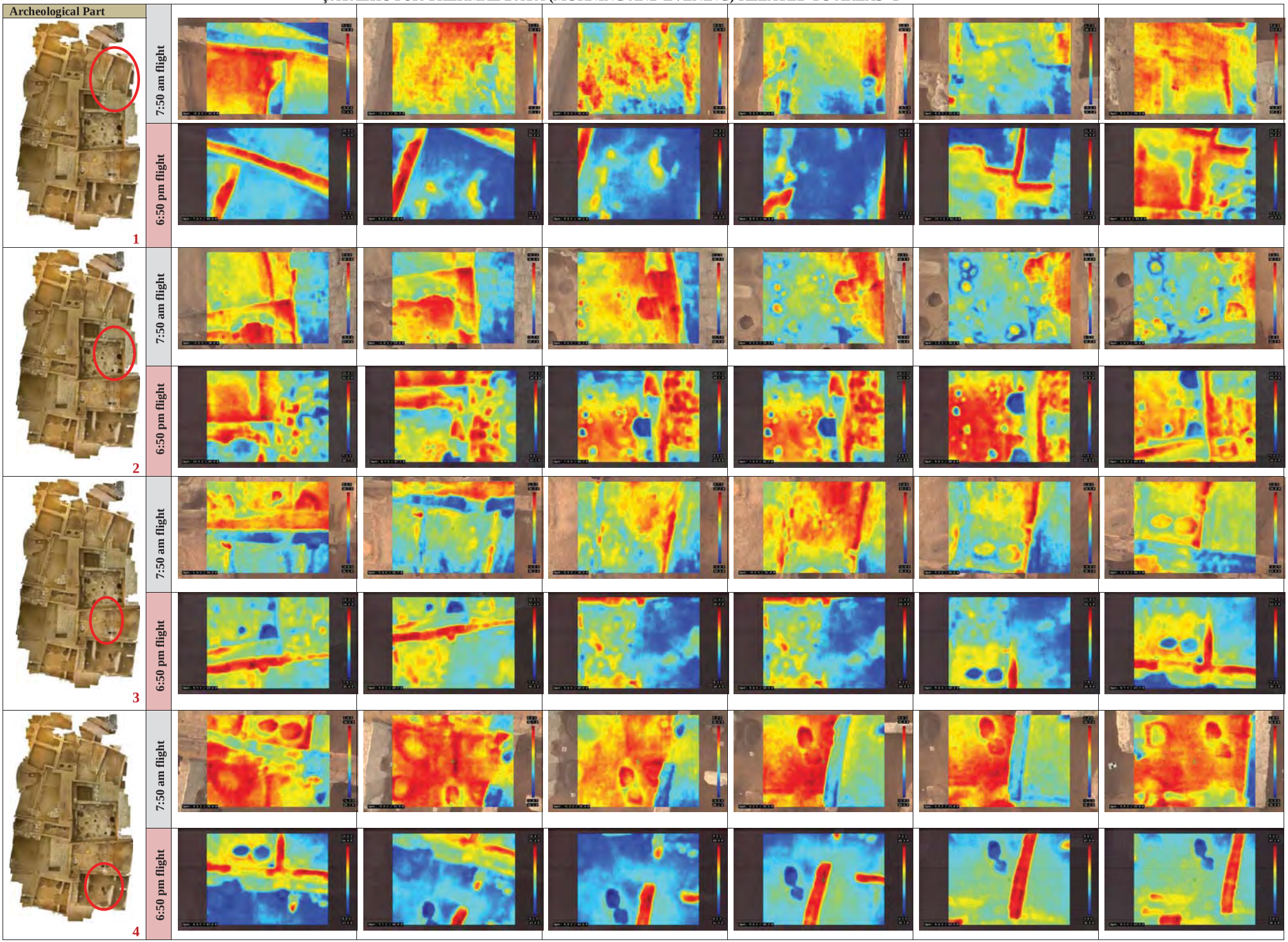

ÇATALHÖYÜK THERMAL DATA (MORNING AND EVENING) RELATED TO AREAS -2
Archeological Part
6:50 pm flight
7:50 am flight
6:50 pm flight
7:50 am flight
6:50 pm flight
7:50 am flight
6:50 pm flight
7:50 am flight
5
9
7
8

ÇATALHÖYÜK THERMAL DATA (MORNING AND EVENING) RELATED TO AREAS -3

ÇATALHÖYÜK THERMAL DATA (MORNING AND EVENING) RELATED TO AREAS -4
Archeological Part
7:50 am Flight
6:50 pm Flight
7:50 am Flight
6:50 pm Flight
7:50 am Flight
6:50 pm Flight
7:50 am Flight
6:50 pm Flight
13
14
15
16

ÇATALHÖYÜK THERMAL DATA (MORNING AND EVENING) RELATED TO AREAS -5

Archeological Part							
 17	7:50 am flight						
	6:50 pm flight						
 18	6:50 pm flight						
 19	6:50 pm flight						
 20	6:50 pm flight						
	6:50 pm flight						
 21	6:50 pm flight						

Çatalhöyük houses are significant with their material, social and ritual. Houses were roughly rectangle, built together very closely, without streets. We know that people were moving around on roofs and accessing their homes down a wooden ladder via an opening in the ceiling. All the houses in Çatalhöyük were in different shape and size but follows a general layout. It has a central room with an owen below the stairs. Raised platforms within the rooms used for sleeping or other domestic activities. Beneath these platforms, inhabitants buried their dead. Side rooms were accessed off the central room providing essential storage areas.

The houses were made of mud-brick. There were the holes in the ceilings. It also appears that in later periods they had even built communal ovens on the rooftops. The renewal of the houses was succeeded by partial demolition and rebuilding on the basis of the debris. This resulted in the approximately sixty feet high mound which consists of almost eighteen levels of settlement.

Even though several flights were done on excavated area, subsurface remains are more visible in 7:50 am and 6:50 pm flight. Field investigations and results of excavation show that the houses are made of mud-brick which excavated ones are visible today on the area. The other features generally appear on the early morning thermal imagery as with lower temperature while higher temperature in the evening. Since mud-brick has higher thermal conductivity than the soil, it retain heat longer. In the morning images, it can be clearly seen that the holes are hot in the morning means keep the heat inside while they seem very cold in the evening flights. They get hot more quickly in the sun and cool just as fast as night like soil. With the help of this property, estimating the potential strength of anomalies in different context becomes easier (Cool, 2015).When the content of adobe is considered, it consist of stones, sand, silt, clay and organic humus. This thermal behavior may related with contents of the material inside and their rates. Even the walls are made of adobe, while they are cold early in the morning, they seem hot in the evening. Contrarily, the floor is hot in the morning however in the evening it becomes cold quickly which helps to recognize the anomalies. These anomalies show similar behavior like walls but presumably depending on the content and depth of the material, they seem hot but not as hot as walls. It should also be considered that inhabitants buried their dead which means it is possible to have features like bones. Thermal conductivity of the bone is between 0.41-0.63 and more than soil (0.3) and mud-brick/adobe has high thermal conductivity almost between 0.6-1.2 in contrast to wood (0.09-0.14). (page,198).

Adobes are dried mud or unburned bricks. Smith (1982) classified adobe bricks into six types as: traditional, semi-stabilized, stabilized, terron(cut sod), pressed adobe and burnt adobe. Each of them has different rates of materials and made somewhat differently. The net results of the thermal properties of adobe bricks is the preservation of cooler night temperatures into the next day and of warmer afternoon temperatures into the following evening (Austin, 1984). A material with high conductivity and low volumetric heat, will have high diffusivity, means that heat travels quickly. However the material with low conductivity and high volumetric heat will retain more heat.

Significantly, in some thermal images, some subsurface architectural remains were distinguished. One of the examples comes from the 1st area. On the floor of the

area estimated to be a room, some subsoil features are visible especially in the evening flight (2nd and 3rd image). Additionally, on the 5th image of the first area, it can be seen hot areas which behaves like walls but not as hot as walls. In the second part, it is easily visible thermal behavior of the holes. Similarly in the third part which is a raised platform, some features can be traced more hot than the floor, cooler than the walls. Similarly on the fourth part, 5th and 6th images, some areas, just behind the holes, can readily be seen as high-value as high value areas. Other example, in 9th part of the area, in the 1st image, while the floor is almost in homogeneous heat, in the evening, some parts cools down faster than other sides of the area. Strong anomalies may refer to materials close to surface. Likewise on the 4th and 5th images, anomalies can be seen around the cold hole. Even it's not visible in normal image, some traces are found in thirteen part, 5th and 6th images, behind the holes. This part seems completely and homogeneously hot early in the morning, however it doesn't get cool in the same way and some parts remain hot. This parts are not visible on normal image but easily can be traced on thermal images. Identically, in the fourteenth part, in the 4th and 6th image, floor of the small room is cold in the morning while some part of it becomes heat faster than the other parts. In the same way, fifteenth part in 4th and 5th photos, similar traces can be seen in the evening flight. With the guide of these data, in the evening flights of 18th, 19th and 20th parts of the archaeological area, some anomalies can be recognized mostly in 19th and 20th part. As unexcavated small part of the area, in the evening images of 21st part, thermal data provide a clear indication of some materials with different thermal conductivity or in different distance from the surface. It can be observed that these high value features heat up differently from the wall and these features save their contours in consecutive images as in 3rd, 4th and 5th images even though these signals are not visible in normal images.

Previous studies have already proved that aerial thermography can be a powerful tool to reveal subsurface remains. This method also provides valuable approach for archaeological investigations and rapid data collection for archaeological documentation. The method for UAV-based thermography outlined in this case study offers a methodology for data acquisition and data processing of thermal images in a short time over archaeological areas. The technique could be a suitable tool for documentation of the areas where to walk or to work on it is strictly forbidden like Çatalhöyük. It could also supply a valuable complement for improved documentation of archaeological features. However it would likely be difficult to get thermal data where the features are covered by dense vegetation.

The aerial thermal imaging conducted here presented valuable insights regarding to a part of excavated area of Çatalhöyük. Aerial thermography with UAV showed its potentials for methodology, data collection and processing over small and indoor areas. Since the flights were conducted in very low height, the resolution was not a problem. This data may help to reveal many features that are not visible on the ground surface of the area. However additional investigations including seasonal flights, inside and outside, between two shelters. Future fieldwork can also aim to solve UAV indoor application problems in order to prevent possible damages such as crashing as we experienced. For this detailed study can be improved to solve GPS connection and

signal to have a georeferenced orthophoto. Future studies also could be to enhance the visibility of archaeological subsurface features by diurnal or seasonal surveys and to help to determine their depths. Also the improvements in UAV and thermal cameras/sensors may facilitate data acquisition of thermal images if the reliability, cost and availability factors are considered which may make aerial thermography as a standard stage in archaeological documentation process.

5.4.5. Eastern Mound North Peak Archaeological Area –hill

There were mainly two aims of this project. The first one was to compare two software while the second one was to combine color and thermal data.

5.4.5.1.Field Work

The main objective of this study is to compare two different software packages for a single application, regarding their workflow, visual appeal, similarity, quality and results for the modelling of hill on archaeological area Çatalhöyük. PhotoScan Pro1.2.6. and Pix4Dmapper Pro (3.2.23). These both software packages are available for windows and MAC. And for image acquisition e-Bee UAV RTK from Sensefly was used with eXom 8.02 mm color camera was used (Figure 5.4.48). TUREF / TM33 (EPSG::5255) was choosen as coordinate system.

The acquisition project of the images was planned in eMotion software. It was acquired 72 images from 63 m flight height, in 7 horizontal strips, with %80 sidelap and %65 overlap with 7 GCPs (Figure 5.4.49). According to the sensor resolution and the acquisition distance ground resolution was 1.03 cm/px. The GCPs were measured with GPS RTK.

Figure 5.4.48: Field work and UAV e-Bee RTK

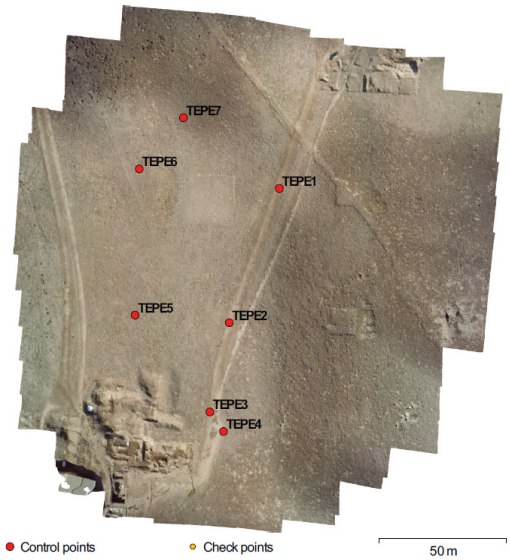

Figure 5.4.49: GCPs location in PhotoScan

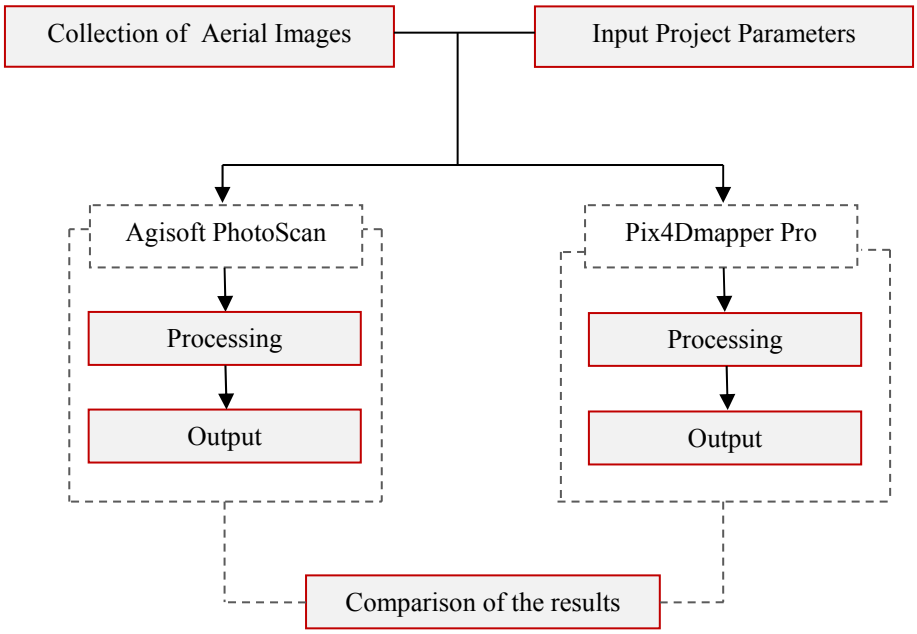

Figure 5.4.50: Basic workflow of methodology

5.4.5.2. Data Processing

In order to process the data, as mentioned in the previous section, PhotoScan Pro1.2.6. and Pix4Dmapper Pro (3.2.23) were tested. Both these softwares are focused on computer vision technology using image matching algorithms combines the automation of computer vision techniques with photogrammetric principles.

The common steps in the standard workflow for both softwares are

-Internal and external orientation parameters calculation (automatic detection of key points and tie points)

-Creation of sparse point cloud

-Creation of dense point cloud model

-Construction of polygonal model
-Texture mapping
-Generation of orthophoto (figure 5.4.51)

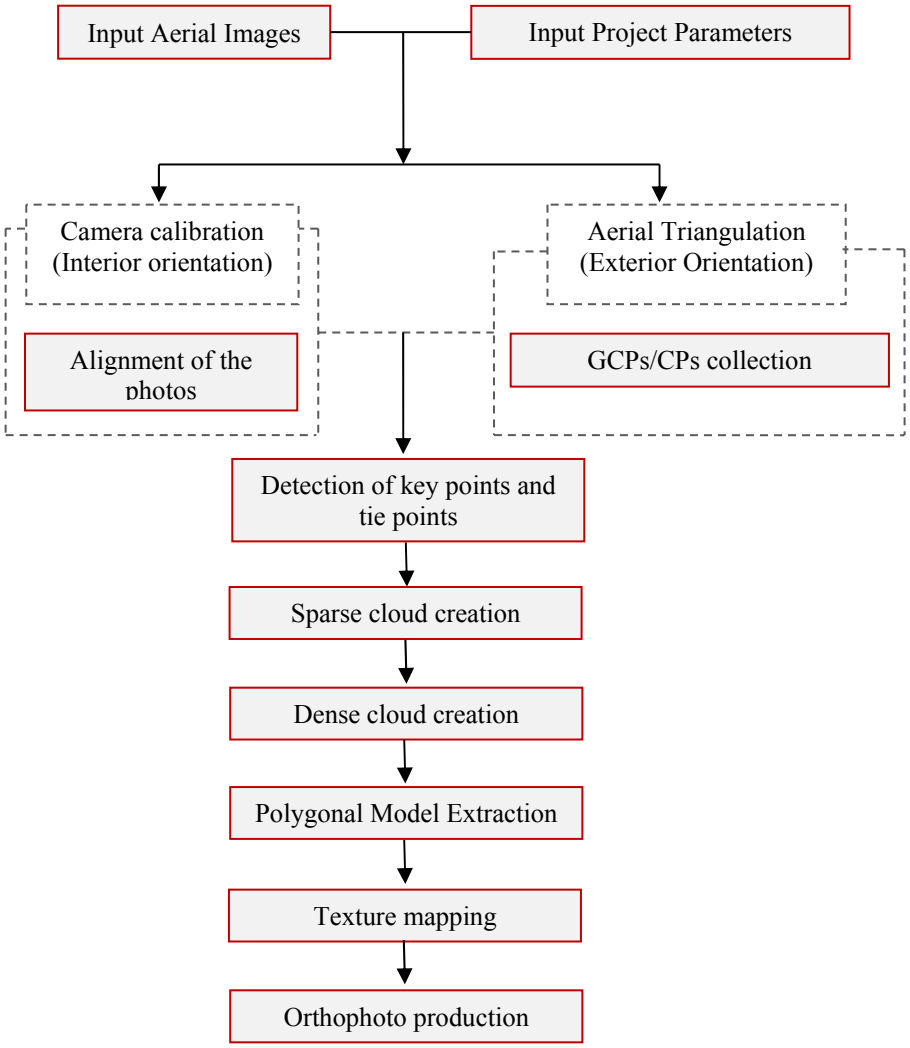

Figure 5.4.51.Common steps in the standard workflow

Interior orientation defines the internal geometry of a camera or sensor as it existed at the time of data capture and shortly it means the process of camera calibration. Interior orientation is primarily used to transform the image pixel coordinate system or other image coordinate measurement system to the image space coordinate system (as described in detail in section 3.4.1.1).

Exterior orientation defines the position and angular orientation associated with an image. Exterior orientation parameters of image are geometric parameters of image, that specify its position and orientation in relation to object of photogrammetric survey in a moment of the survey (as described in detail in section 3.4.1.2).

Estimation of camera orientation parameters helps to alignment of the photos and reconstruction of sparse point cloud. Measurement of GCPs allows linear transformation of model using three parameters for translation (x,y,z) and three for

rotation (omega, phi, kappa). However for this translation at least 3 GCPs must be known. To use GCPs provides higher accuracy and correction of possible distortions.

During the optimization process, the sum of re-projection errors and reference coordinate misalignment errors is minimized. The re-projection error concerns the difference between the control points position defined on the original image and their estimated position during optimization process

To get a reliable comparison between softwares, some points have to be considered. GCPs/CPs should be detected on the same images and the most similar or same settings should be selected (Fiorillo, Limongiello, & Fernández-Palacios, 2016). In this case study the same GCPs were selected and measured in the same images. GCPs were measured with GPS RTK on the field.

Agisoft PhotoScan

Agisoft PhotoScan is a commercial software package. It operates with arbitrary images and is efficient in both controlled and uncontrolled conditions. It allows to align the images and 3D model reconstruction in automated way. Mainly the goal of the photographs processing is to build a textured 3D model. Firstly it searches for common point on photographs and matches them, finds the position of the camera for each photo and refines the camera calibration parameters. This image alignment process has three kinds of parameters: disabled, generic or referenced. Disabled option searches tie points in every possible photo pair while generic option finds tie points in two steps: firstly it makes pairs or groups with subsampled photos then merge these groups using photos with desired accuracy. Referenced option searches tie points using geolocation of the images on the proximity of neighboring images. For this study it was used reference option for the image alignment.

As result of this, a sparse point cloud and set of camera positions are formed. Based on the estimated camera positions, a dense point cloud which may be edited or classified prior to export or proceeding to 3D mesh model generation is built by PhotoScan. This dense point cloud model can be computed in different qualities which mainly shows the number of points. These qualities are ultra high, high, medium, low and lowest. For this case study, high quality and moderate filtering was used in order to get dense point cloud data.

After this step, it reconstructs a 3D polygonal mesh representing the object surface based on point cloud. This mesh can be edited by removing detached components, closing of holes or smoothing etc. It could be exported to softwares. After the geometry is reconstructed, it can be textured and/or used for orthomosaic generation as well as DEM generation process.

The PhotoScan Pro workflow can be classified into four basic steps:
-Image alignment
-Dense point cloud formation
-Mesh creation
-Texture creation

Each of these steps can be run independent of each other and they can be saved separately for later use or revision.

In this project, for the image alignment, for accuracy parameter high setting was chosen while for the pair selection reference setting was used with 50.000 key point limit and 10.000 tie point limit. The second step generation of point cloud model, for quality parameter high was chosen as setting and depth filtering was in moderate setting. The third step to build a mesh model, surface type was in height field while source data was set dense cloud. The other parameters interpolation was enabled, quality of the mesh was set high and depth filtering was moderate. In the last step texture mapping, mapping mode was in orthophoto, blending mode was mosaic while enable color correction and hole filling was set as yes.

Table 5.4.7: Project parameter setting for PhotoScan

Step	Parameter	Setting
Image alignment	Accuracy Pair preselection Key point limit Tie point limit	High Reference 50.000 10.000
Dense point cloud	Quality Depth filtering	High Moderate
Built mesh	Surface type Source data Interpolation Quality Depth filtering	Height field Dense cloud Enabled High Moderate
Texture mapping	Mapping mode Blending mode Enable color correction Enable hole filling	Orthophoto Mosaic Yes Yes
Export orthopohoto	Blending mode	Mosaic

Pix4D

Pix4D is alternative orthomosaic software created in 2011 by a Swiss company of the same name (Gross, 2016). It is used for the generation of point clouds, models, and orthomosaics from photos. The workflow is similar with PhotoScan and has mainly three steps:
-Initial processing (image alignment)
-Point cloud densification
-DSM, Orthomosaic and index
In image alignment different image resolutions may be used (2, 1, 1/2, ¼, 1/8). In point cloud generation step, the original resolution of the images could be used but resampling to half of the original resolution is recommended (Pix4D 2016). Besides, the desired point density of the point cloud could be set as low, optimal and high. Before any processing is done, Pix4D recommends the inclusion of any GCP data

available. GCPs data also allows reduce shift and other errors may be in the final model (Gross, 2016).

Table 5.4.8: Project parameter setting for Pix4Dmapper

Step	Parameter	Setting
Initial processing	Keypoints image scale Matching image pairs Keypoint extraction Calibration Bundle adjustment	Full, Image scale:1 Aerial grid or corridor Targeted number of keypoints: automatic Calibration method: Standard Internal and external parameters optimization: all Classic
oint cloud	Image scale Point density Minimum number of matches	Multiscale, ½ (half image size) Optimal 3
DSM/Orthomosaic	Noise filtering Surface smoothing Raster DSM Export	Yes Yes, type: sharp Generated: yes Method: Inverse distance weightening Merge tiles: yes GeoTIFF

Table 5.4.9: Project parameters in PhotoScan and Pix4Dmapper

Parameters	Agisoft PhotoScan	Pix4Dmapper
Number of cameras	72	72
Aligned cameras	72	72
Covered area	0.319 km²	0.305 km²
GSD	1.03 cm/px	1cm
Sidelap	%80	%80
Overlap	%65	%65
Tie point	118,224	
Dense cloud	83,734,517	187,390,76
Mean key point size	3.17058 px	95820 per image
Number of strips	7	7
Projections	705,403	965,873
Reprojection error	0,675 px	0.161 px
Faces	5,505,412	-----
Vertices	2,757,814	-----
DEM size	14,171x15,188	-----
Orthomosaic size	18,751x19,963	-----

5.4.5.3.Results and Discussion

Comparison of the softwares

With wide use of UAVs increasing in both in the academic and other sectors, it has become important to find quick, reliable and accurate methods for converting images into a single orthomosaic. This research has presented two possible alternative software packages offering highly automated approach PhotoScan Pro and Pix4D.

A first analysis was carried out on geometric accuracy assasment by root mean square errors RMSE. RMSE is the comparison of real world (ground truth) information to estimated (image derived) measurements. In this research totally 7 GCPs were measured on the field and their world location were compared to their estimated location in all orthomosaic by software calculation. In table 5.4.10 it is shown GCPs corresponding RMS errors on XYZ coordinates. The points have been inserted in the same images for each software by the same operator. When it is observed the GCPs errors, in both softwares the errors has no big difference in values. Total RMS erros in Agisoft PhotoScan was 0.67 in X, 0.76 in Y and 0.69 in Z axis and totally 0.513 pix in image, while RMS erros in Pix4D was 0.81 in X, 0.73 Y, 2.01 in Z axis which is the highest value (table 5.4.10)

Table 5.4.10: GCP errors in softwares.

GCPs name	Error X (cm)		Error Y (cm)		Error Z (cm)	
	PhotoScan	Pix4D	PhotoScan	Pix4D	PhotoScan	Pix4D
GCP1	-0.45	0.70	-0.31	-0.05	-0.06	-1.00
GCP2	1.40	-1.40	0.65	-0.50	0.00	1.10
GCP3	0.03	-0.10	1.11	-0.80	1.11	-2.90
GCP4	-0.81	1.20	-1.49	1.20	-1.05	2.60
GCP5	0.02	-0.10	0.03	0.80	0.25	0.30
GCP6	0.31	-0.30	-0.04	0.00	-0.81	0.70
GCP7	-0.51	0.45	0.05	0.06	0.56	0.65
RMSE(cm)	0.67	0.81	0.76	0.73	0.69	2.01

The second comparison was conducted on the camera calibration parameters. The maximum difference was seen in coordinates of principal points (Cx and Cy) in the softwares. The other values don't has very small difference. Mean reprojection error was 0.161 px in Pix4D while in PhotoScan RMS reprojection error was 0.513 px Table 5.4.11It should be defined that a certain amount of the increased error of PhotoScan relative to Pix4D may be due to the presence of image artifacts which made it more difficult to accurately determine the geometric centers of GCPs.

Table 5.4.11: Comparison of camera calibration parameters

Camera	Type	Focal Length	Pixel Size		
eXom	Frame	8.02 mm	1.4 x 1.4 µm		
Parameter	PhotoScan	Pix4D	Parameter	PhotoScan	Pix4D
Cx	10.9263	5.021	F	5728.57	-
Cy	90.3334	3.882	B1	-1.16133	-
K1	0.255687	0.249	B2	-0.728966	-
K2	-0704389	-0.669	P1	0.000304498	0.000
K3	0.5818	0.536	P2	0.00038912	0.000
K4	0	0	P3	0	-
			P4	0	-

According to Gross (2016) study, there is no single bet option for optimization of all criteria, and a software selection should reflect the cost-benefit trade-off between cost, ease of use, geometric accuracy and visual quality (Gross, 2016). In his study, it can be seen that in point of geometric accuracy PhotoScan and Pix4D has no big difference and show very good results. According to his study Pix4D has better quality than PhotoScan while Pix4D is cheaper. Depending on the ease of use PhotoScan is more user-friendly than Pix4D (Figure 5.4.52).

	Geometric accuracy	Visual quality	Cost	Ease of use
ICE	2	1	1	2
Photoscan Pro	1	3	2	1
Pix4D	1	2	3	3

Figure 5.4.52: Overall comparison between the software. Numbers represent the software order for that category with 1 being the highest. Duplicate values were awarded in cases where no statistical difference was observed (Gross, 2016)

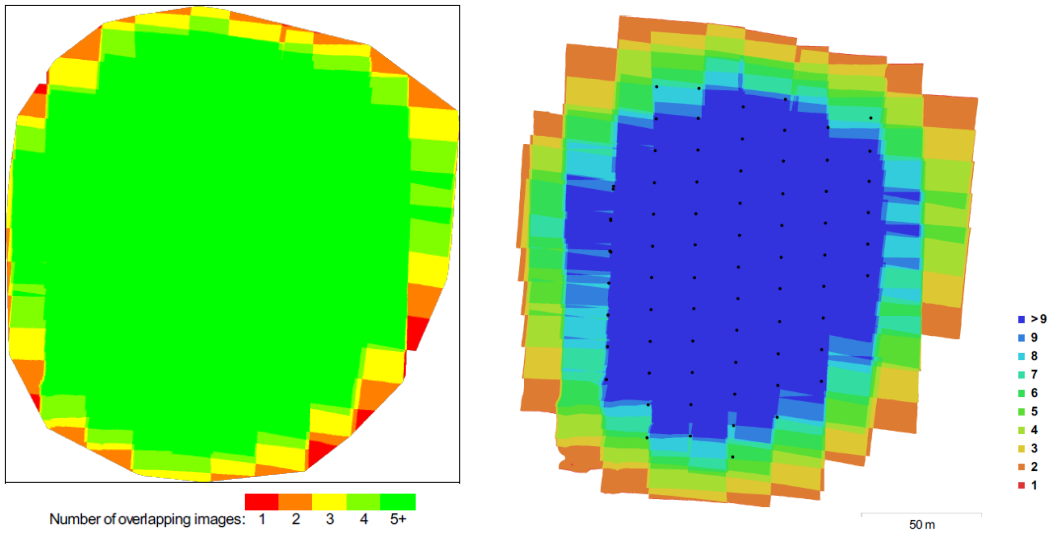

Figure 5.4.53: Number of overlapping images computed for each pixel of the orthomosaic in Pix4D (left). Red and yellow areas indicate low overlap for which poor results may be generated. Green areas indicate an overlap of over 5 images for every pixel. Good quality results will be generated as long as the number of keypoint matches is also sufficient for these areas .
Camera locations and image overlap in PhotoScan (right)

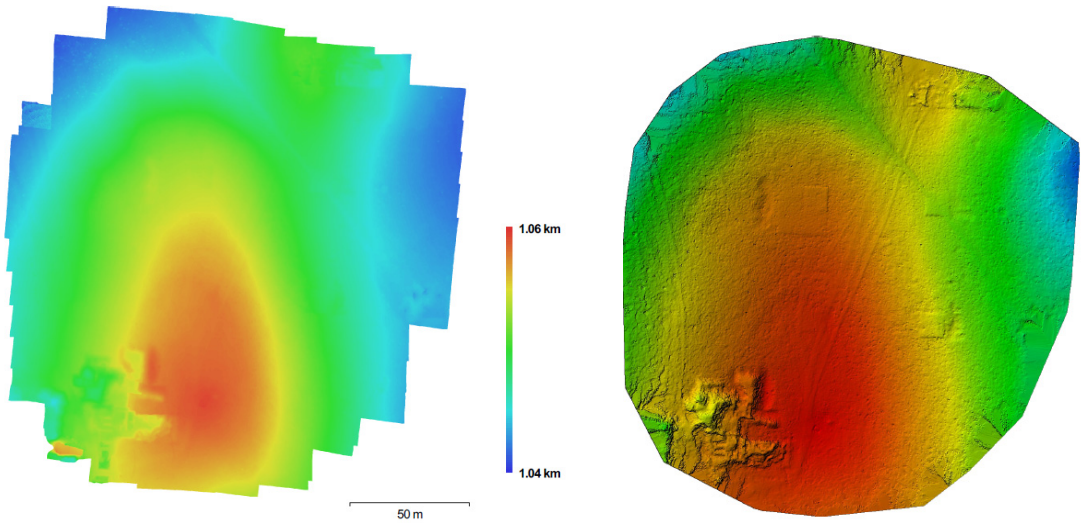

Figure 5.4.54: Figure Reconstructed DEM with resolution 2.06 cm/px and 0.235 points/cm² in PhotoScan (left)Digital urface Model (DSM) in Pix4D (right)

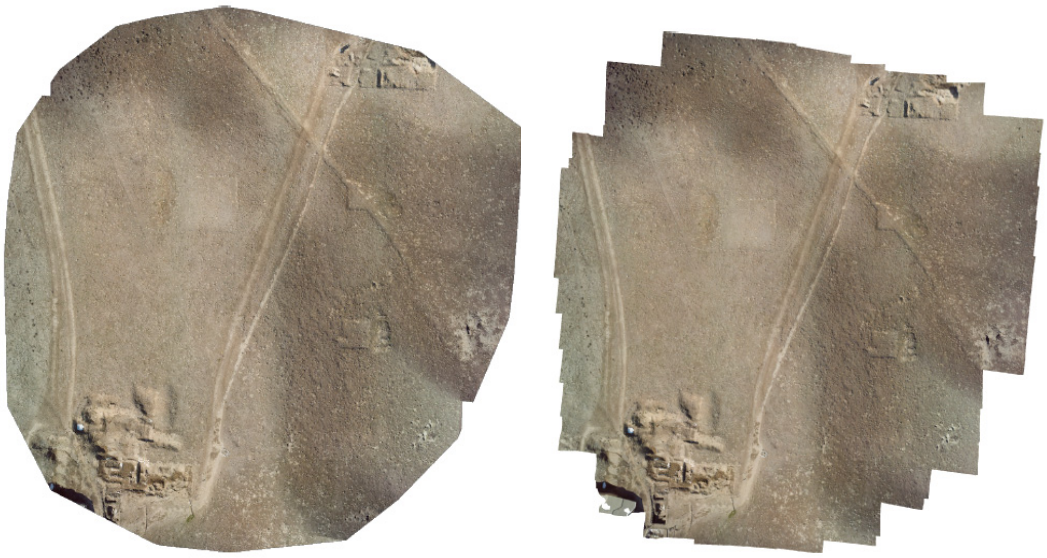

Figure 5.4.55: Reconstructed orthophoto in Pix4D (left)
Reconstructed orthophoto in PhotoScan(right)

Aerial Thermal data results

On Eastern Mound North Peak Hill are which is located in between two shelters with ongoing excavations in Çatalhöyük, only one thermal survey was carried out to check if it would be possible to see the anomalies in the afternoon. The flight was 10 minutes from take-off to land on. The thermal flight was on 4:21 pm in the afternoon while the sunrise was 7:15 am and sunset was 6:48 pm. The flight height was 63 m above the ground. The weather was with some cloudy and there was some wind. The flight was conducted in autonomous mode. On the days of the survey, the temperature variability was 20□. The weather temperature was 12.8 □ when the survey was conducted while it was 2.3 □ early in the morning and 8.2□ after the sunset. The soil temperature was 17□ in the survey time. The weather humidity was %48 while it was %67 early in the morning, then it became %20 in the afternoon and increased again to %55 the soil humidity was in low level.

ÇATALHÖYÜK HILL THERMAL DATA RELATED TO IMAGES -1

IMAGE (COLOR)	 1	 2	 3	 4	 5
IMAGE (THERMAL)	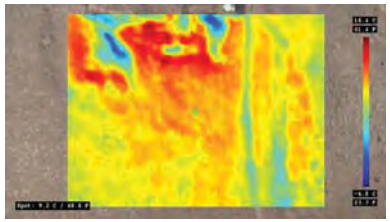 1	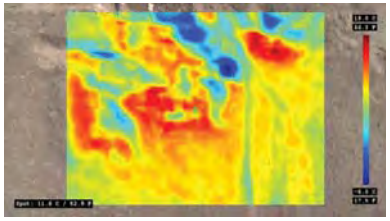 2	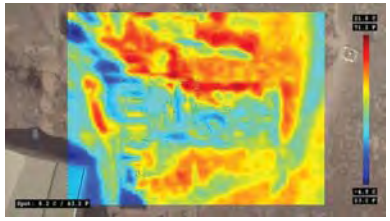 3	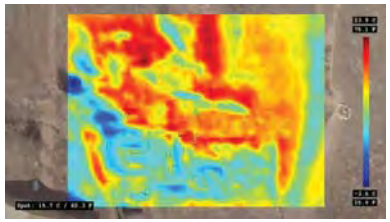 4	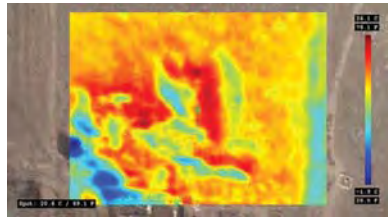 5
IMAGE (COLOR)	 6	 7	 8	 9	 10
IMAGE (THERMAL)	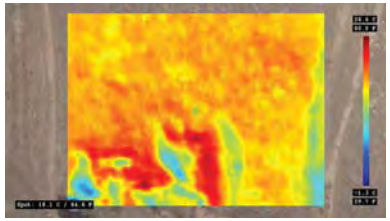 6	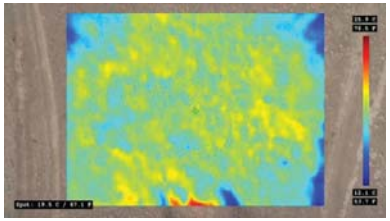 7	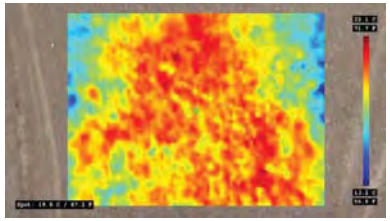 8	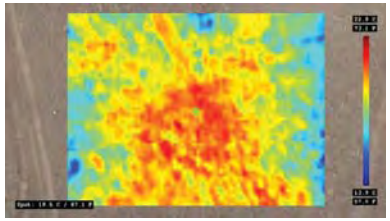 9	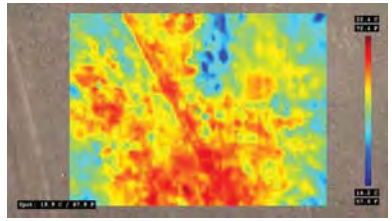 10

ÇATALHÖYÜK HILL THERMAL DATA RELATED TO IMAGES -2

IMAGE (COLOR)	 11	 12	 13	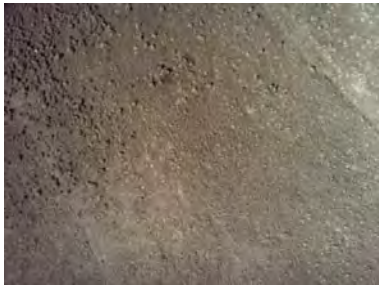 14	 15
IMAGE (THERMAL)	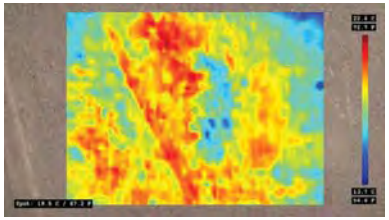 11	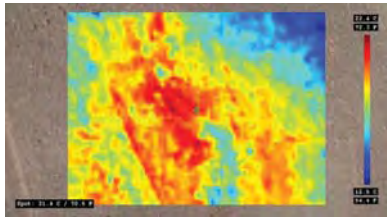 12	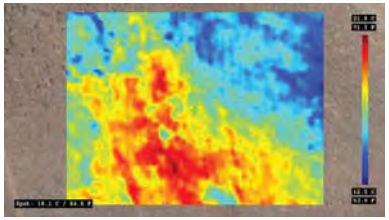 13	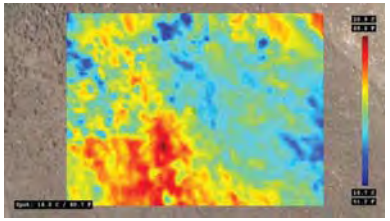 14	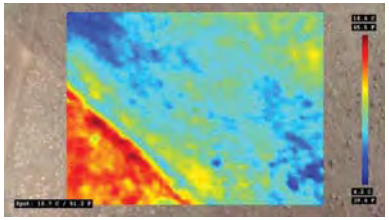 15
IMAGE (COLOR)	 16	 17	 18	 19	 20
IMAGE (THERMAL)	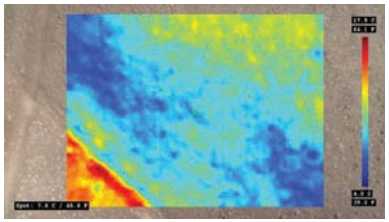 16	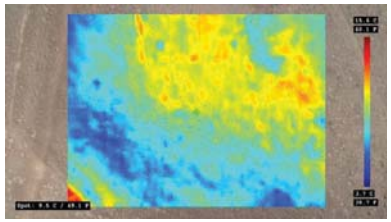 17	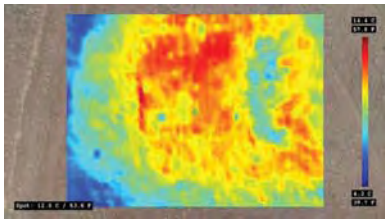 18	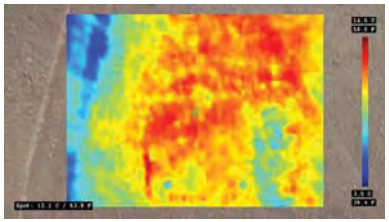 19	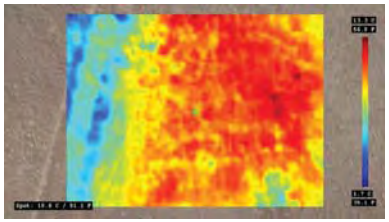 20

ÇATALHÖYÜK HILL THERMAL DATA RELATED TO IMAGES -3

IMAGE (COLOR)	 21	 22	 23	 24	 25
IMAGE (THERMAL)	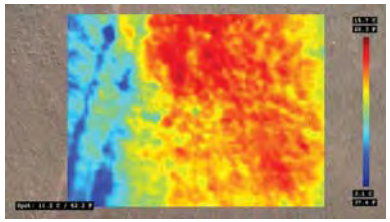 21	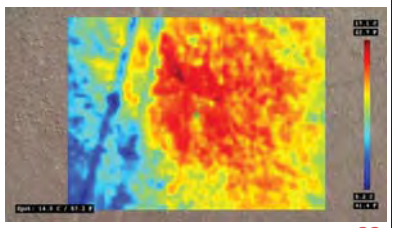 22	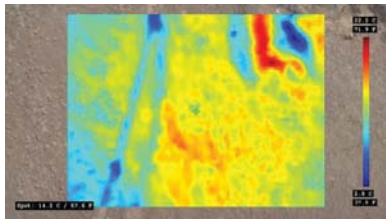 23	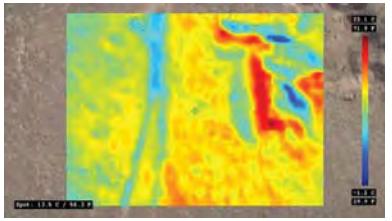 24	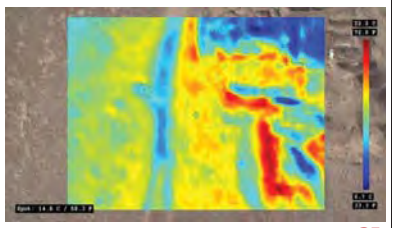 25
IMAGE (COLOR)	 26	 27	 28	 29	 30
IMAGE (THERMAL)	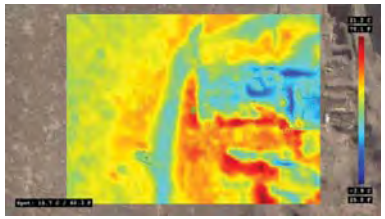 26	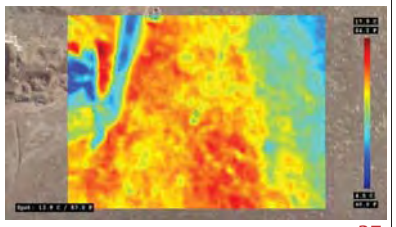 27	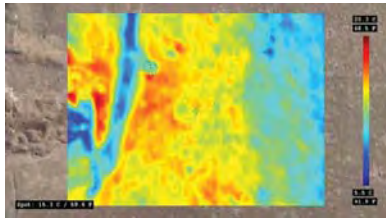 28	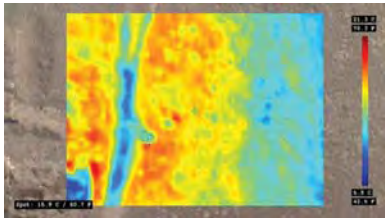 29	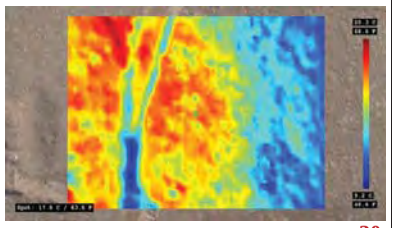 30

ÇATALHÖYÜK HILL THERMAL DATA RELATED TO IMAGES -4

IMAGE (COLOR)	 31	 32	 33	 34	 35
IMAGE (THERMAL)	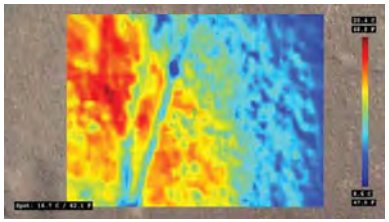 31	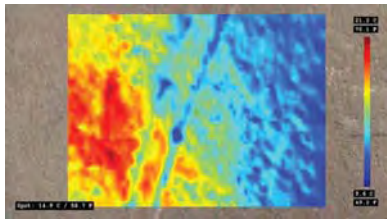 32	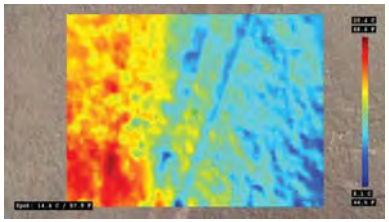 33	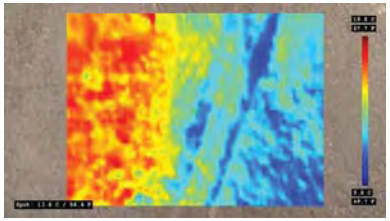 34	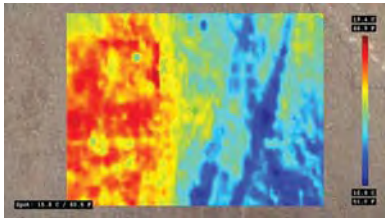 35
IMAGE (COLOR)	 36	 37	 38	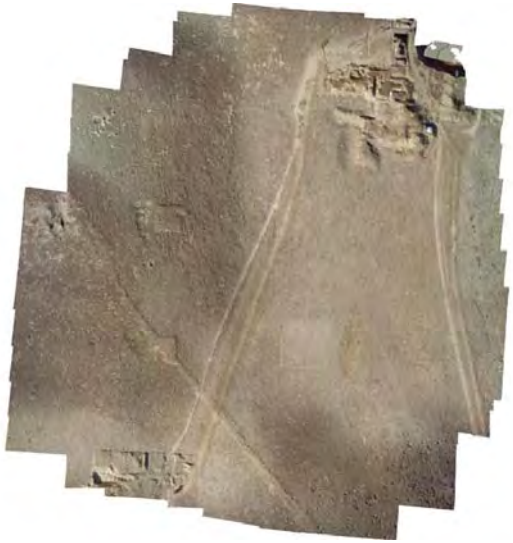 Orthophoto of the IMAGE	
IMAGE (THERMAL)	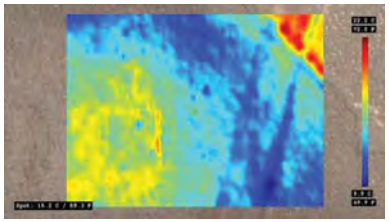 36	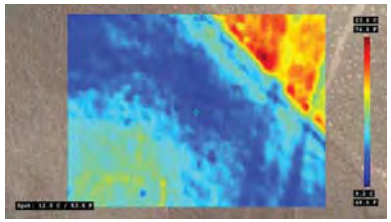 37	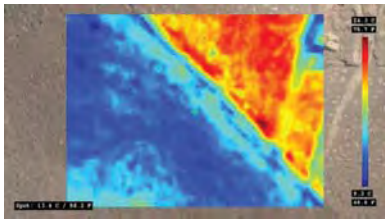 38		

Alignment of thermal images and the creation of orthophoto of thermal images was not possible since it can't get raw thermal images without overlapping. Totally 40 overlapped images were acquired from the survey. It was laready known the significance and the materials of Çatalhöyük houses as described in detail in section 5.4.This hill locates between two archaeological excavation areas. Since previous studies has shown that this hill was full of settlements, there is a high possibility to have some features under the ground.

According to another study leaded by Lunden (1985), to minimize the effect of heterogeneous surface is to perform in clear weather and spring time so the survey was conducted in clear weather in spring. Lunden also adds a suitable time for registration is spring when the surface if the ground is drying out and the fields are without crops. The surveyed area was without any vegetation and crop and commonly covered with soil. When the soil is warming up, the higher thermal inertia can be appeared in soil profile and strengthen the temperature anomalies. Scollar et al. 1990, if the surface layer is composed of homogenous material, it uniformly dampen the thermal responses of any underground features. If the surface layer is heterogonous means if there are human agricultural and construction activities or archaeological materials or etc., they are mostly affected by diurnal variations and they are most visible in the afternoon.

The surveyed area was divide into 38 parts totally (table 5.4.12). When thermal images are evaluated, it can easily be seen that pits, holes and the lines of the roads and the areas without soil seem in different degrees of cold while bumps seem hot (1,2,3,4,5 photos). Since the soil heat more quickly in the sun and cool fastly in the evening, the strength of anomalies could cause thermal conductivity of the material and its density. Since materials with high conductivity and low volumetric heat will have high diffusivity, they don't keep the heat so they seem cold while the surrounding is hot. Similarly in the 8th and 9th photo, it can be clearly recognizable hot areas in different rate. On the 9th and 10th photos, on the right part of the road slightly passing through the image, some cold areas can be appeared and it continues through 11st and 12nd images with the same contours. These anomalies show similar behavior with previously excavated area seen in the photos 1-5. However the cold degree is different from them which may depend on the depth or the content of the material under the ground or may be signal of a hole on the roof. As we know that soil (0.3) and mud-brick/adobe has high thermal conductivity almost between 0.6-1.2 in contrast to wood 0.09-0.14.

Significantly in some thermal images, sharp temperature changes are distinguishable. Examples are easily be read in 13rd, 14th and 15th images. Even though they are in the same surface, lower and upper part of the road heats differently. While upper part is colder but it has some hot areas, the lover part is clearly very hot (15th photo) when it's compared. In 18th and 19th photos, on the same surface, some cold and hot anomalies can easily be recognized. Similarly in 21st photo, very hot region according to surrounding could be a signal for surfaces close to ground. Strong temperature difference can also be seen in 30th photo and continues in consecutive photos 31, 32,33, 34 and 35. In photo 36, an area which heat different from the soil can be seen as well on the cold ground. Another example for sharp temperature difference is

in 37th and 38th photos as well as the soil. Since the survey was carried out in the afternoon, the soil is hot however this heat is not homogenous.

Even the survey was made in the afternoon, depending on the difference thermal properties of the materials some anomalies could be observed. Though previous studies have already identified this method, aerial thermal imaging conducted in this case study have given valuable insights regarding unexcavated part of the area. This data may help to reveal some features that are not clearly visible on the ground, especially more homogenous surfaces. Future studies will be to make diurnal and seasonal observations about the area to determine the anomalies.

6. CONCLUSIONS AND RECOMMENDATIONS

6.1 Discussion

Changing definition of cultural heritage has caused the question of how to express, how to manage to be asked over the time. Today, new concepts such as modern heritage, digital heritage, e-heritage have emerged as well as tangible and intangible heritage. In continuation of this diversity, new studies have started for the protection and documentation of cultural heritage. By the change in definition and scope of the heritage, transmission of the heritage has become more significant and prior.

As a complicated process, recording the physical characteristics of heritage is a keystone for their conservation and a guide for decision makers, conservators and all stakeholders in conservation process as well as understanding the significance of heritage and transmitting it to other generations. Understanding the value of heritage is essential for their conservation and their appropriately assessment.

Selection of suitable technology and application is essential for an improved documentation. The fast developments in digital documentation techniques reformed the practice of cultural heritage documentation. Digital tools have led new openings for each of documentation process, especially for data acquisition, data process, data management and data dissemination. Previous studies have proved that there is no certain rule or formula to determine which technique might be suitable for any situation. Here the relation between required output, needed accuracy, object size and scale becomes the most important indicators.

Today for documentation for cultural heritage, both direct and indirect methods are used depending on the situation. For an improved documentation, the integration of data from different sources and the combination of technogies with related methodologies may be the best solution. Beside direct techniques such as hand measurement, levelling, total station, and GPS, indirect techniques such as remote sensing, tereestrial laser scanning, airborne lidar and aerial photogrammetry have get great interest. Especially for documentation of archaeological and cultural heritage documentation, UAVs has been used widely because of their improvements in sophistication, reliability, cost and ability. With new developments, they have started to be a useful tool for archaeological and cultural heritage documentation. New innovations in camera and sensors facilitated the use of UAVs more effectively.

In this study a comprehensive literature review of cultural heritage definition, current status of cultural heritage documentation was given and used methodologies UAV, Infrared Thermography and Aerial Thermography and their use in different case studies was presented.

Review of UAVs includes categories, advantages and concepts of UAVs with data acquisition, data processing concepts as well as system composition and regulations. The studies have proven that UAV technology has been used diverse applications. The researches indicate that better results can be acquired with autonomus process. Even though the autonomus process has reached a satisfactory level for

automatic tie point extraction and DSM generation, imgae orientation and GCPs measurement take time. It is clear that autonomous flight is demanded, in some cases, manuel flight could be an obligation. In this case, it may be required new methodologies or technologies to get GPS connection, especially in indoor environments. As it was experienced in the case studies, while fixed UAVs can cover larger areas, rotary wing UAVs have the possibility of take-off and land vertically. Regarding the payload-systems, new technologies imay open new oppurtunities for cameras and sensors. The main challenge with UAVs is their durability to environmental conditions. Some stabilizers for payloads or cameras may be helpful to solve this problem. The limitation in payload force to use low weight GNSS/IMU systems which are still expensive. Another issue is related to regulations. The regulations are still under development in many countries and long process to get permission is needed.

Review of Infrared Thermography includes parameters and principles of the technology with data acquisition and data processing concepts. As indicated in many studies, ihis technology is used in diverse applications such as cultural heritage documentation and especially in archaeological areas. As non-destructive technique IRT has several advantegous for the investigation. Non-contact data acquisition, fast surface inspection, ease of use, ability to perform on different areas can be among them. However variable emissivity and some looses in cooling could be some of the advantages. Besides suitable conditions should be provided for a good survey. Main limitation with the thermography is IRT's depth capability. Even it could be observed data till only a few cantimeters of subsurface, this obstacle doesn't impede extensive use of IRT.

A part of the study is dedicated aerial thermography and its applications in archaeology. Although aerial thermography has been used since the 1970s, archaeologists have recognized that aerial images with recording thermal infrared wavelengths of lightcould be a powerful tool for recognizing both surface and subsurface cultural remains after 1970s. However the weather and surface conditions and thermal properties of the material and surface are the main factors directly affect the results, especillay the buried objects are considered. With developin new technologies new thermal cameras and sensors have started to be used with UAVs for detection of subsurface features. However the time of the flight, thermal properties such as thermal conductivity, emissivity, diffusivity and thermal inertia are the most significant indicators effecting the visibility of buried objects. Besides, vegetation, humidity and temperature of the surrounding and surface are significant as well. In aerial thermal surveys, another isuue to be considered is the altitude of UAV. High altitude reduces the image resolution while low altitude helps to get better images. Similarly increasing speed of UAV may cover wider areas, it causes excessive number of blurred images. To fly on lower heights provides images with better quality however because of the limited time of UAV, in many cases, it becomes not possible to cover the area in one flight.Another issue to be considerd the target size for aerial thermographic survey. For aerial thermal surveys, the targets should be made of material with low thermal emissivity such as aluminum or plastic. The bets time for the surveys is spring time, clear weatheri just before the sunrise and after the sunset.

Several case studies were conducted as example for the suitability of UAVs particular in cultural heritage and archaeological area documentation. Flights with color images were mainly used for documentation while flights with thermal camera were aimed to make investigation of buried objects.

In the first example, Harzburger Hof Hotel, it was evaluated to research the potentials of UAVs for inacessible and dangerous areas and for architectural documentation of cultural heritage with required scale. It was aimed to make a documentation for 1:50 scale. The results were satisfied and ground resolution was with 0.94 px error which is acceptable for 1:50 scale drawings. In this study, the flight height was not so high so the result was good and all the details were visible. Since the area was not so big we could get all the data in one flight.

In the second case study, Kubad-Abad Palace, there were mainly two aims. The first one was to see the potentials of UAVs for large scale maps while the second one was to check the accuracy of the orthophoto. The required scale was big as the area to be covered was large,too. In order to cover the larger area, a fixed wing UAV was used. The fixed wing UAVs have ability to fly on higher levels, cover larger areas and have more durability to winds. In order to check the accuracy of orthophoto, ASPRS (The American Society for Photogrammetry and Remote Sensing)'s report, ASPRS Positional Accuracy Standards for Digital Geospatial Data, published in 2014 was taken as reference. Horizontal and vertical accuracy of the data was checked according to this report. The results showed that both horizontal accuracy and vertical accuracy were found at %95 confidence level. As the case study demonstrates, with right parameters and good planning with suitable methodology, high accuracy could be provided.

In the third case study, a significant Villa in Medici Park, Florence was used to see the potentials of UAVs with thermal camera for the investigation of buried objects. Both color and thermal orthophotos were created in photogrammetric software. Thermal images were acquired by getting frames from thermal video and they were processed in thermal software. Because of the vegetation, it was not easy to recognize the features under the ground. Early in the morning and in the evening flights vegetation creates a very strong signature, as the water in trees and plants tends to retain heat much more readily than the soil. So the trees and growded grasses made strong signature in the early morning and evening flights. To evaluate the thermal data, temperature diagrams were prepared and used. INthermal diagrams, continuing heats with high temperature and cooling areas with low temperature were recognizable especially in consecutive images. This method has proven that thermal anomalies can be read not only by the images also with the diagrams and thermal behaviours of the materials can be guessed through the temperature differences.

In the forth case study, there wer mainly two archaeological areas. One of them was Eastern Mound North Peak inside the shelter where the excavation continues. The shelter prevented us to fly autonomously since it was not possible to get GPS signal. In the first attempt, because of loosing signal, UAV crashed and it was broken so the flight was conducted in manual mode. Since it was an inddor place, there was not wind so the images were not affected by any external influence. This study showed that to get astrong GPS signal, some precution should be taken for inddor applications. However in

the literature, there are some studies to solve this problem. Regarding the thermal images, the visibility of anomalies was high in early morning and the evening flights. Small areas which warms up and cools down differently were recognizable in the morning and in the evening images. Since UAV couldn't reach all part of the area, especially where the shelter height is low, also TLS survey was conducted and two data were merged with reference of point clouds. One of the results of this study was that UAV data can be combined with TLS data when there are inaccessible or not measured areas for improved documentation.

In the second part of this case study, one thermal flight was conducted and the results were satisfied. Even the flight was in the afternoon, differently hot and cold areas were visible as positive and negative anomalies. This study shows that if the subsoil features are close to the surface, they can be distinguished even in the afternnon when the soil is hot.

Another aim of this study was to compare two free commonly used software, Agisoft Photoscan and Pix4D. Their performance for data processing and the results were evaluated and compared.According to the results. It was seen that there was slight difference between their RMS erros and in geometric accuracy. According to his study Pix4D has better quality than PhotoScan while Pix4D is cheaper. Depending on the ease of use PhotoScan is more user-friendly than Pix4D.

6.2. Conclusions

Depending on the results of this study, several conclusion remarks can be identified.

- Changing cultural heritage definition will cause new technological improvements which may change the standards and way of the documentation.
- To try to improve the capability of UAVs for indoor applications is required and it may open new use fields of UAVs and research areas for researchers.
- There is no best method or technology for any situation so different methodologies can be improved depending on the situation. Diverse methodologies proposed in this study may give an idea for new methodologies. For an improved documentation, combination of different technologies with appropriate methodology is essential.
- Documentation is an interdisciplinary research. It is always demanded that collaboration of different specialists for better documentation of cultural heritage and share their experiences. It would clearly support better understanding and transmission of the heritage to the future.
- This kind of extensive and improved documentation results wiould help conservators, archaeologists and decision-makers in decision-making and conservation of the herigtae. The appropriate decisions could be taken with only accurate and proper information. Wrong decisions may cause irreversible mistakes which directly affect the future of the heritage.
- Try to improve new methodologies may force the technology to solve the problems and to find the solutions.

- New methodologies for documentation may provide a valuable complement to regional archaeological surveys by revealing the likely location of archaeological features across large areas.
- To have an information of likely location of the subsurface features may provide excavation map and may give an idea to archaeologists about how to continue with the excavation.
- To open new research fields may facilitate many possibilities to make aerial thermography as standard stage in archaeological investigations with imagery data.
- Digitally documented data can more easily be shared with all stakeholders in databases which helps a comprehensive dissemination of the heritage data.
- To create a discussion for availability of this technology for other disciplines give precious contributions for better documentation of cultural heritage.

6.3. Recommendations

Cultural Heritage Documentation is a complex project. It's needed different specialist and the combination of diverse methods. In order to choose the right methodology, it has to be decided the type of cultural heritage for choosing the convenient method. An improved documentation can be achieved with the combination of different methods.

Digital technologies have also affected cultural heritage documentation techniques and application of practice. Although traditional survey methods are still important and could be used in some cases, technological possibilities have given opportunity to support them in different ways to decide the convenient technology and method, depending on the cultural heritage type is crucial problem since each technology has pros and cons in itself.

Likely, TLS (Terrestrial Laser Scanning) has been mostly used for CH documentation in the last years, it has some deficiencies. In order to achieve to an improved documentation, it needs to be combined some other techniques like UAV, since it is not possible to get aerial data with TLS. Even though UAVs has many advantages for CH documentation, its use requires attention and decisions should made before the field work. The type of UAV and other criteria such as its size, capability, application requirements, power, height, endurance and maneuverability are the main criteria for selection of the device. These are also depends on the type of the object to be documented or the size of the area, what kind of output is needed, the accuracy of final product and the aim of the survey. These determinants play a vital role for a successful and improved documentation and should be decide at the beginning of the project. Flight planning and the weather condition are the others factors needs to be careful on the field since they affect the block configuration and the quality of final product, as well. Another key factors is to decide the size of GCPs. Their distribution and size should be sufficient for block configuration. The type of final product should be decide at the beginning of the study. Data management and data processing are the most time-consuming part of the project. In order to fasten this process and to get good results, it is

required to work with a successful, user-friendly and reliable software and a good hardware.

IR Thermography make possible a fast, non-contact and non-destructive detection of the artifacts .Archaeologists have used aerial thermography since 1970's, they have recognized that aerial images with recording thermal infrared wavelengths of light (7.5-13 μm) could be a powerful tool for recognizing both surface and subsurface cultural remains after 1970s and today it has developed and combined with UAV for archaeological area documentation with IR cameras. However many factors have to be considered before field work. This technique mainly depends on capability of the method, the state of environment surrounding of the buried objects and human factors. Before carrying out a project, the type of the UAV (because of endurance in the air), IR sensors resolution, and peculiarities of UAV and IR sensor should be choosen according to desired final product. Besides, the time of flight is another main factor in order to detect archaeological ruins. Early in the morning (before sunrise) and after sunrise give the best results, since temperature difference between the soil and material is maximum. Additionally, the survey has to be conducted in different times of the day to see the difference of temperature and material behavior. Besides the suitable for the application of aerial thermography is the spring time as clear weather, the surface of the ground is drying out and the fields are without crops. Target size is also important for the registration of data. Since IR sensors have relatively low resolution, it's quite difficult to see the targets on the ground. Beside the target size, also the material of it is significant. It should be visible on IR sensors and made of material with low thermal emissivity so they tend to appear dark in thermal images and video.

8. REFERENCES

Abe, T., & Sugimoto, T. (2009). Extremely Shallow Underground Imaging Using Scanning Laser Doppler Vibrometer. *Japanese Journal of Applied Physics, 48*(7S).

Ahmad, A. (2011). Digital Mapping Using Low Altitude UAV. *Pertanika J. Sci. & Technol., 19*, 51-58.

Aicardi, I., Chiabrando, F., Grasso, N., Lingua, A. M., Noardo, F., & Spano, A. (2016). *UAV Photogrammetry with oblique images: first analysis on data acquisition and processing* Paper presented at the XXIII ISPRS Congress:From human history to the future with spatial information, Prague, Czech Republic.

Allinson, D. (2007). *Evaluation of Aerial Thermography to discriminate loft insulation in residental housing.* (Doctor of Philosophy Doctor of Philosophy), University of Nottingham, Nottingham.

Amorim, A. (2011). Methodological Aspects of Architectural Documentation. *Geoinformatics FCE CTU, 6*, 34-39.

Andrews, D., Bedford, J., Blake, B., Bryan, P., Cromwell, T., & Lea, R. (2009). *Measured and Drawn: Techniques and Practice for the Metric Survey of Historic Buildings*. Swindon: English Heritage.

Anuar, A., Khairul, N. T., Wani , S. U., Khairil , A. H., NorHadija, D., Mohd, H., . . . Shahrul, M. A. (2013). *Digital Aerial Imagery of Unmanned Aerial Vehicle for Various Applications*. Paper presented at the IEEE International Conference on Control System, Computing and Engineering, Penang, Malaysia.

Apollonio, F. I., Gaiani, M., & Benedetti, B. (2011). 3D reality-based artefact models for the management of archaeological sites using 3D Gis: a framework starting from the case study of the Pompeii Archaeological Area. *Journal of Archaeological Science, 39*.

Araneo, R., & Celozzi, S. (2003). Numerical Analysis of Subsurface Object Discrimination Systems. *IEEE Transactions on Magnetics, 39*, 1219-1222.

Arık, R. (2000). *Kubad Abad Selçuklu Sarayı ve Çinileri*. İstanbul: Türkiye İş Bankası Kültür Yayınları.

ASHRAE. (2011). *2011 Thermal Guidelines for Data Processing Environments – Expanded Data Center Classes and Usage Guidance*. Retrieved from

Austin, R. (2010). *Unmanned Aircraft Systems : UAVS Design, Development and Deployment*. West Sussex, United Kingdom: John Wiley & Sons Ltd.

Avdelidis, N. P., & Moropoulou, A. (2003). Emissivity considerations in building thermography. *Journal of Energy and Buildings, 35*, 663-667.

Avdelidis, N. P., & Moropoulou, A. (2004). Applications of infrared thermography for the investigation of historic structures. *Journal of Cultural Heritage, 5*, 119-127. doi:10.1016/j.culher.2003.07.002

Azmi, S. M., Ahmad, B., & Ahmad, A. (2014). *Accuracy assessment of topographic mapping using UAV image integrated with satellite images.* Paper presented at the 8th InternationalSymposiumoftheDigitalEarth(ISDE8).

Balsi, M., & Corcione, M. (2005). Thermal detection of buried landmines by local heating. *International Journal of Systems Science, 36*, 589-604.

Barabanov, A. E., & Romaev, D. V. (2009). *Design of helicopter autopilot.* Paper presented at the European Control Conference (ECC), Budapest, Hungary.

Barazzetti, L., Remondino, F., & Scaioni, M. (2009, 2-3 August 2009). *Combined use of photogrammetric and computer vision techniques for fully automated and accurate 3D modeling of terrestrial objects.* Paper presented at the Videometrics, Range Imaging and Applications X, San Diego, CA, USA.

Barazzetti, L., Remondino, F., & Scaioni, M. (2010). Automation in 3D reconstruction: Results on different kinds of close-range blocks. *International Archives of Photogrammetry, Remote Sensing, Spatial Information Science 38*, 55-61.

Barazzetti, L., Remondino, F., Scaioni, M., & Brumana, R. (2010). *Fully Automatic UAV image-based sensor orientation*, Calgary, Canada.

Bartelsen, J., Mayer, H., Hirschmüller, H., Kuhn, A., & Michelini, M. (2012). Orientation and Dense Reconstruciton of Unordered Terrestrial and Aerial Wide Baseline Image Stes. *ISPRS Annals of the Photogrammetry,*

Remote Sensing and Spatial Information Sciences Volume I(Issue 3), 25-30.

Bell, T. H., Barrow, B. J., & Miller, J. T. (2002). Subsurface discrimination using electromagnetic induction sensors. *IEEE Transactions on Geoscience and Remote Sensing, 39*(6), 1286-1293. doi: 10.1109/36.927451

Bellerby, T. J., Noel, M., & Branigan, K. (1990). A thermal method for archaeological prospection:preliminary investigations. *Archaeometry, 32*, 191-203.

Bendea, H., Chiabrandao, F., Giulio Tonolo, F., & Marenchino, D. (2007). *Mapping of archaeological areas using with a low-cost UAV teh Augusta Bagiennorum test site* Paper presented at the XXI International CIPA Symposium, Athens, Greece

Bendea, H., Chiabrando, F., Giulio Tonolo, F., & Marenchino, D. (2007). *Mapping of Archaeological Areas Using a Low-Cost UAV The Augusta Bagiennorum Test Site*. Paper presented at the XXI International Cipa Symposium, Athens, Greece.

Berlin, G. L., Ambler, J. R., Hevly, R. H., & Schaber, G. G. (1977). Identification of a Sinagua agricultural field by aerial thermography, soil chemistry, pollen/plant analysis, and archaeology. *Am. Antiq., 42*, 588-600.

Berni, J. A. J., Zarco-Tejada, P. J., Suarez, L., & Fereres, E. (2009). *IEEE Transactions on Geoscience and Remote Sensing, 47*(3), 722-738. doi: 10.1109/TGRS.2008.2010457

Bhandari, B., Oli, U., Pudasaini, U., & Panta, N. (2015). *Generation of High Resolution DSM Using UAV Images*. Paper presented at the FIG Working Week 2015 "From the Wisdom of the Ages to the Challenges of the Modern World", Sofia, Bulgaria.

Blake, W. H. (2010). *What is the Future of Metric Heritage Documentation and Its Skills?* . Paper presented at the International Archives of Photogrammetry, Remote Sensing and Spatial Information Sciences, Vol. XXXVIII, Part 5 Commission V Symposium, Newcastle upon Tyne.

Boochs, F., Trémeau, A., Murphy, O., Gerke, M., Lerma, J. L., Karmacharya, A., & Karaszewski, M. (2014). *Towards a Knowledge Model Bridging Technologies and Applications in Cultural Heritage Documentation*.

Paper presented at the ISPRS Annals of the Photogrammetry, Remote Sensing and Spatial Information Sciences Technical Commission V Symposium, Riva del Garda, Italy.

Boras, I., Malinovec, M., Stepanic, J., & Svaic, S. (2000). *Detection of underground objects using thermography.* Paper presented at the 15th WCNDT proceedings, Rome.

Boras, I., Malinovec, M., Stepanic, J., & Svaic, S. (2002). *Modelling of buried object detection using thermography.* Paper presented at the QIRT Conference Proceedings, Reims.

Böhler, W., & Marbs, A. (2002). *3D Scanning Instruments.* Paper presented at the CIPA WG6 Scanning for Cultural Heritage Recording, Corfu, Greece.

Brooks, F. D., Buffler, A., & Allie, M. S. (2004). Detection of anti-personnel landmines using neutrons and gamma-rays. *Radiation Physics and Chemistry, 71*(3-4), 749-757. doi:http://dx.doi.org/10.1016/j.radphyschem.2004.04.087

Brown, R., Chalmers, A., Saigol, T., Green, C., & D'Errico, F. (2001). An Automated Laser Scan Survey of the Upper Palaeolithic Rock Shelter of Cap Blanc. *Journal of Archaeological Science, 28*(3), 7.

Brumana, R., Oreni, D., Van Hecke, L., Barazzetti, L., Previtali, M., Roncoroni, F., & Valente, R. (2013). *Combined Geometric and Thermal Analysis From UAV Platforms for Archaeological Heritage Documentation.* Paper presented at the XXIV International Cipa Symposium, Strasbourg, France.

Bryan, P., Blake, B., Bedford, J., Barber, D., & Mills, J. (2009). *Metric Survey Specifications for Cultural Heritage* (D. Andrews Ed. Second Edition ed.). Swindon: English Heritage.

Buck, P. E., Sabol, D. E., & Gillespie, A. R. (2003). Sub-pixel artifact detection using remote sensing. *Journal of Archaeological Science, 30*(8), 973-989.

Budzier, H., & Gerlach, G. (2015). Calibration of uncooled thermal infrared cameras. *Journal of Sensors and Sensor Systems, 4*, 11. doi:10.5194/jsss-4-187-2015

Burns, R. (2006). Photogrammetry: Caltrans Geometronics

Caltrans. (2006). SurveysManual *Photogrammetry Surveys* (pp. 13-63). California: California Department of Transportation.

. Camera Calibration for stereo vision.

Campana, S. (2014). *UAV for archaeological purposes:an overview* (pp. 158).

Carlomagno, G. M., Maio, R. D., Meola, C., & Roberti, N. (2005). Infrared thermography and geophysical techniques in cultural heritage conservation. *Quantitative InfraRed Thermography Journal, 2*(1), 20. doi:http://dx.doi.org/10.3166/qirt.2.5-24

Caroti, G., Martínez-Espejo Zaragoza, I., & Piemonte, A. (2015). *Accuracy Assessment in Structure from Motion 3D Reconstruciton from UAV-Born Images: The Influence of the Data Processing Methods.* Paper presented at the International Conference on Unmanned Aerial Vehicles in Geomatics, Toronto, Canada.

Casana, J., Kantner, J., Wiewel, A., & Cothren, J. (2014). Archaeological aerial thermography: a case study at the Chaco-era Blue J community, New Mexico. *Journal of Archaeological Science, 45*, 207-219. doi:http://dx.doi.org/10.1016/j.jas.2014.02.015

Challis, K., Kincey, M., & Howard, A. (2009). Airborne remote sensing of valley floor geoarchaeology using Daedalus ATM and CASI. *Archaeological Prospects, 16*, 17-33.

Chiabrando, F., Nex, F., Piatti, D., & Rinaudo, F. (2011). UAV and RPV systems for photogrammetric surveys in archaeological areas: two tests in the Piedmont region (Italy). *Journal of Archaeological Science, 38*, 697-710. doi:10.1016/j.jas.2010.10.022

Chiang, W.-K., Tsai, L.-M., Naser, S. E., Habib, A., & Chu, H.-C. (2015). A New Calibration Method Using Low Cost MEM IMUs to Verify the Performance of UAV-Borne MMS Payloads. *Sensors, 15*, 6560-6585. doi:10.3390/s150306560

Church, P., Mcfee, J. E., Gagnon, S., & Wort, P. (2006). Electrical Impedance Tomographic Imaging of Buried Landmines. *IEEE Transactions on Geoscience and Remote Sensing, 44*(9), 2407-2420. doi: 10.1109/TGRS.2006.873208

Clarke, T. A., & J.G., F. (1998). The development of camera calibration methods and models. *Photogrammetric Record, 16*(91), 51-66.

Colomina, I., Aigner, E., Agea, A., Pereira, M., Vitoria, T., Jarauta, R., . . . Hasegawa, J. (2007). *The uVISION project for helicopter-UAV photogrammetry and remote-sensing.* Paper presented at the 7th International Geomatic Week, Barcelona, Spain.

Cowley, D. C. (2010). *Remote Sensing for Archaeological Heritage Management.* Paper presented at the 11th EAC Heritage Management Symposium, Reykjavík, Iceland.

Cramer, M., Stallmann, D., & Haala, N. (2000). Direct Georeferencing Using GPS/Inertial Exterior Orientations for Photogrammetric Applications. *International Archives of Photogrammetry and Remote Sensing, XXXIII*(B-3), 198-205.

Cruz Silva, A. H. (2009). *Neutron Backscattering Technique for the Detection of Buried Organic Objects.* (Master of Science in Physics), UNIVERSIDAD NACIONAL DE COLOMBIA, Bogot´a - Colombia.

D'Ayala, D., & Smars, P. (2003). *Minimum requirement for metric use of non-metric photographic documentation*. Retrieved from Bath, UK:

Dalamagkidis, K., Valavanis, K. P., & Piegl, L. A. (2008, June 25-27, 2008). *A Survey of Unmanned Aircraft Systems Regulation: Status and Future Perspectives.* Paper presented at the 16th Mediterranean Conference on Control and Automation, Ajaccio, France.

Darwin, N., Ahmad, A., & Zainon, O. (2014). *The potential of Unmanned Aerial Vehicle for large scale mapping of coastal area* Paper presented at the 8th InternationalSymposiumoftheDigitalEarth(ISDE8), Sarawak, Malaysia.

Daș, E. (2017). Kubadabad Palace. Retrieved from www.discoverislamicart.org website:

Diaz-Andreu, M., Hobbs, R., Rosser, N., Sharpe, K., & Trinks, I. (2005). Long Meg: Rock Art Recording Using 3D Laser Scanning". *Past: The Newsletter of the Prehistoric Society, 50*, 5.

Durgut, A., & Akçay, Ö. (2016). Termal Kamera Kalibrasyon Şablonlarının Performans Analizi. *Uludağ Üniversitesi Mühendislik Fakültesi Dergisi, 21*(1), 14. doi:10.17482/uujfe.61071

Ehsan, S., & McDonald-Maier, K. D. (2009). *On-board vision processing for small UAVs: Time to rethink strategy," in Adaptive Hardware and Systems.* Paper presented at the NASA/ESA Conference on Adaptive Hardware and Systems (AHS 2009), San Francisco, California.

Eisenbeiß, H. (2004). *A mini unmanned aerial vehicle (UAV): Ssystem overview and image acquisition.* Paper presented at the International Workshop on "Processing and Visualization Using High Resolution Imagery, Pitsanulok, Thailand.

Eisenbeiß, H. (2009). *UAV photogrammetry.* (Doctorate), ETH Zurich, Switzerland. (18515)

Eisenbeiss, H., Lambers, K., & Sauerbier, M. (2005). *Photogrammetric recording of the archaeological site of Pinchango Alto (Palpa, Peru) using a mini helicopter (UAV).* Paper presented at the CAA 2005:The world is in your eyes : CAA 2005 : Computer Applications and Quantitative Methods in Archaeology, Tomar, Portugal.

Eisenbeiss, H., & Zhang, L. (2006). *Comparison of DSMs Generated From Mini UAV Imagery and Terrstrial Laser Scanner in a Cultural Heritage Application.* Paper presented at the ISPRS Commission V Symposium 'Image Engineering and Vision Metrology, Dresden, Germany.

Ellenberg, A., Kontsos, A., Moon, F., & Bartoli, I. (2016). Bridge deck delamination identification from unmanned aerial vehicle infrared imagery. *Automation in Construction, 72*(Part 2), 155-165. doi:http://dx.doi.org/10.1016/j.autcon.2016.08.024

ELtohamy, F., & Hamza, H. E. (2009). *Effect of Ground Control points Location and Distribution on Geometric Correction Accuracy of Remote Sensing Satellite Images*. Paper presented at the 13th International Conference on Aerospcae Sciences & AviationTechnology -ASAT-, Cairo, Egypt.

Europe, C. o. (1985). *Convention for the Protection of the Architectural Heritage of Europe*. Retrieved from Granada:

Everaerts, J. (2008). The use of Unmanned Aerial Vehicles (UAVS) for remote sensing and mapping. . *International Archives of the Photogrammetry, Remote Sensing and SpatialInformation Sciences, XXXVII* (B1), 1187-1192.

Falkner, E., & Morgan, D. (2002). *Aerial Mapping*. Florida Lewis Publishers.

Feifei, X., Zongjian, L., Dezhu, G., & Hua, L. (2012). Study on construction of 3D building based on UAV images. *The International Archives of the Photogrammetry, Remote Sensing and Spatial Information Sciences*, 4.

Fiorillo, F., Fernández-Palacios, B. J., Remondino, F., & Barba, S. (2013). 3D Surveying and modelling of the Archaeological Area of Paestum, Italy. *Virtual Archaeology Review, 4*(8), 6.

Fiorillo, F., Limongiello, M., & Fernández-Palacios, B. J. (2016). Testing GoPro for 3D model reconstruction in narrow spaces. *Acta IMEKO, 5*(2), 64-70.

Floreano, D., & Wood, J. R. (2015). Science, Technology and The Future of Small Autonomous Drones. *International Weekly Journal of Science*(521), 460-466. doi:10.1038/nature14542

Fryskowska, A., Kedzierski, M., Grochala, A., & Braula, A. (2016). *Calibration of Low Cost Color and NIR UAV Cameras.* Paper presented at the XXIII ISPRS Congress: From human history to the future with spatial information, Prague, Czech Republic.

Gašparović, M., & Gajski, D. (2016). *Two-step Camera Calibration Method Developed for Micro UAVs.* Paper presented at the XXIII ISPRS Congress:From human history to the future with spatial information, Prague, Czech Republic.

Gerke, M., & Przybilla, H. (2016). Accuracy Analysis of Photogrammetric UAV Image Blocks: Influence of Onboard RTK-GNSS and Cross Flight Patterns. *Photogrammetrie – Fernerkundung– Geoinformation (PFG)*, 17-30. doi:10.1127/pfg/2016/0284

Gini, R., Pagliari, D., Passoni, D., Pinto, L., Sona, G., & Dosso, P. (2013). *UAV Photogrammetry: Block Triangulation Comparisons.* Paper presented at the UAV-g2013, Rostock, Germany.

Gomez-Lahoz, J., & Gonzalez-Aguilera, D. (2009). Recovering Traditions in the Digital Era: The Use of Blimps for Modelling the Archaeological Cultural Heritage. *Journal of Archaeological Science, 36*, 100-109.

Graça, N., Mitishita, E., & Gonçalves, J. (2014, 17 – 20 November 2014). *Photogrammetric Mapping Using Unmanned Aerial Vehicle* Paper presented at the ISPRS Technical Commission I Symposium, Denver, Colorado, USA.

Grenzdörffer, G. J., Engel, A., & Teichert, B. (2008). *The Photogrammetric Potential of Low-Cost UAVs in Forestry and Agriculture.* Paper presented at the Silk Road for Information from Imagery, Beijing, CHINA.

Grinzato, E., Bressan, C., Marinetti, S., Bison, P., & Bonacina, C. (2002). Monitoring of the Scrovegni Chapel by IR thermography: Giotto at infrared. *Infrared Physics & Technology, 43*(3-5), 5.

Gross, J. W. (2016). *A Comparison of Orthomosaic Software for Use with Ultra High Resolution Imagery of q Wetland Environment*. Paper presented at the IMAGIN's 25 th Annual Conference Great Wolf Lodge Traverse City, Michigan.

GRTI. (2008). *Formation Thermal Conductivity Test and Data Analysis*. Retrieved from

Haala, N. (2011). *Multiray photogrammetry and dense image matching.* Paper presented at the 53rd Photogrammetric Week, Stuttgart, Germany.

Haala, N., Cramer, M., Weimer, F., & Trittler, M. (2011). *Performance Test on UAV-based Photogrammetric Data Collection.* Paper presented at the UAV-g 2011, Zurich, Switzerland.

Haarbrink, R. B., & Eisenbeiß, H. (2008). *Accurate DSM production from unmanned helicopter systems*, Beijing,PRC.

HABS. (1990). Secretary of the Interior's standard and guidelines for architectural and engineering documentation. In U. D. o. Interior (Ed.). Washington,DC: US Department of Interior.

Hadas, Z., Wilner, K., & Ben-Yosef, N. (2003). Introducing anisotropy in the autocorrelation function of natural terrain infrared images. *Optical Engineering, 42*, 1683-1689.

Hagman, F., & Lefebvre, M. (2012). From wasting to saving both energy and money: Aerial Thermography and more. *GIM International*(October), 36-43.

Hammerseth, B. V. (2013). *Autonomous Unmanned Aerial Vehicle in Search and Rescue.* (Master Master of Science in Engineering Cybernetics), Norwegian University of Science and Technology, Norwey.

Hassani, F. (2015). *Documentation of Cultural Heritage Techniques, Potentials and Constraints.* Paper presented at the 25th International CIPA Symposium, Taipei, Taiwan.

Haubeck, K., & Prinz, T. (2013, 4 – 6 September 2013). *UAV-Based low-cost stereo camera system for archaeological surveys- experiences from doliche (Turkey).* Paper presented at the UAV-g2013, Rostock, Germany.

He, J., Li, Y., & Zhang, K. (2012). Research of UAV Flight Planning Parameters. *Scientific Research* (3), 43-45. doi:http://dx.doi.org/10.4236/pos.2012.34006

Heipke, C. (1997). Automation of interior, relative and absolute orientation. *ISPRS Journal of Photogrammetry&Remote Sensing*(57), 1-19.

Heipke, C. (1999). *Automatic Aerial Triangulation: Results of theOEEPE-ISPRS Test and Current Developments* Paper presented at the Photogrammetric Week '99, Heidelberg.

Hendrickx, M., Wouter Gheyle, W., Bonne, J., Bourgeois, J., Wulf, A., & Goossens, R. (2011). The use of stereoscopic images taken from a microdrone for the documentation of heritage: An example from the Tuekta burial mounds in the Russian Altay. *Journal of Archaeological Science, 38*, 11.

Heritage, E. (2011). *3D Laser Scanning for Heritage*. Swindon: English Heritage.

Höhle, J. (2013). *Oblique Aerial Images and Their Use in Cultural Heritage Documentation.* Paper presented at the XXIV International CIPA Symposium, Strasbourg, France.

http://alanya.bel.tr/S/809/Alanya-Castle.

http://ecmweb.com.

http://eijournal.com/news/industry-insights-trends/earth-observation.
http://globalmrr.com/aerotherm/.
http://mittenmang-bs.blogspot.com.tr/2014/05/harzburger-hof-1874-2014-in-memoriam.html.
http://theuav.net/.
http://web.shgm.gov.tr.
http://whc.unesco.org/en/list/1405.
http://www.ai-journal.com/articles/10.5334/ai.1319/.
http://www.catalhoyuk.com/site/architecture.
http://www.charim.net.
http://www.enac.gov.it/.
http://www.faa.gov/uas/.
http://www.flir.com.
http://www.haz.de/Nachrichten/Der-Norden/Uebersicht/Der-Abstieg-eines-Prunk-Hotels-Der-Harzburger-Hof-in-Bad-Harzburg.
http://www.helikites.com.
http://www.monitorday.com/.
http://www.nationalgeographic.com.tr/makale/kesfet/catisma-kesfedilmeden-once/2625.
http://www.naturalhistorymag.com/htmlsite/master.html?http://www.naturalhistorymag.com/htmlsite/0606/0606_feature.html.
http://www.ndr.de/nachrichten/niedersachsen/braunschweig_harz_goettingen/Harzburger-Hof-Verschwindet-der-Schandfleck, h. h.
http://www.newtowninstitute.org.
http://www.oregonnaturalmedicine.com/breast-thermography/researcharticles.
http://www.rottenplaces.de/main/harzburger-hof-6886/.
http://www.tanguayphotomag.biz/.
http://www.turkishculture.org/archaeology/catalhoyuk-1023.htm.
http://www.unisky.it.
http://www.viaduct-diadrasis.net/methods/17.
https://commons.wikimedia.org/wiki/File:Kite_aerial_photo.jpg.
https://en.wikipedia.org/wiki/Heat_transfer.
https://wiki.hexagongeospatial.com.

https://www.khanacademy.org/science/physics/thermodynamics/specific-heat-and-heat-transfer.
https://www.sensefly.com/drones/albris.html.
Ibarra-Castanedo, C., Gonzalez, D., Klein, M., Pilla, M., & Vallerand, S. (2004). Infrared image processing and data analysis. *Infrared Physics & Technology*. doi:10.1016/j.infrared.2004.03.011
ICOMOS. (1931). *The Athens Charter for the Restoration of Historic Monuments*. Retrieved from Athens:
ICOMOS. (1964). *The Venice Charter*. Retrieved from Venice:
ICOMOS. (1987). *The Washington Charter*. Retrieved from Washington, DC:
Imposa, S. (2010). Infrared thermography and Georadar techniques applied to the ‘‘Sala delle Nicchie’’ (Niches Hall) of Palazzo Pitti, Florence (Italy). *Journal of Cultural Heritage, 11*(3), 6.
Imrie, D. A. (2009). Calibrating the thermal camera. *Photonics Spectra, 43*(12).
Ioannidis, C., Potsiou, C., Soile, S., & Badekas, J. (2000, July 16-23, 2000). *Detailed 3D Representations of Archaeological Sites.* Paper presented at the XIXth ISPRS Congress, Amsterdam, The Netherlands.
Ip, A., El-Sheimy, N., & Mostafa, M. (2006). *Performance Analysis of Integrated Sensor Orientation.* Paper presented at the International Archives of Photogrammetry and Remote Sensing, Istanbul.
IUASC, I. U. A. S. C. (2008). *Unmanned Aircraft System:The Global Perspective 2008/2009*. Retrieved from
Jones, T. S., & Kaplan, H. Principles of Infrared and Thermal Testing.
Kandemir-Yücel, A., Tavukcuoglu, A., & Caner-Saltik, E. N. (2007). In situ assessment of structural timber elements of a historic building by infrared thermography and ultrasonic velocity. *Infrared Physics & Technology, 49*, 6. doi:10.1016/j.infrared.2006.06.012
Karras, G. E., & Mavrommati, D. (2001). *Simple calibration techniques for non-metric cameras.* Paper presented at the CIPA International Symposium: Surveying and Documentation of Historic Buildings-Monuments-Sites. Traditional and Modern Methods Potsdam, Germany.
Kendoul, F., Fantoni, I., & Nonami, K. (2009). Optic flow-based vision system for autonomous 3d localization and control of small aerial vehicles.

Robotics and Autonomous Systems, Elseiver, 57(6-7). doi:10.1016/j.robot.2009.02.001

Kersten, T., & Haering, S. (1997). Automatic Interior Orientatio of Digital Aerial Images *Photogrammetric Engineering&Remote Sensing, 63*(8), 1007-1011.

Konoglie, K., & Agrawal, M. (2008). Frameslam: from bundle adjustment to realtime visual mapping. *IEEE Journal of Robotics and Automation, 24*(5), 1066-1077.

Kordatos, E. Z., Exarchos, D. A., Matikas, T. E., Stavrakos, C., & Moropoulou, A. I. (2012). Application of IR thermography to damage characterization of structures and the diagnosis of historic monuments. 5.

Krzystek, P., Heuchel, T., Hirt, U., & Petran, F. (1995). *A New Concept for Automatic Digital Aerial Triangulation*. Paper presented at the Photogrammetric Week '95.

Lambers, K., Eisenbeiss, H., Sauerbier, M., Kupferschmidt, D., Gaisecker, T., Sotoodeh, S., & Hanusch, T. (2007). Combining photogrammetry and laser scanning for the recording and modelling of the Late Intermediate Period site of Pinchango Alto, Palpa, Peru. *Journal of Archaeological Science, 34*, 11. doi:10.1016/j.jas.2006.12.008

Lan, Y., Thomson, S. J., Huang, Y., Hoffmann, W. C., & Zhang, J. (2010). Current status and future directions of precision aerial application for site-specific crop management in the USA. *Computers and Electronics in Agriculture, 74*, 34-38.

Lane, B., & Whitenton, E. P. (2015). *Calibration and Measurement Procedures for a High Magnification Thermal Camera* (Vol. 8098): NIST:National Institute of Standards and Technology.

Lasaponara, R., Coluzzi, R., Gizzi, F. T., & Masini, N. (2010). On the LİDAR contrubiton for the archaeological and geomorphological study of a deserted medieval village in Southern Italy. *Journal of Geophysics and Engineering 7*(2), 155-163.

Lega, M., Kosmatka, J., Ferrara, C., Russo, F., Napoli, R. M. A., & Persechino, G. (2012). Using Advanced Aerial Platforms and Infrared Thermography

to Track Environmental Contamination. *Environmental Forensics Journal, 13*(4), 332-338. doi:http://dx.doi.org/10.1080/15275922.2012.729002

Lega, M., & Teta, R. (2016). Environmental Forensics: Where Techniques And Technologies Enforce Safety And Security Programs. *International Journal of Safety and Security Engineering, 6*(4), 709-719. doi:10.2495/SAFE-V6-N4-709-719

Lerma, L. J., Navarro, S., Cabrelles, M., & Villaverde, V. (2010). Terrestrial Laser Scanning and Close Range Photogrammetry for 3D Archaeological Documentation: The Upper Palaeolithic Cave of Parpallo´ As a Case Study. *Journal of Archaeological Science, 37*, 499-507.

Lester, J., & Bernold, L. E. (2007). Innovative process to characterize buried utilities using ground penetrating radar. *Automation in Construction, 16*, 546-555.

Letellier, R. (2007). *Recording, documentation, and information management for the conservation of heritage places : guiding principles* (R. Letellier Ed.). Los Angeles, US: The Getty Conservation Institute.

Linder, W. (2006). *Digital Photogrammetry*. Netherlands: Springer

Lo Brutto, M., Borruso, A., & A., D. A. (2012). *UAV Systems For Photogrammetric Data Acquisition of Archaeological Sites*. Paper presented at the International Conference on Cultural Heritage, Lemesos, Cyprus.

Lourenço, P. B., Pena, F., & Amado, M. (2010). A Document Management System for the Conservation of Cultural Heritage Buildings. *International Journal of Architectural Heritage: Conservation, Analysis, and Restoration, 5*(1), 101-121. doi:10.1080/15583050903318382

Ludwig, N., Redaelli, V., Rosina, E., & Augelli, F. (2004). Moisture detection in wood and plaster by IR thermography. *Infrared Physics & Technology, 46*(1-2), 6.

Luhmann, T., Ohm, J., Piechel, J., & Thorsten, R. (2010, 21-24 June 2010). *Geometric Calibration of Thermographic Cameras.* Paper presented at the ISPRS Commission V-Close Range Image Measurement Techniques, Newcastle upon Tyne, United Kingdom.

Lunden, B. (1985). Aerial Thermography: A Remote Sensing Technique Applied to Detection of Buried Archaeological Remains at a Site in Dalecarlia, Sweden. *GeografiskaAnnaler. Series A, Physical Geography, 67*(1/2), 161-166.

Machin, G., Simpson, R., & Broussely, M. (2008). *Calibration and validation of thermal imagers.* Paper presented at the QIRT2008: 9th International Conference on Quantitative InfraRed Thermography, Krakow, Poland.

Madding, P. R., Orlove, G. L., & Kaplan, H. (2003). *Twenty-five years of Thermosense: an historical and technological retrospective.* Paper presented at the Thermosense XXV, Orlando, FL.

Mahlein, A. K., Oerke, E. C., Steiner, U., & Dehne, H. W. (2012). Recent advances in sensing plant diseases for precision crop protection. *European Journal of Plant Pathology, 133*(1), 197-209. doi:10.1007/s10658-011-9878-z

Maldague, P. V. X. History of Infrared and Thermal Testing.

Maldague, P. V. X. (2013). *Infrared Thermography for NDT: Potentials and Applications*. Paper presented at the International Symposium on Structural Health Monitoring and Non-Destructive Testing, Insa,Lyon.

Martiny, M., Schiele, R., Gritsch, M., Schulz, A., & Witting, S. (1997). In Situ Calibration for Quantitative Infrared Thermography. *QIRT 96-Eurotherm Series 50*. doi:http://dx.doi.org/10.21611/qirt.1996.001

Mauriello, L. M., & Froehlich, E. J. (2014). *Towards automated thermal profiling of buildings at scale using unmanned aerial vehicles and 3D reconstruction.* Paper presented at the UbiComp '14 Adjunct: ACM International Joint Conference on Pervasive and Ubiquitous Computing, Seattle, Washington.

Meola, C. (2007). Infrared Thermography of masonry structures. *Infrared Physics And Technology, 49*(3), 6.

Mian, O., Lutes, J., Lipa, G., Hutton, J. J., Gavelle, E., & Borghini, S. (2015). Direct Georeferencing on Small Unmanned Aerial Platforms for Improved Reliability and Accuracy of Mapping without the Need for Ground Control Points. *ISPRS – Int. Arch. Photogram. Remote Sens. Spatial Inform. Sci, XL-1/W4*, 397-402.

Mohamed M.R, M., & Hutton, J. (2001, April 24-27, 2001). *Direct Positioning and Orientation Systems, How Do they Work? What is the Attainable Accuracy?* Paper presented at the American Society of Photogrammetry and Remote Sensing Annual Meeting, St. Louis, MO, USA.

Mohamed, M. K., Patra, S., & Lanzon, A. (2011). *Designing Simple Indoor Navigation system for UAVs*. Paper presented at the 19th Mediterranean Conference on Control and Automation, Aquis Corfu Holiday Palace, Corfu, Greece.

Moropoulou, A., Avdelidis, N. P., Koui, M., Delegou, E. T., & Tsiourva, T. (2001). Infrared thermographic assessment of materials and techniques for the protection of cultural heritage. In Z. Y. Tong Q, Zhu Z, (Ed.), (pp. 6). Wuhan, China: SPIE.

Mouget, A., & Lucet, G. (2014). *Photogrammetric archaeological survey with UAV.* Paper presented at the ISPRS Technical Commission V Symposium:Close-range imaging, ranging and applications, Riva del Garda, Italy.

Moukalled, F., Ghaddar, N., Kabbani, H., Khalid, N., & Fawaz, Z. (2006). Numerical and experimental investigation of thermal signatures of buried landmines in dry soil. *Journal of Heat Transfer, 128*, 484-494.

Mozas-Calvache, A., Prez-Garca, J., Cardenal-Escarcena, F., Mata-Castro, E., & Delgado-Garca, J. (2012). Method for photogrammetric surveying of archaeological sites with light aerial platforms. *Journal of Archaeological Science 39*(2), 521-530. doi:10.1016/j.jas.2011.10.007

Muscio, A., & Corticelli, M. A. (2004). Experiments of thermographic landmine detection with reduced

size and compressed time. *Infrared Physics & Technology, 46*, 101-107.

Nex, F., & Remondino, F. (2014). UAV for 3D Mapping Applications: A Review. *Applied Geomatics* (6), 1-15. doi:10.1007/s12518-013-0120-x

Nocerino, E., Menna, F., Remondino, F., & Saleri, R. (2013). *Accuracy adn Bloeck Deformation Analysis in Automatic AUV and Terrestrial Photogrammetry.* Paper presented at the XXIV International CIPA Symposium, Strasbourg, France.

Nuechter, A., Lingemann, K., Hertzberg, J., & Surmann, H. (2007). 6D SLAM for 3D mapping outdoor environments. *Journal of Field Robotics (JFR), Special Issue on Quantitative Performance Evaluation of Robotic and Intelligent Systems, 24*(8-9), 699-722.

Owen, R., Buhalis, D., & Pletinckx, D. (2004). *Identifying Technologies Used in Cultural Heritage.* Paper presented at the The 5 th Internatioanl Symposium on Virtual Reality, Arceology and Cultural Heritage, Belgium.

Paine, D. P., & Kiser, J. D. (2002). *Aerial Photography and Image Interpretation*. New York: John Wiley and Sons.

Paoletti, D., Ambrosini, D., Sfarra, S., & Bisegna, F. (2013). Preventive thermographic diagnosis of historical buildings for consolidation. *Journal of Cultural Heritage, 14*, 6. doi:http://dx.doi.org/10.1016/j.culher.2012.05.005

Patias, P. (2006, 24-29 April 2006). *Cultural Heritage Documentation.* Paper presented at the International Summer School"Digital Recording and 3D Modelling, Aghios Nikolas, Crete, Greece.

Patias, P., Grussenmeyer, P., & Hanke, K. (2008). *Applications in Cultural Heritage Documentation.* Paper presented at the XXIth ISPRS Congress: Silk Road for Information from Imagery, Beijing, China.

Patias, P., Kaimaris, D., Georgiadis, C., Stamnas, A., Antoniadis, D., & Papadimitrakis, D. (2013). *3D Mapping of Cultural Heritage: Special Problems and Best Practices in Extreme Case-Studies.* Paper presented at the XXIV International CIPA Symposium, Strasbourg, France.

Patias, P., & Santana, M. (2009). *CIPA Heritage Documentation: Best Practices and Applications* (E. Stylianidis, P. Patias, & M. Quintero Santana Eds. Vol. XXXVIII-5/C19). Greece: CIPA.

Perez, M., Agüera, F., & Carvajal, F. (2011). Paper presented at the UAV-g 2011:Conference on Unmanned Aerial Vehicle in Geomatics, Zurich, Switzerland.

Pfeifer, N., Glira, P., & Briese, C. (2012). Direct Georeferencing with on Board Navigation Components of Light Weight UAV PLatforms. *International Archives of the Photogrammetry, Remote Sensing and Spatial Information Sciences, XXXIX*(B7), 487-492.

Apero, an Open Source Bundle Adjustment Software for Automatic Calibration adn Orientation of Set of Images, XXXVIII-5 C.F.R. (2011).

Pineda, U., Montés, N., Sánchez, F., Bensadoun, F., & Ruiz, E. (2012). *In-situ calibration experimental method for Infrared thermography applied to the heat transfer analysis for composite parts during manufacturing based on Resin Infusion technique*. Paper presented at the QIRT 2012-11th International Conference on Quantitative InfraRed Thermography.

Polski, P. (2004, 20–23 September 2004). *View of Unmanned Aerial Vehicle Needs.* Paper presented at the AIAA 3rd Unmanned Unlimited Technical Conference, Chical, IL, USA.

Prajwal, M., Jain, R., Srinivasa, V., & Karthik, K. S. (2016). Optimal Number of Ground Control Points for a UAV based Corridor Mapping. *International Journal of Innovative Research in Science, Engineering and Technology, 5*(9), 28-32.

Püschel, H., Sauerbier, M., & Eisenbeiss, H. (2008). *A 3d model of castle Landenberg (CH) from combined photogrammetric processing of terrestrial and UAV-based Images.* Paper presented at the XXIth ISPRS Congress: Silk Road for Information from Imagery, Beijing, China.

Remondino, F. (2014). UAV:Platforms, Regulations, Data Acquisition and Processing. In F. Remondino & S. Campana (Eds.), *3D Recording and Modelling in Archaeology and Cultural Heritage* (pp. 74-87): BAR International Series

Remondino, F., Barazzetti, L., Nex, F., Scaioni, M., & Sarazzi, D. (2011). *UAV Photogrammetry for Mapping and 3D Modelling- Current Status and Future Perspectives-.* Paper presented at the ISPRS ICWG I/V-UAV-g (unmanned aerial vehicle in geomatics) conference, Zurich, Switzerland. 2011.

Remondino, F., Del Pizzo, S., Kersten, T., & Troisi, S. (2012a). *Low-cost and open-source solutions for automated image orientation – A critical overview*. Paper presented at the EuroMed 2012 Conference.

Remondino, F., Del Pizzo, S., Kersten, T., & Troisi, S. (2012b). *Low-cost and open-source solutions for automated image orientation – A critical overview*. Paper presented at the Proc. EuroMed 2012 Conference.

Remondino, F., & Fraser, C. (2006). Digital camera calibration methods: considerations and comparisons. *International Archives of Photogrammetry, Remote Sensing and the Spatial Sciences, 36*(5), 266-272.

Remondino, F., Spera, G. M., Nocerino, E., Menna, F., Nex, F., & Barsanti, G. S. (2015). *Dense image matching: comparisons and analyses.* Paper presented at the Digital Heritage International Congress 2015:Digitization & Acquisition, Computer Graphics & Interaction, Granada, Spain.

Rinaudo, F., Chiabrando, F., Lingua, A., & Spanò, A. (2012). *Archaeological Site Monitoring: UAV Photogrammetry can be an answer.* Paper presented at the XXII ISPRS Congress, Melbourne, Australia.

Rizaldy, A., & Firdaus, W. (2012). *Direct Georeferencing: A New Standart in Photorammetry for High Accuracy Mapping.* Paper presented at the XXII ISPRS Congress, Comission I, WG I/1, Melbourne, Australia.

Rizzi, A., Voltolini, F., Girardi, S., Gonzo, L., & Remondino, F. (2007). *Digital Preservation, Documentation And Analysis of Paintings, Monuments And Large Cultural Heritage With Infrared Technology, Digital Cameras And Range Sensors*. Paper presented at the XXI International CIPA Symposium, Athens, Greece.

Rock, G., Ries, J. B., & Udelhoven, T. (2011). *Sensitivity Analysis of UAV-Photogrammetry for Creating DigitalElevation Models (DEM).* Paper presented at the UAV-g 2011, Conference on Unmanned Aerial Vehicle in Geomatics, Zurich, Switzerland.

Rosina, E., Avdelidis, N. P., Moropoulou, A., Della Tore, S., Pracchi, V., & Suardi, G. (2004). *IRT Monitoring in Planned Preservation of Built Cultural Heritage*. Paper presented at the 16th World Conference on Nondestructive Testing, Montreal.

Rosina, E., & Grinzato, E. (2001). Infrared and thermal testing for conservation of historic buildings *Infrared and Thermal Testing, NonDestructive Testing Handbook* (Vol. 3). Columbus, OH: ASNT.

Ruiz, J. J., Diaz-Mas, L., Perez, F., & Viguria, A. (2013). *Evaluating the accuracy of DEM generation algorithms from UAV Imagery.* Paper presented at the UAV-g2013, Rostock, Germany.

Rüther, H., Mtaloand, G., & Mngumi, E., 2003. (2003). *3D Modelling of Heritage Sites in Africa. A case study in the world heritage site of Kilwa Kisiwani, Tanzania*. Paper presented at the CIPA 2003, XIXth InternationalSymposium, Antalya, Turkey.

Santulli, C. (2007). IR thermography for the detection of buried objects: a short review. *E-Journal of Non-Destructive Testing, 12*(12).

Santulli, C., & Jeronimidis, G. (2006). Measurement of surface void content on balsa wood using IR thermography. *E-Journal of Non-Destructive Testing, 11*(6).

Sauerbier, M., & Eisenbeiss, H. (2010). *UAV for the documentation of archaeological excavations.* Paper presented at the ISPRS 2010:Close Range Image Measurement Techniques, Newcastle upon Tyne.

Schuckman, K., & Renslow, M. (2017). Direct Georeferencing Technology. from Penn State's College of Earth and Mineral Sciences

Sever, T. L., & Wagner, D. W. (1991). Analysis of prehistoric roadways in Chaco Canyon using remotely sensed data. In C. D. Trombold (Ed.), *Ancient Road Networks and Settlement Hierarchies in the New World* (pp. 42-52): Cambridge University Press.

Skarlatos, D., Procopiou, E., Stavrou, G., & Gregoriou, M. (2013). *Accuracy Assessment of Minimum Control Points for UAV Photography and Georeferencing.* . Paper presented at the First Int. Conference On Remote Sensing Geoinformation Environment.

Skarlatos, D., Theodoridou, S., & Glabenas, D. (2004). *Archaeological surveys in Greece using radio controlled helicopter.* Paper presented at the FIG Working Week 2004, Athens, Greece.

Sofia Udin, W., & Ahmad, A. (2012). Large scale mapping using digital imagery of unmanned aerial vehicle. *International Journal of Scientific & Engineering Research, 3*(11).

Spodek, J., & Rosina, E. (2009). Application of Infrared Thermography to Historic Building Investigation. *Journal of Architectural Conservation, 15*(3), 65-81.

Stepanic, J., Malivovec, M., Svaic, S., & Krstelj, V. (2004). Parametrisation of non-homogeneities in buried object detection by means of thermography. *Infrared Physics & Technology, 45*, 201-208.

Strakova, H., & Reznicek, J. (2013). *Documentation of Dumps and Heaps by use of UAV.* Paper presented at the International Multidisciplinary Scientific GeoConference : SGEM : Surveying Geology & mining Ecology Management, Sofia.

Sun, X. M., Zhu, Z. L., Tang, X. Z., Su, H. B., & Zhang, R. H. (2000). A new measuring technique of soil thermal inertia. *Science in China Series E - Technological Sciences, 43*, S62-69.

Suresh, B., Pardha sardhi reddy, V., Vinod, P. S., Ravi Chandra sekhar, B., & Ghali, V. S. (2015). Comparative Data Processing Methods for Non-Stationary Thermal Wave Imaging. *QIRT*. doi:http://dx.doi.org/10.21611/qirt.2015.0105

Tahar, N. K. (2013). *An Evaluation on Different Number of Ground Control Points in Unmanned Aerial Vehicle Photogrammetric Block.* Paper presented at the ISPRS 8th 3DGeoInfo Conference & WG II/2 Workshop, Istanbul, Turkey.

Tahar, N. K., Ahmad, A., Abdul Aziz, W., Mohd Akib, W., & Mohd Naim, W. (2012). Assessment on Ground Control Points in Unmanned Aerial Ssytesm Image Processing for Slope Mapping Studies *International Journal of Scientific & Engineering Research, 3*(11), 1-10.

Tavukçuoğlu, A., Düzgüneş, A., Caner-Saltik, E. N., & Demirci, Ş. (2005). Use of IR thermography for the assessment of surface-water drainage problems in a historical building, Ag˘zıkarahan (Aksaray), Turkey. *NDT E, 38*(5), 9.

Tianyun, X., Xiaocheng, T., Defang, Y., Yonghe, X., & Hongliang, Y. (2015). UAV Remote Sensing Applications in Large-Scale Mapping in the Hilly Region of Tibetan Plateau. *International Journal of Control and Automation, 8*(3), 279-286. doi:http://dx.doi.org/10.14257/ijca.2015.8.3.28

Trimm, W. M. Nondestructive Testing *Infrared and Thermal Testing*.

Turner, D., Lucieer, A., & Watson, C. (2011, 11–15 April 2011). *Development of an Unmanned Aerial Vehicle (UAV) for Hyper Resolution Vineyard Mapping Based on Visible, Multispectral, and Thermal Imagery.* Paper presented at the ISRSE34:34th International Symposium on Remote Sensing of Environment, Sydney, Australia.

Udin, W. S., & Ahmad, A. (2014). *Assessment of Photogrammetric Mapping Accuracy Based on Variation Flying Altitude Using Unmanned Aerial Vehicle.* Paper presented at the 8th International Symposium of the Digital Earth (ISDE8), Malaysia.

UNESCO. (1972). *Photogrammetry applied to the survey of Historic Monuments, of Sites*

and to Archaeology (UNESCO ed.): UNESCO.

UNESCO. (1989). *Recommendation on the Safeguarding of Traditional Culture and Folklore*. Retrieved from Paris:

Valavanis, K. P. (2007). *Advances in Unmanned Aerial Vehicles State of the Art and the Road to Autonomy* (Vol. 33): Springer,.

van Blyenburgh, P. (2006, 9 March 2006). *UAV Systems: Global Review.* Paper presented at the Avionics‘06 Conference, Amsterdam, The Netherlands.

Vanblyenburgh, P. (2006, 9 March 2006). *UAV Systems: Global Review.* Paper presented at the Avionics‘06 Conference, Amsterdam, The Netherlands.

Vecco, M. (2010). A Definition of Cultural Heritage: From the Tangible to the Intangible. *Journal of Cultural Heritage, 11*, 321-324. doi:10.1016/j.culher.2010.01.006

Verhoeven, G. J., Loenders, J., Vermeulen, F., & Docter, R. (2009). Helikite aerial photography or HAP - a versatile means of unmanned, radio controlled low altitude aerial archaeology. *Archaeological Prospection, 16*, 125-138.

Wang, J., Shi, F., Zhang, J., & Liu, Y. (2008). A new calibration model of camera lens distortion. *Pattern Recognition, 41*, 607-615.

Watts, C. A., Ambrosia, G. V., & Hinkley, A. E. (2012). Unmanned Aircraft Systems in Remote Sensing and Scientific Research: Classification and Considerations of Use. *Remote Sensing*(4), 1671-1692. doi:10.3390/rs4061671

Weil, G. J. (2001). Techniques of Infrared Thermographic Leak Testing *Infrared and Thermal Testing, NonDestructive Testing Handbook* (Vol. 3, pp. 7). Columbus, OH: ASNT.

Wendel, A., Maurer, M., Graber, G., Pock, T., & Bischof, H. (2012). *Dense reconstruction on-the-fly.* Paper presented at the IEEE Int. CVPR Conference, Providence, USA.

Wernke, S. A., Adamas, J. A., & Hooten, E. R. (2014). Capturing Complexity: Toward an Integrated Low-Altitude Photogrammetry and Mobile Geographic Information System

Archaeological Registry System. *Advances in Archaeological Practice: A Journal of the Society for American Archaeology, August,2014*(Special Issue on Digital Domains), 17.

Wierzbicki, D., Kedzierski, M., & Fryskowska, A. (2015). *Assessment of the Influence of UAV Image Quality on the Orthophoto Production.* Paper presented at the International Conference on Unmanned Aerial Vehicles in Geomatics, Toronto, Canada.

www.google.com/patents/US20120069193.

www.nordharz-portal.de.

www.noz.de.

Xiang, H., & Tian, L. (2011). Development of a Low-cost Agricultural Remote Sensing System Based on an Autonomous Unmanned Aerial Vehicle (UAV). *Biosystems Enginnering-Elseiver*(108), 174-190. doi:10.1016/j.biosystemseng.2010.11.010

Xie, F., Lin, Z., Gui, D., & Lin, H. (2012). Study on Construction of 3D building Based on UAV Images. *International Archives of Photogrammetry and Remote Sensing, XXXIX*(B1), 469-473.

Xiong, Z. (2009). *Technical Development for Automatic Aerial Triangulation of High Resolution Satellite Imagery*. Retrieved from University of New Brunswick:

Yanagi, H., & Chikatsu, H. (2015). *Camera Calibration in 3D Modelling for UAV Application.* Paper presented at the Indoor-Outdoor Seamless Modelling, Mapping and Navigation, Tokyo, Japan.

Yılmaz, H. M., Yakar, M., Gulec, S. A., & Dulgerler, O. N. (2007). Importance of digital close-range photogrammetry in documentation of cultural heritage. *Journal of Cultural Heritage, 8*, 428-433. doi:10.1016/j.culher.2007.07.004

Yilmaz, H. M., Yakar, M., Mutluoglu, O., & Yildiz, F. (2004). *Selection of the Most Suitable Sizes of Ground Control Points in the Satellite Images.* Paper presented at the 20th ISPRS Congress Istanbul, Turkey.

Z., S., A., E.-P., & I., K. (2011). *Automatic tie-point extraction using advanced approaches.* Paper presented at the ASPRS 2011 Annual Conference, Wisconsin.

Zarco-Tejada, P. J., González-Dugo, V., & Berni, J. A. J. (2011). Fluorescence, temperature and narrow-band indices acquired from a UAV platform for water stress detection using a micro-hyperspectral imager and a thermal camera. *Remote Sensing of Environment, 117*, 322-337. doi:http://dx.doi.org/10.1016/j.rse.2011.10.007

Zhang, J., Wu, Y., Liu, W., & Chen, X. (2010). Novel approach to position and orientation estimation in vision-based UAV navigation

IEEE Transactions on Aerospace and Electronic Systems, 46(2). doi:10.1109/TAES.2010.5461649

Zhang, W., Jiang, T., & Han, M. (2010). *Digital camera calibration method based on PhotoModeler.* Paper presented at the 3rd International Congress on Image and Signal Processing (CISP2010).

Zischinsky, T., Dorffner, L., & Rottensteiner, F. (2000, 16-23 July 2000). *Application of a new model helicopter system in architectural photogrammetry.* Paper presented at the XIXth ISPRS Congress: Geoinformation for all, Amsterdam, The Netherlands.

Zomrawi, N., Hussien, A. M., & Mohamed, H. (2013). Accuracy Evaluation of Digital Aerial Triangulation. *International Journal of Engineering and Innovative Technology (IJEIT), 2*(10), 7-11.

http://guides.archaeologydataservice.ac.uk/g2gp/AerialPht_UAV